UNIVERSITY OF SOUTHAMPTON

FACULTY OF NATURAL AND ENVIRONMENTAL SCIENCES

School of Chemistry

Use of Flow Techniques to Investigate Organic Reactions

by

Thomas Durand

Thesis for the degree of Doctor of Philosophy

October 2016

UNIVERSITY OF SOUTHAMPTON

ABSTRACT

FACULTY OF NATURAL AND ENVIRONMENTAL SCIENCES

SCHOOL OF CHEMISTRY

Doctor of Philosophy

Use of Flow Techniques to Investigate Organic Reactions

by Thomas Durand

Flow chemistry, the basis of petrochemical and bulk chemicals industry, has recently found various applications in fine chemicals production and discovery chemistry with the development of commercially available laboratory equipment. Due to the precise control of the reaction parameters, the potential for automation and sequencing of reactions, the *in situ* analysis and for safety reasons the development of this novel technology has proven to make significant impact within organic chemistry.

By taking advantage of the potential of flow chemistry, the optimisation of difficult batch reactions involved in the total synthesis of epicocconone analogues, and the *in situ* generation of isocyanides were attempted. However, some limitations such as solubility issues and formation of insoluble species made the optimisations complicated.

Then, activation energies and reaction rate constants were determined from the thermolysis of 1,3-dioxin-4-ones by means of *in situ* analysis (UV and IR) and by using conventional and novel kinetic study methods. Good consistency was observed between both procedures. The significant gain in time and the lower consumption of material were the main advantages of this novel methodology which can be used as a reliable tool to accelerate reaction study and process development.

Finally, the flow platform was employed to develop optimisation of reaction methodologies by using the dispersion effect and the “turn off” light concept. Thermolysis of 1,3-dioxin-4-one, Diels-Alder reaction, [2+2] photocycloaddition, photocyclisation and $S_{RN}1$ reactions were used as models for the development of these two methodologies.
The determination of the rate constant of both 1^{st} and 2^{nd} order reactions, the determination of the optimum amount of reagent and the determination of the optimum concentration of starting material were achieved with the dispersion effect methodology. Then, the “turn off” light procedure was developed to rapidly determine the optimum reaction time. Consistent results were obtained for both new methodologies.

Contents

Declaration of authorship

I, Thomas DURAND

declare that this thesis and the work presented in it are my own and has been generated by me as the result of my own original research.

Use of Flow Techniques to Investigate Organic Reactions

I confirm that:

1. This work was done wholly or mainly while in candidature for a research degree at this University;
2. Where any part of this thesis has previously been submitted for a degree or any other qualification at this University or any other institution, this has been clearly stated;
3. Where I have consulted the published work of others, this is always clearly attributed;
4. Where I have quoted from the work of others, the source is always given. With the exception of such quotations, this thesis is entirely my own work;
5. I have acknowledged all main sources of help;
6. Where the thesis is based on work done by myself jointly with others, I have made clear exactly what was done by others and what I have contributed myself;
7. Parts of this work have been published as:

Durand, T.; Henry, C.; Bolien, D.; Harrowven, D. C.; Bloodworth, S.; Franck, X.; Whitby, R. J., *React. Chem. Eng.* **2016**, 1, 82-89.

Signed:

Date:

Acknowledgements

First of all, I would like to thank my supervisor Prof Richard Whitby for his tireless help, warm encouragement and thoughtful guidance during my time at the University of Southampton. I appreciate all his contributions of time, ideas, endless enthusiasm for chemistry which made my Ph.D. experience productive and stimulating. I would also like to thank my co-supervisors Prof David Harrowven for providing useful ideas and excellent feedback from quarterly reports, and Dr Sally Bloodworth for inspirational discussions and all her time spent for correcting this manuscript.

I wish to thank Dr John Langley and Ms Julie Herniman in MS, Dr Neil Wells in NMR and the glassblowing staff at Southampton. A special mention is due to Keith and Mark in stores who as well as providing an excellent service have also been the source of much entertainment over the past 3 years.

I want to express my gratitude to past and present members of the Whitby group, particularly David, Cyril, Andrea, Bogdan, Ayham, Alexis, Alexandre who have not only been a source of ideas but also great people to work with. Special thanks go to Shamim, “my technician”, for his enthusiasm and for the good time we had together in and outside the lab. Beyond the Whitby group there are a great number of people within Chemistry who have become good friends over the years and I am grateful for that friendship.

I would like to thank my family for the support and the encouragement especially during the final step of my Ph.D.

Finally, special thanks go to INTERREG AI-CHEM for funding this project.

Abbreviations

°C	Degrees Celsius
BL	Black light
BORIS	Bristol Online Reaction Investigation Software
BPR	Back pressure regulator
CI	Chemical Ionisation
COSY	Correlation spectroscopy
DCM	Dichloromethane
DEPT	Distortionless enhancement of polarisation transfer
DFT	Density functional theory
DIBAL-H	Diisobutylaluminium hydride
DIPA	Diisopropylamine
DIPEA	Diisopropylethylamine
DMAD	Dimethyl acetylenedicarboxylate
DMF	Dimethylformamide
DMSO	Dimethyl sulfoxide
E_a	Activation energy
EI	Electron Impact
equiv.	Equivalent(s)
ES	Electrospray
FMO	Frontier molecular orbital
FR	Flow rate
g	Gram(s)
GC	Gas chromatography
h	Hour(s)
HMBC	Heteronuclear multiple bond correlation spectroscopy
HOMO	Highest occupied molecular orbital
HPLC	High performance liquid chromatography
HRMS	High resolution mass spectrometry
HSQC	Heteronuclear single quantum correlation spectroscopy
i.d.	Internal diameter
IPA	Isopropyl alcohol
IR	Infrared
IS	Internal standard
LCMS	Liquid Chromatography Mass Spectrometry
lit.	literature
LRMS	Low resolution mass spectrometry
LUMO	lowest unoccupied molecular orbital
M	Molarity in moles per litre
MACOS	Microwave-assisted continuous flow organic synthesis
m.p.	Melting point
m/z	Mass Charge Ratio
MCR	Multi-component reaction
mg	Milligram(s)
min	Minute(s)
mL	Millilitre(s)
MLR	Multi linear regression
mmol	Millimole(s)
mol	Mole(s)
MS	Mass spectrometry
MW	Molecular Weight
NMR	Nuclear magnetic resonance
OFET	Organic field-effect transistor
OPA	Orthogonal projection approach
PET	Petroleum ether

PFA	Perfluoroalkoxy (polymer)
PSI	Pounds per square inch
PTSA	*p*-toluenesulfonic acid
RBF	Round-bottom flask
Re	Reynolds number
R*f*	Retardation factor
r.t.	Room temperature
RT	Reaction time
RTD	Residence time distribution
sat	Saturated
s/sec	Second(s)
SS	Stainless steel
TBAA	Tetrabutylammonium azide
TFA	Trifluoroacetic acid
THF	Tetrahydrofuran
TLC	Thin layer chromatography
UV	Ultraviolet
vis	Visible (light)
ε	Coefficient of extinction (UV)
µL	Microlitre(s)

1 Chapter 1: Flow chemistry - A new tool for chemists?

1.1 Context

Nowadays, with the competitive nature of the chemical industry, the production of pharmaceuticals, agrochemicals, high-performance polymers, paints, pigments, perfumes and fuel additives is in constant intensification. Moreover, due to the continuous pressure to deliver new and successful compounds within short deadlines and in order to be competitive in a fast changing market, the research process is improving and industrial companies are going through continuous developments. Innovations and new strategies towards more sustainable, cost-effective and greener synthetic procedures are necessary[1] from early discovery to production. A future that has lower energy consumption, uses less solvent and produces less waste is essential.

In this context, aided by the progress of computational techniques and data analysis devices, continuous flow processing is developing as one of the techniques that can considerably impact on synthetic procedures. More recently, continuous flow processes have gained much more attention from organic chemists and have found applications for the preparation of fine chemicals such as Active Pharmaceutical Ingredients (APIs) or natural products.[2] Although chemical industries still rely on batch reactors, continuous processing is slowly gaining ground and promising perspectives can be supposed for this novel technology.[3]

Figure 1.1 highlights the evolution of the number of publications related to "flow chemistry" processes for the last 20 years and the substantial increase confirms that this technology is attracting lots of interests.

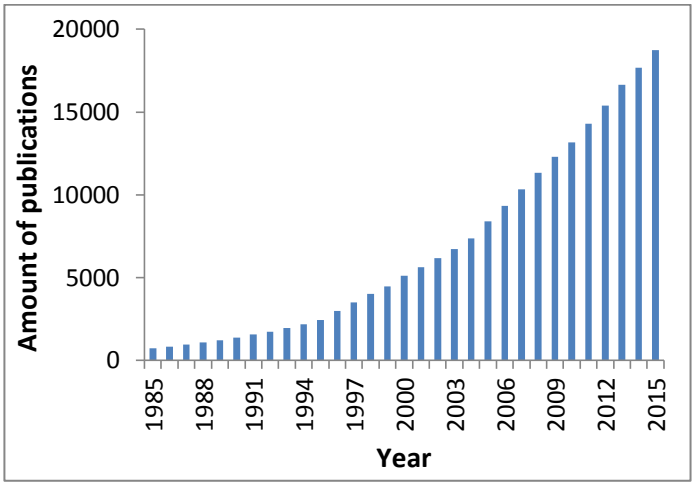

Figure 1.1: Number of publications related to "flow chemistry" technology. Literature search on Reaxys.[4]

1.2 What is flow chemistry?

Flow chemistry can be defined as a continuous process with four main components: pumps, tubing, a mixer and a reactor. This concept works according to a constant input and output flow rather than producing single batches. The different reactive species are mixing and going through a tube or a chip reactor where the reaction occurs. The product is collected at the exit in a suitable reservoir. The stoichiometry is defined by the concentration of the reagent solutions and their relative flow rates when they mix. The reaction time is defined by the ratio of the volume of the reactor to the flow rate after the mixer.

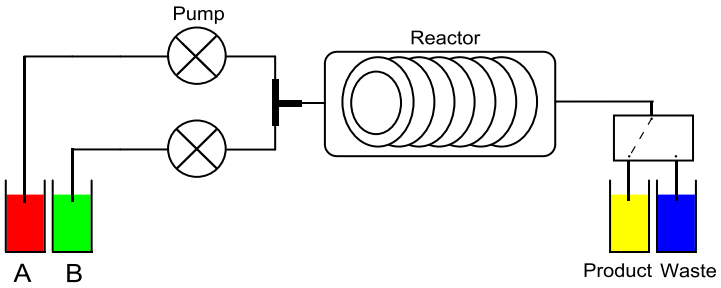

Figure 1.2: General scheme for a flow reactor.

1.3 Advantages of flow chemistry

Flow chemistry has several inherent advantages compared to the conventional batch chemistry.[3, 5]

Precise control of reaction parameters:

The reaction time is precisely controlled by the selected flow rate. Moreover, computer-controlled systems enable the reduction of variations and errors induced by the operator, and thus increase reproducibility.

Fast assembly of apparatus:

The different commercial flow platforms are made up of different standard single units (pumps, reactor, tubing, mixer, back pressure regulator, cooling loop, injection loop) which can be easily assembled and customised with purification, analysis (in-line IR or UV spectrometer) and collection units in order to design the required system for the target transformation. A series of reactors can be easily connected together to perform sequential reactions.

High level of automation:

Flow chemistry can perform a series of reactions entirely controlled by a computer. On the provided software, the operator just needs to program a series of experiments with the

various experimental conditions and run them without direct supervision. In this way, this fully automated system can be particularly useful for kinetic studies when the same setup is used for a series of experiments with different flow rates and temperatures.

In situ analysis:

Real-time monitoring with *in situ* analysis allows the determination of the composition of the reaction mixture at the exit of the reactor. This can be very useful for reaction optimisation and changing reaction conditions rapidly. In specific cases, the series of spectra recorded during an experiment can be processed with relevant software to quickly extract useful information such as reaction rate constants and activation energies for kinetic studies.

Efficient heat transfer and easy scale-up:

Due to their higher surface-to-volume ratios than batch systems, heat transfer in flow reactors is much faster, which means that the reaction mixture quickly reaches the desired temperature. For very exothermic reactions such as nitration, this efficient heat transfer allows excellent temperature control and avoids thermal runaway.[6] Scale-up of a reaction in flow means adding several reactors in parallel or leaving the reaction running with the same parameters, whereas in batch, the reactor size is increased leading to a dramatic decrease in the surface-to-volume ratio and consequently in the heat transfer. This loss in heat transfer efficiency can induce dramatic changes in the scale up experiment (different yield, selectivity…).

Increased safety:

Flow platforms are closed systems and are made up of resistant tubing which limits the exposure to hazardous compounds. Moreover, with the efficient heat transfer and the small amount of material in the reactor, hazardous experiments such as nitration or those involving azide are more accessible.[6-7]

Access to new reaction conditions:

Flow reactors can be used under high pressure and temperature. With the use of a back pressure regulator, the reaction mixture can be heated beyond the boiling point of the solvent.

1.4 Disadvantages of flow chemistry

Although the various advantages described previously make flow chemistry very attractive, there are also a few drawbacks.

Cost:

Flow chemistry is still a new technology and flow kits are not mass-produced. Indeed, in 2014, Vapourtec Company sold the 200th flow platform. Moreover, a small number of specialised companies are providing this advanced equipment which explains the low competitive market and the rather expensive cost. Regarding the different units and spare parts of the flow platform, their replacement is rather expensive (pumps, reactor, valves). Moreover, only few suppliers are selling ferrules, check valves, tubing, back pressure regulators, seals and mixers. Therefore, it is very costly to research in this area.

Maintenance:

Flow chemistry platforms are made up of various mechanical and electrical components which need to be fixed when they break-down. For this reason, standard mechanical skills are required to keep the flow machine working properly. When a replacement is needed, an engineer can come to the laboratory but this servicing is rather expensive.

Chemistry limitation:

First of all, for the Vapourtec platform, corrosive components such as strong acids are prohibited because they can damage the pumps. Then, most of the flow machines have not been designed to work with non-homogeneous reaction mixtures especially with solid materials. For this reason, solubility is a key factor and working with organometallic reagents or non-soluble products can be an issue.

Visibility of the reaction:

Flow platforms are closed systems and in most cases, reactions are run with stainless steel reactors which are not transparent. For this reason, it is not always easy to assess the progress of a reaction. The operator has to rely on the information provided by the software (pressure, temperature, flow rate) to monitor the chemical reaction.

Communication between the different devices:

The different devices used for the customisation of the flow platform such as the IR and UV spectrometers, the syringe pumps, the HPLC, improve its versatility but, at the same time, increase the communication problems. Indeed, each device is controlled by different non-open source software which make the automated connection and communication between each other very complicated.

1.5 Flow equipment

Over the last few decades, a wide range of flow chemistry platforms have become commercially available. Flow equipment exist in various scales, from micro-scale (μL/min) to meso-scale (mL/min) and even larger (L/h). The easy customization of the platforms by adding or removing various units (pumps, injection loops, PFA reactor, SS reactor, photochemical reactor, autosampler/collector, *in situ* analysis) allows the access to a wide range of chemical applications. These advanced and fully automated systems give new perspectives in the field of organic synthesis as they can perform complex and sequential chemical reactions with only a few mouse clicks and with low interactions from the operator. Several suppliers, which are continuously improving their equipment to build the most sophisticated machine, are selling them at different prices and for different applications. The main ones are RS-400 and easy-Medchem by Vapourtec, Asia 130 by Syrris, FlowSyn Multi-X by Uniqsis and Phoenix flow reactor/H-cube by ThalesNano. Various parameters of these flow platforms are highlighted in the following Table 1.1.

The RS-400 is the flow platform used in Prof R. J. Whitby's laboratory (Figure 1.3). This versatile machine offers the flexibility to tackle challenging problems by modifying the system configuration. Various reactors are available to carry out experiments: the air-heated plastic reactor (perfluoroalkoxy polymer) is convenient for reaction up to 150 °C and allows the user to monitor the progress of the reaction (transparent reactor-visual monitoring). Then, the air-heated stainless steel reactor is suitable for reactions performed in harsher conditions (higher pressure and temperature up to 250 °C). Home-made reactors to perform specific reactions are also adaptable to this system. For example, we designed a flow photochemical reactor[8] and a coiled stainless steel reactor immersed in oil for kinetic investigations. Gas-exchange reactors are also commercially available. The reagents can either be injected from stock bottles or injection loops and the T-mixer achieves their efficient mixing. At the exit of the reactor, *in situ* analysis (UV-vis or IR) gives access to real-time monitoring of the reaction mixture which is then collected in a single flask or by means of an autocollector.

RS-400 (R2+/R2+/R4) by Vapourtec®[9]	
	The RS-400 is a flow platform with 4 HPLC pumps, tube reactors, injection loops, an autosampler and collector, manually controlled or fully automated with the flow commander software. Upgrades with cryo-reactor, packed column reactor, photochemical reactor and gas-liquid reactor are possible - Flow rate: 0.1 to 10 mL/min - Pressure limit: 50 bar - Temperature: r.t. to 250 °C
Asia 130 by Syrris®[10]	
	The Asia 130 provides a full range of equipment: syringe pump, tube reactor, microreactor, injection loops, product collector and back pressure controller for super heating. - Flow rate: 1 µL to 10 mL/min - Pressure limit: 20 bar - Temperature: - 15 °C to 150 °C
FlowSyn Multi-X by Uniqsis®[11]	
	The FlowSyn Multi-X is a flow platform with 2 HPLC pumps, coiled reactor, chip reactor, column reactor and fraction collector, manually controlled or fully automated with the flow software. Various upgrades are possible such as the incorporation of a cryo-reactor. - Flow rate: up to 20 mL/min - Pressure limit: 97 bar - Temperature: up to 260 °C
Phoenix flow reactor by ThalesNano®[12]	
	The Phoenix flow reactor can perform very high temperature homogeneous and heterogeneous reactions using loops or cartridges. This platform is compatible with the H-cube (see below). - Flow rate: up to 25 mL/min - Pressure limit: 100 bar - Temperature: up to 450 °C
H-cube by ThalesNano®[12]	
	The H-cube is a continuous-flow hydrogenation reactor with *in situ* generation of hydrogen and a disposable catalyst cartridge (Pd/C). - Flow rate: 0.3 to 3 mL/min - Pressure limit: 100 bar - Temperature: up to 100 °C

Table 1.1: Most popular commercially available flow kits.

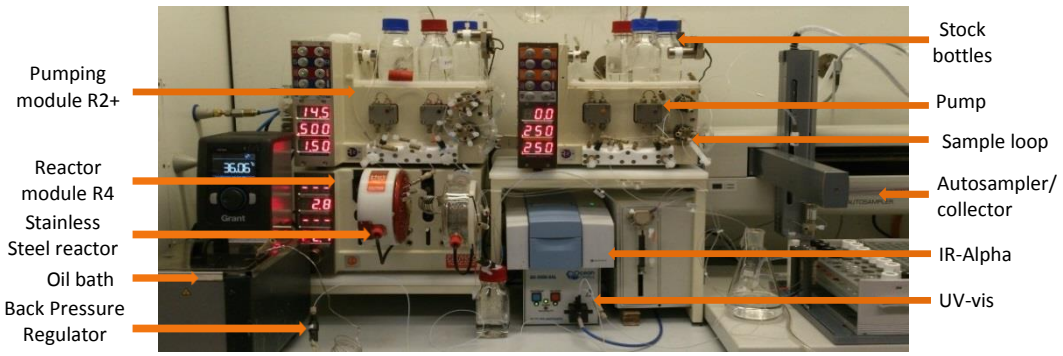

Figure 1.3: Flow chemistry platform (RS-400) set-up in a fume cupboard and equipped with a 10 mL Stainless Steel reactor, IR (Bruker Alpha) and UV-vis (Ocean Optics) spectrometers, and an autosampler/collector. This different devices are controlled with software: Flow commander (flow platform), OPUS (IR) and SpectraSuite (UV-vis).

1.6 Aims and overview of the thesis

1.6.1 Flow chemistry - A tool for optimisation of complicated batch reactions

According to various published examples,[13] it has been described that flow chemistry can dramatically improve low yielding reactions performed in batch. Better heat transfer, access to very high temperatures, good mixing and precise control of reaction time are the main reasons of these improvements. Based on these promising flow results, the aim of this chapter was to optimise in flow the final steps of the synthesis of 2nd generation epicocconone analogues due to rather poor results in batch (Collaboration with the Franck research group (IRCOF, COBRA Laboratory, Rouen))

1.6.2 *In situ* generation of isocyanides, indispensable building blocks of multi-component reactions (MCRs)

Isocyanides are important building blocks which can be used in multi-component reactions such as the Passerini or the Ugi reactions. With flow chemistry, they can be generated *in situ* and then be engaged in sequential reactions to form new components. In this context, the "clean" *in situ* generation of isocyanides was investigated.

1.6.3 Thermolysis of 1,3-dioxin-4-ones under flow, fast generation of kinetic data using in-line analysis

Using a novel methodology developed in 2011,[14] we highlighted the power of our mesoscale platform to quickly generate kinetic information. The thermolysis of various 1,3-dioxin-4-ones were used as model reactions to show the excellent consistency between the "Push-out" methodology and the conventional one.

1.6.4 Flow chemistry - A tool for fast optimisation of reaction conditions

Finally, the dispersion phenomenon occurring in flow chemistry and generating a gradient of concentration was used to quickly optimise photochemical reaction conditions. Then, using flow photochemistry, a novel methodology was developed to quickly determine the optimum reaction time.

2 Chapter 2: Flow chemistry - A tool for optimisation of complicated batch reactions

2.1 Introduction to flow optimisation of difficult batch reactions

The application of flow chemistry to organic syntheses offers several advantages over traditional batch chemistry such as the improvement of the reaction yield, purity, selectivity, scalability and reproducibility.[5a] These benefits are mainly related to the good spatial, thermal, and temporal control offered by continuous flow processes. In this context, many reactions such as oxidation,[13a] reduction,[13b] electrophilic aromatic substitution (e.g. halogenation,[15] Friedel-Craft aminoalkylation[16]), organometallic reactions (Suzuki coupling,[17] Sonogashira coupling,[18] Heck reaction,[19] Grignard[20]), Knoevenagel condensation,[21] reactions involving very short-lived highly reactive intermediates[22] and many others were widely improved and developed by using flow chemistry. Moreover, several batch organic syntheses with successive protection-deprotection steps due to sensitive functional groups were considerably improved and shortened with flow processes by avoiding these additional steps. Examples were developed with reactions involving organolithium compounds (very reactive species towards electrophiles) bearing unprotected groups such as ketone,[22] alkoxy-carbonyl[23] or nitro[24] by taking advantage of the precise residence time control that flow processing offers.

Some of the optimised reactions mentioned previously are described below with comparison of the flow and batch mode results.

Kawaguchi *et al.*[13a] reported that Swern oxidation can be performed with flow mode at temperatures between -20 and 20 °C, much higher temperatures than those required for conventional batch reactors (-50 °C or below). The efficient flow mixing prevented the by-product formation via the Pummerer rearrangement and substantially increased the yield of the reaction (Table 2.1).

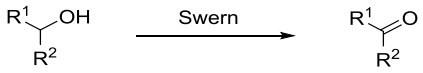

2.1 **2.2**

System	Alcohol **2.1**	Temperature (°C)	Yield of the oxidised product **2.2** (%)
flow	1-decanol	-20	75
flow	1-decanol	20	71
batch	1-decanol	-20	11
flow	2-octanol	-20	95
flow	2-octanol	20	89
batch	2-octanol	-20	20

Table 2.1: Swern oxidation of alcohols by using flow and batch systems.

Then, Midorikawa *et al.*[15] showed that the use of flow chemistry enables better selective monoiodination of aromatic compounds compared to batch mode due to efficient mixing.

The monoiodo compounds **2.4** and **2.7** are less reactive than the parent compounds because the iodo group deactivates the aromatic ring. However, in batch mode, the formation of the diiodo compounds **2.5** and **2.8** can be ascribed to "disguised chemical selectivity" because the reaction is faster than the mixing.[15] The use of flow chemistry with efficient mixing turns out to be a good solution to solve this selectivity issue (Scheme 2.1).

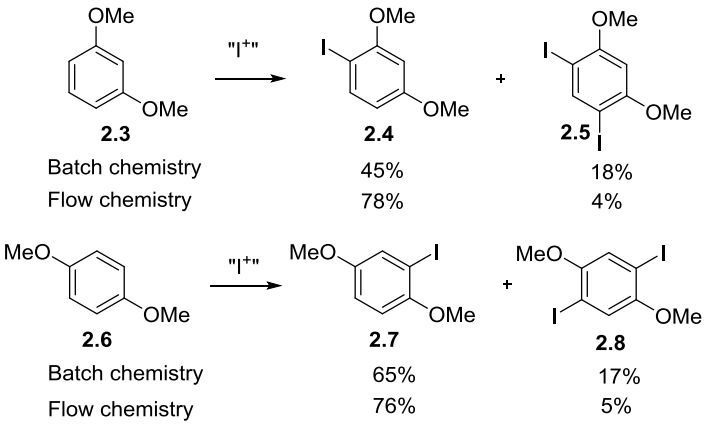

Scheme 2.1: Product selectivity of iodination of aromatic compounds with electrochemically generated "I^+".

Finally, flow chemistry has demonstrated its potential regarding the protecting-group-free synthesis. Belardi *et al.*[25] described in 2008 the total synthesis of the Macbecin I using traditional batch chemistry (Scheme 2.2).

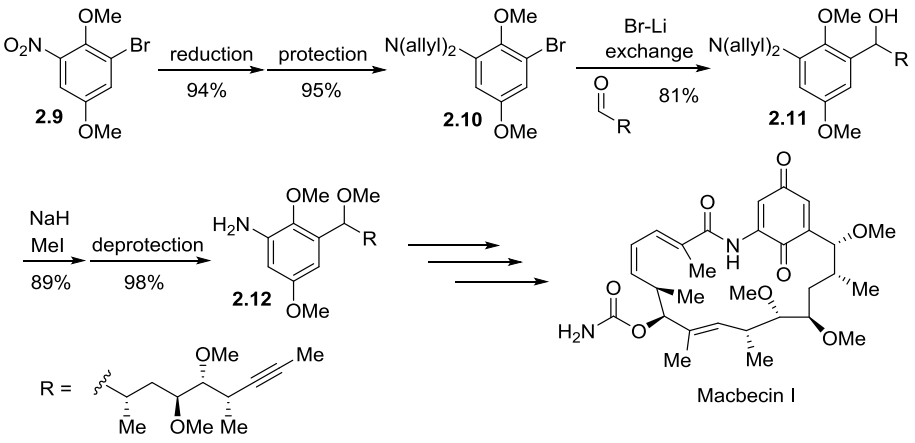

Scheme 2.2: Synthesis of Macbecin I in batch mode.

Due to the very difficult formation *m*-nitro-substituted aryllithium compounds in traditional chemistry, **2.9** was reduced and the amine was protected to form **2.10**. Then, **2.11** was obtained after reaction between the aryllithium bearing a protected amino group and an

aldehyde. After methylation, the amino group was deprotected to give **2.12**. The overall yield was 63% for this 5 step synthesis.

To compare, the transformation employing a *m*-nitro-substituted aryllithium by using a continuous flow process (precise residence time control) turns out to be a possible and promising alternative straightforward route (Scheme 2.3). The reaction between **2.13** and PhLi followed by sequential reactions with an aldehyde and Me_2SO_4 gave compound **2.16** in 73% yield. The target compound **2.12** was obtained by a simple reduction of the nitro group, avoiding protection-deprotection steps.[24]

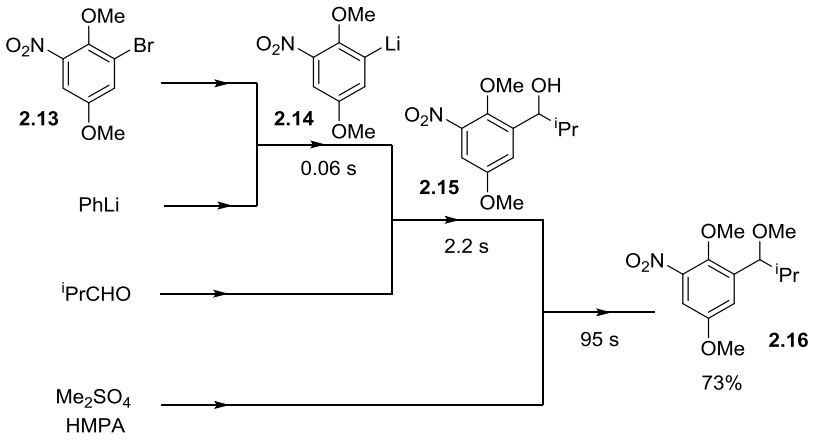

Scheme 2.3: Protecting-group-free alternative route to Macbecin I.

In the following section, flow chemistry was used in order to improve and optimise low yielding reactions performed in batch chemistry. Indeed, developing a collaboration with the Franck research group (IRCOF, COBRA Laboratory, Rouen) working on the synthesis of epicocconone analogues, low yields were obtained during key steps, and the use of flow chemistry was investigated as a possible solution.

2.2 Introduction to epicocconone and the synthesis of epicocconone analogues

Epicocconone (**2.17**), a natural product isolated from the fungus *Epicoccum nigrum*,[26] has remarkable properties. Indeed, this molecule is well soluble in water and in lipid bilayers, and the masked aldehyde can react with an amine to form an enamine which is highly fluorescent in the red region (around 600 nm) (Scheme 2.4). Therefore, this molecule has found biological applications such as in live-cell imaging[27] due to its large Stokes shift.

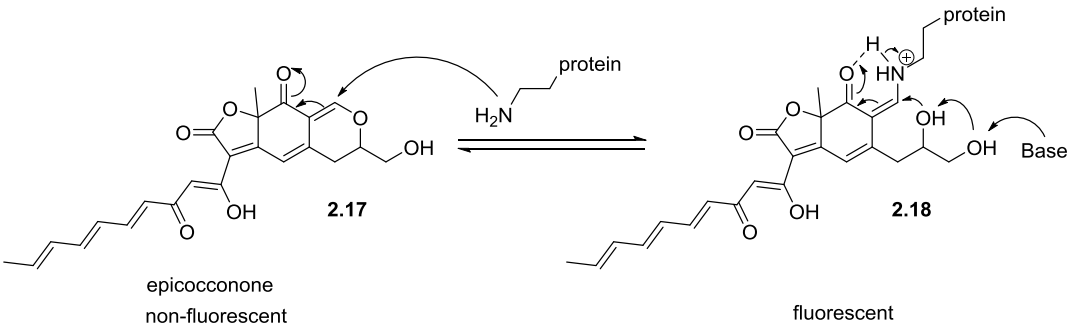

Scheme 2.4: Mechanism of the reversible protein fixation on the epicocconone (**2.17**).

However, due to the low photostability of epicocconone, the Franck research group worked on the development of a strategy for the synthesis of epicocconone analogues by replacing the ketotriene or the triene tail by an aromatic ring and the final methyl alcohol by a dimethyl group. The straightforward route will provide access to a wide range of polyfunctional fluorophores[28] based on the same design as the epicocconone while increasing the photostability (no photo-isomerisation or photo-oxidation and less reversible cyclisation with the tertiary alcohol). The retrosynthesis of the 1st generation epicocconone analogues **2.19**, characterised by a single keto group (Scheme 2.5, in green) next to the final aromatic ring, and 2nd generation epicocconone analogues **2.20**, characterised by a β-ketoenol side chain as in the natural product (Schemes 2.5, in orange) next to the final aromatic ring, can be described with 3 key steps (Scheme 2.5).[29] The tricycle species **2.19** or **2.20** were obtained by trapping of an acylketene with **2.21** followed by an intramolecular Knoevenagel condensation. **2.21** was synthesised from the oxidative dearomatisation of **2.22**, which was previously prepared by alkylation of the commercially available **2.23** or **2.24**.

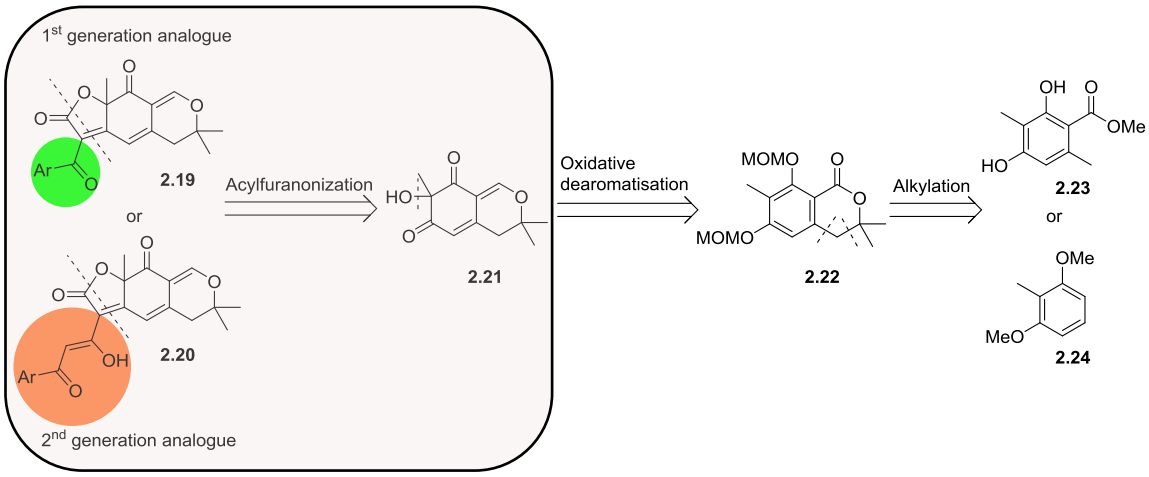

Scheme 2.5: Retrosynthetic analysis of epicoconnone analogues **2.19** and **2.20**.

The final step of the synthesis of epicoconnone analogues, the acylfuranonization, was performed between **2.21** and an acylketene. This acylketene, a very unstable intermediate, was obtained by thermal fragmentation of a 1,3-dioxin-4-one via a retro Diels-Alder reaction. Preliminary studies on this final step were performed by the Frank research group using 3-hydroxy-3-methylbutan-2-one (**2.25**) and various 1,3-dioxin-4-ones, and really promising results were obtained for these model syntheses of the 1st and 2nd generation analogues (Tables 2.2 and 2.3).[30]

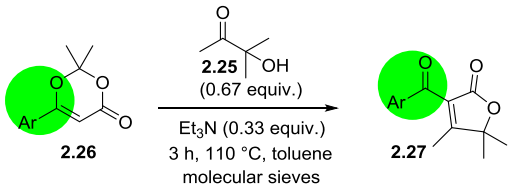

Entry	Ar	**2.27** (Yield)
1	phenyl	**2.27a** (90%)
2	*p*-methoxyphenyl	**2.27b** (71%)
3	furyl	**2.27c** (65%)

Table 2.2: Model synthesis of first generation epicocconone analogues.[30]

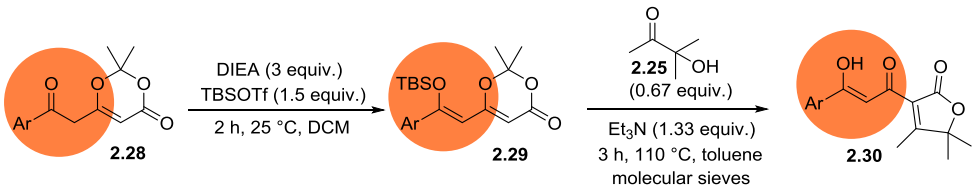

Entry[a]	Ar	**2.29**[a] (Yield)	**2.30** (Yield)
1	phenyl	**2.29a** (98%)	**2.30a** (91%)
2	*p*-cyanophenyl	**2.29b** (88%)	**2.30b** (50%)

Table 2.3: Model synthesis of second generation epicocconone analogues.[30]
[a] For the unprotected system, the intramolecular trapping compound was the main product.

These model conditions were then transferred to the target synthesis using alcohol **2.21** instead of 3-hydroxy-3-methylbutan-2-one (**2.25**).

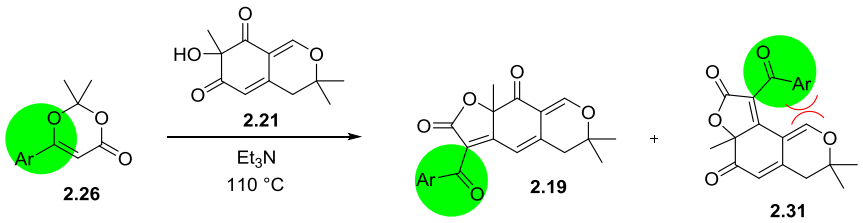

Entry[a]	Ar	**2.19** (Yield)	**2.31** (Yield)
1	phenyl	**2.19a** (60%)	**2.31a** (< 2%)
2	*p*-methoxyphenyl	**2.19b** (86%)	**2.31b** (< 2%)
3	2-naphthyl	**2.19d** (64%)	**2.31d** (< 2%)

Table 2.4: Synthesis of first generation epicocconone analogues.[29, 31]

[a] Reaction conducted in one pot with: **2.26** (1 equiv.), **2.21** (0.67 equiv.), Et_3N (1.33 equiv.), molecular sieves (4 Å), toluene at 110 °C during 3 h.

For the one-pot synthesis of the 1st generation analogues, furanones **2.19** and **2.31** were obtained from the trapping of the acylketene, prepared from the thermolysis of the 1,3-dioxin-4-one **2.26**, by the alcohol **2.21** followed by a Knoevenagel condensation.[29, 31] Starting with different dioxinones **2.26**, a library of 1st generation epicocconone analogues **2.19** was synthesised in rather good yields (Table 2.4, entries 1-3). In each case, a non-isolatable amount of the undesired regioisomer **2.31** was obtained and the steric constraint can be an explanation of the low yield (< 2%).[29]

For the one-pot synthesis of the 2nd generation analogues, the first attempt was tried with the same synthetic route as the 1st generation but starting with an unprotected dioxinone **2.28a** bearing an additional keto group. As expected, the desired product **2.20a** was not obtained and 2 side reactions were observed: the intramolecular trapping of the unstable acylketene **2.32** by the unprotected ketone to form 6-phenyl-4-hydroxy-2*H*-pyran-2-one (**2.33**) (Scheme 2.6), and the decarboxylation of **2.34** due to the small amount of water in the media leading to β-keto acid **2.35** (Scheme 2.7).[29]

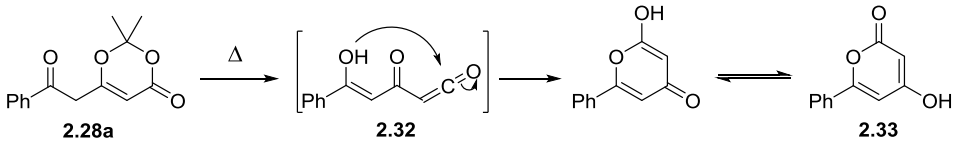

Scheme 2.6: Intramolecular trapping of the acylketene **2.32** for the unprotected system.

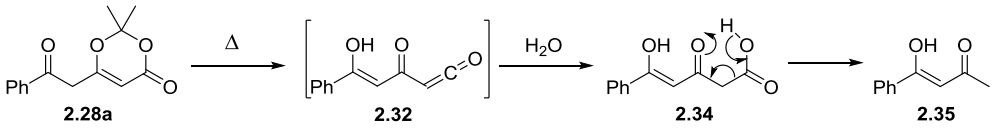

Scheme 2.7: decarboxylation due to the small amount of water in the media.

For these reasons, the protection of the aryl ketone as a silyl enol ether was considered (as for the model synthesis, Table 2.3) and the synthesis of the 2nd generation epicocconone analogues **2.20** was performed (Table 2.5).[31]

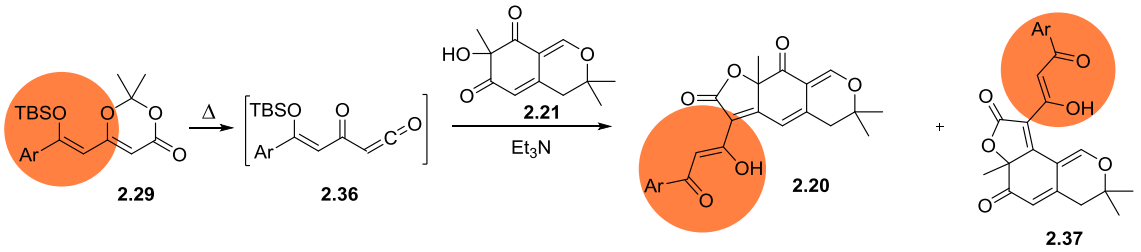

Entry[a]	Ar	**2.20** (Yield)	**2.37** (Yield)
1	phenyl	**2.20a** (39%)	**2.37a** (0%)
2	*p*-cyanophenyl	**2.20b** (3%)	**2.37b** (0%)
3	2-naphthyl	**2.20c** (26%)	**2.37c** (0%)
4	*p*-methoxyphenyl	**2.20d** (15%)	**2.37d** (0%)
5	6-chloro-3-pyridyl	**2.20e** (15%)	**2.37e** (0%)
6	4-(prop-2-ynyloxy)phenyl	**2.20f** (14%)	**2.37f** (0%)

Table 2.5: Synthesis of second generation epicocconone analogues.[31]

[a] Reaction conducted in one pot with: **2.29** (1 equiv.), **2.21** (0.67 equiv.), Et_3N (1.33 equiv.), molecular sieves (4 Å), toluene at 110 °C during 3 h.

The different yields described in Table 2.5 are rather poor for the one-pot synthesis of the 2nd generation epicocconone analogues **2.20** (3-39%). No traces of the undesired regioisomers **2.37** were observed. The deprotected product **2.20** was isolated at the end of each reaction, probably due to the deprotection of the dioxinone **2.29** with the high temperature experimental conditions. Therefore, the poor yields can be explained by the competitive intramolecular trapping of the acylketene and the formation of the decarboxylated product, which are probably faster than the trapping by alcohol **2.21**.[31a]

Having these batch results from the Franck research group, the aim of our project was to try this final acylfuranonization using our flow Vapourtec platform in order to improve the yields of the 2nd generation epicocconone analogues by decreasing the formation of by-products (intramolecular trapping product and decarboxylated product) and by avoiding the protection of 1,3-dioxin-4-ones. The efficient heat transfer and the good mixing offered by continuous flow processes can help in the increase of the yield.

2.3 Results and discussions

2.3.1 Synthesis of 2,2-dimethyl-6-(2-(2-naphthyl)-2-oxoethyl)-4*H*-1,3-dioxin-4-one (2.28c), precursor of a 2nd generation epicocconone analogue

Before studying the acylfuranonization for the 2nd generation epicocconone analogue, 2,2-dimethyl-6-(2-(2-naphthyl)-2-oxoethyl)-4*H*-1,3-dioxin-4-one (**2.28c**) was prepared as described in Scheme 2.8.[29]

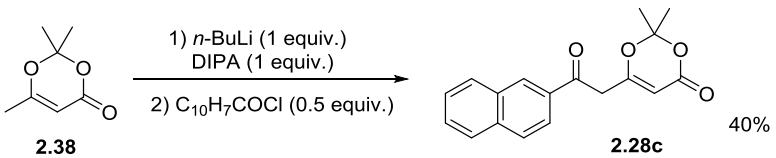

Scheme 2.8: Synthesis of 2,2-dimethyl-6-(2-(2-naphthyl)-2-oxoethyl)-4*H*-1,3-dioxin-4-one (**2.28c**).

2.28c was obtained in 40% yield by condensation of the lithium enolate of commercially available 2,6-trimethyl-4*H*-1,3-dioxin-4-one (**2.38**) and the naphthoyl chloride. This 1,3-dioxin-4-one **2.28c** was used in our investigations to improve the yields of the 2nd generation epicocconone analogues.

2.3.2 Optimisation experiments towards the synthesis of 2nd generation epicocconone analogues

During the batch synthesis of the 2nd generation epicocconone analogues described previously (Table 2.5),[31] the additions of alcohol **2.21** and Et_3N were performed simultaneously and could be an explanation of the significant amount of intramolecular trapping and therefore the poor yields obtained. For this reason, we decided to try the optimisation of both steps one after the other (1st step: reaction between 1,3-dioxin-4-one **2.28c** and alcohol, 2nd step: addition of Et_3N (Knoevenagel condensation)).

2.3.2.1 Optimisation of the trapping of the acylketene by an alcohol - Model reactions

Due to the small amount of alcohol **2.21** in our laboratory (100 mg provided by the Franck research group), the optimisation of the trapping of the acylketene was first performed on model reactions using simple alcohols (EtOH, *t*-BuOH, IPA and 3-hydroxy-3-methylbutan-2-one (**2.25**)) under various experimental conditions. It was then envisaged that the best conditions found with the model reactions would be applied to the synthesis of the 2nd generation epicocconone analogue using 1,3-dioxin-4-one **2.28c** and alcohol **2.21**.

For each reaction condition described (Table 2.6), a 5 mL plug of a mixture of **2.28c** and ROH in the corresponding dry solvent was injected into the flow set-up (Figure 2.1) using a sample loop. At the exit of the reactor (90 - 150 °C), the reaction mixture was collected, the solvent was evaporated under reduced pressure (except for DMSO-*d6*), and NMR samples were prepared. The different compounds observed in the ^1H NMR spectra were quantified in molecular percentage ($\%_{mol}$) and the results are described in Table 2.6 (The identification of each compound was performed with NMR data from the literature[32]). **2.39** and **2.39'** are the only tautomers in each reaction mixtures.

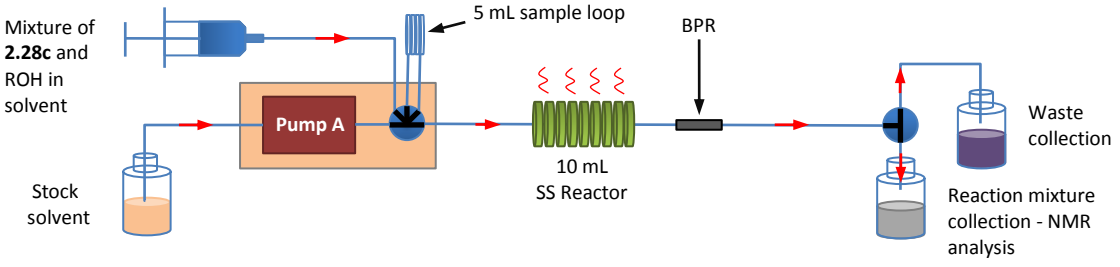

Figure 2.1: Flow set-up for the optimisation of the trapping of the acylketene by an alcohol - Sample loop configuration.

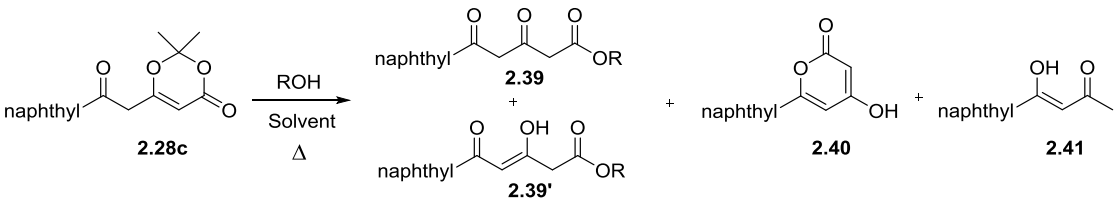

Entry	ROH	**2.28c** (equiv.)	ROH (equiv.)	[**2.28c**] (g/L)	Reaction time (min)	Solvent	Temp. (°C)	%$_{mol}$ **2.28c**	%$_{mol}$ **2.39 + 2.39'**	%$_{mol}$ **2.40**	%$_{mol}$ **2.41**
1	EtOH	1	0.67	1	10	MeCN	100	50	28	5	17
							110	13	46	7	34
							120	0	50	7	43
							130	0	48	6	46
							140	0	39	6	55
							150	0	28	5	67
2	EtOH	1	0.25	1	10	MeCN	90	78	8	3	11
							100	52	14	5	29
							110	14	23	8	55
							120	0	24	8	68
							130	0	22	7	71
							140	0	17	6	77
							150	0	11	5	84
3	EtOH	1	0.67	0.5	10	MeCN	90	79	11	2	8
							100	50	26	6	18
							110	13	44	9	34
							120	0	45	10	45
							130	0	41	9	50
							140	0	34	9	57
							150	0	26	8	66
4	*t*-BuOH	1	0.67	1	10	MeCN	90	81	5	4	10
							100	50	15	9	26
							110	15	24	13	48
							120	0	25	14	61
							130	0	14	12	74
							140	0	6	12	82
							150	0	0	10	90
5	*t*-BuOH	1	5	1	10	MeCN	110	14	63	14	9
							120	0	72	15	13
							130	0	63	20	17
							140	0	49	24	27
6	EtOH	1	0.67	1	10	DMSO-*d6*	90	68	0	20	12
							100	38	0	45	17
							110	6	0	68	26
							120	0	0	70	30
							130	0	0	70	30
							140	0	0	71	29
							150	0	0	75	25
7	*t*-BuOH	1	0.67	1	10	DMSO-*d6*	90	70	0	17	13
							100	39	0	37	24
							110	7	0	60	33
							120	0	0	66	34
							130	0	0	69	31
							140	0	0	69	31
							150	0	0	65	35
8	IPA	1	0.67	1	10	toluene	90	68	29	0	3
							100	42	50	0	8
							110	13	67	0	20
							120	1	69	0	30
							130	0	65	0	35
							140	0	58	0	42
							150	0	49	0	51
9	*t*-BuOH	1	0.67	1	10	toluene	110	9	49	0	42
							120	0	40	0	60
							130	0	25	0	75
							140	0	14	0	86
10	*t*-BuOH	1	1	1	10	toluene	120	0	61	0	39
					40			0	48	0	52
11	*t*-BuOH	1	1	4	20	toluene	120	0	82	0	18
12	*t*-BuOH	1	1	8	10	toluene	120	0	89	0	11
					40			0	88	0	12
13	*t*-BuOH	1	1	24	10	toluene	120	0	94	0	6
14		1	1	24	10	toluene	110	12	85	0	3
							120	0	97	0	3

Table 2.6: Optimisation of the trapping of the acylketene with various alcohols.

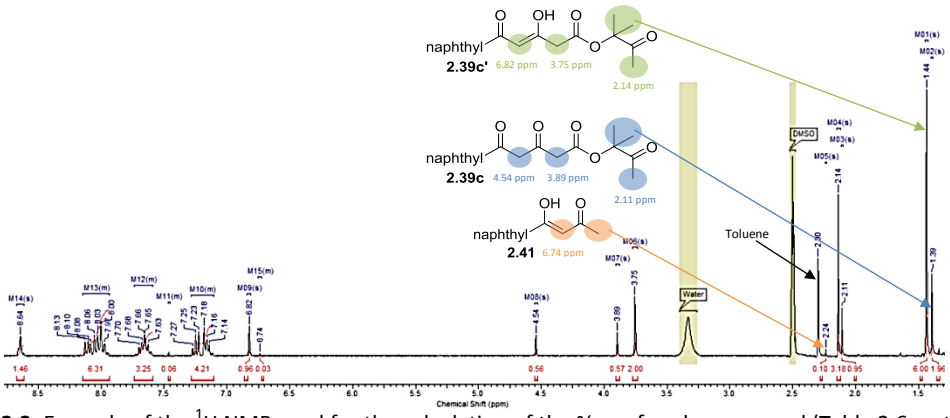

Figure 2.2: Example of the ^{1}H NMR used for the calculation of the $\%_{mol}$ of each compound (Table 2.6, entry 14).

By comparing entries 1 to 5 (10 min reaction time, MeCN), an increase in the amount of alcohol ROH (EtOH or *t*-BuOH) increased the amount of desired products **2.39** and **2.39'** while decreasing the amount of decarboxylated product **2.41**. With 5 equivalents of alcohol (entry 5), the $\%_{mol}$ of **2.39** and **2.39'** was maximum ($72\%_{mol}$). However, due to the high value and difficult synthesis of alcohol **2.21**, it will not be possible to exceed 1 equivalent in the target synthesis of epicocconone analogues. The decrease of the concentration of **2.28c** from 1 to 0.5 g/L (entry 1 *vs.* 3) did not induce positive results. For entries 1 to 5, the optimum temperature was about 120 °C (100% conversion and highest amount of desired products **2.39** and **2.39'**).

The use of a more polar solvent (DMSO) was not convincing because products **2.39** and **2.39'** were not obtained. The δ-lactone compound **2.40** was the main product (entries 6 and 7).

Using toluene as solvent was promising because the amount of desired products increased (entry 9 *vs.* 4) and the intramolecular trapping reaction to form **2.40** did not occur. An increase of the amount of alcohol up to 1 equivalent and an increased concentration of **2.28c** from 1 to 24 g/L with a reaction time of 10 min (entries 9 to 13) gave promising results with low formation of **2.41**.

Finally, using the previous optimised conditions, the trapping of the acylketene was performed with 3-hydroxy-3-methylbutan-2-one (**2.25**) as alcohol (entry 14). Indeed, the structures of this tertiary alcohol and alcohol **2.21** used in the synthesis of the epicocconone analogues are very close. A large amount of **2.39** and **2.39'** were obtained ($97\%_{mol}$) with low formation of **2.41** ($3\%_{mol}$) and no formation of the δ-lactone product **2.40**.

2.3.2.2 Optimisation of the Knoevenagel condensation - Model reaction

As a first attempt, the flow acylfuranonization with pre-mixing of the reaction mixture containing 1,3-dioxin-4-one **2.28c**, alcohol **2.25** and triethylamine was performed. The optimised conditions described previously (Table 2.6, entry 14) with dry toluene and addition

of 1.1 equivalent of Et_3N were used for the preparation of this reaction mixture. A 5 mL plug of this solution was injected into the flow set-up (Figure 2.3). At the exit of the reactor, the media was collected, the solvent was evaporated under reduced pressure and the crude mixture was analysed by NMR spectroscopy. Only 11%$_{mol}$ of the desired products **2.30c** and **2.30c'** were obtained. However, a large amount of the δ-lactone product **2.40** (85%$_{mol}$) was observed (Scheme 2.9).

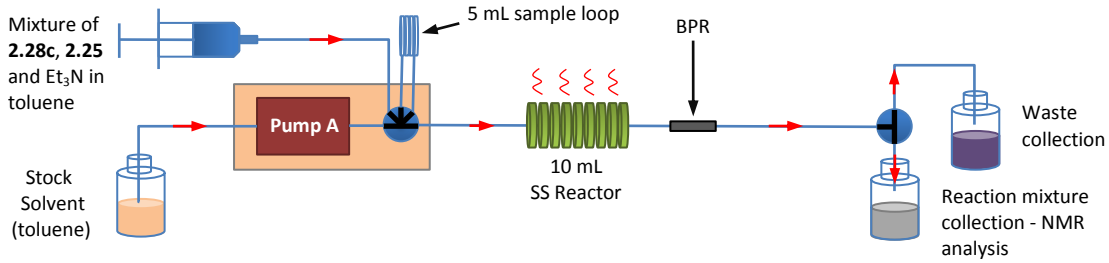

Figure 2.3: Flow set-up for the acylfuranonization with pre-mixing of **2.28c**, **2.25** and Et_3N.

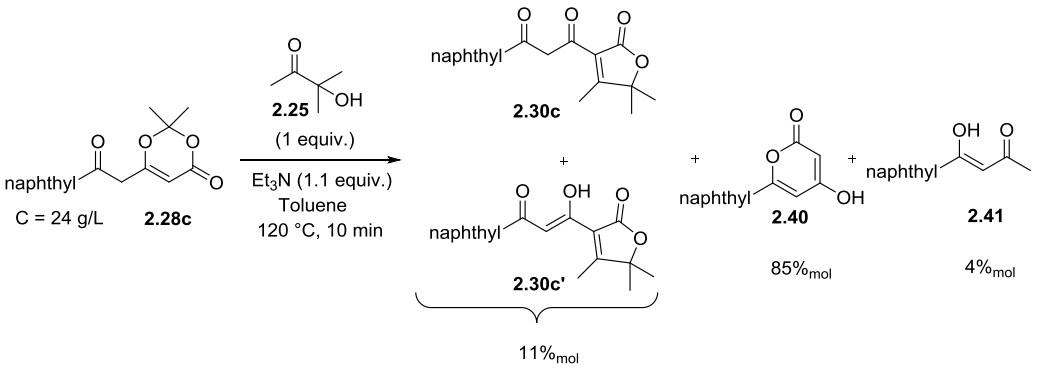

Scheme 2.9: Acylfuranonization with pre-mixing of **2.28c**, **2.25** and Et_3N.

Due to these poor results (Scheme 2.9) and as explained previously, it was decided to try the same reaction in two successive steps (Table 2.7) in order to avoid the formation of the δ-lactone compound **2.40** as the main product:

1st step: fragmentation in flow of the 1,3-dioxin-4-one **2.28c** and trapping of the acylketene by alcohol **2.25**.

2nd step: Knoevenagel condensation in flow or batch.

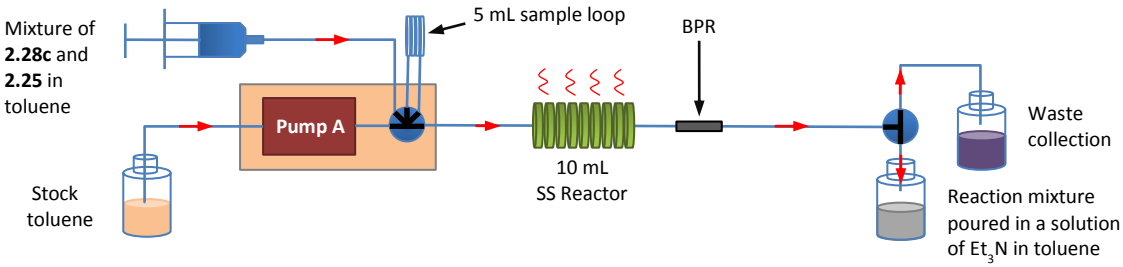

Figure 2.4: Flow set-up for the optimisation of the two-step process (Table 2.7, entries 2, 3 and 4).

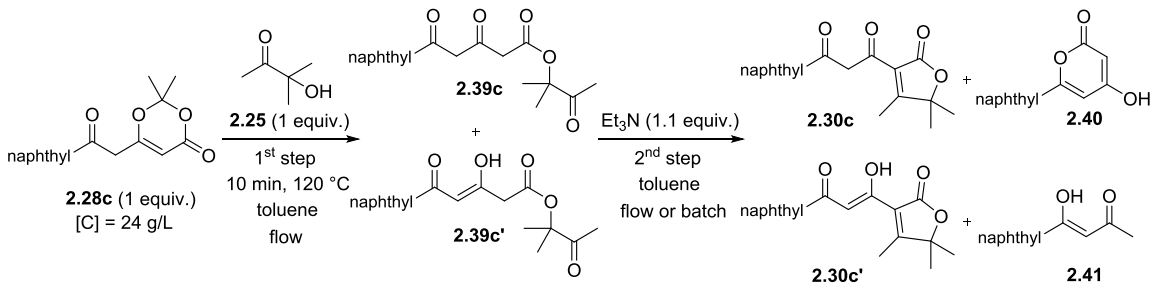

Entry[a]	2nd step (Knoevenagel condensation)							
	Et_3N (equiv.)	Solvent	RT[b] (min)	Temperature (°C)	%mol **2.39c + 2.39c'**	%mol (yield) **2.30c + 2.30c'**	%mol **2.40**	%mol **2.41**
1[c]	1.1	toluene	10	30	0	96	0	4
				60	0	96	0	4
				80	0	96	0	4
				100	0	91	3	6
				120	0	76	8	16
				140	0	54	9	37
				160	0	52	6	42
2[d]	1.1	toluene	15	30	41	51	0	8
			30	30	0	91	0	9
			60	30	0	91	0	9
3[d]	1.1	toluene	15	70	0	93	0	7
4[d]	1.1	toluene	15	90	0	93 (94%)	2	5

Table 2.7: The optimised two-step process - model reaction.

[a] 1st step (ketene formation and trapping with **2.25**) performed in flow: Injection of a 5 mL plug of a mixture of **2.28c** and **2.25** in toluene at the indicated conditions. [b] Reaction Time. [c] 2nd step performed in flow: Addition of Et_3N to the collected crude mixture dissolved in 40 mL of toluene. For each selected temperature, injection of a 5 mL plug of this solution. NMR analysis in DMSO-*d6* (%mol). [d] 2nd step performed in batch: the crude mixture was poured into a 20 mL solution of Et_3N in toluene and left to stir at the indicated conditions. NMR analysis in DMSO-*d6* (%mol).

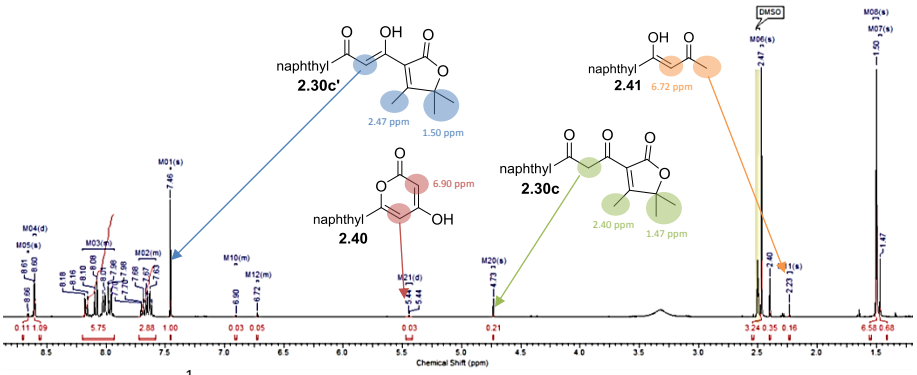

Figure 2.5: Example of the ^1H NMR used for the calculation of the %mol of each compound (Table 2.7, entry 4).

Table 2.7 describes the results obtained during the optimisation of the two-step process: trapping of the acylketene by alcohol **2.25** (1st step) followed by Knoevenagel condensation (2nd step). For the trapping step by alcohol **2.25**, the previous optimised conditions were kept (Table 2.6, entry 14).

The first attempt of this two-step process (entry 1) was fully performed with the flow machine. The Knoevenagel reaction gave the best results for temperatures between 30 and 80 °C (96%mol of products **2.30c** and **2.30c'**). No δ-lactone product **2.40** was observed. However, these two reactions were not run in sequence (isolation of **2.39c** and **2.39c'** in the middle of

the process) and the experimental time was long. In order to cut this time down, we could have tested the sequential reactions in flow but we decided to try the 1st step in flow and the 2nd in batch (simple set-up). For this purpose, a solution of 1,3-dioxin-4-one **2.28c** with alcohol **2.25** was injected into the flow machine and at the exit of the reactor, the reaction mixture was poured in a solution containing Et_3N (entries 2-4). Good results were observed for a Knoevenagel condensation performed at 30 °C and for a reaction time between 30 and 60 min (91%$_{mol}$ of products **2.30c** and **2.30c'**, no δ-lactone product **2.40**) (entry 2). An increase of the temperature to 70 °C (entry 3) or 90 °C (entry 4) with a decrease of the reaction time to 15 min gave similar results (93%$_{mol}$ of products **2.30c** and **2.30c'**). For entry 4, **2.30c** and **2.30c'** were isolated in 94% yield (over 2 steps) with a ratio **2.30c**/**2.30c'** = 10/90. Due to the low amount of compounds **2.40** and **2.41** formed in these conditions, no purification was performed at the end of this model reaction.

The optimised conditions found for the model reaction (Table 2.7, entry 4) were then applied to the synthesis of the 2nd generation epicocconone analogues using 1,3-dioxin-4-one **2.28c** and alcohol **2.21**.

2.3.3 Application of the optimised conditions to the synthesis of 2nd generation epicocconone analogues

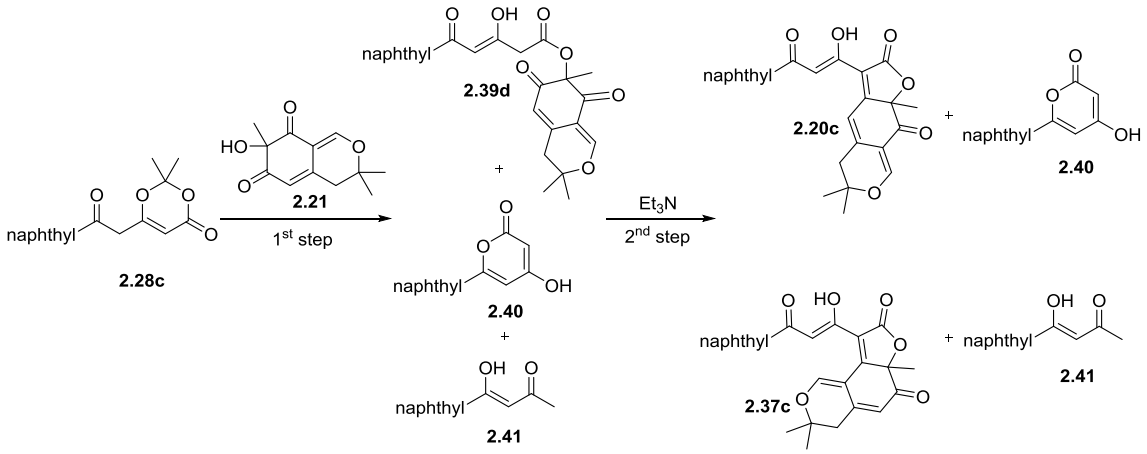

Entry	1st step (trapping step)[a]									2nd step (Knoevenagel condensation)							
	2.28c (equiv.)	**2.21** (equiv.)	[**2.28c**] (g/L)	solvent	RT[b] (min)	Temp. (°C)	%$_{mol}$ (yield) **2.39d**	**2.40**	**2.41**	Et_3N (equiv.)	RT[b] (min)	Temp. (°C)	%$_{mol}$ (yield) **2.39d**	**2.20c**	**2.37c**	**2.40**	**2.41**
1[c]	1	1	5	toluene	10	120	50	11	39	1.1	30	25	13	20	16	11	40
2[d]	1	1	12	tol./DCM 1/1	10	120	54	9	37	1.1	45	60	15	16	19	9	41
3[d]	1	0.9	24	toluene	10	120	83	/[f]	17	1.1	960	60	0	39 (13%)	40	/[f]	21
4[e]	1	0.5	24	toluene	10	120	52 (61%)	19	29	/	/	/	/	/	/	/	/

Table 2.8: The optimised two-step process - target reaction.

[a] 1st step performed in flow: Injection of a plug (1, 2 or 5 mL) of a mixture of **2.28c** and **2.21** in toluene at the indicated conditions. NMR analysis (%$_{mol}$ and yield). [b] Reaction Time. [c] 2nd step: Addition of Et_3N in the NMR tube containing the crude mixture. NMR analysis (%$_{mol}$). [d] 2nd step performed in batch: the collected reaction mixture was poured into a 5 mL solution of Et_3N in toluene and left to stir at the indicated conditions. NMR analysis (%$_{mol}$ and yield). [e] Step performed in flow at the indicated conditions. NMR analysis (%$_{mol}$ and yield). [f] When the NMR analysis was run in $CDCl_3$, **2.40** was not observed (not soluble).

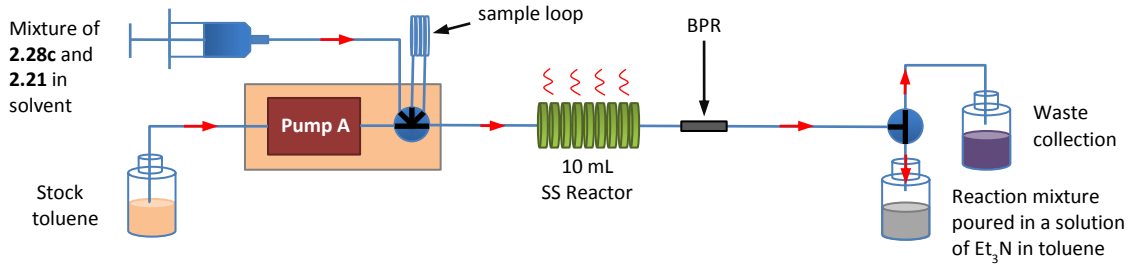

Figure 2.6: Flow set-up for the optimisation of the two-step process (Table 2.8, entries 2, 3 and 4).

Table 2.8 describes the different results obtained during the optimisation of the two-step process: trapping of the acylketene by alcohol **2.21** (1st step) followed by Knoevenagel condensation (2nd step). In the different attempts (entries 1 to 4), some minor unknown impurities observed on the ^{1}H NMR spectra were not considered in the molecular percentage calculations. As a first attempt (entry 1), the optimised conditions found for the model reaction (Table 2.6, entry 14) could not be applied due to the low solubility of alcohol **2.21** in toluene. Therefore, the initial concentration of 1,3-dioxin-4-one **2.28c** was decreased to 5 g/L. At the end of the first step, 1,3-dioxin-4-one **2.28c** was totally converted but alcohol **2.21** was still observed from NMR analysis (Ratio integration ^{1}H NMR: **2.21**/**2.39d** = 0.77). After the Knoevenagel condensation (2nd step), the crude NMR highlighted a mixture of compounds **2.39d**, **2.20c** (20%$_{mol}$), **2.37c**, **2.40**, **2.41** and few other unknown impurities. In these conditions, the decarboxylated compound **2.41** was the main product (40%$_{mol}$).

During the model reaction studies, it was noticed that the increase of the initial concentration of 1,3-dioxin-4-one decreased the formation of the decarboxylated compound (Table 2.6, entries 10, 11, 12 and 13). Therefore, using a mixture of toluene and DCM as solvent, the initial concentration of 1,3-dioxin-4-one **2.28c** was increased to 12 g/L with a good solubility of alcohol **2.21** (entry 2). With the same 1st step reaction time (10 min), alcohol **2.21** was still observed from NMR analysis performed at the end of the trapping reaction (Ratio integration ^{1}H NMR: **2.21**/**2.39d** = 1). Moreover, similar molecular percentages were obtained after the 2nd step even for a longer reaction time and higher temperature (entry 1 *vs.* 2).

In order to avoid the collection of unreacted alcohol **2.21** at the end of the first step, its initial amount was decreased from 1 to 0.9 equivalents (entry 3). The initial concentration of 1,3-dioxin-4-one **2.28c** was increased to 24 g/L. With these experimental conditions, the reaction mixture was turbid but the attempt was performed. During the flow reaction (1st step), the pressure of the Vapourtec platform was very high (turbid plug) but we managed to collect the crude product at the exit of the reactor. At the end of this 1st step, the amount of alcohol **2.21** was lower (Ratio integration ^{1}H NMR: **2.21**/**2.39d** = 0.38). Then, after 960 min at 60 °C, the Knoevenagel reaction (2nd step) was complete. An NMR analysis of the crude mixture

highlighted both isomers **2.20c** and **2.37c** in similar amount (39%$_{mol}$ *vs.* 40%$_{mol}$). However, the amount of decarboxylated compound **2.41** decreased (21%$_{mol}$) due to the initial higher concentration of dioxinone **2.28c**. The crude mixture was then purified and compound **2.20c** was isolated in 13% yield.

For entry 4, the amount of alcohol **2.21** was decreased to 0.5 equivalents to avoid its collection at the end of the trapping step. However, under these conditions, a large amount of compound **2.40** was formed due to the excess of 1,3-dioxin-4-one **2.28c**. Moreover, owing to the poor solubility of **2.40** in toluene, blockages occurred in the flow reactor. The use of MeCN instead of toluene as stock solvent enabled the solubilisation of **2.40** and the collection of the reaction mixture. At the end of the trapping step, the NMR analysis still highlighted alcohol **2.21** (Ratio integration ^{1}H NMR **2.21**/**2.39d** = 0.19) and enabled the calculation of the yield by addition of an internal standard (NMR yield = 61%).

Due to various issues encountered during the optimisation of the two-step process using alcohol **2.21** (low solubility of alcohol **2.21** in toluene, blockage due to the formation of the insoluble compound **2.40** in toluene), no improvements were performed in the synthesis in flow of the 2nd generation epicocconone analogues compared to the batch results. Indeed, our best yield in flow for the synthesis of **2.20c** was 13% (Table 2.8, entry 3) whereas the best yield in batch was 26% (Table 2.5, entry 3).

During our optimisation studies, the Franck research group tried this two-step process in batch starting from the unprotected 1,3-dioxin-4-one **2.28** and by adding first the alcohol and then the triethylamine. By this procedure, they managed to increase their previous yields (Table 2.5 *vs.* Table 2.9).

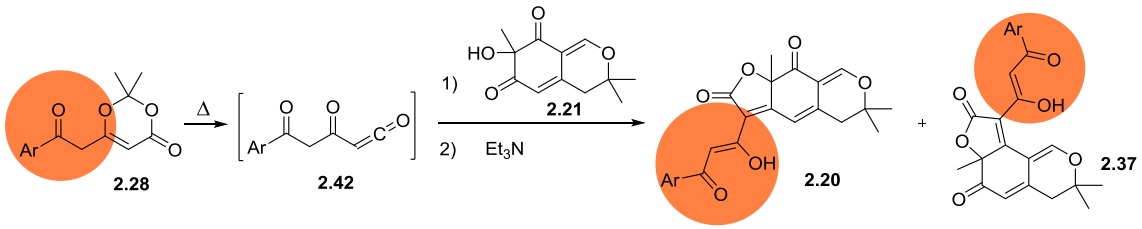

Entry[a]	Ar	**2.20** (Yield)	**2.37** (Yield)
1	phenyl	**2.20a** (35%)	**2.37a** (0%)
2	2-naphthyl	**2.20c** (33%)	**2.37c** (0%)
3	*p*-methoxyphenyl	**2.20d** (30%)	**2.37d** (0%)
4	6-chloro-3-pyridyl	**2.20e** (27%)	**2.37e** (0%)

Table 2.9: Synthesis of second generation epicocconone analogues.[29]

[a] One-pot reaction with 2 successive steps. 1st step: **2.28** (1 equiv.), **2.21** (0.67 equiv.), molecular sieves (4 Å), toluene at 110 °C during 20 min. 2nd step: addition of Et_3N (1.33 equiv.), toluene at 110 °C during 1 h.

2.3.4 Towards the total synthesis of epicocconone

Epicocconone is a natural product isolated from the fungus *Epicoccum nigrum*[26] and no total syntheses have been developed so far. For this reason, using the same key reactions as described in the synthesis of the 1st and 2nd generation analogues, the following retrosynthesis (Scheme 2.10) could be a possible pathway to form this natural product.

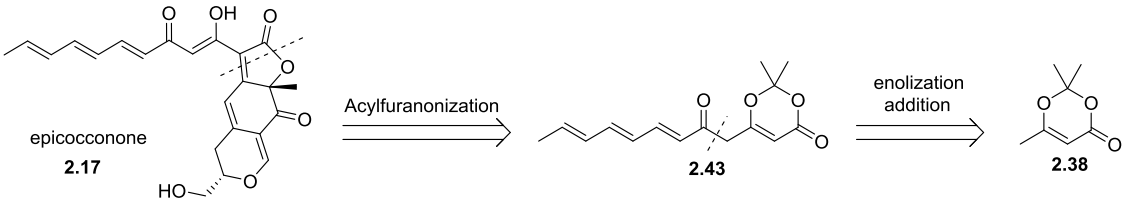

Scheme 2.10: Retrosynthetic route towards the synthesis of the epicocconone.

Epicocconone can be obtained by trapping of an acylketene, prepared by thermolysis of **2.43**, with the corresponding alcohol and followed by an intramolecular Knoevenagel condensation. Then, **2.43** can be synthesised by the direct functionalization of the lithium enolate derived from the commercially available 1,3-dioxin-4-one **2.38** (Scheme 2.10).

The introduction of the 'keto triene' group on 1,3-dioxin-4-one **2.43** (Scheme 2.10) was more difficult than the 'keto naphtalene' highlighted on 1,3-dioxin-4-one **2.28c**, precursor of 2nd generation epicocconone analogues. Indeed, the major issue was the low photostability of the heptatriene chain.[28-29]

The following 4 steps were performed in batch for the synthesis of the 'keto triene dioxinone' **2.43** (Scheme 2.11). First, ethyl octa-2,4,6-trienoate (**2.45**) was obtained in 94% yield from sorbaldehyde (**2.44**) via a Wittig-Horner reaction with phosphonoacetate. Then, the carboxylic acid **2.46** was prepared in 60% yield after hydrolysis of **2.45**. Two different routes were then investigated to form 1,3-dioxin-4-one **2.43**. In a first attempt, the Weinreb amide **2.47** was synthesised in good yield (90%) but the formation of 1,3-dioxin-4-one **2.43** from this amide was not possible. The other route was to prepare and condense the acyl chloride **2.48** with the lithium enolate of commercially available 2,2,6-trimethyl-4*H*-1,3-dioxin-4-one (**2.38**). Following this route, 1,3-dioxin-4-one **2.43** was isolated in 22% yield. The final steps would be the trapping of the acylketene, obtained with the thermolysis of **2.43**, by the mono-protected alcohol **2.49**, followed by the Knoevenagel condensation and the deprotection of the primary alcohol. However, alcohol **2.49** has not been synthesised yet by the Franck research group. Indeed, the diastereoselectivity obtained during the oxidative dearomatisation reaction[33] did not match with the natural product. The development of a diastereoselective oxidative

dearomatisation reaction to form alcohol **2.49** with the right stereochemistry is currently in progress in the Franck research group.

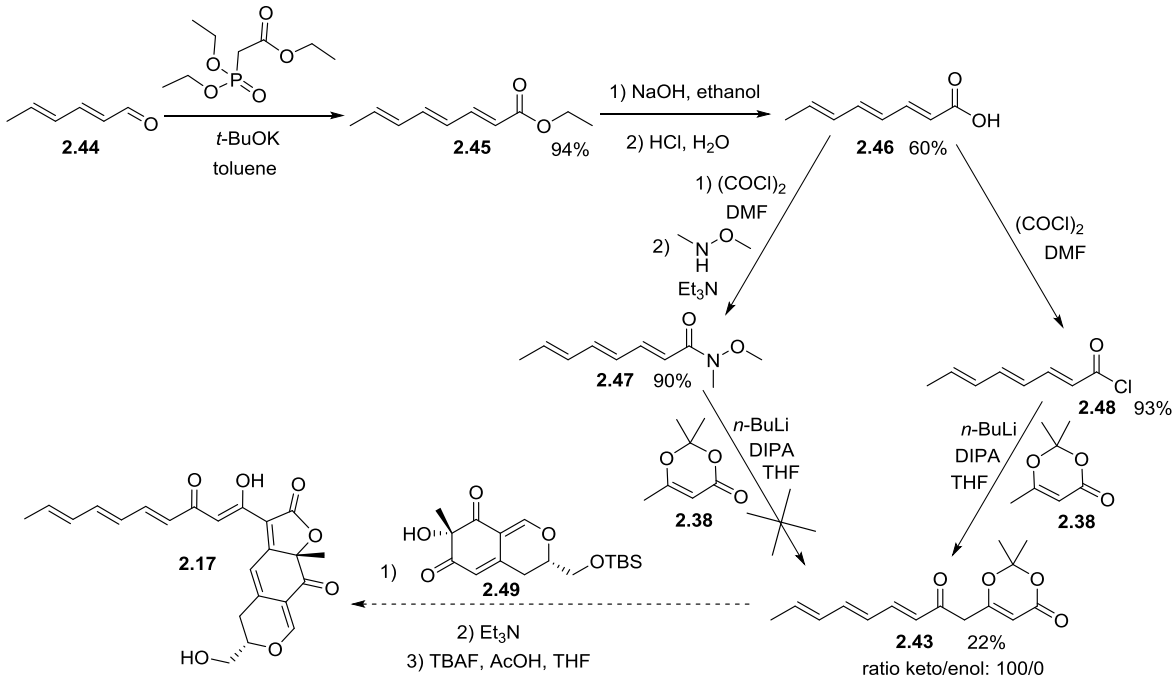

Scheme 2.11: Towards the synthesis of epicocconone.

Instead of using alcohol **2.49**, preliminary flow thermolyses of **2.43** followed by trapping of the acylketene with simpler alcohols were performed (Schemes 2.12 and 2.13).

First of all, the thermolysis of 1,3-dioxin-4-one **2.43** was performed in the presence of ethanol (Scheme 2.12) using the same optimised conditions as Table 2.7, entry 4 (Injection into the flow machine of a 1 mL plug of a mixture of **2.43** and EtOH in dry toluene with the indicated conditions). At the exit of the reactor, the reaction mixture was collected, the solvent was evaporated under reduced pressure and the ^{1}H NMR (DMSO-*d6*) of the reaction mixture identifies compound **2.50** as the main tautomer with some impurities (probably the intramolecular trapping product and the decarboxylated product due to the small amount of water in the media). However, product **2.50** could not be isolated in pure state.

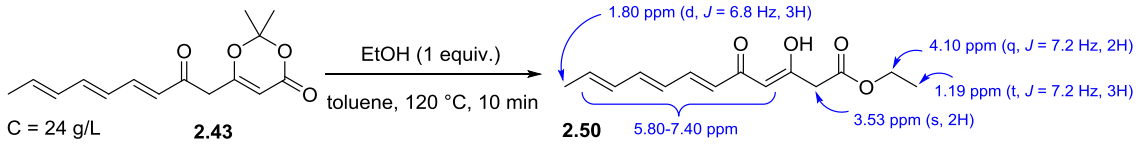

Scheme 2.12: Towards the synthesis of epicocconone.

In the same way, the trapping of the acylketene, prepared from the thermolysis of **2.43**, with 3-hydroxy-3-methylbutan-2-one (**2.25**) followed by the Knoevenagel condensation (Scheme 2.13) was performed using the same optimised conditions as Table 2.7, entry 4 (1st step: Injection into the flow machine of a 1 mL plug of a mixture of **2.35** and alcohol **2.25** in dry toluene with the indicated conditions. 2nd step: At the exit of the flow reactor, the reaction mixture was poured into a 10 mL solution of Et_3N in dry toluene. The media was left to stir at the indicated time and temperature). At the end of the 2nd step, the solvent was evaporated under reduced pressure and the ^1H NMR (DMSO-*d6*) of the reaction mixture identifies compound **2.51** with some impurities (probably the intramolecular trapping product and the decarboxylated product due to the small amount of water in the media). However, product **2.51** could not be isolated in a pure state.

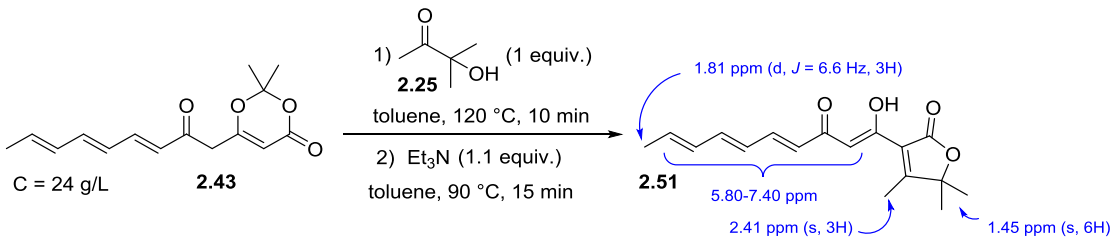

Scheme 2.13: Towards the synthesis of epicocconone.

These results are promising towards the total synthesis of epicocconone. Once alcohol **2.49** will be synthesised by the Franck research group at the University of Rouen, attempts and optimisations based on this model reaction conditions (Scheme 2.13) would be investigated.

To sum up, promising results were obtained on the preliminary optimisation experiments towards the synthesis of 2nd generation epicocconone analogues. Indeed, over 2 successive steps, compounds **2.30c** and **2.30c'** were obtained in 94% yield. However, the application of these optimised conditions on the target reaction between compounds **2.28c** and **2.21** was not possible due to solubility issues. For this flow synthesis, 13% was the best yield optained. No improvement was performed compared to the batch one (33%).

Towards the total synthesis of epicocconone, complementary investigations will have to be undertaken between dioxinone **2.43** and first the model alcohol **2.25,** and finally the target alcohol **2.49**.

3 Chapter 3: *In situ* generation of isocyanides, indispensable building blocks of multi-component reactions (MCRs)

Isocyanides, organic compounds bearing the functional group -NC, belong to an intriguing family in organic chemistry. Indeed, the versatile reactivity of the carbon atom which is able to act as a nucleophile or an electrophile[34] has been widely developed in many different multi-component reactions (MCRs). These useful and high atom efficiency reactions combine multiple reagents in one-pot to form a new product where most of the starting atoms are involved. The Ugi reaction (Scheme 3.1) is one of the most common multi-component reactions with high atom economy as it involves four different reagents to form the desired bis-amide and water.

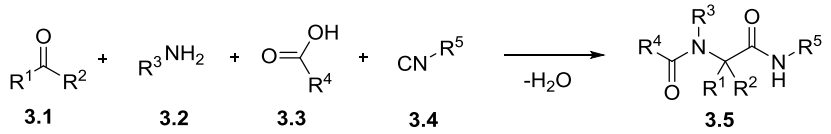

Scheme 3.1: 2 The Ugi reaction.

3.1 Introduction to isocyanides

3.1.1 Properties of isocyanides

In spite of the significant potential of isocyanide chemistry, the very unpleasant odour and toxicity were probably the main reasons of the underdevelopment during many years.[35] However, with the recent advances in continuous flow processes, these major limitations are controlled with these closed systems and new explorations of isocyanide chemistry can be performed.

Like the carbon monoxide functional group, isocyanides can be described by two resonance forms, one with a carbon-nitrogen triple bond and a formal positive charge on the nitrogen and a formal negative charge on the carbon, and one with a carbon-nitrogen double bond with a carbenic structure (Scheme 3.2).

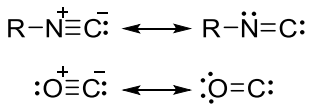

Scheme 3.2: Two resonance forms of isocyanides and carbon monoxide.

Carbon-nitrogen bonds of isocyanides exhibit sharp signals in the IR spectra at approximately 2110-2165 cm^{-1},[36] which is similar to carbon monoxide (about 2140 cm^{-1}).

3.1.2 General preparations of isocyanides

Due to their unique reactivity in MCRs, isocyanides represent an important category of monomers and they have become ideal targets for synthesis.

The first preparation of an isocyanide was performed by Lieke in 1859.[37] This reaction involved ally iodide (**3.6**) and silver cyanide to form allyl isocyanide (**3.7**) (Scheme 3.3) although he thought at that time that the product was a cyanide.

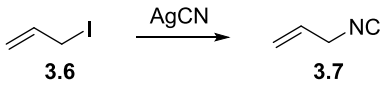

3.6 **3.7**

Scheme 3.3: First isocyanide preparation.

The development of classical isocyanide syntheses was then performed by Gautier[38] and Hofmann in 1867.[39] Then, for about a century, synthesis of isocyanides was investigated in moderation especially due to the very unpleasant and piercing odour (about 10 isocyanide syntheses were developed between 1867 and 1958).[35]

New perspectives in the synthesis of isocyanides began in 1958 with the development of a new methodology: the formylation of primary amines **3.8** followed by dehydration of the formamide **3.9** (Scheme 3.4). For the formylation step, various reagents such as alkyl formates[40] or formic acid[41] can be employed. Then, several dehydration methods are available, the most convenient being a combination of $POCl_3$ and trimethylamine,[42] a combination of triphenylphosphine, carbon tetrachloride and trimethylamine,[43] *p*-tosyl chloride or the Burgess's reagent.[44] Other reagents have been reported to dehydrate formamides including triflic anhydride,[45] cyanuric chloride,[46] chlorophosphates,[47] diphosgene[48] and triphosgene.[49] Today, the dehydration of formamides is the most common reaction for the synthesis of isocyanides.

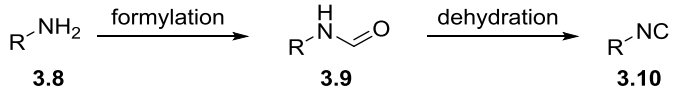

3.8 **3.9** **3.10**

Scheme 3.4: Synthesis of isocyanides **3.10** from primary amines **3.8**.

The Hofmann carbylamine reaction[50] using phase transfer catalysis is another process for the synthesis of isocyanides **3.12** (Scheme 3.5). However, this reaction encountered limitations due to the low yields and experimental difficulties.

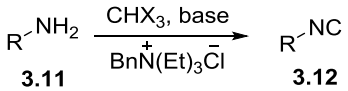

3.11 **3.12**

Scheme 3.5: The Hofmann carbylamine reaction.

Another route to the synthesis of isocyanides has been recently described starting from benzylic or tertiary alcohols.[51] This one-pot synthesis involved the following three steps: The modified Ritter reaction with trimethylsilyl cyanide and acid, the neutralization with base and the dehydration with tosyl chloride and pyridine to lead to the corresponding isocyanide (Scheme 3.6).

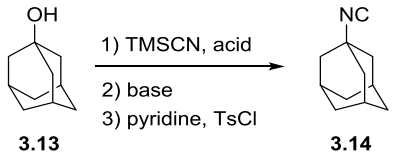

Scheme 3.6: One-pot synthesis of isocyanide **3.14** from adamantan-1-ol (**3.13**).

The ring opening-reaction of oxazoles **3.15** described by Pirrung *et al*.[52] provides another methodology for the synthesis of unsaturated isocyanides **3.16** (Scheme 3.7).

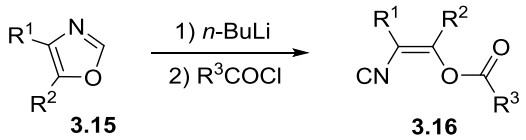

Scheme 3.7: Synthesis of unsaturated isocyanides **3.16**.

Ley *et al*.[53] have developed the solid-supported phosphine **3.18** which generates primary, secondary and tertiary alkyl isocyanides **3.19** by reduction of isothiocyanates **3.17** (Scheme 3.8).

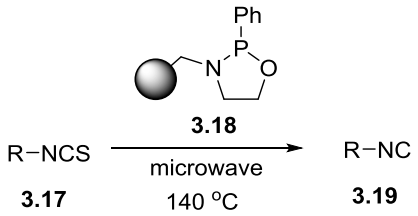

Scheme 3.8: Synthesis of isocyanides **3.19** from isothiocyanate **3.17**.

Other methods developed by Gassman[54] and Barton[55] enable the generation of β-hydroxy isocyanides and vinyl isocyanides.

3.1.3 Isocyanides in MCRs

A MCR is a combination of 3 or more reagents in one-pot to form a new product where most of the atoms are involved. Great interest in this kind of reaction derives from the atom economy and the low generation of waste. Isocyanides are able to react either as nucleophiles

or as electrophiles, and this versatile property makes this functional group the most widely used in MCRs. For example, the multi-component Passerini and Ugi reactions are initiated with the reaction of the isocyanide with an electrophile through the terminal carbon. In turn, this generates an electrophile which can be finally trapped by a nucleophile.

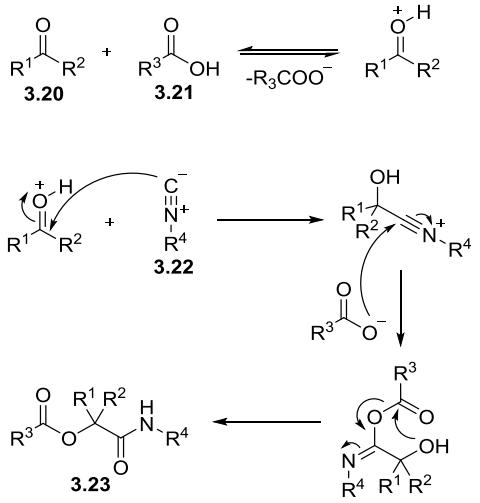

Scheme 3.9: Mechanism of the Passerini reaction.

The Passerini three-component reaction (Scheme 3.9) involves an aldehyde or a ketone **3.20**, a carboxylic acid **3.21** and an isocyanide **3.22** to form a α-acyloxy amine **3.23** with excellent atom economy as all atoms are incorporated in the final product. This reaction, discovered in 1921,[56] has been widely used especially in the formation of peptidomimetic compounds.[57]

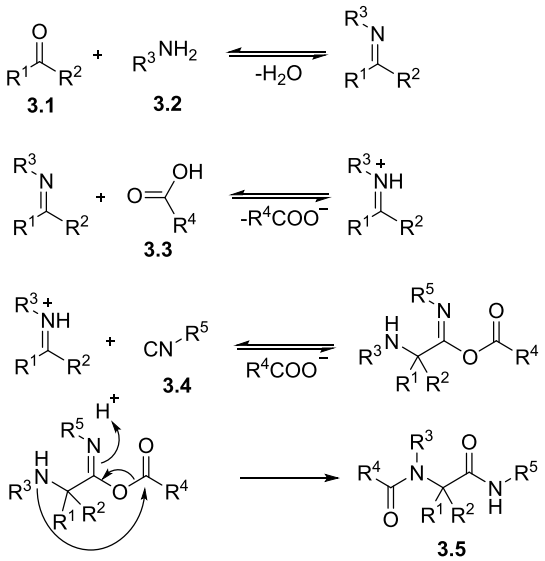

Scheme 3.10: Mechanism of the Ugi reaction.

The Ugi four-component reaction (Scheme 3.10), first reported in 1959,[58] involves an aldehyde or a ketone **3.1**, an amine **3.2**, a carboxylic acid **3.3** and an isocyanide **3.4** to form a bis(amide) **3.5**. As with the Passerini reaction, a new stereocentre is generated and the reaction is atom economical. This reaction has been widely used in peptide synthesis.[59]

3.1.4 Reaction of isocyanides in continuous flow process

Using a mesofluidic flow reactor, Ley *et al*.[60] synthesised a variety of 4,5-disubstituted oxazoles **3.24** from the reaction between isocyanide **3.25** and acid chloride **3.26** (Figure 3.1). Both reagents were injected through the flow reactor. The solid-supported base **3.27** contained in the first column enabled the base-catalysed intramolecular cyclisation. Finally, the second post-reactor column containing a primary amine-functionalized resin enabled the efficient clean-up sequence (scavenged the unreacted acid chloride). With this system, a library of 36 different oxazoles in yields between 83 and 99% were synthesised.

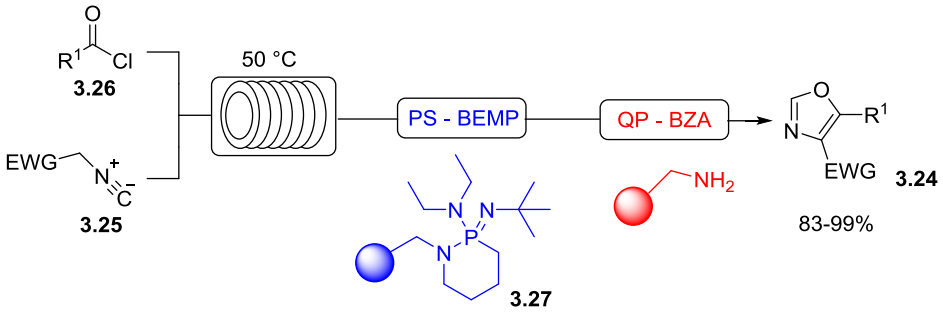

Figure 3.1: Flow synthesis of 4,5-disubstituted oxazoles **3.24** from isocyanides **3.25** and acids chloride **3.26**.

Organ *et al*.[61] investigated under MACOS conditions (microwave-assisted continuous flow organic synthesis) the formation of tetra substituted furans from DMAD (**3.28**), substituted benzaldehyde (e.g. 4-nitrobenzaldehyde (**3.29**)) and cyclohexyl isocyanide (**3.30**). In the example described in Figure 3.2, the resulting substituted furan **3.31** was isolated in 79% yield.

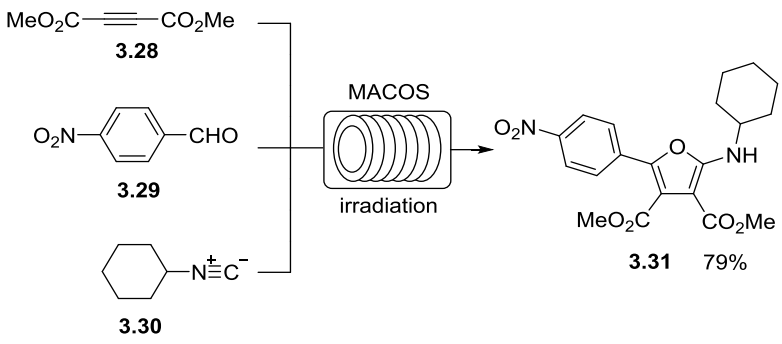

Figure 3.2: Synthesis under MACOS conditions of tetra substituted furan **3.31**.

3.1.5 Generation and reaction of isocyanides in continuous flow process

The *in situ* generation of isocyanides in a continuous flow process has recently been developed by Kim *et al*.[62] With this system, the rapid formation of the desired Passerini or Ugi product thanks to the cascade generation, extraction, separation and reaction of isocyanides and the low exposure to its extremely unpleasant odour are the main advantages.

For this study, the dehydration of *N*-substituted formamides was used as a model reaction for the *in situ* generation of isocyanides which were then engaged in a continuous-flow Passerini or Ugi multi-component reaction. For this purpose, an amide and diisopropylethylamine (DIPEA) were injected into the flow reactor at the same time as a solution of $POCl_3$ in toluene. After a residence time of 6 min at room temperature and by using ultrasound to avoid the precipitation of insoluble salts, the dehydration of the amide was achieved. The injection of water to the reaction mixture enabled the solubilisation of unwanted salts and the resulting aqueous layer was removed. The purified solution of isocyanide was then engaged in MCRs including Passerini and Ugi reactions. Bis(amide) Ugi products **3.32** were obtained in around 80% yield (Figure 3.3).

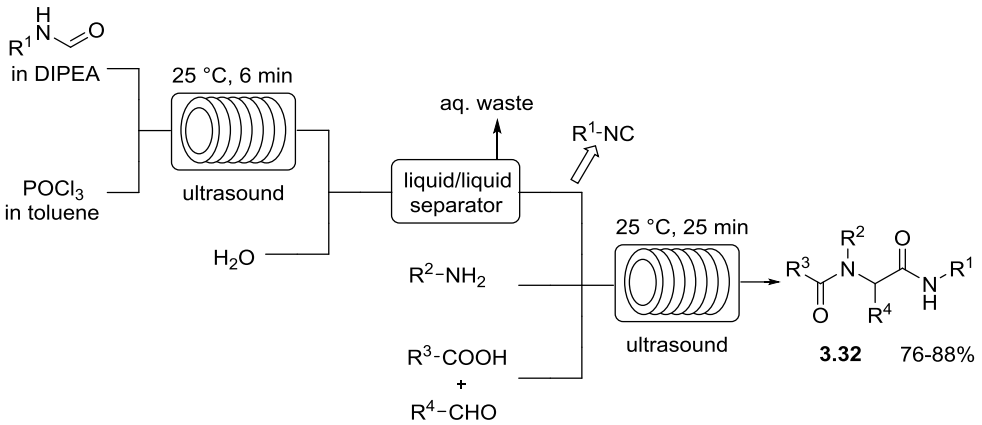

Figure 3.3: *In situ* generation, extraction, separation and reaction of isocyanides to synthesise bis(amide) Ugi products **3.32**.

Passerini and Ugi reactions have been widely used in the synthesis of peptidomimetic scaffolds. In this context, Kappe *et al*.[63] employed the *in situ* generation of isocyanides in continuous flow process for the synthesis of peptoids via the Ugi four-component reaction (Figure 3.4).

Based on the similar reaction as described by Kim *et al.*, **3.33** and the dehydrating Burgess reagent were mixed for the *in situ* formation of isocyanides. The stream was mixed with paraformaldehyde, *tert*-butylamine and the outcome of the azide formation (reaction between **3.34** + TBAA). After 5 min of reaction time, the Ugi reaction yielded the bis(amide) **3.35** in 80% yield before the macrocyclisation.

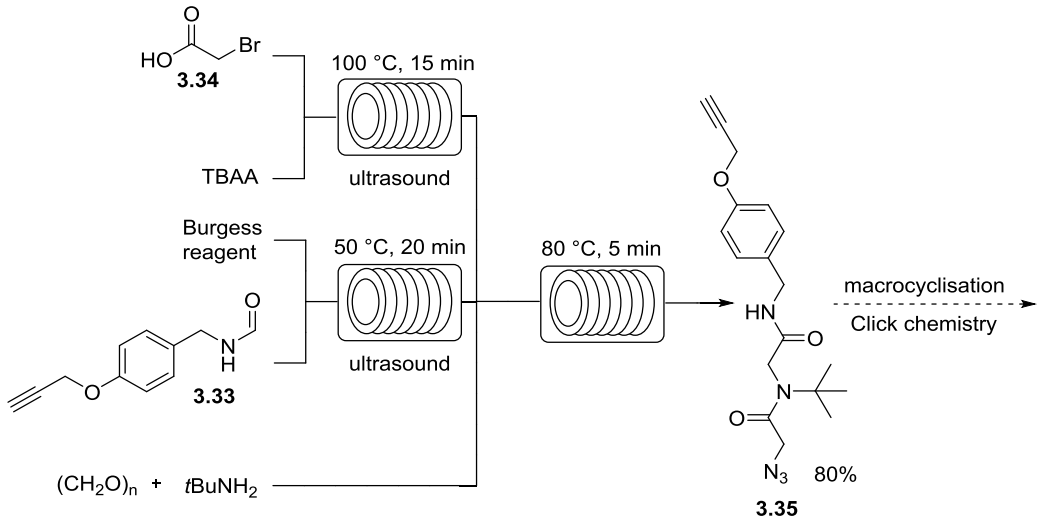

Figure 3.4: *In situ* generation and reaction of isocyanides to synthesise linear peptidomimetic scaffolds **3.35** via a Ugi reaction.

3.2 Results and discussions

3.2.1 Preliminary studies on a possible alternative *in situ* generation of isocyanides in continuous flow process

In situ generation of isocyanides under continuous flow conditions have been successfully performed using the dehydration of *N*-substituted formamides.[62-63] However, the generation of waste due to the use of dehydrating reagents can be an issue in sequential flow reactions as they can interact later on with other reagents or induce solubility problems in the case of salt formation. For this reason, we decided to study an alternative way for the *in situ* generation of isocyanides in continuous flow process using thermal fragmentations with formation of inert waste such as benzene or cyclohexadiene.

It has been demonstrated that bicyclo[2.2.1]hepta-2,5-dien-7-one (**3.36**) fragments even at temperatures below ambient to form benzene and carbon monoxide (Scheme 3.11).[64] These bonds are ruptured because the product formed, the benzene, is a very stable aromatic structure.

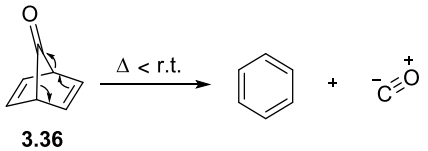

Scheme 3.11: fragmentation of bicyclo[2.2.1]hepta-2,5-dien-7-one (**3.36**) to form benzene and carbon monoxide.

Based on these results, the idea was to synthesise similar compounds as **3.36** but by replacing the carbonyl group by an imine group in order to generate isocyanides by thermal or photochemical fragmentation.

Preliminary DFT calculations (B3LYP/6-31G(d)) using Spartan software were performed by Prof R. J. Whitby to determine the energy required for the fragmentation of the model ketones **3.36** and **3.37**, and the model imines **3.38a** and **3.39a**. They were compared to the experimental values (Table 3.1).

Compounds	Theoretical values (DFT calculation)			Experimental values			
	E_a (kJ/mol)	$\Delta G^{\ddagger}$ (25 °C) (kJ/mol)	$\Delta G^{\ddagger}$ (125 °C) (kJ/mol)	E_a (kJ/mol)	$\Delta G^{\ddagger}$ (25 °C) (kJ/mol)	$\Delta G^{\ddagger}$ (125 °C) (kJ/mol)	Half-life[a]
 **3.36**	61.4	50.1	49.1	66.9[65]	62.8[65]	--	6.7×10^{-5} s at 25 °C
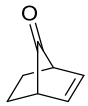 **3.37**	133.3	121.5	120.6	146[66]	133.9[67]	--	9 min 15 s at 125 °C
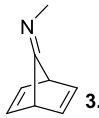 **3.38a**	108.5	97.1	96.7	--	--	--	0.4 s at 125 °C
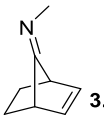 **3.39a**	206.2	190	189.5	--	--	--	19000 years at 125 °C

Table 3.1: Theoretical and experimental E_a and $\Delta G^{\ddagger}$ regarding the fragmentation of ketones **3.36** and **3.37**, and imines **3.38** and **3.39**. [a] The half-lives were calculated thanks to the theoretical value and the calculator provided on the following website: http://www.unige.ch/sciences/chiorg/lacour/correl

The theoretical predictions obtained for ketones **3.36** and **3.37** are in accordance with the experimental values found in the literature. Ketone **3.36** fragments spontaneously as its half-life at 25 °C is below 1 second (6.7×10^{-5} s). This is the lowest activation energy. However, no experimental values were found for the fragmentations of imines **3.38a** and **3.39a**. The DFT calculations and the calculated half-lives highlight that the fragmentation of imine **3.38a** is much faster than **3.39a**.

Having these preliminary DFT calculations, we first attempted the synthesis of imine **3.38** starting from norbornadiene (**3.40**) (Scheme 3.12). Then, even with a very high calculated half-life, the synthesis of imine **3.39** was attempted starting from norbornene (**3.41**) (Scheme 3.13).

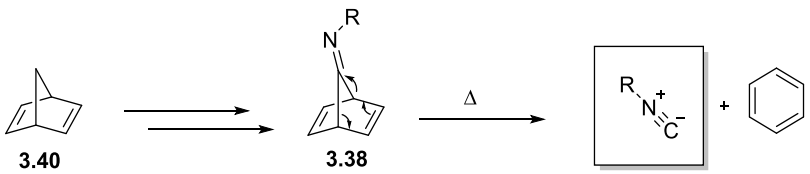

Scheme 3.12: Possible synthesis of isocyanides from norbornadiene (**3.40**).

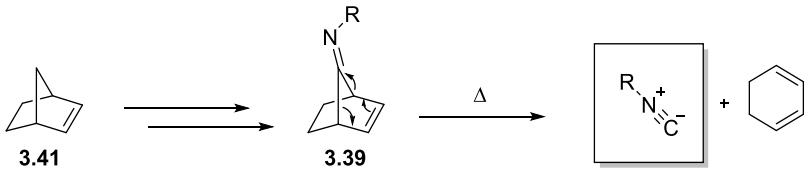

Scheme 3.13: Possible synthesis of isocyanides from norbornene (**3.41**).

3.2.2 Norbornadiene routes: Towards the synthesis of imine 3.38

In order to synthesise imine **3.38**, two different routes starting from norbornadiene (**3.40**) (Schemes 3.14 and 3.15) were attempted. The formation of ketone **3.36** was avoided during the synthesis due to its fast decomposition at room temperature.

3.2.2.1 1st Route to imine 3.38

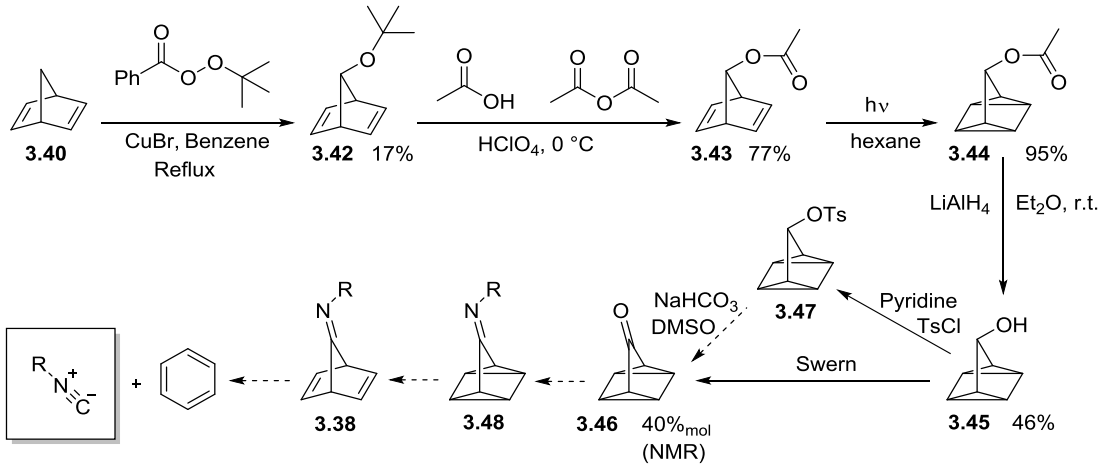

Scheme 3.14: Towards the synthesis of imine **3.38**.

Regarding the procedure described by Story *et al.*,[68] 7-*t*-butoxynorbornadiene (**3.42**) was obtained via a radical reaction with *t*-butyl perbenzoate and norbornadiene (**3.40**). The low yield obtained (17%) is in accordance with the literature (20%).[68] Then, 7-norbornadienyl acetate (**3.43**) was prepared in 77% yield from **3.42** in the presence of perchloric acid.[69] Due to its strong oxidizing and acidic properties, the same reaction was tried with sulphuric acid instead. However, the yield decreased to 27%. The [2+2] reaction leading to compound **3.44** was performed using the photo flow reactor. Compared to the literature procedure performed in batch and using a 450 W Mercury Arc lamp for 5 h,[70] compound **3.44** was synthesised in 95% yield after 28 min of irradiation with the photoflow UVC lamp (9 W). The reduction of ester **3.44** with lithium aluminium hydride led to the formation of the corresponding alcohol **3.45** in 46% yield.[71] However, as reported in the literature,[70] the purification of this alcohol was very complicated even with a basic alumina column. Indeed, the purity of the product after column

was not better than the crude mixture (purity = 78%). Finally, a Swern reaction was tried.[72] The reaction was complete but only 40%$_{mol}$ of the target compound **3.46** was obtained (^{1}H NMR ratio). The other main compound highlighted in the crude mixture was the 7-norbornadienol (**3.50**). This crude mixture containing both compounds **3.46** and **3.50** has not been purified. Due to this poor result, a described alternative route performing the tosylation of alcohol **3.45** followed by a DMSO-$NaHCO_3$ oxidation to form **3.46** with good yields (80% yield for both steps)[71] was considered. Unfortunately, after the tosylation of alcohol **3.45**, the purification on silica gel of the crude mixture, containing a mixture of **3.47**, TsCl and 7-norbornadienol (**3.50**), decomposed and only PTSA and TsCl were recovered in the fractions.

Due to the low yields, the difficulties in the purification of alcohol **3.45**, the difficulties in the formation of ketone **3.46** and the remaining steps to generate imine **3.38**, a possible precursor of isocyanides, it was decided to investigate another route.

3.2.2.2 2nd Route to imine 3.38

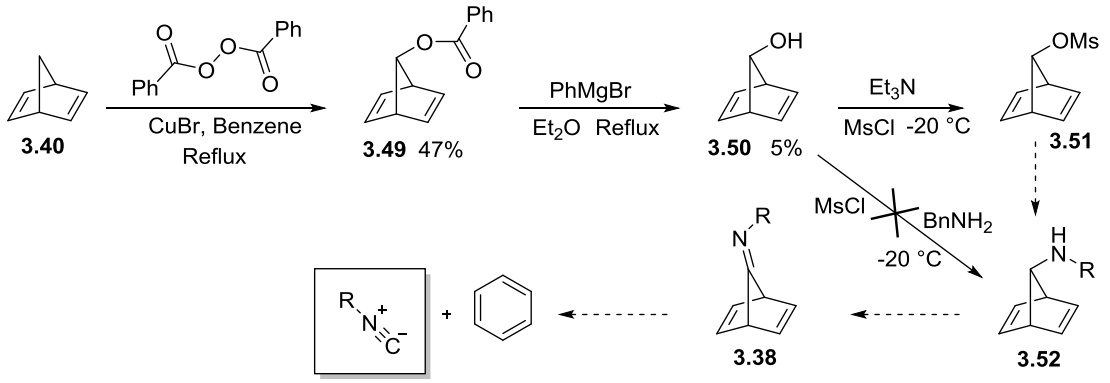

Scheme 3.15: Towards the synthesis of imine **3.38**.

According to Story *et al.,*[68] "when benzoyl peroxide is used in place of *t*-butyl perbenzoate with norbornadiene (**3.40**), 7-benzoxynorbornadiene (**3.49**) is obtained in 38% yield". Indeed, in this synthesis, product **3.49** was isolated in 47% yield. Compared to the 1st Route, this first yield was much better. However, the conversion of ester **3.49** to tertiary alcohol **3.50** using a Grignard reagent was very problematic and more particularly the purification. In the literature,[73] a distillation was performed, but this purification process was complicated to employ on a small scale (less than 0.5 g of starting material **3.49** engaged in the conversion). Therefore, columns were tried but neither silica nor basic alumina columns led to pure alcohol **3.50** (best purity = 50%). According to the method of Bentley,[74] the mesylation of the impure alcohol **3.50** was investigated. After 30 min at -20 °C, the reaction was complete and the ^{1}H NMR of the crude mixture indicated that the 7-norbornadienyl methanesulfonate (**3.51**) (3%$_{mol}$) had been formed with a large amount of methanesulfonyl chloride (64%$_{mol}$) and

Et_3N (32%$_{mol}$), and a small amount of 7-chlorononbornadiene (1%$_{mol}$). However, after standing the NMR tube at 5 °C for 4 h, the 7-norbornadienyl methanesulfonate (**3.51**) disappeared completely due to its low stability. For this reason, we decided to try the one pot mesylation of **3.50** followed by the nucleophilic substitution with the benzylamine but the desired product **3.52** was not generated.

At this time of the investigations, Routes 1 and 2 were not very promising towards the synthesis of imine **3.38**, a possible precursor of isocyanides. For this reason, even with a very long predicted fragmentation half-life (Table 3.1), the synthesis of imine **3.39** from norbornene (**3.41**) was attempted.

3.2.3 Norbornene route: Towards the synthesis of imine 3.39b

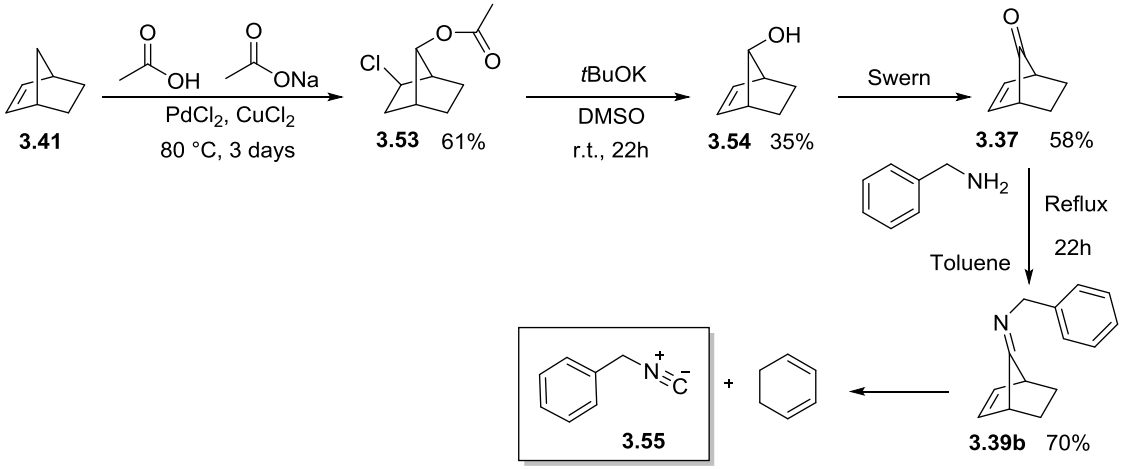

Scheme 3.16: Towards the synthesis of imine **3.39b**.

According to the literature procedure,[75] norbornenol (**3.54**) was synthesised in two steps. First, 2-chloro-7-acetoxynorbornane (**3.53**) was obtained in 61% yield by heating norbornene (**3.41**) with cupric chloride, sodium acetate in glacial acetic acid and a catalytic amount of palladium chloride. This reaction involves a nucleophilic attack of the acetate anion on the π bond to form the β-acetoxyalkyl palladium chloride. The heterolytic cleavage to form a carbocation followed by a rearrangement and the combination with the chlorine anion led to the desired product **3.53** (Scheme 3.17).

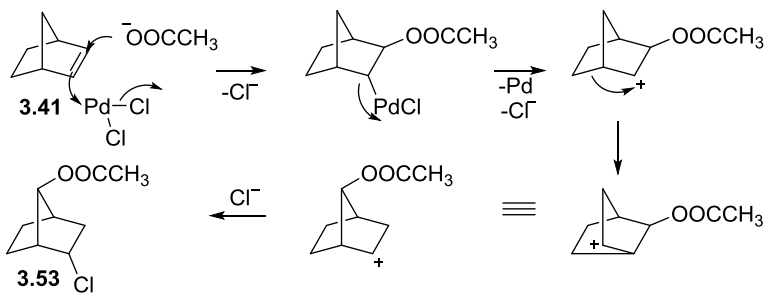

Scheme 3.17: Possible mechanism for the formation of **3.53**.

Then, using potassium *tert*-butoxide, **3.53** was converted into the corresponding alcohol **3.54** in 35% yield. After a Swern oxidation of alcohol **3.54** affording the corresponding ketone **3.37** (58%, purity = 87%), imine **3.39b** was prepared in 70% yield (purity = 75%). However, this imine was particularly unstable because after standing our sample at room temperature for one day, it was partially hydrolysed (22% of conversion) to ketone **3.37** (Figure 3.5(b)). This hydrolysis was probably due to a small amount of water in the sample and the acidity of the glassware. This mixture of **3.39b** and **3.37** (^{1}H NMR ratio imine **3.39b**/ketone **3.37** = 3.51) was used for different fragmentation tests with our flow machine.

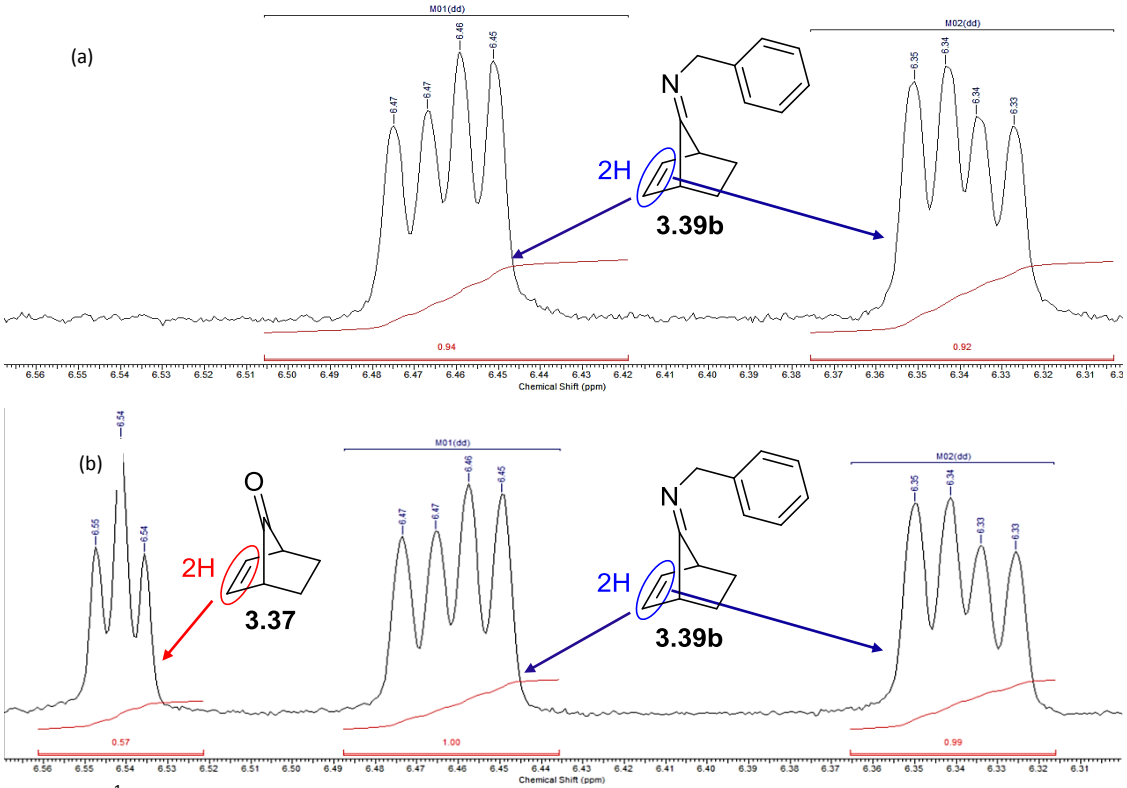

Figure 3.5: ^{1}H NMR of (a) imine **3.39b** (b) imine **3.39b** and and ketone **3.37** (24 h later) due to the partial hydrolysis (NMR ratio imine **3.39b**/ketone **3.37** = 1/(0.57/2) = 3.51).

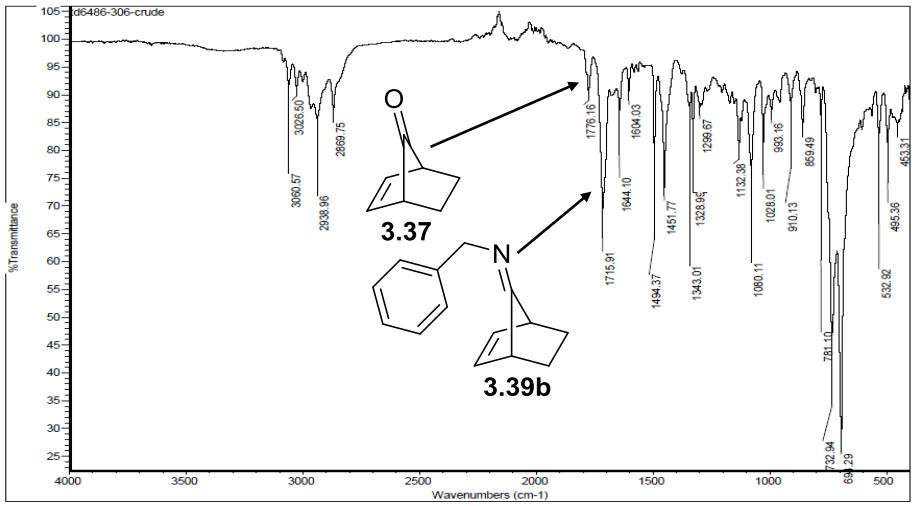

Figure 3.6: IR spectra of the mixture of imine **3.39b** and and ketone **3.37**.

3.2.4 Fragmentation tests

Using our Vapourtec flow platform, the access to very high temperature thanks to the use of a back pressure regulator is possible. According the DFT calculations (Table 3.1), the half-lives at 125 °C of imine **3.39b** and ketone **3.37** are 19000 years and 9 min 15 seconds respectively. However, these half-lives are probably lower if we perform the fragmentation at 250 °C in toluene. The IR spectra of the initial mixture of imine **3.39b** and ketone **3.37** revealed characteristic stretching peaks at 1715 cm^{-1} (major peak-imine) and 1776 cm^{-1} (minor peak-ketone) (Figure 3.6). The mixture of imine **3.39b** and ketone **3.37** used for the fragmentation tests highlighted an NMR ratio imine/ketone = 3.51 (Figure 3.5(b)).

Two different samples of a mixture of imine **3.39b** and ketone **3.37** were injected into the stainless steel flow reactor (Figure 3.7) at the indicated flow rate, temperature and concentration (Table 3.2, entries 1 and 2). In-line IR measurements enabled the monitoring of the reaction with the possible disappearance of characteristic stretching peaks of the imine **3.39b** and ketone **3.37** (1715 and 1776 cm^{-1} respectively) and the possible appearance of characteristic stretching peaks of the carbon monoxide or isocyanides (in the range 2110-2165 cm^{-1}). The different recorded IR spectra were processed with BORIS software. Moreover, at the exit of the reactor, the reaction mixture was collected, the solvent was evaporated under reduced pressure and an NMR analysis was performed. By comparing the NMR ratio imine **3.39b**/ketone **3.37** at the end of each attempt to the initial ratio (= 3.51) and by analysing the different IR spectra, investigations can be made about the fragmentation of the mixture of imine **3.39b** and ketone **3.37**.

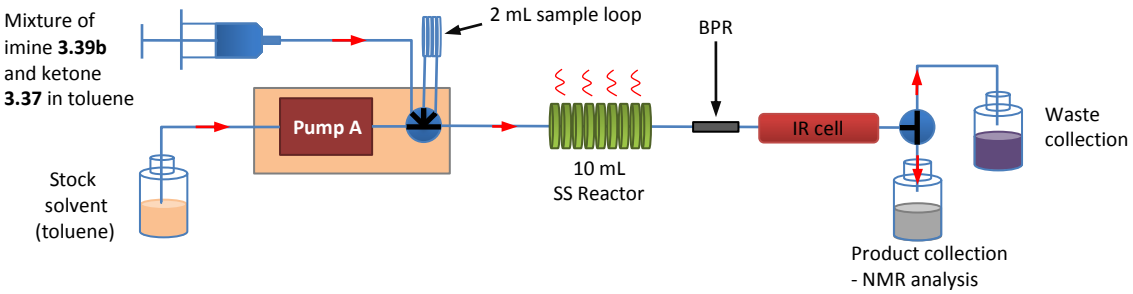

Figure 3.7: Flow set-up for the fragmentation tests towards the formation of isocyanides.

Entry	Volume sample (mL)	Conc. sample (mg/mL)	Temp. reactor (°C)	Flow rate (mL/min)	Reaction time (min)	^{1}H NMR ratio Imine **3.39b**/ ketone **3.37**	IR detection
1	0.4	22.75	250	0.25	40	3.4	Peak at 1715 cm^{-1} Tiny peak around 2120 cm^{-1}
2	0.3	76.7	250	0.25	40	4.6	Peak at 1715 cm^{-1} Tiny peak around 2125 cm^{-1}

Table 3.2: Reaction conditions and analytical results for the fragmentation of the mixture of **3.39b** and **3.37**.

The fragmentation tests (Table 3.2, entries 1 and 2) were quickly performed after the NMR analysis (Figure 3.5(b)) to not be disturbed by the continual hydrolysis of imine **3.39b**.
As a first attempt (entry 1), a sample containing the mixture of imine **3.39b** and ketone **3.37** in toluene ([C] = 22.75 mg/mL) was injected into the flow set up (Figure 3.7) for a reaction time of 40 min and with the flow reactor heated to 250 °C. The recorded IR spectra processed with BORIS software (OPA processing, compilation of all the spectra recorded and generation of the estimated IR spectrum of the reaction mixture (See chapter 4 for more explanations about BORIS software)) highlighted a characteristic peak around 1715 cm^{-1} (imine) and a very tiny peak at around 2120 cm^{-1} (Figure 3.8). Regarding the NMR analysis of the reaction mixture collected at the exit of the reactor (Figure 3.9), the resonance signals of imine **3.39b** and ketone **3.37** were still highlighted with a NMR ratio = 3.39. This ratio is similar to the initial one (NMR ratio = 3.51) so we can assume that the signal at 2120 cm^{-1} is a mixture of carbon monoxide and isocyanide **3.55**.

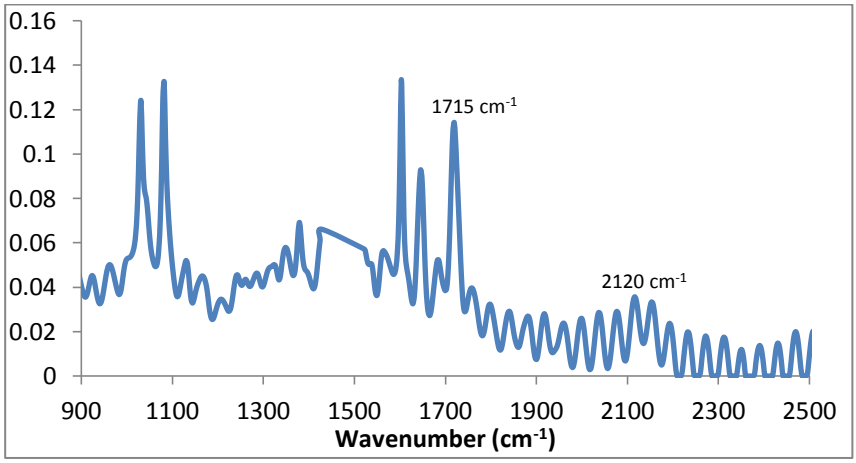

Figure 3.8: Estimated IR spectrum of the collected reaction mixture generated using BORIS software and OPA processing (entry 1).

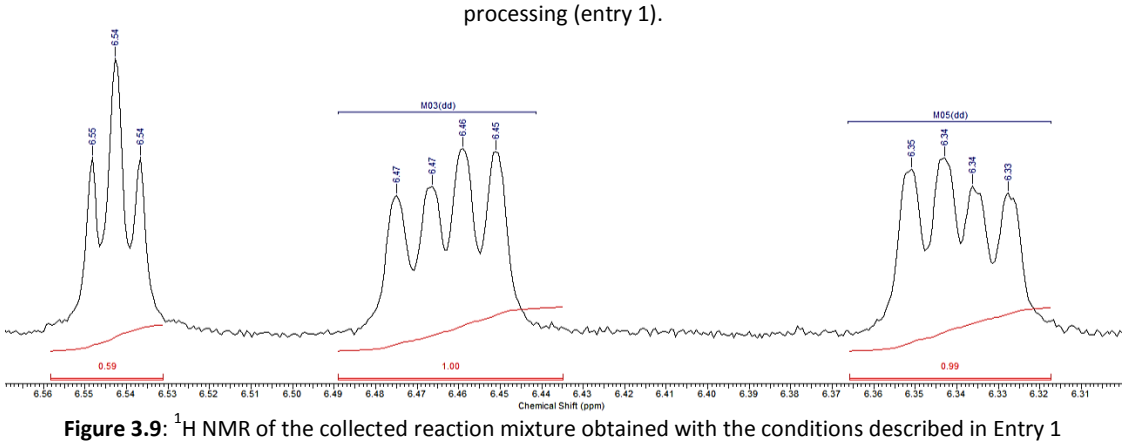

Figure 3.9: ^{1}H NMR of the collected reaction mixture obtained with the conditions described in Entry 1 (NMR ratio imine **3.39b**/ketone **3.37** = 1/(0.59/2) = 3.39).

As a second attempt (entry 2), in order to try to intensify the signal at around 2120 cm^{-1} in the IR spectrum, the concentration of the injected sample was increased to 76.7 mg/mL and

the other experimental conditions remained unchanged. The recorded IR spectra processed with BORIS software highlighted a characteristic peak around 1715 cm^{-1} (imine) and a tiny peak at around 2125 cm^{-1} (Figure 3.10). Regarding the NMR analysis of the reaction mixture collected at the exit of the reactor (Figure 3.11), the resonance signals of imine **3.39b** and ketone **3.37** were still highlighted with a NMR ratio = 4.55. This ratio is higher than the initial one (NMR ratio = 3.51) which means that the amount of ketone **3.37** decreased faster than the amount of imine **3.39b**. Therefore, the signal at 2125 cm^{-1} is probably a mixture of carbon monoxide and isocyanide **3.55** with a higher amount of CO.

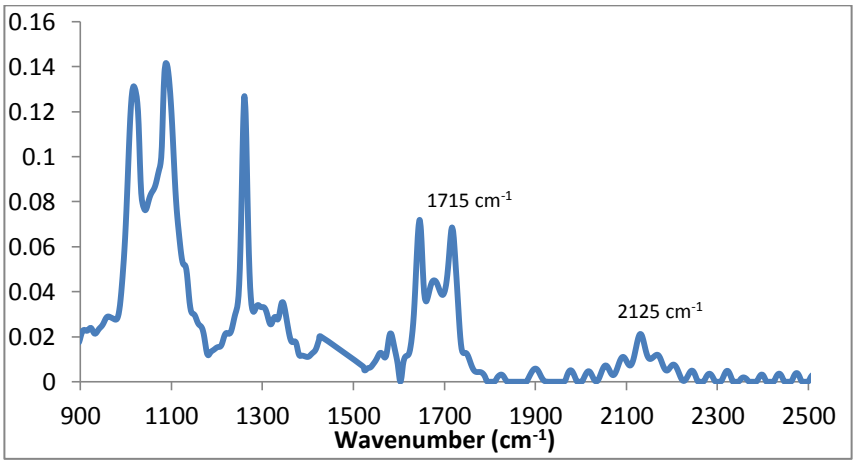

Figure 3.10: Estimated IR spectrum of the collected reaction mixture generated using BORIS software and OPA processing (entry 2).

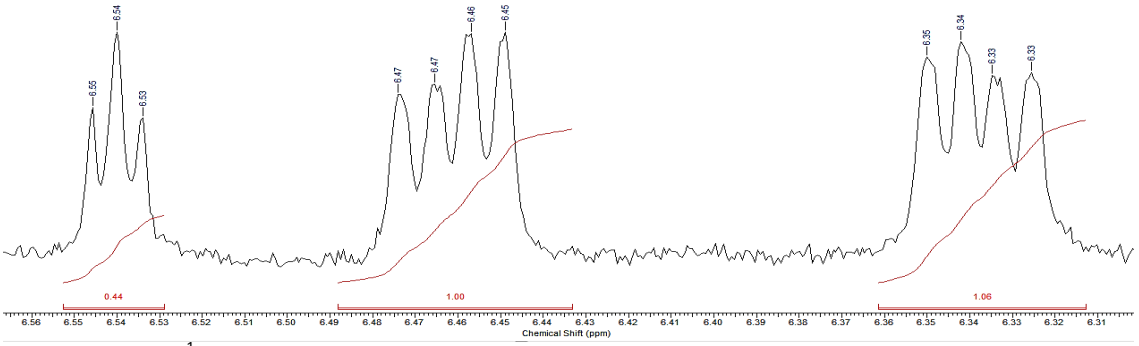

Figure 3.11: ^{1}H NMR of the collected reaction mixture obtained with the conditions described in Entry 2 (NMR ratio imine **3.39b**/ketone **3.37** = 1/(0.44/2) = 4.55).

To sum up with these two attempts, we cannot assure that we managed to generate *in situ* isocyanides. Indeed, with an initial mixture of ketone **3.37** and imine **3.39b**, both fragmentations could have occurred and we cannot distinguish between the generated carbon monoxide and isocyanide as they have similar stretching peaks in their IR spectra. The use of a pure precursor is essential. However, the sequential reactions starting with the fragmentation of our mixture of ketone **3.37** and imine **3.39b** followed by the reaction with the Passerini or Ugi reagents could have been a good test of the success of *in situ* isocyanide generation.

With both norbornadiene and norbornene routes described for the synthesis of isocyanide precursors, the results were not promising. Indeed, difficult purifications, volatile products or low yields were the main drawbacks which prevent the reliable synthesis of the target imines **3.38** and **3.39**. Moreover, the instability of imine **3.39b** (fast hydrolysis) was another issue towards the *in situ* isocyanide generation. For these reasons, another system employing either a thermal (e.g. Retro Diels-Alder reaction) or a photochemical fragmentation as a key step would be interesting to study and investigate in order to develop an efficient in-line isonitrile generation.

4 Chapter 4: Thermolysis of 1,3-dioxin-4-ones under flow; fast generation of kinetic data using in-line analysis

4.1 Introduction to kinetic studies

Over the last few decades, advances in research have highlighted the potential of continuous flow processes in a wide range of chemical applications. In the context of kinetic studies, flow chemistry provides many advantages over classical batch experiments such as the minimisation of waste,[5b] the low consumption of reagents and fully automated systems for convenient replication of experiments. Moreover, in-line analysis of the reaction mixture enables direct monitoring of a chemical reaction and the rapid acquisition of data while breaking the gap between the synthetic and the analytical part. Consequently, flow chemistry with in-line monitoring turns out to be an efficient and reliable process for the acquisition of kinetic information. Several examples using in-line analysis such as UV,[76] IR,[77] Raman,[78] fluorescence,[79] NMR,[80] MS[81] and HPLC[82] have already shown their efficiency for kinetic studies conducted under steady-state flow conditions. In opposition, other examples using off-line analysis (UV[83] or NMR[84]) to perform kinetic study highlight the laborious process to collect kinetic data. However, regarding the kinetic study conducted under steady state flow conditions and in-line analysis, the main drawback is that each reaction time needs a different flow rate so 25-30 individual experiments need to be conducted to carry out a complete kinetic study. An elegant, but limited solution is to change the position of the analytical probe along the reactor pathway to provide the reaction time information.[85] A more general solution to providing a very fast kinetic study method was described by Mozharov *et al*.[14] Using microreactors with in-line monitoring (Raman spectroscopy), this method is based in a step-change in flow rate to generate from a single flow experiment time-series data. The gain in time (approximately 3-4 times faster) and the lower consumption of material are the main advantages of this novel methodology. More recently, a similar method based on the use of a flow rate ramp instead of a step change in flow rate between two steady states was reported by Moore *et al*.[86] This modification was explained by the "uncertainty in the accurate determination of residence time"[86] due to the "non-instantaneous step change in flow rates".[86] However, the application of this linear-residence-time-ramp method requires specific technology with uninterrupted flow-rate adjustment which is not possible with most of the available flow platforms. Therefore, the method highlighted by Mozharov,[14] which is called the "push-out" method in the present report, was used as a reference to develop our kinetic studies with our mesoscale flow chemistry platform. Being widely used in the previous chapter regarding the synthesis of analogues of epicocconone, the thermolysis of 1,3-dioxin-4-ones

was chosen as a model reaction (Scheme 4.1) to illustrate the procedure with our Vapourtec platform. To monitor the reactions, in-line UV and IR as well as off-line NMR analysis were employed and the kinetic results were compared to validate the novel process.

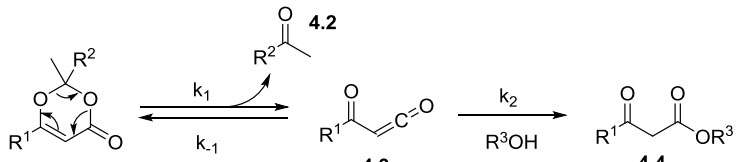

2.38, $R^1 = R^2 = Me$
2.26, R^1 = aryl and R^2 = Me
4.1, R^1 = Me and R^2 = aryl

Scheme 4.1: Thermal cycloreversion of 1,3-dioxin-4-ones and acylketene trapping.

4.2 Results and discussion: Synthesis of a range of 1,3-dioxin-4-ones

In order to investigate the influence of substituent effects upon the thermolysis, a series of 1,3-dioxin-4-ones (**2.26**, **4.1**) with different substituents at the 2- and 6-positions (R_1 = methyl, aryl ≠ R_2 = methyl, aryl) were prepared.

4.2.1 Synthesis of 1,3-dioxin-4-ones 2.26 (R^1 = aryl and R^2 = methyl)

4.2.1.1 First synthetic route to 1,3-dioxin-4-ones 2.26

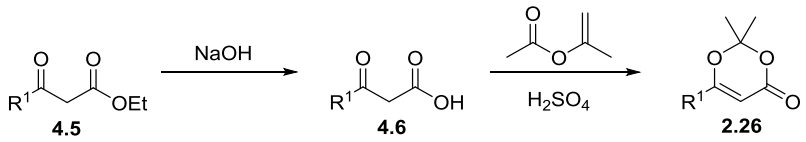

Entry	R^1	scale (mmol)	**4.6**[a] (yield)	**2.26**[b] (yield)
1	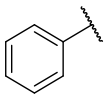	10	**4.6a** (63%)[c]	**2.26a** (66%)[c]
2	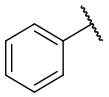	200	**4.6a** (44%)[d]	-

Table 4.1: Synthesis in batch of **2.26a** (R^1 = phenyl) from ethyl benzoylacetate (**4.5a**) (R^1 = phenyl).
[a] Reaction conducted with: ethyl benzolyacetate (**4.5a**, 1 equiv.) and sodium hydroxide (1 equiv.) at 0 °C for 3 h and then r.t. for 20 h. [b] Reaction conducted with: **4.6a** (1 equiv.), isoprenyl acetate (3.7 equiv.) and sulfuric acid (0.2 equiv.) at 0 °C for 3 h. [c] Isolated Yields. [d] Calculated yield from the crude NMR (mixture of acetophenone and **4.6a**).

The first synthetic route tried towards the formation of 1,3-dioxin-4-ones **2.26** is described in Table 4.1.[87] On small scale, benzoyl acetic acid (**4.6a**) was prepared in good yield (63%) by hydrolysis of ethyl benzoylacetate (**4.5a**). However, after 2 days, the pure isolated compound **4.6a** was completely decomposed into acetophenone. On larger scale, the yield decreased to 44% because a large amount of acetophenone (decarboxylation of **4.6a**) was formed (29% yield). 1,3-Dioxin-4-one **2.26a** was obtained in 66% yield by treatment of the β-keto acid **4.6a** with a mixture of sulfuric acid and isopropenyl acetate. Owing to the instability of the β-keto acid **4.6a** (decarboxylation), a second synthetic route was studied.

4.2.1.2 Second synthetic route to 1,3-dioxin-4-ones 2.26

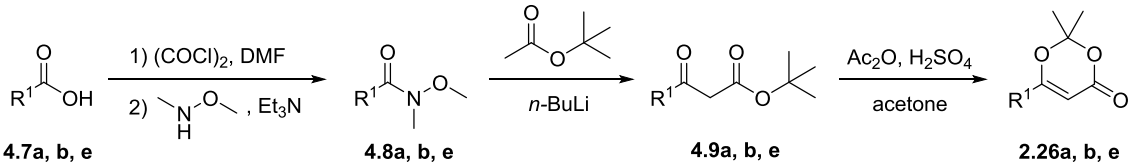

4.7a, b, e **4.8a, b, e** **4.9a, b, e** **2.26a, b, e**

Entry	R^1	**4.8**[a] (yield)[d]	**4.9**[b] (yield)[d]	**2.26**[c] (yield)[d]
1		**4.8a** (68%)	**4.9a** (81%)	**2.26a** (48%)
2	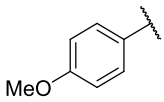	**4.8b** (95%)	**4.9b** (96%)	**2.26b** (89%)
3	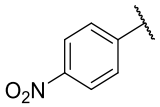	**4.8e** (92%)	**4.9e** (47%)	**2.26e** (37%)

Table 4.2: Synthesis in batch of 1,3-dioxin-4-ones **2.26a, b, e** from benzoic acids **4.7a, b, e**.
[a] Reaction conducted with: 1) benzoic acid **4.7a, b, e** (1 equiv.), $(COCl)_2$ (1.25 equiv.) and DMF (0.004 equiv.) at r.t. for 3 h. 2) N,O-dimethylhydroxylamine (1.4 equiv.) and Et_3N (3 equiv.) at r.t. for 12 h. [b] Reaction conducted with: *n*-BuLi (3.1 equiv.) and DIPA (3 equiv.) at 0 °C for 45 min and then *t*-butylacetate (3 equiv.) and Weinreb amide **4.8a, b, e** (1 equiv.) at -78 °C for 1 h 45 min. [c] Reaction conducted with: acetic anhydride (15 equiv.), sulfuric acid (1 equiv.), acetone (10 equiv.) and *t*-butylester **4.9a, b, e** (1 equiv.) at r.t. for 1 h. [d] Isolated yields.

The second synthetic route towards the formation of 1,3-dioxin-4-ones **2.26** is described in Table 4.2.[29-30, 88] β-Substituted-β-keto *tert*-butyl esters **4.9** were synthesised in good yields from Weinreb amides[89] **4.8** previously obtained from benzoic acids **4.7**. Finally, 1,3-dioxin-4-ones **2.26** were prepared from condensation between **4.9** and acetone under acidic conditions.[90]

4.2.2 Synthesis of 1,3-dioxin-4-ones 4.1 (R^1 = methyl and R^2 = aryl)

4.2.2.1 First synthetic route to 1,3-dioxin-4-ones 4.1

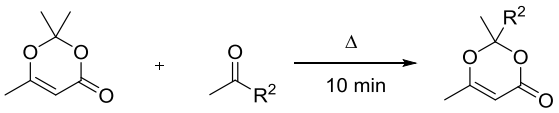

2.38 **4.10a-c** **4.1a-c**

Entry	R^2	Dioxinone **2.38** (equiv.)	Ketone **4.10a-c** (equiv.)	Solvent	Temperature (°C)	**4.1** (yield)
1	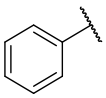	1	1.5	MeCN	150	**4.1a** (≈ 2%)[a]
2	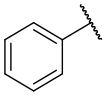	1	10	-	150	**4.1a** (31%)[b]
3	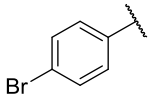	1	10	-	150	**4.1b** (0%)
4	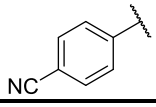	1	5	MeCN	180	**4.1c** (0%)

Table 4.3: Synthesis in flow of 1,3-dioxin-4-ones **4.1a-c** from 2,2,6-trimethyl-4*H*-1,3-dioxin-4-one (**2.38**).
[a] Calculated yield from the crude NMR. [b] Isolated yield.

Towards the synthesis of 1,3-dioxin-4-ones **4.1**, the first attempts performed were the thermolysis in flow of 2,2,6-trimethyl-4*H*-1,3-dioxin-4-one (**2.38**) followed by cyclisation with ketone **4.10** (Table 4.3). With 10 equiv. of ketone **4.10a**, the dioxinone **4.1a** was obtained in 31% yield. However, 1,3-dioxin-4-ones **4.1b** and **4.1c** were not formed in the conditions described. Therefore, in order to enlarge our range of 1,3-dioxin-4-ones, a second synthetic route was studied.

4.2.2.2 Second synthetic route to 1,3-dioxin-4-ones 4.1

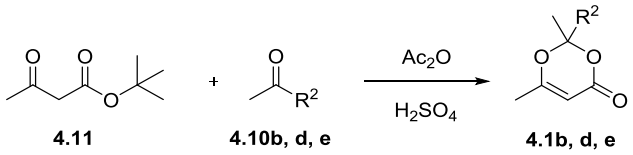

4.11 **4.10b, d, e** **4.1b, d, e**

Entry	R^2	**4.1**[a] (yield)[b]
1	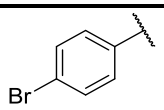	**4.1b** (18%)
2	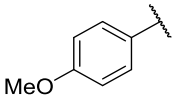	**4.1d** (20%)
3	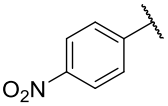	**4.1e** (0%)

Table 4.4: Synthesis in batch of 1,3-dioxin-4-ones **4.1b, d, e** from *tert*-butyl acetoacetate (**4.11**).
[a] Reaction conducted with: sulfuric acid (1 equiv.), *tert*-butyl acetoacetate (**4.11**, 1 equiv.), ketone **4.10b, d, e** (2 equiv.), acetic anhydride (3.5 equiv.) for 16-43 h at 0-15 °C. [b] Isolated yields.

This second synthetic route is based on the condensation between the β-keto *tert*-butyl ester **4.11** and the ketone **4.10** in acidic conditions (Table 4.4).[91] Following this procedure, Haddad *et al*.[91] managed to synthesise **4.1a** in 70% yield. Regarding our results, **4.1b** and **4.1d** were prepared in low yield (18 and 20% respectively). With the same reaction conditions, **4.1e** was not formed.

4.3 Results and discussion: Kinetic study of the thermolysis of 1,3-dioxin-4-ones

4.3.1 Fragmentation of 1,3-dioxin-4-ones in the presence of excess of alcohol: a 1st order reaction

The fragmentation of 1,3-dioxin-4-ones *via* a retro Diels-Alder reaction[92] to afford highly reactive acylketenes which can be trapped by a nucleophile and more particularly by an alcohol leading to β-ketoesters has been widely studied in the literature (Scheme 4.1).[93] The particular thermal fragmentation of 2,2,6-trimethyl-4*H*-1,3-dioxin-4-one (**2.38**) followed by the

trapping of the acylketene intermediate **4.3a** in the presence of an excess of alcohol (Scheme 4.2) has been described as a first order reaction.[94] Indeed, the reaction between the acylketene **4.3a** and the alcohol is much faster than the reverse reaction (Diels-Alder reaction) between the same acylketene **4.3a** and acetone (k_2[EtOH] >> k_{-1}[acetone]).[94-95] Thus, the kinetic expression of this reaction (Equation 4.1) can be simplified as a first-order rate equation (Equation 4.2). The integrated first-order rate law gives Equation 4.3.

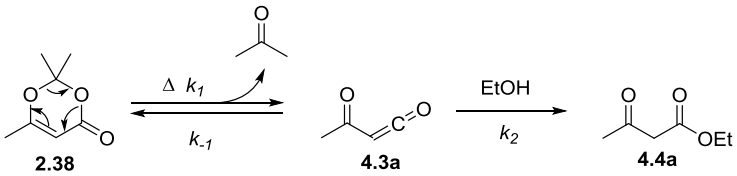

2.38 **4.3a** **4.4a**

Scheme 4.2: Thermal fragmentation of 2,2,6-trimethyl-4*H*-1,3-dioxine-4-one (**2.38**) followed by trapping with EtOH.

$$\frac{\mathrm{d}[\mathbf{2.38}]}{\mathrm{dt}} = \frac{k_1 k_2[\mathbf{2.38}][\mathrm{EtOH}]}{k_{-1}[\mathrm{acetone}] + k_2[\mathrm{EtOH}]}$$

Equation 4.1: Rate equation of the thermolysis of 1,3-dioxin-4-one **2.38** followed by trapping with EtOH.

$$\frac{\mathrm{d}[\mathbf{2.38}]}{\mathrm{dt}} = k_1[\mathbf{2.38}]$$

Equation 4.2: Simplified first-order rate equation.

$$\ln[\mathbf{2.38}]_t = -k_1 t_R + \ln[\mathbf{2.38}]_0$$

Equation 4.3: Integrated first-order rate equation.

As a first experiment, we checked that the reverse reaction (Diels-Alder reaction) between the acylketene **4.3a** and acetone was not significant by showing that the measured reaction rate constant k_1 did not change with the amount of alcohol. For this purpose, the kinetic studies of the fragmentation of 2,2,6-trimethyl-4*H*-1,3-dioxine-4-one (**2.38**) in the presence of 1, 2 and 4 equivalents of EtOH were performed under flow conditions at 120 °C using the conventional kinetic study method (steady-state method) with off-line ^{1}H NMR analysis. Between 1 and 4 equivalents of EtOH, kinetic measurements gave constant and consistent first-order reaction rate constants (k_1 = 1.85 x 10^{-3} s^{-1} ± 1%) (See experimental part).

During our kinetic experiments, an excess of alcohol (4 equivalents) was premixed with the corresponding 1,3-dioxin-4-one to avoid possible side reactions: condensation of the acylketene with the enol form of **4.2** (e.g. to form 2,6-dimethyl-4*H*-pyran-4-one from **4.3a** and the enol form of acetone)[93b] and [4 + 2] dimerization of the acylketene (e.g. to form dehydro acetic acid from **4.3a**).[93b]

4.3.2 Push-out methodology - Fast kinetic study procedure in 3 key steps

As described in section 4.1, a novel kinetic study methodology, called the push-out method and based in a step-change in flow rate (low flow rate F_1 and high flow ate F_2) to generate from a single flow experiment time-series data, was recently reported.[14] This methodology dramatically speeds up data acquisition and reduces experimental time to solve kinetic investigations. Indeed, to perform a complete kinetic study with the conventional method (steady-state method), 25-30 experiments (5 different reaction times per temperature, 5-6 different temperatures) are required for about 6-7 hours of work, whereas the push-out method can solve the kinetic study in only 7-8 experiments in about 2 hours. Initially developed for microfluidic flow platforms, this methodology was transferred to our meso-scale Vapourtec platform with in-line or off-line analysis and the reliability of our results was demonstrated.

The push-out procedure towards the fast acquisition of kinetic data is divided into the following 3 key steps:

Step I: Injection of the reaction mixture and stabilisation of the system at low flow rate F_1 until the steady-state 1 is reached (Figure 4.1). In these conditions, a high conversion is observed. For a typical experiment, F_1 = 1 mL/min, which means that the specific position R_1, located at the end of the 10 mL reactor, had 10 min reaction time (Figure 4.1).

Step II: Introduction of the step-change in flow rate by pushing the reaction mixture out of the reactor at a high flow rate F_2 and rapid analysis of the stream with the in-line spectrometer (UV or IR) or off-line ^{1}H NMR analysis. For a typical experiment, F_2 = 10 mL/min. During this step-change, 2 other specific positions were used as examples to highlight two different reaction times. First, the position R_3 (Figure 4.1), which is located just at the entrance of the 10 mL reactor, will have 1 min reaction time at high flow rate F_2. Then, the position R_2 (Figure 4.1), which is located just in the middle of the 10 mL reactor (5 mL away from the entrance), had 5 min reaction time at low flow rate F_1 (during the steady state 1), and will have 30 seconds reaction time at high flow rate F_2. Therefore, this position R_2 will have 5 min and 30 seconds reaction time. In this way, the transitional period between the 2 steady-states give spectroscopic information across a gradient of reaction time (typically between 1 and 10 min for F_1 = 1 mL/min and F_2 = 10 mL/min) within the reactor.

Step III: Stabilisation of the system at high flow rate F_2 till a second steady-state is detected (steady-state 2). A low conversion is observed. Then, the reaction is stopped (Figure 4.1).

A complete kinetic study is achieved by repeating these 3 steps at several temperatures.

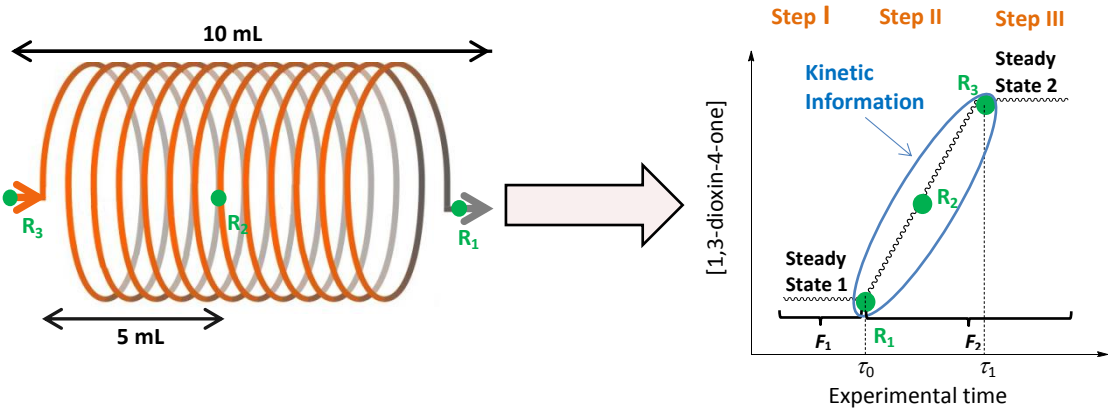

Figure 4.1: Flow reactor with kinetic study acquisition. The transitional period between the 2 steady-states give kinetic information across a gradient of residence time within the reactor (e.g. R_1, R_2 and R_3 data points).

4.3.3 Push-out methodology - Acquisition of the kinetic data

BORIS software (Bristol Online Reaction Investigation Software), a chemometric tool developed by Bristol Chemometrics Group and GlaxoSmithKline, was used to process the various in-line spectra collected during the 3 steps described previously. The use of chemometric methods for quantitative analysis of in-line spectra during process monitoring has been well developed and enables the detection of individual components from complex mixtures.[96]

The Orthogonal Projection Approach[97] (OPA, calibration-less method), a multivariate curve resolution of spectra by alternating least squares method (MCR-ALS)[98] included in BORIS software, was applied for the processing of our multi-component UV or IR data and for the reconstruction of the different reactant concentrations. This method is particularly useful when overlaps occur between different components. During the kinetic studies of the thermolysis of 1,3-dioxin-4-ones, the OPA method processed our analytical data with 2 spectral components resolution (component 1: 1,3-dioxin-4-one and component 2: the corresponding ketone **4.2** and the β-ketoester **4.4**). The ketone and the β-ketoester were identified as a single component in the OPA process since their ratio did not change during the thermolysis. Processing with 3 spectral components resolution did not resolve the kinetic study (see experimental part). In addition to the generation of the plot of the evolution of the relative concentration of each component *vs.* the experimental time (Figure 4.2(a)), the OPA

method generated the estimated spectra of each component. In all cases, the estimated spectra of the 1,3-dioxin-4-one was consistent with the experimental one.

The Multivariate Linear Regression (MLR) included in BORIS software, was another method employed for the processing of our multi-component UV or IR data. This methodology reconstructed the concentration profile of a component from the given pure component spectrum (Reference). After processing with this method, the generated concentration profile of 1,3-dioxin-4-one under push-out conditions was similar to Figure 4.2(a).

Finally, the height of non-overlapping peak processing, also included in BORIS software, was the last method used for our kinetic study resolution. This simple method determined the relative concentration of each component by measuring the height of a peak (absorbance) at a selected wavelength. The main limitation of this approach was to find a specific wavelength for each species without overlap during the reaction. When the resolution was possible, the generated concentration profile of 1,3-dioxin-4-one under push-out conditions was similar to Figure 4.2(a).

In Figure 4.2(b), the different parts of a push-out experiment at one specific temperature (steady-state 1, transitional period and steady-state 2) relative to the 3 key steps previously described are observed. From the transitional period of each push-out experiment performed at the indicated temperature, the logarithm of [1,3-dioxin-4-one] (ln[**2.38**] in Figure 4.2(c)) is plotted against the reaction time t_r calculated from Equation 4.4.[14] The incorporation of a correction due to the thermal expansion of the solvent was performed in this calculation of t_r. In order to do this, τ_0 was estimated from the first inflection point of the push-out experiment and τ_1 was calculated from the flow rate corrected for thermal expansion of the solvent (Equation 4.5). The first order reaction rate constants are obtained from the slope of the different straight lines (Figure 4.2(c)). Finally, the Arrhenius plot of the reaction rate constants against the reciprocal of temperature (Figure 4.2(d)) enables the calculation of the activation energy E_a of 1,3-dioxin-4-one thermolysis.

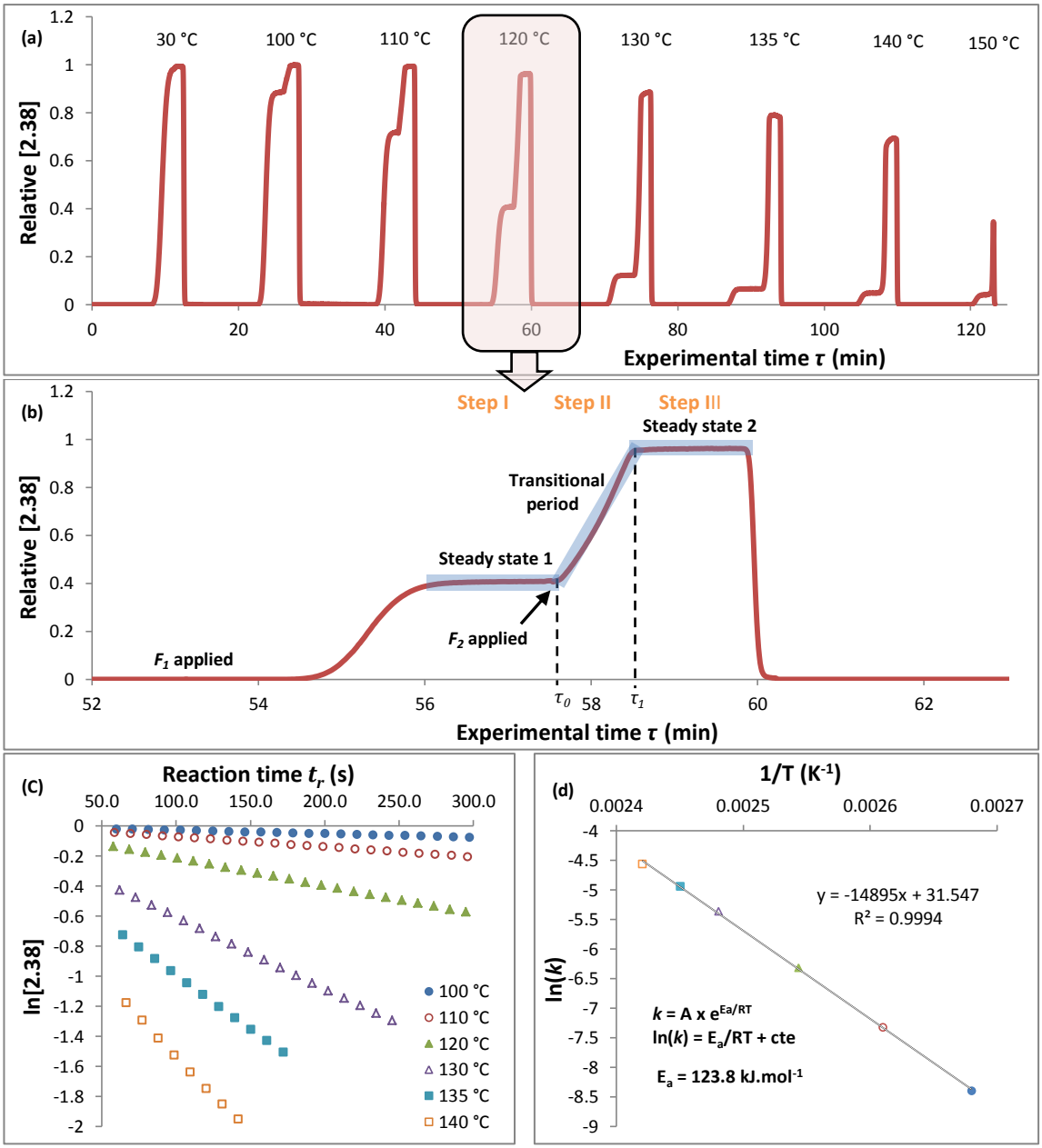

Figure 4.2: Acquisition of the kinetic data from push-out experiments (this example is Table 4.7 entry 1). (a) Concentration profile of 2,2,6-trimethyl-4*H*-1,3-dioxin-4-one (**2.38**) during flow thermolysis obtained from push-out experiments with in-line monitoring at each of the temperature indicated. Processing of the UV spectra with the OPA method. (b) Zoom in on the push-out experiment at 120 °C. (c) First-order kinetics of thermolysis of **2.38**. (d) Arrhenius plot and calculation of activation energy from $\ln(k) = E_a/RT + cte$ with E_a the Activation energy ($J.mol^{-1}$), R the universal gas constant ($J.K^{-1}.mol^{-1}$), T the temperature (K) and k the first-order reaction rate constant (s^{-1}).

$$t_r = \frac{F_2 - F_1}{F_1}\tau + \frac{F_2}{F_1}\tau_1 - \tau_0$$

with t_r = reaction time (s)
F_2 = high flow rate (mL/s)
F_1 = low flow rate (mL/s)
τ_o = estimated start of step II - first inflection point (s)
τ_1 = calculated end of step II - Equation 4.5 - second inflection point (s)
τ = experimental time (s)

Equation 4.4: Determination of the reaction time t_r from the different push-out parameters.

$$\tau_1 = \tau_0 + \frac{V}{F_2(1 + \alpha\Delta T)}$$

with τ_1 = calculated end of step II - 2nd inflection point (s)
τ_o = estimated start of step II - first inflection point (s)
F_2 = high flow rate (mL/s)
α = expansion coefficient of solvent ($°C^{-1}$)
= 0.00137 $°C^{-1}$ for MeCN
V = volume of the reactor (mL)
T = temperature (°C)

Equation 4.5: Correction for thermal expansion of the solvent.

4.3.4 Configuration of the flow platform for the push-out methodology

To perform the kinetic studies, the Vapourtec R series system (R2+/R4) was employed (Figure 4.3). This platform is equipped with one Knauer HPLC pump, a home-made Stainless Steel reactor (10 mL capacity, 1 mm i.d.) heated by immersion in a high temperature silicone oil bath (Grant Optima™ TXF200), a cooling loop (100 cm, 1 mm i.d.) immersed in an ice bath, a Back Pressure Regulator to allow the heating of solvents beyond the boiling point and an in-line IR or UV spectrometer integrated into the flow system. Both analytical systems use flow cells specially designed for flow chemistry. The in-line IR measurements were recorded on an alpha transmission FT-IR from Bruker at room temperature. Harrick Demountable Liquid Flow cell with NaCl windows was connected to the flow system and enables the liquid going through the spectrometer. Each spectrum was recorded every 3.75 seconds with the OPUS software. The in-line UV spectra were acquired on Ocean Optics DH-2000-BAL spectrometer using a Type 583-F Starna fluorimeter flow cell (path length: 1 mm, volume: 0.011 mL) from Starna Scientific. UV spectra were recorded every 1.2 seconds with the SpectraSuite software. When needed for off-line reaction analysis (NMR), the system was connected to a Gilson Prep Fraction Collector.

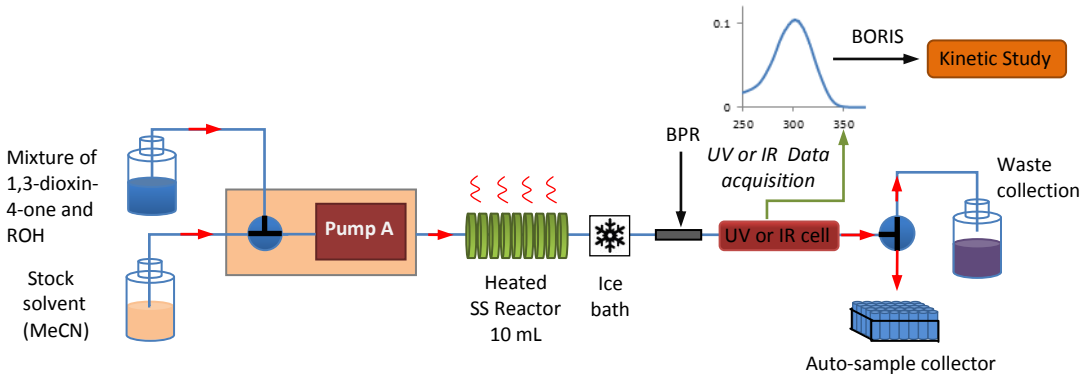

Figure 4.3: Flow set-up for the kinetic studies of the fragmentation of 1,3-dioxin-4-ones **2.38**, **2.26** and **4.1** in the presence of an excess of alcohol.

4.3.5 Air-heated system issues

Using the commercial double coiled air-heated stainless steel reactor provided with the Vapourtec platform (Figure 4.6), a difference was observed between the steady-state and the push-out reaction rate constants measured at high temperature (130 °C) for the thermolysis of **2.38** (Table 4.5). Moreover, according to Figure 4.4, two different measures of reaction rate constants *k* were observed during the push-out experiment in this commercial reactor. These two inconsistent results/measures are explained by the inefficient heat transfer in air and the unequal heating of the inner and outer air-heated stainless steel reactor coils (under control of a single thermocouple). In comparison, consistent first-order reaction rate constants were measured between steady-state and push-out method performed with

oil-heating (Table 4.5 and Figures 4.7-4.8). Additionally, homogeneity of the temperature across the reactor immersed in oil results in a linear plot of ln[**2.38**] *vs.* reaction time during the push-out experiment (Figure 4.5). The same comparison was performed between the reaction rate constants obtained in the air-heated and an oil heated PFA reactor (Table 4.6). The smaller rate constants obtained with the air-heated compared to the oil-heated PFA reactor (and oil-heated stainless steel reactor) are due to lower thermal transfer in air.

Having these preliminary results, the home-made oil heated reactor was employed in all kinetic experiments performed in this chapter.

Entry	Kinetic study method	Commercial air-heated stainless steel reactor $k \times 10^{-3}$ (s^{-1})	Home-made oil-heated stainless steel reactor $k \times 10^{-3}$ (s^{-1})
1	Steady-state	3.99	4.92
2	Push-out	5.86	4.70

Table 4.5: Reaction rate constants measured during the thermolysis of 2,2,6-trimethyl-4*H*-1,3-dioxin-4-one (**2.38**) in the presence of EtOH (4 equiv.) in acetonitrile at 130 °C with either the commercial double coiled air-heated or the oil heated reactor with in-line UV analysis. The push-out procedure was performed with F_1 = 1 mL/min and F_2 = 10 mL/min. The steady state one was carried out with a series of flow rates: 3, 5, 7 and 10 mL/min. Processing of the data with the OPA method.

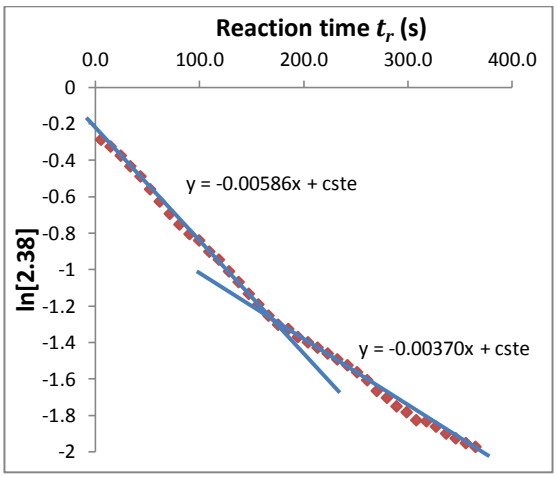

Figure 4.4: ln [**2.38**] plotted against the reaction time from push-out experiments of the thermolysis of **2.38** with 4 equiv. of EtOH in MeCN - Double coiled air-heated reactor at 130 °C - In-line UV monitoring and OPA processing.

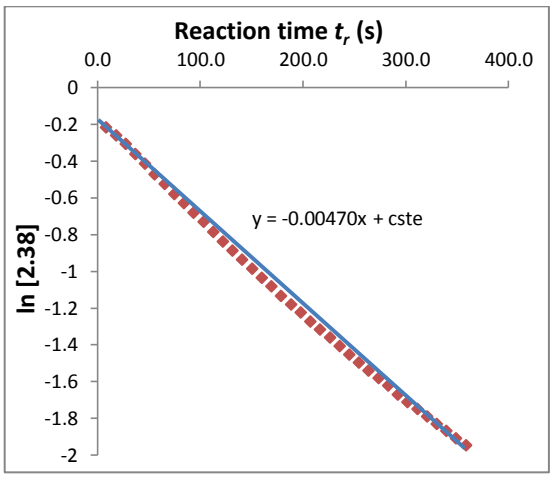

Figure 4.5 ln [**2.38**] plotted against the reaction time from push-out experiments of the thermolysis of **2.38** with 4 equiv. of EtOH in MeCN - Oil-heated reactor at 130 °C - In-line UV monitoring and OPA processing.

Figure 4.6: 10 mL double coiled air-heated Vapourtec SS reactor.

Figure 4.7: Silicon oil bath Grant with immersed SS reactor.

Figure 4.8: 10 mL home-made stainless steel reactor (immersed in silicon oil).

Entry	Kinetic study method	Commercial air-heated PFA reactor[a]	Oil-heated PFA reactor[a]	Home-made oil-heated stainless steel reactor[b]
		k x 10^{-3} (s^{-1})	k x 10^{-3} (s^{-1})	k x 10^{-3} (s^{-1})
1	Steady-state	0.77	1.20	-
2	Push-out	0.72	1.10	1.17

Table 4.6: Reaction rate constants measured during the thermolysis of 2,2,6-trimethyl-4*H*-1,3-dioxin-4-one (**2.38**) in the presence of EtOH (4 equiv.) in acetonitrile at 115 °C with either the commercial air-heated PFA reactor or the oil-heated PFA reactor or the home-made oil-heated stainless steel reactor. The push-out procedure was performed with F_1 = 1 mL/min and F_2 = 10 mL/min. The steady state one was carried out with a series of flow rates: 3, 5, 7 and 10 mL/min.
[a] Reaction rate constants obtained from in-line UV analysis and OPA processing. [b] Reaction rate constant obtained from in-line IR analysis and OPA processing.

4.3.6 Dispersion issues

Using our meso-scale Vapourtec platform (tube diameter of 1 mm) with a range of flow rates between 0.1 and 20 mL.min^{-1}, laminar flow occurs (Reynolds number < 2000) and significant Taylor dispersion is expected (see section 5.1 for detailed explanations about dispersion). The determination of this dispersion can be performed by measuring the residence time distribution (RTD) of a very short plug of material going through a tube.

The aim of this investigation is to determine the effects of dispersion occurring during push-out experiments on the kinetic results. For this purpose, Figure 4.9 highlights the dispersion of 10 µL sample of a solution of benzophenone in MeCN going through our home-made coiled stainless steel reactor (Figure 4.8, 10 mL capacity, 1 mm internal diameter) at different flow rates (0.1, 1, and 10 mL.min^{-1}) and at different temperatures (30 and 120 °C). High temperatures and low flow rates reduced the dispersion effects due to increased diffusion mixing across the tube. Moreover, the Taylor dispersion in a reactor coil is reduced (peak height higher) compared to a linear one due to Dean circulation.[99] Cyril Henry demonstrated this effect in his Thesis[100] by comparing the maximum UV absorbance of a small plug of material going through a linear reactor and a reactor coil. Significant difference was observed: Maximum UV absorbance for the linear reactor was about 30-40% lower than the reactor coil. The experiment at 10 mL.min^{-1} and at 30 °C highlights the highest dispersion and represents the worst case. For the same temperatures, the dispersions at 1 and 10 mL.min^{-1} (typical flow rates employed in the push-out experiments) are almost identical.

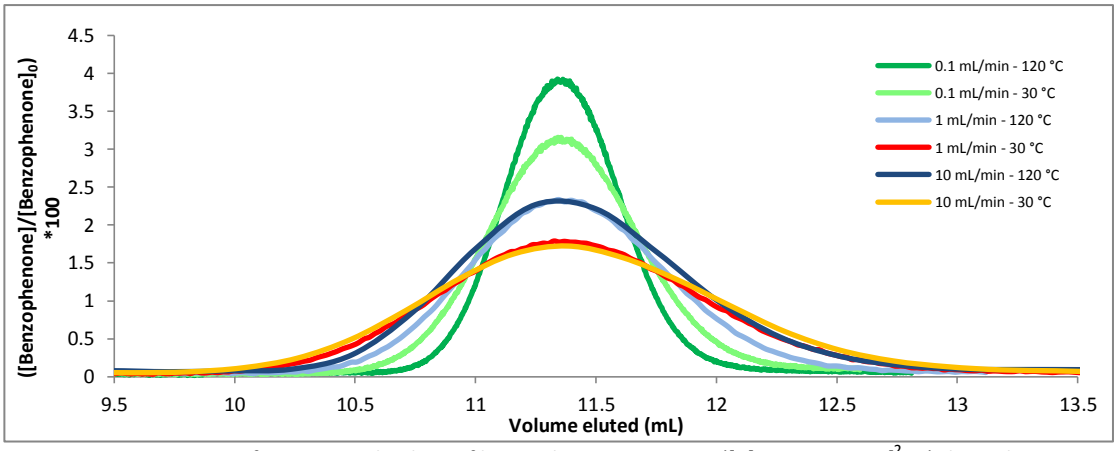

Figure 4.9: Dispersion of 10 µL sample plugs of benzophenone in MeCN ($[C]_0 = 1.015 \times 10^{-2}$ M) through a 10 mL home-made coiled stainless steel tubing at 30 and 120 °C and at the indicated flow rates - In-line UV analysis and height of non-overlapping peak processing at 250 nm.

As the RTD is symmetrical, the average reaction time and the observed reaction time are similar. For our dispersion profiles performed between 0.1 and 10 mL/min at 30 and 120 °C, the average retention time and the retention time of the top of the peak are almost identical. Therefore, the average conversion will be very close to that expected. The worst case dispersion profile (10 mL/min, 30 °C) was used as a model to simulate the effect of dispersion upon calculated kinetic parameters of 1st and 2nd order reactions under push-out conditions. The theoretical reaction rate constants chosen for the longest reaction time were set to a corresponding 80% conversion. We observed that the influence of dispersion was insignificant except at the beginning and the end of the push-out experiment. A slight deviation can be seen at the beginning and the end of plot relative [A] *vs.* experimental time (Figure 4.10) and the corresponding kinetic plots (ln[A] *vs.* reaction time for a first-order relation) (see experimental part). However, this dispersion effect was negligible during the calculation of the reaction rate constants under our push-out conditions.

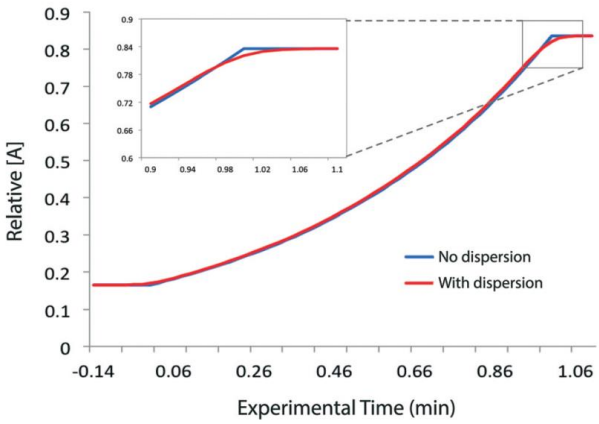

Figure 4.10: Calculated reagent concentration profile during a push-out experiment (flow rates going from 1 to 10 mL/min) and for a 1st order reaction (A -> B) (blue line). The reagent concentration profile with dispersion (red line) was calculated by redistribution of the data point of the reagent concentration profile with no dispersion (blue line) according to the worst case dispersion profile (dispersion profile of benzophenone in MeCN at 30 °C and 10 mL/min in a 10 mL reactor).

4.3.7 Kinetic study of the fragmentation of 2,2,6-trimethyl-4*H*-1,3-dioxin-4-one (2.38)

Entry[a]	Kinetic study method	Analytical technique	Processing method	F_1 (mL.min^{-1})	F_2 (mL.min^{-1})	ROH	k x 10^{-3} (s^{-1}) 100 °C	110	115	120	125	130	135	140	E_a (kJ/mol)
1	Push-out	In-line UV	OPA	1	10	EtOH	0.23	0.66	-	1.81	-	4.70	7.17	10.44	123.8
2	Push-out	In-line UV	Peak height[b]	1	10	EtOH	0.23	0.65		1.82		4.74	7.07	10.81	123.8
3	Steady-state	In-line UV	OPA	-	-	EtOH	0.24	0.68	-	1.89	-	4.92	-	-	126.7
4	Push-out	In-line IR	OPA	1	10	EtOH	0.27	0.71	1.17	1.92	3.16	5.06	7.97	11.38	123.5
5	Push-out	In-line IR	Peak height[b]	1	10	EtOH	0.25	0.66	1.09	1.80	3.04	4.78	7.56	11.36	125.0
6	Steady-state	In-line IR	OPA	-	-	EtOH	-	0.72	-	1.83	3.15	5.11	-	11.96	124.4
7	Push-out	In-line UV	OPA	10	1	EtOH	-	0.62	0.96	1.66	2.80	4.47	-	-	128.7
8	Push-out	In-line IR	OPA	1	2	EtOH	-	0.66	1.26	1.96	2.93	4.80	-	-	123.9
9	Push-out	In-line UV	OPA	1	2	EtOH	-	-	1.03	1.74	2.89	4.82	-	11.30	128.2
10	Steady-state	Off-line NMR	-	-	-	EtOH	-	0.65	-	1.89	2.97	5.13	-	12.52	129.9
11	Steady-state	Off-line NMR	-	-	-	BnOH	-	0.67	-	1.79	2.85	4.88	7.74	-	127.9

Table 4.7: Reaction rate constants and activation energies of the thermolysis of **2.38** with 4 equiv. of alcohol using different kinetic study methods, analytical technics and processing methods.
[a] For paired entries 1 + 2, 4 + 5 and 8 + 9, in-line UV and IR spectra were obtained from the same kinetic experiment. For entries 3, 6, 7, 10 and 11, UV, IR or NMR data were obtained from an individual kinetic experiment. [b] Peak height refers to the height of non-overlapping peak processing.

The kinetic studies results of the thermolysis of 2,2,6-trimethyl-4*H*-1,3-dioxin-4-one (**2.38**) followed by trapping with alcohol (4 equiv.) in MeCN are described in Table 4.7. Between the push-out and the traditional steady-state method, the reaction rate constants obtained after OPA resolution highlight good consistency with both in-line UV and IR analyses (entry 1 *vs.* 3 and entry 4 *vs.* 6). Moreover, good correlation between both calibration-less processing methods (OPA and height of non-overlapping peak) was underlined (entry 1 *vs.* 2 and entry 4 *vs.* 5). Calculation of kinetic information by measuring the peak height of **2.38** (relative to peak height of (**2.38**)$_0$ determined from the reference experiment at 30 °C) was possible with the height of non-overlapping peak method since clear UV or IR peaks were obtained (no overlaps between the reagent and product peaks). Good agreement between the different analytical techniques (in-line UV and IR, and off-line ^{1}H NMR) was observed (entry 3 *vs.* 6 *vs.* 10). Kinetic results in entries 10 and 11 were obtained by the calculation of the ratio [**2.38**]/[**2.38**]$_0$ from ^{1}H NMR analysis (see experimental part). Since β-ketoester **4.4a** obtained from the trapping with EtOH was probably volatile (we were concerned about the amount of β-ketoester **4.4a** we might have lost during the preparation of the NMR tubes), the kinetic experiment via off-line NMR analysis was repeated with BnOH and similar results were obtained (entry 11), which confirms the reliability of our previous experiment (entry 10) and the independence of the trapping nucleophile on the kinetic results. No traces of side products

were seen on the NMR analysis. During our standard push-out experiments (F_1 = 1 mL/min and F_2 = 10 mL/min), the data acquisition time of the kinetic data rich region (transitional period) was short (about 1 min) and could be problematic for long time scan spectrometers. The use of the "reverse push-out" method (F_1 = 10 mL/min and F_2 = 1 mL/min) was a solution as the transitional period extends to about 10 min and thus, the amount of data acquired from the kinetic rich region increased. Moreover, the non-ideality of the step change methodology due to the non-instantaneous flow rate adjustment was minimised under these conditions. Indeed, Mozharov *et al.*[14] showed that the accuracy of the non-ideal step change methodology can increase with the reduction of the coefficient $\Delta\tau(F_2/F_1)$, where $\Delta\tau$ is the interval between consecutive measurements. With the reverse push-out conditions $\Delta\tau(F_2/F_1)$ = 0.12 (in-line UV) and 0.375 (in-line IR) whereas with the standard push-out conditions $\Delta\tau(F_2/F_1)$ = 12 (in-line UV) and 37.5 (in-line IR). The kinetic study results with the reverse push-out method (entry 7) were consistent with the standard push-out kinetic study results. The only disadvantage is the high consumption of reagent during the equilibrium at the first steady-state. To overcome this drawback, kinetic study experiments with a smaller step-change in flow rate between F_1 = 1 mL/min and F_2 = 2 mL/min turns out to be a good alternative even if the conversion time window is very small (5 min). Indeed, $\Delta\tau(F_2/F_1)$ = 2.4 (in-line UV) and 7.5 (in-line IR) are smaller than the standard ones and good kinetic results were observed (entries 8 and 9).

Overall, a very good consistency was observed for the reaction rate constants *k* and activation energies E_a (E_a = 126.7 ± 3.2 kJ.mol^{-1}, consistent with E_a = 130.1 ± 4.6 kJ.mol^{-1} reported by Clemens[94]) using different kinetic study methods, analytical techniques and processing methods.

4.3.8 Kinetic study of the fragmentation of 1,3-dioxin-4-ones 2.26 and 4.1

In order to explore the substituent effects on kinetic data (*k* and E_a), the thermolysis of a series of 1,3-dioxin-4-ones previously synthesised (**2.26a-b, e** and **4.1a-b, d**) or obtained from our collaboration with the Franck research group at the University of Rouen (**2.26c-d**)[29, 88] was performed in the presence of 4 equiv. of EtOH in MeCN according to the kinetic study methods, analytical techniques and processing methods already described (Tables 4.8 and 4.9).

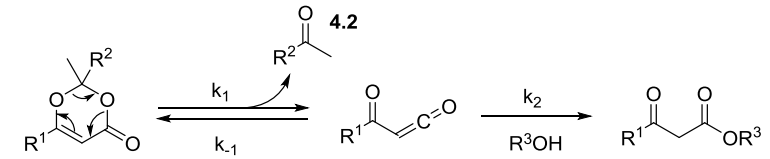

4.1, R^1 = Me and R^2 = aryl
2.26, R^1 = aryl and R^2 = Me

1,3-dioxin-4-one	R^1	R^2	β-ketoester **4.4**	R^3
4.1a	Me	Ph	**4.4a**	Et
4.1d	Me	*p*-$MeOC_6H_4$	**4.4a**	Et
4.1b	Me	*p*-BrC_6H_4	**4.4a**	Et
2.26a	Ph	Me	**4.4b**	Et
2.26b	*p*-$MeOC_6H_4$	Me	**4.4c**	Et
2.26c	2-furyl	Me	**4.4d**	Et
2.26d	2-naphthyl	Me	**4.4e**	Et
2.26e	*p*-$NO_2C_6H_4$	Me	**4.4f**	Et

Table 4.8: Fragmentation of different 1,3-dioxin-4-ones **4.1** and **2.26** followed by trapping with an alcohol.

Entry[a]	1,3-dioxin-4-one	Kinetic study method	Analytical technic	*k* x 10^{-3} (s^{-1}) 85 °C	90	95	100	105	110	115	120	125	130	E_a (kJ/mol)
1	**4.1a**	Push-out	In-line UV	-	0.24	0.45	0.76	1.32	2.19	3.54	5.75	-	-	125.2
2	**4.1a**	Push-out	In-line UV	-	-	0.47	0.71	1.43	2.28	3.81	5.89	-	-	124.9
3	**4.1a**	Push-out	In-line IR	-	-	0.48	0.74	1.27	2.08	3.55	5.84	-	-	121.4
4	**4.1a**	Steady-state	In-line UV	-	-	-	0.80	1.31	2.30	3.70	6.16	-	-	124.9
5[b]	**4.1a**	Steady-state	Off-line NMR	-	-	-	0.79	1.24	2.33	3.29	6.26	-	-	124.6
6	**4.1d**	Push-out	In-line UV	1.66	2.78	4.71	7.55	11.49	17.18	-	-	-	-	107.2
7	**4.1d**	Push-out	In-line UV	1.74	2.90	4.94	7.83	11.66	17.34	-	-	-	-	105.2
8	**4.1d**	Push-out	In-line IR	-	2.65	4.52	7.15	11.11	-	-	-	-	-	108.6
9	**4.1d**	Steady-state	In-line UV	-	2.69	4.84	7.62	11.33	-	-	-	-	-	109.0
10	**4.1b**	Push-out	In-line UV	-	-	-	0.59	0.94	1.59	2.68	4.54	7.80	-	128.3
11	**4.1b**	Push-out	In-line UV	-	-	-	0.53	0.95	1.60	2.83	4.48	7.42	-	130.1
12	**4.1b**	Push-out	In-line IR	-	-	-	0.56	1.06	1.82	2.91	-	7.47	-	126.6
13	**4.1b**	Push-out	Off-line NMR	-	-	-	0.55	0.95	1.62	2.60	-	7.42	-	128.0
14	**2.26a**	Push-out	In-line UV	-	-	-	-	0.32	0.55	0.93	1.56	2.58	4.04	128.6
15	**2.26b**	Push-out	In-line UV	-	-	-	-	-	0.44	0.76	1.30	-	3.62	136.0
16	**2.26c**	Push-out	In-line UV	-	0.37	0.61	1.05	1.72	2.99	4.95	-	-	-	122.3
17	**2.26d**	Push-out	In-line UV	-	-	-	0.21	0.34	0.59	0.96	1.60	-	3.98	124.0
18	**2.26e**	Push-out	In-line UV	-	-	-	0.57	0.91	1.53	2.47	4.15	-	-	120.9

Table 4.9: Reaction rate constants and activation energies of the thermolysis of substituted 1,3-dioxin-4-ones (**4.1** and **2.26**) with 4 equiv. of EtOH using different kinetic study methods, analytical technics and processing methods (OPA and MLR).
[a] For paired entries 1 + 2, 6 + 7, 10 + 11 and 12 + 13, reaction rate constants were calculated from the same kinetic experiment. For the other entries, the analytical data were obtained from an individual kinetic experiment. In-line data processed using OPA except data from entries 2, 7 and 11 processed using MLR. [b] BnOH (4 equiv.) used as trapping alcohol.

Between the in-line UV and IR monitoring, the kinetic data of the thermolysis of **4.1a** obtained from the push-out method with OPA or MLR processing were consistent (entry 1 *vs*. 2 *vs.* 3). Different methods and analytical techniques were used to determine the kinetics of the

fragmentation of both **4.1a** (entries 1-5) and **4.1d** (entries 6-9), and gave good correlation between the reaction rate constants *k* and activation energies E_a. Therefore, the kinetic studies of the thermolysis of **4.1b** and **2.26a-e** were performed using only the push-out experiment (entries 10-18). Excellent linear Arrhenius plots were obtained for the decomposition of **2.38**, **4.1a, b, d** and **2.26a-e** (Figure 4.11). Overall, the activation energies of **2.38**, **4.1a, b, d** and **2.26a-e** are very close except for **4.1d** (R^2 = *p*-$MeOC_6H_4$) with a significant decrease in E_a and **2.26b** (R^1 = *p*-$MeOC_6H_4$) with an increase in E_a, which suggests a transition state with the C2-O1 bond substantially broken (Figure 4.12). Furthermore, in few examples, the very close reaction rate constants but with different activation energies suggests that the entropic effects are significant. The reorganisation of solvent molecules around the charges can be an explanation of these observations.

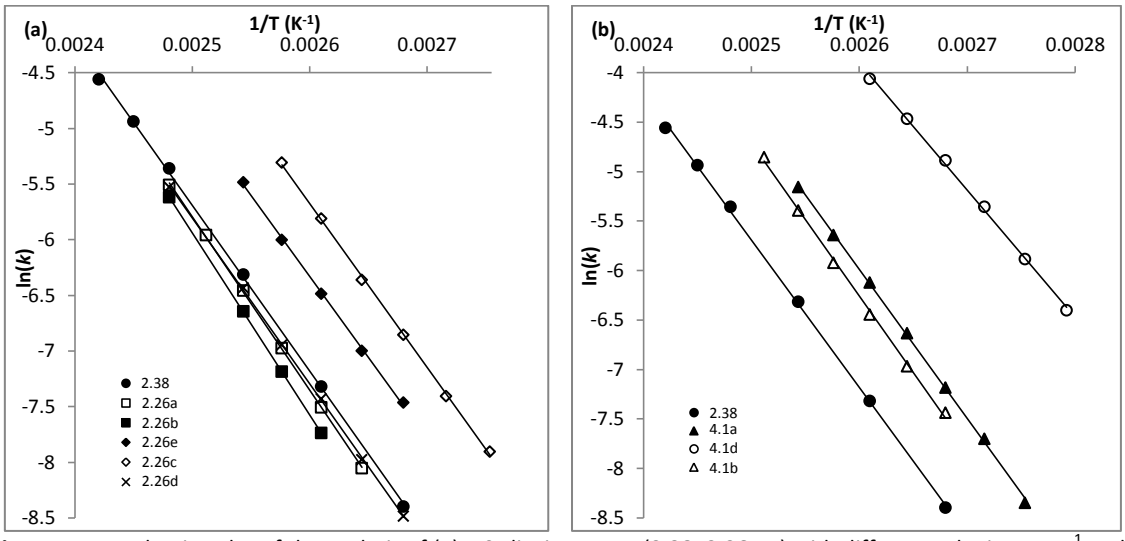

Figure 4.11: Arrhenius plot of thermolysis of (a) 1,3-dioxin-4-ones (**2.38**, **2.26a-e**) with different substituents R^1 and (b) 1,3-dioxoin-4-ones (**2.38**, **4.1a, b, d**) with different substituents R^2 under push-out conditions and OPA processing.

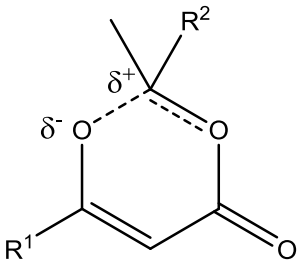

Figure 4.12: Transition state.

The OPA resolution used for our kinetic investigation was particularly powerful compared to the height of non-overlapping peak processing especially when overlaps occurred during the reaction. During the thermolysis of **4.1a, b, d**, significant overlap was noticed

between the UV spectra of the 1,3-dioxin-4-one and the released ketone **4.2**. An example of this overlap between the UV absorption of 1,3-dioxin-4-one **4.1a** and the acetophenone is highlighted in Figure 4.13. To prove the ability of the OPA resolution to distinguish between the UV spectra of the 1,3-dioxin-4-one and the released ketone **4.2**, and to give consistent results (entries 1, 6 and 10), the same datasets were processed with the MLR method (entries 2, 7, 11) and the same push-out experiments were performed with IR monitoring (entries 3, 8 and 12). The close results confirm the reliability of the OPA processing. For **4.1a**, the kinetic results obtained with the steady-state method and ^{1}H NMR analysis (entry 5) were consistent with the OPA and MLR resolutions (entries 1, 2, 3 and 4). For **4.1b**, the push-out experiment with off-line ^{1}H NMR monitoring (collection of 20 samples thanks to a fraction collector after application of the high flow rate) was tried (entry 13). Excellent consistency between the off-line ^{1}H NMR, the in-line UV and the in-line IR analysis was obtained (entries 13 *vs.* 10 *vs.* 12).

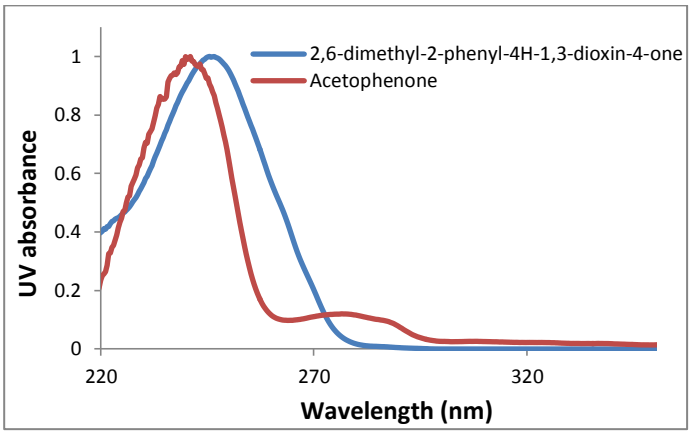

Figure 4.13: UV spectra of **4.1a** and acetophenone.

To sum up, the application of the push-out methodology was developed to our meso-scale Vapourtec platform to rapidly collect kinetic information. The use of in-line UV and IR monitoring for spectra collection followed by OPA or MLR processing (or height of non-overlapping peak processing when distinct peaks) gave results in agreement with the off-line ^{1}H NMR analysis. This powerful methodology offers very interesting feature such as cutting down the time spent to solve kinetic investigations and can be used as a reliable tool to accelerate reaction study and process development.

5 Chapter 5: Flow chemistry - A tool for fast optimisation of reaction conditions

5.1 Introduction to dispersion phenomena in flow chemistry

5.1.1 Characterisation of the flow regime and Taylor dispersion

In fluid mechanics, the Reynolds number (Re) is used to determine the flow regime of a system. By definition, this number is the ratio of inertial forces to viscous forces (Equation 5.1). Laminar flow occurs at low Reynolds number (Re < 2000) when a fluid flows in parallel layers, without disruption between the layers. Turbulent flow occurs at high Reynolds number (Re > 4000) when a fluid flows with lots of instabilities. The meso-scale Vapourtec system is designed to work with flow rates between 0.1 and 20 mL.min^{-1}, and tube diameters of 1 mm. Under these conditions, the flow regime is laminar (Table 5.1) (Reynolds number < 2000). To reach the turbulent conditions using water as a fluid, the Vapourtec system should provide a minimum flow rate of 168 mL/min for a tube diameter of 1 mm or employ a maximum tube diameter of 6 µm for a flow rate of 20 mL/min. These parametres are too extreme and cannot be applied with our flow machine.

$$Re = \frac{Inertial\ forces}{Viscous\ forces} = \frac{\rho VD}{\mu} = \frac{QD}{\nu A}$$

with, ρ = density of the fluid (kg/m^3)
V = velocity of the fluid (m/s)
D = Hydraulic diameter of the pipe (m)
μ = dynamic viscosity of the fluid (Pa.s, N.s/m^2, or kg/(m.s))
Q = flow rate (m^3/s)
A = Pipe's cross section area (m^2)
ν = kinematic viscosity (m^2/s)

Equation 5.1: Reynolds number.

Flow rates (mL.min^{-1})	0.1	0.5	1	2	5	7	10	20
Reynolds number	2.4	11.9	23.8	47.5	118.9	166.4	237.7	475.5

Table 5.1: Reynolds number of the water at different flow rates and using the Vapourtec system with tube diameters of 1 mm.

When carrying out flow chemistry using plugs of material, the extent to which these spread out (mix with adjacent solvent) is important. One mechanism is Taylor dispersion, described by Taylor in his original paper,[101] and occurs via the combined actions of the variation of the cross-sectional velocity of the fluid and the radial diffusion of the molecules.
In laminar conditions, the velocity profile of a fluid is not uniform over the cross section of the tube. The velocity of the fluid decreases radially from a maximum at the centre of the cylinder to a minimum at the wall of the cylinder (Figure 5.1). This parabolic velocity distribution spreads the injected sample plug down the length of the tube. In the Taylor dispersion, radial

diffusion reduces the along-tube spreading as solute molecules move between the layers of different linear velocity, to an extent averaging the effect. Therefore, this radial diffusion tends to keep the molecules distribution together. In his recent paper,[102] Jensen described the importance of mixing and dispersion in different flow systems: for instance, most of the micro-scale systems are described as providing plug flow behaviour (low dispersion) which means that the radial diffusion across a channel is much faster than the along-tube spreading down the channel. This is the case when either the velocity is very low or when the radial distances are very small. However, with the Vapourtec system, the Taylor dispersion is not negligible, which means that the radial diffusion doesn't compensate for the parabolic velocity distribution. The action of these 2 effects (low radial diffusion and high along-tube spreading) develops a symmetrical concentration distribution at the exit of the reactor.

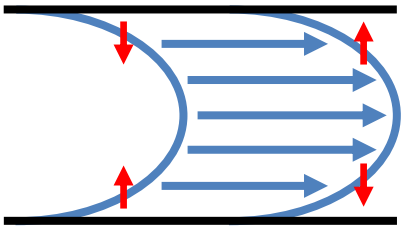

Figure 5.1: Velocity profile (blue arrows) in laminar conditions with slow radial diffusion (red arrows).

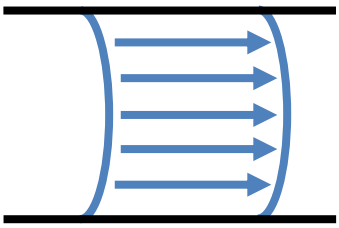

Figure 5.2: Average velocity profile when there is rapid mixing between the laminar layers either through turbulence or diffusion.

5.1.2 Principle of the dispersion in flow systems

With the Vapourtec system, the effect of dispersion is that a sample plug of material going through a reactor tubing at a particular flow rate will experience a range of residence times and will spread. This spreading will imply a larger plug at the exit of the reactor. Indeed, for a 10 mL injected plug going through a 10 mL Stainless Steel reactor at 1 mL/min, the collected plug will be over 12 min (Figure 5.3). Moreover, in comparison to the theoretical undispersed UV profile, a gradient of concentration of the injected material varying between [C] = 0 and [C] = C_0 is described at the beginning and the end of the experimental UV profile (Figures 5.3 and 5.4). Although spreading out of plug-ends is normally a problem, we show later how we can make use of the concentration profiles generated in novel methods to rapidly gain reaction information.

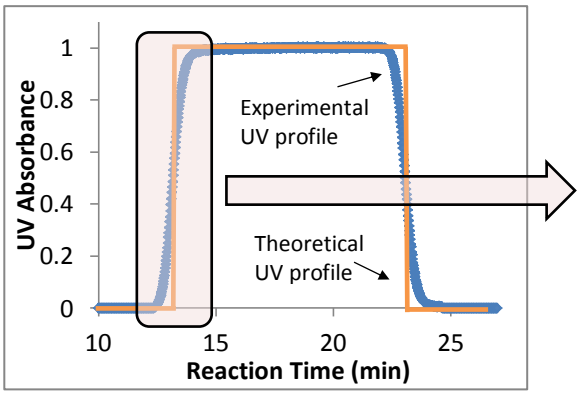

Figure 5.3: Dispersion profile of a 10 mL sample plug of 2,2,6-trimethyl-4*H*-1,3-dioxin-4-one in acetonitrile through a 10 mL Stainless Steel reactor at 1 mL/min - Theoretical undispersed UV profile *vs.* experimental UV profile.

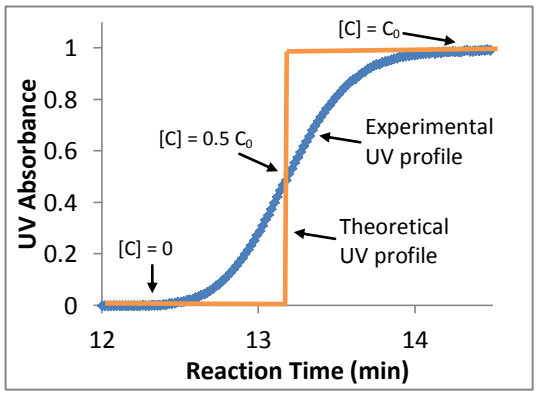

Figure 5.4: Zoom in on the dispersion profile of a 10 mL sample plug - Gradient of concentration between 0 and C_0 - Theoretical undispersed UV profile *vs.* experimental UV profile.

5.1.3 Preliminary study of the dispersion in flow chemistry

5.1.3.1 Influence of the flow rate and the temperature

To quantify dispersions effects in flow chemistry, the residence time distribution (RTD) can be measured. Indeed, the form of the dispersion has the same residence time distribution (RTD) as that measured for a very short plug of material traversing the tube. Therefore, to assess the influence of the flow rate and the temperature on the dispersion, the following measurements of RTD were performed by introducing a very small volume of a solution of benzophenone (10 µL at $[benzophenone]_0$) into a coiled tubular reactor of 10 mL capacity and 1 mm i.d.. Series of injections passing through the reactor at various flow rates (from 0.1 to 10 mL/min) were performed at 30 and 120 °C and analysed by in-line UV detection. After processing the spectra, the following Figures 5.5 and 5.6 were obtained.

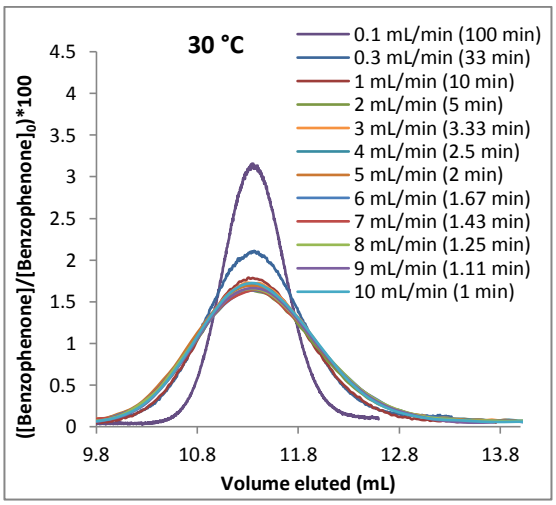

Figure 5.5: Dispersion of 10 µL sample plugs of benzophenone in MeCN ($[C]_0 = 1.015 \times 10^{-2}$ M) through a 10 mL home-made coiled stainless steel tubing at 30 °C and at the indicated flow rates.

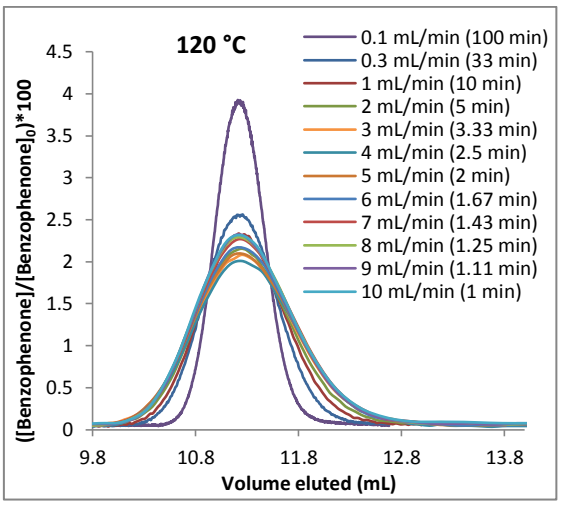

Figure 5.6: Dispersion of 10 µL sample plugs of benzophenone in MeCN ($[C]_0 = 1.015 \times 10^{-2}$ M) through a 10 mL home-made coiled stainless steel tubing at 120 °C and at the indicated flow rates.

At the same temperature, the dispersion profile is much narrower and higher at very low flow rate due to the non-negligible radial diffusion. Indeed, a dramatic difference can be noticed between 0.1 mL.min^{-1} (residence time = 100 min) and 1 mL.min^{-1} (residence time = 10 min). However, between 1 mL.min^{-1} (residence time = 10 min) and 10 mL.min^{-1} (residence time = 1 min), the changes in the dispersion profile are not significant and can be explained by the Dean circulation which increases when the flow rate increases, and which compensates the dispersion effect.[99]

At the same flow rate, the dispersion is considerably reduced at higher temperature. This can be explained by the highest radial diffusion rate at high temperature which tends to keep the sample plug together.

5.1.3.2 The dispersion caused by the UV cell and the reactor

Flow experiments are often monitored by in-line UV or IR analysis. Therefore, extra tubing (tubing + cell) is added at the end of the reactor and dispersion effects are increased. To assess the influence of the length of tubing and more particularly the influence of the incorporation of the UV cell on the dispersion, the following experiments were performed. First of all, a sample plug of a solution of benzophenone in MeCN was injected straight into the UV cell without connecting any reactor. The length of tubing between the injector and the UV cell is about 40 cm (1 mm i.d.) and the dispersion is highlighted by the blue curve (Figure 5.7). Then, a 10 mL Stainless Steel reactor was incorporated to the flow system and a sample plug of a solution of benzophenone in MeCN was injected. The length of tubing between the injector and the UV cell is about 1300 cm (reactor length + tubing, 1 mm i.d.) and the red dispersion profile was obtained (Figure 5.7). Finally, the dispersion caused by the reactor (green curve, about 1260 cm, 1 mm i.d.) was calculated by deducting the dispersion caused by the UV cell (blue curve) to the dispersion caused by the whole system (red curve).

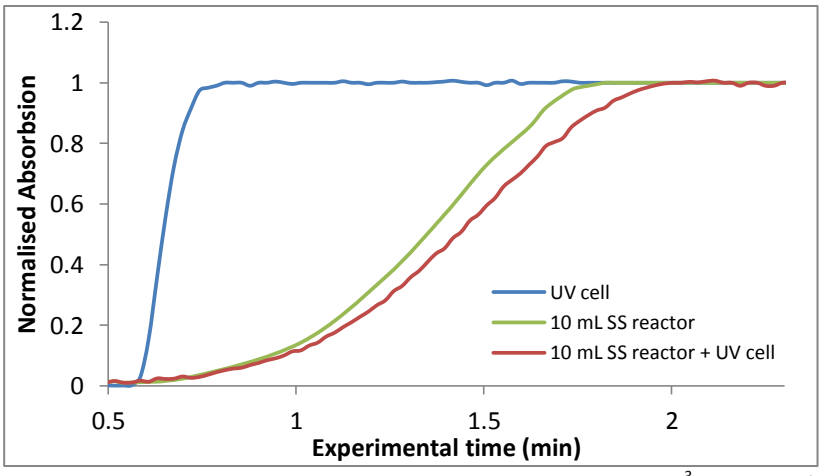

Figure 5.7: Dispersion of 5 mL sample plug of benzophenone in MeCN ([C_0] = 9.5 x 10^{-3} M) at 1 mL/min through the indicated flow system.

With these experiments, we can clearly distinguish the dispersion caused by the reactor and the UV cell. Moreover, these experiments reveal the significant effect of the tube length on the dispersion. Indeed, the dispersion is mainly caused by the contact between the liquid and the surface of the tube. Therefore, increasing the length of tubing increases dispersion effects.

In summary, it has been demonstrated with these preliminary results that the Taylor dispersion can be determined by experimental observations using in-line analysis. This dispersion can be influenced by several parameters such as the flow rate, the temperature, the length of tubing and its radius. A complementary study of these parameters was performed by Cyril Henry during his Ph.D. thesis. Indeed, regarding the influence of the tube length on the dispersion, his experimental results were confirmed by the theoretical calculations (Taylor dispersion model). Then, the effects of other parameters on the dispersion such as the reactor shape (linear *vs*. coiled) and the reactor material (PFA *vs.* SS) were studied.[100]

5.2 Application of concentration gradients generated using dispersion with 1st and 2nd order reactions

5.2.1 The process

In this section, using the dispersion generating concentration gradients, the aim was to rapidly determine how conversions were related to the starting concentration of substrates. At the same time, the application of concentration gradients generated using dispersion to gain kinetic information was carried out on 1st order (thermolysis of 2,2,6-trimethyl-4*H*-1,3-dioxin-4-one (**2.38**)) and 2nd order (Diels-Alder) reactions. To perform these experiments, the starting materials were mixed in the corresponding solvent, and 5 mL plugs of this solution were injected at 0.3 mL/min (residence time in the SS reactor = 33 min) into the flow set-up (Figure 5.8) at different temperatures. The reaction mixture dispersed first in the 10 ml PFA loop creating a gradient of concentration between 0 and C_0. Then, this dispersed plug went through the Stainless Steel reactor, the reaction occurred and in-line (IR) and/or off-line (GC) analyses were performed to identify the concentration profiles.

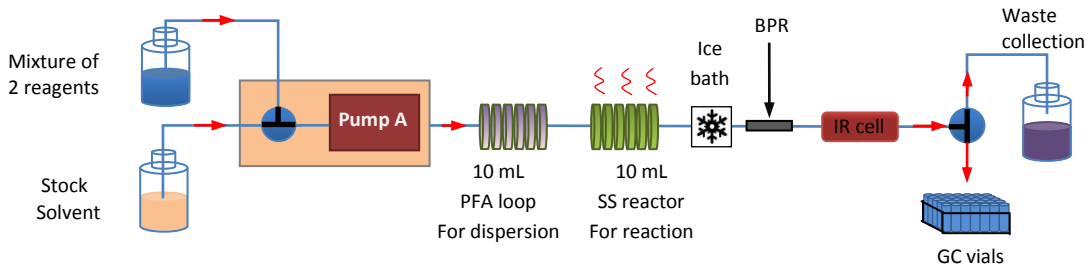

Figure 5.8: Flow set-up for the application of the concentration gradient methodology on 1st and 2nd order reactions - Bottle feed configuration.

5.2.2 1st order reaction

For this study, the fragmentation of the 2,2,6-trimethyl-4*H*-1,3-dioxin-4-one (**2.38**) in the presence of an excess of EtOH was used as a model reaction (Scheme 5.1). Indeed, as explained in the previous section 4.3.1, the thermolysis of **2.38** with an excess of EtOH is considered as a 1st order process because the rate of the Diels-Alder reaction of **4.3a** with acetone is not significant compared to the rate of trapping of **4.3a** by EtOH.

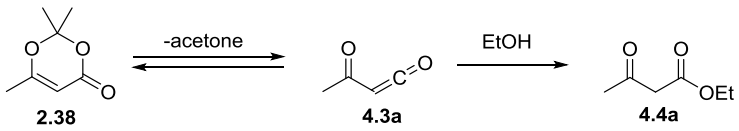

Scheme 5.1: Fragmentation of 2,2,6-trimethyl-4*H*-1,3-dioxin-4-one (**2.38**) via a retro Diels-Alder reaction and trapping of the intermediate **4.3a** by EtOH.

For the application of the concentration gradient methodology on this 1st order reaction, different plugs were injected into the flow set-up (Figure 5.8) heated to different temperatures. The concentration profiles of the reagent and the product recorded using in-line IR analysis are highlighted in the following Figure 5.9.

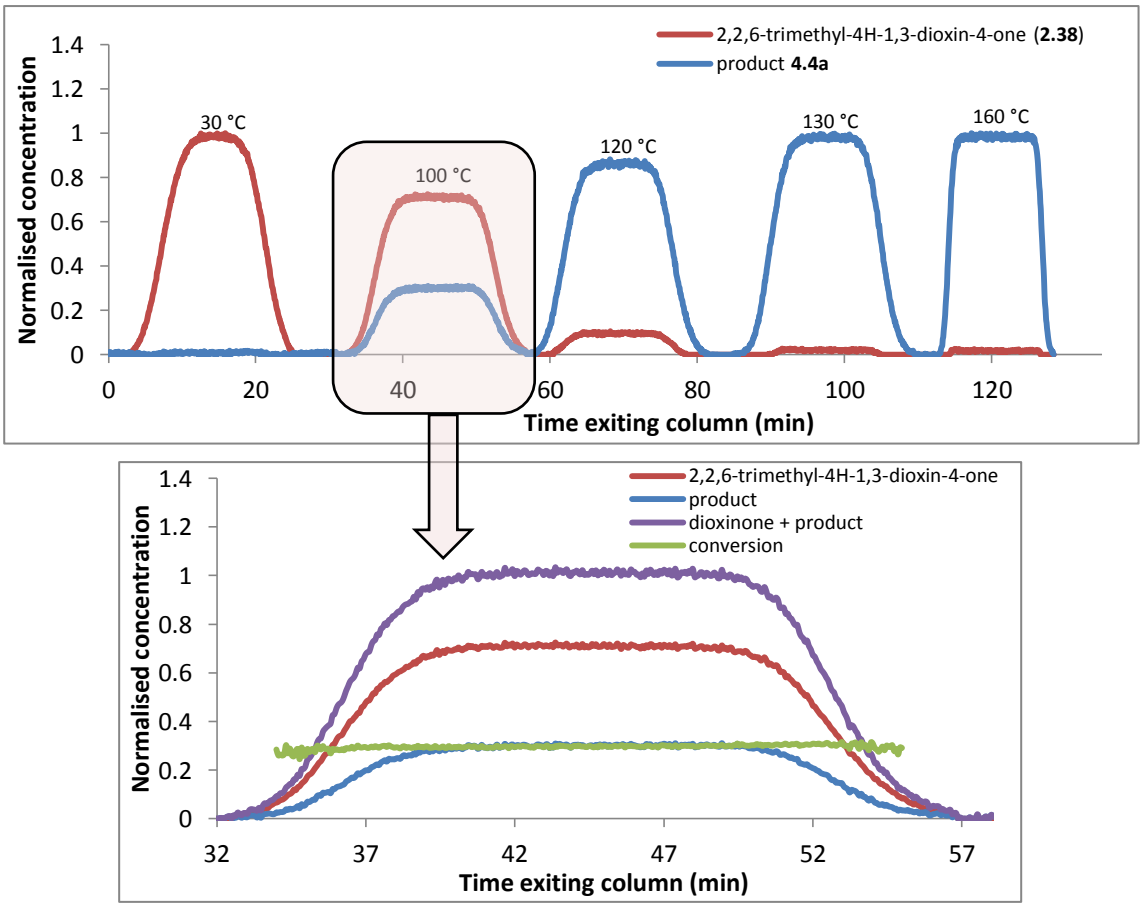

Figure 5.9: Series of 5 mL plug injections of 2,2,6-trimethyl-4*H*-1,3-dioxin-4-one (**2.38**) and EtOH in MeCN at 0.3 mL/min through the 10 mL PFA loop (r.t., residence time = 33 min) and followed by the 10 mL heated reactor (at the indicated temperature, RT = 33 min). In-line IR detection and OPA processing using BORIS software. 0% and 100% conversion respectively conducted at 30 and 160 °C were performed to normalise the data. Zoom in on the sample plug injected into the flow system at 100 °C. Calculation of the conversion at 100 °C according to Equation 5.2.

$$\text{Conversion}_t = 1 - \frac{[\text{dioxinone}]_t}{[\text{dioxinone}]_o} = 1 - \frac{[\text{dioxinone}]_t}{[\text{dioxinone}]_t + [\text{product}]_t}$$

Equation 5.2: Formula used for the calculation of the conversion at a given moment.

First of all, this experiment has been performed to confirm that using the dispersion effect, the conversion of a first order reaction is independent of the initial starting material concentration ($t_{1/2}$ = ln(2)/*k* = constant). Indeed, along the concentration gradient of the 2,2,6-trimethyl-4*H*-1,3-dioxin-4-one (0 < C < 0.7 x C_0), the conversion profile of the reaction is constant.

Then, by using these dispersion data, kinetic information of this first order reaction was extracted. The integrated first-order rate equation is described by Equation 5.3. By plotting $\ln[\mathbf{2.38}]_0$ *vs.* $\ln[\mathbf{2.38}]_t$ from the dispersion curve data (Figure 5.9) (with $[\mathbf{2.38}]_0$ = $[\text{dioxinone } \mathbf{2.38}]_t$ + $[\text{product } \mathbf{4.4a}]_t$), a straight line of slope 1 and intercept kt_R was obtained (Figure 5.10).

$$\ln[\mathbf{2.38}]_0 = \ln[\mathbf{2.38}]_t + kt_R$$

Equation 5.3: Integrated first-order rate equation.

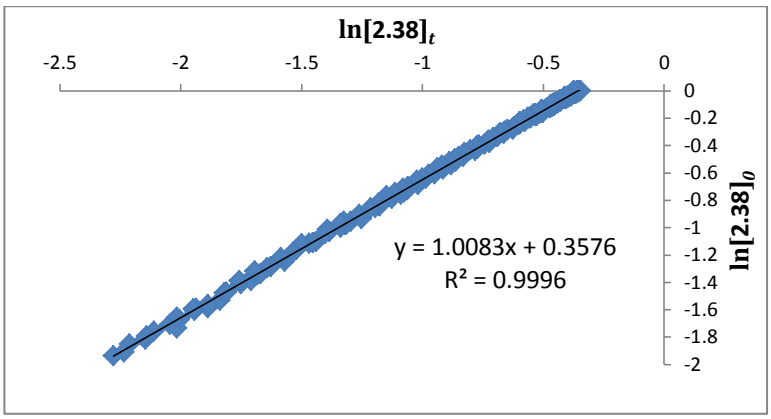

Figure 5.10: Plot of $\ln[\mathbf{2.38}]_0$ *vs*. $\ln[\mathbf{2.38}]_t$.

From this intercept, *k* (100 °C) = 0.18 x 10^{-3} s^{-1} (with t_R = 2000 s) which is almost identical to the one calculated with the "push-out" method (Table 4.7, entry 1, *k* (100 °C) = 0.23 x 10^{-3} s^{-1}).

5.2.3 2nd order reaction

The Diels-Alder reaction was used as a model 2nd order reaction. This [4 + 2] cycloaddition involving a conjugated diene and a dienophile to form a substituted cyclohexene with good control over regio and stereochemical properties has been described many times in

continuous flow processes.[103] For our investigations, the Diels-Alder reaction between isoprene (**5.1**) and methyl acrylate (**5.2**) was studied (Scheme 5.2).

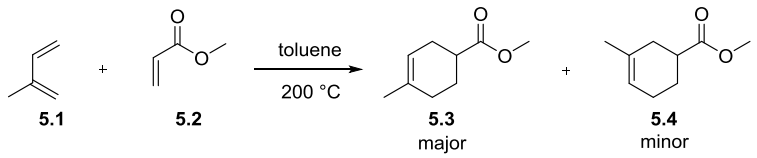

Scheme 5.2: Diels-Alder reaction between isoprene (**5.1**) and methyl acrylate (**5.2**). Formation of both 3-methyl **5.4** and 4-methyl isomers **5.3**.

During this reaction, the two cyclohexene isomers **5.3** and **5.4** are formed because two modes of addition are possible. However, the 4-methyl product **5.3** is chiefly produced.[104] Using frontier molecular orbital arguments, the determination of the major isomer to be formed is easily found. The HOMO of the isoprene (**5.1**) is interacting with the LUMO of the methyl acrylate (**5.2**) in such a way that the larger and smaller coefficients (sizes) of orbitals can respectively place side by side (Scheme 5.3). To highlight the regioselectivity of this reaction, a 2 mL plug of a mixture of isoprene (1 equiv.) and methyl acrylate (1 equiv.) in toluene ([C] = 1.98 M) was injected into the flow set-up (Figure 5.8 without the initial 10 mL PFA loop). After 50 min at 200 °C, the reaction mixture was collected at the end of the reactor and purified on silica gel. A mixture of both isomers **5.3** and **5.4** was isolated (48%) with a ratio 4-methyl/3-methyl = 65/35. To compare with the literature, Hosomi *et al.*[105] carried out this experiment in batch mode for 6 h at 120 °C in toluene. A mixture of both isomers **5.3** and **5.4** was isolated (83%) with a ratio 4-methyl/3-methyl = 70/30. In our case, the reaction was probably not complete after 50 min of reaction because the yield is about half that described by Hosomi.

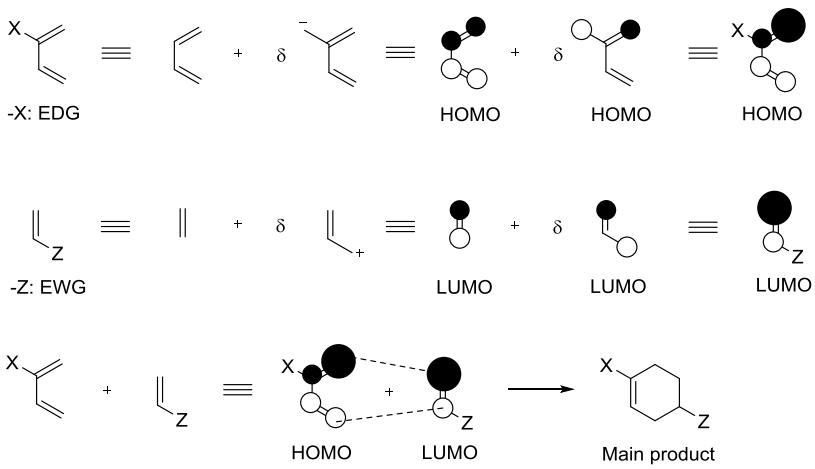

Scheme 5.3: FMO arguments to describe the major isomer to be formed in the studied Diels-Alder reaction.

For the application of the dispersion phenomenon on this 2nd order reaction, only one plug containing the starting materials in toluene was injected into the flow set-up (Figure 5.8) heated to 200 °C. The concentration profiles of the methyl acrylate (**5.2**) and the products (both isomers **5.3** and **5.4**) recorded using an in-line IR spectrometer and off-line GC analysis are highlighted in the following Figure 5.11.

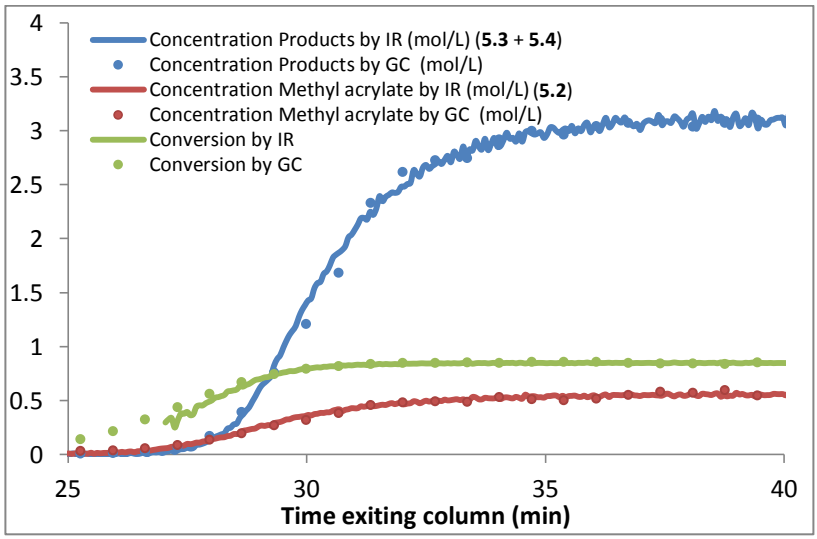

Figure 5.11: 5 mL plug injection of isoprene (**5.1**) and methyl acrylate (**5.2**) in toluene at 0.3 mL/min and through the 10 mL PFA loop followed by the 10 mL heated reactor (200 °C). Concentration profile of the methyl acrylate (**5.2**) and the products (both isomers **5.3** + **5.4**) obtained after conversion of the peak area (GC) into molar units using calibration curves (in dots). Concentration profile of the methyl acrylate (**5.2**) and the products **5.3** + **5.4** obtained after normalisation of the IR data processed with BORIS (in solid lines). Calculation of the conversion according to the GC and IR data and using Equation 5.4.

$$\text{Conversion}_t = 1 - \frac{[\text{methyl acrylate}]_t}{[\text{methyl acrylate}]_0} = 1 - \frac{[\text{methyl acrylate}]_t}{[\text{methyl acrylate}]_t + [\text{products}]_t}$$

Equation 5.4: Formula used for the calculation of the conversion.

First of all, a good overlap is noticed between the different results (concentration profiles and conversion) obtained from in-line IR and off-line GC analysis. By opposition to the 1st order reaction results, the conversion of a 2nd order reaction is dependant to the initial starting material concentration ($t_{1/2}$ = 1/([C_0] x *k*)). Indeed, the conversion is smaller with the low initial starting material concentration and grows till a maximum (85%) for the highest concentration.

Then, by using these dispersion data, kinetic information of this second order reaction was extracted. The integrated second-order rate equation is described by Equation 5.5. By plotting $1/[\mathbf{5.2}]_t$ *vs.* $1/[\mathbf{5.2}]_0$ from the dispersion curve data (Figure 5.11) (with $[\mathbf{5.2}]_0$ = [methyl acrylate **5.2**]$_t$ + [products **5.3** + **5.4**]$_t$), a straight line of slope around 1 and intercept kt_R was obtained (Figure 5.12).

$$\frac{1}{[\mathbf{5.2}]_t} = \frac{1}{[\mathbf{5.2}]_0} + kt_R$$

Equation 5.5: Integrated second-order rate equation.

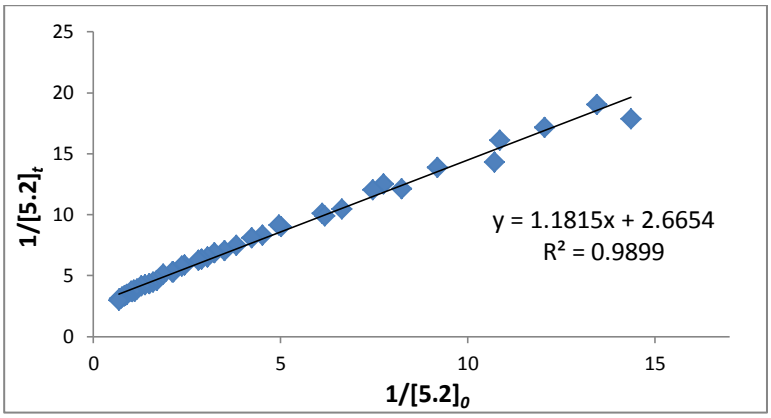

Figure 5.12: Plot of 1/ln[**5.2**]$_t$ *vs*. 1/ln[**5.2**]$_{0.}$

From this intercept, k (200 °C) = 1.33 x 10^{-3} L.mol^{-1}.s^{-1} (with t_R = 2000 s).

As a summary, the application of the concentration gradient methodology on the thermolysis of 2,2,6-trimethyl-4*H*-1,3-dioxin-4-one (**2.38**) (1st order reaction) and on the Diels-Alder reaction between the isoprene (**5.1**) and the methyl acrylate (**5.2**) (2nd order reaction) enables the rapid calculation of reaction rate constants. Using this methodology with various temperatures, the activation energy can be calculated.

5.3 Application of dispersion in flow: a novel methodology towards the fast optimisation of photochemical reaction conditions

5.3.1 Principle of this novel methodology

Based on the dispersion phenomenon which occurs in flow tubes and on a former Ph.D. student's study,[100] we developed with Prof Richard J. Whitby a novel methodology for the fast optimisation of reaction conditions. As explained before, a plug of solution injected into a tube spreads down the length of this tube and a concentration gradient can be recorded at the exit. These concentration gradient experiments under flow conditions were conducted using a Vapourtec R series system with a 10 mL capacity PFA loop for dispersion of compounds, a photoflow PFA reactor (14.1, 28.0 or 31.8 mL capacity) of 1 mm internal diameter equipped with a UV lamp (UV-A/B or C 9 W or 36 W) and an automated sample collector for off-line analysis (Figure 5.13).

Two different cases were studied in the next sections 5.3.3 and 5.3.4.

In the first case, if the reaction to optimise; A + B → C is performed by mixing a continuous flow of A ([A] = A_0) with a flow of a dispersed plug of B (0 ≤ [B] ≤ B_0), different equivalents of B

can react with the same amount of A during one single experiment. The different experimental conditions can be studied by collecting samples at the outlet of the reactor and further off-line GC analysis.

In a second case, if the reaction to optimise is B → C (with compound A as an internal standard), the influence of the concentration of reagent B on the conversion and the yield of the reaction can be investigated. The different experimental conditions can be studied by collecting samples at the outlet of the reactor and further off-line GC analysis.

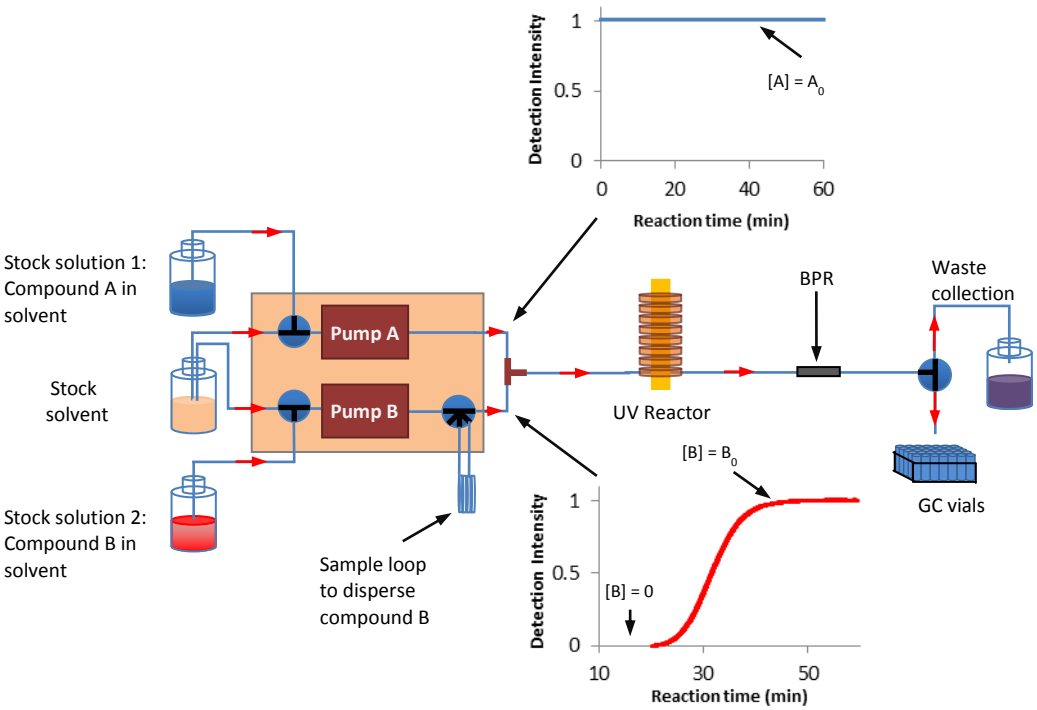

Figure 5.13: Flow set-up for concentration gradient experiments.

Thanks to this novel concentration gradient methodology, a large amount of experimental conditions can be investigated with only one attempt (different amount of dispersed compound B reacting with the same amount of A, various concentration of B) and therefore optimisation of reaction conditions can be performed very quickly.

5.3.2 Photochemistry

Photochemical reactions were used as models to study the two cases described above ([2 + 2] photocycloaddition and photocyclisation of stilbene). For this reason, before discussing the results, a rapid overview of photochemistry and more particularly flow photochemistry is provided.

5.3.2.1 Batch photochemistry *vs*. flow photochemistry

Photochemistry is based on the absorption of light by a molecule (UV or visible) to provide the required energy to cause a reaction. In many cases, photochemical reactions allow the synthesis of polycycles or highly functionalized molecules without adding extra reagents, and therefore minimising waste generation. Photochemistry is probably one of the most attractive 'clean' chemistry techniques.

Despite being a reagentless method, the amount of photochemistry applications in industry is very low (e.g. Vitamin D synthesis).[106] Indeed, conventional batch reactors have limited applications especially for large scale photochemical synthesis. First of all, the lack of scalability of the light source remains one of the main drawbacks because most photoreactions occur within a short distance from the lamp. As shown in Figure 5.14, the transmittance decreases rapidly with distance from the lamp. In these conditions, the light is totally absorbed for a distance higher than 2 mm. Consequently, using a larger batch reactor will reduce the amount of photons with the distance from the light (Equations 5.6 and 5.7) and therefore, will reduce the throughput. Secondly, most of the batch photoreactors are equipped with medium pressure mercury lamps (> 125 W) emitting intense UV broadband radiation and heat (about 600 °C). Therefore, the reactor must be equipped with an appropriate water-cooled system and be shielded to protect the user. Finally, it is very difficult to get full conversion for large scale batch photochemical reactor because the reaction solution close to the lamp screens the rest of the solution from UV irradiation. For this reason, attempts to increase the conversion can lead to the over-irradiation of the reaction mixture and therefore the formation of side products. These different constraints make batch photochemical reactions very challenging.

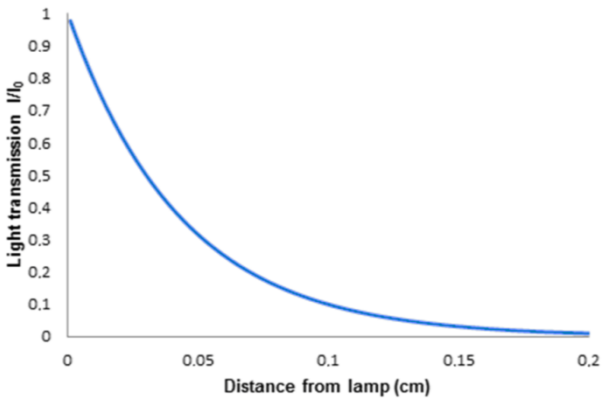

Figure 5.14: Light transmission profile of a solution at 0.05 M, ε_{254} = 200 $M^{-1}.cm^{-1}$ *vs.* the distance from the lamp.[107]

$$A = \varepsilon LC$$

Equation 5.6: Beer-Lambert law.

$$A = -\log\frac{I}{I_0}$$

Equation 5.7: Relation between absorbance and transmittance.

To overcome these various limitations, the advantages offer by photoflow reactors lead the chemists to perform general improvements in photochemistry:

- easy scale-up as no change in the reactor size is required

- efficient and homogeneous irradiation by minimizing light transmission versus distance constraint
- precise control of the reaction time to avoid over irradiation and formation of unwanted products
- use of low energy and interchangeable lamps which allows the control of irradiation wavelengths centred around 254 nm (UV-C), 313 nm (UV-B) or 370 nm (UV-A)
- access to in-line analysis

5.3.2.2 Design of coiled photoflow reactors

Based on the work of Booker-Milburn and co-workers,[108] former Ph.D. students David Bolien, Cyril Henry and Mubina Mohamed working for Prof Richard J. Whitby and Prof David C. Harrowven constructed a photochemical reactor (Reactor 1) for use under flow mode.

Reactor 1: 36.0 m of PFA tubing (capacity = 28.0 mL, double coiled) was wrapped around a Quartz cylinder (38 mm i.d., length = 20 cm) containing the low energy interchangeable UV lamp (Philips 2-pin PL-S 9 W UV-A/B or C). Perfluoroalkoxy polymer (PFA) tubing was used for the design of the reactor because the absorbance of the light is very low above 230 nm.[109] Even if the UV lamp does not heat too much (around 50-60 °C), a condenser tubing was coiled to maintain the system at ambient temperature. Between the PFA and the condenser tubing, a layer of aluminium foil was placed to maximise the efficiency of the light inside the reactor and to protect the user from UV irradiation. The different parts of this set-up are described in Figure 5.15.[8]

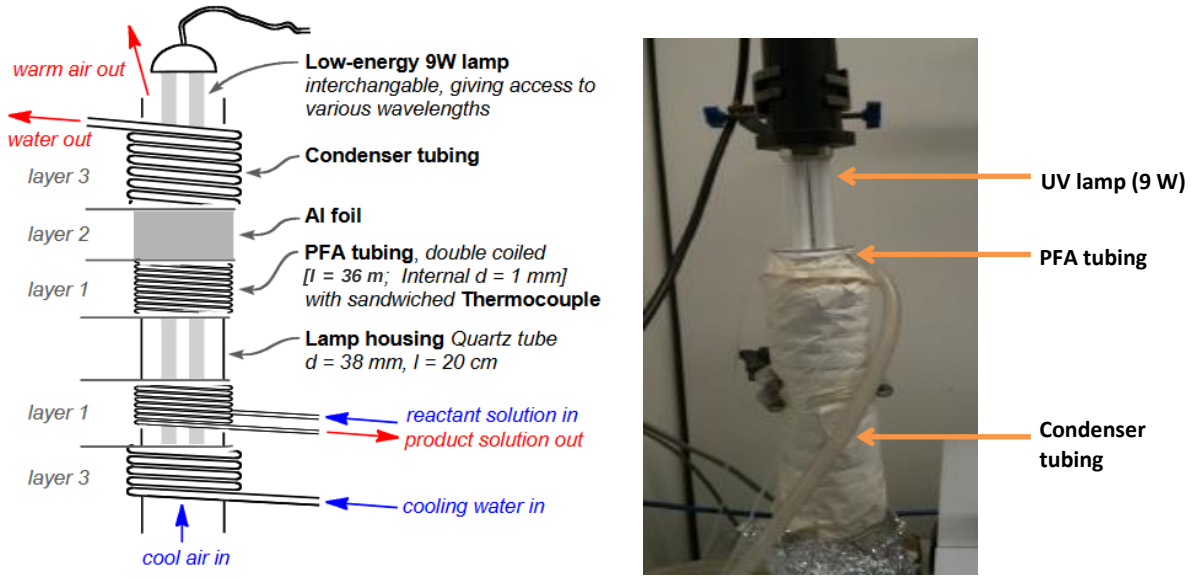

Figure 5.15: Photochemical set-up featuring a double layer of PFA tubing (28.0 mL capacity, 1 mm i.d.) and interchangeable UV lamp (Philips 2-pin PL-S 9 W UV-A/B or C).

Based on the same design as described in Figure 5.15, 2 other photochemical reactors were built with only one layer of PFA tubing wrapped around the quartz cylinder.

Reactor 2: 18.0 m of PFA tubing (capacity = 14.1 mL, single coiled) was wrapped around a Quartz cylinder (38 mm i.d., length = 20 cm) containing the low energy interchangeable UV lamp (Philips 2-pin PL-S 9 W UV-A/B or C).

Reactor 3: 40.5 m of PFA tubing (capacity = 31.8 mL, single coiled) was wrapped around a Quartz cylinder (47 mm i.d., length = 41 cm) containing the low energy interchangeable UV lamp (Philips 4-pin PL-L 36 W UV-A/B or C).

The different UV lamps are relatively cheap, around £10 for the 9 W and £30 for the 36 W and very easy to interchange. The 2 or 4-pin lamps from Philips just need to be clicked in the corresponding lamp holder. The photochemical set-up is robust and easily integrated in any continuous flow processes.

Until 2013, the majority of the photochemical reactors were designed with high power mercury lamps (> 125 W) which emit intense UV irradiation across a broad area of the UV spectrum.[108, 110] This broad range of wavelengths was one of the main disadvantages of these lamps because UV irradiation can excite more than the desired chromophore, leading to unwanted products. The use of filters to control the wavelength leads to very poor power efficiency and increases heat generation. More recently, a second generation of photochemical reactor was built with low power mercury lamps (< 36 W) which allow the selection of the irradiation wavelength by simply changing the light bulb (UV-A, B or C).[8, 111]

5.3.3 Application of the concentration gradient methodology on a [2 + 2] photocycloaddition (A + B → C)

5.3.3.1 Preliminary study of [2 + 2] cycloadditions towards the application of the concentration gradient methodology (A + B → C)

The [2 + 2] photocycloaddition has been widely described in the literature[112] as it is a very useful reaction in organic synthesis since two new C-C bonds are created. In several total syntheses,[113] this reaction can provide key intermediates towards the formation of target molecules. The enone-alkene cycloaddition, probably the most useful photochemical reaction to organic chemists, is a light induced combination of an excited state enone with a ground state alkene to form a cyclobutane. A maximum of four new chiral centres can be formed in the target cyclobutane molecule. The first [2 + 2] photocycloaddition was observed by Ciamician and Silber in 1908 with the intramolecular cyclisation of carvone (**5.5**) to camphorcarvone (**5.6**) by irradiation with sunlight (Scheme 5.4).[114]

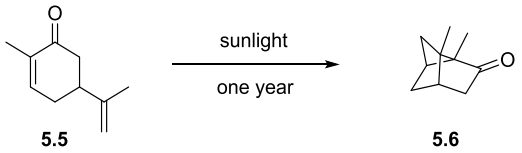

Scheme 5.4: Synthesis of camphorcarvone.

During the last few years, the number of [2 + 2] photocycloaddition applications in flow chemistry has increased intensively due to major advances in continuous flow processes (productivity, efficiency). The first step towards the application of the concentration gradient methodology was to identify in the literature a simple model [2 + 2] photocycloaddition. In 2011, Fukuyama *et al*.[115] performed [2 + 2] cycloadditions of cyclohexenones **5.7** with olefins **5.8** in a microflow system using a 15 W black light (Scheme 5.5). This reaction gave promising yields but poor diastereoselectivity.

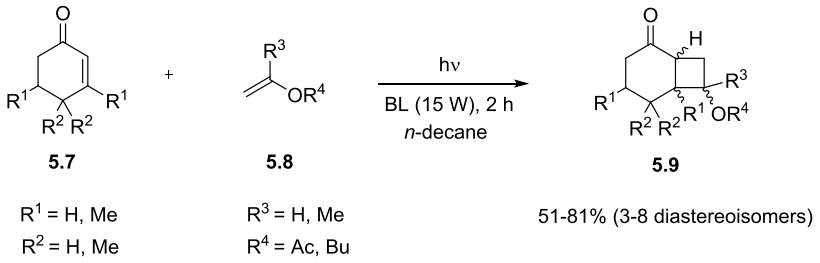

Scheme 5.5: [2 + 2] photocycloaddition in microflow system of cyclohexenones and olefins.[115]

According to Fukuyama's reaction conditions, the [2 + 2] cycloaddition (Scheme 5.6) of cyclohex-2-enone (**5.7a**) with vinyl acetate (**5.8a**) was investigated with our Vapourtec machine equipped with the photoflow reactor (UV-A lamp 9 W). After analysis by GC-MS, the isolated crude mixture highlighted 4 isomeric products and cyclohex-2-enone dimers. No products were isolated as pure compounds. Due to the formation of this mixture, this reaction was not kept as model for further dispersion studies.

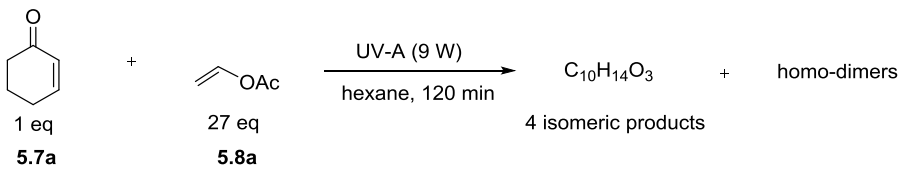

Scheme 5.6: [2 + 2] photocycloaddition in flow of cyclohex-2-enone (**5.7a**) and vinyl acetate (**5.8a**).

In 1994, Weedon *et al*.[116] highlighted the formation of seven racemic cycloadducts (**5.10**-**5.16**) during the photocycloaddition of cyclohex-2-enone (**5.7a**) to ethoxyethene (**5.9**), in

the respective ratio 23/28/7/23/7/2/10 (Scheme 5.7). The regioisomeric ratio of head-to-head to head-to-tail cycloadducts was 19/81. In addition to diastereoselectivity limitations, this experiment emphasises the regioselectivity issues of [2 + 2] cycloadditions.

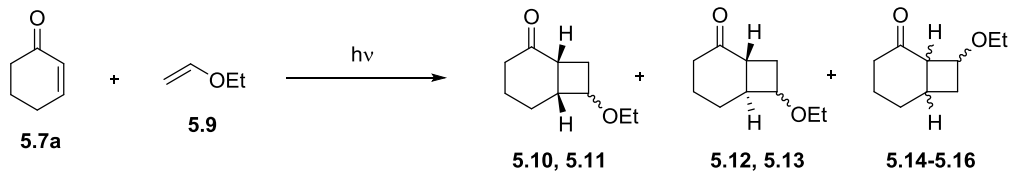

Scheme 5.7: [2 + 2] photocycloaddition in batch of cyclohex-2-enone (**5.7a**) and ethoxyethene (**5.9**).[116]

Based on previous literature and experimental results (Schemes 5.5, 5.6 and 5.7), the use of a symmetric alkene turns out to be the ideal solution to minimise the formation of diastereosiomers and to avoid regioselectivity issues (head-to-head *vs*. head-to-tail product). The reaction between cyclohex-2-enone (**5.7a**) and tetramethylethylene (**5.17**)[117] to form a mixture of trans and cis 7,7,8,8-tetramethylbicyclo[4.2.0]octan-2-ones **5.18** and **5.19** as major products was used as a first model to develop the concentration gradient methodology to optimise a photochemical reaction.

As a preliminary experiment, this reaction was investigated (Scheme 5.8) with our Vapourtec system. Using one single pump and the 28.0 mL double coiled photoflow reactor (UV-A lamp, 9 W), a mixture of cyclohex-2-enone (**5.7a**, 1 equiv.) and tetramethylethylene (**5.17**, 19 equiv.) in THF ($[C_{cyclohexenone}]$ = 0.052 M) was injected into the flow machine without dispersion loop. After 140 min, the reaction mixture was collected at the end of the reactor and purified on silica gel. The reaction was not 100% complete because cyclohex-2 enone (**5.7a**) was observed on TLC. A mixture of both diastereoisomers **5.18** and **5.19** was isolated (36% yield) with a ratio trans/cis = 90/10. The trans diastereoisomer **5.18** appeared to be the major product as previously reported.[117b] No oxetane or dimers were formed under these conditions. However, the unsaturated cyclohexanone (called open cyclobutane in this report) **5.20** was formed in 3% yield according to a Norrish type II fragmentation of the photoreactive cyclobutanes **5.18** and **5.19**.[117a]

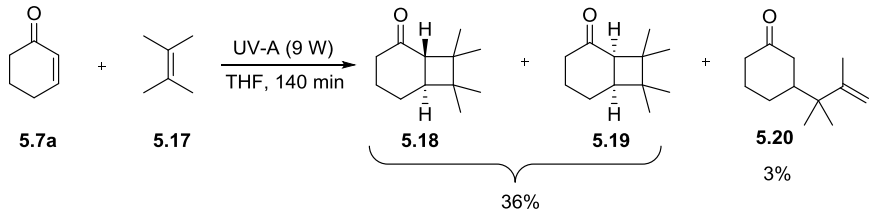

Scheme 5.8: [2 + 2] photocycloaddition of cyclohex-2-enone (**5.7a**) and tetramethylethylene (**5.17**) - Model reaction for concentration gradient studies.

Although the yield was not high, this reaction was used as a model for further optimisations by applying the concentration gradient methodology.

5.3.3.2 Application of the concentration gradient methodology to the [2 + 2] photocycloaddition of cyclohex-2-enone and tetramethylethylene (A + B → C)

The concentration gradient methodology was tested using the [2 + 2] photocycloaddition of cyclohex-2-enone and tetramethylethylene. In order to develop this methodology and find the optimum conditions, various concentration gradient experiments were performed (dispersion of tetramethylethylene with constant amount of cyclohex-2-enone, dispersion of cyclohex-2-enone with constant amount of tetramethylethylene, dispersion experiment with different photoflow reactor design and volume, and dispersion experiment with different UV lamp power). Before discussing the different results, the general methodology of experimental data acquisition (conversion, yield) is described.

5.3.3.2.1 General methodology for the concentration gradient process and data acquisition (A + B → C)

In the following general description of the methodology, 'reagent B' is the dispersed reagent and 'reagent A' is the non-dispersed one. The graphs used to illustrate the methodology were taken from a specific example (reagent A: cyclohex-2-enone (**5.7a**, 1 equiv.) and reagent B: tetramethylethylene (**5.17**, 19.6 equiv.)). However, in the results section, an experiment with dispersion of cyclohex-2-enone was performed but the process and the data acquisition is the same.

Step 1: The first step towards the acquisition of the experimental information (conversion, yield) is the generation of the gradient of concentration of the reagent to disperse (reagent B). A plug of this reagent was injected into the flow set-up (Figure 5.16) at a specific flow rate. This plug dispersed in the 10 mL loop to generate the gradient of concentration which was recorded via an in-line UV or IR spectrometer. After processing the spectra with BORIS software (OPA processing or height of non-overlapping peaks processing), the gradient of concentration profile was generated (Figure 5.17).

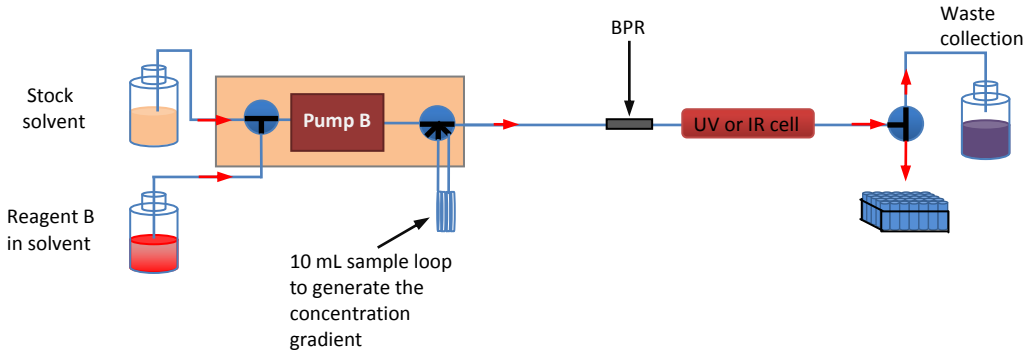

Figure 5.16: Flow set-up for the generation of concentration gradient profile.

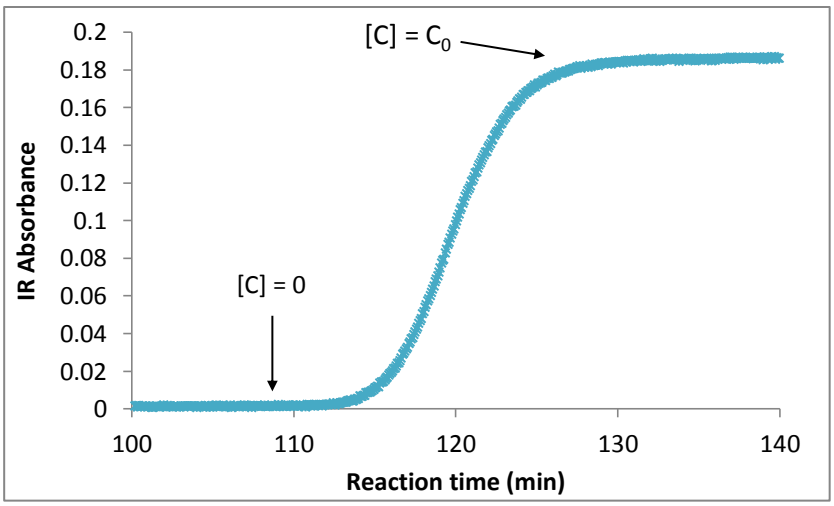

Figure 5.17: Example of concentration gradient profile of a 10 mL plug of reagent B (tetramethylethylene in MeCN ($[C_0]$ = 0.4 M)) after going through a 10 mL PFA loop at 0.1 mL/min. In-line IR detection and height of non-overlapping peaks processing at 1160 nm.

Step 2: The second step consists of performing the [2 + 2] photocycloaddition with dispersion of reagent B using the flow set-up described below (Figure 5.18). Reagent A, which was mixed with an internal standard and MeCN, was injected straight into the UV reactor whereas reagent B, which was mixed with MeCN, dispersed in the 10 mL loop. At the exit of the loop, the flow with the dispersed concentration of reagent B was inserted into a flow of constant concentration of reagent A and internal standard. Therefore, thanks to the concentration gradient, different amount of reagent B can mix with the same amount of reagent A with only one experiment. The combination of these two flows with different experimental conditions went through the UV reactor and samples were collected and analysed via off-line GC analysis (Figure 5.19). For each concentration gradient experiment, the sampling rate was precisely determined.

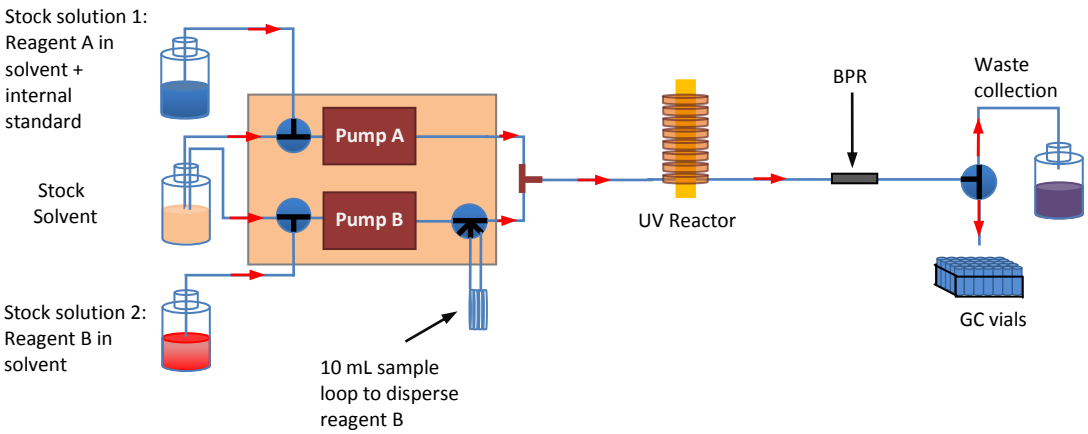

Figure 5.18: Flow set-up for the application of the concentration gradient methodology on the [2 + 2] photocycloaddition.

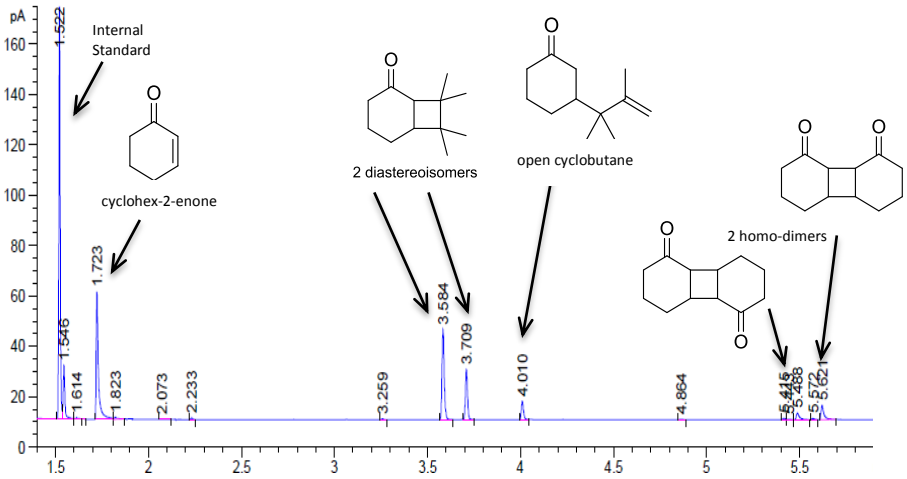

Figure 5.19: Example of a GC analysis during the concentration gradient experiment. In this case, the dispersed reagent B was the tetramethylethylene (**5.17**) and the reagent A was the cyclohex-2-enone (**5.7a**). *N*-butyl ether was used as an internal standard. With low amount of tetramethylethylene, dimers of cyclohex-2-enone were formed.

Step 3: Based on the series of GC analysis obtained, the ratios of the peak area of each compound over the peak area of the internal standard (IS) were calculated and the following Figure 5.20 was generated. Then, the concentration gradient profile of reagent B obtained during step 1 was incorporated with few normalisations to get Figure 5.21. Indeed, as the flow used to collect the samples for GC analysis (Figure 5.20) was twice as high (0.2 mL/min in the example) as the flow used to record the concentration gradient profile (Figure 5.17) (0.1 mL/min in the example), the x-axis scale (time) of the concentration gradient profile was doubled. In the same time, the maximum of the concentration gradient profile was normalised with the maximum peak area 2 diastereoisomers/peak area IS. The determination of the right position of the concentration gradient curve on the x-axis was the main difficulty in this incorporation (See experimental part for explanations).

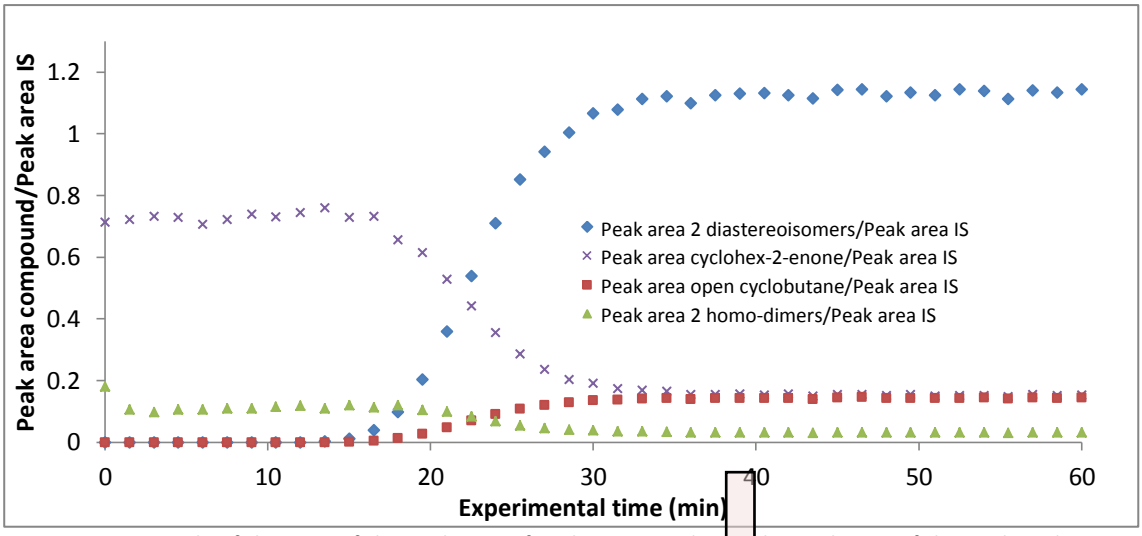

Figure 5.20: Example of the ratio of the peak area of each compound over the peak area of the IS plotted against the experimental time. In this experiment, the dispersed reagent B, the tetramethylethylene (**5.17**, $[B_0]$ = 1 M, 19.6 equiv.), and the reagent A, the cyclohex-2-enone (**5.7a**, $[A_0]$ = 0.051 M, 1 equiv.), were injected into the flow system at 0.1 mL/min respectively. The UV reactor (28 mL capacity) was equipped with a UV-A lamp (9 W). *N*-butyl ether was used as an internal standard [IS] = 0.044 M.

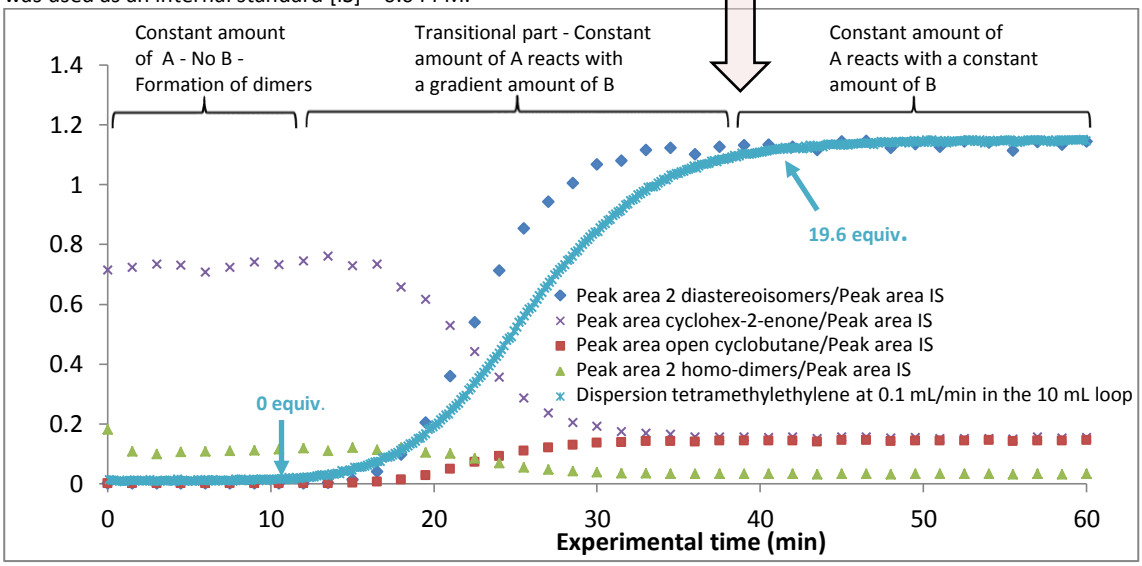

Figure 5.21: Example of the ratio of the peak area of each compound over the peak area of the IS plotted against the experimental time. Incorporation of the concentration gradient profile of reagent B (gradient of concentration tetramethylethylene from 1 to 19.6 equiv.) obtained in step 1.

Step 4: Once data in Figure 5.21 were obtained, the conversion and the yield for each GC analysis were calculated using Equations 5.8 and 5.9 respectively. They were plotted in the following Figure 5.22.

$$\text{Conversion}_t = 1 - \frac{(\text{Peak area cyclohex} - 2 - \text{enone/ Peak area internal standard})_t}{(\text{Peak area cyclohex} - 2 - \text{enone/ Peak area internal standard})_0}$$

Equation 5.8: Formula used for the calculation of the conversion at a given moment.

$$\text{Yield}_t = \frac{\text{n(2 diastereoisomeres)}_t}{\text{n(2 diastereoisomeres)}_{theoretical}}$$

Equation 5.9: Formula used for the calculation of the yield at a given moment.

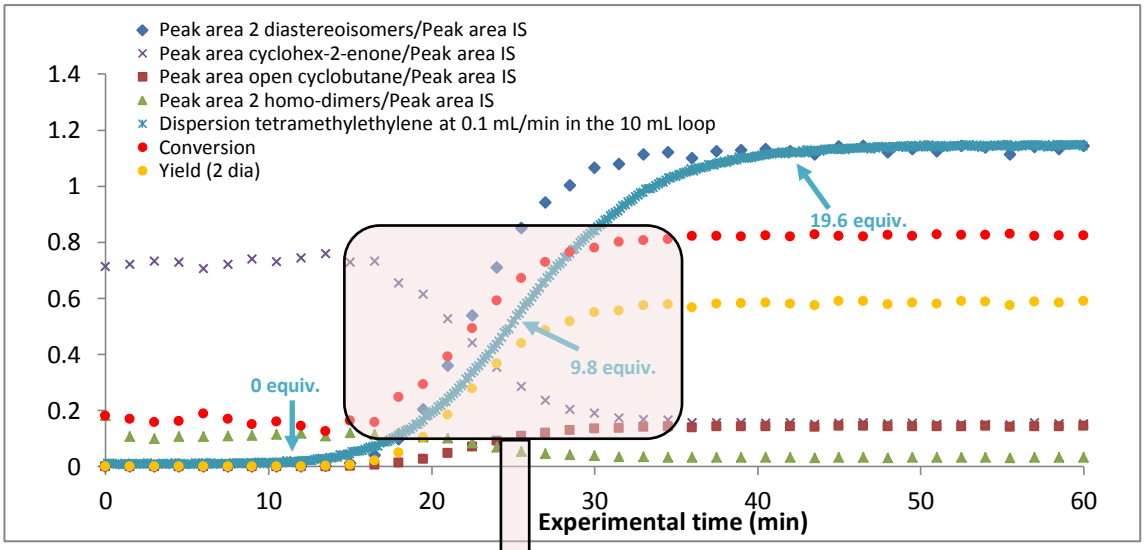

Figure 5.22: Example of the ratios of the peak area of each compound over the peak area of the IS plotted against the experimental time. Incorporation of the concentration gradient profile of reagent B (tetramethylethylene) and calculation of the conversion and the yield.

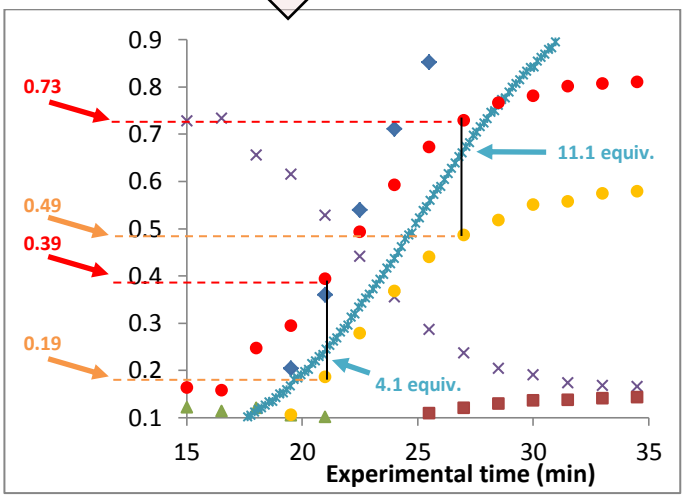

Figure 5.23: Two specific series of point towards the generation of the curves highlighting the evolution of the conversion and the yield according to the equivalents of dispersed reagent B (tetramethylethylene) (Figures 5.24 and 5.25).

Step 5: Using this previous Figure 5.22, the conversion and the yield can be plotted against the equivalents of dispersed reagent B. Indeed, for specific experimental times, equivalents of reagent B, conversion and yield are aligned (Figure 5.23). Using this series of specific data, the following Figures 5.24 and 5.25 can be obtained. Two examples at 4.1 and 11.1 equivalents of reagent B (tetramethylethylene) are highlighted to explain the methodology (Figure 5.23).

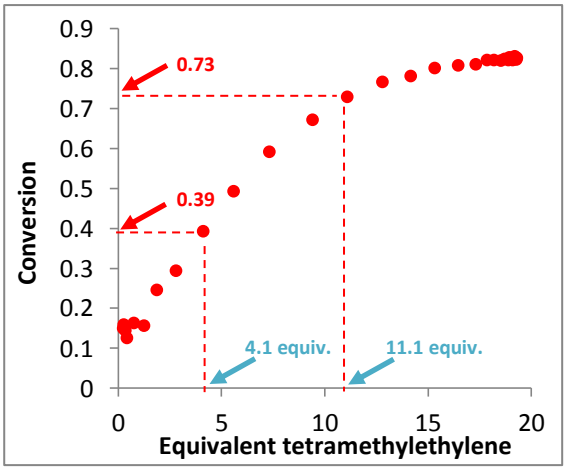

Figure 5.24: Evolution of the conversion according to the equivalent of reagent B (tetramethylethylene).

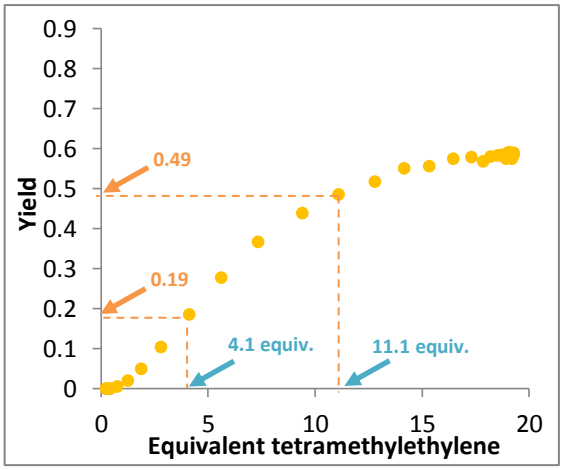

Figure 5.25: Evolution of the yield according to the equivalent of reagent B (tetramethylethylene).

The rapid generation of these two curves is very useful towards the optimisation of reaction conditions. Indeed, the optimum conditions (optimum amount of reagent B) are highlighted to get the best conversion and yield.

5.3.3.2.2 Results of the concentration gradient experiments using the [2 + 2] photocycloaddition of cyclohex-2-enone to tetramethylethylene as a model reaction (A + B → C)

Using the methodology previously described, concentration gradient experiments were performed with different reactors: a double coiled 28.0 mL photoflow reactor equipped with a 9 W UV-A lamp (Tables 5.2 and 5.5), a single coiled 14.1 mL photoflow reactor equipped with a 9 W UV-A lamp (Table 5.3) and a single coiled 31.8 mL photoflow reactor equipped with a 36 W UV-A lamp (Table 5.4).

Dispersion results using the double coiled 28.0 mL photoflow reactor - UV-A (9 W):

Entry	Reagent A	Reagent B	Internal Standard	Reagent A			Reagent B (dispersed)			IS	Reaction time (min)
				equiv.	[A][a] (M)	flow rate (mL/min)	equiv.	[B][b] (M)	flow rate (mL/min)	[IS][c] (M)	
1			dibutyl ether	1	0.051	0.1	5	0.26	0.1	0.044	140
2	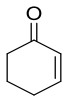		dibutyl ether	1	0.051	0.1	19.6	1	0.1	0.044	140

Table 5.2: Concentration gradient experiments performed with the double coiled 28.0 mL photoflow reactor.
[a] [A] Concentration of reagent A in the stock solution 1, [b] [B] Concentration of reagent B in the stock solution 2, [c] [IS] Concentration of Internal Standard in the stock solution 1.

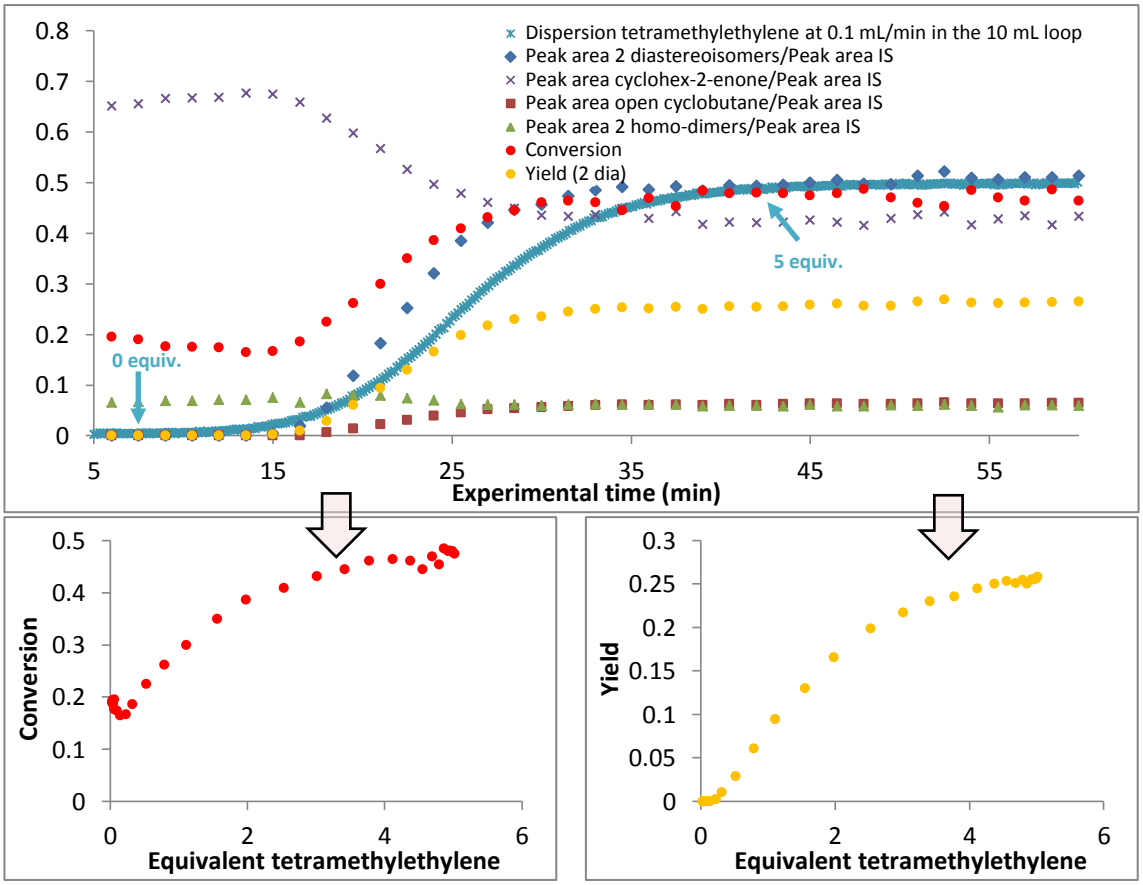

Figure 5.26: Concentration gradient results Table 5.2, entry 1.

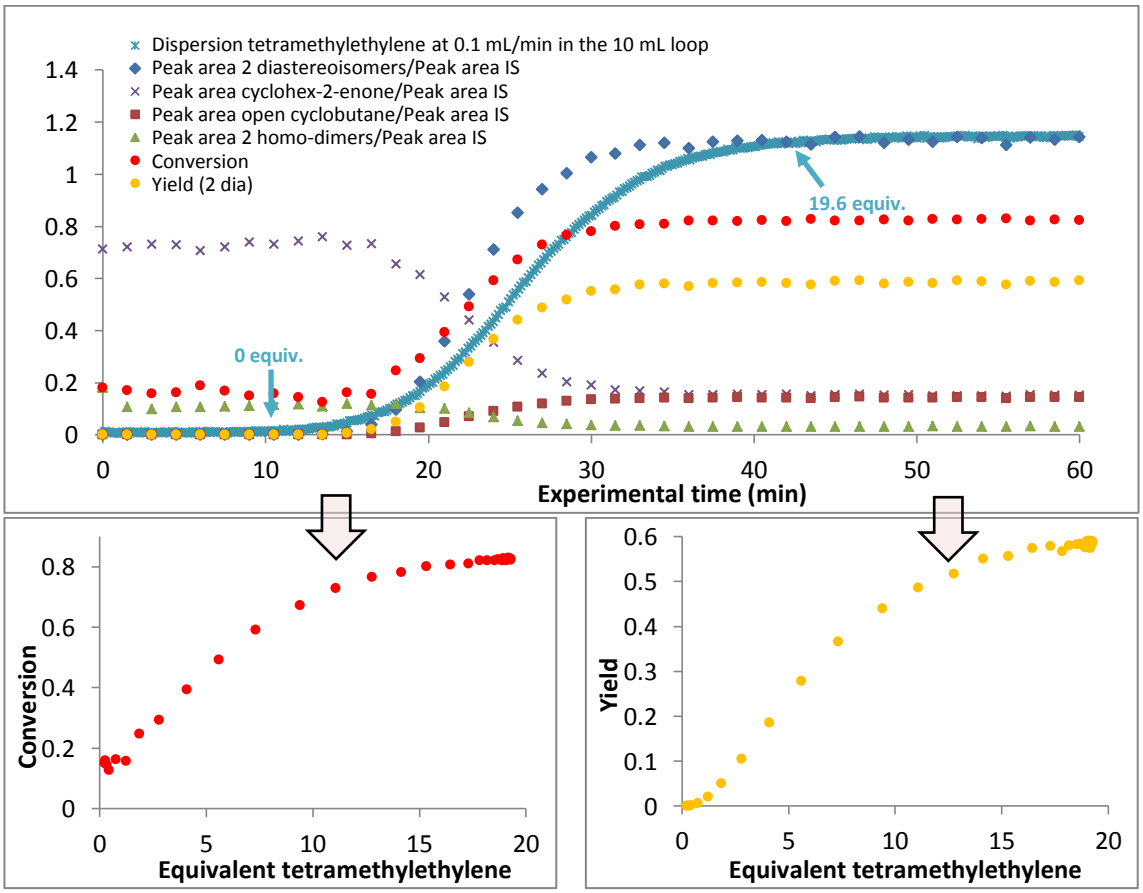

Figure 5.27: Concentration gradient results Table 5.2, entry 2.

These two first experiments were performed with the injection of a constant amount of cyclohex-2-enone (**5.7a**) (1 equiv., [C] = 0.051 M) into a gradient of concentration of tetramethylethylene (**5.17**) (0 to 5 equivalents for entry 1 and 0 to 19.6 equivalents for entry 2). In Figure 5.26, the conversion and the yield stabilise at 48% and 26% respectively from about 4 equivalents of tetramethylethylene. However, this stabilisation is not confirmed when the dispersed amount of tetramethylethylene is increased to 19.6 equivalents (Figure 5.27). Indeed, the stabilisation of the conversion and the yield is observed at 82% and 58% respectively from about 16 equivalents of tetramethylethylene. These slightly inconsistent results obtained between entry 1 and 2 are highlighted in the following Figure 5.28 (poor overlap). During the increase of the amount of **5.17**, we can notice the decrease of the amount of dimer.

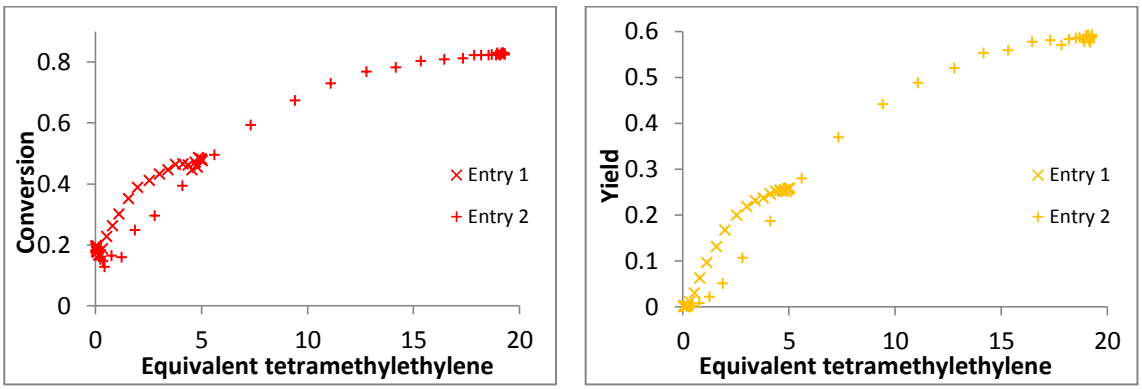

Figure 5.28: Evolution of conversion and yield for Table 5.2, entries 1 and 2.

In order to find an explanation for this inconsistency which might be from the use of a double coiled photoflow reactor, the same experiments were tried with single coiled ones (Tables 5.3 and 5.4).

Dispersion results using the single coiled 14.1 mL photoflow reactor - UV-A (9 W):

Entry	Reagent A	Reagent B	Internal Standard	Reagent A			Reagent B (dispersed)			IS	Reaction time (min)
				equiv.	[A][a] (M)	flow rate (mL/min)	equiv.	[B][b] (M)	flow rate (mL/min)	[IS][c] (M)	
1	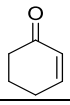		dibutyl ether	1	0.051	0.05	5	0.26	0.05	0.044	140
2	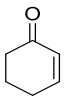		dibutyl ether	1	0.051	0.05	19.6	1	0.05	0.044	140
3	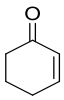		dibutyl ether	1	0.153	0.05	5	0.77	0.05	0.131	140
4	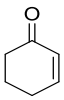		dibutyl ether	1	0.153	0.05	19.6	2.99	0.05	0.131	140

Table 5.3: Concentration gradient experiments performed with the single coiled 14.1 mL photoflow reactor.
[a] [A] Concentration of reagent A in the stock solution 1, [b] [B] Concentration of reagent B in the stock solution 2, [c] [IS] Concentration of Internal Standard in the stock solution 1.

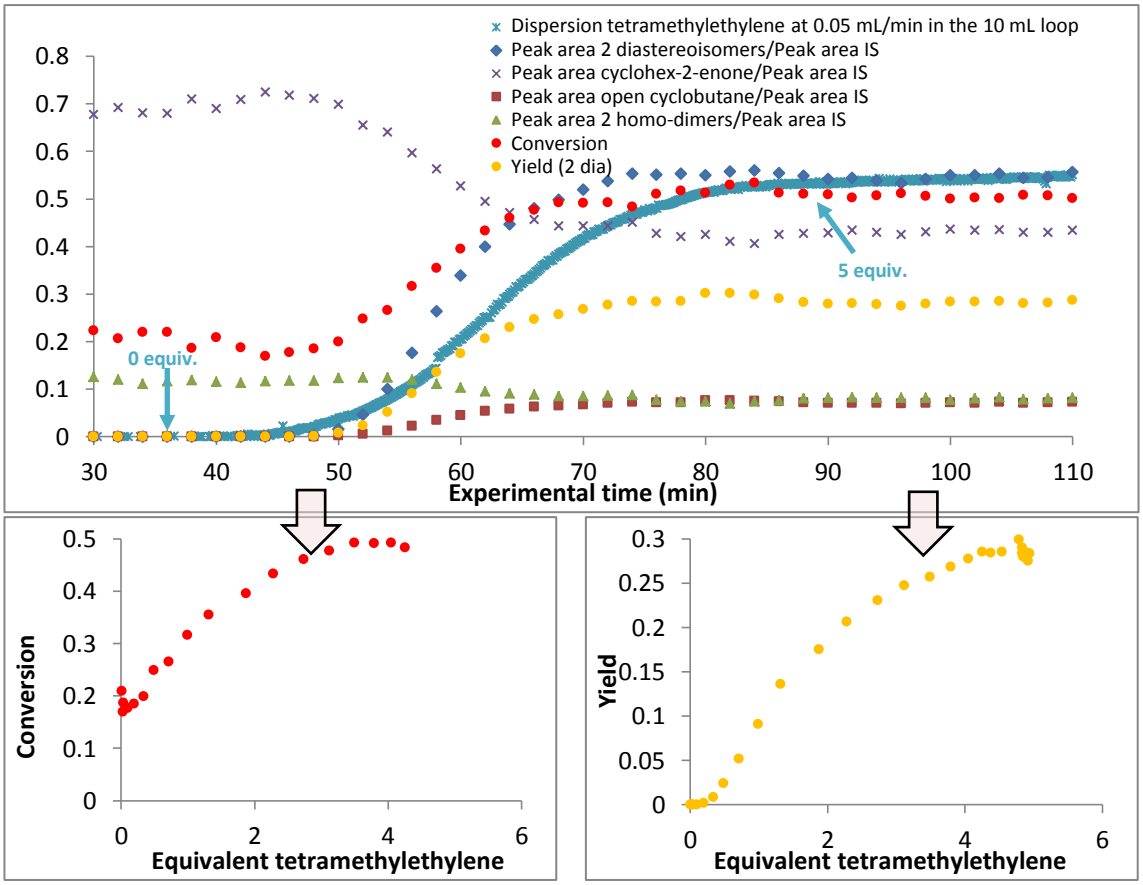

Figure 5.29: Concentration gradient results Table 5.3, entry 1.

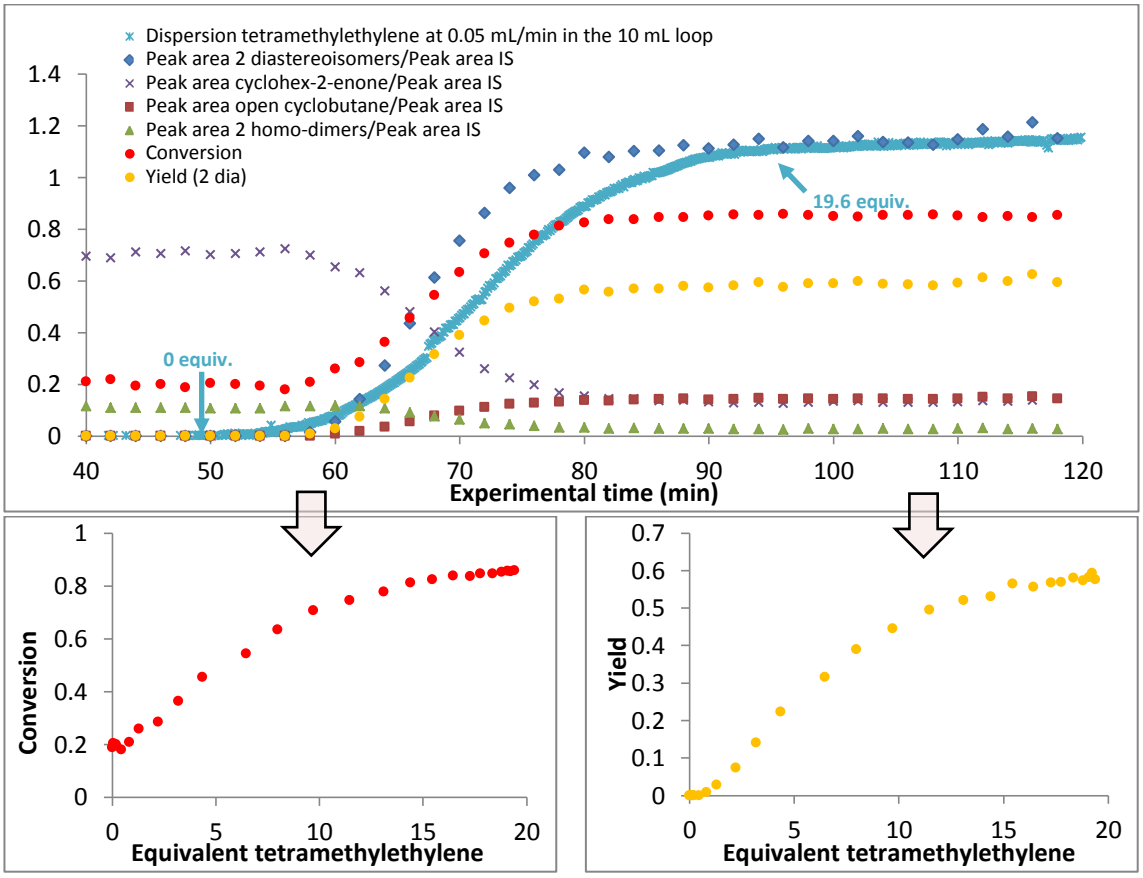

Figure 5.30: Concentration gradient results Table 5.3, entry 2.

As previously stated, these two experiments (Figures 5.29 and 5.30) were performed with the same parameters as Table 5.2, entries 1 and 2 but using a single coiled photoflow reactor (14.1 mL, UV-A 9W). The results are similar and the slight inconsistencies between the 5 and 19.6 equivalents experiments are still present (Figure 5.31). The double coiled photoflow reactor is not the cause of this difference but the dispersion profile position on the x-axis (difficulty to find an accurate position on the x-axis, see experimental part for methodology) might be another potential explanation.

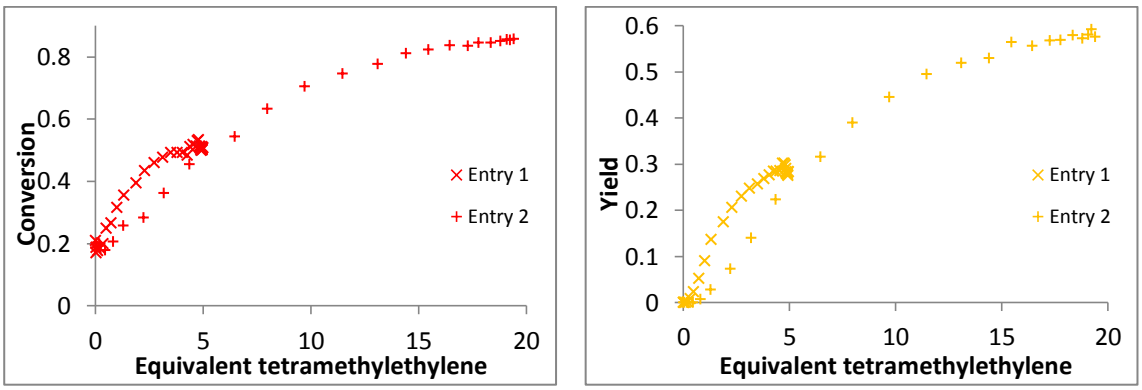

Figure 5.31: Evolution of conversion and yield for Table 5.3, entries 1 and 2.

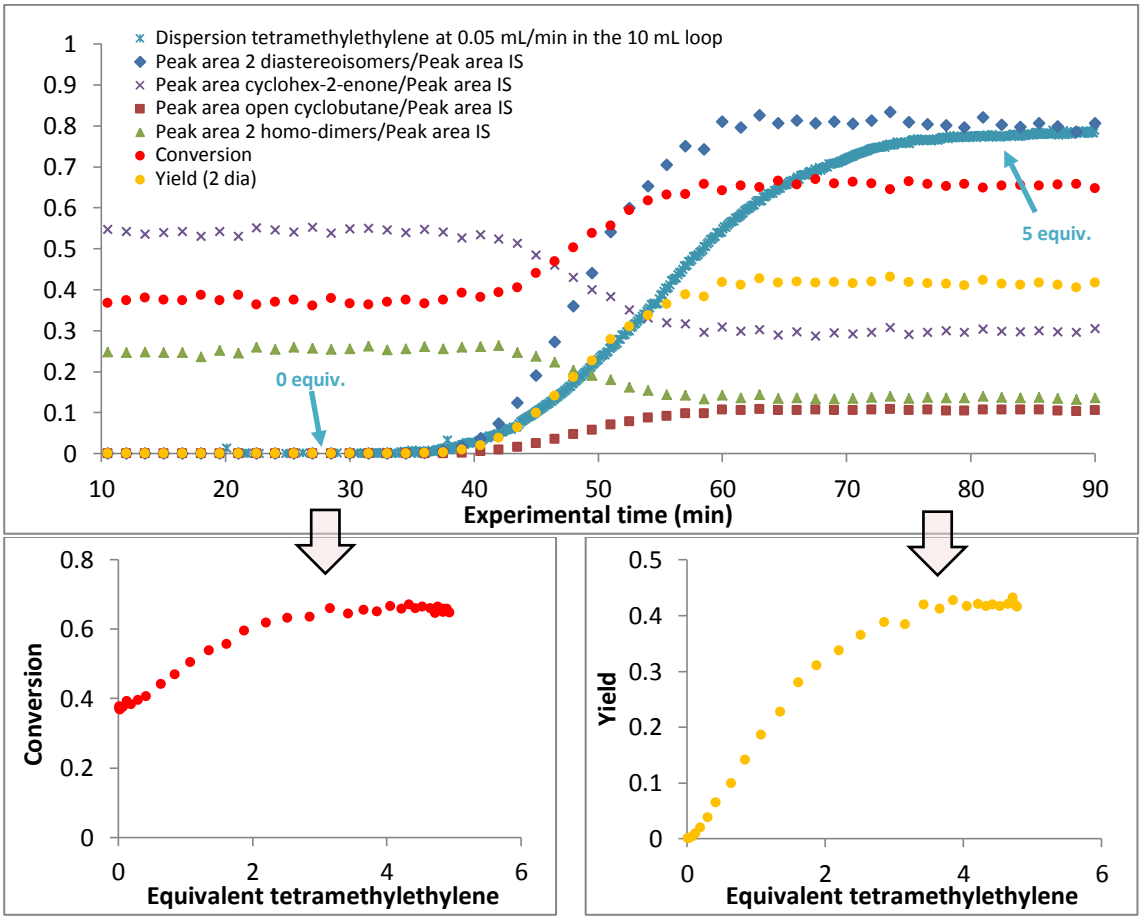

Figure 5.32: Concentration gradient results Table 5.3, entry 3.

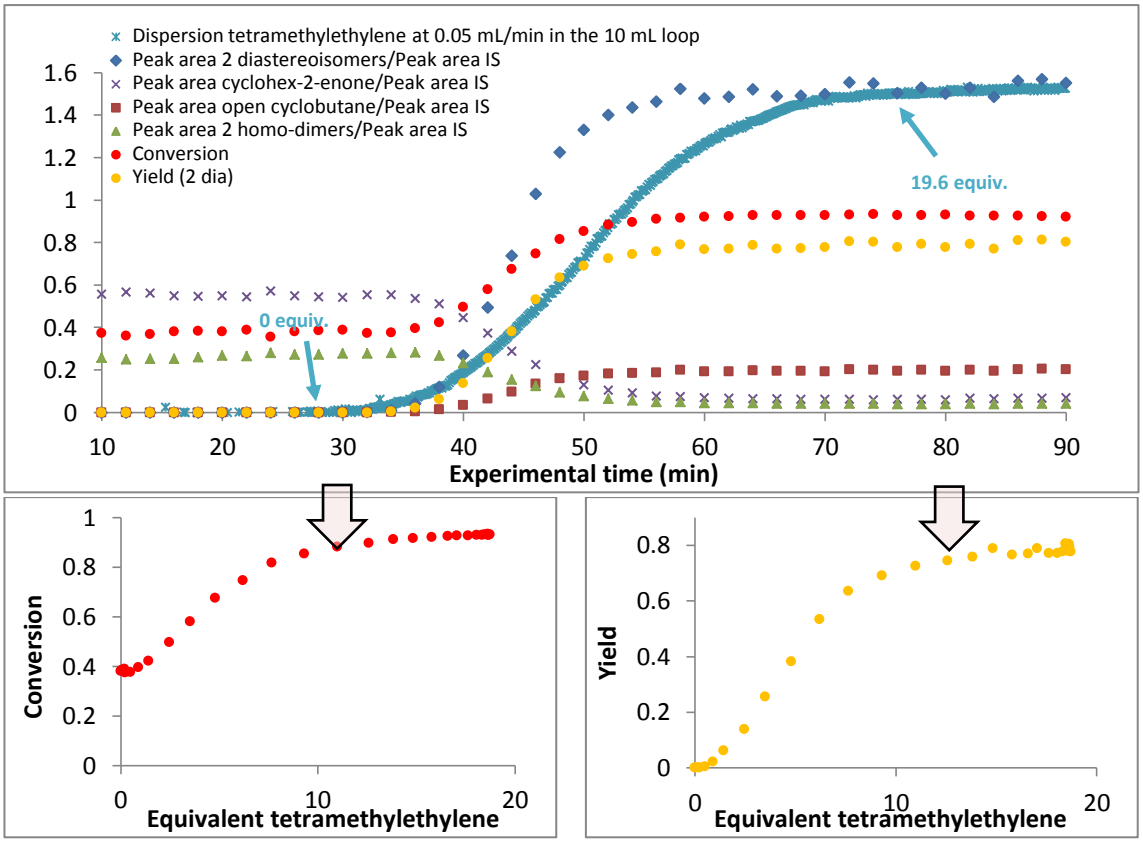

Figure 5.33: Concentration gradient results Table 5.3, entry 4.

In the previous Figures 5.32 and 5.33 (Table 5.3, entries 3 and 4), the initial concentrations of cyclohex-2-enone (**5.7a**) and tetramethylethylene (**5.17**) were tripled compared to entries 1 and 2. The other reaction parameters remained the same. 2nd order reactions occurred during these experiments so tripling the initial concentration increases the overall conversions (e.g. max conversion = 93% (Figure 5.33) *vs.* max conversion = 84% (Figure 5.30)). A larger amount of dimer is formed before the dispersion of the tetramethylethylene and a larger amount of diastereoisomers is generated after the dispersion. Consequently, the maximum yields are increased (e.g. max yield = 80% (Figure 5.33) *vs.* max yield = 60% (Figure 5.30)). As the previous entries 1 and 2 (Tables 5.2 and 5.3), a slight difference is observed between the dispersion of 5 and 19.6 equivalents of tetramethylethylene (Figure 5.34).

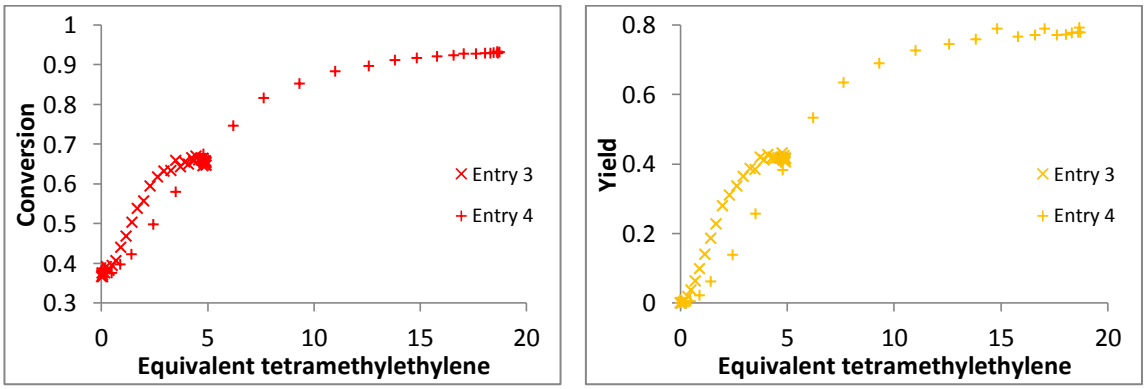

Figure 5.34: Evolution of conversion and yield for Table 5.3, entries 3 and 4.

Dispersion results using the single coiled 31.8 mL photoflow reactor - UV-A (36 W):

Entry	Reagent A	Reagent B	Internal Standard	Reagent A			Reagent B (dispersed)			IS	Reaction time (min)
				equiv.	[A][a] (M)	flow rate (mL/min)	equiv.	[B][b] (M)	flow rate (mL/min)	[IS][c] (M)	
1	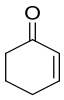		dibutyl ether	1	0.051	0.113	5	0.26	0.113	0.044	140
2			dibutyl ether	1	0.051	0.113	19.6	1	0.113	0.044	140
3	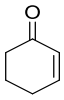		dibutyl ether	1	0.153	0.113	5	0.77	0.113	0.131	140
4			dibutyl ether	1	0.153	0.113	19.6	2.99	0.113	0.131	140

Table 5.4: Concentration gradient experiments performed with the single coiled 31.8 mL photoflow reactor. [a] [A] Concentration of reagent A in the stock solution 1, [b] [B] Concentration of reagent B in the stock solution 2, [c] [IS] Concentration of Internal Standard in the stock solution 1.

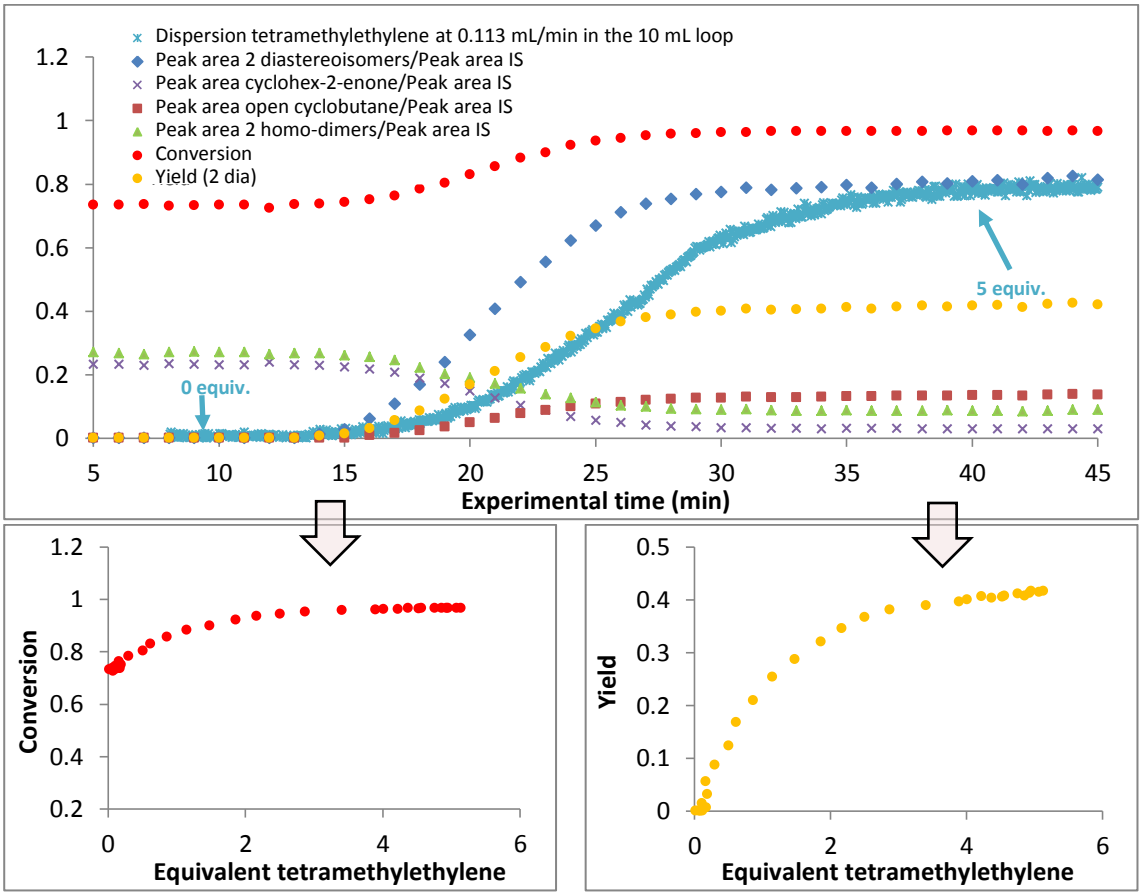

Figure 5.35: Concentration gradient results Table 5.4, entry 1.

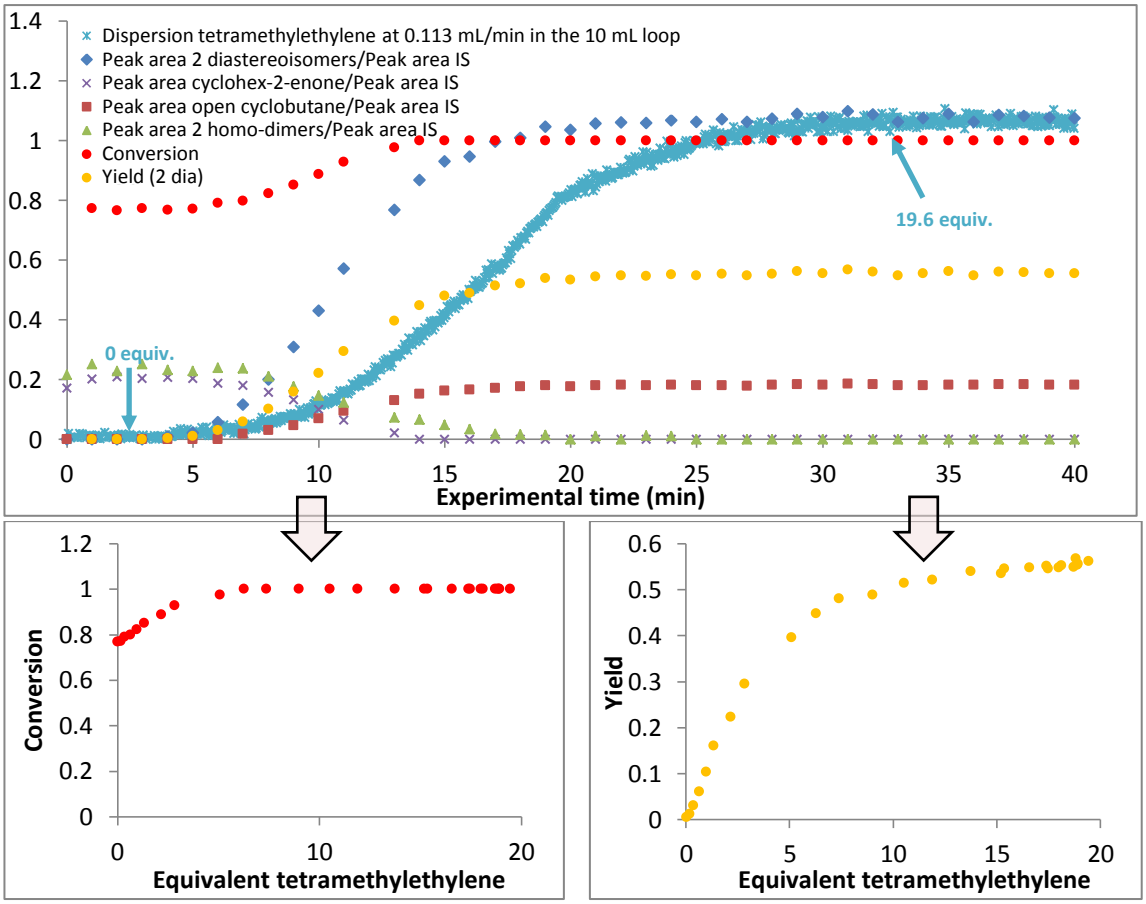

Figure 5.36: Concentration gradient results Table 5.4, entry 2.

These two experiments (Figures 5.35 and 5.36) were performed with the same parameters as Tables 5.2 and 5.3, entries 1 and 2 but using a single coiled photoflow reactor equipped with a 36 W UV-A lamp. With these reaction conditions and this higher power lamp, the reaction proceeds to completion, and the conversion and the yield increase much faster with the amount of tetramethylethylene (e.g. yield = 40% for 5 equivalents of tetramethylethylene (Figure 5.36) *vs*. yield = 30% for 5 equivalents of tetramethylethylene (Figure 5.30)). However, as observed previously, a small deviation is noticed between the dispersion of 5 and 19.6 equivalents of tetramethylethylene (Figure 5.37).

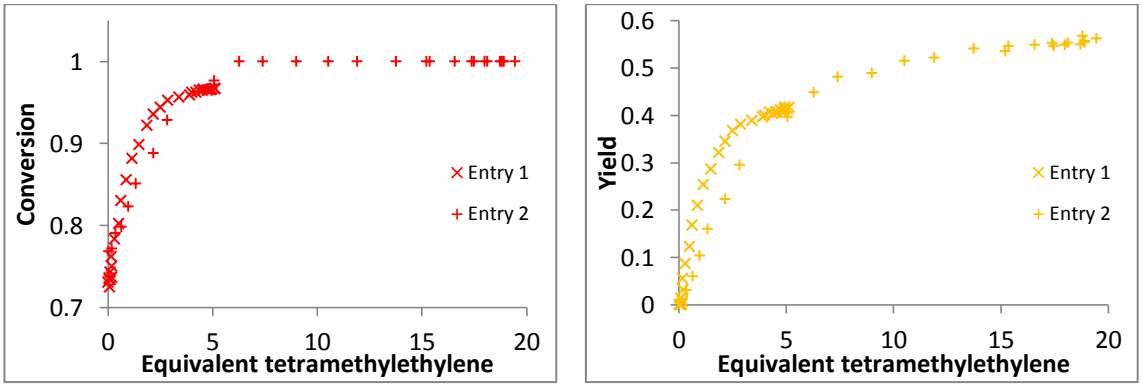

Figure 5.37: Evolution of conversion and yield for Table 5.4, entries 1 and 2.

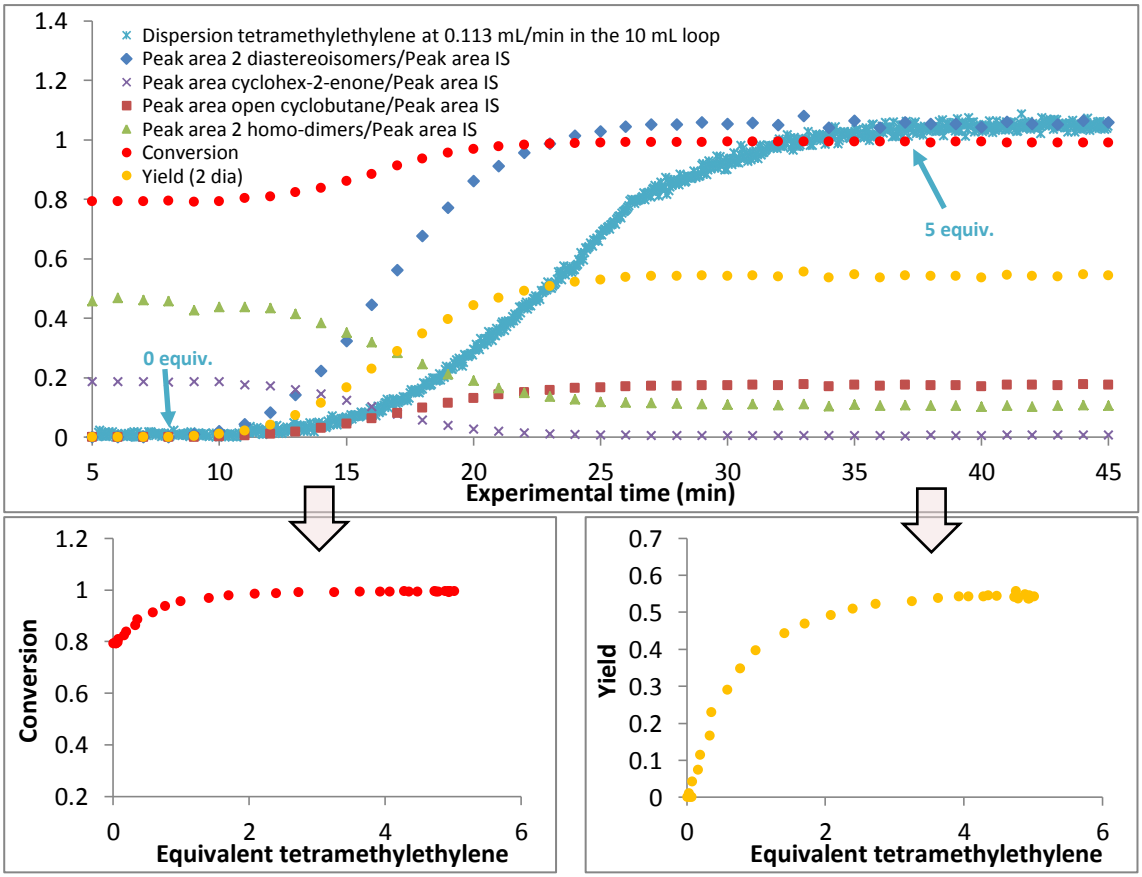

Figure 5.38: Concentration gradient results Table 5.4, entry 3.

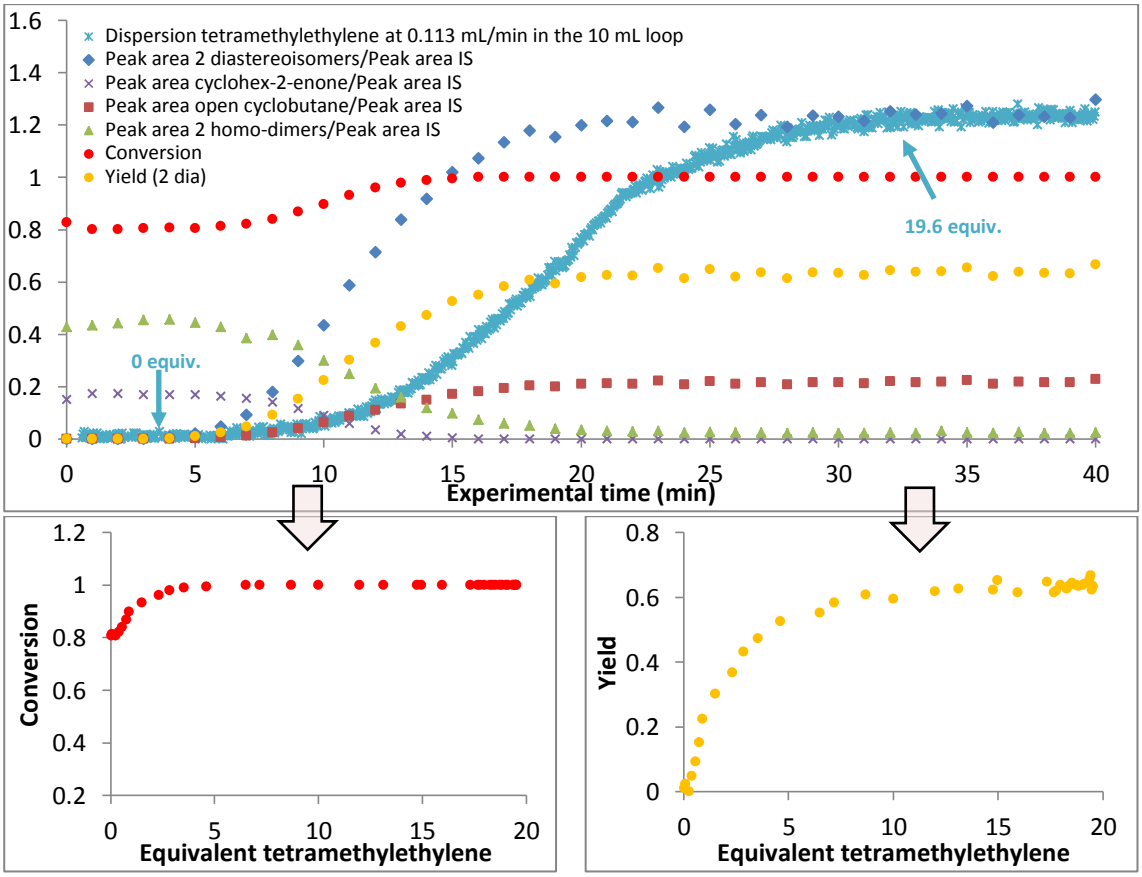

Figure 5.39: Concentration gradient results Table 5.4, entry 4.

In the previous Figures 5.38 and 5.39, the initial concentration of tetramethylethylene and cyclohex-2-enone were tripled to highlight the influence of the concentration in a second order reaction. For this purpose, for the same amount of tetramethylethylene, the conversion and yield are higher in these cases (Figure 5.39) than with the lower concentration (Figure 5.36). However, with the same conditions, the maximum yield with the 36 W lamp (63%, Figure 5.39) is lower than using the 9 W lamp (80%, Figure 5.33). This difference can be explained by the degradation of the starting material and diastereoisomers due to the over exposure to the high energy UV irradiation.

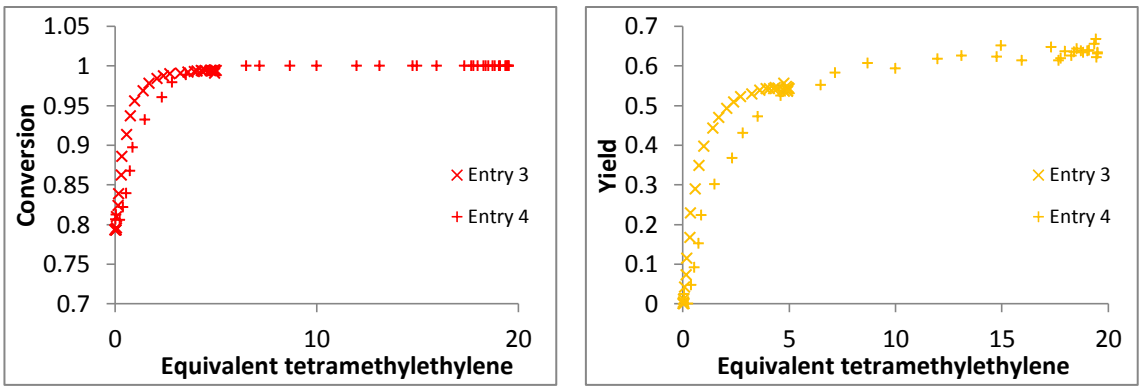

Figure 5.40: Evolution of conversion and yield for Table 5.4, entries 3 and 4.

Dispersion results using the double coiled 28.0 mL photoflow reactor - UV-A (9 W) - Dispersion of cyclohex-2-enone:

Entry	Reagent A	Reagent B	Internal Standard	Reagent A			Reagent B (dispersed)			IS	Reaction time (min)
				equiv.	[A][a] (M)	flow rate (mL/min)	equiv.	[B][b] (M)	flow rate (mL/min)	[IS][c] (M)	
1			dibutyl ether	19.4	0.99	0.1	1	0.051	0.1	0.044	140

Table 5.5: Concentration gradient experiments performed with the double coiled 28.0 mL photoflow reactor.
[a] [A] Concentration of reagent A in the stock solution 1, [b] [B] Concentration of reagent B in the stock solution 2, [c] [IS] Concentration of Internal Standard in the stock solution 1.

For this experiment (Table 5.5, Figure 5.41), a concentration gradient of cyclohex-2-enone (0 to 1 equiv.) was injected into a constant amount of tetramethylethylene (19.4 equiv., [C] = 0.99 M). This dispersion attempt gives access to lower ratios between the initial amount of cyclohex-2-enone and tetramethylethylene (1 to 19.6 was the lowest ratio tried in the previous experiments). The conversion of the reaction is constant with the amount of cyclohex-2-enone injected (about 80%). However, the yield reaches a maximum (80%) for about 0.5 equivalent of ketone (ratio ketone/tetramethylethylene = 1/38.8). As it is the cyclohex-2-enone which is absorbing the light, there is a balance between not absorbing the

light at low concentrations to the situation where there is not enough light for complete reaction at high concentration. This experiment is particularly interesting because it clearly highlights the conditions for which the yield is maximum.

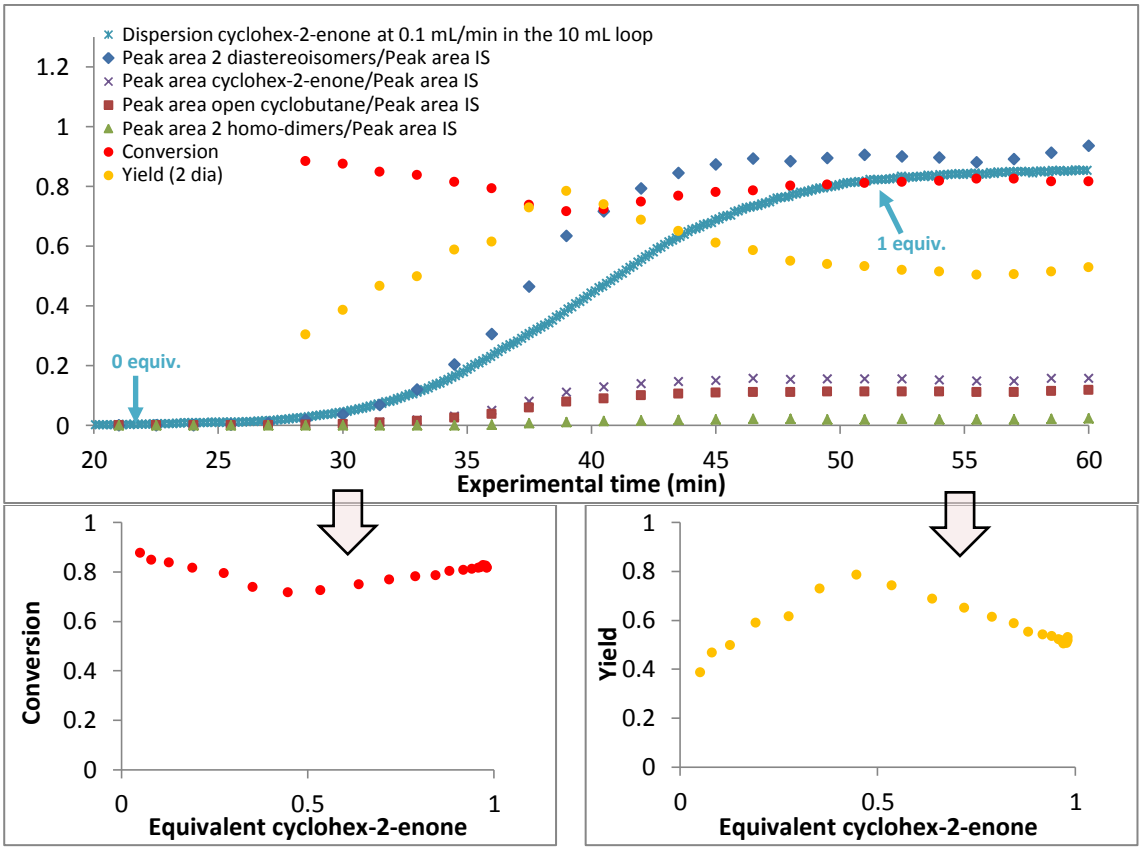

Figure 5.41: Concentration gradient results Table 5.5, entry 1.

With this series of experiments, it has been shown that it is possible to monitor crucial information (evolution of the amount of the different compounds, conversion and yield according to the amount of the dispersed reagent) using this novel concentration gradient methodology. In spite of small inconsistencies observed between a few experiments, the power and efficiency of such a method remains in the rapid generation of this crucial set of information towards the fast optimisation of reaction conditions. After complementary investigations especially on the development of an in-line monitoring (UV or IR), time saving and reduction of waste material would be much more significant and will increase the efficiency and the power of this methodology.

5.3.4 Application of the concentration gradient methodology to the Mallory photocyclisation (B → C)

5.3.4.1 Preliminary study on the Mallory photocyclisation of cis-stilbene towards the application of the concentration gradient methodology (B → C)

Over the past few decades, π-conjugated compounds have attracted lots of interests in organic synthesis due to their various applications in electronics and more particularly in semiconductors.[118] Due to their high chemical stability on exposure to air and light, and their high OFET performance, phenacenes are promising organic electronic materials.[119] The Mallory photocyclisation[120] is the typical reaction for the synthesis phenacene skeletons but very few literature publications are available with the development of this reaction under flow conditions.[121] For this reason, we decided to apply our new concentration gradient methodology using this photocyclisation.

Photolysis of cis-stilbene (**5.21**) induces the reversible cyclisation to dihydrophenanthrene (**5.22**), an intermediate which can be irreversibly oxidised with hydrogen acceptors such as iodine, oxygen or cyclohexene to form **5.23** (Scheme 5.9). Moreover, cis-stilbene (**5.21**) undergoes photoisomerisation to trans-stilbene (**5.24**) (Scheme 5.10) which can then dimerise to form a mixture of **5.25** and **5.26** (Scheme 5.11) in high concentration conditions.[122]

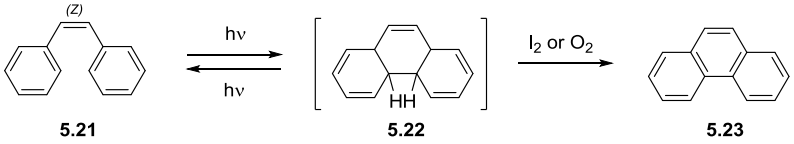

5.21 **5.22** **5.23**

Scheme 5.9: Photolysis of cis-stilbene.

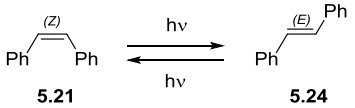

5.21 **5.24**

Scheme 5.10: Photoisomerisation of stilbene.

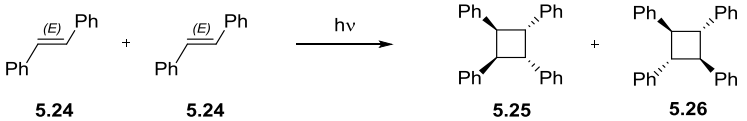

5.24 **5.24** **5.25** **5.26**

Scheme 5.11: Photodimerisation of trans-stilbene.

As preliminary experiments, the photocyclisation of cis-stilbene (**5.21**) was performed using a Vapourtec system equipped with the 31.8 mL single coiled photoreactor. As described by Bedekar *et al.*,[123] the first attempt was performed with the cyclohexene (2 equiv.) as

hydrogen acceptor. With the conditions described in Scheme 5.12, only 50% conversion was noticed after 30 min reaction time. However, as described by Okamoto *et al.*,[121c] using a catalytic amount of iodine (0.1 equiv.) instead of cyclohexene proceeded to better results with full conversion and 96% yield (Scheme 5.12). No dimers were formed with this low concentration [C] = 0.005 M.

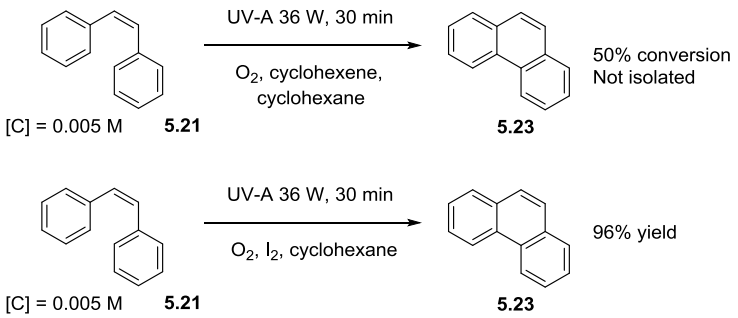

Scheme 5.12: Phenanthrene synthesis in flow chemistry using cyclohexene and iodine as hydrogen acceptors.

According to these results, iodine was kept as hydrogen acceptor for our concentration gradient experiments.

5.3.4.2 Application of the concentration gradient methodology to the photocyclisation of cis-stilbene (B → C)

5.3.4.2.1 General methodology for the concentration gradient process and data acquisition (B → C)

Based on a comparable general methodology to that described in section 5.3.3.2.1, the following 5 steps were performed during the concentration gradient process and data acquisition.

Step 1: Generation of the gradient of concentration of the dispersed reagent B (cis-stilbene (**5.21**)) using the flow set up described in Figure 5.16.

Step 2: Photocyclisation with dispersion of reagent B (cis-stilbene) using the flow set-up described in Figure 5.42. Compound A (internal standard) was injected straight into the UV reactor whereas reagent B dispersed in the 10 mL loop. At the exit of the loop, the flow with the dispersed concentration of reagent B was inserted into a flow of constant concentration of internal standard. At the exit of the reactor, the sample collection and off-line GC analysis enable the determination of the reaction mixture composition, the conversion and the yield according to the reaction time.

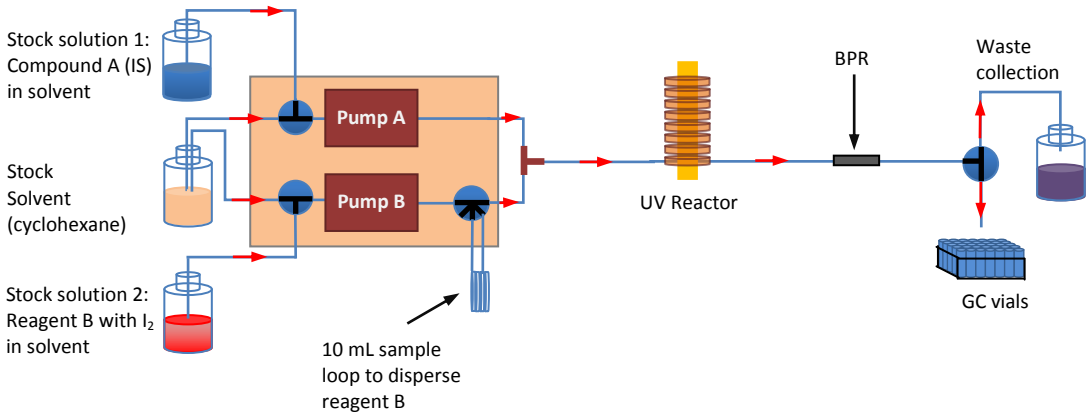

Figure 5.42: Flow set-up for the application of the concentration gradient methodology on the photocyclisation of cis-stilbene (**5.21**).

Step 3: Calculation of the ratios of the peak area of each compound over the peak area of the internal standard (IS) thanks to the GC analysis and generation of the graph with these ratios plotted against the experimental time. Then, incorporation with few normalisations of the gradient of concentration curve obtained during step 1.

Step 4: Calculation of the conversion and yield for each GC analysis using equations 5.10 and 5.11 respectively and incorporation of the corresponding values into the graph plotting the different ratios against the reaction time.

$$\text{Conversion}_t = 1 - \frac{(\text{Peak area cis} - \text{stilbene/ Peak area internal standard})_t}{(\text{Peak area cis} - \text{stilbene/ Peak area internal standard})_{0\,t}}$$

Equation 5.10: Formula used for the calculation of the conversion at a given moment.

$$\text{Yield}_t = \frac{\text{n(phenanthrene)}_t}{\text{n(phenanthrene)}_{theoretical\,t}}$$

Equation 5.11: Formula used for the calculation of the yield at a given moment.

Step 5: Generation of the graph with the conversion and the yield plotted against the initial concentration of the cis-stilbene.

5.3.4.2.2 Results of the concentration gradient experiments using the photocyclisation of cis-stilbene as a model reaction (B → C)

Using the methodology previously described, different concentration gradient experiments were performed. As the UV absorption of the cis-stilbene is in the range 240-320 nm,[124] attempts were investigated with 3 different UV lamps (UV-A, B and C 36 W) (Table 5.6).

Entry	Compound A Internal Standard	Reagent B	Compound A (IS)		Reagent B (dispersed)		Reaction time (min)	UV lamp	UV reactor
			[A][a] (M)	flow rate (mL/min)	[B][b] (M)	flow rate (mL/min)			
1	dibutyl ether		0.36	0.353	0.1	0.353	45	UV-A 36 W	Single coiled 31.8 mL
2	dibutyl ether		0.36	0.353	0.1	0.353	45	UV-B 36 W	Single coiled 31.8 mL
3	dibutyl ether		0.36	0.353	0.1	0.353	45	UV-C 36 W	Single coiled 31.8 mL

Table 5.6: Concentration gradient experiments performed with the single coiled 31.8 mL photoflow reactor. [a] [A] Concentration of compound A (Internal standard) in the stock solution 1, [b] [B] Concentration of reagent B in the stock solution 2.

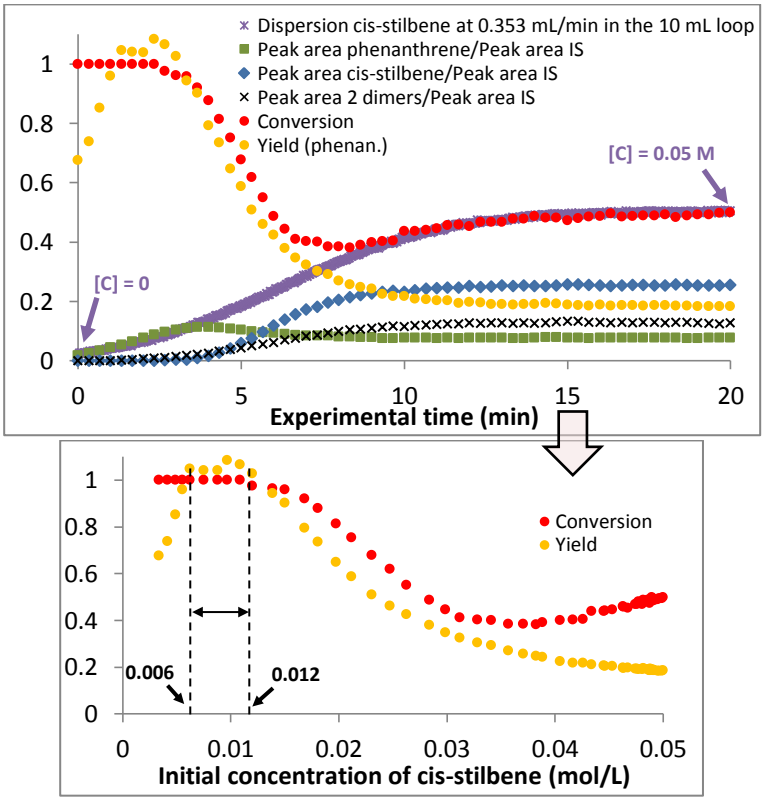

Figure 5.43: Concentration gradient results Table 5.6, entry 1 (UV-A).

From this first concentration gradient experiment performed with the UV-A lamp (Figure 5.43), the evolution of the conversion and the yield according to the initial concentration of cis-stilbene ($[C]_0$ = 0.05 M) is clearly highlighted. For the reaction conditions described in Table 5.6 (entry 1), an initial concentration of cis-stilbene between 0.006 and 0.012 M leads to the highest conversion and yield (around 1 and 1 respectively), and low formation of dimers. For an initial concentration of cis-stilbene at 0.012 M, a production efficiency of 91 mg/h of phenanthrene is obtained. For lower initial concentrations, the reaction is complete but the yield decreases, probably because of the over irradiation and the degradation of the product. For concentrations higher than 0.012 M, the decrease of the

conversion and the yield is due to the over concentration of the reaction mixture compared to the amount of photons provided in 45 min by the UV-A lamp (36 W). Moreover, the increase of the formation of dimers with the increase of the initial concentration is another explanation of the decrease of the yield.

For the experiment with the UV-B lamp (Figure 5.44), the maximum yield and conversion (around 1 and 1 respectively) are obtained for an initial concentration between 0.012 and 0.025 M. The production efficiency of phenanthrene is 189 mg/h for an initial concentration of cis-stilbene at 0.025 M and a 36 W UV-B lamp. This production is slightly better than the one mentioned by Okamoto with an initial concentration of cis-stilbene at 0.005 M, a 8 min reaction time and with a 450 W high pressure Hg lamp (175 mg/h).[121c] For lower concentration than 0.012 M, the decrease of the yield is probably due to the same reasons as the UV-A lamp. For higher concentration than 0.025 M, the formation of dimers is the explanation for the decrease of the yield.

Finally, for the experiment with the UV-C lamp (Figure 5.45), the maximum yield and conversion (around 1 and 1 respectively) are obtained for an initial concentration between 0.016 and 0.021 M. The production efficiency of phenanthrene is 158 mg/h for an initial concentration of cis-stilbene at 0.021 M.

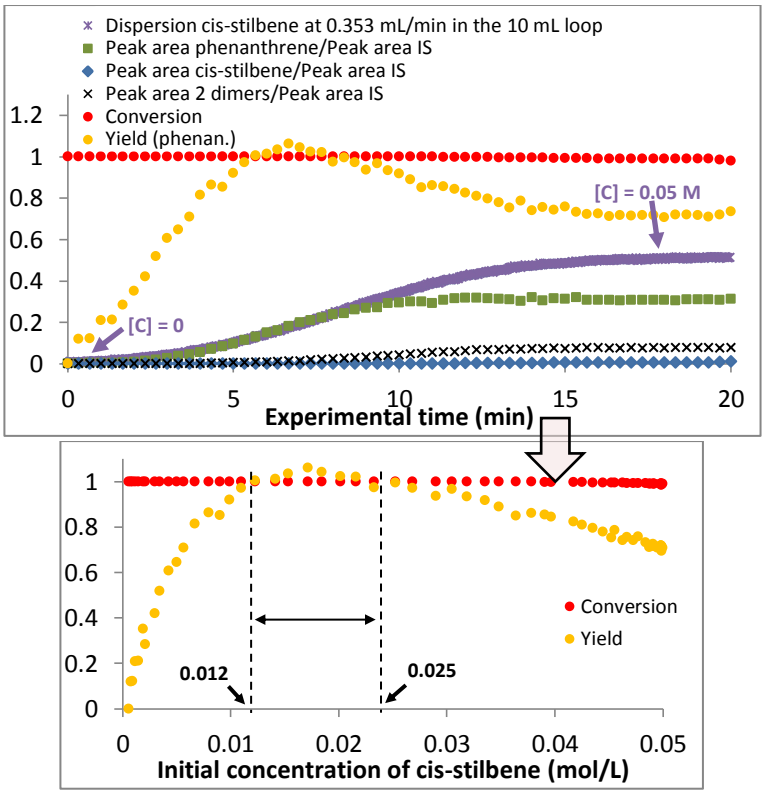

Figure 5.44: Concentration gradient results Table 5.6, entry 2 (UV-B).

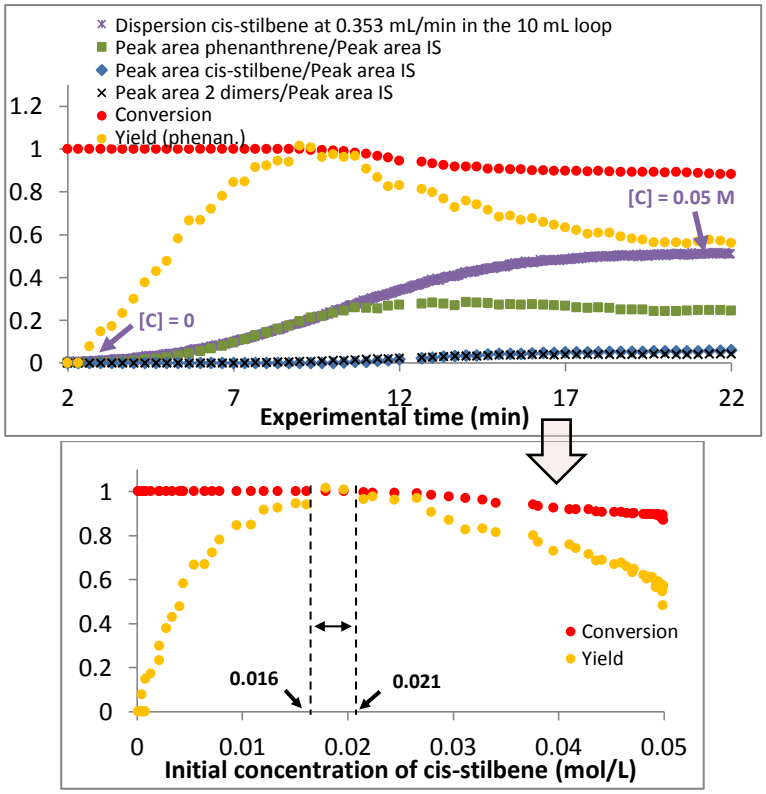

Figure 5.45: Concentration gradient results Table 5.6, entry 3 (UV-C).

With these three different experiments, it has been emphasised that the concentration gradient experiment can enable identification of the optimum initial reaction mixture concentration to get the best conversion and yield. According to our results, a mixture of cis-stilbene in cyclohexane ([cis-stilbene] = 0.025 M) going through the 31.8 mL photoflow reactor for 45 min and equipped with the UV-B lamp (36 W) led to the best conversion, yield, productivity and low formation of dimers.

The concentration gradient methodology employed for the model 2nd and 1st order photoreactions (A + B → C ([2 + 2] photocycloaddition) and B → C (photocyclisation)) quickly highlights the optimum reaction conditions (optimum ratio A/B or optimum initial concentration of B) to get the best conversion and yield. This methodology was studied with photochemical reactions but the application on thermal reactions could be possible. Using this concentration gradient process, the promising and consistent results emphasise the efficiency of flow chemistry to quickly produce a large amount of relevant data towards the fast optimisation of reaction conditions.

5.4 Turn off light methodology in photoflow chemistry

5.4.1 Principle of this novel methodology

In the context of optimisation of reaction conditions, the determination of the optimum reaction time remains one of the main goals. For this purpose, we developed with Prof Richard J. Whitby another novel methodology using our photoflow reactors to quickly find the optimum reaction time.

The turn off light experiments under flow conditions were conducted using a Vapourtec R series system with a single coiled photoflow PFA reactor (14.1 or 31.8 mL capacity) of 1 mm internal diameter equipped with a UV lamp (UV-A/B or C 9 W or 36 W) and an automated sample collector (Figure 5.46).

The general principle of this methodology is described as follows: the starting materials (Reagent A or Reagents A + B or Reagents A + B + C) are injected into the UV reactor (capacity = V_0) with the light on at a constant flow rate FR. Once the reactor is entirely filled up with the reaction mixture, the UV lamp is turned off and the content of the reactor is pushed out with the stock solvent. At the end of the reactor, the mixture is collected in vials for off-line GC analysis. After turning off the light and before pushing out the content of the reactor, Figure 5.47 highlights 3 different reaction times according to the position in the tube. Thanks to the GC analyses, the different mixture compositions can be determined according to the reaction time ($0 < RT < V_0/FR$), and the corresponding conversion and yield can be calculated (Equations 5.12 and 5.13). In the following sections 5.4.3 to 5.4.6, this methodology was investigated with several photochemical reactions (A → D, A + B → D and A + B + C → D). Dispersion was not considered in this methodology.

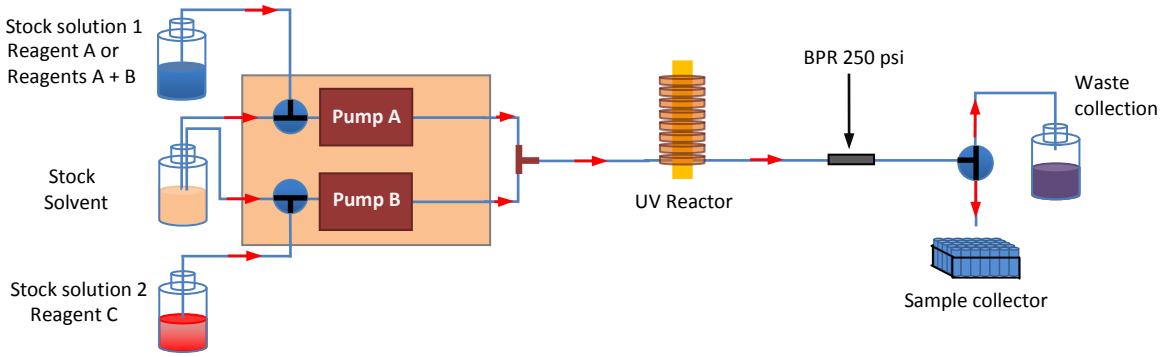

Figure 5.46: Flow set-up for turn off light methodology.

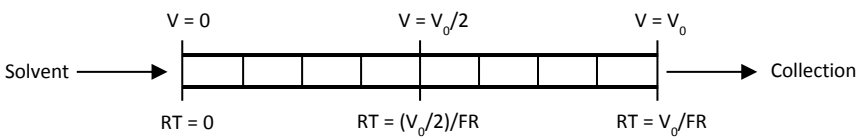

Figure 5.47: Turn off light methodology - Reaction times according to the position in the UV reactor.

$$\text{Conversion}_t = 1 - \frac{(\text{Peak area reagent A/ Peak area internal standard})_t}{(\text{Peak area reagent A/ Peak area internal standard})_0}$$

Equation 5.12: Formula used for the calculation of the conversion at a given moment.

$$\text{Yield}_t = \frac{\text{n(product)}_t}{\text{n(product)}_{theoretical}}$$

Equation 5.13: Formula used for the calculation of the yield at a given moment.

5.4.2 Correction to apply to the turn off light methodology for the determination of the optimum reaction time

During a photoflow chemical reaction, the intensity of the light is not homogeneous throughout the UV reactor. Indeed, the amount of photons is higher in the middle of the reactor than at the entrance and the end, creating a difference of efficiency between the reaction occurring in the middle and the ends. For the turn off light experiments, the lower efficiency at the ends is an issue as it increases the reaction time. Therefore, to assess this difference of intensity/efficiency, the reaction between the cyclohex-2-enone (1 equiv., [C] = 0.025 M) and the tetramethylethylene (19.6 equiv.) was used as a model. The reaction mixture was injected into the photoflow reactor (light turned off). Once the reactor was entirely filled up, the pump was turned off, the light was turned on and the reaction was left to proceed. After the indicated reaction time, the light was turned off and the content of the reactor was pushed out, collected in GC vials and analysed. From these GC data (Figures 5.48 and 5.50), the efficiency/intensity of the UV lamp (UV-A 9 W and 36 W inside the 14.1 and 31.8 mL UV reactor respectively) according to the area in the UV reactor was generated (Figures 5.49 and 5.51). These data were used in the following sections 5.4.3 to 5.4.6 for the determination of the real reaction time (corrected reaction time). Details about the correction process are described in the experimental part.

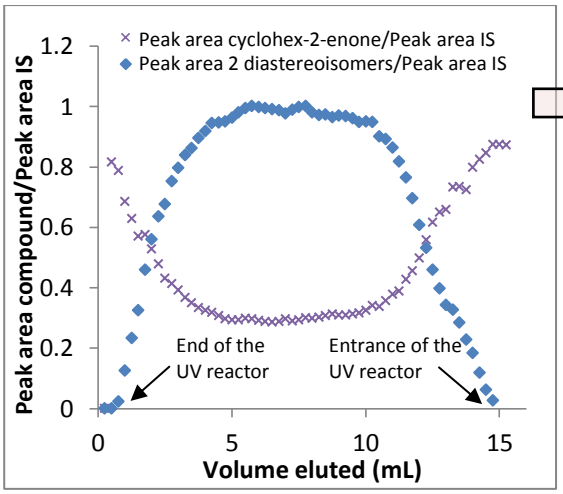

Figure 5.48: GC data of the different vials collected at the exit of the reactor (14.1 mL, UV-A 9 W) - light on during 60 min.

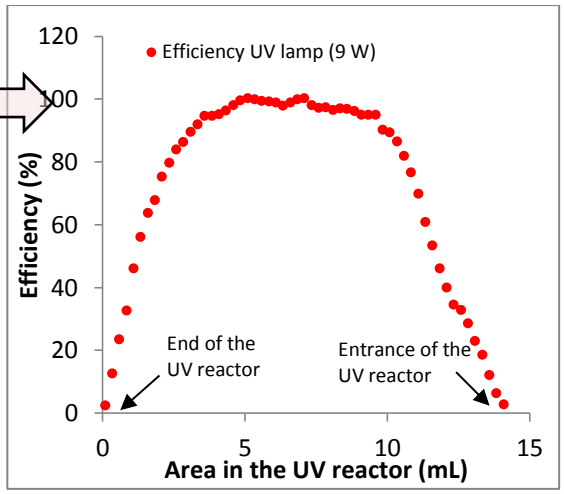

Figure 5.49: Conversion of the GC data into % efficiency of the lamp according to the area in the UV reactor (14.1 mL, UV-A 9W).

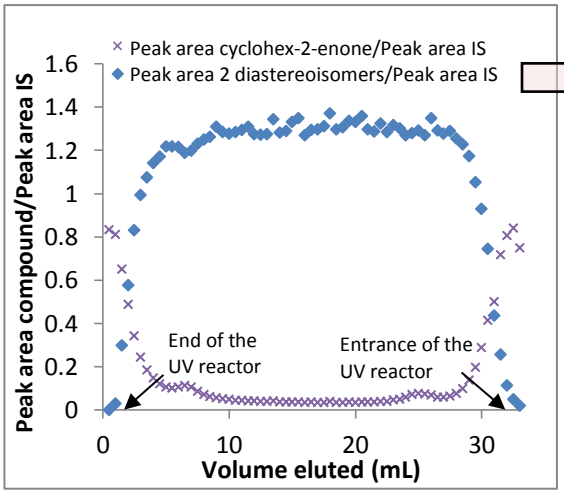

Figure 5.50: GC data of the different vials collected at the exit of the reactor (31.8 mL, UV-A 36 W) - light on during 30 min.

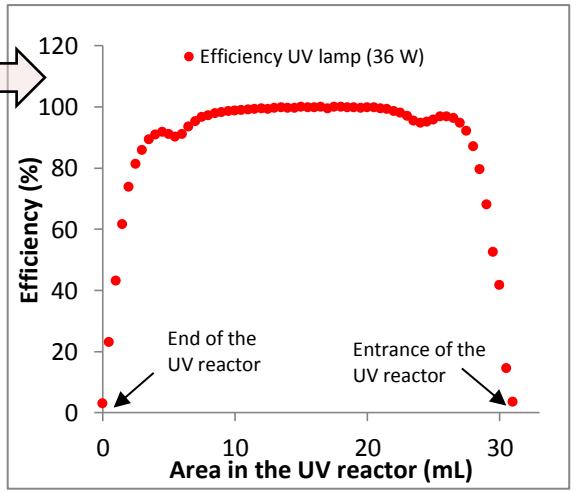

Figure 5.51: Conversion of the GC data into % efficiency of the lamp according to the area in the UV reactor (31.8 mL, UV-A 36 W). The dips at each ends are due to the locating clips on the lamp.

5.4.3 Application of this turn off light methodology on a [2 + 2] photocycloaddition between the cyclohex-2-enone and the tetramethylethylene (A + B → D)

The first photochemical reaction investigated with this novel methodology was the 2nd order [2 + 2] photo-cycloaddition between the cyclohex-2-enone and the tetramethylethylene (Scheme 5.13). The different attempts performed with this methodology and the different results after GC analysis and processing of the data (see experimental part) are highlighted in the following Table 5.7 and Figures 5.52 to 5.56.

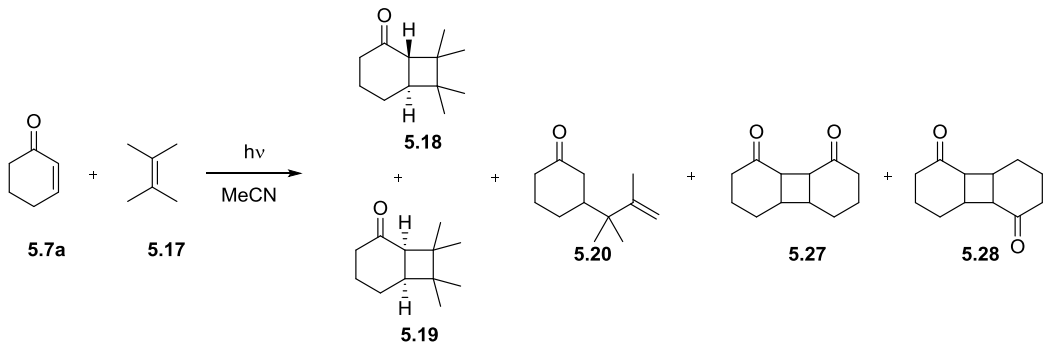

Scheme 5.13: [2 + 2] photocycloaddition of cyclohex-2-enone and tetramethylethylene - Turn off light experiments.

Entry	Reagent A	Reagent B	Internal Standard	Reaction conditions								
				equiv. A	[A][a] (M)	equiv. B	[B][b] (M)	[IS][c] (M)	flow rate (mL/min)	Reaction time (min)	UV lamp	UV reactor
1			dibutyl ether	1	0.025	19.6	0.50	0.022	0.058	240	UV-A 9 W	Single coiled 14.1 mL
2			dibutyl ether	1	0.025	19.6	0.50	0.022	0.058	240	UV-C 9 W	Single coiled 14.1 mL
3			dibutyl ether	1	0.025	19.6	0.50	0.022	0.133	240	UV-A 36 W	Single coiled 31.8 mL
4			dibutyl ether	1	0.025	19.6	0.50	0.022	0.133	240	UV-B 36 W	Single coiled 31.8 mL
5	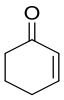		dibutyl ether	1	0.025	19.6	0.50	0.022	0.133	240	UV-C 36 W	Single coiled 31.8 mL

Table 5.7: Turn off light experiments performed in the single coiled 14.1 and 31.8 mL photoflow reactors.
[a] [A] Concentration of reagent A in the stock solution 1. [b] [B] Concentration of reagent B in the stock solution 1. [c] [IS] Concentration of Internal Standard in the stock solution 1.

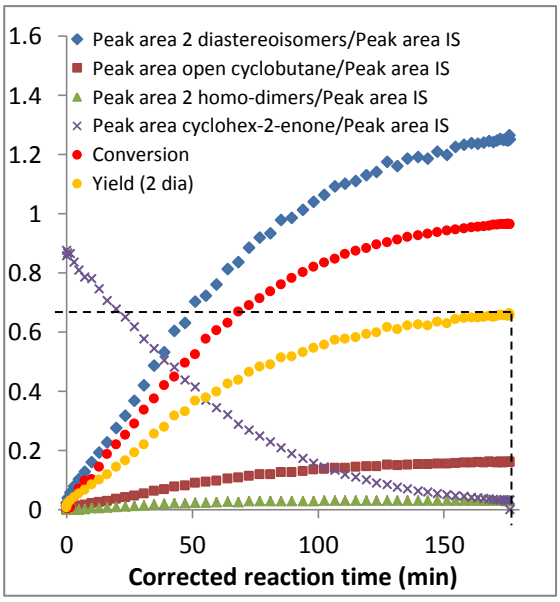

Figure 5.52: Turn off light results - Table 5.7, entry 1 (UV-A 9 W).

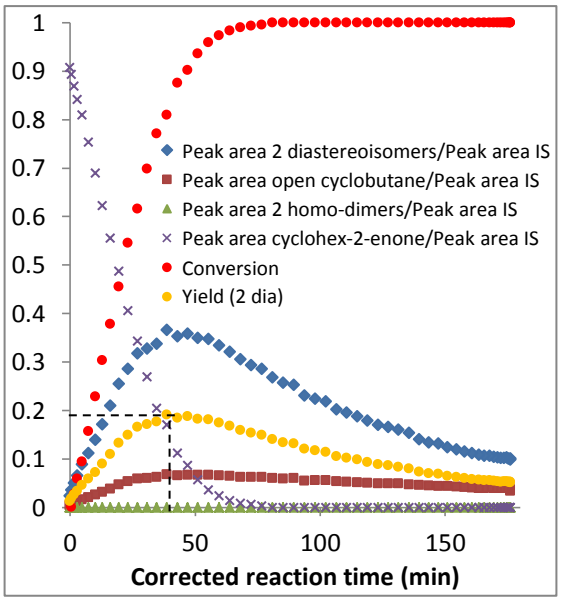

Figure 5.53: Turn off light results - Table 5.7, entry 2 (UV-C 9 W).

These first two attempts were performed with the low energy UV-A and UV-C lamps (9 W) (Figures 5.52 and 5.53 respectively). 66% and 19% are the maximum yields obtained after 175 and 45 min respectively (corrected reaction time). For the UV-C experiment, the degradation of the product after about 45 min is due to the over exposure of the reaction mixture to the higher energy UV irradiation (UV-C). In the range of reaction time studied, this degradation is not present with the UV-A lamp.

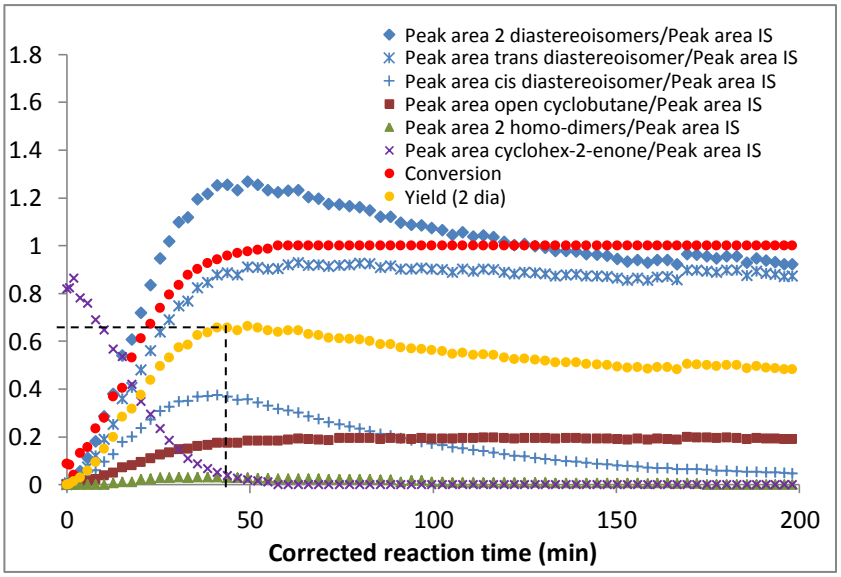

Figure 5.54: Turn off light results - Table 5.7, entry 3 (UV-A 36 W).

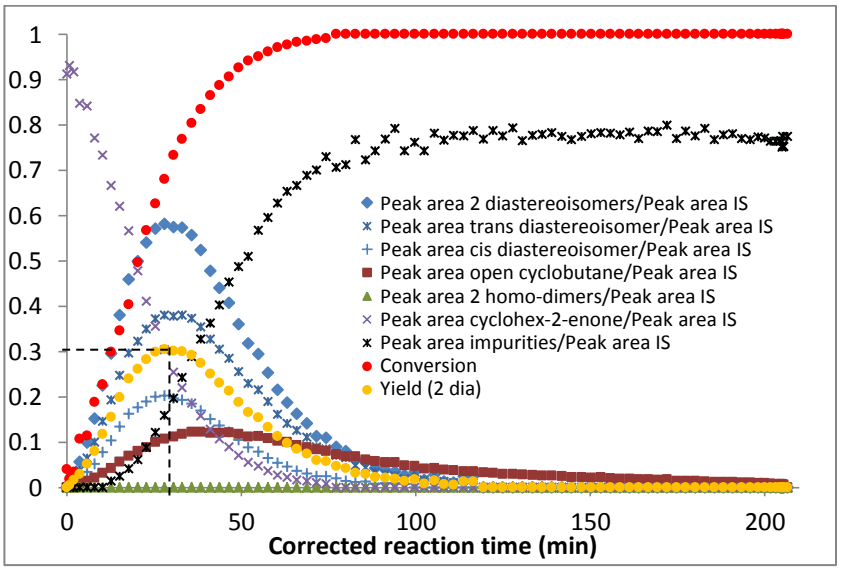

Figure 5.55: Turn off light results - Table 5.7, entry 4 (UV-B 36 W).

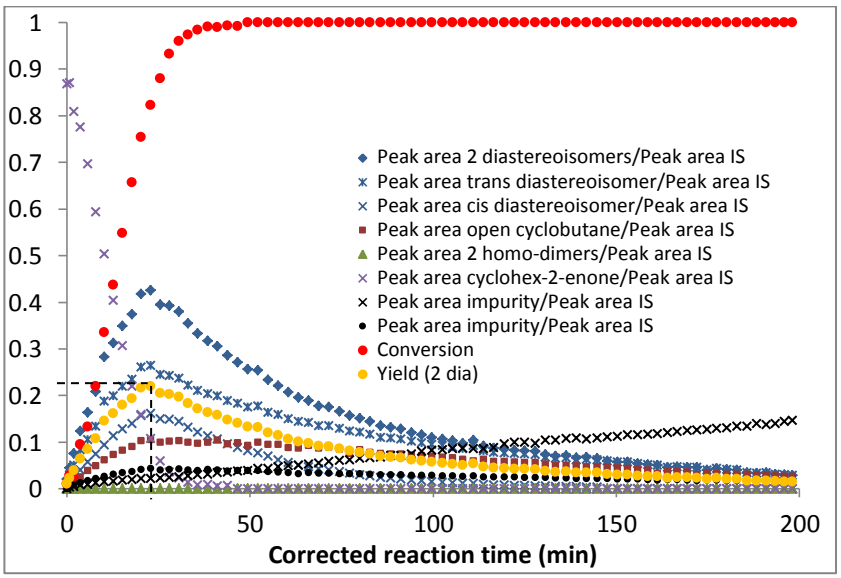

Figure 5.56: Turn off light results - Table 5.7, entry 5 (UV-C 36 W).

These 3 last attempts were performed with a higher power UV-A, B and C lamps (36 W) (Figures 5.54, 5.55 and 5.56 respectively). 65%, 30% and 22% (UV-A, B and C) are the maximum yields obtained after 45, 28 and 23 min respectively (corrected reaction time). Compared to the lower energy lamps (Figures 5.52 and 5.53), the maximum yields are consistent but are achieved after a shorter reaction time. Regarding the UV-B and C experiments (Figures 5.55 and 5.56), complete degradation of the product was observed for long reaction time, due to over exposure of the reaction mixture to the higher energy radiations. Regarding the UV-A experiments (Figure 5.54), specific degradation of the cis-diastereoisomer is highlighted after about 45 min.

5.4.4 Application of this turn off light methodology on a [2 + 2] photocycloaddition between the 2,2,6-trimethyl-4*H*-1,3-dioxin-4-one and the tetramethylethylene (A + B → D)

5.4.4.1 Preliminary study on the [2 + 2] photocycloaddition between the 2,2,6-trimethyl-4*H*-1,3-dioxin-4-one and the tetramethylethylene

As the 2,2,6-trimethyl-4*H*-11,3-dioxin-4-one (**2.38**) was widely used during the kinetic study section, the [2 + 2] photocycloaddition between this dioxinone and the tetramethylethylene (**5.17**) was tried using the turn off light methodology.

As a preliminary experiment and based on Baldwin's study,[125] the synthesis of **5.29** (Scheme 5.14) was investigated using our Vapourtec system. Equipped with the 28.0 mL double coiled photoflow reactor (UV-C lamp, 9 W), a mixture of dioxinone **2.38** (1 equiv.) and tetramethylethylene (**5.17**, 20 equiv.) in MeCN ($[C_{dioxinone}]$ = 0.05 M) was injected into the flow set-up. After 120 min (88 min corrected reaction time), the reaction mixture was collected at the end of the reactor and purified on silica gel. The target product **5.29** was isolated in low yield (22%). The same experiment was performed with the UV-A and UV-B lamp but no product was formed (2,2,6-trimethyl-4*H*-1,3-dioxin-4-one absorbs at 245 nm). In order to find the optimum reaction time and increase the yield of this reaction, the turn off light experiment was applied.

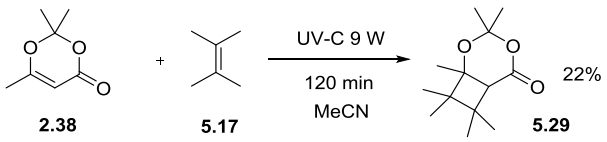

Scheme 5.14: [2 + 2] photocycloaddition of 2,2,6-trimethyl-4*H*-11,3-dioxin-4-one (**2.38**) and tetramethylethylene (**5.17**).

5.4.4.2 Application of the turn off light experiment

The attempt performed with this methodology and the results after GC analysis and processing of the data are highlighted in the following Table 5.8 and Figure 5.57.

Entry	Reagent A	Reagent B	Internal Standard	Reaction conditions								
				equiv. A	[A][a] (M)	equiv. B	[B][b] (M)	[IS][c] (M)	flow rate (mL/min)	Reaction time (min)	UV lamp	UV reactor
1	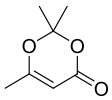		dibutyl ether	1	0.05	20	1	0.044	0.116	120	UV-C 9 W	Single coiled 14.1 mL

Table 5.8: Turn off light experiments performed in the single coiled 14.1 mL photoflow reactor.
[a] [A] Concentration of reagent A in the stock solution 1. [b] [B] Concentration of reagent B in the stock solution 1. [c] [IS] Concentration of Internal Standard in the stock solution 1.

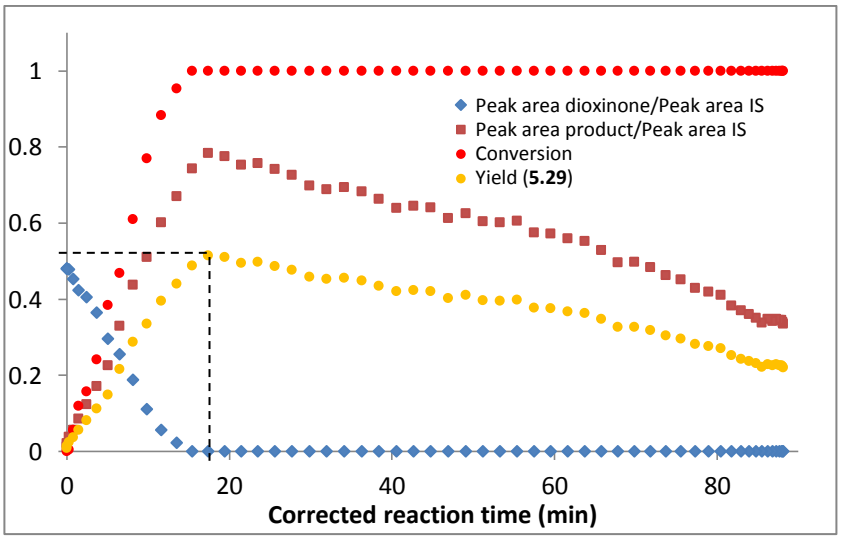

Figure 5.57: Evolution of Peak area compounds/Peak area IS, conversion and yield according to the corrected reaction time (UV-C 9 W).

Having these results, the best conversion and yield (100 and 53% respectively) are obtained after 18 min (corrected reaction time). During the preliminary experiment (Scheme 5.14), the reaction time applied (120 min, 88 min corrected reaction time) was too long and over-irradiation is the reason of the degradation of the product and the low yield of the reaction.

5.4.5 Application of this turn off light methodology on the photocyclisation of cis-stilbene (A → D)

As a third model reaction for the application of the turn off light methodology, the 1st order photocyclisation of cis-stilbene (**5.21**), the so-called Mallory photocyclisation, to afford phenanthrene (**5.23**) was investigated (Scheme 5.15). As the UV absorption of the cis-stilbene is in the range 240-320 nm,[124] turn off light experiments with UV-A, B and C lamps were

performed. The following Table 5.9 and Figures 5.58 to 5.63 describe the various attempts with different initial conditions carried out with the 31.8 mL photoflow reactor.

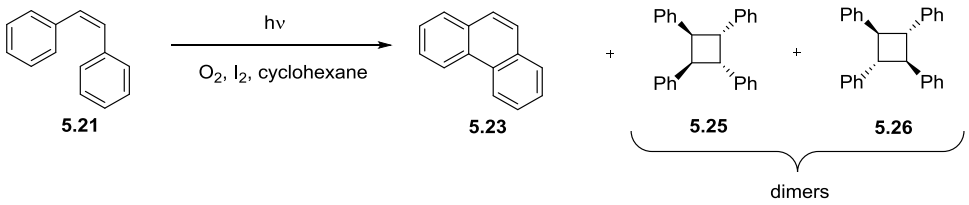

Scheme 5.15: Photocyclisation of cis-stilbene - Turn off light experiments.

Entry	Reagent A	Internal Standard	Reaction conditions					
			[A][a] (M)	[IS][b] (M)	flow rate (mL/min)	Reaction time (min)	UV lamp	UV reactor
1		dibutyl ether	0.0050	0.018	0.707	45	UV-A 36 W	Single coiled 31.8 mL
2		dibutyl ether	0.050	0.18	0.177	180	UV-A 36 W	Single coiled 31.8 mL
3		dibutyl ether	0.0050	0.018	0.707	45	UV-B 36 W	Single coiled 31.8 mL
4		dibutyl ether	0.050	0.18	0.177	180	UV-B 36 W	Single coiled 31.8 mL
5		dibutyl ether	0.0050	0.018	0.707	45	UV-C 36 W	Single coiled 31.8 mL
6		dibutyl ether	0.050	0.18	0.177	180	UV-C 36 W	Single coiled 31.8 mL

Table 5.9: Turn off light experiments performed in the single coiled 31.8 mL photoflow reactor.
[a] [A] Concentration of reagent A in the stock solution 1. [b] [IS] Concentration of Internal Standard in the stock solution 1.

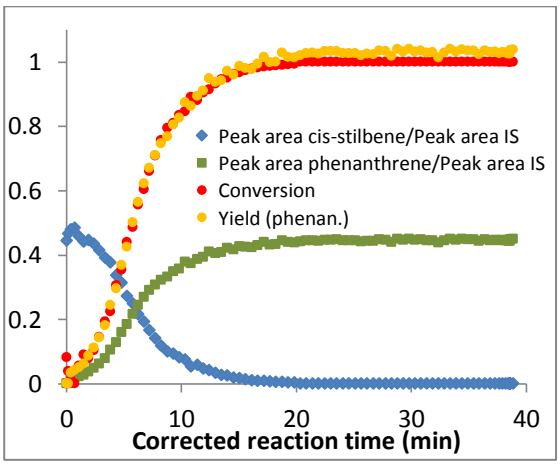

Figure 5.58: Turn off light results - Table 5.9, entry 1 (UV-A).

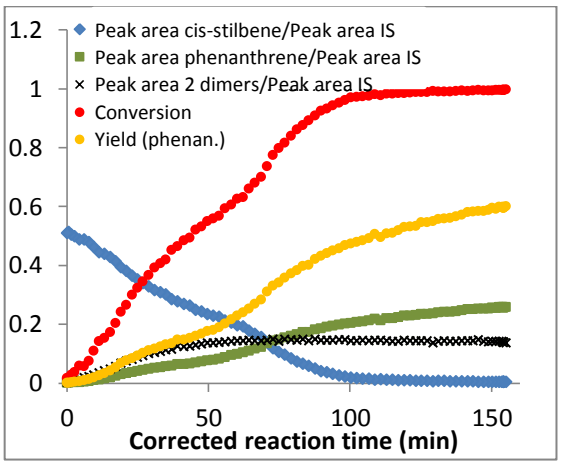

Figure 5.59: Turn off light results - Table 5.9, entry 2 (UV-A). The odd behaviour is due to the formation of dimers which are poorly soluble in cyclohexane (blockage)

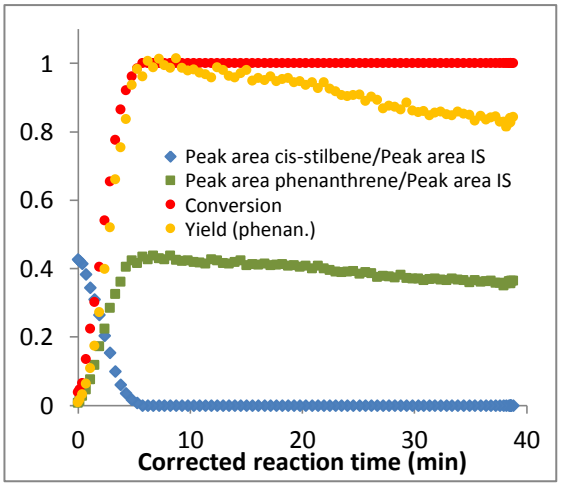

Figure 5.60: Turn off light results - Table 5.9, entry 3 (UV-B).

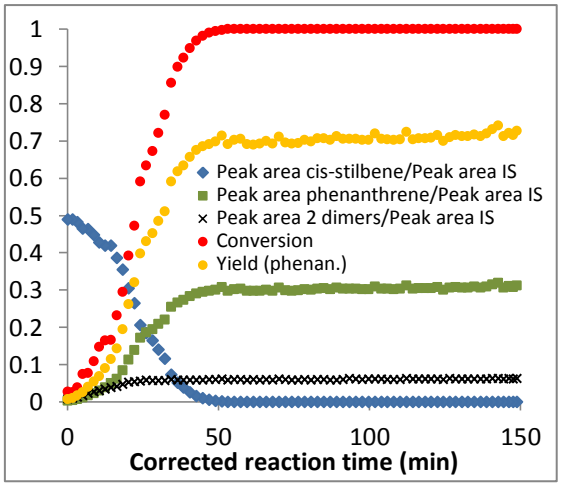

Figure 5.61: Turn off light results - Table 5.9, entry 4 (UV-B).

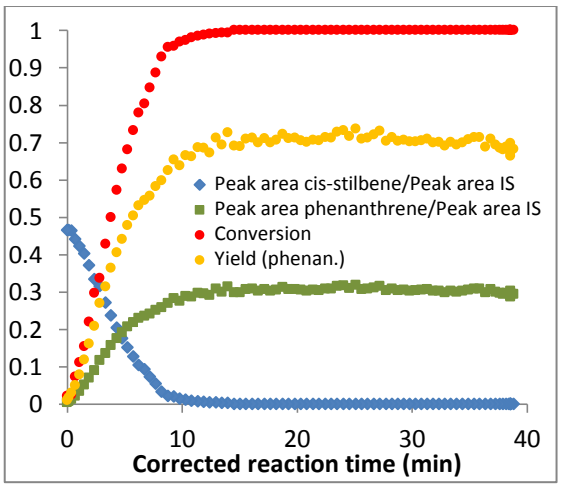

Figure 5.62: Turn off light results - Table 5.9, entry 5 (UV-C).

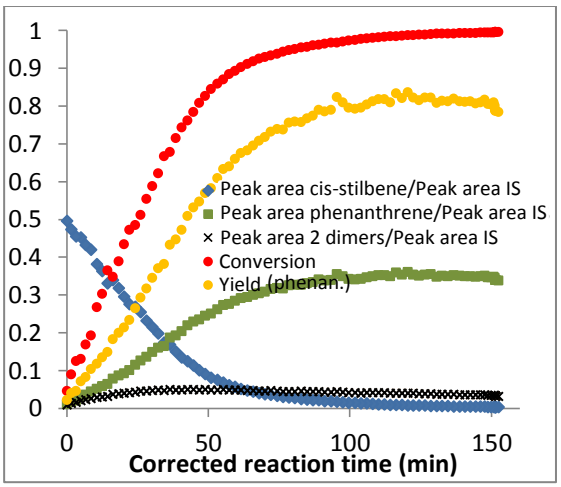

Figure 5.63: Turn off light results - Table 5.9, entry 6 (UV-C).

For low concentration of cis-stilbene ([C] = 0.005 M) (Table 5.9, entries 1, 3 and 5), the UV-A and UV-B lamps highlights the best results with 100% yield for reaction times of 16 and 6 min respectively (Figures 5.58 and 5.60). To confirm Figure 5.58 results, the cyclisation experiment with exactly the same initial conditions and equipment ([cis-stilbene] = 0.005 M, 31.8 mL single coiled reactor, UV-A 36 W) was performed for a reaction time of 30 min (26 min corrected reaction time) (Scheme 5.16). The phenanthrene was isolated in 96% yield which is consistent with the turn off light data (96% *vs.* 100%). No dimers were formed.

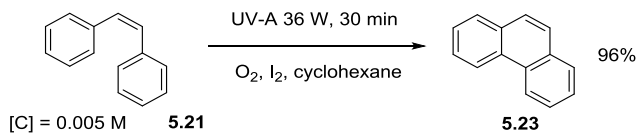

Scheme 5.16: Phenanthrene synthesis in flow chemistry - Low concentration.

For higher concentration of cis-stilbene ([C] = 0.050 M) (Table 5.9, entries 2, 4 and 6), the best results are obtained with the UV-C lamp (80% yield after 95 min) (Figure 5.63). For these 3 different attempts (Figures 5.59, 5.61 and 5.63), the formation of dimers of the stilbene **5.25** and **5.26** is observed. In the same way, to confirm Figure 5.59 results, the cyclisation experiment with exactly the same initial conditions and equipment ([cis-stilbene] = 0.050 M, 31.8 mL single coiled reactor, UV-A 36 W) was performed for a reaction time of 180 min (156 min corrected reaction time) (Scheme 5.17). The phenanthrene was isolated in 55% yield which is consistent with the GC data (55% *vs.* 60%).

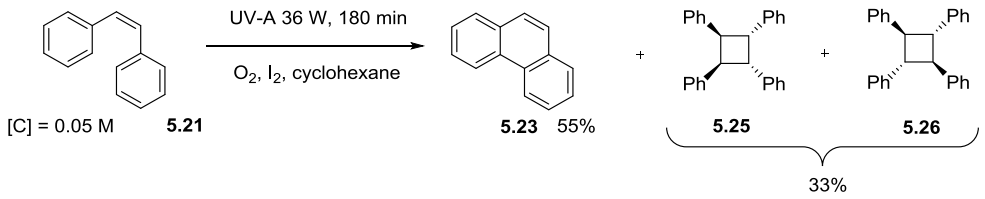

Scheme 5.17: Phenanthrene synthesis in flow chemistry - High concentration.

5.4.6 Application of this turn off light methodology on a $S_{RN}1$ reaction (A + B + C → D)

5.4.6.1 Preliminary study on the $S_{RN}1$ reaction

The $S_{RN}1$ reaction has been widely used in organic synthesis to achieve new carbon-carbon bonds. The mechanism of this reaction is described in the following Scheme 5.18.

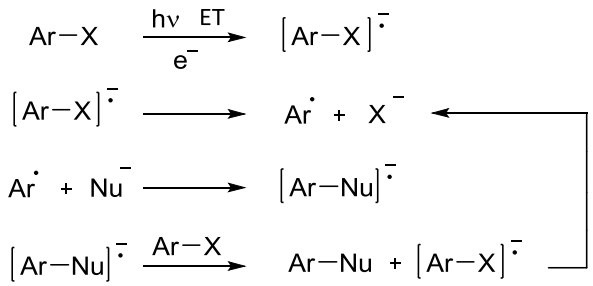

Scheme 5.18: Mechanism of $S_{RN}1$ reactions.

Based on the work developed by Beugelmans,[126] the $S_{RN}1$ reaction between 2-bromobenzonitrile (**5.30**) and ethyl 2-cyanoacetate (**5.31**) was used as a final model to illustrate our new turn off light methodology. As the UV absorption of the 2-bromobenzonitrile is in the range 260-300 nm, the preliminary synthesis of the ethyl 2-cyano-2-(2-cyanophenyl)acetate (**5.32**) was performed using the UV-B lamp. With complete conversion, 50% yield was obtained for a reaction time of 120 min (104 min corrected reaction time) (Scheme 5.19).

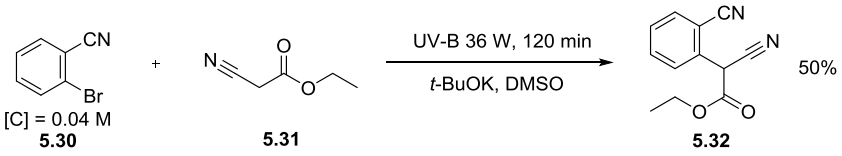

Scheme 5.19: Formation of ethyl 2-cyano-2-(2-cyanophenyl)acetate (**5.32**) through a $S_{RN}1$ reaction.

5.4.6.2 Application of the turn off light experiment

Based on this preliminary result (Scheme 5.19), investigations about the optimum reaction time were carried out using the turn off light methodology (Table 5.10 and Figure 5.64). For this particular reaction, the *in situ* formation of ethyl 2-cyano-2-(2-cyanophenyl)acetate salt requires the addition of acid (TFA) before GC analysis.

Reaction conditions											
Reagent A		Reagent B		IS		Reagent C			Reaction time (min)	UV lamp	UV reactor[e]
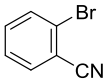		*t*-BuOK		Triethylene glycol dimethyl ether		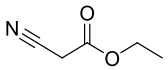					
Stock solution 1						Stock solution 2					
equiv. A	[A][a] (M)	equiv. B	[B][b] (M)	[IS][c] (M)	flow rate (mL/min)	equiv. C	[C][d] (M)	flow rate (mL/min)			
1	0.080	4	0.32	0.092	0.133	4	0.32	0.133	120	UV-B 36 W	Single Coiled 31.8 mL

Table 5.10: Turn off light experiment performed in the single coiled 31.8 mL photoflow reactors.
[a] [A] Concentration of reagent A in the stock solution 1. [b] [B] Concentration of reagent B in the stock solution 1. [c] [IS] Concentration of IS in the stock solution 1. [d] [C] Concentration of reagent C in the stock solution 2. [e] At the end of the UV reactor and before the collection in the GC vials, a flow of a solution of TFA in DMSO was injected in the reaction mixture.

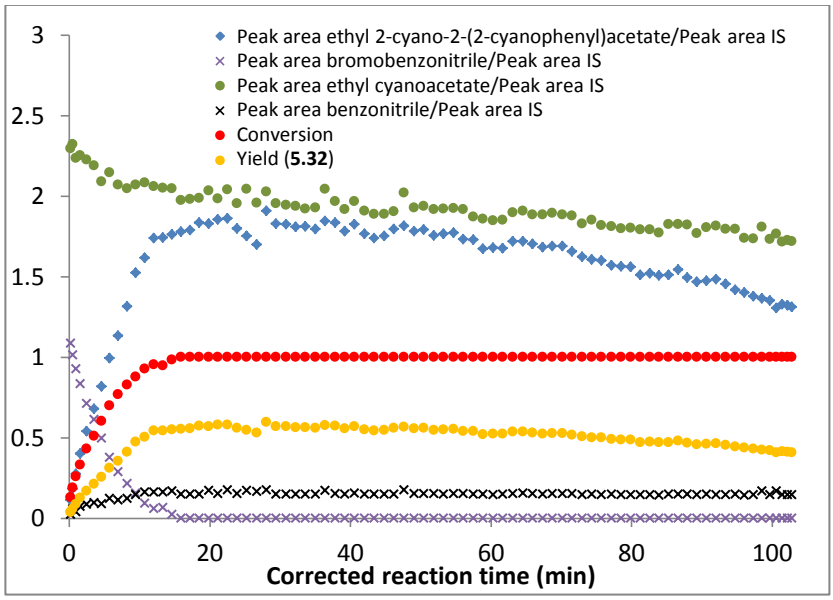

Figure 5.64: Turn off light results - Table 5.10.

According to Figure 5.64, the best yield obtained during this turn off light experiment is 55% which remains constant between 10 and 50 min of reaction time. This medium yield can be explained by the formation of benzonitrile by-product by a C-Br cleavage during the irradiation. Degradation of the product is highlighted after 50 min of irradiation. For the same reaction conditions, good consistency was obtained between the preliminary experiment yield (Scheme 5.19) and the turn off light yield for 104 min corrected reaction time (50% *vs*. 43%).

To conclude with the turn off light experiments, it has been shown with these 4 model reactions ([2 + 2] photocycloadditions, Mallory photocyclisation, and $S_{RN}1$ reaction) that it is possible to quickly find with our single coiled photoflow reactor the optimum reaction time. Consistent values of yield were obtained between the reaction at a particular reaction time and the turn off light results which highlight the reliability of the method. This new method is intended to be broadly applicable to a wide range of chemical reactions (e.g. thermal reactions) for which optimum reaction time needs to be determined.

6 Conclusion and future work

During this Ph.D. thesis, the potential of flow chemistry has been demonstrated (precise control of reaction parameters, high level of automation, in-line analysis, efficient heat transfer and access to more hazardous reactions).

After unfavourable results in the optimisation of final steps of the synthesis of epicocconone analogues and in the *in situ* generation of isocyanides, the development of an efficient and innovative methodology based in a step-change in flow rate and in-line analysis for rapid acquisition of kinetic information has been described (Figure 6.1). This powerful procedure, developed using the thermolysis of 1,3-dioxoin-4-ones as model reactions (1st order), offers very interesting feature such as cutting down the time spent to solve kinetic investigations and can be used as a reliable tool to accelerate reaction study and process development. The application of this procedure to 2nd order reactions could be an interesting target for future research.

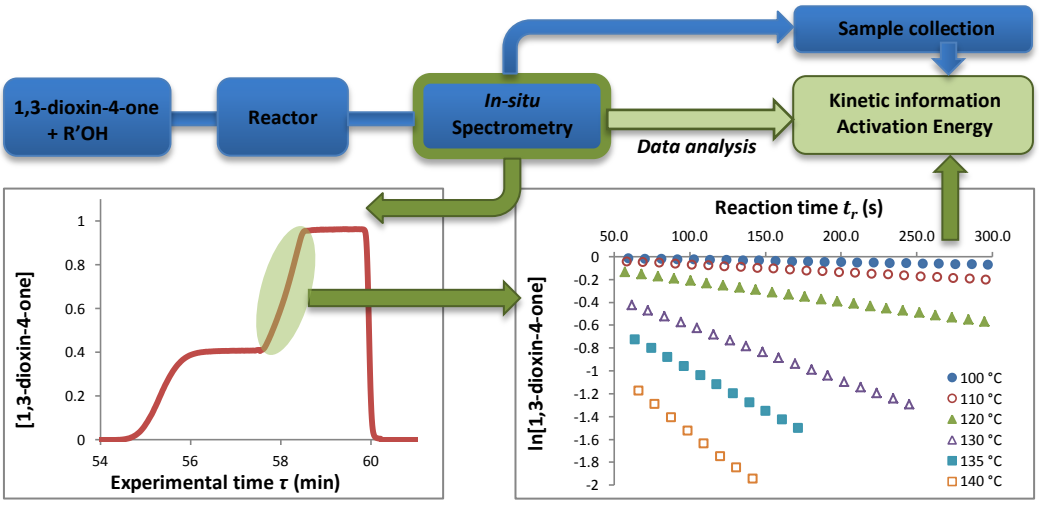

Figure 6.1: Overall view of the fast kinetic study procedure: The push-out method

Then, other novel methodologies were developed to quickly optimise reaction conditions. The concentration gradient procedure based on the dispersion phenomenon was first investigated for the fast determination of kinetic information of 1st (thermolysis of 2,2,6-trimethyl-4*H*-1,3-dioxin-4-one) and 2nd order reactions (Diels-Alder reaction). This methodology will be pursued with other reactions to highlight its reliability. Then, this concentration gradient methodology was developed to rapidly extract reaction information like the conversion or the yield as a function of the amount of dispersed reagent (Figures 6.2

and 6.3). The entire profile can be extracted with only one experiment whereas conventional methodologies will require one reaction for each desired data point.

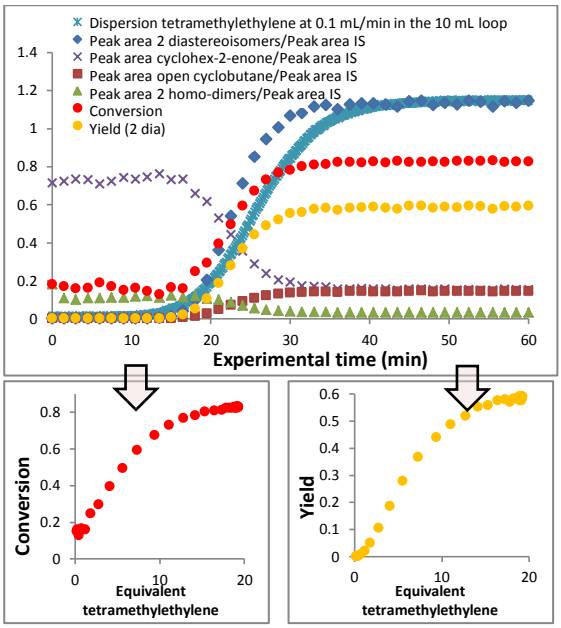

Figure 6.2: Concentration gradient procedure, [2 + 2] photocycloaddition.

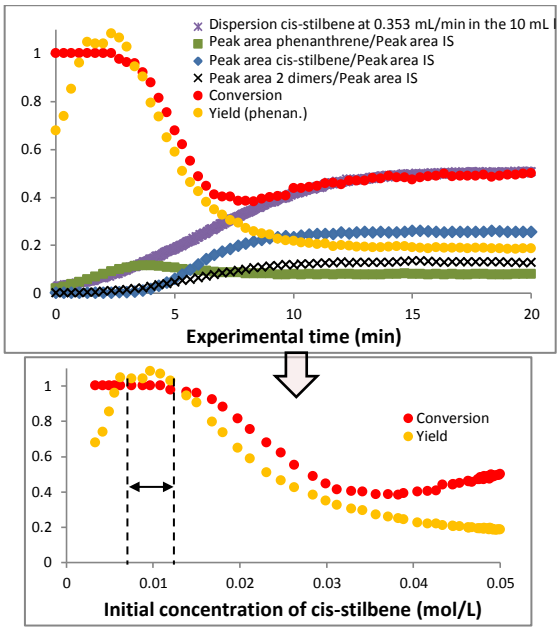

Figure 6.3: Concentration gradient procedure, Mallory photocyclisation.

Finally, the turn off light methodology applied to [2 + 2] photocycloadditions, photocyclisations and $S_{RN}1$ reactions demonstrated the efficiency and the reliability of the procedure for the fast determination of the optimum reaction time. The application of this procedure to thermal reactions would be an interesting target for future research.

The development of these efficient and innovative methodologies is really promising towards the fast optimisation of reaction conditions using continuous flow processing as they can considerably impact on synthetic procedures and chemical engineering.

7 Experimental Part

7.1 Instrumentation, general analytical techniques and general procedures in flow chemistry

NMR Analysis: NMR spectra were recorded on Bruker AV-300 (300/75 MHz) or Bruker DPX-400 (400/100 MHz) spectrometers in the deuterated solvents indicated ($CDCl_3$ or DMSO-d_6) at 298 K. The residual peak of the solvent was used as reference for ^1H spectra (7.27 ppm for $CDCl_3$ and 2.50 ppm for DMSO-d_6) and ^{13}C spectra (77.00 ppm for $CDCl_3$ and 39.51 ppm for DMSO-d_6). The information related to the spectra are written as follows: the chemical shift δ (in ppm), the multiplicity (s = singlet, d = doublet, t = triplet, q = quartet, quin = quintet, sxt = sextet, m = multiplet), the coupling constant *J* (in Hz), the integration and the atom concerned. DEPT, COSY, HSQC and HMBC correlation experiments were used to aid assignment of spectra. The numbered assignment for proton and carbon signals is for identification purposes only and does not represent the systematic IUPAC numbering.

Mass Spectrometry Analysis: Electron impact ionisation mass spectra (EI) and chemical ionisation (CI) were recorded on a ThermoQuest TraceMS GCMS. Electrospray mass spectra (ES) were recorded using Microsaic 4000 MID quadrupole spectrometer using ES^+ or ES^- ionisation. The electrospray is previously linked to an HPLC (HP Agilent 1100 platform) using a Sigma Aldrich Hypersil ODS C18 column (5 µm, 4.6 x 150 mm). The gradient was 20-95% MeCN in water within 10 min and 2 min hold. The column was kept at 30 °C. The UV detection was a summed signal from wavelength of 210 nm to 350 nm.

Accurate mass spectra were recorded on a VG analytical 70-250-SE double focussing mass spectrometer using electron impact ionisation (EI) at 70eV or a Bruker Apex III using electrospray ionisation or Orbitrap - Biomax 088259.

Infrared Analysis: Infrared spectra were run as neat films on a Thermo Nicolet 380 FT-IR spectrometer with a Smart Orbit Goldengate ATR attachment.

All *in situ* IR measurements were recorded on Bruker ALPHA FT-IR Universal Sampling Module at room temperature using OPUS Software. Harrick's DLC 2™ Demountable Liquid Flow Cell with NaCl windows and 100 µm spacers was connected to the flow system at the indicated positions.

Absorptions are given in wavenumbers (cm^{-1}). Peaks are recorded as s (strong), m (medium), w (weak), sh (shoulder) and br (broad).

UV-vis Analysis: Ultra Violet measurements were recorded with the Ocean Optics DH-2000-BAL UV spectrometer at room temperature using SpectraSuite Software. All *in situ* UV measurements were performed with a Type 583-F Starna® fluorimeter flow cell (path length: 1 mm, volume: 0.011 mL). The other UV measurements were run with UV Fused Quartz cuvette (path length: 10 mm, volume: 3.5 mL). The wavelengths are given in nanometers and the corresponding extinction coefficient in $M^{-1}.cm^{-1}$.

Melting Points: Melting points were recorded on a GallenKamp melting point apparatus and are uncorrected.

GC Analysis: GC was performed on a Hewlett Packard HP 6890 series GC system, using a HP-5 (cross-linked 5% Ph Me siloxane) 30 m column, with a film thickness of 0.25 µm and 0.32 mm internal diameter. The carrier gas was helium and the flow rate was 2.7 mL min^{-1}. The injector is maintaining at 300 °C with 1 µL injection. The run start at 80 °C with a gradient of 25 °C/min until 275 °C which is hold during 4 min.

HPLC Analysis: All HPLC experiments were run on HP Agilent 1100 platform using a Zorbax SB-C18 column (1.8 micron, 3.0 x 50 mm rapid resolution). The gradient was 20-95% MeCN in water over 10 min and a 5 min hold. The column was kept at 60 °C. The UV detection was a summed signal from wavelength of 190 nm to 400 nm

TLC Analysis: TLC was performed using Merck silica gel 60 Å F_{254} plates with detection by UV and/or various stains (phosphomolybdic acid, potassium permanganate, iodine, 5% sulfuric acid in methanol).

DFT Calculation: DFT calculations (B3LYP/6-31G(d)) using Spartan software were performed by Prof Richard J. Whitby.

General Experimental Procedures: When needed, experiments were performed under argon or nitrogen atmosphere. The glassware was dried in an oven (160 °C for at least 12 h) before cooling in a sealed desiccator over silica gel.

DCM, DMSO and MeCN were freshly distilled from CaH_2. Et_2O, THF and toluene were freshly distilled from sodium/benzophenone. *n*-BuLi was used as a 2.5 M solution in hexane and was stored at 4 °C. All other solvents and commercially available reagents were used as received or purified using standard procedures.

Purifications were performed using either silica gel 60A from Fisher Scientific or basic alumina Brockman I deactivated with 6% of H_2O (for acid sensitive products). Columns were packed and run under light pressure. Solvent compositions are described as ratios prior to mixing.

Flow Experiments: The Vapourtec® R series Integrated Flow Chemistry System (R2+/R2+/R4) was the platform used for the flow experiments. Various configurations (bottle-feed, sample loop, Stainless Steel and PFA reactor) and customisation of this platform (photochemical flow reactor, Grant Optima™ TXF200 heated bath with high temperature silicone oil with home-made Stainless Steel reactor, UV and IR spectrometers, sample collector, auto sampler, Gilson Prep Fraction Collector) enables a large access of reaction conditions and analyses. Flow consumables such as HPLC fittings, ferrules, check valves, tubing, back pressure regulators, seals and mixers were employed to perform the various flow reactions and to ensure the proper functioning of the platform.

General Procedure for a Thermal Reaction in Flow: Using the flow machine (Vapourtec R2+/R2+/R4), the thermal reactions were performed either with bottle-feed or sample loop (10 µL, 2, 5 or 10 mL) configurations. Two types of reactor were employed: either the Stainless Steel reactor (SS, 10 mL capacity, ambient to 250 °C) or the plastic reactor (PFA, 5 or 10 mL capacity, ambient to 150 °C). The SS reactor was connected to a 100 cm cooling loop (1 mm i.d.). To increase the boiling point of the solvent, an appropriate Back-Pressure Regulator (BPR) was connected to the exit of the reactor (40, 100 or 250 psi). During an experiment, the stock solution was injected straight into the reactor or into the sample loop, and pumped at the indicated flow rate FR (which corresponds to a residence time RT = Volume reactor/FR) and at the indicated temperature. At the end of the reaction, when indicated, the mixture was pumped through an in-line spectrometer (UV or IR), was then collected either by sample collector or into a round bottom flask and then treated as described.

General Procedure for a Photochemical Reaction in Flow: Using the flow machine (Vapourtec R2+/ R2+/R4), the photochemical reactions were performed either with bottle-feed or sample loop (2, 5 or 10 mL) configurations. The reaction mixture was degassed by sonication whilst being saturated with nitrogen gas or air. Before starting the reaction, the indicated UV lamp (Philips 2-pin PL-S 9 W UV-A/B/C or Philips 4-pin PL-L 36 W UV-A/B/C) was switched on and left to warm up for 10-15 minutes. The water cooling system was turned on. During an experiment, the stock solution was injected straight into the UV reactor (single or double coiled with 14.1, 28.0 or 31.8 mL capacity) or into the sample loop and pumped at the indicated flow rate FR (which corresponds to a residence time RT = Volume reactor/FR). At the end of the reaction, when indicated, the mixture was pumped through an in-line spectrometer (UV or IR), was then collected either by sample collector or into a round bottom flask and then treated as described.

7.2 Procedures and analytical data

7.2.1 Chapter 2: Flow chemistry - A tool for optimisation of complicated batch reactions

2,2-Dimethyl-6-(2-(2-naphthyl)-2-oxoethyl)-4*H*-1,3-dioxin-4-one (**2.28c**)

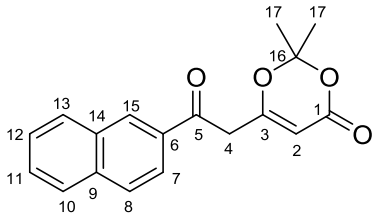

$C_{18}H_{16}O_4$

MW = 296.32 g.mol $^{-1}$

R*f* = 0.19 (hexane/acetone, 8:2)

Pale yellow solid

Yield = 40%

m.p. = 104 °C

In a RBF flushed with argon, *n*-BuLi at 2.5 M in hexane (4.04 mL, 10.1 mmol) was slowly added at -78 °C to a 50 mL THF solution containing DIPA (1.40 mL, 10.0 mmol). After 30 min at 0 °C, the media was cooled again at -78 °C and 2,2,6-trimethyl-4*H*-1,3-dioxin-4-one (**2.38**, 1.33 mL, 10.0 mmol) was added dropwise. Finally, after 50 min at -78 °C, naphthoyl chloride (0.95 g, 5.0 mmol) was added dropwise at this temperature. After the addition was complete, the media was left at -40 °C for 2 h and 30 min. The reaction mixture was quenched at 0 °C with HCl (20 mL of 1 M aq.) and extracted three times with EtOAc (3 x 50 mL). The combined organic layers were the washed with brine (3 x 50 mL), dried over $MgSO_4$, filtered and the solvent was evaporated under reduced pressure to afford the crude product. This crude material was then purified on silica gel (hexane/acetone, 8:2) to give the title compound **2.28c** (0.60 g, 2.0 mmol, 40%) as a pale yellow solid, m.p. = 104 °C (lit. m.p. = 119 °C, lit. yield = 43%).[29] NMR data are consistent with the literature.[29, 32]

^{1}H NMR (400 MHz, $CDCl_3$) δ ppm: 8.46 (d, *J* = 1.0 Hz, 1H, ArH), 8.03-7.88 (m, 4H, ArH), 7.69-7.57 (m, 2H, ArH), 5.48 (s, 1H, H-2), 4.04 (s, 2H, H-4), 1.73 (s, 6H, H-17).

^{13}C NMR (75 MHz, $CDCl_3$) δ ppm: 192.9 (C, C-5), 165.2 (C, C-3), 160.7 (C, C-1), 135.9 (C), 133.2 (C), 132.4 (C), 130.4 (CH), 129.6 (CH), 129.1 (CH), 128.9 (CH), 127.9 (CH), 127.2 (CH), 123.5 (CH), 107.3 (C, C-16), 97.0 (CH, C-2), 43.4 (CH_2, C-4), 25.0 (CH_3, C-17).

UV (MeCN) C = 1.88x10^{-5} M, $\lambda = 250.75$ nm, $\varepsilon = 48983$ M^{-1}.cm^{-1}.

IR ν_{max}(neat)/cm^{-1} = 1724 (s), 1676 (m), 1371 (m), 1272 (m), 1179 (m), 811 (s), 764 (m), 472 (m).

(*Z*)-3-(3-Hydroxy-3-(naphthalen-2-yl)acryloyl)-4,5,5-trimethylfuran-2(5*H*)-one (**2.30c'**) and 1-(Naphthalen-2-yl)-3-(4,5,5-trimethyl-2-oxo-2,5-dihydrofuran-3-yl)propane-1,3-dione (**2.30c**)

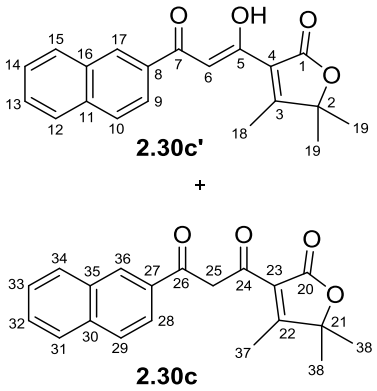

$C_{20}H_{18}O_4$

MW = 322.35 g.mol^{-1}

Yellow-orange solid

Purity = 93%

Yield = 94%

Ratio keto/enol: 10/90

m.p. = 132 °C

In a RBF flushed with argon, 2,2-dimethyl-6-(2-(2-naphthyl)-2-oxoethyl)-4*H*-1,3-dioxin-4-one (**2.28c**, 122 mg, 0.412 mmol) and dried 3-hydroxy-3-methylbutan-2-one (**2.25** distilled over CaH_2, 41.9 mg, 0.412 mmol) were dissolved in dried toluene (distilled) to make a 5 mL solution ([dioxinone] = 24 g/L). This solution was injected into the flow set-up described below using the sample loop configuration. Then, the content of the loop was pushed by toluene (Stock solvent) into the flow stream. The residence time was set at 10 min (flow = 1 mL/min) and the oil bath was heated to 120 °C. The 10 mL Stainless Steel reactor was connected to a cooling loop (100 cm, 1 mm i.d.) followed by a backpressure regulator (250 psi). At the end of the reaction, the product was poured into a 20 mL solution of toluene containing triethylamine (63 µL, 0.45 mmol) and heated to 90 °C. After 15 min of mixing at this temperature, the crude mixture was evaporated and concentrated under reduced pressure. To remove water, the crude mixture was dissolved in EtOAc (20 mL) and dried over $MgSO_4$. The organic layer was filtered and the solvent was evaporated under reduced pressure to afford the desired product (134 mg (purity = 93%), 0.387 mmol, 94%) as a yellow-orange solid, m.p. = 132 °C. No purification was performed. The ^{1}H NMR spectrum reported on the following page identified the Knoevenagel products **2.30c'** and **2.30c** (about 93%$_{mol}$) with a small amount of decarboxylated product **2.41** (about 4.5%$_{mol}$) and δ-lactone product **2.40** (about 2.5%$_{mol}$).

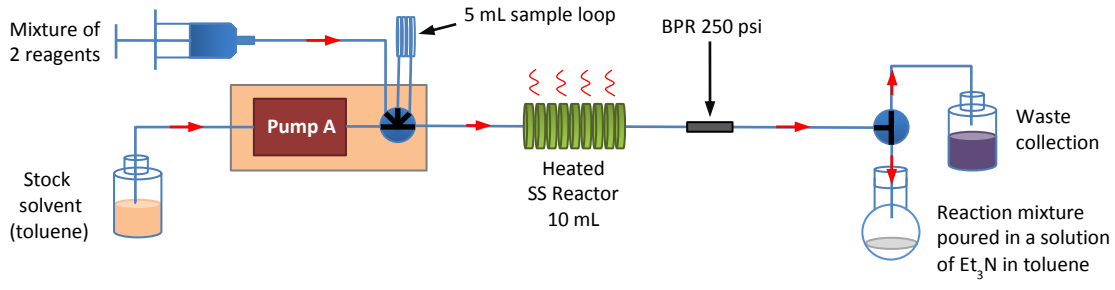

Figure 7.1: Flow set-up for the synthesis of **2.30c** and **2.30c'**- Sample loop configuration.

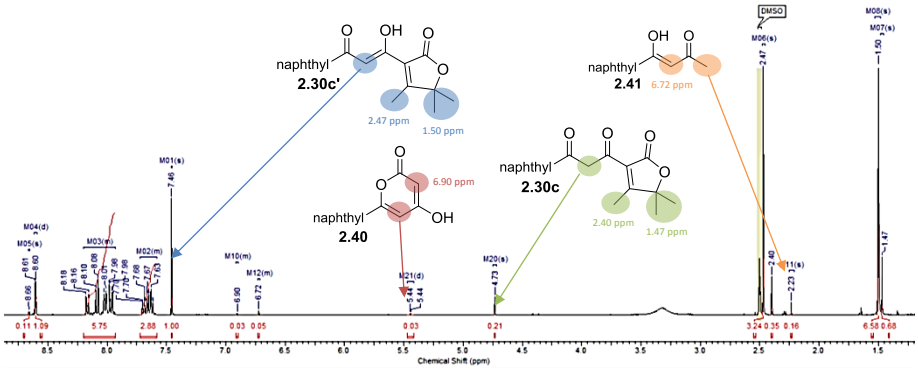

Keto form (**2.30c**):

^{1}H NMR (400 MHz, DMSO-d_6) δ ppm: 8.66 (s, 1H, ArH), 8.20-7.93 (m, 4H, ArH), 7.72-7.58 (m, 2H, ArH), 4.73 (s, 2H, H-25), 2.40 (s, 3H, H-37), 1.47 (s, 6H, H-38).

Enol form (**2.30c'**):

^{1}H NMR (400 MHz, DMSO-d_6) δ ppm: 8.61 (d, *J* = 1.5 Hz, 1H, ArH), 8.20-7.93 (m, 4H, ArH), 7.72-7.58 (m, 2H, ArH), 7.46 (s, 1H, H-6), 2.47 (s, 3H, H-18), 1.50 (s, 6H, H-19).

^{13}C NMR (100 MHz, DMSO-d_6) δ ppm: 187.3 (C, C-7), 180.2 (C, C-3), 177.7 (C, C-5), 168.2 (C, C-1), 135.1 (C), 132.2 (C, C-8), 131.9 (C), 129.6 (CH), 128.8 (CH), 128.8 (CH), 128.6 (CH), 127.7 (CH), 127.1 (CH), 122.9 (CH), 119.1 (C, C-4), 96.9 (CH, C-6), 86.0 (C, C-2), 23.9 (CH_3, C-19), 13.6 (CH_3, C-18).

UV (MeCN) C = 4.4x10^{-5} M, λ = 348.85 nm, ε = 22954 M^{-1}.cm^{-1}.

IR ν_{max} (neat)/cm^{-1} = 2982 (w), 2926 (w), 2360 (w), 1745 (s), 1494 (m), 1271 (m), 1191 (m), 804 (s), 466 (s).

LRMS (LC/ES$^-$): m/z = 321, 100% [M-H]$^-$.

HRMS (ES$^+$): Found 345.1101 Da, $C_{20}H_{18}NaO_4$ [M+Na]$^+$ requires 345.1097 Da.

(*Z*)-3-(1-Hydroxy-3-(naphthalen-2-yl)-3-oxoprop-1-en-1-yl)-6,6,9a-trimethyl-5,6-dihydro-2*H*-furo[3,2-g]isochromene-2,9(9a*H*)-dione (**2.20c**)

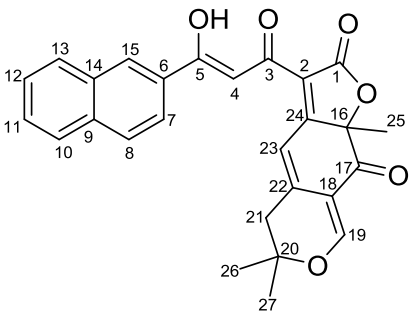

$C_{27}H_{22}O_6$

MW = 442.46 g.mol^{-1}

R*f* = 0.46 (EtOAc/hexane, 1:1)

Pale yellow solid

Yield = 13%

In a vial flushed with argon, 2,2-dimethyl-6-(2-(2-naphthyl)-2-oxoethyl)-4*H*-1,3-dioxin-4-one (**2.28c**, 24 mg, 0.081 mmol) and 7-hydroxy-3,3,7-trimethyl-3*H*-isochromene-6,8(4*H*,7*H*)-dione (**2.21**, 16 mg, 0.072 mmol) were mixed in dried toluene (distilled) to make a 1 mL solution

([dioxinone] = 24 g/L). This solution was injected into the flow set-up described below using the sample loop configuration. Then, the content of the loop was pushed by toluene (Stock solvent) into the flow stream. The residence time was set at 10 min (flow = 1 mL/min) and the oil bath was heated to 120 °C. The 10 mL Stainless Steel reactor was connected to a cooling loop (100 cm, 1 mm i.d.) followed by a backpressure regulator (250 psi). At the end of the reaction, the product was poured into a 5 mL solution of toluene containing triethylamine (12 µL, 0.088 mmol) and heated to 60 °C. After 16 h of mixing at this temperature, the crude mixture was quenched with HCl (0.13 mL of 1 M aq.). The aqueous layer was extracted three times with EtOAc (3 x 10 mL). The combined organic layers were washed with brine (2 x 15 mL), dried over $MgSO_4$, filtered and the solvent was evaporated under reduced pressure to afford the crude product **2.20c**. This crude mixture was then purified on silica gel (EtOAc/hexane, 1:1) to give the title compound **2.20c** (4 mg, 0.009 mmol, 13%) as a pale yellow solid. (lit. yield = 33%).[29] NMR data are consistent with the literature.[29]

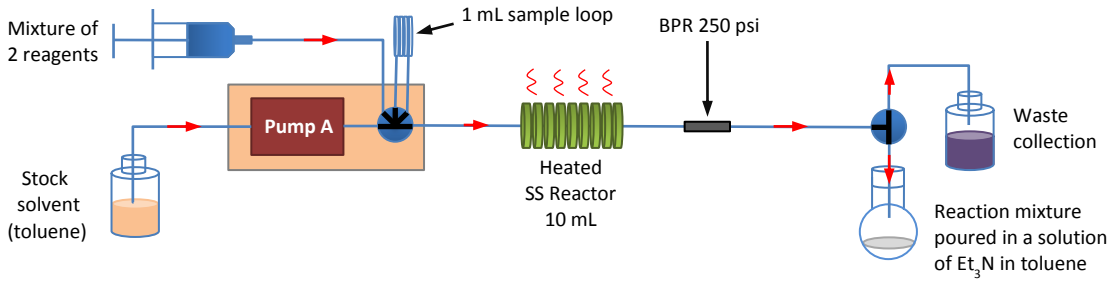

Figure 7.2: Flow set-up for the synthesis of **2.20c** - Sample loop configuration.

^{1}H NMR (300 MHz, $CDCl_3$) δ ppm: 8.57 (s, 1H), 8.10-7.99 (m, 2H), 7.96-7.87 (m, 2H), 7.79 (d, *J* = 1.1 Hz, 1H), 7.67 (s, 1H), 7.65-7.53 (m, 2H), 7.15 (d, *J* = 1.5 Hz, 1H), 2.78 (d, *J* = 17.0 Hz, 1H), 2.74 (d, *J* = 17.0 Hz, 1H), 1.76 (s, 3H, C*H*$_3$), 1.49 (s, 3H, C*H*$_3$), 1.42 (s, 3H, C*H*$_3$).

(2*E*,4*E*,6*E*)-Ethyl octa-2,4,6-trienoate (**2.45**) and (2*Z*,4*E*,6*E*)- Ethyl octa-2,4,6-trienoate (**2.45'**)

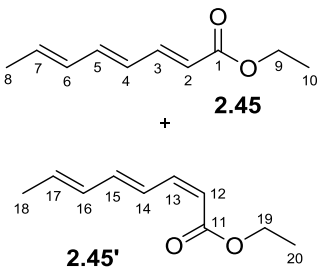

$C_{10}H_{14}O_2$

MW = 166.22 g.mol^{-1}

R*f* = 0.54 (hexane/acetone, 7:3)

Orange brown solid

Yield = 94%

Ratio *E*/*Z*: 86/14

m.p. = 30 °C

Ethyl 2-(diethoxyphosphoryl)acetate (1.77 mL, 8.92 mmol) was added dropwise at 25 °C to a stirred solution of toluene (35 mL) and potassium *tert*-butoxide (1.00 g, 8.92 mmol).

Dissolution of the potassium *tert*-butoxide was incomplete but the reaction was carried out. The white viscous mixture was stirred for 1 h and the sorbaldehyde (**2.44**, 0.990 mL, 8.92 mmol) was then added slowly. The colour changed immediately to red/brown. Using a water bath, the temperature was maintained between 20 and 25 °C because this reaction was exothermic. The reaction was then stirred overnight (14 h) at r.t. TLC showed the total conversion of the starting materials. To this mixture was added 60 mL of water with 15 mL of toluene, and the media was stirred for 30 min. The phases were separated and the aqueous layer was extracted twice with toluene (2 x 50 mL). The combined organic layers were washed with brine (50 mL), dried over $MgSO_4$, filtered and the solvent was evaporated under reduced pressure to afford the title compounds **2.45** and **2.45'** (1.40 g, 8.42 mmol, 94%) as an orange brown solid, m.p. = 30 °C (lit. m.p. = 30 °C,[127] lit. yield = 100%[128]). The NMR highlights the ratio *E/Z*: 86/14. They are consistent with the literature.[129]

E form (**2.45**):

^{1}H NMR (300 MHz, $CDCl_3$) δ ppm: 7.30 (dd, *J* = 15.5, 11.0 Hz, 1H), 6.53 (dd, *J* = 15.0, 11.0 Hz, 1H), 6.27-6.07 (m, 2H), 6.02-5.88 (m, 1H), 5.84 (d, *J* = 15.3 Hz, 1H, H-2), 4.20 (q, *J* = 7.2 Hz, 2H, H-9), 1.84 (d, *J* = 6.8 Hz, 3H, H-8), 1.30 (t, *J* = 7.2 Hz, 3H, H-10).

^{13}C NMR (75 MHz, $CDCl_3$) δ ppm: 167.2 (C, C-1), 144.8 (CH), 141.0 (CH), 135.0 (CH), 131.2 (CH), 127.6 (CH), 120.0 (CH), 60.2 (CH_2, C-9), 18.6 (CH_3), 14.3 (CH_3).

Z form (**2.45'**):

^{1}H NMR (300 MHz, $CDCl_3$) δ ppm: 7.37 (dd, *J* = 15.4, 11.3 Hz, 1H), 6.88 (dd, *J* = 14.7, 11.3 Hz, 1H), 5.73-6.57 (m, 4H), 4.21 (q, *J* = 7.2 Hz, 2H, H-19), 1.92 (d, *J* = 5.3 Hz, 3H, H-18), 1.31 (t, *J* = 7.2 Hz, 3H, H-20).

(2*E*,4*E*,6*E*)-Octa-2,4,6-trienoic acid (**2.46**) and (2*Z*,4*E*,6*E*)-Octa-2,4,6-trienoic acid (**2.46'**)

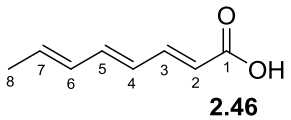

2.46

+

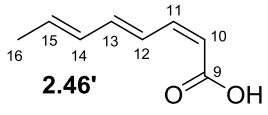

2.46'

$C_8H_{10}O_2$

MW = 138.16 g.mol^{-1}

White solid

Yield = 61%

Ratio *E/Z*: 92/8

m.p. = 170 °C

In a RBF flushed with argon, ethyl octa-2,4,6-trienoates (*E* and *Z*) (**2.45** and **2.45'**, 1.40 g, 8.42 mmol) were dissolved at r.t. in 7 mL of ethanol. Then, NaOH (10.5 mL of 2 M aq., 21.0 mmol) was added dropwise to the mixture. Using a water bath, the temperature was maintained between 20 and 25 °C during this addition. The mixture was stirred at r.t. for 18 h. Evaporation of the solvent under reduced pressure afforded the sodium octa-2,4,6-trienoate as an orange

oil. 20 mL of deionised water were added to the concentrated crude oil followed by 0.23 g of charcoal. The mixture was stirred at 40 °C for one hour, filtered on celite to remove the charcoal and washed with water (10 mL). An orange solution was obtained.

The crude mixture was then reloaded into a flask and the temperature was cooled down between 0 and 10 °C. Without exceeding 20 °C, HCl (21.0 mL of 1 M aq., 21.0 mmol) was added and the solution changed from orange translucent to turbid soft yellow (mixing during 25 min at r.t.). The mixture was then filtered, washed with 10 mL of deionised water and dried under reduced pressure to obtain the title compounds **2.46** and **2.46'** (0.71 g, 5.1 mmol, 61%) as a white solid, m.p. = 170 °C (lit. m.p. = 188 °C,[130] lit. yield = 77%[128]). The NMR highlights the ratio *E/Z*: 92/8. They are consistent with the literature.[130] The *Z* form is not entirely described due to some overlaps with the *E* form on the ^{1}H NMR.

E form (**2.46**):

^{1}H NMR (300 MHz, DMSO-d_6) δ ppm: 12.15 (br s, 1H, OH), 7.18 (dd, *J* = 15.4, 11.3 Hz, 1H), 6.65 (dd, *J* = 14.8, 10.8 Hz, 1H), 6.30 (dd, *J* = 15.0, 11.3 Hz, 1H), 6.20 (ddd, *J* = 14.9, 10.9, 1.5 Hz, 1H), 5.96 (dq, *J* = 15.0, 6.6 Hz, 1H, H-7), 5.84 (d, *J* = 15.0 Hz, 1H, H-2), 1.79 (d, *J* = 6.6 Hz, 3H, H-8); [Selected peaks for the *Z* form are: 7.29 (dd, *J* = 15.5, 11.5 Hz, 1H), 7.04 (dd, *J* = 14.5, 11.5 Hz, 1H), 6.40 (dd, *J* = 15.0, 11.5 Hz, 1H)].

^{13}C NMR (75 MHz, DMSO-d_6) δ ppm: 167.6 (C, C-1), 144.3 (CH), 140.7 (CH), 134.8 (CH), 131.3 (CH), 127.7 (CH), 121.0 (CH), 18.3 (CH_3, C-8).

(2*E*,4*E*,6*E*)-Ethyl octa-2,4,6-trienoate (**2.47**) and (2*Z*,4*E*,6*E*)-Ethyl octa-2,4,6-trienoate (**2.47'**)

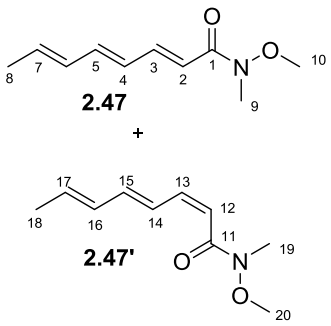

$C_{10}H_{15}NO_2$

MW = 181.23 g.mol $^{-1}$

R*f* = 0.52 (hexane/acetone, 1:1)

Yellow oil

Yield = 90%

Ratio *E/Z*: 90/10

In a RBF flushed with argon, oxalyl chloride (0.375 mL, 4.36 mmol) and DMF (1.1 µL, 0.014 mmol) were added all at one time at r.t. to a CH_2Cl_2 solution (50 mL) containing octa-2,4,6-trienoic acids (**2.46** and **2.46'**, 0.482 g, 3.49 mmol). After 2 h, the media was evaporated under reduced pressure to remove the excess of oxalyl chloride. Afterwards, CH_2Cl_2 (30 mL), N,O-dimethylhydroxylamine (0.476 g, 4.88 mmol) and Et_3N (1.46 mL, 10.5 mmol) were successively added at r.t.. After adding the Et_3N, a white fume appeared and disappeared progressively. The media was stirred for 16 h and the reaction was quenched at r.t. with 15 mL

of $NaHCO_{3\ sat}$ and extracted twice with 15 mL of CH_2Cl_2. The combined organic layers were then washed four times with 20 mL of NH_4Cl_{sat}, dried over $MgSO_4$, filtered and the solvent was evaporated under reduced pressure to afford the title compounds **2.47** and **2.47'** (0.57 g, 3.1 mmol, 90%) as a yellow oil. The NMR highlights the ratio *E/Z*: 90/10. The *Z* form is not entirely described due to some overlaps with the *E* form on the ^{1}H NMR.

E form (**2.47**):

^{1}H NMR (400 MHz, $CDCl_3$) δ ppm: 7.35 (dd, *J* = 15.2, 11.3 Hz, 1H, H-3), 6.53 (dd, *J* = 14.9, 10.9 Hz, 1H, H-5), 6.44 (d, *J* = 15.2 Hz, 1H, H-2), 6.27 (dd, *J* = 14.9, 11.3 Hz, 1H, H-4), 6.16 (ddd, *J* = 14.9, 10.9, 1.0 Hz, 1H, H-6), 5.92 (dq, *J* = 14.9, 7.1 Hz, 1H, H-7), 3.71 (s, 3H, CH_3), 3.25 (s, 3H, CH_3), 1.83 (dd, *J* = 7.1, 1.2 Hz, 3H, H-8); [Selected peaks for the *Z* form are: 7.41 (dd, *J* = 15.0, 11.0 Hz, 1H), 6.88 (dd, *J* = 15.0, 11.0 Hz, 1H), 6.36 (dd, *J* = 15.0, 11.0 Hz, 1H)].

^{13}C NMR (100 MHz, $CDCl_3$) δ ppm: 167.4 (C, C-1), 143.6 (CH, C-3), 140.4 (CH, C-5), 134.3 (CH, C-7), 131.3 (CH, C-6), 128.2 (CH, C-4), 117.8 (CH, C-2), 61.7 (CH_3), 32.5 (CH_3), 18.5 (CH_3, C-8).

UV (MeCN) C = 3.66x10^{-5} M, $\lambda = 298.4$ nm, $\varepsilon = 32131$ M^{-1}.cm^{-1}.

IR ν_{max} (neat)/cm^{-1} = 2936 (br), 1649 (m), 1603 (s), 1413 (m), 1376 (m), 1087 (m), 999 (s), 435 (m).

LRMS (LC/ES$^+$): m/z = 182, 50% $[M+H]^+$; 204, 60% $[M+Na]^+$; 385, 100% $[2M+Na]^+$.

HRMS (ES$^+$): Found 204.0997 Da, $C_{10}H_{15}NNaO_2$ $[M+Na]^+$ requires 204.0995 Da.

2,2-Dimethyl-6-((3*E*,5*E*,7*E*)-2-oxonona-3,5,7-trien-1-yl)-4*H*-1,3-dioxin-4-one (**2.43**)

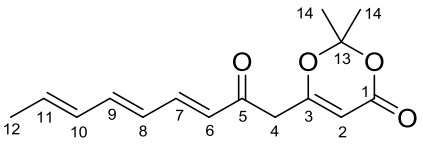

$C_{15}H_{18}O_4$

MW = 262.30 g.mol^{-1}

R*f* = 0.32 (hexane/acetone, 7:3)

Yellow solid

Yield = 22%

m.p. = 66 °C

In a RBF flushed with argon, $(COCl)_2$ (0.400 mL, 4.52 mmol) and DMF (1.1 µL, 0.014 mmol) were added all at one time at room temperature to a 50 mL solution of CH_2Cl_2 containing octa-2,4,6-trienoic acids (**2.46** and **2.46'**, 0.500 g, 3.62 mmol). After 3 h, the media was evaporated under reduced pressure to remove the excess of oxalyl chloride and to isolate 0.530 g of octa-2,4,6-trienoyl chloride (93%). Then, in another RBF flushed with argon, *n*-BuLi at 2.5 M in hexane (4.20 mL, 10.5 mmol) was slowly added at -78 °C to a 50 mL THF solution containing DIPA (1.42 mL, 10.2 mmol). After 45 min at 0 °C, the media was cooled again at -78 °C and 2,2,6-trimethyl-4*H*-1,3-dioxin-4-one (**2.38**, 1.35 mL, 10.2 mmol) was added dropwise. After 30 min at -78 °C, octa-2,4,6-trienoyl chloride (0.530 g, 3.38 mmol) previously isolated and dissolved in 5 mL of THF was added at -50 °C. After 3 h 15 min at -40 °C, the reaction was

complete. It was quenched at 0 °C with $NaHCO_{3\,sat}$ (20 mL) and extracted three times with EtOAc (3 x 70 mL). The combined organic layers were washed with NH_4Cl_{sat} (3 x 50 mL), dried over $MgSO_4$, filtered and the solvent was evaporated under reduced pressure to afford the crude product. This crude mixture was then purified on silica gel (hexane/acetone, 8:2) to give the title compound **2.43** (192 mg, 0.732 mmol, 22%) as a yellow solid, m.p. = 66 °C.

^{1}H NMR (400 MHz, $CDCl_3$) δ ppm: 7.24 (dd, *J* = 15.2, 11.2 Hz, 1H, H-7), 6.64 (dd, *J* = 15.2, 10.6 Hz, 1H, H-9), 6.22 (dd, *J* = 15.2, 11.2 Hz, 1H, H-8), 6.20 (*J*-coupling not resolved due to an overlap with H-6 and H-8, 1H, H-10), 6.17 (d, *J* = 15.3 Hz, 1H, H-6), 6.04 (dq, *J* = 14.5, 7.0 Hz, 1H, H-11), 5.38 (s, 1H, H-2), 3.46 (s, 2H, H-4), 1.86 (d, *J* = 7.1 Hz, 3H, H-12), 1.71 (s, 6H, H-14).

^{13}C NMR (100 MHz, $CDCl_3$) δ ppm: 192.2 (C, C-5), 165.1 (C, C-3), 160.7 (C, C-1), 145.2 (CH, C-7), 143.9 (CH, C-9), 137.0 (CH, C-11), 131.2 (CH, C-10), 127.5 (CH, C-8), 126.8 (CH, C-6), 107.2 (C, C-13), 96.6 (CH, C-2), 45.3 (CH_2, C-4), 25.0 (CH_3, C-14), 18.7 (CH_3, C-12).

IR ν_{max} (neat)/cm^{-1} = 1725 (m), 1610 (m), 1390 (w), 1268 (w), 1188 (s), 998 (s), 808 (m), 499 (w).

UV (MeCN) $C = 4.24x10^{-5}\ M, \lambda_1 = 251.12\ nm, \varepsilon_1 = 10397\ M^{-1}.cm^{-1}, \lambda_2 = 321.31\ nm, \varepsilon_2 = 30665\ M^{-1}.cm^{-1}$.

LRMS (LC/ES$^-$): m/z = 203, 100% $[M\text{-acetone-H}]^-$, 261, 40% $[M\text{-H}]^-$.

HRMS (ES$^+$): Found 227.0682 Da, $C_{12}H_{12}NaO_3$ $[M\text{-acetone+Na}]^+$ requires 227.0679 Da.

7.2.2 Chapter 3: *In situ* generation of isocyanides, indispensable building blocks of multi-component reactions (MCRs)

7.2.2.1 Synthesis

7-*t*-Butoxynorbornadiene (**3.42**)

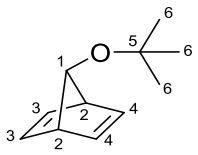

$C_{11}H_{16}O$

MW = 164.25 $g.mol^{-1}$

Colourless oil

Purity = 95%

Yield = 17%

Following the procedure described by Story,[68] in a 50 mL RBF flushed with argon, norbornadiene (**3.40**, 10.0 mL, 98.3 mmol) and cuprous bromide (21 mg, 0.15 mmol) were added all at one time to 20 mL of benzene. Argon was introduced continuously, and, after heating the media to reflux, a solution of *t*-butyl perbenzoate (7.28 mL, 38.3 mmol) in benzene (5 mL) was added over 1 hour to the stirred reaction mixture. After the end of the addition, the media was heated to the reflux temperature for an additional 1 h. To check that the *t*-butyl perbenzoate was completely reacted, an IR of the reaction mixture was performed. *t*-Butyl perbenzoate absorbs in the infrared at 5.65 - 5.70 µm. However, no characteristic peaks were noticed in this area. It is important to check the presence of this compound because during a

distillation, it can lead to an explosion. Afterwards, the media was cooled down to r.t., washed with brine (3 x 25 mL) to remove copper salts, and with 10% aqueous NaOH (3 x 25 mL) to remove benzoic acid. The organic layer was then washed again with brine (3 x 25 mL), dried over $MgSO_4$ and filtered. The crude mixture was then purified by distillation under lower pressure. First, the benzene and the excess of norbornadiene (**3.40**) were removed at r.t. under approximately 200 mmHg. Then, the pressure was slowly lowered to 10 - 15 mmHg and the product was collected until the temperature reached 100 - 120 °C. Traces of norbornadiene and benzene were identified on the ^{1}H NMR, but after leaving the flask open over night, the title compound **3.42** (1.14 g (purity = 95%), 6.59 mmol, 17%) was obtained as a colourless oil (lit. yield = 20%).[68] NMR data are consistent with the literature.[131]

^{1}H NMR (400 MHz, $CDCl_3$) δ ppm: 6.65 (dd, *J* = 2.1, 2.0 Hz, 2H, C*H*=C*H*), 6.62-6.56 (m, 2H, C*H*=C*H*), 3.81-3.77 (m, 1H, H-1), 3.43-3.38 (m, 2H, H-2), 1.15 (s, 9H, H-6).

^{13}C NMR (100 MHz, $CDCl_3$) δ ppm: 139.8 (CH, *C*H=*C*H), 137.3 (CH, *C*H=*C*H), 104.3 (CH, C-1), 73.6 (C, C-5), 55.5 (CH, C-2), 28.3 (CH_3, C-6).

7-Norbornadienyl acetate (**3.43**)

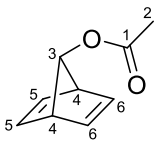

$C_9H_{10}O_2$

MW = 150.07 g.mol^{-1}

Light yellow oil

Yield = 77%

Following the procedure described by Story,[69] in a RBF previously flushed with nitrogen, 7-*t*-butoxynorbornadiene (**3.42**, 55 mg, 0.32 mmol) was slowly added to a mixture of glacial acetic acid (0.550 mL, 9.61 mmol) and acetic anhydride (0.106 mL, 1.12 mmol). The media was stirred at r.t. for 30 min. Then, the reaction mixture was cooled down in an ice bath and quickly added to a precooled solution of perchloric acid at 60% (54 µL, 0.50 mmol). The yellow mixture was swirled in an ice bath for exactly 1 min. The media was then transferred into a separatory funnel containing about 5 mL of ice and water. The aqueous layer was extracted three times with DCM (3 x 5 mL). The combined organic layers were washed with saturated sodium bicarbonate (2 x 5 mL), brine (2 x 5 mL), dried over $MgSO_4$, filtered, and the solvent was evaporated under reduced pressure to afford the desired product **3.43** (37 mg, 0.25 mmol, 77%) as a light yellow oil (lit. yield = 73%).[69] NMR data are consistent with the literature.[70, 131a]

^{1}H NMR (400 MHz, $CDCl_3$) δ ppm: 6.72 (dd, *J* = 2.3, 2.2 Hz, 2H, C*H*=C*H*), 6.61-6.58 (m, 2H, C*H*=C*H*), 4.60-4.57 (m, 1H, H-3), 3.64-3.60 (m, 2H, H-4), 1.99 (s, 3H, H-2).

^{13}C NMR (100 MHz, $CDCl_3$) δ ppm: 171.0 (C, C-1), 140.3 (CH, *C*H=*C*H), 137.8 (CH, *C*H=*C*H), 99.3 (CH, C-3), 52.4 (CH, C-4), 21.1 (CH_3, C-2).

7-Acetoxy quadricyclane (**3.44**)

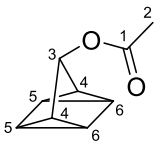

$C_9H_{10}O_2$

MW = 150.07 g.mol $^{-1}$

Yellow oil

Yield = 95%

In a RBF previously flushed with nitrogen, 7-norbornadienyl acetate (**3.43**, 61 mg, 0.37 mmol) was dissolved in 10 mL of hexane. This solution was degassed by sonication whilst being saturated with nitrogen gas. Using the sample loop configuration, the reaction mixture was injected into the 28 mL length photoflow reactor (UV-C lamp, 9W) at 1 mL/min. The crude mixture was collected at the output of the reactor and evaporation of the solvent under reduced pressure afforded the desired product **3.44** (53 mg, 0.35 mmol, 95%) as a yellow oil (lit. yield = 63%).[131a] NMR data are consistent with the literature.[70, 131a]

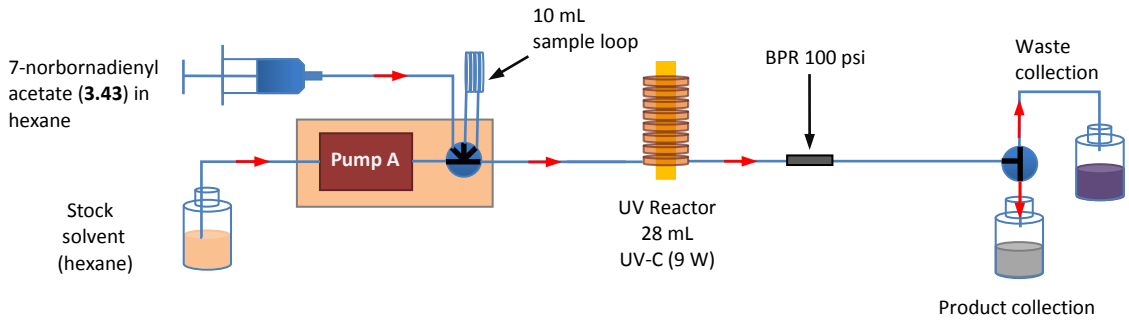

Figure 7.3: Flow set-up for the synthesis of the 7-acetoxy quadricyclane (**3.44**) - Sample loop configuration.

^{1}H NMR (400 MHz, $CDCl_3$) δ ppm: 5.63 (t, *J* = 1.7 Hz, 1H, H-3), 2.12 (s, 3H, H-2), 1.83 (ddd, *J* = 5.6, 4.3, 2.2 Hz, 2H, H-5/6), 1.61 (ddd, *J* = 5.5, 4.0, 2.3 Hz, 2H, H-5/6), 1.53 (ddd, *J* = 4.3, 4.3, 1.6 Hz, 2H, H-4).

^{13}C NMR (100 MHz, $CDCl_3$) δ ppm: 171.8 (C, C-1), 82.3 (CH, C-3), 25.6 (CH, C-4), 21.4 (CH_3, C-2), 15.9 (CH, C-5/6), 14.6 (CH, C-5/6).

7-Quadricyclanol (**3.45**)

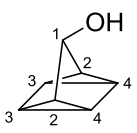

C_7H_8O

MW = 108.14 g.mol $^{-1}$

R*f* = 0.38 (Et_2O/PET, 1:1)

Yellow oil

Purity = 78%

Yield = 46%

Following the procedure described by Lustgarten,[71] in a RBF previously flushed with nitrogen, 7-acetoxy quadricyclane (**3.44**, 300 mg, 2.00 mmol) was dissolved in 15 mL of anhydrous diethyl ether. This solution was added over 30 min to a cold (0 °C) mixture of lithium aluminium hydride (128 mg, 3.36 mmol) and anhydrous ether (17 mL). This mixture was allowed to stir at r.t. for an additional 30 min and then cooled down to 0 °C. 20 mL of aqueous saturated Rochelle's salt were added to quench the reaction. The aqueous layer was extracted three times with ether (3 x 20 mL). The combined organic layers were washed with brine (3 x 20 mL), dried over $MgSO_4$, filtered and the solvent was evaporated under reduced pressure to afford the crude product. This yellow crude oil was then purified on basic alumina (Et_2O/PET, 1:1) to give the title compound **3.45** (126 mg (purity = 78%), 0.909 mmol, 46%) as a yellow oil (lit. yield = 96%).[71] Using either silica gel or basic alumina, it was very difficult to obtain a pure product. NMR data are consistent with the literature.[70, 131a]

^{1}H NMR (400 MHz, $CDCl_3$) δ ppm: 4.90 (br s, 1H, H-1), 1.82-1.74 (m, 2H, H-3/4), 1.60-1.55 (m, 2H, H-3/4), 1.39 (ddd, *J* = 4.2, 4.1, 1.6 Hz, 2H, H-2), 1.35 (br s, 1H, OH).

^{13}C NMR (100 MHz, $CDCl_3$) δ ppm: 79.3 (CH, C-1), 28.8 (CH, C-2), 15.6 (CH, C-3/4), 14.7 (CH, C-3/4).

Tetracyclo[3.2.0.0^{2,7}.0^{4,6}]heptan-3-one (**3.46**)

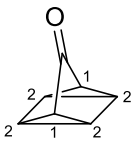

C_7H_6O

MW = 106.12 g.mol^{-1}

Yellow oil

Following the procedure described by the patent from Srinivasu,[72] in a RBF flushed with nitrogen, DMSO (34 µL, 0.47 mmol) in 0.5 mL of DCM was slowly added at -78 °C to a solution of oxalyl chloride (20 µL, 0.24 mmol) in 0.5 mL of DCM. The media was stirred for 10 min. Then, a solution of 7-quadricyclanol (**3.45**, 21 mg, 0.20 mmol) in 0.5 mL of DCM was slowly added followed by a solution of Et_3N (143 µL, 1.03 mmol) in 0.1 mL of DCM. The media was stirred at -78 °C for 35 min and then warmed to r.t. 5 mL of water with 2 mL of HCl (1 M aq.) were added to the mixture and the media was stirred at r.t. for 30 min. The aqueous layer was extracted three times with DCM (3 x 5 mL). The combined organic layers were washed with brine (2 x 5 mL), dried over $MgSO_4$, filtered and the solvent was evaporated under reduced pressure to afford the crude mixture. ^{1}H NMR data showed the presence of a 4:6 mixture of tetracyclo[3.2.0.0^{2,7}.0^{4,6}]heptan-3-one (**3.46**) and 7-norbornadienol (**3.50**) in the crude. Tetracycloheptan-3-one (**3.46**) has not been isolated. NMR data of tetracycloheptan-3-one (**3.46**) contained in the crude mixture are consistent with the literature.[131a]

^{1}H NMR (400 MHz, $CDCl_3$) δ ppm: 2.24 (d, *J* = 4.3 Hz, 4H, H-2), 1.12 (t, *J* = 4.2 Hz, 2H, H-1).

3-Tosyloxytetracyclo[3.2.0.0^{2,7}.0^{4,6}]heptane (**3.47**)

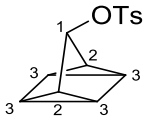

$C_{14}H_{14}O_3S$

MW = 262.32 g.mol^{-1}

R*f* = 0.15 (hexane/EtOAc, 6:4)

Following the procedure described by Gassman,[132] in a RBF previously flushed with nitrogen, *p*-toluenesulfonyl chloride (120 mg, 0.629 mmol) was added over a 30 min period to a cold (-10 °C) solution of 7-quadricyclanol (**3.45**, 40 mg, 0.37 mmol) dissolved in dry pyridine (0.333 mL, 4.12 mmol). The solution was let to stand at -10 °C for 12 h. The reaction mixture was then added to a cold solution of hydrochloric acid (2 mL of 2 M aq.). The mixture was poured into a separatory funnel and the aqueous layer was extracted three times with DCM (3 x 5 mL). The combined organic layers were then washed with brine (3 x 5 mL), dried over $MgSO_4$, filtered, and the solvent was evaporated under reduced pressure to afford the crude mixture. ^{1}H NMR data showed the presence of a 35:45:20 mixture of 3-tosyloxytetracyclo[3.2.0.0^{2,7}.0^{4,6}]heptane (**3.47**), TsCl, and 7-norbornadienol (**3.50**) in the crude. This crude mixture was then purified on silica gel (hexane/EtOAc, 6:4) but only the excess of TsCl and PTSA were collected in the fractions. NMR data of 3-tosyloxytetracyclo[3.2.0.0^{2,7}.0^{4,6}]heptane (**3.47**) contained in the crude product are consistent with the literature.[71]

^{1}H NMR (400 MHz, $CDCl_3$) δ ppm: 7.88 (d, *J* = 8.3 Hz, 2H, ArH), 7.35 (d, *J* = 7.8 Hz, 2H, ArH), 5.48 (t, *J* = 1.7 Hz, 1H, H-1), 2.46 (s, 3H, C*H*$_3$), 1.87-1.80 (m, 2H, H-2), 1.46-1.40 (m, 4H, H-3).

7-Benzoyloxybicyclo[2.2.1]hepta-2,5-diene (**3.49**)

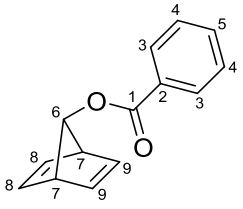

$C_{14}H_{12}O_2$

MW = 212.25 g.mol^{-1}

R*f* = 0.5 (PET/EtOAc, 9:1)

White solid

Yield = 47%

m.p. = 50 °C

Following the procedure described by Fairlamb,[133] in a 50 mL RBF flushed with argon, norbornadiene (**3.40**, 5.00 mL, 49.2 mmol) and cuprous bromide (77 mg, 0.53 mmol) were added to 10 mL of benzene. Argon was introduced continuously, and, after heating the media to 40 °C, a solution of benzoyl peroxide (12.23 g, 37.86 mmol) in 12.5 mL of benzene was added over 2 hours to the stirred reaction mixture. After the end of the addition, the media

was heated to the reflux temperature for 3 days. After one day, the mixture turned green. After 3 days, the brown mixture was cooled down to r.t., washed with saturated sodium carbonate (3 x 10 mL), brine, dried over $MgSO_4$, filtered and the solvent was evaporated under reduced pressure to afford the crude product. This crude mixture was then purified on silica gel (PET/EtOAc, 95:5) to give the title compound **3.49** (2.16 g, 10.2 mmol, 47%) as a white solid, m.p. = 50 °C (lit. m.p. = 54 °C,[134] lit. yield = 34%[133]). NMR data are consistent with the literature.[133]

^{1}H NMR (400 MHz, $CDCl_3$) δ ppm: 8.02-7.96 (m, 2H, H-3), 7.55 (tt, *J* = 7.5, 1.5 Hz, 1H, H-5), 7.42 (dd, *J* = 7.8, 7.8 Hz, 2H, H-4), 6.78 (dd, *J* = 2.2, 2.1 Hz, 2H, C*H*=C*H*), 6.69-6.63 (m, 2H, C*H*=C*H*), 4.89-4.81 (m, 1H, H-6), 3.77-3.71 (m, 2H, H-7).

^{13}C NMR (100 MHz, $CDCl_3$) δ ppm: 166.5 (C, C-1), 140.3 (CH, *C*H=*C*H), 137.9 (CH, *C*H=*C*H), 132.9 (CH, C-5), 130.3 (C, C-2), 129.6 (CH, C-3), 128.3 (CH, C-4), 99.5 (CH, C-6), 52.6 (CH, C-7).

7-Norbornadienol (**3.50**)

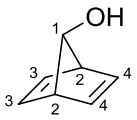

C_7H_8O

MW = 108.14 g.mol^{-1}

R*f* = 0.37 (hexane/ether, 6:4)

NMR Yield (crude mixture) = 57%

Light yellow oil

Purity = 50%

Yield (after purification) = 5%

From the procedure described by Tsuji,[73] in a RBF flushed with nitrogen, a solution of benzoylnorbornadiene (**3.49**, 448 mg, 2.11 mmol) in 2 mL of anhydrous ether was added slowly to a solution of phenylmagnesium bromide (951 mg, 5.25 mmol) in 3 mL of dry ether. After refluxing for 2 hours, the media was mixed with 20 mL saturated aqueous solution of ammonium chloride. The aqueous layer was extracted three times with ether (3 x 10 mL). The combined organic layers were washed with brine (2 x 10mL), dried over $MgSO_4$, filtered and the solvent was slowly evaporated under reduced pressure to afford the crude volatile product. An internal standard (toluene) was used to determine the crude NMR yield (130 mg, 1.20 mmol, 57%). This crude product was mixed with hexane and the triphenylmethanol precipitates. After filtration and evaporation, the residue was purified on silica gel (hexane/ether, 6:4) to give the title compound **3.50** (22 mg (purity = 50%), 0.10 mmol, 5%) as a light yellow oil with traces of hexane and few impurities (lit. yield = 83% after distillation).[73] Even with a basic alumina column, the purification of this volatile alcohol was very complicated. NMR data are consistent with the literature.[74]

^{1}H NMR (400 MHz, $CDCl_3$) δ ppm: 6.69-6.65 (m, 2H, C*H*=C*H*), 6.62 (dd, *J* = 2.3, 2.2 Hz, 2H, C*H*=C*H*), 3.90 (d, *J* = 12.5 Hz, 1H, H-1), 3.51-3.45 (m, 2H, H-2), 3.10 (d, *J* = 13.2 Hz, 1H, OH).

^{13}C NMR (100 MHz, $CDCl_3$) δ ppm: 139.0 (CH, *C*H=*C*H), 138.2 (CH, *C*H=*C*H), 102.3 (CH, C-1), 56.0 (CH, C-2).

7-Norbornadienyl methanesulfonate (**3.51**)

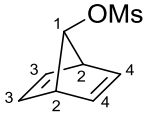

$C_8H_{10}O_3S$

MW = 186.22 g.mol $^{-1}$

From the procedure described by Bentley,[74] in a RBF flushed with nitrogen, a solution of 7-norbornadienol (**3.50**, 18 mg, 0.17 mmol) and triethylamine (50 µL, 0.36 mmol) in anhydrous chloroform (2 mL) was cooled to -20 °C. Methanesulfonyl chloride (67 µL, 0.20 mmol) was added slowly and stirring was continued for 30 min at the same temperature. A ^{1}H NMR of the crude mixture was performed and identified the presence of a 64:32:3:1 mixture of MsCl, Et_3N, 7-norbornadienyl methanesulfonate (**3.51**) and 7-chloronorbornadiene. After standing at 5 °C for 4 h, the NMR tube was run again and 7-norbornadienyl methanesulfonate (**3.51**) was not identified. It was probably converted into 7-chloronorbornadiene. 7-norbornadienyl methanesulfonate (**3.51**) has not been isolated. NMR data of 7-norbornadienyl methanesulfonate (**3.51**) contained in the crude mixture (after 30 min of reaction time at -20 °C) are consistent with the literature.[74]

^{1}H NMR (400 MHz, $CDCl_3$) δ ppm: 6.65 (dd, *J* = 2.2, 2.1 Hz, 2H, C*H*=C*H*), 6.55 (m, 2H, C*H*=C*H*), 4.40 (s, 1H, H-1), 3.64 (m, 2H, H-2), 2.92 (s, 3H, CH_3).

2-Chloro-7-acetoxynorbornane (**3.53**)

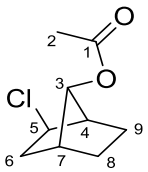

$C_9H_{13}ClO_2$

MW = 188.65 g.mol $^{-1}$

R*f* = 0.5 (hexane/Et_2O, 7:3)

Light yellow oil

Yield = 61%

Following the procedure described by Baird,[75] in a RBF flushed with nitrogen, norbornene (**3.41**, 5.50 g, 58.4 mmol), anhydrous sodium acetate (4.65 g, 56.7 mmol), anhydrous cupric chloride (13.18 g, 98.00 mmol) and anhydrous palladium chloride (260 mg, 1.47 mmol) were added to glacial acetic acid (55.34 mL, 966.6 mmol). The reaction mixture was heated to 80 °C

and stirred for 68 hours. The media was then cooled down, filtered, and the filter cake was washed twice with glacial acetic acid (2 x 15 mL). Water (200 mL) was added to the combined filtrate and washings. The aqueous layer was extracted four times with *n*-pentane (4 x 60 mL). The combined organic layers were washed with saturated sodium carbonate solution (2 x 100 mL), with brine (2 x 100 mL), dried over $MgSO_4$, filtered and the solvent was evaporated under reduced pressure to afford the crude product. This crude mixture was then purified on silica gel (hexane/Et_2O, 7:3) to give the title compound **3.53** (6.50 g, 34.5 mmol, 61%) as a light yellow oil (lit. yield = 84% after distillation).[75] NMR data are consistent with the literature.[75]

^{1}H NMR (400 MHz, $CDCl_3$) δ ppm: 4.72-4.67 (m, 1H, H-3), 3.97 (ddd, *J* = 8.0, 4.0, 1.0 Hz, 1H, H-5), 2.62 (d, *J* = 4.4 Hz, 1H, H-4), 2.37-2.32 (m, 1H, H-7), 2.32-2.26 (m, 1H, *endo*/exo-H-6), 2.16 (dd, *J* = 13.5, 8.3 Hz, 1H, *endo*/exo-H-6), 2.07 (s, 3H, H-2), 1.77 (dddd, *J* = 12.4, 12.0, 4.7, 4.6 Hz, 1H, *endo/*exo-H-9), 1.68-1.57 (m, 1H, *endo*/exo-H-8), 1.23 (ddd, *J* = 12.8, 10.0, 4.0 Hz, 1H, *endo*/exo-H-9), 1.14 (ddd, *J* = 12.0, 10.2, 4.3 Hz, 1H, *endo*/exo-H-8).

^{13}C NMR (100 MHz, $CDCl_3$) δ ppm: 171.3 (C, C-1), 80.3 (CH, C-3), 59.5 (CH, C-5), 46.4 (CH, C-4), 41.6 (CH_2, C-6), 39.2 (CH, C-7), 24.9 (CH_2, C-9), 23.9 (CH_2, C-8), 21.2 (CH_3, C-2).

7-Norbornenol (**3.54**)

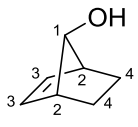

$C_7H_{10}O$

MW = 110.16 g.mol $^{-1}$

R*f* = 0.55 (DCM/Et_2O, 7:3)

colourless oil

Yield = 35%

Following the procedure described by Baird,[75] in a RBF flushed with nitrogen, a solution of potassium *t*-butoxide (9.13 g, 81.4 mmol) in 80 mL of dimethyl sulfoxide was added all at one time to a solution of 2-chloro-syn-7-acetoxynorbornane (**3.53**, 6.50 g, 34.5 mmol) in 16 mL of dimethyl sulfoxide. The solution turned brown straight after the addition of *t*-BuOK. The media was stirred overnight (22 h) at room temperature. Afterwards, 65 mL of water were added to the reaction mixture and it was stirred for one hour. The aqueous layer was extracted four times with ether (4 x 150 mL). The combined organic layers were washed with water (2 x 200 mL), with brine (2 x 200 mL), dried over $MgSO_4$, filtered and the solvent was evaporated under reduced pressure to afford the crude product. This crude mixture was then purified twice on silica gel (DCM/Et_2O, 7:3) to give the title compound **3.54** (1.34 g, 12.2 mmol, 35%) as a colourless oil (lit. yield = 70%).[75] NMR data are consistent with the literature.[72, 74, 135]

^{1}H NMR (400 MHz, $CDCl_3$) δ ppm: 6.07 (dd, *J* = 2.2, 2.0 Hz, 2H, H-3), 3.77 (d, *J* = 10.8 Hz, 1H, H-1), 2.81-2.71 (m, 2H, H-2), 1.95 (d, *J* = 11.5 Hz, 1H, OH), 1.79-1.66 (m, 2H, *exo*-H-4), 0.93 (dd, *J* = 11.5, 3.9 Hz, 2H, *endo*-H-4).

^{13}C NMR (100 MHz, $CDCl_3$) δ ppm: 132.3 (CH, C-3), 87.2 (CH, C-1), 47.6 (CH, C-2), 22.2 (CH_2, C-4).

Bicyclo[2.2.1]hept-2-en-7-one (**3.37**)

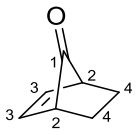

C_7H_8O

MW = 108.14 g.mol^{-1}

R*f* = 0.8 (DCM/Et_2O, 8:2)

Light yellow oil

Purity = 87%

Yield = 58%

Following the procedure described by the patent from Srinivasu,[72] in a RBF flushed with nitrogen, DMSO (430 µL, 6.06 mmol) in 6 mL of DCM was added slowly at -78 °C to a solution of oxalyl chloride (256 µL, 3.03 mmol) in 6 mL of DCM. The media was stirred for 10 min. Then, a solution of 7-norbornenol (**3.54**, 278 mg, 2.52 mmol) in 6 mL of DCM was slowly added followed by a solution of Et_3N (1.83 mL, 13.1 mmol) in 2 mL of DCM. The media was stirred at -78 °C for 1 h 40 min and then warmed to r.t. 6 mL of water were added and the media was stirred at r.t. for 30 min. 20 mL of water were added with 20 mL of HCl (1 M aq.) and the solution was stirred for 10 min. The aqueous layer was extracted three times with DCM (3 x 50 mL). The combined organic layers were washed with brine (2 x 50 mL), dried over $MgSO_4$, filtered and the solvent was evaporated under reduced pressure to afford the crude product. Few millilitres of bleach were added in the trap of the rotary evaporator to remove the unpleasant odour of the dimethyl sulfide. The crude product was then purified on silica gel (DCM/Et_2O, 8:2) to give the title compound **3.37** (182 mg (purity = 87%), 1.46 mmol, 58%) as a light yellow oil (lit. yield = 49%).[72] NMR data are consistent with the literature.[72]

^{1}H NMR (400 MHz, $CDCl_3$) δ ppm: 6.54 (dd, *J* = 2.5, 2.3 Hz, 2H, H-3), 2.83 (dt, *J* = 3.9, 2.2 Hz, 2H, H-2), 2.03-1.93 (m, 2H, *endo/exo*-H-4), 1.26-1.19 (m, 2H, *endo/exo*-H-4).

^{13}C NMR (100 MHz, $CDCl_3$) δ ppm: 206.0 (C, C-1), 133.3 (CH, C-3), 45.3 (CH, C-2), 21.0 (CH_2, C-4).

N-Benzylbicyclo[2.2.1]hept-2-en-7-imine (**3.39b**)

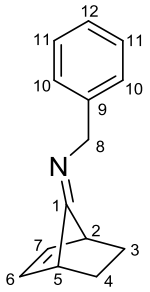

$C_{14}H_{15}N$

MW = 197.28 g.mol^{-1}

Yellow oil

Purity = 75%

Yield = 70%

In a RBF previously dry and flushed with nitrogen, 3 Å molecular sieves were added to a solution of ketone **3.37** (136 mg, 1.25 mmol) in 11 mL of toluene. Then, benzylamine (137 µL, 1.25 mmol) was quickly added to the reaction mixture. The media was stirred for 22 h at 80 °C. It was then filtered on celite, and the cake was washed few times with toluene. Evaporation of the solvent under reduced pressure afforded the crude product **3.39b** (230 mg (purity = 75%), 0.87 mmol, 70%) as a yellow oil. The impurities highlighted in the synthesis of bicyclo[2.2.1]hept-2-en-7-one (**3.37**) were recovered at the end of this reaction.

^{1}H NMR (400 MHz, $CDCl_3$) δ ppm: 7.39-7.20 (m, 5H, ArH), 6.46 (dd, *J* = 6.1, 3.2 Hz, 1H, H-6/7), 6.34 (dd, *J* = 6.2, 3.3 Hz, 1H, H-6/7), 4.45 (d, *J* = 14.0 Hz, 1H, H-8), 4.41 (d, *J* = 14.0 Hz, 1H, H-8), 3.51 (dd, *J* = 3.5, 3.4 Hz, 1H, H-2/5), 3.04 (dd, *J* = 3.5, 3.4 Hz, 1H, H-2/5), 1.93 (ddd, *J* = 9.3, 7.1, 3.9 Hz, 1H, endo/exo-H-3/4), 1.82 (ddd, *J* = 9.3, 7.1, 3.9 Hz, 1H, endo/exo-H-3/4), 1.23 (dd, *J* = 10.0, 2.0 Hz, 1H, endo/exo-H-3/4), 1.18 (dd, *J* = 10.0, 2.0 Hz, 1H, endo/exo-H-3/4).

^{13}C NMR (100 MHz, $CDCl_3$) δ ppm: 181.3 (C, C-1), 139.8, 135.8, 133.5, 128.4, 127.7, 126.7, 56.5, 45.6, 37.5, 22.9, 22.6.

IR ν_{max} (neat)/cm^{-1} = 2938 (w), 1716 (s), 1451 (m), 1080 (m), 859 (w), 734 (s), 694 (s).

Due to the fast hydrolysis of the target compound in the RBF, no other analyses were performed (After one day, 22% of conversion to the bicyclo[2.2.1]hept-2-en-7-one (**3.37**), ^{1}H NMR ratio imine **3.39b**/ketone **3.37** = 3.51).

7.2.2.2 Fragmentation tests towards the formation of isocyanides

Experimental set-up and Instrumentation: Using the flow machine (Vapourtec R2+/R2+/R4), fragmentation tests of the mixture of imine **3.39b** and ketone **3.37** (Ratio imine/ketone = 3.51) were carried out with the commercial air-heated stainless steel reactor (10 mL capacity, 1 mm i.d.). The reactor was connected to a cooling loop (100 cm, 1 mm i.d.) immersed in an ice bath followed by a backpressure regulator. In-line IR measurements were recorded on an alpha transmission FT-IR from Bruker integrated into the flow system thanks to a Harrick DLC2™ demountable liquid flow cell with NaCl windows. IR spectra were collected with an interval of 6

sec. At the exit of the reactor, the reaction mixture was collected, the solvent was evaporated under reduced pressure and the sample was analysed by NMR spectroscopy.

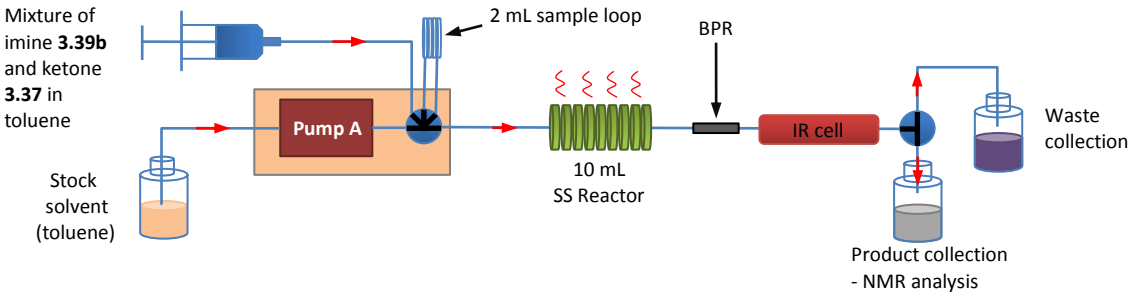

Figure 7.4: Flow set-up for the fragmentation tests towards the formation of isocyanides.

General procedure for the fragmentation tests: At the indicated concentration, a sample of imine **3.39b** and ketone **3.37** (Ratio imine/ketone = 3.51) in dry toluene was prepared and injected into the 2 mL loop. Solvent (toluene) was pumped at the indicated flow rate and the reactor was set to a temperature. Once the temperature was stable, the valve was switched to the loop and the content was injected into the reactor. At the end of the reactor, the reaction was monitored by in-line IR analysis. Spectra were recorded every 6 seconds. For each attempt, the reaction mixture was collected, the solvent was evaporated under reduced pressure and the resulting sample was analysed by NMR spectroscopy. IR spectra were processed with BORIS software (OPA processing).

Sample	Weight imine **3.39b** + ketone **3.37** (mg)	Volume sample (mL)	Concentration sample (mg/mL)	Temp. reactor (°C)	Flow rate (mL/min)	Reaction time (min)
1	9.1	0.4	22.75	250	0.25	40
2	23	0.3	76.7	250	0.25	40

Table 7.1: Reaction conditions for the fragmentation tests.

7.2.3 Chapter 4: Kinetic Studies

3-Oxo-3-phenylpropanoic acid (**4.6a**) and (*Z*)-3-Hydroxy-3-phenylacrylic acid (**4.6a'**)

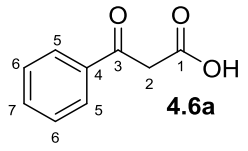

+

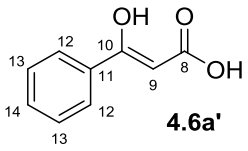

$C_9H_8O_3$

MW = 164.16 g.mol $^{-1}$

White solid

Yield = 63%

Ratio keto/enol: 79/21

m.p. = 85 °C

In a RBF flushed with argon, the mixture of β-keto acid **4.6a** and the enol form **4.6a'** were prepared from a mixture of ethyl benzoylacetate (**4.5a**, 1.73 mL, 10.0 mmol) and sodium hydroxide (20 mL of 0.53 M aq., 10.5 mmol). The mixture was stirred at 0 °C during 3 h and then left to stand at room temperature for 20 h. The reaction mixture was washed with diethyl ether and acidified with hydrochloric acid (1.30 mL at 36% in 11.7 mL of water, 15.0 mmol). The collected solid was then dissolved in diethyl ether, dried over $MgSO_4$, filtered and the solvent was evaporated under reduced pressure to afford the title compounds **4.6a** and **4.6a'** (1.04 g, 6.34 mmol, 63%) as a white solid, m.p. = 85 °C (lit. m.p. = 80 °C).[136] NMR data are consistent with the literature.[137]

Keto form (**4.6a**):

^{1}H NMR (300 MHz, $CDCl_3$) δ ppm: 8.00 (d, *J* = 8.0 Hz, 2H, H-5), 7.69 (t, *J* = 7.5 Hz, 1H, H-7), 7.55 (t, *J* = 7.7 Hz, 2H, H-6), 4.11 (s, 2H, H-2).

Enol form (**4.6a'**):

^{1}H NMR (300 MHz, $CDCl_3$) δ ppm: 7.82 (d, *J* = 8.0 Hz, 2H, H-12), 7.50-7.42 (m, 3H, H-13, 14), 5.74 (s, 1H, H-9).

7.2.3.1 GENERAL PROCEDURE A: Synthesis of Weinreb amides

In a RBF flushed with argon, oxalyl chloride (1.25 equiv.) and dimethylformamide (0.004 equiv.) were added at room temperature to a solution of CH_2Cl_2 with benzoic acid (1 equiv., 0.1 - 0.3 mol.L^{-1}). After 3 h, the media was evaporated under reduced pressure to remove the excess of oxalyl chloride. Then, N,O-dimethylhydroxylamine (1.4 equiv.) and Et_3N (3 equiv.) were added at room temperature to a solution of CH_2Cl_2 (0.1 - 0.3 mol.L^{-1}) with the isolated acyl chloride. After half a day, the reaction was quenched at room temperature with $NaHCO_{3\,sat}$ and extracted twice with CH_2Cl_2. The combined organic layers were then washed four times with NH_4Cl_{sat} and once with $NaCl_{sat}$. The organic layer was then dried over $MgSO_4$, filtered and the solvent was evaporated under reduced pressure to afford the desired Weinreb amide.

N-Methoxy-*N*-methylbenzamide (**4.8a**)

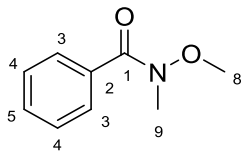

$C_9H_{11}NO_2$

MW = 165.19 g.mol^{-1}

Yellow oil

Yield = 68%

From benzoic acid (**4.7a**, 7.39 g, 60.5 mmol), the reaction was performed as detailed in the general procedure **A** to give the title amide **4.8a** (6.83 g, 41.3 mmol, 68%) as a yellow oil (lit. yield = 98%).[30] NMR data are consistent with the literature.[138]

^{1}H NMR (400 MHz, $CDCl_3$) δ ppm: 7.75-7.64 (m, 2H, H-3), 7.51-7.36 (m, 3H, H-4, 5), 3.56 (s, 3H, H-8), 3.36 (s, 3H, H-9).

^{13}C NMR (100 MHz, $CDCl_3$) δ ppm: 169.5 (C, C-1), 133.8 (C, C-2), 130.1 (CH, C-5), 127.7 (CH, C-3), 127.6 (CH, C-4), 60.6 (CH_3, C-8), 33.3 (CH_3, C-9).

N,4-Dimethoxy-*N*-methylbenzamide (**4.8b**)

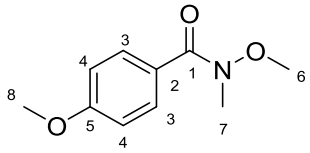

$C_{10}H_{13}NO_3$

MW = 195.22 g.mol^{-1}

Yellow oil

Yield = 95%

From *p*-methoxybenzoic acid (**4.7b**, 10.0 g, 65.7 mmol), the reaction was performed as detailed in the general procedure **A** to give the title amide **4.8b** (12.2 g, 62.5 mmol, 95%) as a yellow oil (lit. yield = 95%).[30] NMR data are consistent with the literature.[30]

^{1}H NMR (300 MHz, $CDCl_3$) δ ppm: 7.73 (d, *J* = 9.0 Hz, 2H, H-3), 6.91 (d, *J* = 9.0 Hz, 2H, H-4), 3.85 (s, 3H, H-8), 3.56 (s, 3H, H-6), 3.36 (s, 3H, H-7).

^{13}C NMR (75 MHz, $CDCl_3$) δ ppm: 169.3 (C, C-1), 161.5 (C, C-5), 130.5 (CH, C-3), 126.0 (C, C-2), 113.2 (CH, C-4), 60.8 (CH_3, C-6), 55.3 (CH_3, C-8), 33.9 (CH_3, C-7).

N-Methoxy-*N*-methyl-4-nitrobenzamide (**4.8e**)

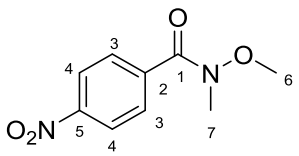

$C_9H_{10}N_2O_4$

MW = 210.19 g.mol^{-1}

Yellow solid

Yield = 92%

m.p. = 75 °C

From *p*-nitrobenzoic acid (**4.7e**, 2.39 g, 14.3 mmol), the reaction was performed as detailed in the general procedure **A** to give the title amide **4.8e** (2.77 g, 13.2 mmol, 92%) as a yellow solid, m.p. = 75 °C (lit. m.p. = 72 °C,[139] lit. yield = 96%[31b]). NMR data are consistent with the literature.[139]

^{1}H NMR (300 MHz, $CDCl_3$) δ ppm: 8.20 (d, *J* = 9.0 Hz, 2H, H-3/4), 7.77 (d, *J* = 9.0 Hz, 2H, H-3/4), 3.46 (s, 3H, C*H*$_3$), 3.33 (s, 3H, C*H*$_3$).

7.2.3.2 GENERAL PROCEDURE B: Synthesis of *t*-butylesters

In a RBF flushed with argon, *n*-butyllithium (2.5 M in hexane, 3.1 equiv.) was slowly added at -78 °C to a THF solution (0.1 mol.L^{-1}) containing diisopropylamine (3 equiv.). After 45 min at 0 °C, the media was cooled again to -78 °C and *t*-butylacetate (3 equiv.) was slowly added followed by the Weinreb amide (1 equiv.). After 1 h 45 min, the reaction was quenched at room temperature with $NaHCO_{3\ sat}$ and extracted three times with EtOAc. The combined organic layers were then washed four times with NH_4Cl_{sat}, dried over $MgSO_4$, filtered and the solvent was evaporated under reduced pressure to afford the desired *t*-butylester.

t-Butyl 3-oxo-3-phenylpropanoate (**4.9a**) and (*Z*)-*t*-Butyl 3-hydroxy-3-phenylacrylate (**4.9a'**)

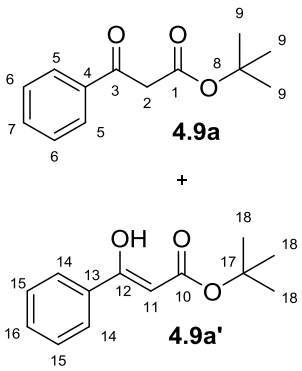

$C_{13}H_{16}O_3$

MW = 220.27 g.mol^{-1}

Orange oil

Purity = 81%

Yield = 81%

Ratio keto/enol: 89/11

From the Weinreb amide **4.8a** (2.00 g, 12.1 mmol), the reaction was performed as detailed in the general procedure **B** to give the title compounds **4.9a** and **4.9a'** (2.67 g (purity = 81%), 9.82 mmol, 81%) as an orange oil (lit. yield = 99%).[30] NMR data are consistent with the literature.[140]

Keto form (**4.9a**):

^{1}H NMR (300 MHz, $CDCl_3$) δ ppm: 7.87 (d, *J* = 7.7 Hz, 2H, H-5), 7.52 (tt, *J* = 7.5, 1.5 Hz, 1H, H-7), 7.41 (t, *J* = 7.5 Hz, 2H, H-6), 3.83 (s, 2H, H-2), 1.36 (s, 9H, H-9).

Enol form (**4.9a'**):

^{1}H NMR (300 MHz, $CDCl_3$) δ ppm: 12.65 (s, 1H, OH), 7.69 (dd, *J* = 8.0, 1.6 Hz, 2H, H-14), 7.37-7.30 (m, 3H, H-15, 16), 5.51 (s, 1H, H-11), 1.47 (s, 9H, H-18).

t-Butyl 3-(4-methoxyphenyl)-3-oxopropanoate (**4.9b**) and (*Z*)-*t*-Butyl 3-hydroxy-3-(4-methoxyphenyl)acrylate (**4.9b'**)

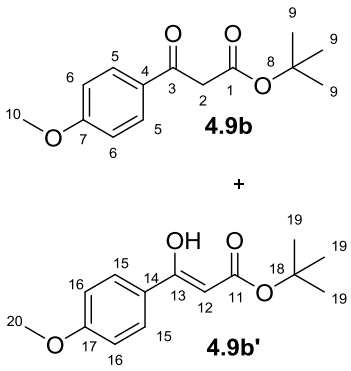

$C_{14}H_{18}O_4$

MW = 250.29 g.mol $^{-1}$

Orange oil

Yield = 96%

Ratio keto/enol: 96/4

From the Weinreb amide **4.8b** (3.00 g, 15.4 mmol), the reaction was performed as detailed in the general procedure **B** to give the title compounds **4.9b** and **4.9b'** (3.69 g, 14.7 mmol, 96%) as an orange oil (lit. yield = 98%).[30] NMR data are consistent with the literature.[30]

Keto form (**4.9b**):

^{1}H NMR (400 MHz, $CDCl_3$) δ ppm: 7.91 (d, *J* = 8.7 Hz, 2H, H-5), 6.93 (d, *J* = 9.1 Hz, 2H, H-6), 3.85 (s, 3H, H-10), 3.83 (s, 2H, H-2), 1.43 (s, 9H, H-9).

^{13}C NMR (100 MHz, $CDCl_3$) δ ppm: 191.4 (C, C-3), 166.9 (C, C-1), 163.8 (C, C-7), 130.8 (CH, C-5), 129.3 (C, C-4), 113.8 (CH, C-6), 81.7 (C, C-8), 55.4 (CH_3, C-10), 47.1 (CH_2, C-2), 27.9 (CH_3, C-9).

Enol form (**4.9b'**):

^{1}H NMR (400 MHz, $CDCl_3$) δ ppm: 12.77 (s, 1H, OH), 7.70 (d, *J* = 8.6 Hz, 2H, H-15), 6.89 (d, *J* = 8.6 Hz, 2H, H-16), 5.48 (s, 1H, H-12), 3.85 (s, 3H, H-20), 1.52 (s, 9H, H-19).

t-Butyl 3-(4-nitrophenyl)-3-oxopropanoate (**4.9e**) and (*Z*)-*t*-Butyl 3-hydroxy-3-(4-nitrophenyl)acrylate (**4.9e'**)

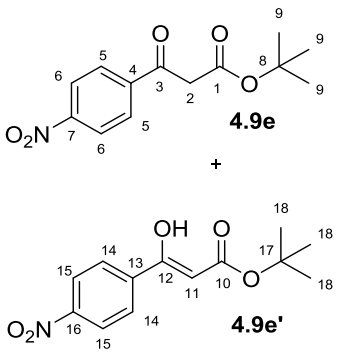

$C_{13}H_{15}NO_5$

MW = 265.26 g.mol $^{-1}$

R*f* = 0.62 (hexane/EtOAc, 8:2)

Yellow oil

Yield = 47%

Ratio keto/enol: 53/47

From the Weinreb amide **4.8e** (2.77 g, 13.2 mmol), the reaction was performed as detailed in the general procedure **B**. The crude mixture was then purified on silica gel (hexane/EtOAc, 8:2) to give the title compounds **4.9e** and **4.9e'** (1.65 g, 6.22 mmol, 47%) as a yellow oil (lit.

yield = 85%).[31b] The ^{1}H NMR spectrum reported below identified the keto and enol forms. NMR data are consistent with the literature.[140]

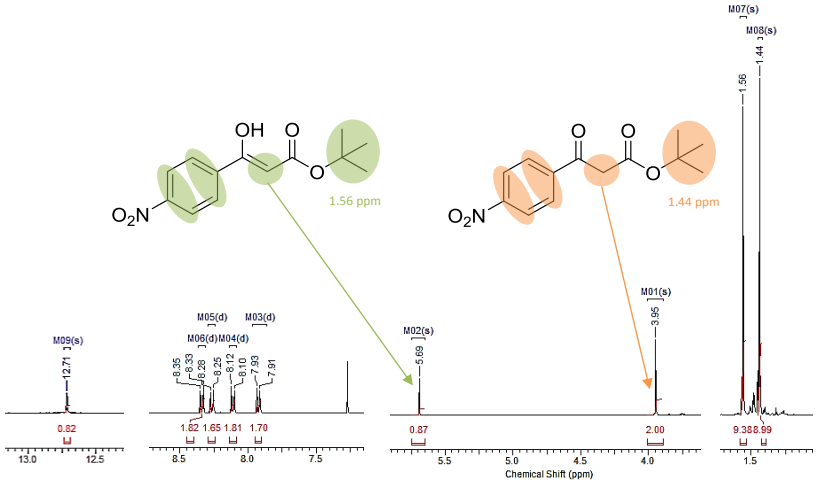

Keto form (**4.9e**):

^{1}H NMR (400 MHz, $CDCl_3$) δ ppm: 8.34 (d, *J* = 8.7 Hz, 2H, H-5/6), 8.11 (d, *J* = 8.7 Hz, 2H, H-5/6), 3.95 (s, 2H, H-2), 1.44 (s, 9H, H-9).

Enol form (**4.9e'**):

^{1}H NMR (400 MHz, $CDCl_3$) δ ppm: 12.71 (s, 1H, OH), 8.27 (d, *J* = 8.7 Hz, 2H, H-14/15), 7.92 (d, *J* = 8.7 Hz, 2H, H-14/15), 5.69 (s, 1H, H-11), 1.56 (s, 9H, H-18).

7.2.3.3 GENERAL PROCEDURE C: Synthesis of 1,3-dioxin-4-ones (R^1 = aryl and R^2 = methyl)

In a RBF flushed with argon, acetic anhydride (15 equiv.) followed by sulfuric acid (1 equiv.) were slowly added at 0°C to a mixture of acetone (10 equiv.) and *t*-butylester (1 equiv.). The solution was then allowed to warm slowly to room temperature over 15 min. After 1 h, the reaction was quenched at room temperature with $Na_2CO_{3\ aq}$ (30 equiv.) and EtOAc were added. The biphasic solution was then allowed to stir for 1 h 40 min and the aqueous layer was extracted three times with EtOAc. The combined organic layers were then washed with NH_4Cl_{sat}, dried over $MgSO_4$, filtered and the solvent was evaporated under reduced pressure to afford the desired dioxinone.

2,2-Dimethyl-6-phenyl-4*H*-1,3-dioxin-4-one (**2.26a**)

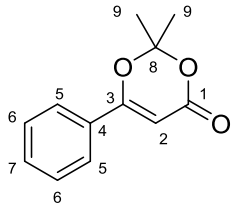

$C_{12}H_{12}O_3$

MW = 204.23 g.mol $^{-1}$

R*f* = 0.35 (hexane/EtOAc, 8:2)

Yellow solid

Yield = 48%

m.p. = 59 °C

From the mixture of **4.9a** and **4.9a'** (1.57 g, 7.13 mmol), the reaction was performed as detailed in the general procedure **C**. The crude mixture was purified on silica gel (hexane/EtOAc, 8:2) to give the title dioxinone **2.26a** (0.710 g, 3.48 mmol, 48%) as a yellow solid, m.p. = 59 °C (lit. m.p. = 66 °C, lit. yield = 73%).[30] NMR data are consistent with the literature.[29]

^{1}H NMR (400 MHz, $CDCl_3$) δ ppm: 7.71 (d, *J* = 7.4 Hz, 2H, H-5), 7.57-7.42 (m, 3H, H-6, 7), 5.91 (s, 1H, H-2), 1.82 (s, 6H, H-9).

^{13}C NMR (100 MHz, $CDCl_3$) δ ppm: 165.0 (C, C-3), 161.9 (C, C-1), 132.1 (CH, C-7), 131.1 (C, C-4), 128.8 (CH, C-6), 126.3 (CH, C-5), 106.6 (C, C-8), 91.3 (CH, C-2), 25.0 (CH_3, C-9).

6-(4-Methoxyphenyl)-2,2-dimethyl-4*H*-1,3-dioxin-4-one (**2.26b**)

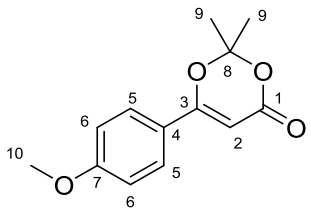

$C_{13}H_{14}O_4$

MW = 234.25 g.mol $^{-1}$

White solid

Yield = 39%

m.p. = 74 °C

From the mixture of **4.9b** and **4.9b'** (1.00 g, 4.00 mmol), the reaction was performed as detailed in the general procedure **C**. A recrystallization of the crude solid from hexane gave the title dioxinone **2.26b** (0.370 g, 1.58 mmol, 39%) as a white solid, m.p. = 74 °C (lit. m.p. = 68 °C, lit. yield = 82%).[30] NMR data are consistent with the literature.[29]

^{1}H NMR (400 MHz, $CDCl_3$) δ ppm: 7.65 (d, *J* = 9.1 Hz, 2H, H-5), 6.95 (d, *J* = 9.1 Hz, 2H, H-6), 5.79 (s, 1H, H-2), 3.86 (s, 3H, H-10), 1.79 (s, 6H, H-9).

^{13}C NMR (100 MHz, $CDCl_3$) δ ppm: 164.9 (C, C-3), 162.8 (C, C-7), 162.1 (C, C-1), 128.1 (CH, C-5), 123.3 (C, C-4), 114.2 (CH, C-6), 106.3 (C, C-8), 89.4 (CH, C-2), 55.4 (CH_3, C-10), 25.0 (CH_3, C-9).

2,2-Dimethyl-6-(4-nitrophenyl)-4*H*-1,3-dioxin-4-one (**2.26e**)

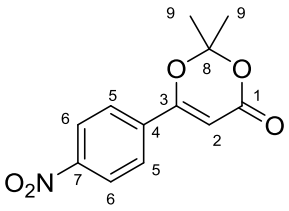

$C_{12}H_{11}NO_5$

MW = 249.22 g.mol $^{-1}$

Yellow solid

Yield = 37%

m.p. = 150 °C

From the mixture of **4.9e** and **4.9e'** (0.990 g, 3.73 mmol), the reaction was performed as detailed in the general procedure **C**. A recrystallization of the crude solid from Et_2O gave the title dioxinone **2.26e** (0.340 g, 1.36 mmol, 37%) as a yellow solid, m.p. = 150 °C (lit. m.p. = 142 °C).[87] NMR data are consistent with the literature.[87]

^{1}H NMR (400 MHz, $CDCl_3$) δ ppm: 8.31 (d, *J* = 9.0 Hz, 2H, H-6), 7.88 (d, *J* = 9.0 Hz, 2H, H-5), 6.03 (s, 1H, H-2), 1.84 (s, 6H, H-9).

^{13}C NMR (100 MHz, $CDCl_3$) δ ppm: 162.3 (C, C-3), 160.8 (C, C-1), 149.7 (C, C-7), 136.9 (C, C-4), 127.2 (CH, C-5), 124.0 (CH, C-6), 107.4 (C, C-8), 94.1 (CH, C-2), 25.1 (CH_3, C-9).

7.2.3.4 GENERAL PROCEDURE D: Synthesis of 1,3-dioxin-4-ones (R^1 = methyl and R^2 = aryl)

In a RBF flushed with argon, concentrated sulfuric acid (1 equiv.) was added dropwise to a cold solution (-10 °C) of *tert*-butyl acetoacetate (1 equiv.) and the corresponding acetophenone (2 equiv.) in acetic anhydride (3.5 equiv.). The mixture was stirred for 16 - 43 h at 0 - 15 °C, then carefully transferred to an ice-cooled saturated solution of potassium carbonate (50 - 70 mL) and stirred for 30 min at room temperature. The aqueous layer was extracted with DCM (3 x 100 mL), and the combined organic layers were washed with brine (3 x 100 mL), dried over $MgSO_4$, filtered and the solvent was evaporated under reduced pressure to afford the crude dioxinone.

2-(4-Bromophenyl)-2,6-dimethyl-4*H*-1,3-dioxin-4-one (**4.1b**)

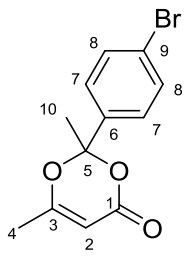

$C_{12}H_{11}BrO_3$

MW = 283.12 g.mol $^{-1}$

R*f* = 0.17 (hexane/EtOAc, 85:15)

White solid

Yield = 18%

m.p. = 100 °C

From the 4-bromoacetophenone (**4.10b**, 4.88 g, 24.5 mmol), the reaction was performed as detailed in the general procedure **D**. The reaction mixture was stirred for 43 h at 0 °C. The crude mixture was purified on silica gel (hexane/Et_2O, 85:15) to remove the excess of 4-bromoacetophenone and impurities. This column was followed by a recrystallization in 5 mL of hexane at 65 °C to give the title compound **4.1b** (0.600 g, 2.12 mmol, 18%) as a white solid, m.p. = 100 °C.

^{1}H NMR (400 MHz, $CDCl_3$) δ ppm: 7.52 (d, *J* = 8.6 Hz, 2H, H-8), 7.34 (d, *J* = 8.6 Hz, 2H, H-7), 5.18 (d, *J* = 1.0 Hz, 1H, H-2), 2.01 (d, *J* = 1.0 Hz, 3H, H-4), 1.87 (s, 3H, H-10).

^{13}C NMR (100 MHz, $CDCl_3$) δ ppm: 169.0 (C, C-3), 160.9 (C, C-1), 139.6 (C, C-6), 131.8 (CH, C-8), 126.7 (CH, C-7), 123.3 (C, C-9), 106.1 (C, C-5), 96.6 (CH, C-2), 29.3 (CH_3, C-10), 20.0 (CH_3, C-4).

UV (MeCN) C = 5.09x10^{-5} M, $\lambda_1 = 229.75$ nm, $\varepsilon_1 = 12161$ M^{-1}.cm^{-1}, $\lambda_2 = 246.63$ nm, $\varepsilon_2 = 7898$ M^{-1}.cm^{-1}.

IR ν_{max} (neat)/cm^{-1} = 1716 (m), 1387 (m), 1171 (m), 969 (m), 824 (s).

LRMS (LC/ES$^+$): m/z = 199, 25% [1-(4-bromophenyl)ethanone(^{79}Br)+H]$^+$; 201, 25% [1-(4-bromophenyl)ethanone(^{81}Br)+H]$^+$; 283, 100% [M(^{79}Br)+H]$^+$; 285, 100% [M(^{81}Br)+H]$^+$, 300, 25% [M(^{79}Br)+NH_4]$^+$; 302, 25% [M(^{81}Br)+NH_4]$^+$; 305, 20% [M(^{79}Br)+Na]$^+$; 307, 20% [M(^{81}Br)+Na]$^+$.

HRMS (ES$^+$): Found 304.9786 Da, $C_{12}H_{11}BrNaO_3$ [M+Na]$^+$ requires 304.9784 Da.

2-(4-Methoxyphenyl)-2,6-dimethyl-4*H*-1,3-dioxin-4-one (**4.1d**)

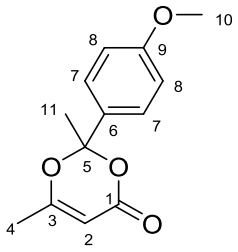

$C_{13}H_{14}O_4$

MW = 234.25 g.mol^{-1}

R*f* = 0.1 (hexane/EtOAc, 9:1)

Yellow solid

Yield = 20%

m.p. = 70 °C

From the 4-methoxacetophenone (**4.10d**, 9.06 g, 60.3 mmol), the reaction was performed as detailed in the general procedure **D**. The reaction mixture was stirred for 16 h at 15 °C. The crude oil was purified on silica gel (hexane/EtOAc, 9:1) to remove the excess of 4-methoxyacetophenone and impurities. This column was followed by a recrystallization in 60 mL of hexane at 60 °C to give the title compound **4.1d** (1.41 g, 6.02 mmol, 20%) as a yellow solid, m.p. = 70 °C.

^{1}H NMR (400 MHz, $CDCl_3$) δ ppm: 7.38 (d, *J* = 8.6 Hz, 2H, H-7), 6.89 (d, *J* = 8.6 Hz, 2H, H-8), 5.17 (d, *J* = 1.0 Hz, 1H, H-2), 3.81 (s, 3H, H-10), 2.00 (s, 3H, H-4), 1.87 (s, 3H, H-11).

^{13}C NMR (100 MHz, $CDCl_3$) δ ppm: 168.9 (C, C-3), 161.4 (C, C-1), 160.0 (C, C-9), 132.5 (C, C-6), 126.3 (CH, C-7), 113.9 (CH, C-8), 106.7 (C, C-5), 96.4 (CH, C-2), 55.3 (CH_3, C-10), 29.5 (CH_3, C-11), 20.1 (CH_3, C-4).

UV (MeCN) C = 7.56x10^{-5} M, λ_1 = 230.50 nm, ε_1 = 10966 M^{-1}.cm^{-1}, λ_2 = 245.88 nm, ε_2 = 7725 M^{-1}.cm^{-1}.

IR ν_{max} (neat)/cm^{-1} = 1710 (m), 1351 (m), 1244 (m), 1163 (m), 840 (m).

LRMS (LC/ES$^+$): m/z = 151, 70% [1-(4-methoxyphenyl)ethanone+H]$^+$; 235, 100% [M+H]$^+$; 257, 10% [M+Na]$^+$; 469, 10% [2M+H]$^+$; 486, 10% [2M+NH_4]$^+$; 491, 25% [2M+Na]$^+$.

HRMS (ES$^+$): Found 257.0783 Da, $C_{13}H_{14}NaO_4$ [M+Na]$^+$ requires 257.0784 Da.

2,6-Dimethyl-2-phenyl-4*H*-1,3-dioxin-4-one (**4.1a**)

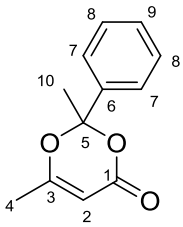

$C_{12}H_{12}O_3$

MW = 204.22 g.mol^{-1}

R*f* = 0.22 (hexane/EtOAc, 9:1)

Pale yellow solid

Yield = 31%

m.p. = 89 °C

A solution flushed with argon of 2,2,6-trimethyl-4*H*-1,3-dioxin-4-one (**2.38**, 1.30 mL, 9.78 mmol) and acetophenone (11.41 mL, 97.80 mmol) was injected into the flow set-up described below using the bottle feed configuration. Once the mixture was entirely injected, it was then pushed into the reactor by acetonitrile (Stock solvent). The residence time was set at 10 min (flow rate = 1 mL/min) and the 10 mL Stainless Steel reactor, connected to a cooling loop (100 cm, 1 mm i.d.) followed by a backpressure regulator (250 psi), was heated to 150 °C. A brown liquid mixture was collected and isolated with a lot of acetophenone due to the large excess of this reagent. A distillation at 70 °C and under reduced pressure was performed to remove this excess. The crude mixture was then purified on silica gel (hexane/EtOAc, 9:1) to give the title compound **4.1a** (0.620 g, 3.04 mmol, 31%) as pale yellow solid, m.p. = 89 °C (lit. m.p. = 93 °C).[141] NMR data are consistent with the literature.[142]

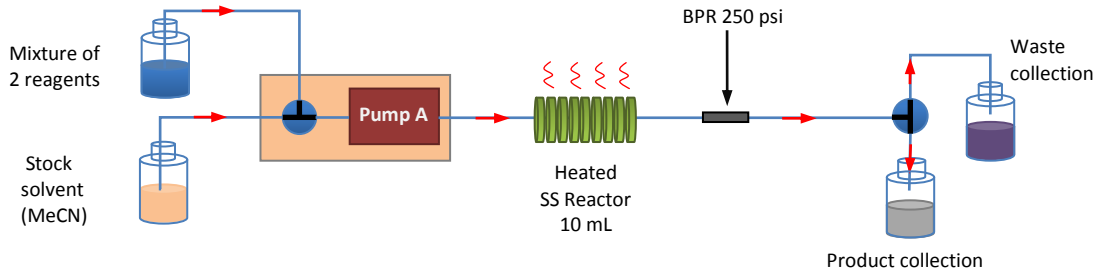

Figure 7.5: Flow set-up for the synthesis of the 2,6-dimethyl-2-phenyl-4*H*-1,3-dioxin-4-one - Bottle-feed configuration.

^{1}H NMR (400 MHz, $CDCl_3$) δ ppm: 7.49-7.44 (m, 2H, H-7), 7.40-7.35 (m, 3H, H-8, 9), 5.17 (d, *J* = 0.9 Hz, 1H, H-2), 2.01 (d, *J* = 0.9 Hz, 3H, H-4), 1.89 (s, 3H, H-10).

^{13}C NMR (100 MHz, $CDCl_3$) δ ppm: 169.1 (C, C-3), 161.3 (C, C-1), 140.5 (C, C-6), 129.1 (CH, C-8 or C-9), 128.6 (CH, C-8 or C-9), 124.9 (CH, C-7), 106.6 (C, C-5), 96.6 (CH, C-2), 29.5 (CH_3, C-10), 20.1 (CH_3, C-4).

UV (MeCN) C = 1.37x10^{-4} M, λ = 246.63 nm, ε = 6708 M^{-1}.cm^{-1}.

IR ν_{max} (neat)/cm^{-1} = 1713 (s), 1353 (m), 1171 (m), 972 (m), 831 (m).

7.2.3.5 GENERAL PROCEDURE E: Kinetic Studies

Experimental set-up and Instrumentation: Using the flow machine (Vapourtec R2+/R2+/R4), kinetic studies experiments were carried out with a home-made stainless steel reactor (10 mL capacity, 1 mm i.d.). Heating of the reactor was performed by immersion in a high temperature silicone oil bath (Grant Optima™ TXF200). The reactor was connected to a cooling loop (100 cm, 1 mm i.d.) immersed in an ice bath and followed by a backpressure regulator. In-line IR measurements were recorded on an alpha transmission FT-IR from Bruker integrated into the flow system thanks to a Harrick DLC2™ demountable liquid flow cell with NaCl windows. IR spectra were collected with an interval of 3.75 sec. In-line UV measurements were recorded on an Ocean Optics DH-2000-BAL spectrometer integrated into the flow system with a Type 583-F Starna® fluorimeter flow cell (1 mm path length, 0.011 mL volume). UV spectra were recorded with an interval of 1.2 sec. When needed for off-line reaction analysis (GC or NMR), the system was connected to a Gilson Prep Fraction Collector.

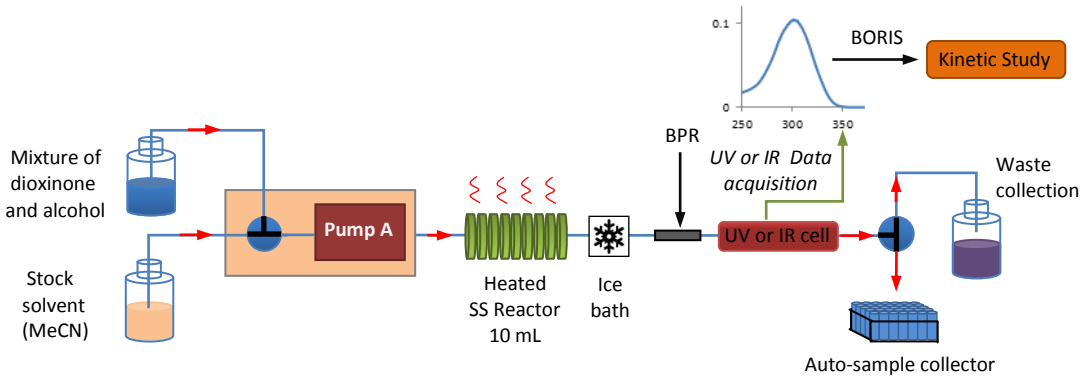

Figure 7.6: Flow set-up for the kinetic studies of the fragmentation of 1,3-dioxin-4-ones in presence of an excess of alcohol - Bottle-feed configuration.

General procedure of Push-Out Kinetic Studies: A solution of dioxinone (1 equiv., [dioxinone] = 1 mM for UV analysis or 0.015 - 0.3 M for IR analysis) and alcohol (4 equiv.) in dry acetonitrile was prepared. Solvent (dry acetonitrile) was pumped at flow rate F_1 and the reactor was set to

the temperature of interest. Once the temperature was stable, the feeding valve was switched to the reagent solution at the same flow rate F_1. At the end of the reactor, the reaction was monitored by in-line analysis (UV or IR) or off-line NMR. The flow rate was switched to flow rate F_2 when the steady state of conversion was reached (stability of the spectra) and the mixture exiting the reactor was monitored until a second steady state was reached. The feeding valve was immediately returned to solvent feed until no further absorption was noticed on the monitoring and the flow rate was returned to F_1. This procedure was repeated at several reaction temperatures (4-5 different temperatures for a complete study). Data sampling rate was determined by the acquisition parameters. IR and UV spectra were processed with BORIS software to perform the kinetic resolution (OPA processing, height of non-overlapping peaks processing or MLR processing) and by using the spectra of 0% and 100% conversion experiments respectively conducted at 30 °C and 160 °C as references to scale the spectroscopic data between 0 and 1.

General procedure of Steady-State Kinetic Studies: A solution of dioxinone (1 equiv., [dioxinone] = 1 mM for UV analysis or 0.015 - 0.3 M for IR analysis) and alcohol (4 equiv.) in dry acetonitrile was prepared. Solvent (dry acetonitrile) was pumped at a given flow rate and the reactor was set to a given temperature. Once the temperature was stable, the feeding valve was switched to the reagent solution and the mixture exiting the reactor was monitored by *in situ* analysis (UV or IR). When the steady state of the conversion was reached, the feeding valve was returned to the solvent feed and the procedure was repeated at the next flow rate whilst maintaining the same reaction temperature. The completed cycle of multiple experiments (typically five within a cycle, across a range of flow rates from 1 mL min^{-1} to 10 mL min^{-1}) was itself repeated at several temperatures. The reaction time was calculated from each flow rate displayed on the flow system with a correction for thermal expansion of acetonitrile according to $Flow_{effective} = Flow_{pump} (1 + \alpha\Delta T)$ where α = the expansion coefficient of the solvent.[143] IR and UV spectra were processed with BORIS software by calibration-less methods (OPA processing or height of non-overlapping peaks processing) and by using the spectra of 0% and 100% conversion experiments respectively conducted at 30 °C and 160 °C as references to scale the spectroscopic data between 0 and 1. In the following Figure 7.7, a typical dioxinone concentration profile for the steady-state method is described and the flow rates effective to use in the calculations. Analysis of ^{1}H NMR data was carried out manually (see section ^{1}H NMR Analysis).

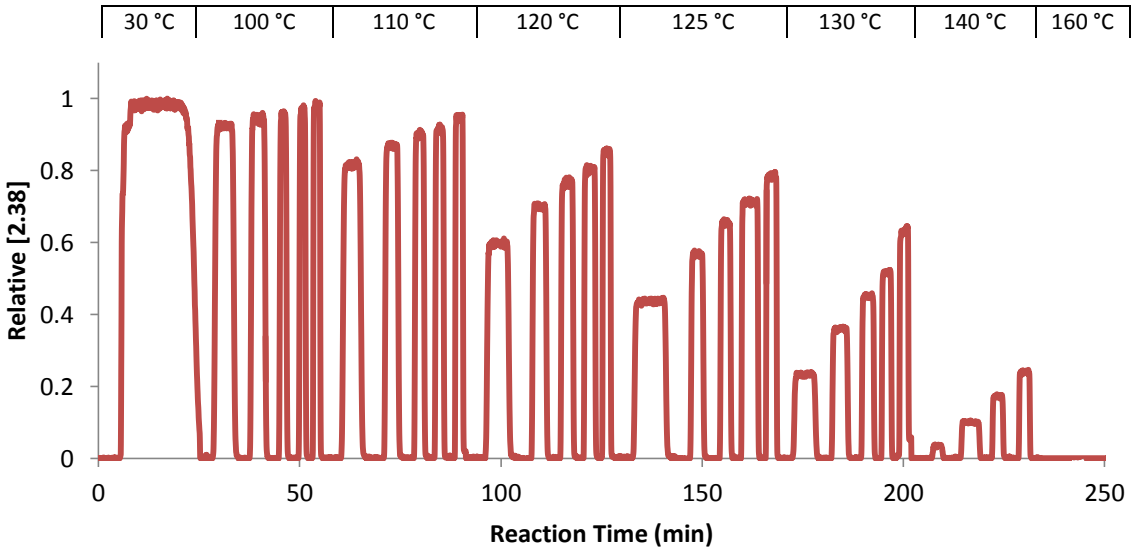

Flow pump ($mL.min^{-1}$)	Flow effective ($mL.min^{-1}$)					
	100 °C	110 °C	120 °C	125 °C	130 °C	140 °C
2	2.19728	2.22468	2.25208	2.26578	2.27948	2.30688
3	3.29592	3.33702	3.37812	3.39867	3.41922	3.46032
4	4.39456	4.44936	4.50416	4.53156	4.55896	4.61376
5	5.4932	5.56170	5.63020	5.66445	5.69870	5.76720
7	7.69048	7.78638	7.88228	7.93023	7.97818	-

Figure 7.7: Concentration profile of 2,2,6-trimethyl-4*H*-1,3-dioxin-4-one (**2.38**) after thermolysis in the presence of EtOH (4 equiv.) under steady-state conditions. Processing of the IR spectra with the OPA method. Tabulation of the flow rates effective after correction due to the expansion coefficient of the solvent.

<u>General procedure for data processing:</u>

<u>Orthogonal Projection Approach processing:</u>

To perform the OPA resolution of the UV or IR spectra collected during the push-out or steady state kinetic experiments, Bristol Online Investigation Software was used. First of all, the number of spectral components was chosen (set at 2 for thermolysis, Component 1: 1,3-dioxin-4-one and Component 2: mixture of ketone **4.2** and β-ketoester **4.4**). The software cannot distinguish **4.2** and **4.4** as they keep the same ratio during the thermolysis. Then, the resolution was performed through alternating least squares cycles. The OPA resolution stopped when the different spectra (relative to the number of spectral components initially chosen) with the highest dissimilarities are distinguished. The estimated spectra (plot of absorbance *vs.* wavelength/wavenumber) and concentration profiles (plot of relative concentration of the component *vs.* experimental time) were generated and sent to an Excel sheet allowing the calculation of the kinetic data. In all cases, the estimated spectra generated for the 1,3-dioxin-4-one was consistent with the pure one (Figure 7.9(c) *vs.* 7.10). Examples of OPA resolutions of UV and IR spectra from thermolysis of 1,3-dioxin-4-one **4.1d** (Scheme 7.1) under push-out conditions are described in Figures 7.8-7.15.

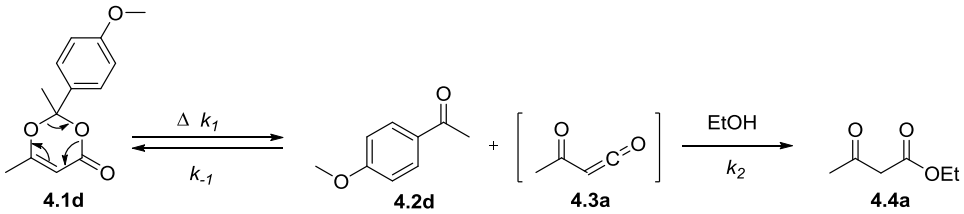

Scheme 7.1: Thermolysis of **4.1d** and acylketene trapping by EtOH.

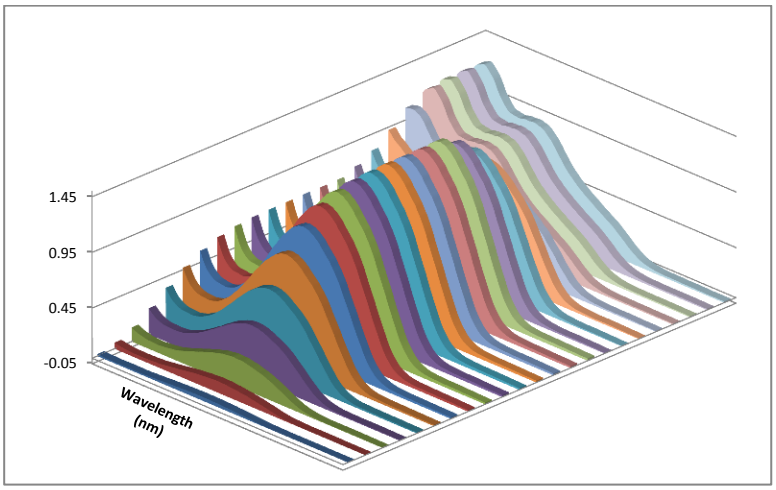

Figure 7.8: in-line UV spectra collected during thermolysis of **4.1d** in the presence of 4 equiv. of EtOH in MeCN at 85 °C under push-out conditions (Table 4.9, Entry 6 85 °C). From the series of UV spectra collected for each temperature, the OPA resolution generates the push-out profiles of Components 1 and 2 (Figures 7.9(a) and 7.9(b)) and the estimated UV spectra (Figures 7.9(c) and 7.9(d)).

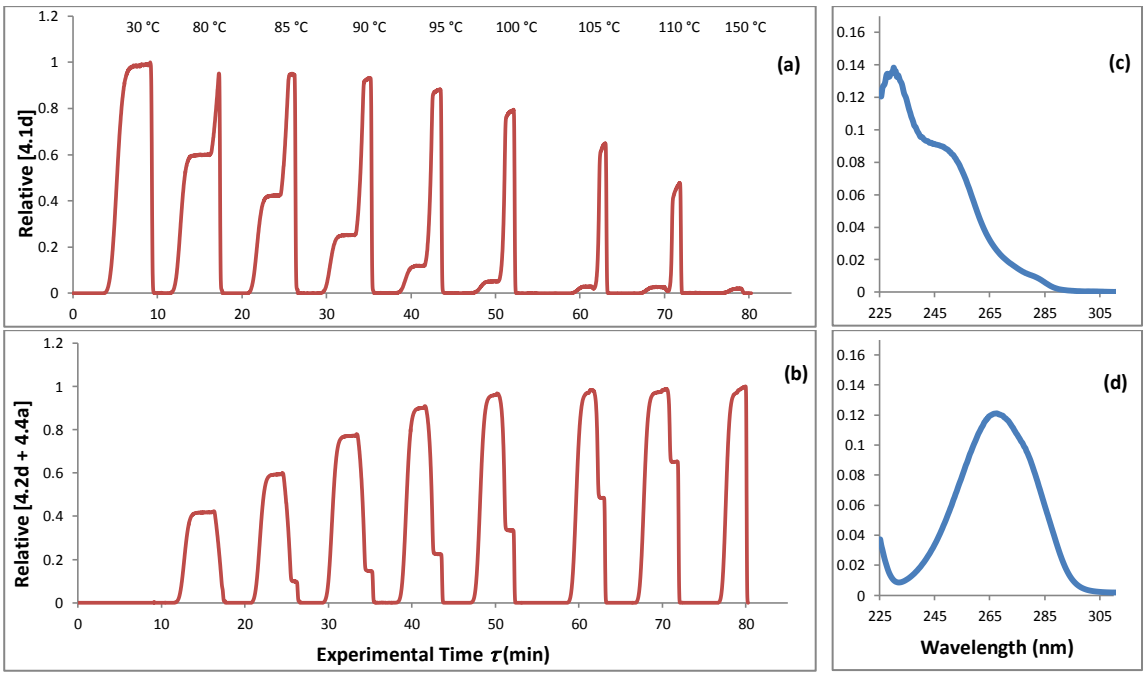

Figure 7.9: OPA resolution of the in-line UV spectra collected during the thermolysis of **4.1d** with 4 equiv. of EtOH in MeCN under push-out conditions. Selection of 2 spectral components in the OPA method. Generation of the corresponding (a) concentration profile of Component 1 **4.1d** (b) concentration profile of Component 2 (mixture of **4.2d** and **4.4a**) (c) estimated UV spectrum of Component 1 **4.1d** and (d) estimated UV spectrum of Component 2 (mixture of **4.2d** and **4.4a**).

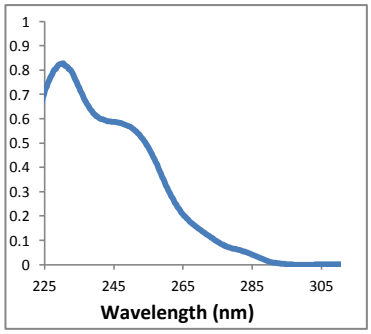

Figure 7.10: Pure UV spectrum of **4.1d**.

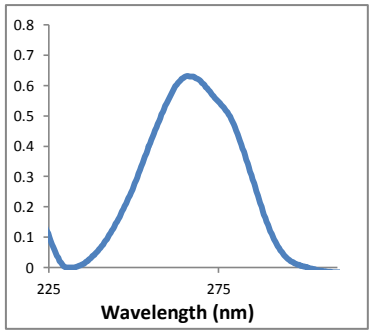

Figure 7.11: Pure UV spectrum of **4.2d**.

As previously stated, **4.2d** and **4.4a** are identified as a single component during the OPA resolution. Indeed, the ratio does not change during the thermolysis. Therefore, the OPA method does not make any distinctions. An example of OPA resolution with 3 spectral components is described in Figure 7.12. Due to this constant ratio between **4.2d** and **4.4a** and the weak signal of **4.4a**, the method does not resolve the request.

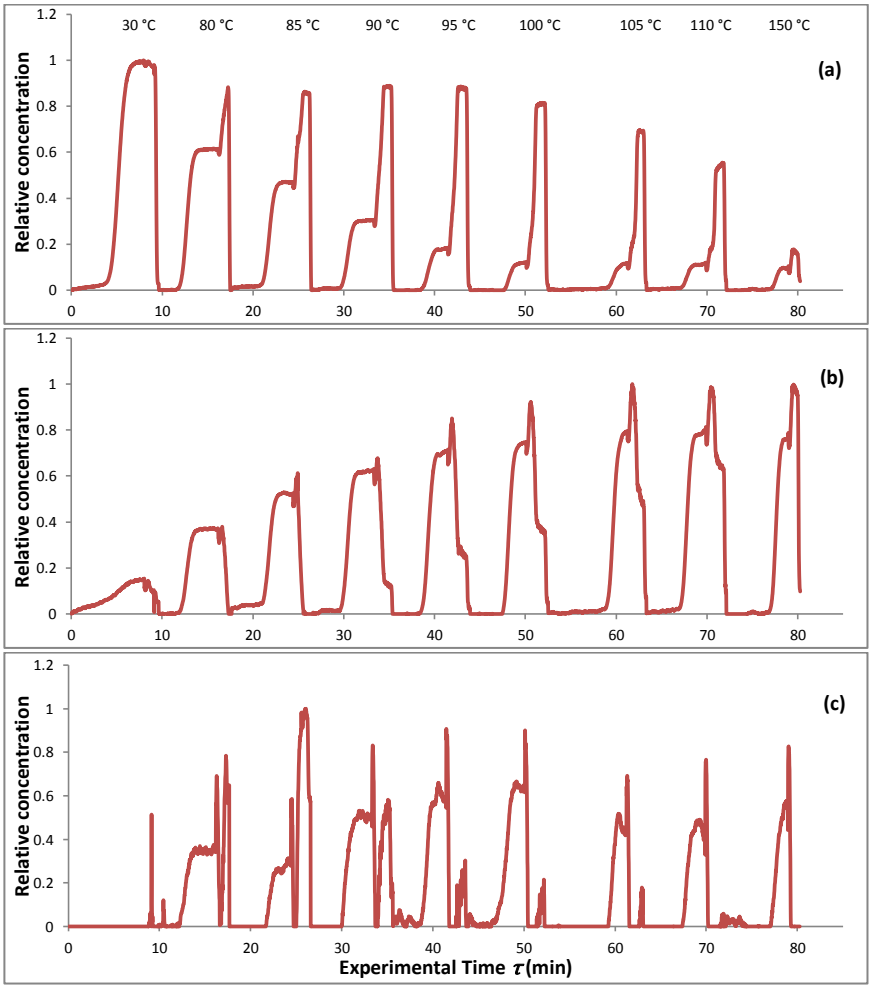

Figure 7.12: OPA resolution of the in-line UV spectra collected during the thermolysis of **4.1d** with 4 equiv. of EtOH in MeCN under push-out conditions (same dataset as used for resolution in Figure 7.9). Selection of 3 spectral components in the OPA method. Generation of the corresponding (a) concentration profile of Component 1 (b) concentration profile of Component 2 (c) and concentration profile of Component 3.

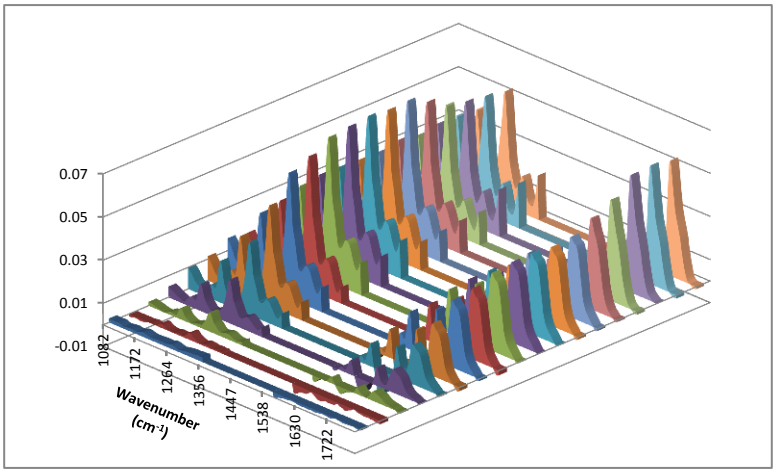

Figure 7.13: in-line IR spectra collected during thermolysis of **4.1d** in the presence of 4 equiv. of EtOH in MeCN at 85 °C under push-out conditions (Table 4.9, Entry 8 85 °C). From the series of IR spectra collected for each temperature, the OPA resolution generates the push-out profiles of Components 1 and 2 (Figures 7.14(a) and 7.14(b)) and the estimated IR spectra (Figures 7.14(c) and 7.14(d)).

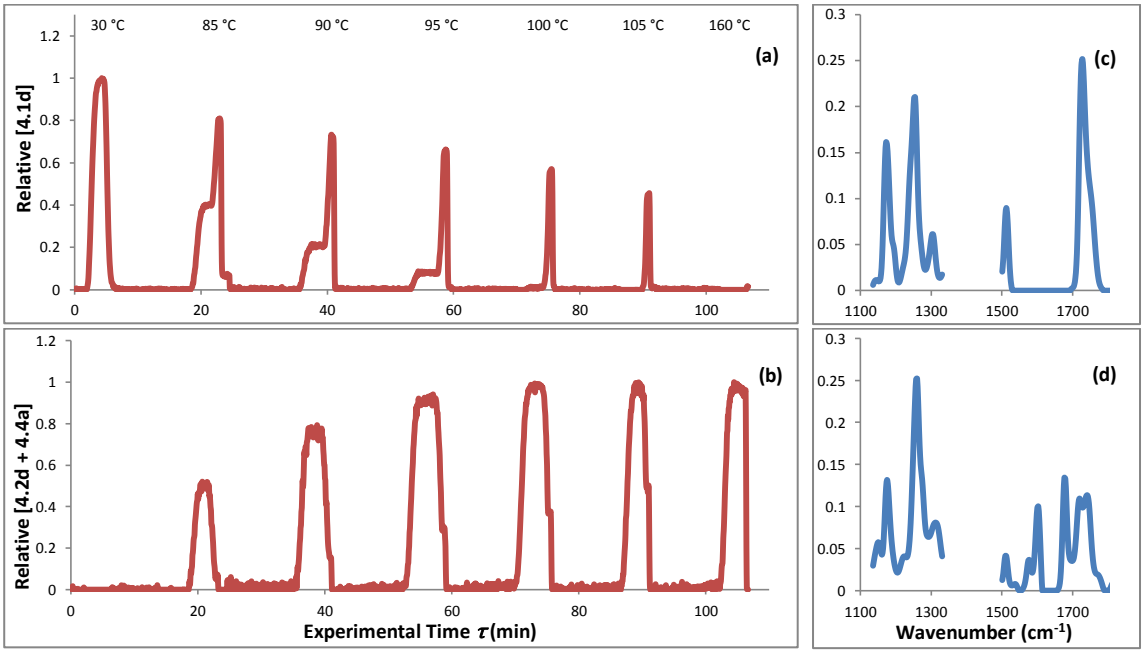

Figure 7.14: OPA resolution of the in-line IR spectra collected during the thermolysis of **4.1d** with 4 equiv. of EtOH in MeCN under push-out conditions. Selection of 2 spectral components in the OPA method and selection of the range of wavenumber to consider in the OPA resolution (removal of the area with noise). Generation of the corresponding (a) concentration profile of Component 1 **4.1d** (b) concentration profile of Component 2 (mixture of **4.2d** and **4.4a**) (c) estimated IR spectrum of Component 1 **4.1d** and (d) estimated IR spectrum of Component 2 (mixture of **4.2d** and **4.4a**).

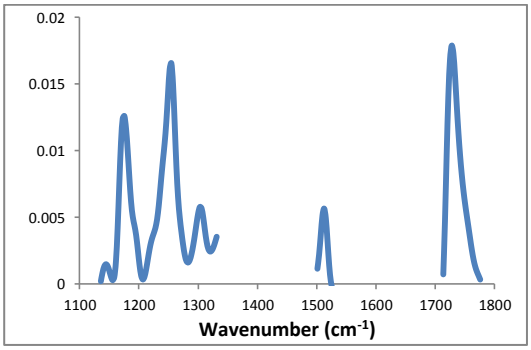

Figure 7.15: Pure IR spectrum of **4.1d**.

Height of non-overlapping peak processing:

Height of non-overlapping peak processing, conducted using Bristol Online Reaction Investigation Software (BORIS), determines the UV or IR peak height above zero (Absorbance) at a selected wavelength/wavenumber and scales the spectroscopic data between 0 and 1 by using the spectra of 0% and 100% conversion experiments respectively conducted at 30 °C and 160 °C as references. Clear peaks need to be selected (no overlaps between peaks). For each wavelength/wavenumber selected, the relative absorbance profiles (plot of relative peak height of the component *vs.* experimental time) were generated and sent to an Excel sheet allowing the calculation of the kinetic data.

Multivariate Linear Regression processing:

Multivariate Linear Regression processing conducted using Bristol Online Reaction Investigation Software (BORIS), estimates the concentration profiles of the components from the given pure components spectra (References) and scales the spectroscopic data between 0 and 1 by using the spectra of 0% and 100% conversion experiments respectively conducted at 30 °C and 160 °C as references. In our MLR processing, paired pure spectra of 1,3-dioxin-4-one and the released ketone **4.2** were used as references for the resolution. For each 1,3-dioxin-4-one and ketone **4.2**, the concentration profiles (plot of relative concentration of the component *vs.* experimental time) were generated and sent to an Excel sheet allowing the calculation of the kinetic data.

Table Data, Arrhenius Plots and NMR of the products:

Table 4.7 Data:

Entry 1: Thermolysis of **2.38** in the presence of 4 equiv. EtOH using push-out method, in-line UV analysis and OPA processing. F_1 = 1 mL.min^{-1} and F_2 = 10 mL.min^{-1}

Temp. °C	*k*	ln(*k*)	1/T (K^{-1})
100	**0.000225300**	-8.39807	0.00267988
110	**0.000660526**	-7.32247	0.00260994
120	**0.001808672**	-6.31516	0.00254355
130	**0.004704682**	-5.35920	0.00248046
135	**0.007174536**	-4.93722	0.00245008
140	**0.010443578**	-4.56177	0.00242042

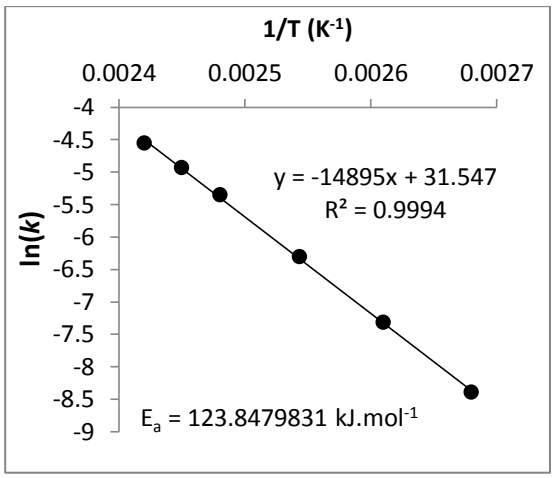

Entry 2: Thermolysis of **2.38** in the presence of 4 equiv. EtOH using push-out method, in-line UV analysis and height of non-overlapping peak processing at 245 nm. F_1 = 1 mL.min^{-1} and F_2 = 10 mL.min^{-1}

Temp. °C	*k*	ln(*k*)	1/T (K^{-1})
100	**0.000232959**	-8.36464	0.00267988
110	**0.000646222**	-7.34436	0.00260994
120	**0.001823268**	-6.30712	0.00254355
130	**0.004736555**	-5.35244	0.00248046
135	**0.007071116**	-4.95173	0.00245008
140	**0.010811649**	-4.52713	0.00242042

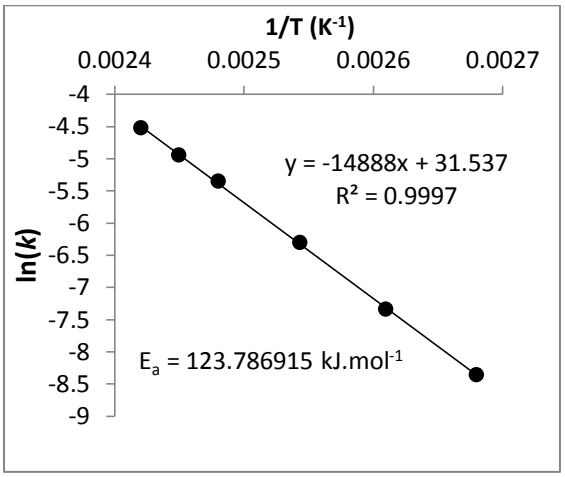

Entry 3: Thermolysis of **2.38** in the presence of 4 equiv. EtOH using steady-state method, in-line UV analysis and OPA processing.

Temp. °C	*k*	ln(*k*)	1/T (K^{-1})
100	**0.000237024**	-8.34735	0.00267988
110	**0.000677258**	-7.29746	0.00260994
120	**0.001893935**	-6.26910	0.00254355
130	**0.004921215**	-5.31420	0.00248046

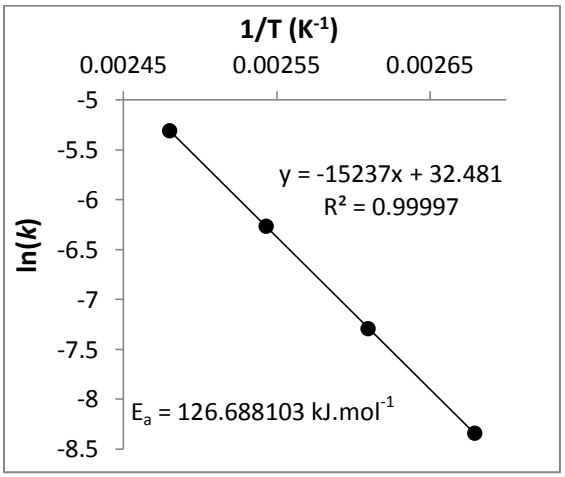

Entry 4: Thermolysis of **2.38** in the presence of 4 equiv. EtOH using push-out method, in-line IR analysis and OPA processing. F_1 = 1 mL.min^{-1} and F_2 = 10 mL.min^{-1}

Temp. °C	*k*	ln(*k*)	1/T (K^{-1})
100	**0.000268034**	-8.22440	0.00267988
105	**0.000411167**	-7.79651	0.00264445
110	**0.000705572**	-7.25650	0.00260994
115	**0.001167875**	-6.75257	0.00257632
120	**0.001915560**	-6.25775	0.00254355
125	**0.003164512**	-5.75576	0.00251161
130	**0.005064222**	-5.28555	0.00248046
135	**0.007967575**	-4.83238	0.00245008
140	**0.011582578**	-4.45825	0.00242042

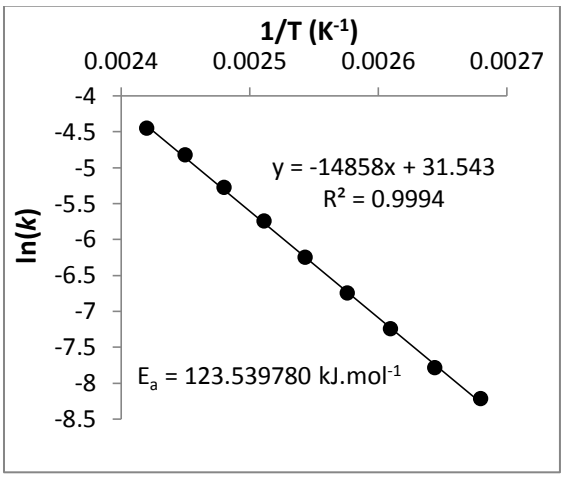

Entry 5: Thermolysis of **2.38** in the presence of 4 equiv. EtOH using push-out method, in-line IR analysis and height of non-overlapping peak processing at 1640 cm^{-1}. F_1 = 1 $mL.min^{-1}$ and F_2 = 10 $mL.min^{-1}$

Temp. °C	*k*	ln(*k*)	1/T (K^{-1})
100	**0.000247606**	-8.30367	0.00267988
105	**0.000382279**	-7.86936	0.00264445
110	**0.000660319**	-7.32279	0.00260994
115	**0.001089549**	-6.82199	0.00257632
120	**0.001804247**	-6.31761	0.00254355
125	**0.003039696**	-5.79600	0.00251161
130	**0.004777281**	-5.34388	0.00248046
135	**0.007564617**	-4.88427	0.00245008
140	**0.011361675**	-4.47751	0.00242042

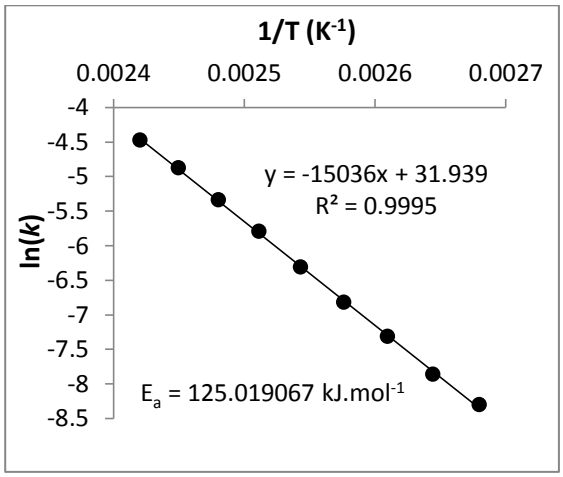

Entry 6: Thermolysis of **2.38** in the presence of 4 equiv. EtOH using steady-state method, in-line IR analysis and OPA processing.

Temp. °C	*k*	ln(*k*)	1/T (K^{-1})
110	**0.000720672**	-7.23533	0.00260994
120	**0.001834821**	-6.30081	0.00254355
125	**0.003145287**	-5.76185	0.00251161
130	**0.005110373**	-5.27648	0.00248046
140	**0.011962562**	-4.42597	0.00242042

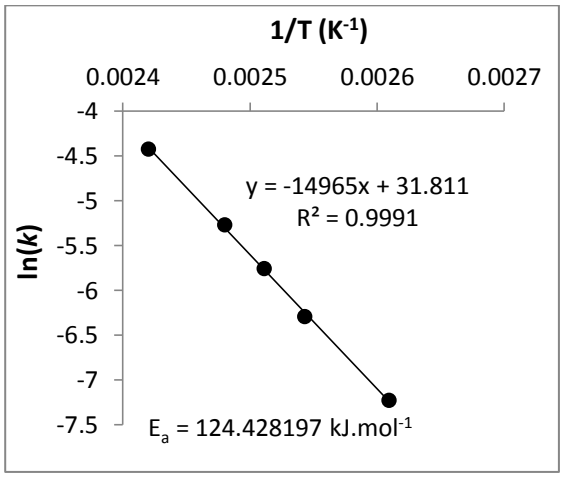

Entry 7: Thermolysis of **2.38** in the presence of 4 equiv. EtOH using reverse push-out method, in-line UV analysis and OPA processing. F_1 = 10 $mL.min^{-1}$ and F_2 = 1 $mL.min^{-1}$

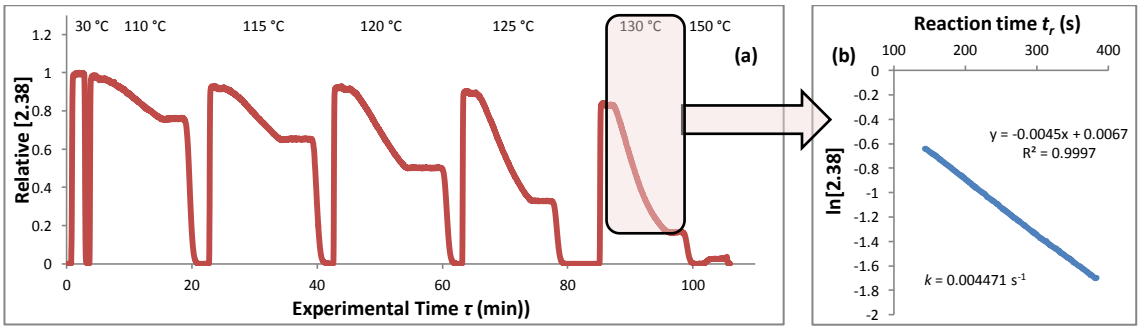

Figure 7.16: (a) OPA resolution of the in-line UV spectra collected during the thermolysis of **2.38** with 4 equiv. of EtOH in MeCN under reverse push-out conditions. (b) Calculation of the reaction rate constant at 130 °C from the kinetic plot of 253 data points (*vs.* 22 data points for the standard push-out experiment at 130 °C) - Extended transitional part.

Temp. °C	*k*	ln(*k*)	1/T (K^{-1})
110	**0.000623600**	-7.38000	0.00260994
115	**0.000955728**	-6.95304	0.00257632
120	**0.001657503**	-6.40244	0.00254355
125	**0.002795612**	-5.87970	0.00251161
130	**0.004470768**	-5.41019	0.00248046

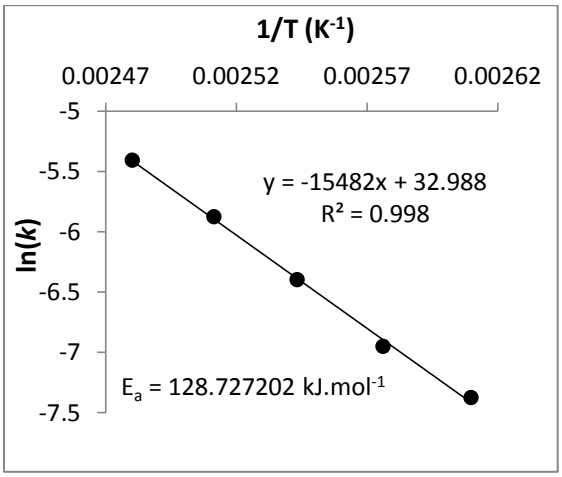

Entry 8: Thermolysis of **2.38** in the presence of 4 equiv. EtOH using push-out method, in-line IR analysis and OPA processing. F_1 = 1 mL.min^{-1} and F_2 = 2 mL.min^{-1}

Temp. °C	*k*	ln(*k*)	1/T (K^{-1})
110	**0.000658092**	-7.32617	0.00260994
115	**0.001256256**	-6.67962	0.00257632
120	**0.001962024**	-6.23378	0.00254355
125	**0.002926425**	-5.83397	0.00251161
130	**0.004801202**	-5.33889	0.00248046

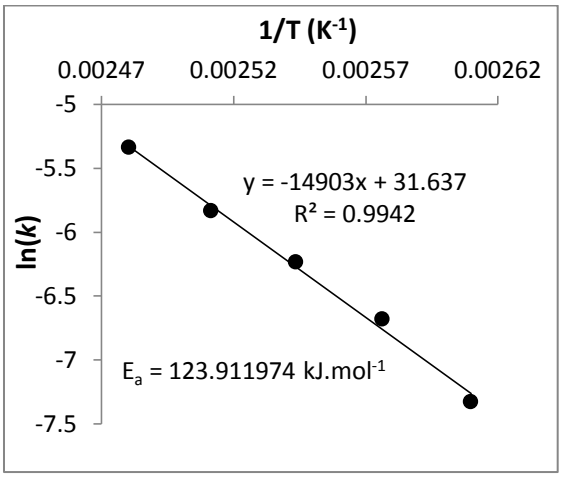

Entry 9: Thermolysis of **2.38** in the presence of 4 equiv. EtOH using push-out method, in-line UV analysis and OPA processing. F_1 = 1 mL.min^{-1} and F_2 = 2 mL.min^{-1}

Temp. °C	*k*	ln(*k*)	1/T (K^{-1})
115	**0.001029629**	-6.87856	0.00257632
120	**0.001743752**	-6.35172	0.00254355
125	**0.002893492**	-5.84529	0.00251161
130	**0.004822791**	-5.33440	0.00248046
140	**0.011302172**	-4.48276	0.00242042

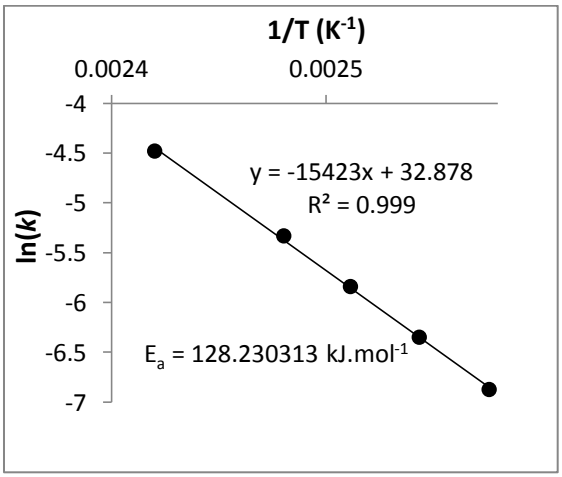

Entry 10: Thermolysis of **2.38** in the presence of 4 equiv. EtOH using steady-state method and off-line ^{1}H NMR analysis.

Temp. °C	*k*	ln(*k*)	1/T (K^{-1})
110	**0.000650812**	-7.33729	0.00260994
120	**0.001891984**	-6.27013	0.00254355
125	**0.002966663**	-5.82032	0.00251161
130	**0.005133186**	-5.27203	0.00248046
140	**0.012523923**	-4.38011	0.00242042

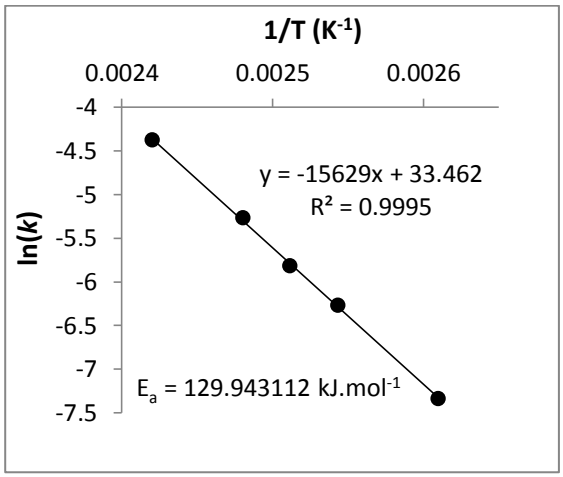

Entry 11: Thermolysis of **2.38** in the presence of 4 equiv. BnOH using steady-state method and off-line ^{1}H NMR analysis.

Temp. °C	*k*	ln(*k*)	1/T (K^{-1})
110	**0.000664943**	-7.31581	0.00260994
120	**0.001788730**	-6.32625	0.00254355
125	**0.002847009**	-5.86149	0.00251161
130	**0.004875351**	-5.32356	0.00248046
135	**0.007744443**	-4.86078	0.00245008

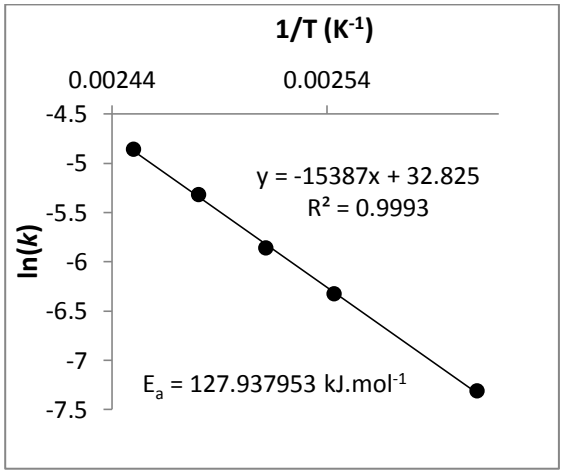

Table 4.9 Data:

Entry 1: Thermolysis of **4.1a** in the presence of 4 equiv. EtOH using push-out method, in-line UV analysis and OPA processing. F_1 = 1 mL.min^{-1} and F_2 = 10 mL.min^{-1}

Temp. °C	*k*	ln(*k*)	1/T (K^{-1})
90	**0.000235949**	-8.35189	0.00275368
95	**0.000451353**	-7.70326	0.00271628
100	**0.000757243**	-7.18583	0.00267988
105	**0.001315017**	-6.63391	0.00264445
110	**0.002190678**	-6.12354	0.00260994
115	**0.003540051**	-5.64361	0.00257632
120	**0.005745694**	-5.15930	0.00254355

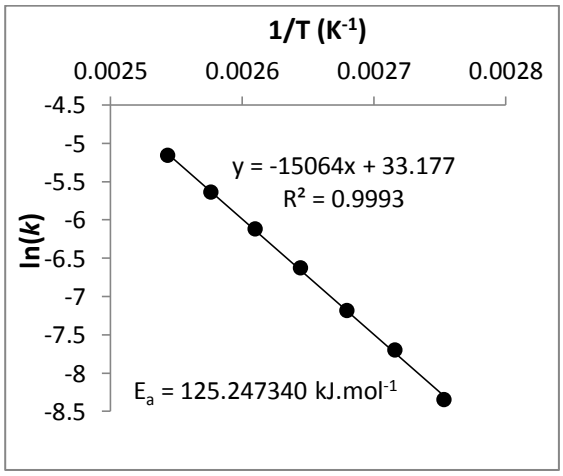

Entry 2: Thermolysis of **4.1a** in the presence of 4 equiv. EtOH using push-out method, in-line UV analysis and MLR processing. F_1 = 1 mL.min^{-1} and F_2 = 10 mL.min^{-1}

Temp. °C	*k*	ln(*k*)	1/T (K^{-1})
95	**0.000467969**	-7.66711	0.00271628
100	**0.000712897**	-7.24617	0.00267988
105	**0.001426878**	-6.55227	0.00264445
110	**0.002284696**	-6.08152	0.00260994
115	**0.003807766**	-5.57071	0.00257632
120	**0.005890714**	-5.13438	0.00254355

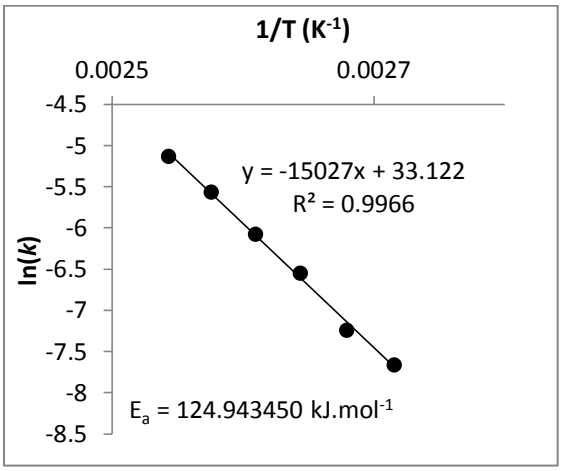

Entry 3: Thermolysis of **4.1a** in the presence of 4 equiv. EtOH using push-out method, in-line IR analysis and OPA processing. F_1 = 1 ml.min^{-1} and F_2 = 10 mL.min^{-1}

Temp. °C	*k*	ln(*k*)	1/T (K^{-1})
95	**0.000482914**	-7.63567	0.00271628
100	**0.000738087**	-7.21145	0.00267988
105	**0.001272883**	-6.66647	0.00264445
110	**0.002077854**	-6.17642	0.00260994
115	**0.003547972**	-5.64138	0.00257632
120	**0.005840732**	-5.14290	0.00254355

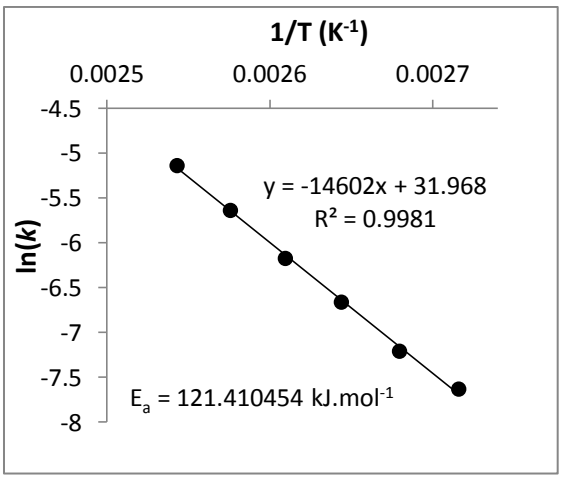

Entry 4: Thermolysis of **4.1a** in the presence of 4 equiv. EtOH using steady-state method, in-line UV analysis and OPA processing.

Temp. °C	*k*	ln(*k*)	1/T (K^{-1})
100	**0.000799534**	-7.13148	0.00267988
105	**0.001312299**	-6.63597	0.00264445
110	**0.002298925**	-6.07531	0.00260994
115	**0.003703033**	-5.59860	0.00257632
120	**0.006155691**	-5.09038	0.00254355

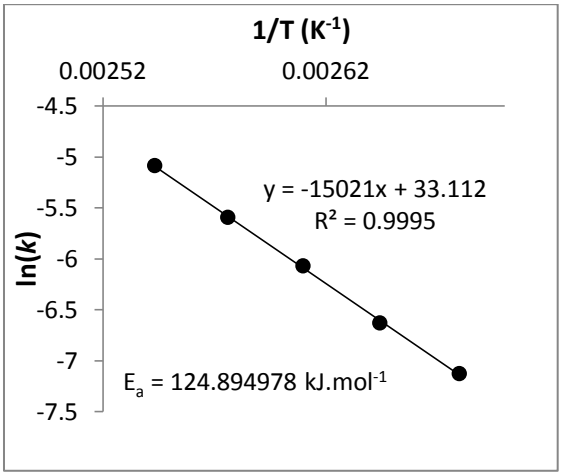

Entry 5: Thermolysis of **4.1a** in the presence of 4 equiv. BnOH using steady-state method and off-line ^{1}H NMR analysis

Temp. °C	*k*	ln(*k*)	1/T (K^{-1})
100	**0.000792559**	-7.14024	0.00267988
105	**0.001237786**	-6.69443	0.00264445
110	**0.002330798**	-6.06154	0.00260994
115	**0.003288001**	-5.71748	0.00257632
120	**0.006263254**	-5.07306	0.00254355

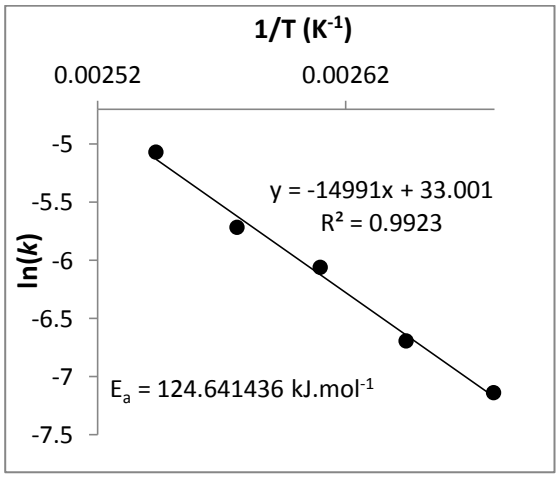

Entry 6: Thermolysis of **4.1d** in the presence of 4 equiv. EtOH using push-out method, in-line UV analysis and OPA processing. F_1 = 1 mL.min^{-1} and F_2 = 10 mL.min^{-1}

Temp. °C	*k*	ln(*k*)	1/T (K^{-1})
85	**0.001657298**	-6.40257	0.00279212
90	**0.002778499**	-5.88584	0.00275368
95	**0.004707618**	-5.35857	0.00271628
100	**0.007551304**	-4.88604	0.00267988
105	**0.011486105**	-4.46662	0.00264445
110	**0.017175729**	-4.06426	0.00260994

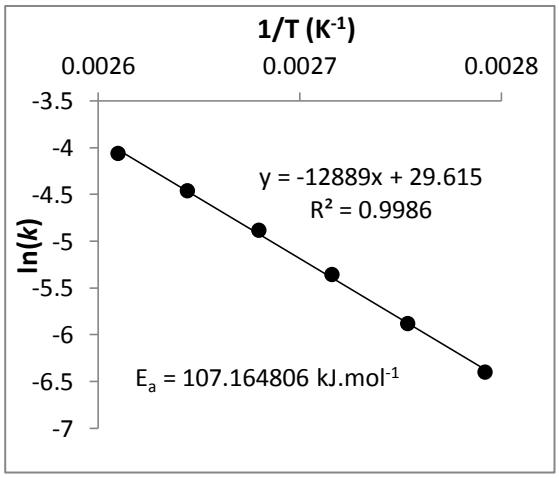

Entry 7: Thermolysis of **4.1d** in the presence of 4 equiv. EtOH using push-out method, in-line UV analysis and MLR processing. F_1 = 1 mL.min^{-1} and F_2 = 10 mL.min^{-1}

Temp. °C	*k*	ln(*k*)	1/T (K^{-1})
85	**0.00174496**	-6.35102	0.00279212
90	**0.002904377**	-5.84154	0.00275368
95	**0.004944215**	-5.30954	0.00271628
100	**0.007827803**	-4.85007	0.00267988
105	**0.011663276**	-4.45131	0.00264445
110	**0.017339691**	-4.05476	0.00260994

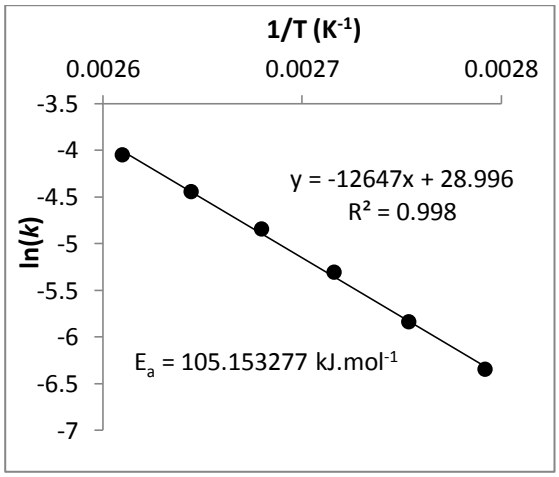

Entry 8: Thermolysis of **4.1d** in the presence of 4 equiv. EtOH using push-out method, in-line IR analysis and OPA processing. F_1 = 1 mL.min^{-1} and F_2 = 10 mL.min^{-1}

Temp. °C	*k*	ln(*k*)	1/T (K^{-1})
90	**0.002653613**	-5.93183	0.00275368
95	**0.004515082**	-5.40033	0.00271628
100	**0.007151931**	-4.94037	0.00267988
105	**0.011110539**	-4.49986	0.00264445

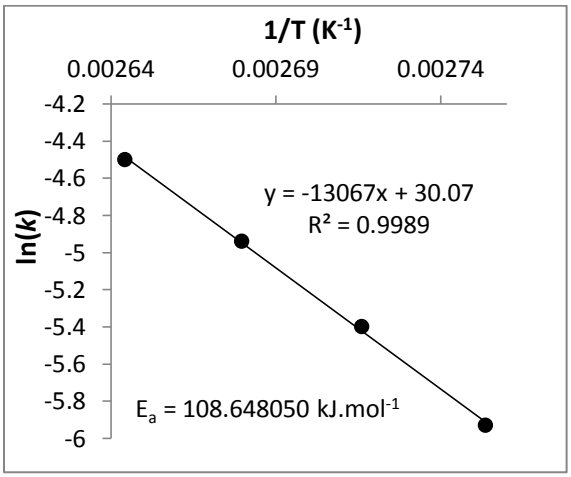

Entry 9: Thermolysis of **4.1d** in the presence of 4 equiv. EtOH using steady-state method, in-line UV analysis and OPA processing.

Temp. °C	*k*	ln(*k*)	1/T (K^{-1})
90	**0.002689176**	-5.91852	0.00275368
95	**0.004834908**	-5.33189	0.00271628
100	**0.007619779**	-4.87701	0.00267988
105	**0.011332349**	-4.48009	0.00264445

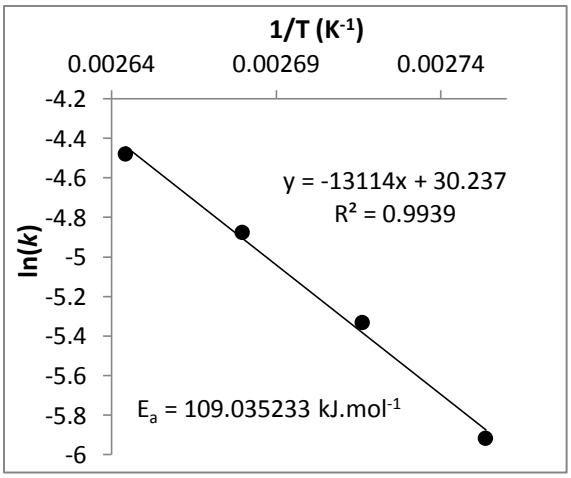

Entry 10: Thermolysis of **4.1b** in the presence of 4 equiv. EtOH using push-out method, in-line UV analysis and OPA processing. F_1 = 1 mL.min^{-1} and F_2 = 10 mL.min^{-1}

Temp. °C	*k*	ln(*k*)	1/T (K^{-1})
100	**0.000587258**	-7.44005	0.00267988
105	**0.000940204**	-6.96941	0.00264445
110	**0.001587826**	-6.44539	0.00260994
115	**0.002680919**	-5.92160	0.00257632
120	**0.004544167**	-5.39391	0.00254355
125	**0.007797548**	-4.85395	0.00251161

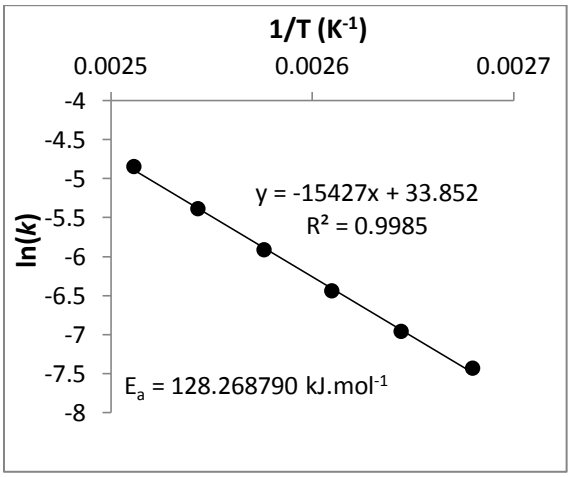

Entry 11: Thermolysis of **4.1b** in the presence of 4 equiv. EtOH using push-out method, in-line UV analysis and MLR processing. F_1 = 1 mL.min^{-1} and F_2 = 10 mL.min^{-1}

Temp. °C	*k*	ln(*k*)	1/T (K^{-1})
100	**0.000531043**	-7.54067	0.00267988
105	**0.000945996**	-6.96327	0.00264445
110	**0.001595969**	-6.44027	0.00260994
115	**0.002833114**	-5.86638	0.00257632
120	**0.004478312**	-5.40851	0.00254355
125	**0.00742144**	-4.90338	0.00251161

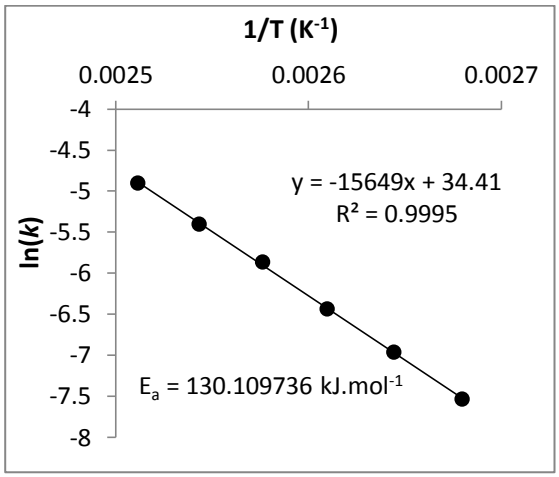

Entry 12: Thermolysis of **4.1b** in the presence of 4 equiv. EtOH using push-out method, in-line IR analysis and OPA processing. F_1 = 1 mL.min^{-1} and F_2 = 10 mL.min^{-1}

Temp. °C	*k*	ln(*k*)	1/T (K^{-1})
100	**0.000559079**	-7.48922	0.00267988
105	**0.001062288**	-6.84733	0.00264445
110	**0.001821606**	-6.30804	0.00260994
115	**0.002906250**	-5.84089	0.00257632
125	**0.007468588**	-4.89705	0.00251161

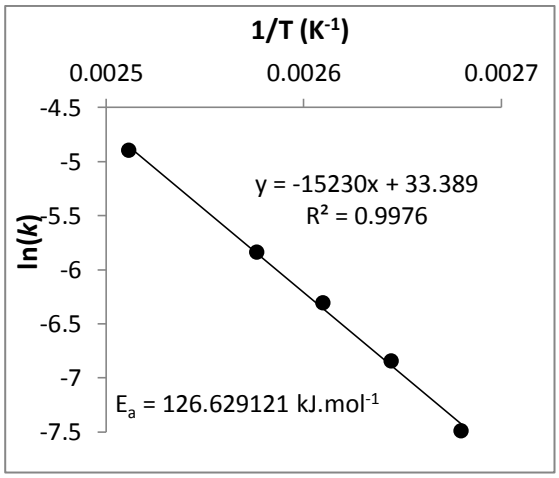

Entry 13: Thermolysis of **4.1b** in the presence of 4 equiv. EtOH using push-out method and off-line ^{1}H NMR analysis. F_1 = 1 mL.min^{-1} and F_2 = 10 mL.min^{-1}

Temp. °C	*k*	ln(*k*)	1/T (K^{-1})
100	**0.000549312**	-7.50684	0.00267988
105	**0.000949227**	-6.95986	0.00264445
110	**0.001618969**	-6.42597	0.00260994
115	**0.002595547**	-5.95396	0.00257632
125	**0.007418929**	-4.90372	0.00251161

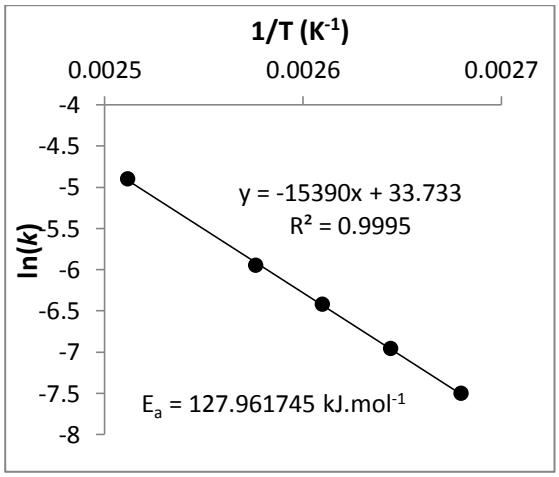

Entry 14: Thermolysis of **2.26a** in the presence of 4 equiv. EtOH using push-out method, in-line UV analysis and OPA processing. F_1 = 1 mL.min^{-1} and F_2 = 10 mL.min^{-1}

Temp. °C	*k*	ln(*k*)	1/T (K^{-1})
105	**0.000317165**	-8.05609	0.00264445
110	**0.000549577**	-7.50636	0.00260994
115	**0.000934674**	-6.97531	0.00257632
120	**0.001564908**	-6.45993	0.00254355
125	**0.002577148**	-5.96107	0.00251161
130	**0.004044506**	-5.51040	0.00248046

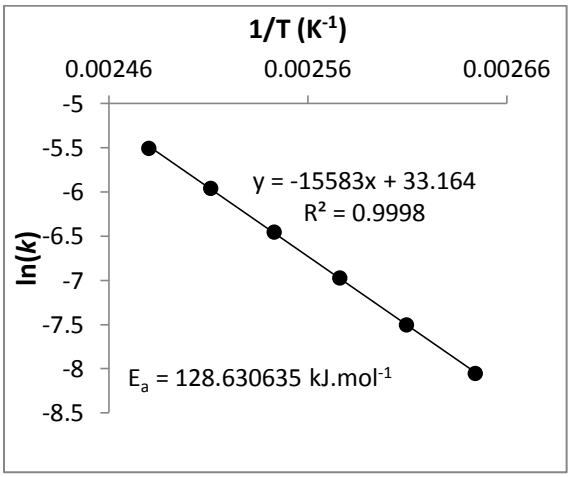

Entry 15: Thermolysis of **2.26b** in the presence of 4 equiv. EtOH using push-out method, in-line UV analysis and OPA processing. F_1 = 1 mL.min^{-1} and F_2 = 10 mL.min^{-1}

Temp. °C	*k*	ln(*k*)	1/T (K^{-1})
110	**0.000436225**	-7.73735	0.00260994
115	**0.000755304**	-7.18839	0.00257632
120	**0.001300208**	-6.64523	0.00254355
130	**0.003623828**	-5.62022	0.00248046

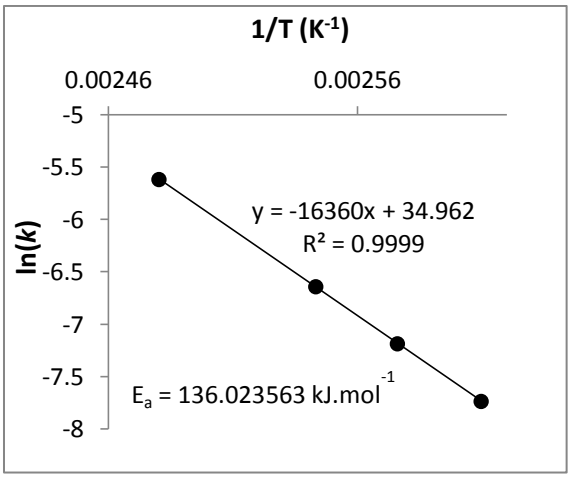

Entry 16: Thermolysis of **2.26c** in the presence of 4 equiv. EtOH using push-out method, in-line UV analysis and OPA processing. F_1 = 1 mL.min^{-1} and F_2 = 10 mL.min^{-1}

Temp. °C	*k*	ln(*k*)	1/T (K^{-1})
90	**0.000369181**	-7.90422	0.00275368
95	**0.000605304**	-7.40978	0.00271628
100	**0.001052721**	-6.85638	0.00267988
105	**0.001720652**	-6.36505	0.00264445
110	**0.002992631**	-5.81160	0.00260994
115	**0.004949794**	-5.30841	0.00257632

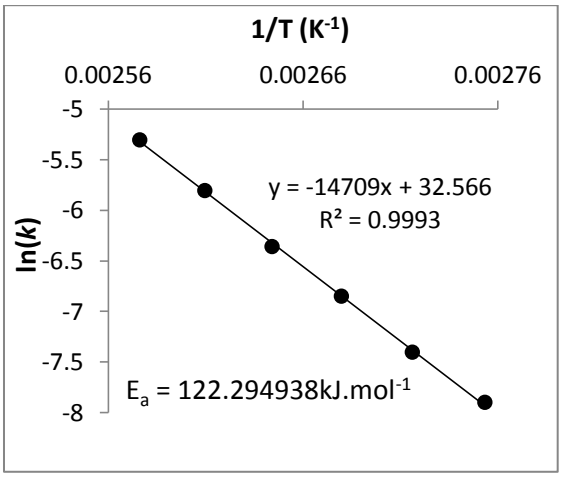

Entry 17: Thermolysis of **2.26d** in the presence of 4 equiv. EtOH using push-out method, in-line UV analysis and OPA processing. F_1 = 1 mL.min^{-1} and F_2 = 10 mL.min^{-1}

Temp. °C	*k*	ln(*k*)	1/T (K^{-1})
100	**0.000206094**	-8.48718	0.00267988
105	**0.000343122**	-7.97742	0.00264445
110	**0.000591477**	-7.43289	0.00260994
115	**0.000962230**	-6.94626	0.00257632
120	**0.001602055**	-6.43647	0.00254355
130	**0.003978796**	-5.52678	0.00248046

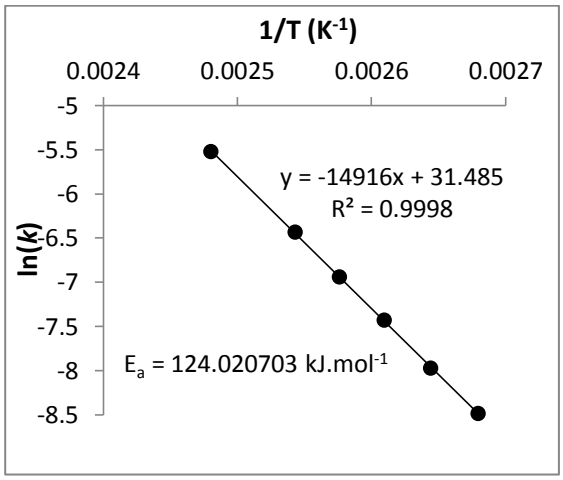

Entry 18: Thermolysis of **2.26e** in the presence of 4 equiv. EtOH using push-out method, in-line UV analysis and OPA processing. F_1 = 1 mL.min^{-1} and F_2 = 10 mL.min^{-1}

Temp. °C	*k*	ln(*k*)	1/T (K^{-1})
100	**0.000573185**	-7.46430	0.00267988
105	**0.000909735**	-7.00236	0.00264445
110	**0.001525452**	-6.48546	0.00260994
115	**0.002472934**	-6.00235	0.00257632
120	**0.004149356**	-5.48480	0.00254355

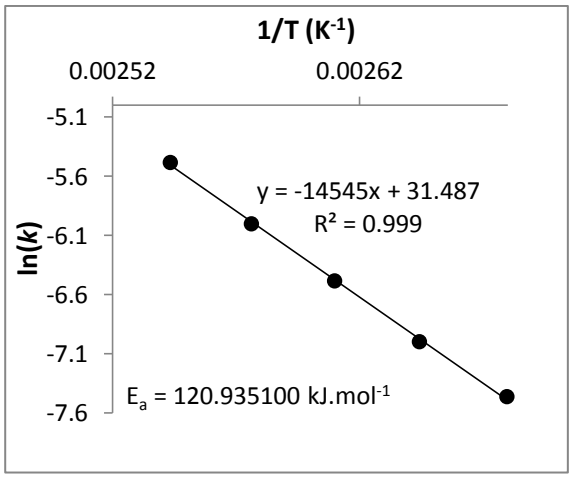

Off-Line ^{1}H NMR Analysis

General Methods: ^{1}H NMR spectra of crude samples were obtained from AV-300 or DPX-400 MHz spectrometer in $CDCl_3$ after solvent removal under reduced pressure from fractions collected under steady-state conditions as described in the general procedure. Chemical shifts for proton are reported in ppm and are referenced to the residual peak of the solvent. Reaction rate constants for thermolysis of 1,3-dioxin-4-one **2.38**, **4.1a** and **4.1b** at different temperatures were determined from the peak integrals indicated. In plotting ln([**1,3-dioxin-4-one**]/[**1,3-dioxin-4-one**]$_0$), it is assumed that [**1,3-dioxin-4-one**]$_0$ ≡ [**1,3-dioxin-4-one** + **4.4** + **4.4**$_{tautomer}$] where **4.4** is the β-keto ester product of ketene trapping by EtOH or BnOH. In other cases, it is assumed that [**1,3-dioxin-4-one**]$_0$ ≡ [**1,3-dioxin-4-one** + **4.2**] where **4.2** is the non-volatile ketone product. No evidence of competing [4+2] self-cycloaddition of **4.3** was

observed in the ^{1}H NMR spectrum. Activation energies for thermolysis of **2.38**, **4.1a** and **4.1b** calculated from the reaction rate constants reported below, are given in the previous section.

Reaction Rate Constant Data:

Table 4.7, Entry 10: Thermolysis of **2.38** in the presence of 4 equiv. EtOH under steady-state conditions

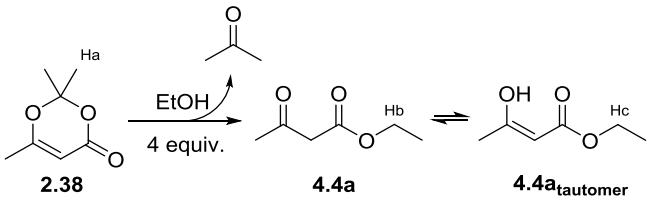

Peaks used in calculation of [**2.38**]/[**2.38** + **4.4a** + **4.4a**$_{tautomer}$]:

^{1}H NMR (300 MHz, $CDCl_3$) δ ppm: 1.69 (s, 6H, Ha), 4.20 (q, *J* = 7.0 Hz, 2H, Hb), 4.19 (q, *J* = 7.0 Hz, 2H, Hc).

Figure 7.17 shows sample data collected from experiments carried out at 130 °C.

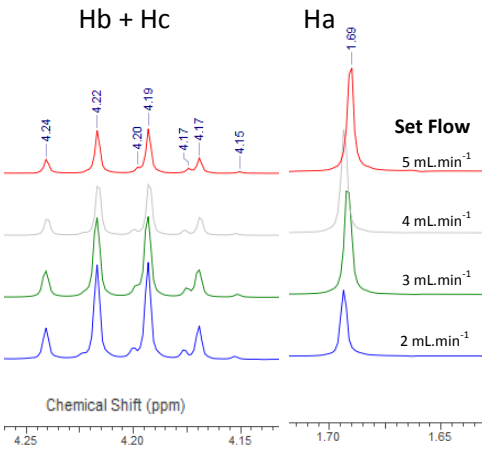

Figure 7.17

Reaction temperature = 110 °C			
Set flow (mL.min^{-1})	Effective flow (mL.min^{-1})	Reaction time (sec.)	ln([**2.38**]/[**2.38** + **4.4a** + **4.4a**$_{tautomer}$])
7	7.786	75.208	-0.029558802
5	5.562	105.292	-0.048790164
4	4.449	131.614	-0.062974799
3	3.337	175.486	-0.09531018

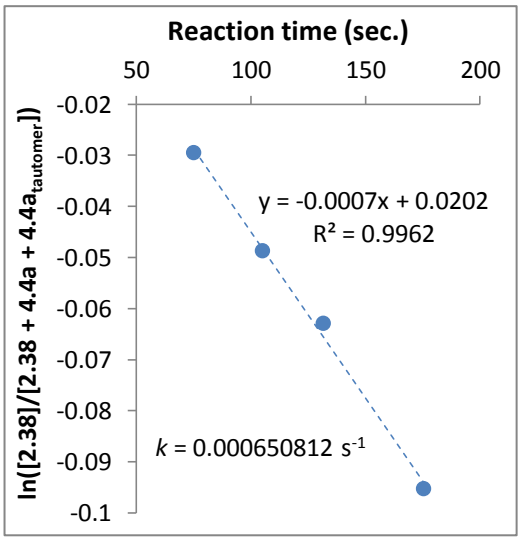

Reaction temperature = 120 °C			
Set flow ($mL.min^{-1}$)	Effective flow ($mL.min^{-1}$)	Reaction time (sec.)	ln([**2.38**]/[**2.38** + **4.4a** + **4.4a**$_{tautomer}$])
7	7.882	74.293	-0.131028262
5	5.630	104.011	-0.186479567
4	4.504	130.013	-0.235072122
3	3.378	173.351	-0.318453731

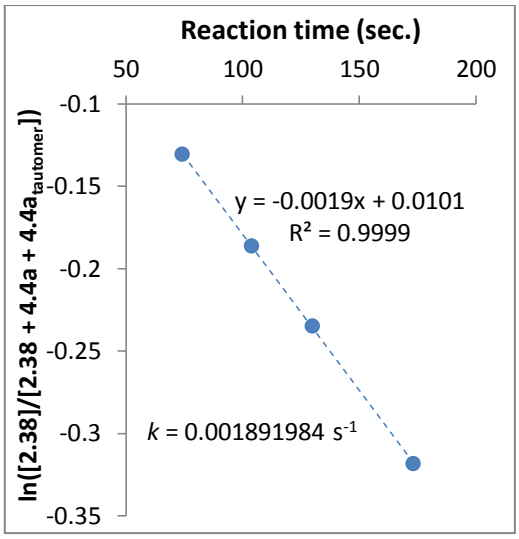

Reaction temperature = 125 °C			
Set flow ($mL.min^{-1}$)	Effective flow ($mL.min^{-1}$)	Reaction time (sec.)	ln([**2.38**]/[**2.38** + **4.4a** + **4.4a**$_{tautomer}$])
7	7.930	73.844	-0.207014169
5	5.664	103.382	-0.296394013
4	4.532	129.227	-0.381855242
3	3.399	172.303	-0.497740384

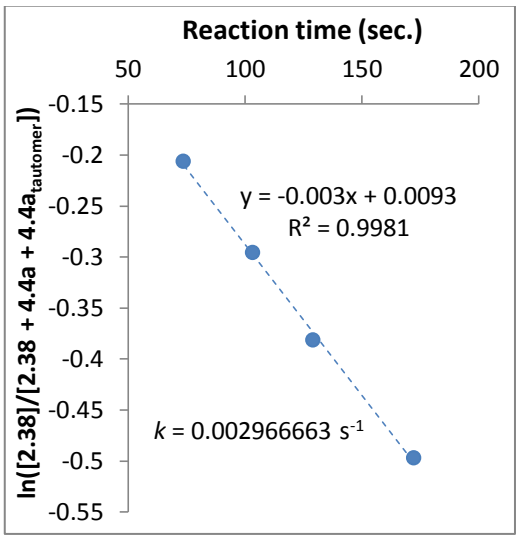

Reaction temperature = 130 °C			
Set flow ($mL.min^{-1}$)	Effective flow ($mL.min^{-1}$)	Reaction time (sec.)	ln([**2.38**]/[**2.38** + **4.4a** + **4.4a**$_{tautomer}$])
5	5.699	102.760	-0.476234179
4	4.559	128.450	-0.612479277
3	3.419	171.267	-0.819779831
2	2.279	256.901	-1.269760545

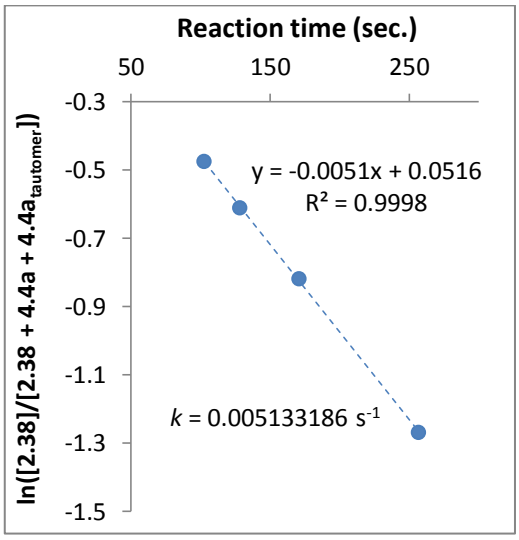

Reaction temperature = 140 °C			
Set flow (mL.min^{-1})	Effective flow (mL.min^{-1})	Reaction time (sec.)	ln([**2.38**]/[**2.38** + **4.4a** + **4.4a**$_{tautomer}$])
5	5.767	101.540	-1.239822457
4	4.614	126.925	-1.561297537
3	3.460	169.233	-2.088153482

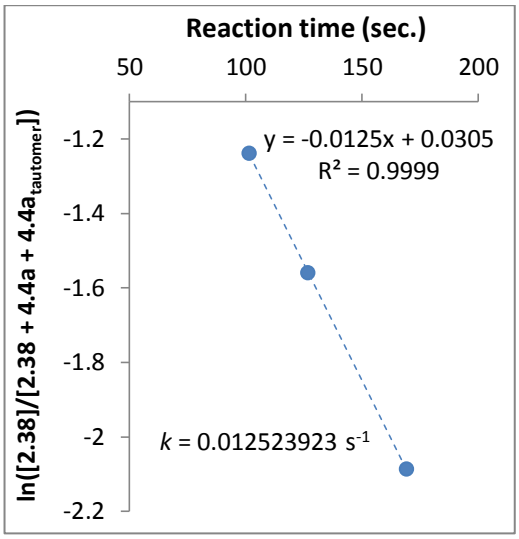

Table 4.7, Entry 11: Thermolysis of **2.38** in the presence of 4 equiv. BnOH under steady-state conditions

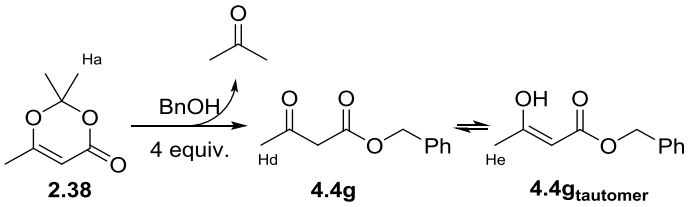

Peaks used in calculation of [**2.38**]/[**2.38** + **4.4g** + **4.4g**$_{tautomer}$]:

^{1}H NMR (400 MHz, $CDCl_3$) δ ppm: 1.69 (s, 6H, Ha), 2.20 (s, 3H, Hd), 1.99 (s, 3H, He).

Figure 7.18 shows sample data collected from experiments carried out at 125 °C.

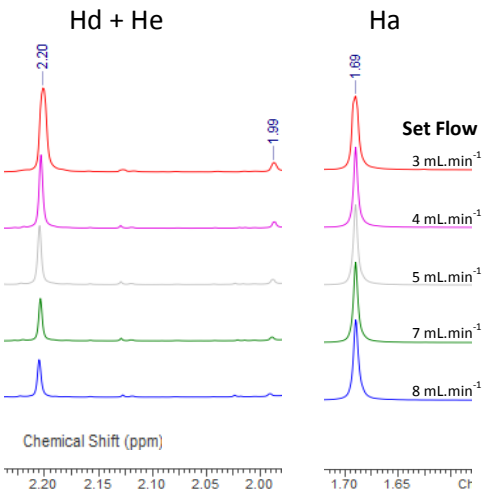

Figure 7.18

Reaction temperature = 110 °C			
Set flow (mL.min^{-1})	Effective flow (mL.min^{-1})	Reaction time (sec.)	ln([**2.38**]/[**2.38** + **4.4g** + **4.4g**$_{tautomer}$])
8	8.899	65.807	-0.032789823
7	7.786	75.208	-0.039220713
5	5.562	105.292	-0.055119299
4	4.449	131.614	-0.070769071
3	3.337	175.486	-0.107358518

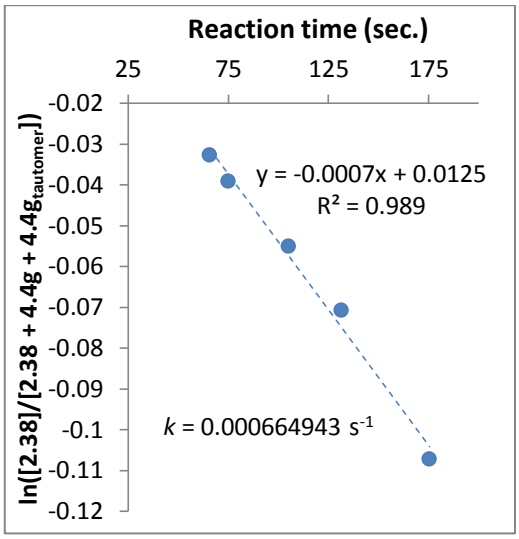

Reaction temperature = 120 °C			
Set flow (mL.min^{-1})	Effective flow (mL.min^{-1})	Reaction time (sec.)	ln([**2.38**]/[**2.38** + **4.4g** + **4.4g**$_{tautomer}$])
8	9.008	65.007	-0.095310180
7	7.882	74.293	-0.110348057
5	5.630	104.011	-0.162685582
4	4.504	130.013	-0.220473323
3	3.378	173.351	-0.285178942

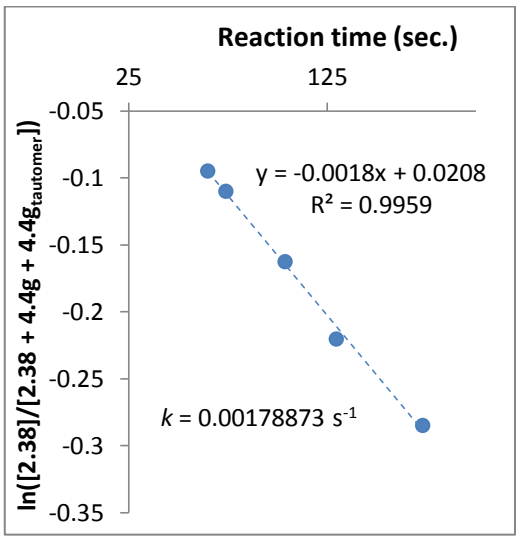

Reaction temperature = 125 °C			
Set flow (mL.min^{-1})	Effective flow (mL.min^{-1})	Reaction time (sec.)	ln([**2.38**]/[**2.38** + **4.4g** + **4.4g**$_{tautomer}$])
8	9.063	64.614	-0.162685582
7	7.930	73.844	-0.182321557
5	5.664	103.382	-0.267479365
4	4.532	129.227	-0.331698958
3	3.399	172.303	-0.470003629

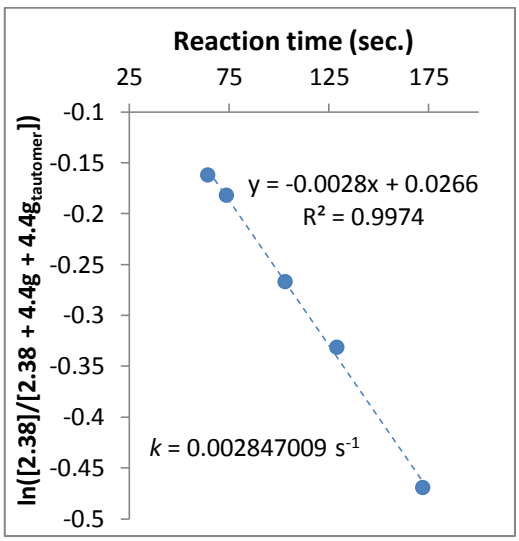

Reaction temperature = 130 °C			
Set flow (mL.min^{-1})	Effective flow (mL.min^{-1})	Reaction time (sec.)	ln([**2.38**]/[**2.38** + **4.4g** + **4.4g**$_{tautomer}$])
8	9.118	64.225	-0.257222865
7	7.978	73.400	-0.312374685
5	5.699	102.760	-0.440403159
4	4.559	128.450	-0.576613364
3	3.419	171.267	-0.782378314

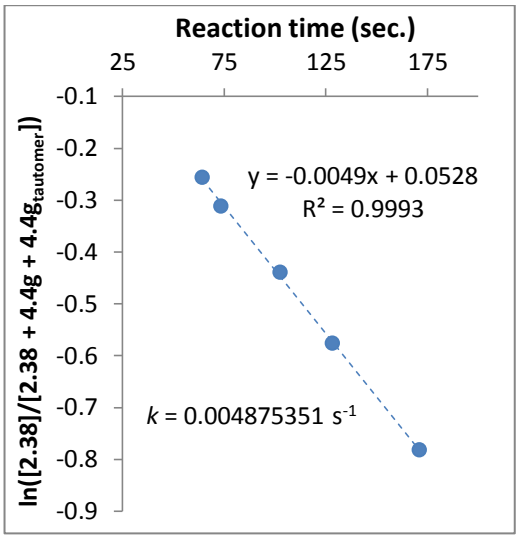

Reaction temperature = 135 °C			
Set flow (mL.min^{-1})	Effective flow (mL.min^{-1})	Reaction time (sec.)	ln([**2.38**]/[**2.38** + **4.4g** + **4.4g**$_{tautomer}$])
8	9.173	63.841	-0.429615568
7	8.026	72.962	-0.500775288
5	5.733	102.146	-0.756121980
4	4.586	127.683	-0.900161350
3	3.440	170.244	-1.264126727

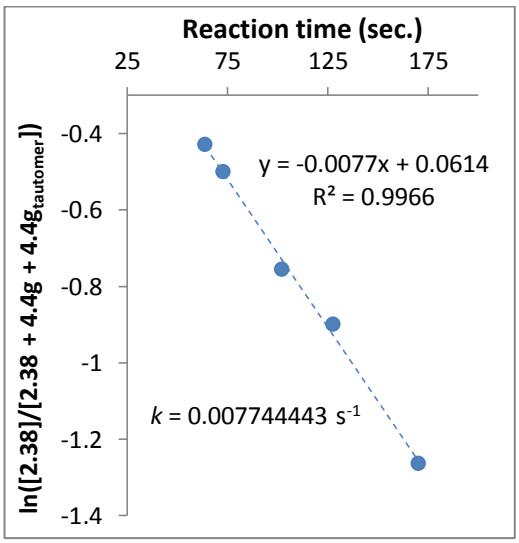

Table 4.9, Entry 5: Thermolysis of **4.1a** in the presence of 4 equiv. BnOH under steady-state conditions

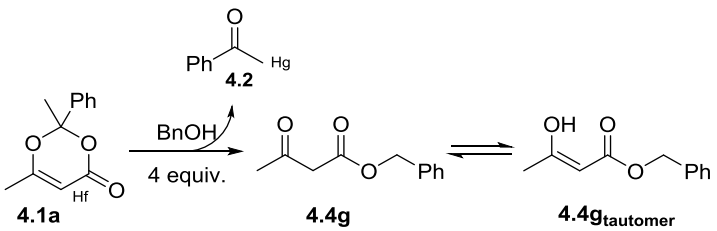

Peaks used in calculation of [**4.1a**]/[**4.1a** + **4.2**]:

^{1}H NMR (400 MHz, $CDCl_3$) δ ppm: 5.15 (q, *J* = 0.7 Hz, 1H, Hf), 2.61 (s, 3H, Hg).

Figure 7.19 shows sample data collected from experiments carried out at 105 °C.

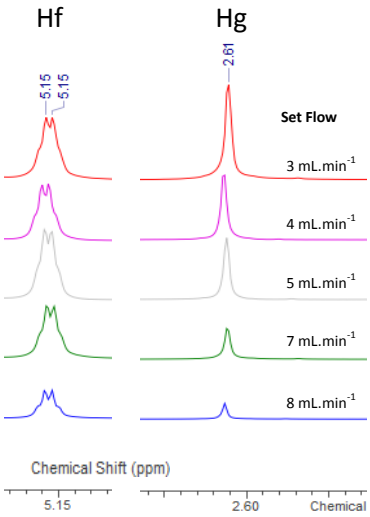

Figure 7.19

Reaction temperature = 100 °C			
Set flow (mL.min^{-1})	Effective flow (mL.min^{-1})	Reaction time (sec.)	ln([**4.1a**]/[**4.1a** + **4.2**])
8	8.789	66.628	-0.046025822
7	7.690	76.146	-0.049480057
5	5.493	106.605	-0.076540077
4	4.395	133.256	-0.097374164
3	3.296	177.674	-0.132171773

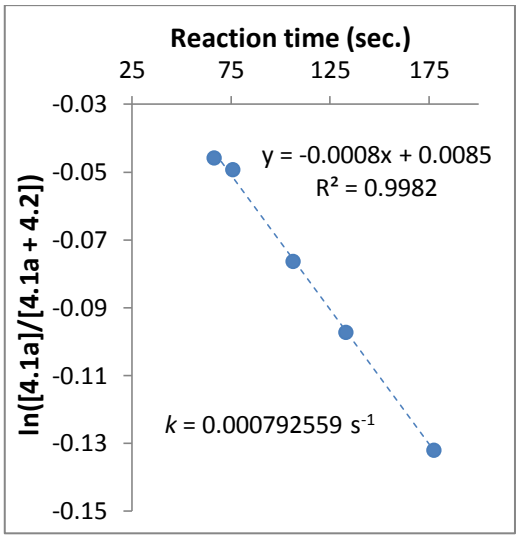

Reaction temperature = 105 °C			
Set flow (mL.min^{-1})	Effective flow (mL.min^{-1})	Reaction time (sec.)	ln([**4.1a**]/[**4.1a** + **4.2**])
8	8.844	66.215	-0.067822596
7	7.738	75.674	-0.078692269
5	5.527	105.944	-0.120901773
4	4.422	132.430	-0.171422266
3	3.316	176.573	-0.197298011

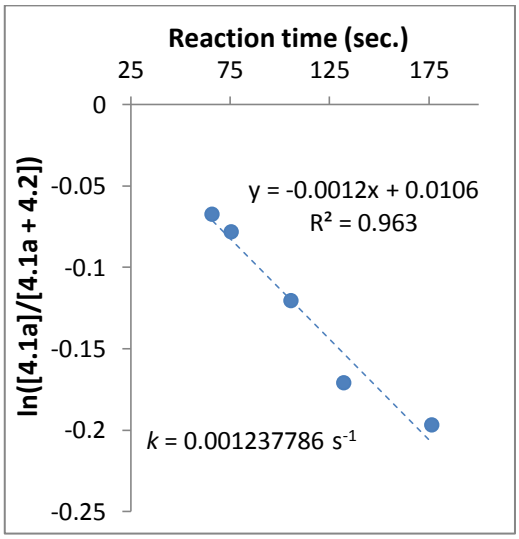

Reaction temperature = 110 °C			
Set flow ($mL.min^{-1}$)	Effective flow ($mL.min^{-1}$)	Reaction time (sec.)	ln([**4.1a**]/[**4.1a** + **4.2**])
8	8.899	65.807	-0.110900696
7	7.786	75.208	-0.159630146
5	5.562	105.292	-0.213574100
4	4.449	131.614	-0.275103290

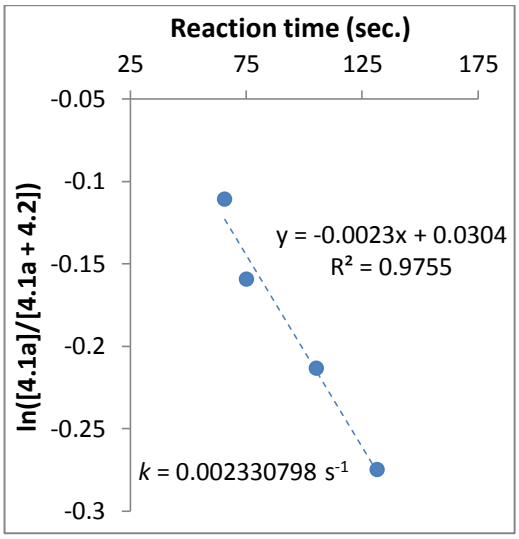

Reaction temperature = 115 °C			
Set flow ($mL.min^{-1}$)	Effective flow ($mL.min^{-1}$)	Reaction time (sec.)	ln([**4.1a**]/[**4.1a** + **4.2**])
8	8.954	65.404	-0.199441439
7	7.834	74.748	-0.233288000
5	5.596	104.647	-0.316669609
4	4.477	130.809	-0.415293197
3	3.358	174.412	-0.558327958

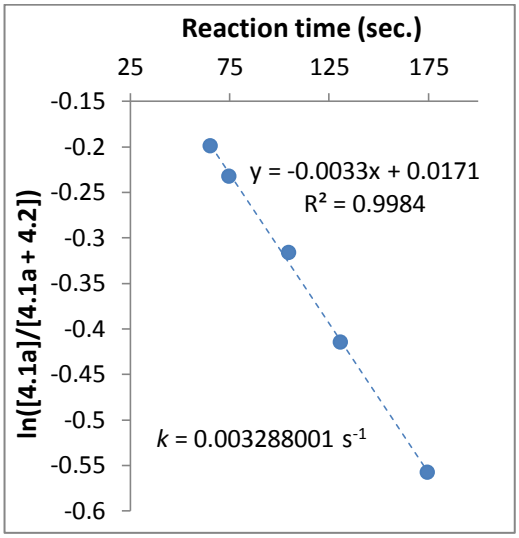

Reaction temperature = 120 °C			
Set flow ($mL.min^{-1}$)	Effective flow ($mL.min^{-1}$)	Reaction time (sec.)	ln([**4.1a**]/[**4.1a** + **4.2**])
8	9.008	65.007	-0.299516530
7	7.882	74.293	-0.399155939
5	5.630	104.011	-0.537623817
4	4.504	130.013	-0.701550591
3	3.378	173.351	-1.001946176

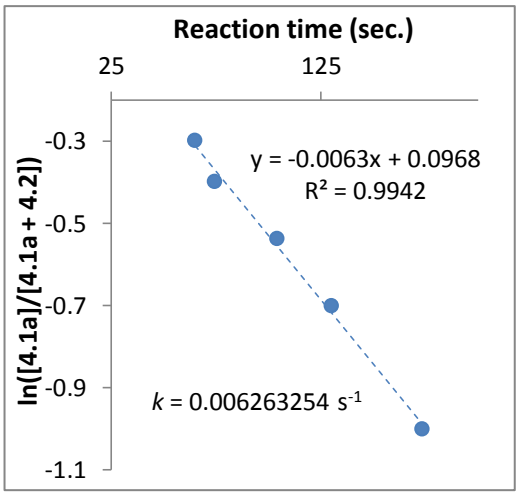

Table 4.9, Entry 13: Thermolysis of **4.1b** in the presence of 4 equiv. EtOH under push-out conditions where F_1 = 1 mL.min^{-1} and F_2 = 10 mL.min^{-1}

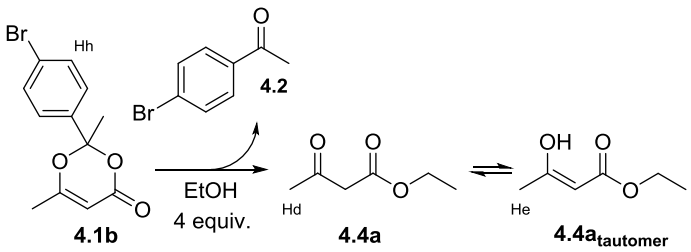

Peaks used in calculation of [**4.1b**]/[**4.1b** + **4.4a** + **4.4a**$_{tautomer}$]:

^{1}H NMR (400 MHz, CDCl$_3$) δ ppm: 7.51 (2H, d, *J* = 8.8 Hz, Hh), 2.20 (3H, s, Hd), 1.99 (3H, s, He).

Figure 7.20 shows sample data collected from experiments carried out at 115 °C.

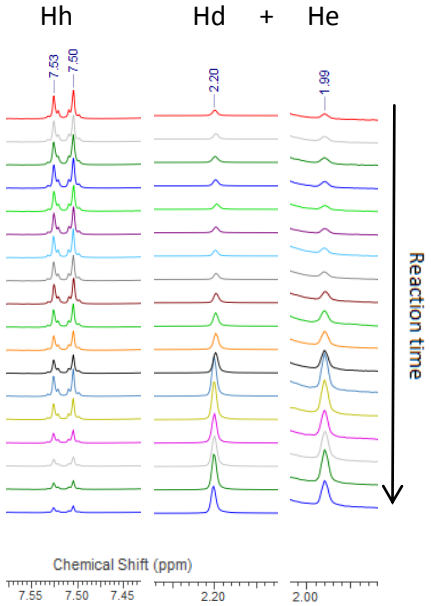

Figure 7.20

Reaction temperature = 100 °C	
Reaction time (sec.)	ln([**4.1b**]/[**4.1b** + **4.4a** + **4.4a**$_{tautomer}$])
373.856	-0.249144053
332.942	-0.228462713
292.028	-0.199783384
251.114	-0.178721941
210.200	-0.152762755
169.285	-0.135472513
128.371	-0.113574114
87.457	-0.092781733

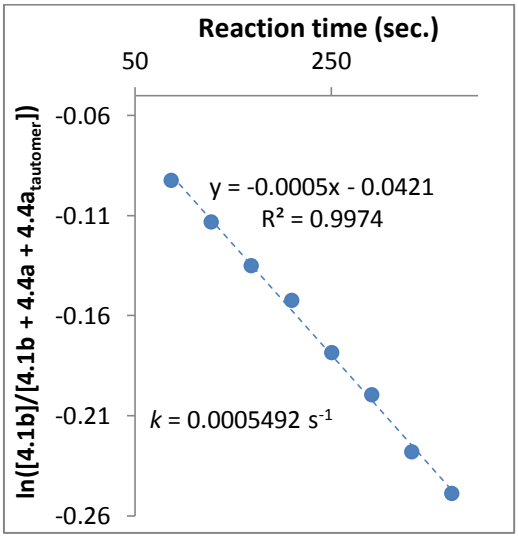

Reaction temperature = 105 °C	
Reaction time (sec.)	ln([**4.1b**]/[**4.1b** + **4.4a** + **4.4a**$_{tautomer}$])
327.821	-0.374910440
287.160	-0.333116529
246.500	-0.298044859
205.839	-0.253865450
165.178	-0.216807733
124.518	-0.183745045
83.857	-0.141339117

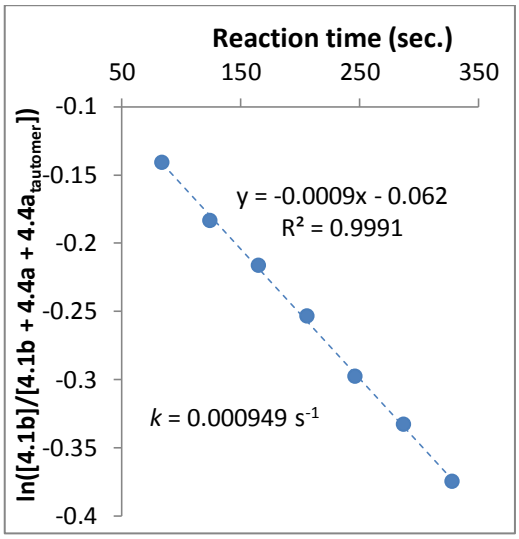

Reaction temperature = 110 °C	
Reaction time (sec.)	ln([**4.1b**]/[**4.1b** + **4.4a** + **4.4a**$_{tautomer}$])
322.801	-0.635446467
282.390	-0.575067892
241.980	-0.505175891
201.570	-0.440797019
161.159	-0.381680203
120.749	-0.317428466
80.339	-0.244492140
39.928	-0.179364963

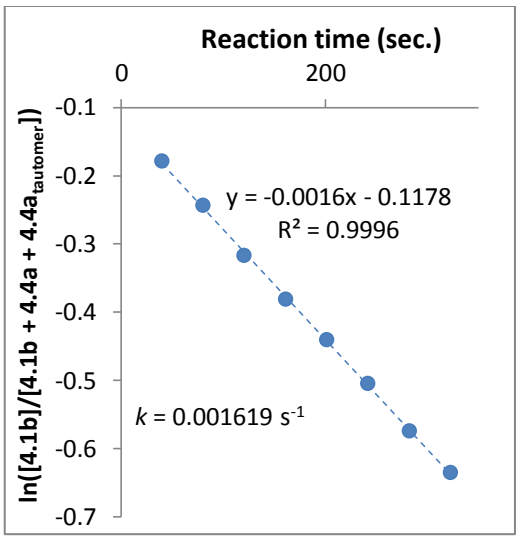

Reaction temperature = 115 °C	
Reaction time (sec.)	ln([**4.1b**]/[**4.1b** + **4.4a** + **4.4a**$_{tautomer}$])
277.715	-0.901691932
237.552	-0.774188391
197.389	-0.671625014
157.226	-0.565446708
117.063	-0.463927941
76.900	-0.362114667

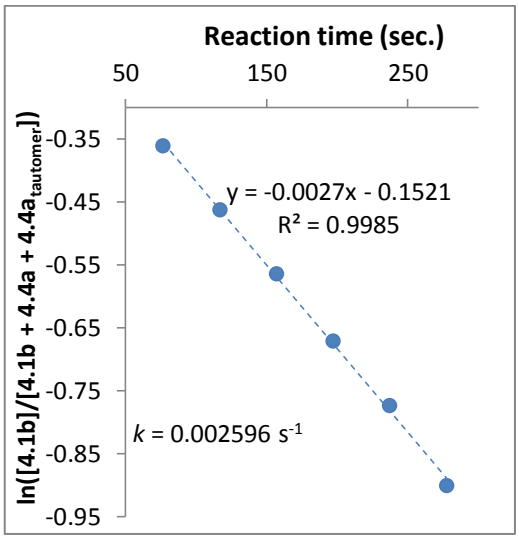

Reaction temperature = 125 °C	
Reaction time (sec.)	ln([**4.1b**]/[**4.1b** + **4.4a** + **4.4a**$_{tautomer}$])
268.640	-2.297367567
228.962	-1.912239482
189.285	-1.646903854
149.608	-1.399769060
109.931	-1.056511615
70.253	-0.783491672
30.576	-0.499275928

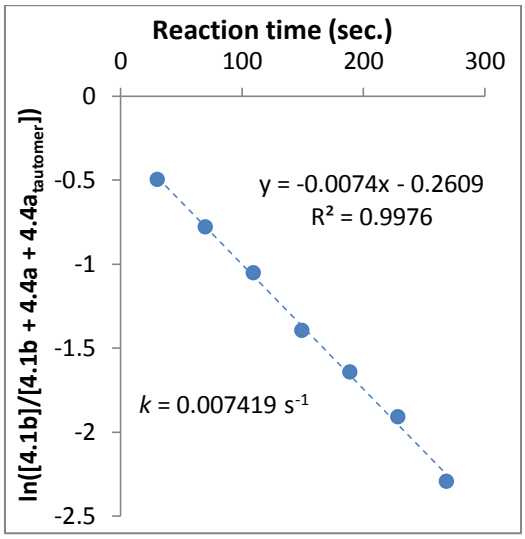

Alcohol Stoichiometry Experiments

Four different solutions of 2,2,6-trimethyl-4*H*-1,3-dioxin-4-one (**2.38**) ([**2.38**] = 0.3 mM) with ethanol (0.5, 1.0, 2.0 or 4.0 equiv.) in dry acetonitrile (100 mL) were prepared. For each solution and by following the steady-state kinetic study procedure, cycle of experiments were performed at 120 °C and sample were collected at the exit of the reactor. After evaporation of the solvent under reduced pressure, off-line ^{1}H NMR analysis was carried out according to the general method described previously, assuming that [**2.38**]$_0$ ≡ [**2.38** + **4.4a** + **4.4a**$_{tautomer}$]. First-order reaction rate constants for thermolysis of **2.38** were determined from integration of identical peak to that described in previously, *i.e.* peaks used in calculation of [**2.38**]/[**2.38** + **4.4a** + **4.4a**$_{tautomer}$]: δ ppm: 1.69 (s, 6H, Ha), 4.20 (q, *J* = 7.0 Hz, 2H, Hb), 4.19 (q, *J* = 7.0 Hz, 2H, Hc).

0.5 equiv. EtOH			
Set flow (mL.min^{-1})	Effective flow (mL.min^{-1})	Reaction time (sec.)	ln([**2.38**]/[**2.38** + **4.4a** + **4.4a**$_{tautomer}$])
9	10.134	57.784	-0.062974799
7	7.882	74.293	-0.086177696
5	5.630	104.011	-0.126632651
3	3.378	173.351	-0.219135530
2	2.252	260.026	-0.347129531

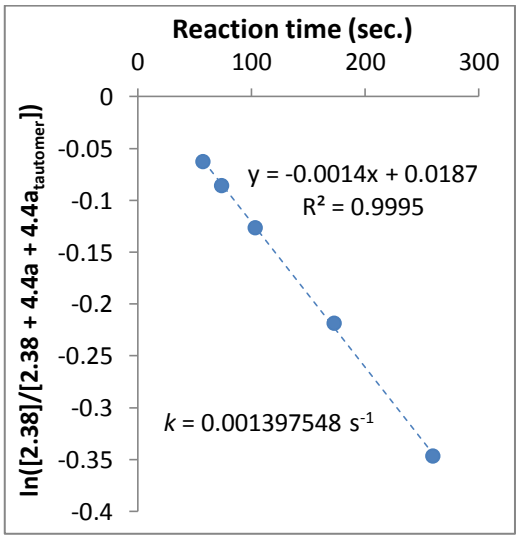

1.0 equiv. EtOH			
Set flow ($mL.min^{-1}$)	Effective flow ($mL.min^{-1}$)	Reaction time (sec.)	ln([**2.38**]/[**2.38** + **4.4a** + **4.4a**$_{tautomer}$])
9	10.134	57.784	-0.095310180
7	7.882	74.293	-0.122217633
5	5.630	104.011	-0.178146185
4	4.504	130.013	-0.227135573
3	3.378	173.351	-0.307484700
2	2.252	260.026	-0.463734016

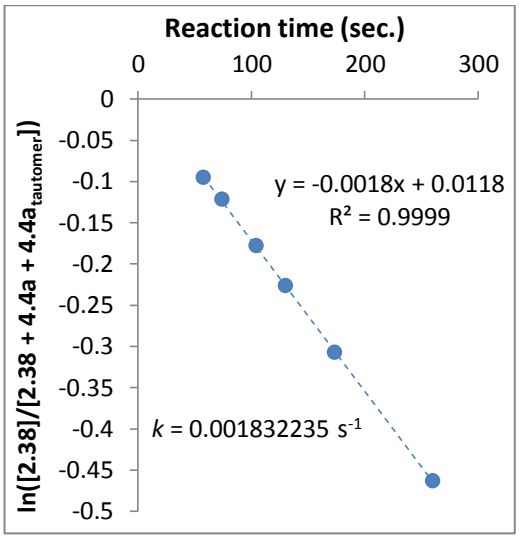

2.0 equiv. EtOH			
Set flow ($mL.min^{-1}$)	Effective flow ($mL.min^{-1}$)	Reaction time (sec.)	ln([**2.38**]/[**2.38** + **4.4a** + **4.4a**$_{tautomer}$])
9	10.134	57.784	-0.095310180
7	7.882	74.293	-0.122217633
5	5.630	104.011	-0.186479567
4	4.504	130.013	-0.235072122
3	3.378	173.351	-0.311154429
2	2.252	260.026	-0.473123757

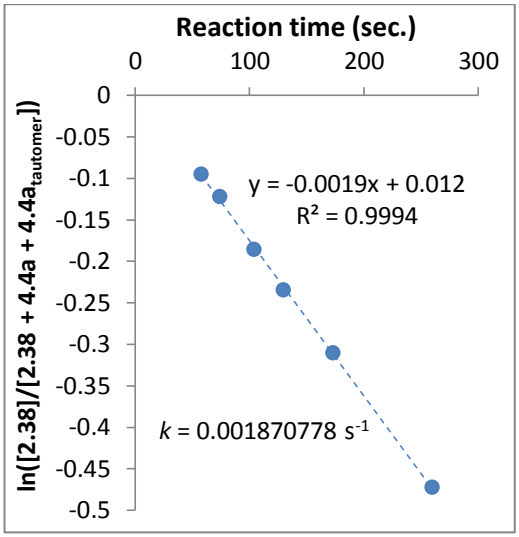

4.0 equiv. EtOH			
Set flow ($mL.min^{-1}$)	Effective flow ($mL.min^{-1}$)	Reaction time (sec.)	ln([**2.38**]/[**2.38** + **4.4a** + **4.4a**$_{tautomer}$])
7	7.882	74.293	-0.131028262
5	5.630	104.011	-0.190620360
4	4.504	130.013	-0.235072122
3	3.378	173.351	-0.314810740

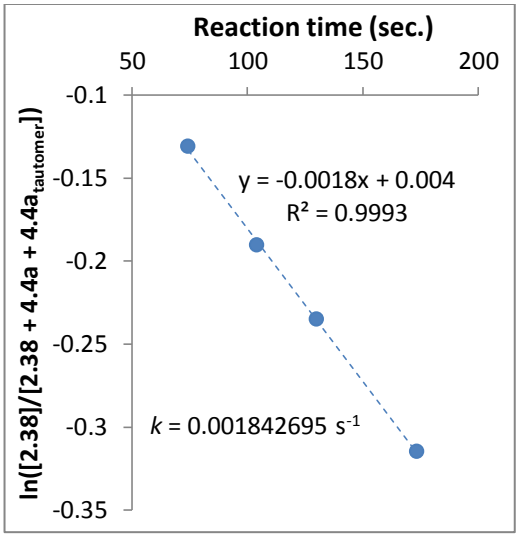

7.2.3.6 GENERAL PROCEDURE F: Synthesis of kinetic study products

After few kinetic studies, the reactor was heated to 160 °C, and the mixture of dioxinone (1 equiv.) and alcohol (4 equiv.) was injected into the flow machine. The residence time was set at 10 min. The crude mixture was collected in a single RBF, concentrated under reduced pressure and analysed by NMR spectroscopy.

Ethyl 3-oxobutanoate (**4.4a**) and Ethyl (*Z*)-3-hydroxybut-2-enoate (**4.4a'**)

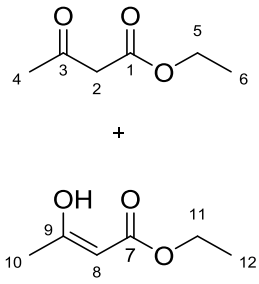

$C_6H_{10}O_3$

MW = 130.06 g.mol $^{-1}$

Ratio Keto/Enol: 92/8

Yield = 84% at 160 °C

From the mixture of 2,2,6-trimethyl-4*H*-1,3-dioxin-4-one (**2.38**, 6.52 mg, 45.9 µmol) and ethanol (10.7 µL, 183 µmol) in acetonitrile (3 mL, [**2.38**] = 0.015 M), the reaction was performed as detailed in the general procedure **F**. The crude products were isolated (5.00 mg, 38.4 µmol, 84%) and analysed. A mixture of the Keto and Enol forms **4.4a** and **4.4a'** was highlighted (92/8). NMR data are consistent with the literature.[144]

Keto form (**4.4a**):

^{1}H NMR (300 MHz, $CDCl_3$) δ ppm: 4.20 (q, *J* = 7.1 Hz, 2H, H-5), 3.43 (s, 2H, H-2), 2.26 (s, 3H, H-4), 1.27 (t, *J* = 7.2 Hz, 3H, H-6).

^{13}C NMR (75 MHz, $CDCl_3$) δ ppm: 200.6, 167.1, 61.3, 50.1, 30.1, 14.0.

Enol form (**4.4a'**):

^{1}H NMR (300 MHz, $CDCl_3$) δ ppm: 12.09 (s, 1H, OH), 4.96 (s, 1H, H-8), 4.19 (q, *J*-coupling not resolved due to an overlap with H-5, 2H, H-11), 1.94 (s, 3H, H-10), 1.27 (t, *J*-coupling not resolved due to an overlap with H-6, 3H, H-12).

Ethyl 3-oxo-3-phenylpropanoate (**4.4b**) and Ethyl (*Z*)-3-hydroxy-3-phenylacrylate (**4.4b'**)

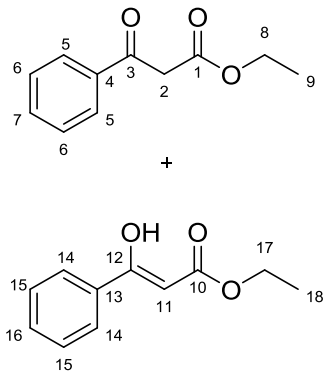

$C_{11}H_{12}O_3$

MW = 192.08 g.mol $^{-1}$

Ratio Keto/Enol: 79/21

Yield = 93% at 160 °C

From the mixture of 2,2-dimethyl-6-phenyl-4*H*-1,3-dioxin-4-one (**2.26a**, 5.54 mg, 27.1 µmol) and ethanol (6.34 µL, 109 µmol) in acetonitrile (1.8 mL, [**2.26a**] = 0.015 M), the reaction was performed as detailed in the general procedure **F**. The crude products were isolated (4.85 mg, 25.2 µmol, 93%) and analysed. A mixture of the Keto and Enol forms **4.4b** and **4.4b'** was highlighted (79/21). NMR data are consistent with the literature.[145]

Keto form (**4.4b**):

^{1}H NMR (300 MHz, $CDCl_3$) δ ppm: 7.99-7.93 (m, 2H, H-5), 7.61 (tt, *J* = 7.3, 1.5 Hz, 1H, H-7), 7.50 (dd, *J* = 7.5, 7.5 Hz, 2H, H-6), 4.23 (q, *J* = 7.0 Hz, 2H, H-8), 4.00 (s, 2H, H-2), 1.27 (t, *J* = 7.2 Hz, 3H, H-9).

Enol form (**4.4b'**):

^{1}H NMR (300 MHz, $CDCl_3$) δ ppm:, 12.59 (s, 1H, OH), 7.79 (dd, *J* = 8.1, 1.5 Hz, 2H, H-14), 7.46-7.41 (m, 3H, H-15, 16), 5.68 (s, 1H, H-11), 4.28 (q, *J* = 7.2 Hz, 2H, H-17), 1.35 (t, *J* = 7.2 Hz, 3H, H-18).

Ethyl 3-(4-methoxyphenyl)-3-oxopropanoate (**4.4c**) and Ethyl (*Z*)-3-hydroxy-3-(4-methoxyphenyl)acrylate (**4.4c'**)

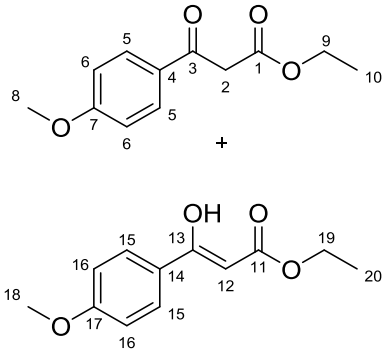

$C_{12}H_{14}O_4$

MW = 222.09 g.mol $^{-1}$

Ratio Keto/Enol: 90/10

Purity = 96%

Yield = 94% at 160 °C

From the mixture of 6-(4-methoxyphenyl)-2,2-dimethyl-4*H*-1,3-dioxin-4-one (**2.26b**, 5.45 mg, 23.3 µmol) and ethanol (5.43 µL, 93.1 µmol) in acetonitrile (1.5 mL, [**2.26b**] = 0.015 M), the

reaction was performed as detailed in the general procedure **F**. The crude products were isolated (5.00 mg (purity = 96%), 21.6 µmol, 94%) and analysed. A mixture of the Keto and Enol forms **4.4c** and **4.4c'**was highlighted (90/10). Moreover, a small amount of decarboxylated product (1-(4-methoxyphenyl)ethanone) ($4\%_{mol}$) was obtained, probably due to the presence of a small amount of water in the media. NMR data are consistent with the literature.[146]

Keto form (**4.4c**):

^{1}H NMR (300 MHz, $CDCl_3$) δ ppm: 7.94 (d, *J* = 9.0 Hz, 2H, H-5), 6.96 (d, *J* = 9.0 Hz, 2H, H-6), 4.22 (q, *J* = 7.1 Hz, 2H, H-9), 3.95 (s, 2H, H-2), 3.89 (s, 3H, H-8), 1.27 (t, *J* = 7.1 Hz, 3H, H-10).

Enol form (**4.4c'**):

^{1}H NMR (300 MHz, $CDCl_3$) δ ppm: 12.64 (s, 1H, OH), 7.75 (d, *J* = 9.0 Hz, 2H, H-15), 6.93 (d, *J*-coupling not resolved due to an overlap with H-6, 2H, H-16), 5.59 (s, 1H, H-12), 4.27 (q, *J* = 7.0 Hz, 2H, H-19), 3.86 (s, 3H, H-18), 1.34 (t, *J* = 7.2 Hz, 3H, H-20).

Ethyl 3-(4-nitrophenyl)-3-oxopropanoate (**4.4f**) and Ethyl (*Z*)-3-hydroxy-3-(4-nitrophenyl)acrylate (**4.4f'**)

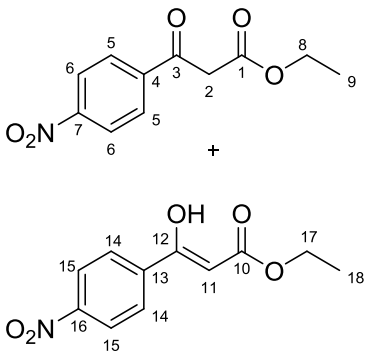

$C_{11}H_{11}NO_5$

MW = 237.06 g.mol $^{-1}$

Ratio Keto/Enol: 1/1

Purity = 75%

Yield = 64% at 160 °C

From the mixture of 2,2-dimethyl-6-(4-nitrophenyl)-4*H*-1,3-dioxin-4-one (**2.26e**, 5.85 mg, 23.5 µmol) and ethanol (5.48 µL, 93.9 µmol) in acetonitrile (1.5 mL, [**2.26e**] = 0.015 M), the reaction was performed as detailed in the general procedure **F**. The crude products were isolated (4.70 mg (purity = 75%), 14.9 µmol, 64%) and analysed. A mixture of the Keto and Enol forms **4.4f** and **4.4f'** was highlighted (1/1). Moreover, decarboxylated product (1-(4-nitrophenyl)ethanone) ($32\%_{mol}$) was obtained, probably due to the presence of a small amount of water in the media. NMR data are consistent with the literature.[147]

Keto form (**4.4f**):

^{1}H NMR (300 MHz, $CDCl_3$) δ ppm: 8.35 (d, *J* = 8.8 Hz, 2H, H-6), 8.12 (d, *J* = 9.0 Hz, 2H, H-5), 4.23 (q, *J* = 7.2 Hz, 2H, H-8), 4.04 (s, 2H, H-2), 1.36 (t, *J* = 7.2 Hz, 3H, H-9).

Enol form (**4.4f'**):

^{1}H NMR (300 MHz, $CDCl_3$) δ ppm: 12.58 (s, 1H, OH), 8.28 (d, *J* = 9.0 Hz, 2H, H-15), 7.95 (d, *J* = 9.0 Hz, 2H, H-14), 5.77 (s, 1H, H-11), 4.31 (q, *J* = 7.2 Hz, 2H, H-17), 1.27 (t, *J* = 7.2 Hz, 3H, H-18).

Ethyl 3-(furan-2-yl)-3-oxopropanoate (**4.4d**) and Ethyl (*Z*)-3-(furan-2-yl)-3-hydroxyacrylate (**4.4d'**)

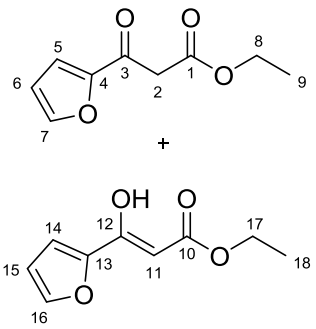

$C_9H_{10}O_4$

MW = 182.06 g.mol $^{-1}$

Ratio Keto/Enol: 92/8

Yield = 72% at 160 °C

From the mixture of 6-(furan-2-yl)-2,2-dimethyl-4*H*-1,3-dioxin-4-one (**2.26c**, 5.61 mg, 29.0 µmol) and ethanol (6.75 µL, 116 µmol) in acetonitrile (1.9 mL, [**2.26c**] = 0.015 M), the reaction was performed as detailed in the general procedure **F**. The crude products were isolated (3.80 mg, 20.9 µmol, 72%) and analysed. A mixture of the Keto and Enol forms **4.4d** and **4.4d'** was highlighted (92/8). NMR data are consistent with the literature.[148]

Keto form (**4.4d**):

^{1}H NMR (300 MHz, $CDCl_3$) δ ppm: 7.62 (dd, *J* = 1.7, 0.8 Hz, 1H, ArH), 7.29 (dd, *J* = 3.6, 0.8 Hz, 1H, ArH), 6.58 (dd, *J* = 3.6, 1.7 Hz, 1H, ArH), 4.22 (q, *J* = 7.2 Hz, 2H, H-8), 3.86 (s, 2H, H-2), 1.27 (t, *J* = 7.2 Hz, 3H, H-9).

Enol form (**4.4d'**):

^{1}H NMR (300 MHz, $CDCl_3$) δ ppm: 12.17 (s, 1H, OH), 7.51-7.49 (m, 1H, ArH), 6.94 (d, *J* = 3.6 Hz, 1H, ArH), 6.51 (dd, *J* = 3.4, 1.9 Hz, 1H, ArH), 5.62 (s, 1H, H-11), 4.26 (q, *J* = 7.2 Hz, 2H, H-17), 1.33 (t, *J* = 7.2 Hz, 3H, H-18).

Ethyl 3-(naphthalen-2-yl)-3-oxopropanoate (**4.4e**) and Ethyl (*Z*)-3-hydroxy-3-(naphthalen-2-yl)acrylate (**4.4e'**)

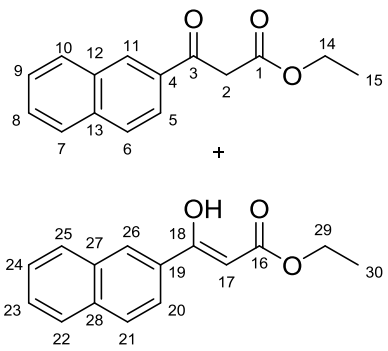

$C_{15}H_{14}O_3$

MW = 242.09 g.mol $^{-1}$

Ratio Keto/Enol: 79/21

Purity = 75%

Yield = 63% at 160 °C

From the mixture of 2,2-dimethyl-6-(naphthalen-2-yl)-4*H*-1,3-dioxin-4-one (**2.26d**, 5.45 mg,

21.0 µmol) and ethanol (5.01 µL, 86.0 µmol) in acetonitrile (1.4 mL, [**2.26d**] = 0.015 M), the reaction was performed as detailed in the general procedure **F**. The crude products were isolated (4.40 mg (purity = 75%), 13.5 µmol, 63%) and analysed. A mixture of the Keto and Enol forms **4.4e** and **4.4e'** was highlighted (79/21). Moreover, decarboxylated product (1-(naphthalen-2-yl)ethanone) (32%$_{mol}$) was obtained, probably due to the presence of a small amount of water in the media. NMR data are consistent with the literature.[149]

Keto form (**4.4e**):

^{1}H NMR (300 MHz, $CDCl_3$) δ ppm: 8.47 (s, 1H, H-11), 8.08-7.83 (m, 4H, ArH), 7.69-7.50 (m, 2H, ArH), 4.24 (q, *J* = 7.1 Hz, 2H, H-14), 4.13 (s, 2H, H-2), 1.27 (t, *J* = 7.1 Hz, 3H, H-15).

Enol form (**4.4e'**):

^{1}H NMR (300 MHz, $CDCl_3$) δ ppm: 12.68 (s, 1H, OH), 8.38 (s, 1H, H-26), 8.08-7.83 (m, 4H, ArH), 7.69-7.50 (m, 2H, ArH), 5.82 (s, 1H, H-17), 4.31 (q, *J* = 7.0 Hz, 2H, H-29), 1.37 (t, *J* = 7.0 Hz, 3H, H-30).

7.2.3.7 Simulated dispersion effects upon 1st and 2nd order kinetics

For a 1st order reaction (A → B) and 2nd order reaction (2A → B), reagent concentration profiles were determined under push-out conditions with flow rates going from 1 mL.min^{-1} to 10 mL.min^{-1}. At t = 0, the flow rate is switched from 1 to 10 mL.min^{-1} (reaction time = 10 min.). Figures 7.21(a) and 7.22(a) show the calculated profiles. For each data point of the calculated reagent concentration profiles, the dispersion profile obtained at 10 mL.min^{-1} and 30 °C for benzophenone (Figure 4.9 section 4.3.6) was then used to simulate the effect of dispersion. Figures 7.21(b) and 7.22(b) show the simulated profiles.

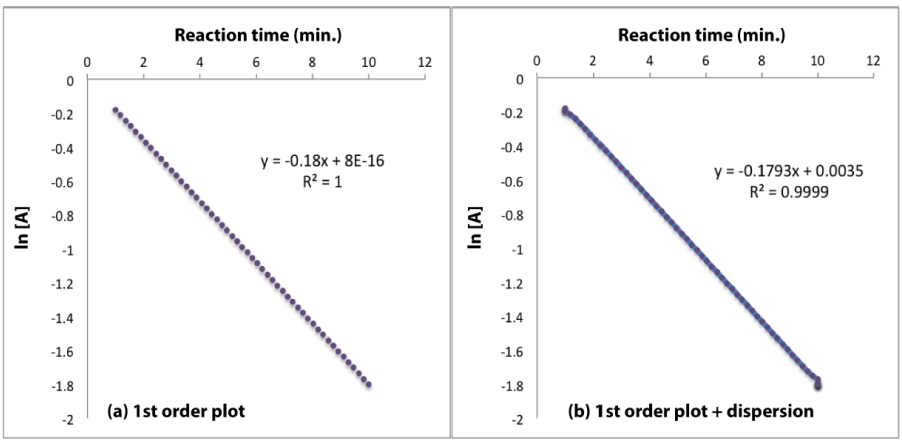

Figure 7.21: Calculated reagent concentration profile for (a) a first order reaction (b) a first order reaction with dispersion.

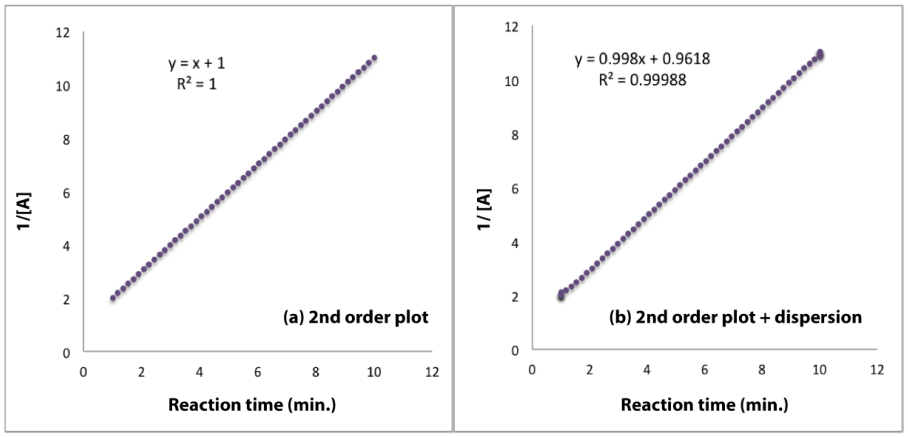

Figure 7.22: Calculated reagent concentration profile for (a) a second order reaction (b) a second order reaction with dispersion.

7.2.4 Chapter 5: Flow chemistry, a tool for fast optimisation of reaction conditions

7.2.4.1 Synthesis

Methyl 4-methylcyclohex-3-ene-1-carboxylate (**5.3**) and Methyl 3-methylcyclohex-3-ene-1-carboxylate (**5.4**)

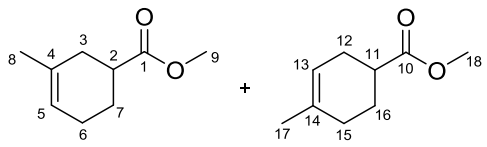

5.4 + **5.3**

$C_9H_{14}O_2$

MW = 154.21 g.mol $^{-1}$

R*f* = 0.40 (DCM)

Yellow oil

Yield = 48%

Ratio 3-methyl isomer/4-methyl

Ratio isomer: 35/65

In a RBF flushed with nitrogen, isoprene (**5.1**, 0.396 mL, 3.96 mmol) and methyl acrylate (**5.2**, 0.357 mL, 3.96 mmol) were mixed with dried toluene (1.24 mL) to make a 2 mL solution. The solution was degassed by sonication whilst being saturated with nitrogen, and injected into the flow set-up described below using the sample loop configuration. Then, the content of the loop was pushed by toluene (Stock solvent) into the flow stream. The residence time was set at 50 min (flow = 0.2 mL/min) and the 10 mL length Stainless Steel reactor, connected to a cooling loop (100 cm, 1 mm i.d.) followed by a backpressure regulator (250 psi), was heated to 200 °C. After collection and evaporation of the solvent under reduced pressure, the crude product was purified on silica gel (DCM) to give a mixture of the title compounds **5.4** and **5.3** (295 mg, 1.91 mmol, 48%) as a yellow oil. The ^{1}H NMR identified the ratio 3-methyl isomer/4-methyl isomer: 35/65. NMR data are consistent with the literature.[150]

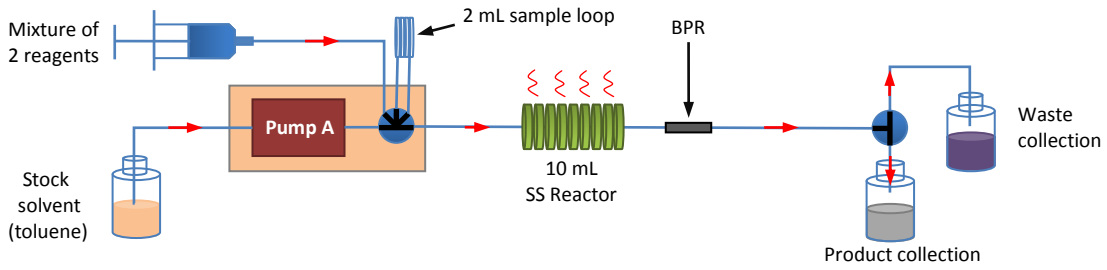

Figure 7.23: Flow set-up for the synthesis of methyl 3-methylcyclohex-3-ene-1-carboxylate (**5.4**) and methyl 4-methylcyclohex-3-ene-1-carboxylate (**5.3**) - Sample loop configuration.

Methyl 3-methylcyclohex-3-ene-1-carboxylate (**5.4**):

^{1}H NMR (400 MHz, $CDCl_3$) δ ppm: 5.38 (br s, 1H, H-5), 3.69 (s, 3H, H-9), 2.62-2.54 (m, 1H, H-2), 2.18-2.10 (m, 2H, H-3), 2.10-2.04 (m, 2H, H-6), 1.96-1.91 (m, 1H, H-7/7'), 1.67 (s, 3H, H-8), 1.63-1.56 (m, 1H, H-7/7').

^{13}C NMR (100 MHz, $CDCl_3$) δ ppm: 176.4 (C, C-1), 132.3 (C, C-4), 120.6 (CH, C-5), 51.6 (CH_3, C-9), 39.8 (CH, C-2), 32.1 (CH_2, C-3), 24.9 (CH_2, C-7), 24.5 (CH_2, C-6), 23.5 (CH_3, C-8).

Methyl 4-methylcyclohex-3-ene-1-carboxylate (**5.3**):

^{1}H NMR (400 MHz, $CDCl_3$) δ ppm: 5.38 (br s, 1H, H-13), 3.68 (s, 3H, H-18), 2.53-2.45 (m, 1H, H-11), 2.25-2.19 (m, 2H, H-12), 2.03-1.96 (m, 3H, H-15, 16/16'), 1.77-1.69 (m, 1H, H-16/16'), 1.65 (s, 3H, H-17).

^{13}C NMR (100 MHz, $CDCl_3$) δ ppm: 176.5 (C, C-10), 133.7 (C, C-14), 119.2 (CH, C-13), 51.6 (CH_3, C-18), 39.1 (CH, C-11), 29.3 (CH_2, C-15), 27.7 (CH_2, C-12), 25.5 (CH_2, C-16), 23.4 (CH_3, C-17).

IR (MeCN) ν_{max}/cm^{-1} = 2927 (br), 1733 (s), 1435 (m), 1305 (w), 1223 (m), 1165 (s), 1025 (w).

7,7,8,8-Tetramethylbicyclo[4.2.0]octan-2-one (**5.18** and **5.19**)

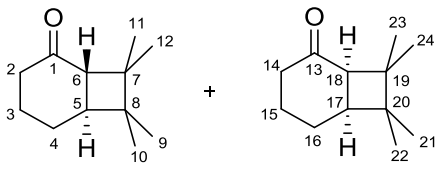

trans **5.18** + cis **5.19**

$C_{12}H_{20}O$

MW = 180.29 g.mol^{-1}

R*f* $_{trans}$= 0.67 (hexane/Et_2O, 4:6)

R*f* $_{cis}$= 0.47 (toluene/Et_2O, 9:1)

Colourless oil

Yield = 36%

Ratio trans/cis: 90/10

In a RBF flushed with nitrogen, cyclohex-2-enone (**5.7a**, 77.0 µL, 0.800 mmol) was mixed with tetramethylethylene (**5.17**, 15.2 mL, 15.2 mmol, 1 M in THF). The solution was degassed by sonication whilst being saturated with nitrogen. With the bottle-feed configuration, the

reaction mixture was injected into the double coiled photochemical flow reactor (capacity: 28.0 mL) at 0.2 mL/min (residence time = 140 min) using a UV-A lamp (9 W). Once the mixture was entirely injected, it was pushed by acetonitrile (Stock solvent) into the flow stream. The reactor was connected to a backpressure regulator (100 psi). After collection and evaporation of the solvent under reduced pressure, the crude mixture was purified twice on silica gel (first: hexane/Et_2O, 9:1, second: toluene/Et_2O, 97:3) to give the diastereoisomers trans **5.18** (46.0 mg, 255 µmol) and cis **5.19** (5.0 mg, 28 µmol) as colourless oils (51.0 mg, 283 µmol, 36%). The reaction was not 100% complete because some cyclohex-2-enone was isolated during the purification.

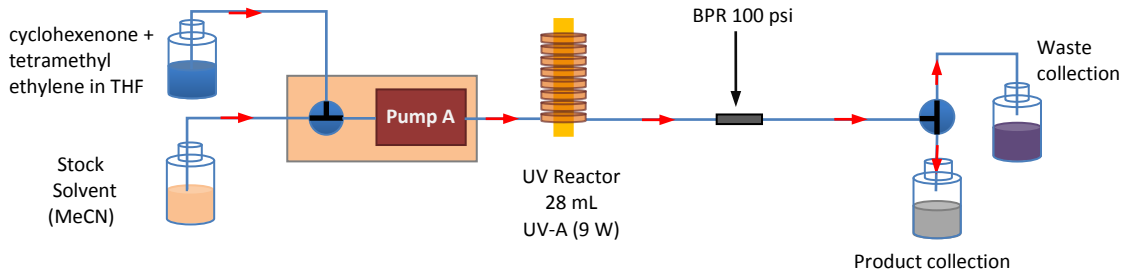

Figure 7.24: Flow set-up for the synthesis of the 7,7,8,8-tetramethylbicyclo[4.2.0]octan-2-one - Bottle-feed configuration.

Diastereoisomer trans (**5.18**):

^{1}H NMR (400 MHz, $CDCl_3$) δ ppm: 2.42 (d, *J* = 13.5 Hz, 1H, H-6), 2.21-2.13 (m, 2H, H-2), 2.13-2.08 (m, 1H, H-3/3'), 2.08-2.03 (m, 1H, H-5), 1.85-1.72 (m, 1H, H-3/3'), 1.71-1.63 (m, 1H, H-4/4'), 1.48 (dddd, *J* = 12.0, 11.8, 11.6, 4.6 Hz, 1H, H-4/4'), 1.19 (s, 3H, H-11/12), 1.02 (s, 3H, H-9/10), 0.93 (s, 3H, H-11/12), 0.90 (s, 3H, H-9/10).

^{13}C NMR (100 MHz, $CDCl_3$) δ ppm: 209.4 (C, C-1), 56.6 (CH, C-6), 51.4 (CH, C-5), 43.4 (C, C-7/8), 42.6 (C, C-7/8), 41.2 (C H_2, C-2), 28.0 (C H_2, C-3), 25.1 (C H_2, C-4), 23.6 (C H_3 C-11/12), 22.9 (C H_3, C-9/10), 19.3 (C H_3, C-11/12), 18.5 (CH_3, C-9/10).

LRMS (GC/EI$^+$): m/z = 41, 20%; 55, 20%; 69, 20%; 83, 100%; 98, 60%; 180, 10% $[M]^+$.

HRMS (EI$^+$): Found 180.15124 Da, $C_{12}H_{20}O_1$ $[M]^+$ requires 180.15087 Da.

Diastereoisomer cis (**5.19**):

^{1}H NMR (400 MHz, $CDCl_3$) δ ppm: 2.73 (d, *J* = 9.3 Hz, 1H, H-18), 2.40 (br d, *J* = 18.3 Hz, 1H, H-14/14'), 2.20 (ddd, *J* = 10.0, 9.2, 9.0 Hz, 1H, H-17), 2.11 (ddd, *J* = 18.3, 12.5, 5.9 Hz, 1H, H-14/14'), 2.00-1.91 (m, 1H, H-15/15'), 1.90-1.79 (m, 1H, H-16/16'), 1.67 (dddd, *J* = 13.6, 12.6, 10.4, 3.0 Hz, 1H, H-16/16'), 1.58-1.48 (m, 1H, H-15/15'), 1.11 (s, 3H, H-21/22), 1.06 (s, 3H, H-23/24), 1.04 (s, 3H, H-23/24), 0.93 (s, 3H, H-21/22).

^{13}C NMR (100 MHz, $CDCl_3$) δ ppm: 214.3 (C, C-13), 50.5 (CH, C-18), 44.4 (C, C-19/20), 42.5 (CH, C-17), 41.2 (CH_2, C-14), 39.6 (C, C-19/20), 27.1 (CH_3, C-21/22), 26.3 (CH_3, C-23/24), 24.0 (CH_2, C-16), 23.0 (CH_3, C-23/24), 21.9 (CH_2, C-15), 19.1 (CH_3, C-21/22).

UV (MeCN) C = 5.55x10^{-3} M, $\lambda = 280.22$ nm, $\varepsilon = 53$ M^{-1}.cm^{-1}.

IR (MeCN) ν_{max}/cm^{-1} = 3631 (br), 2946 (s), 1688 (s), 1634 (s), 1059 (w).

LRMS (GC/EI$^+$): m/z = 41, 30%; 55, 20%; 69, 40%; 83, 100%; 98, 70%; 180, 10% [M]$^+$.

HRMS (EI$^+$): Found 180.15095 Da, $C_{12}H_{20}O_1$ [M]$^+$ requires 180.15087 Da.

3-(2,3-Dimethylbut-3-en-2-yl)cyclohexan-1-one (**5.20**)

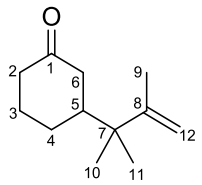

$C_{12}H_{20}O$

MW = 180.29 g.mol^{-1}

R*f* = 0.51 (toluene/Et_2O, 9:1)

Colourless oil

Yield = 3%

This compound was obtained during the 7,7,8,8-tetramethylbicyclo[4.2.0]octan-2-one synthesis (see above for procedure). It was isolated during the second crude purification on silica gel (toluene/Et_2O, 97:3). The title compound **5.20** (3.9 mg, 22 µmol, 3%) was obtained as a colourless oil. This compound was observed during the concentration gradient experiments.

^{1}H NMR (400 MHz, $CDCl_3$) δ ppm: 4.80 (s, 1H, H-12/12'), 4.73 (s, 1H, H-12/12'), 2.41-2.33 (m, 1H, H-2/2'), 2.30 (dd, *J* = 13.5, 3.0 Hz, 1H, H-6/6'), 2.26-2.18 (m, 1H, H-2/2'), 2.15-2.08 (m, 1H, H-3/3'), 2.04 (dd, *J* = 13.5, 13.0 Hz, 1H, H-6/6'), 1.87-1.76 (m, 2H, H-4/4', 5), 1.69 (s, 3H, H-9), 1.57-1.49 (m, 1H, H-3/3'), 1.39-1.29 (m, 1H, H-4/4'), 1.05 (s, 3H, H-10/11), 1.01 (s, 3H, H-10/11).

^{13}C NMR (100 MHz, $CDCl_3$) δ ppm: 212.8 (C, C-1), 151.3 (C, C-8), 110.5 (CH_2, C-12), 45.1 (CH, C-5), 43.6 (CH_2, C-6), 41.4 (CH_2, C-2), 41.2 (C, C-7), 26.2 (CH_2, C-4), 25.7 (CH_2, C-3), 23.5 (CH_3, C-10/11), 23.1 (CH_3, C-10/11), 19.3 (CH_3, C-9).

IR (MeCN) ν_{max}/cm^{-1} = 3628 (br), 2943 (s), 1708 (s), 1632 (s).

LRMS (GC/EI$^+$): m/z = 41, 70% [M-$C_9H_{15}O$]$^+$; 55, 95%; 69, 100%; 83, 95% [M-C_6H_9O]$^+$; 97, 85% [M-C_6H_{11}]$^+$.

HRMS (EI$^+$): Found 180.15134 Da, $C_{12}H_{20}O_1$ [M]$^+$ requires 180.15087 Da.

Decahydrobiphenylene-1,8-dione (**5.27**)

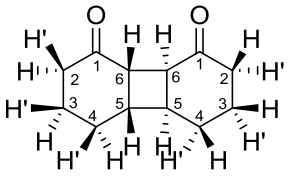

$C_{12}H_{16}O_2$

MW = 192.26 g.mol $^{-1}$

R*f* = 0.19 (hexane/Et_2O, 4:6)

Yellow solid

Yield = 6%

m.p. = 80 °C

This compound was obtained during the following 7,7,8,8-tetramethylbicyclo[4.2.0]octan-2-one synthesis. In a RBF flushed with nitrogen, cyclohex-2-enone (**5.7a**, 90.0 µL, 0.926 mmol) was mixed with tetramethylethylene (**5.17**, 1.80 mL, 1.80 mmol, 1 M in THF) and 9 mL of MeCN. The solution was degassed by sonication whilst being saturated with nitrogen. With the bottle-feed configuration (Figure 7.24), the reaction mixture was injected into the double coiled photochemical flow reactor (capacity: 28.0 mL) at 0.233 mL/min (residence time = 120 min) using a UV-A lamp (9 W). Once the mixture was entirely injected, it was pushed by acetonitrile (Stock solvent) into the flow stream. The reactor was connected to a backpressure regulator (100 psi). After collection and evaporation of the solvent under reduced pressure, the crude mixture was purified on silica gel (hexane/Et_2O, 4:6) to give the title compound **5.27** (5.4 mg, 28 µmol, 6%) as a yellow solid, m.p. = 80 °C (lit. m.p. = 75 °C).[151] NMR data are consistent with the literature.[152]

^{1}H NMR (400 MHz, $CDCl_3$) δ ppm: 3.12 (d, *J* = 7.1 Hz, 2H, H-6), 2.91-2.73 (m, 2H, H-5), 2.42 (ddd, *J* = 14.0, 4.5 Hz, 2H, H-2'), 2.28 (ddd, *J* = 13.0, 5.0 Hz, 2H, H-2), 2.07-1.94 (m, 2H, H-3'), 1.87 (ddddd, *J* = 13.0, 13.0, 13.0, 4.0, 4.0 Hz, 2H, H-3), 1.78-1.67 (m, 2H, H-4'), 1.52 (br d, *J* = 13.9 Hz, 2H, H-4).

^{13}C NMR (100 MHz, $CDCl_3$) δ ppm: 213.2 (C, C-1), 47.6, 41.1, 40.2, 25.1, 22.8.

Octahydrobiphenylene-1,5(2H,4bH)-dione (**5.28**)

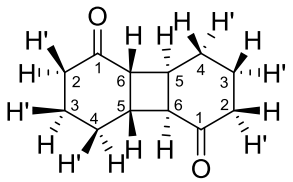

$C_{12}H_{16}O_2$

MW = 192.26 g.mol $^{-1}$

R*f* = 0.11 (hexane/Et_2O, 4:6)

Yellow solid

Yield = 2%

m.p. = 55 °C

In the same way, this compound was obtained during the following 7,7,8,8-tetramethylbicyclo[4.2.0]octan-2-one synthesis. In a RBF flushed with nitrogen, cyclohex-2-enone (**5.7a**, 90.0 µL, 0.926 mmol) was mixed with tetramethylethylene (**5.17**, 1.80 mL, 1.80

mmol, 1 M in THF) and 9 mL of MeCN. The solution was degassed by sonication whilst being saturated with nitrogen. With the bottle-feed configuration (Figure 7.24), the reaction mixture was injected into the double coiled photochemical flow reactor (capacity: 28.0 mL) at 0.233 mL/min (residence time = 120 min) using a UV-A lamp (9 W). Once the mixture was entirely injected, it was pushed by acetonitrile (Stock solvent) into the flow stream. The reactor was connected to a backpressure regulator (100 psi). After collection and evaporation of the solvent under reduced pressure, the crude mixture was purified on silica gel (hexane/Et_2O, 4:6) to give the title compound **5.28** (1.5 mg, 7.8 µmol, 2%) as a yellow solid, m.p. = 55 °C (lit. m.p. = 53 °C).[151] NMR data are consistent with the literature.[153]

^{1}H NMR (400 MHz, $CDCl_3$) δ ppm: 3.08-2.96 (m, 2H), 2.64 (dd, *J* = 7.5, 7.5 Hz, 2H), 2.42 (ddd, *J* = 16.0, 5.0, 5.0 Hz, 2H), 2.32-2.18 (m, 2H), 2.04-1.78 (m, 6H), 1.74-1.60 (m, 2H).

1,3,3,7,7,8,8-Heptamethyl-2,4-dioxabicyclo[4.2.0]octan-5-one (**5.29**)

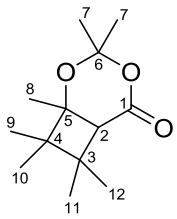

$C_{13}H_{22}O_3$

MW = 226.32 g.mol $^{-1}$

R*f* = 0.36 (hexane/Et_2O, 1:1)

Colourless oil

Yield = 22%

In a RBF flushed with nitrogen, 2,2,6-trimethyl-4*H*-1,3-dioxin-4-one (**2.38**, 66.3 µL, 0.500 mmol) and tetramethylethylene (**5.17**, 1.19 mL, 10.0 mmol) were mixed with dried MeCN (8.75 mL) to make a 10 mL solution. The solution was degassed by sonication whilst being saturated with nitrogen, and injected into a 10 mL sample loop. Then, the content of the loop was pushed by MeCN (Stock solvent) into the double coiled photochemical flow reactor (capacity: 28.0 mL) at 0.233 mL/min (residence time = 120 min) using a UV-C lamp (9 W). The reactor was connected to a backpressure regulator (100 psi). After collection and evaporation of the solvent under reduced pressure, the crude mixture was purified twice on silica gel (first: hexane/Et_2O, 1:1, second: hexane/Et_2O, 8:2) to give the title compound **5.29** (25 mg, 0.11 mmol, 22%) as a colourless oil. The single ^{1}H NMR shift mentioned in the literature[125] is consistent with our data.

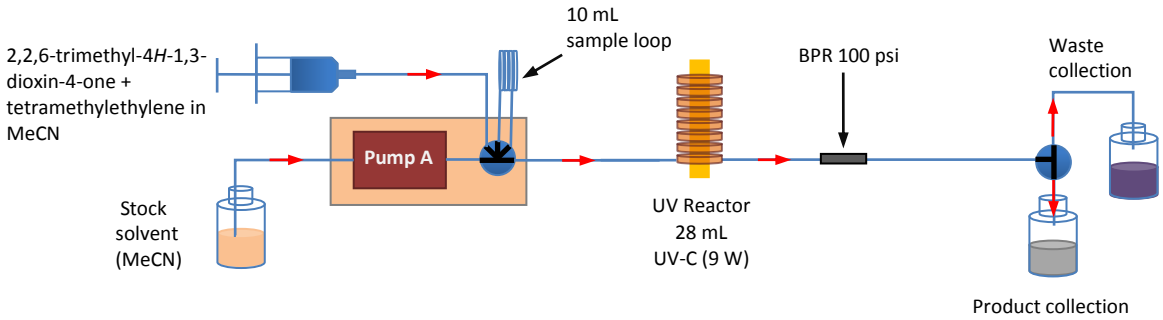

Figure 7.25: Flow set-up for the synthesis 1,3,3,7,7,8,8-heptamethyl-2,4-dioxabicyclo[4.2.0]octan-5-one (**5.29**) - Sample loop configuration.

^{1}H NMR (400 MHz, $CDCl_3$) δ ppm: 2.59 (s, 1H, H-2), 1.57 (s, 3H, CH_3), 1.55 (s, 3H, CH_3), 1.45 (s, 3H, CH_3), 1.18 (s, 3H, CH_3), 1.05 (s, 3H, CH_3), 0.97 (s, 6H, H-7).

^{13}C NMR (100 MHz, $CDCl_3$) δ ppm: 169.1 (C, C-1), 105.2 (C), 76.6 (C), 49.1 (C), 45.4 (C), 40.5 (C), 29.3 (CH_3), 29.0 (CH_3), 26.8 (CH_3), 23.4 (CH_3), 21.7 (CH_3), 20.7 (CH_3), 20.2 (CH_3).

LRMS (LC/ES$^+$): m/z = 169, 100% $[M\text{-acetone}+H]^+$; 249, 20% $[M+Na]^+$; 475, 20% $[2M+Na]^+$.

HRMS (EI$^+$): Found 226.15746 Da, $C_{13}H_{22}O_3$ $[M]^+$ requires 226.15635 Da.

Phenanthrene (**5.23**)

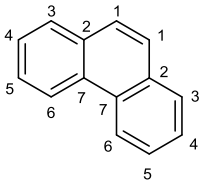

$C_{14}H_{10}$

MW = 178.23 g.mol $^{-1}$

White solid

Yield = 96%

m.p. = 100 °C

In a RBF flushed with nitrogen, cis-stilbene (**5.21**, 50.0 µL, 0.280 mmol) and iodine (7.1 mg, 0.028 mmol) were mixed with 50 mL of cyclohexane and the solution was saturated with O_2. With the bottle-feed configuration (Figure 7.26), the reaction mixture was injected into the single coiled photochemical flow reactor (capacity: 31.8 mL) at 1.06 mL/min (residence time = 30 min) using a UV-A lamp (36 W). Once the mixture was entirely injected, it was pushed by cyclohexane (Stock solvent) into the flow stream. The reactor was connected to a backpressure regulator (100 psi). After collection, the crude mixture was washed with a saturated solution of sodium thiosulfate (20 mL), water (20 mL) and brine (2 x 20 mL). The organic layer was finally dried over $MgSO_4$, filtered and the solvent was evaporated under reduced pressure to afford the desired product **5.23** (48 mg, 0.27 mmol, 96%) as a white solid, m.p. = 100 °C (lit. m.p. = 96 °C).[154] NMR data are consistent with the literature.[154-155]

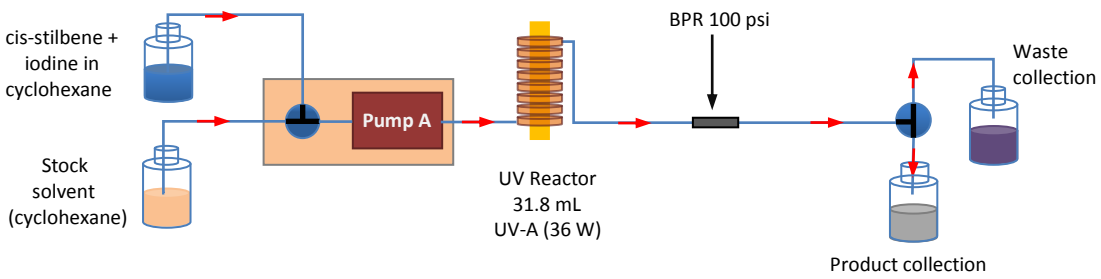

Figure 7.26: Flow set-up for the synthesis of the Phenanthrene - Bottle-feed configuration.

^{1}H NMR (400 MHz, $CDCl_3$) δ ppm: 8.74 (d, *J* = 8.1 Hz, 2H, H-6), 7.94 (dd, *J* = 7.7, 1.3 Hz, 2H, H-3), 7.79 (s, 2H, H-1), 7.70 (ddd, *J* = 8.2, 7.0, 1.6 Hz, 2H, H-5), 7.65 (ddd, *J* = 8.0, 7.0, 1.2 Hz, 2H, H-4).

^{13}C NMR (100 MHz, $CDCl_3$) δ ppm: 132.0 (C, C-2/7), 130.3 (C, C-2/7), 128.5 (CH, C-3), 126.9 (CH, C-1), 126.5 (CH, C-4, 5), 122.6 (CH, C-6).

1,2,3,4-Tetraphenylcyclobutane (**5.25** and **5.26**)

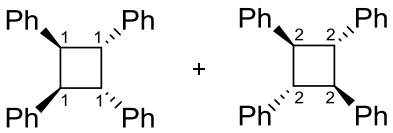

5.25 **5.26**

$C_{28}H_{24}$

MW = 360.19 g.mol $^{-1}$

R*f*(**5.25**) = 0.36 (hexane/EtOAc, 95:5)

R*f*(**5.26**) = 0.44 (hexane/EtOAc, 95:5)

Yellow solid

Yield = 33%

Ratio **5.25**/**5.26**: 66/34

m.p. = 170 °C

This mixture of isomers was obtained during the phenanthrene synthesis. In a RBF flushed with nitrogen, cis-stilbene (**5.21**, 445 µL, 2.50 mmol) and iodine (60.0 mg, 0.236 mmol) were mixed with 50 mL of cyclohexane and the solution was saturated with O_2. With the bottle-feed configuration (Figure 7.26), the reaction mixture was injected into the single coiled photochemical flow reactor (capacity: 31.8 mL) at 0.176 mL/min (residence time = 180 min) using a UV-A lamp (36 W). Once the mixture was entirely injected, it was pushed by cyclohexane (Stock solvent) into the flow stream. The reactor was connected to a backpressure regulator (100 psi). After collection, the crude mixture was washed with a saturated solution of sodium thiosulfate (2 x 20 mL), water (20 mL) and brine (2 x 20 mL). The organic layer was finally dried over $MgSO_4$. After filtration and evaporation of the solvent under reduced pressure, the crude mixture was purified on silica gel (hexane/EtOAc, 95:5) to give phenanthrene (**5.23**, 245 mg, 1.37 mmol, 55%) as a white solid and the mixture of title compounds **5.25** and **5.26** (150 mg, 0.416 mmol, 33%) as a yellow solid, m.p. = 170 °C (lit. m.p. = 158 °C).[156] NMR data are consistent with the literature.[157]

Isomer **5.25**:

^{1}H NMR (400 MHz, $CDCl_3$) δ ppm: 7.33-7.00 (m, 20H, ArH), 4.45 (s, 4H, H-1).

Isomer **5.26**:

^{1}H NMR (400 MHz, $CDCl_3$) δ ppm: 7.33-7.00 (m, 20H, ArH), 3.67 (s, 4H, H-1).

Ethyl 2-cyano-2-(2-cyanophenyl)acetate (**5.32**)

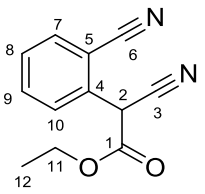

$C_{12}H_{10}N_2O_2$

MW = 214.22 g.mol $^{-1}$

R*f* = 0.63 (hexane/EtOAc, 7:3)

White solid

Yield = 50%

m.p. = 70 °C

Following the procedure described by Beugelmans,[126] in a RBF flushed with nitrogen, ethyl 2-cyanoacetate (**5.31**, 168 µL, 1.58 mmol), 2-bromobenzonitrile (**5.30**, 72.0 mg, 0.396 mmol) and *t*-BuOK (178 mg, 1.58 mmol) were mixed with 10 mL of DMSO. The solution was degassed by sonication whilst being saturated with nitrogen. With the bottle-feed configuration (Figure 7.27), the reaction mixture was injected into the single coiled photochemical flow reactor (capacity: 31.8 mL) at 0.265 mL/min (residence time = 120 min) using a UV-B lamp (36 W). Once the mixture was entirely injected, it was pushed by DMSO (Stock solvent) into the flow stream. The reactor was connected to a backpressure regulator (100 psi). After collection, the crude mixture was quenched with addition of 20 mL of water and 3 mL of an aqueous solution of NH_4Cl. The aqueous layer was extracted 4 times with DCM (4 x 20 mL). The combined organic layers were washed with brine (3 x 20 mL), dried over $MgSO_4$, filtered and the solvent was evaporated under reduced pressure to afford the crude product. This crude mixture was then purified on silica gel (toluene/EtOAc, 8:2) to give the title compound **5.32** (42.0 mg, 0.196 mmol, 50%) as a white solid, m.p. = 70 °C (lit. m.p. = 69 °C).[126] NMR data are consistent with the literature.[126]

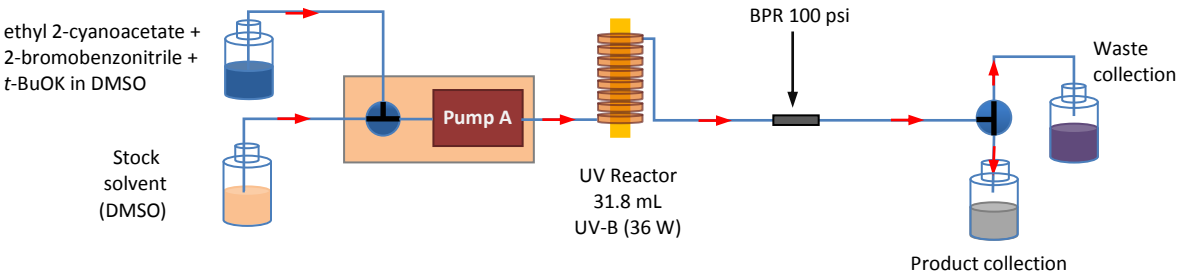

Figure 7.27: Flow set-up for the synthesis of the ethyl 2-cyano-2-(2-cyanophenyl)acetate - Bottle-feed configuration.

^{1}H NMR (400 MHz, $CDCl_3$) δ ppm: 7.79-7.70 (m, 3H, ArH), 7.56 (ddd, *J* = 8.0, 7.2, 2.0 Hz, 1H, ArH), 5.17 (s, 1H, H-2), 4.38-4.24 (m, 2H, H-11), 1.33 (t, *J* = 7.1 Hz, 3H, H-12).

^{13}C NMR (100 MHz, $CDCl_3$) δ ppm: 163.3 (C, C-1), 133.8 (CH), 133.4 (CH and C), 129.9 (CH), 129.1 (CH), 116.3 (C), 114.4 (C), 112.98 (C), 64.1 (CH_2, C-11), 41.8 (CH, C-2), 13.8 (CH_3, C-12).

UV (DMSO) C = 5.58x10^{-4} M, $\lambda_1 = 275.01$ nm, $\varepsilon_1 = 1106$ M^{-1}.cm^{-1}, $\lambda_2 = 282.45$ nm, $\varepsilon_2 = 1032$ M^{-1}.cm^{-1}.

7.2.4.2 GENERAL PROCEDURES: Concentration gradient experiments

7.2.4.2.1 Preliminary study of the dispersion in flow chemistry: Influence of the flow rate and the temperature

Experimental set-up and Instrumentation: Using the flow machine (Vapourtec R2+/R4), dispersion experiments were carried out using one single pump with a 10 µL sample loop, a home-made coiled stainless steel reactor (10 mL capacity, 1 mm i.d.) immersed in a high temperature silicone oil bath (Grant Optima™ TXF200), an ice bath, a 250 psi BPR and in-line UV acquisition (Ocean Optics DH-2000-BAL spectrometer)

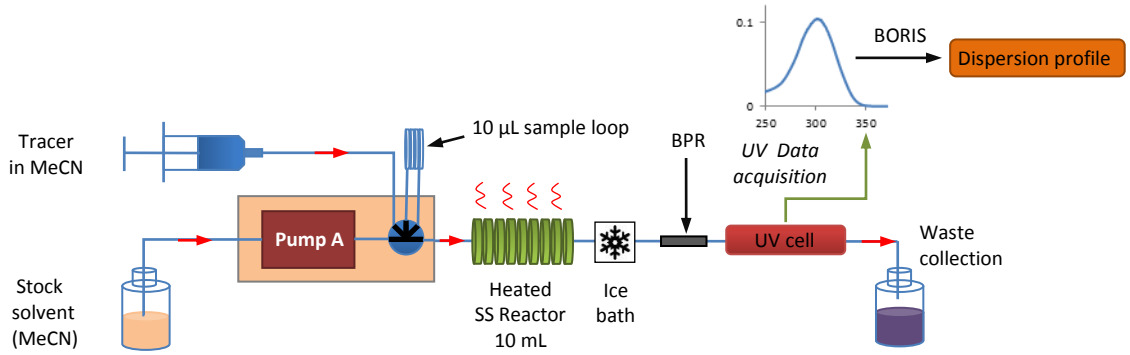

Figure 7.28: Flow set-up for the dispersion experiments - Sample loop configuration.

General procedure for the generation of the dispersion profile: Dispersion profiles were obtained from the experimental set-up described above (sample loop configuration) at flow rates between 0.1 and 10 mL min^{-1} and the reactor heated to 30 °C and 120 °C. For each experiment, 10 µL of a solution of tracer in MeCN ($[C_0]$ = 1.015 × 10^{-2} M) were injected into a sample loop and pushed by the stock solvent (MeCN). In-line UV detection was used and the data sampling rate was determined by the acquisition parameters. The spectra were processed using BORIS software by calibration-less method (height of non-overlapping peak processing at 250 nm). UV absorbance was converted into molar units using a calibration curve and the calculation of $([C]/[C]_0)$ x 100 was performed. In order to compare the dispersion profile at each individual flow rate, the different curves were aligned at the same volume eluted which can be calculated as follow: volume eluted (mL) = time (min) × $Flow_{effective}$ ($mL.min^{-1}$). Each $Flow_{effective}$ were calculated from each flow rate displayed on the flow system with a correction for thermal expansion of acetonitrile according to $Flow_{effective} = Flow_{pump}(1 + \alpha\Delta T)$ where α = the expansion coefficient of the solvent.

Dispersion profile of sample plugs of benzophenone

Calibration curve obtained from the processing of UV spectra using BORIS software (height of non-overlapping peak processing at 250 nm).

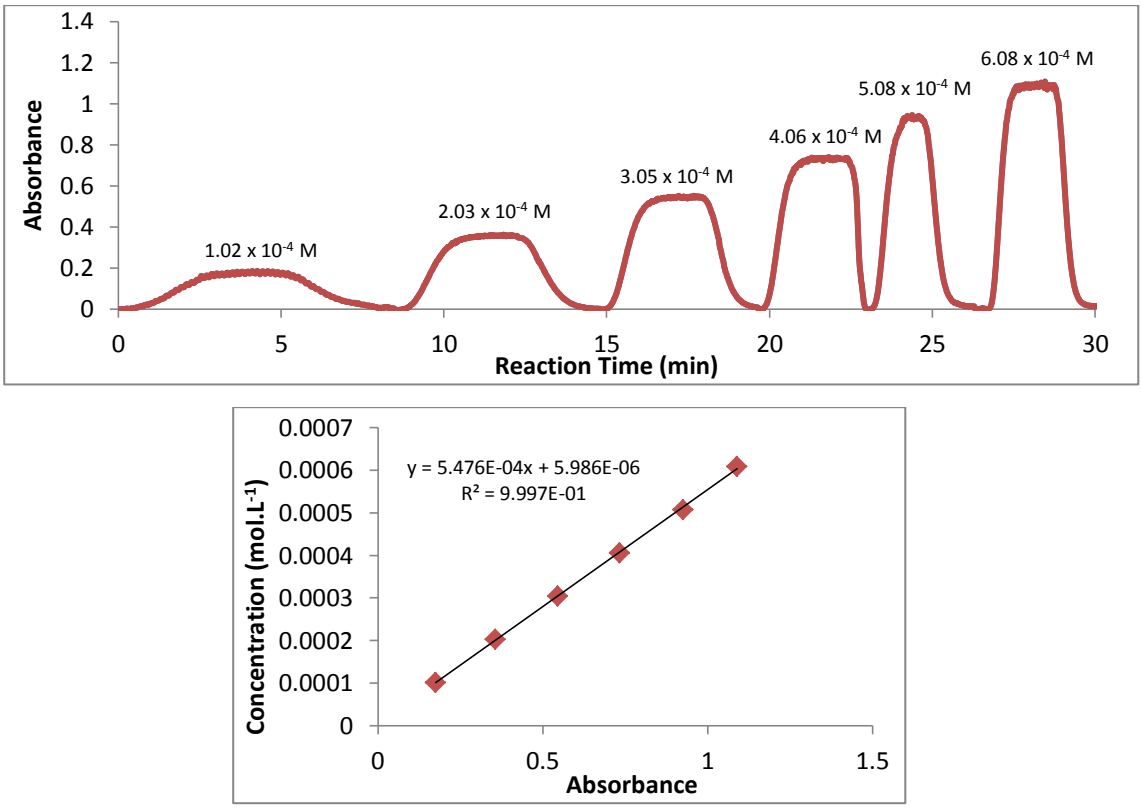

Figure 7.29: Calibration curve to get the concentration of benzophenone solutions according to the UV absorbance.

Using the general procedure described above with the calibration curve (Figure 7.29), the following Figures 7.30 and 7.31 were obtained.

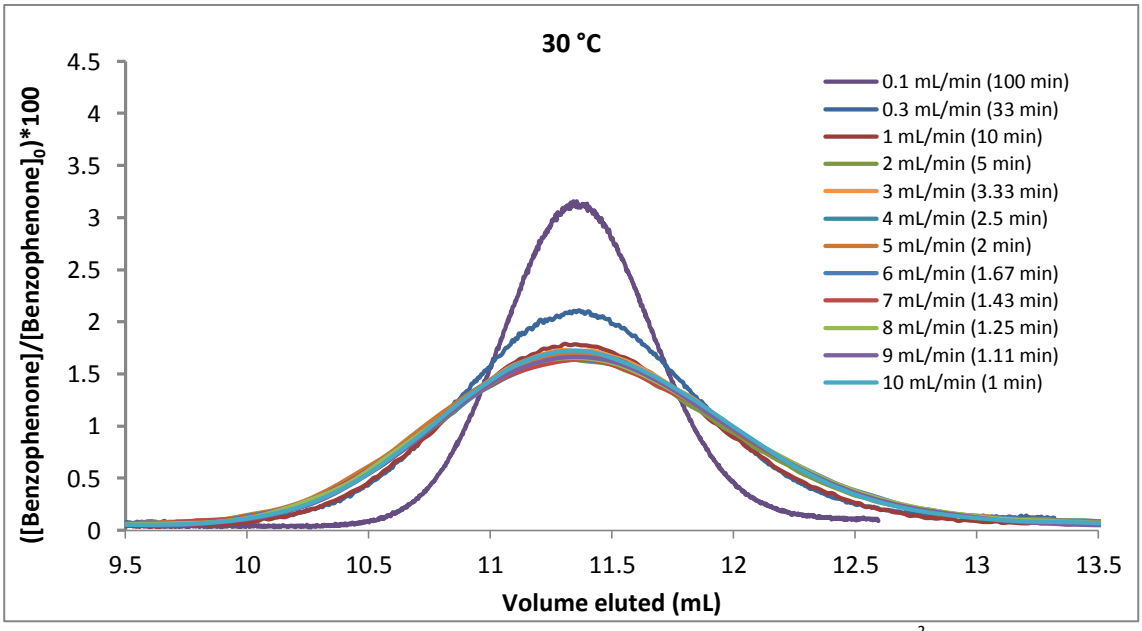

Figure 7.30: Dispersion of a 10 µL sample plug of benzophenone in MeCN ($[C]_0$=1.015 × 10^{-2} M) through 10 mL home-made coiled stainless steel tubing of 1 mm i.d. at 30 °C and the indicated flow rates.

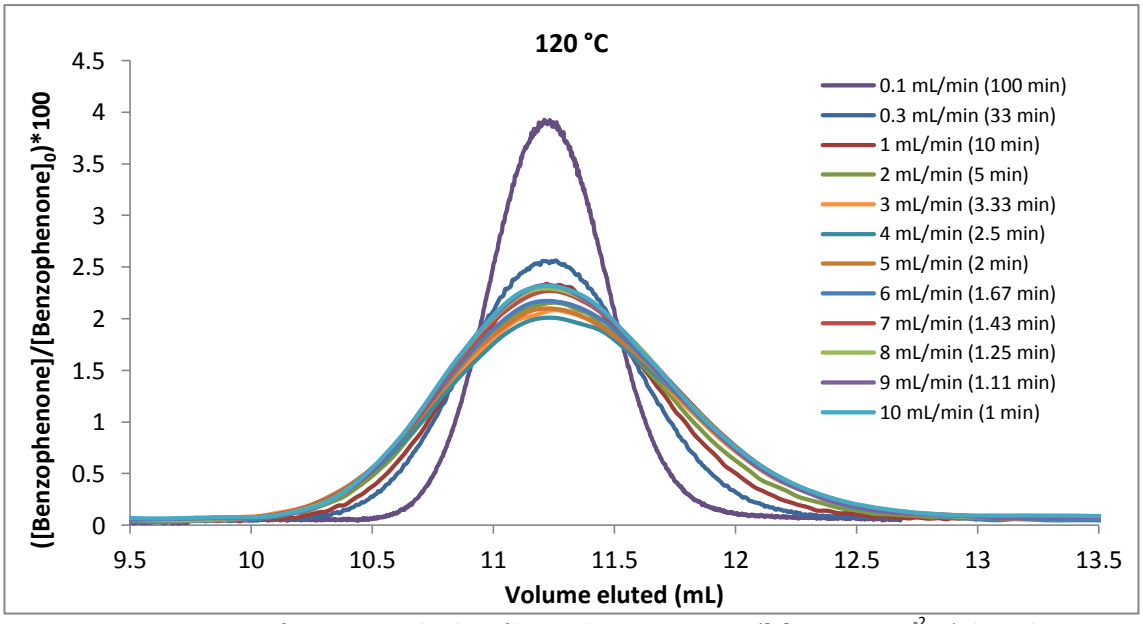

Figure 7.31: Dispersion of a 10 µL sample plug of benzophenone in MeCN ($[C]_0$=1.015 × 10^{-2} M) through 10 mL home-made coiled stainless steel tubing of 1 mm i.d. at 120 °C and the indicated flow rates.

7.2.4.2.2 Preliminary study of the dispersion in flow chemistry: the dispersion caused by the UV cell and the reactor

Experimental set-up and Instrumentation: Using the flow machine (Vapourtec R2+/R4), dispersion experiments were carried out using one single pump with a 5 mL sample loop. In the study of the dispersion caused by the UV cell, the sample loop was connected straight to the UV cell (Figure 7.32). In the study of the dispersion caused by the 10 mL Stainless Steel reactor + the UV cell, the sample loop was connected first to the reactor followed by the UV cell (Figure 7.33).

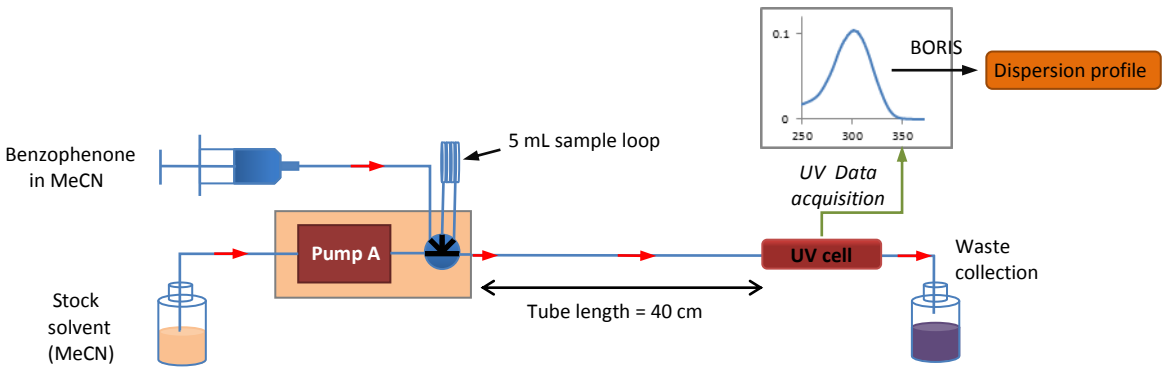

Figure 7.32: Flow set-up for the measurement of the dispersion caused by the UV cell - Sample loop configuration.

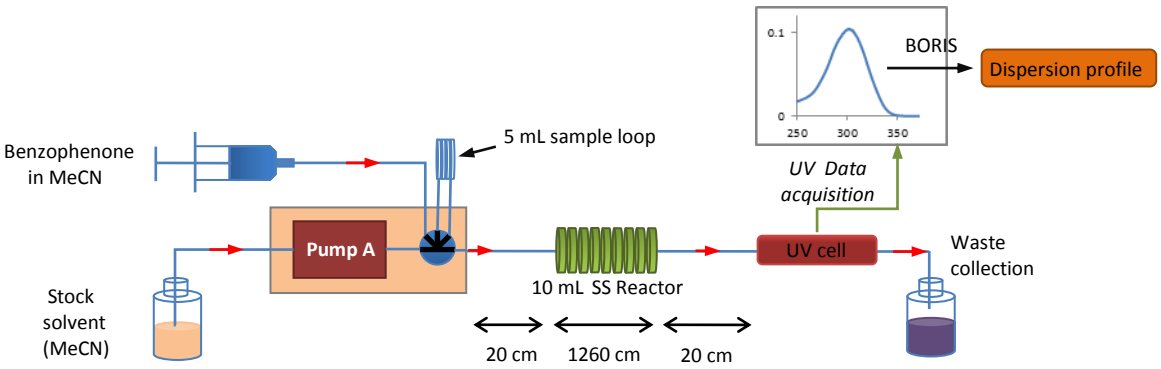

Figure 7.33: Flow set-up for the measurement of the dispersion caused by the 10 mL reactor + the UV cell - Sample loop configuration.

General procedure to quantify the dispersion caused by the UV cell and the 10 mL reactor:

5 mL of a solution of benzophenone in MeCN ($[C_0]$ = 9.5 × 10^{-3} M) were injected into a 5 mL sample loop and pushed by the stock solvent (MeCN) at 1 mL/min. The system was left at r.t. Using the flow set-up without reactor (Figure 7.32), the sample plug went straight through the UV cell (tube length = 40 cm, 1 mm i.d.). Using the flow set-up with the 10 mL SS reactor and the UV cell (tube length = 1300 cm, 1 mm i.d.) (Figure 7.33), the sample plug went first through the reactor and then through the UV cell. For each flow set-up, the dispersion of the sample plugs was analysed and recorded by in-line UV detection and the data sampling rate was determined by the acquisition parameters. The spectra were processed using BORIS software with a calibration-less method (height of non-overlapping peak processing at 250 nm). After normalisation, the dispersion curves of the UV cell (blue) and the 10 mL SS reactor + UV cell (red) were obtained. The dispersion curve of the 10 mL reactor (green) (tube length = 1260 cm, 1 mm i.d.) was calculated from subtraction of the UV cell dispersion (blue) to the 10 mL reactor + UV cell dispersion (red) (Figure 7.34).

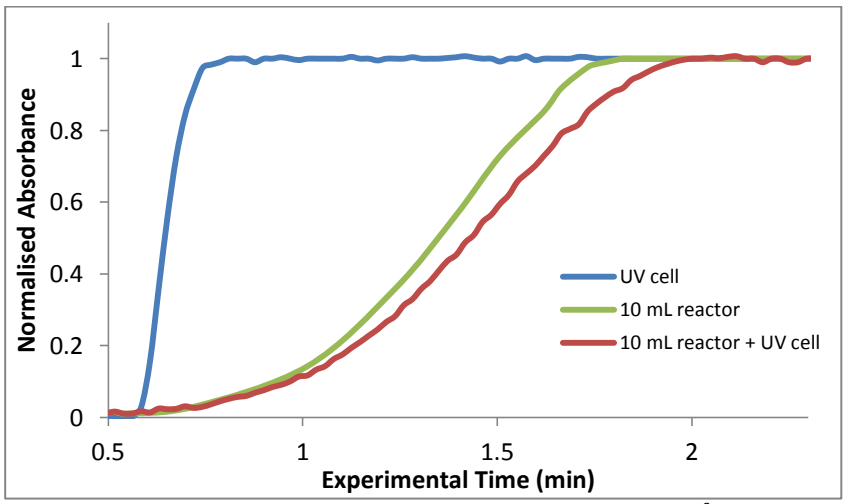

Figure 7.34: Dispersion of 5 mL sample plug of benzophenone in MeCN ($[C_0]$ = 9.5 x 10^{-3} M) at 1 mL/min through the flow system indicated.

7.2.4.2.3 Use of dispersion generated concentration gradient with 1st and 2nd order reactions

Experimental set-up for the application of the concentration gradient methodology on 1st and 2nd order reactions: Using the flow machine (Vapourtec R2+/R4), the experiments were carried out using one single pump with the bottle feed configuration, a PFA loop (10 mL capacity, 1 mm i.d.), a home-made coiled stainless steel reactor (10 mL capacity, 1 mm i.d.) immersed in a high temperature silicone oil bath (Grant Optima™ TXF200), an ice bath, a 250 psi BPR, an in-line IR spectrometer (alpha transmission FT-IR from Bruker) and, when mentioned, GC vials for off-line analysis.

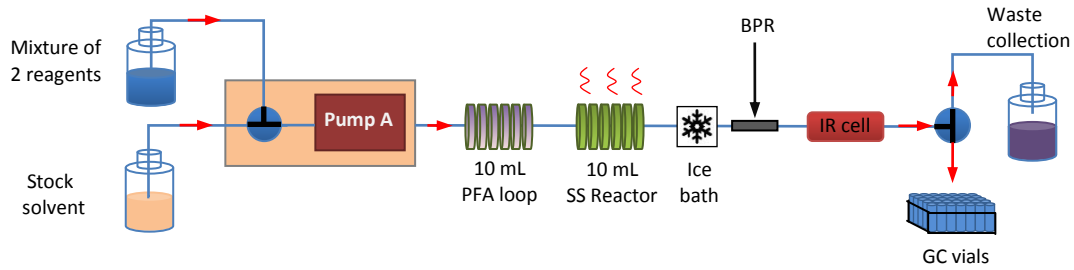

Figure 7.35: Flow set-up for the application of the concentration gradient methodology on 1st and 2nd order reactions - Bottle feed configuration.

General procedure for the application of the concentration gradient methodology on 1st and 2nd order reactions: In a RBF flushed with nitrogen, the different reagents were mixed together with the corresponding solvent. The reaction mixture was degassed by sonication whilst being saturated with nitrogen. Solvent was pumped at the indicated flow rate and the reactor was set to a temperature. Once the temperature was stable, the feeding valve was switched to the reagent solution and 5 mL of the reaction mixture was injected. At the end of the sample plug injection, the feeding valve was returned to the solvent feed. When indicated, this procedure was repeated at several reaction temperatures. The sample plug dispersed first in the 10 mL PFA loop and then the reaction occurred in the heated stainless steel reactor. In-line IR detection was used and the data sampling rate was determined by the acquisition parameters. The spectra were processed using BORIS software by calibration-less methods (OPA processing or height of non-overlapping peaks processing). When indicated, the reaction mixture was collected in vials for GC analysis.

Application of the concentration gradient methodology on a 1st order reaction: Using the general procedure described above, the concentration gradient methodology was first applied to a 1st order reaction. A solution of 2,2,6-trimethyl-4*H*-1,3-dioxin-4-one (**2.38**, 1.50 mL, 11.3 mmol) and EtOH (2.64 mL, 45.2 mmol) in 100 mL of MeCN was prepared ([$C_{dioxinone}$] = 0.11 M).

As described in Figure 7.36, series of reactions mixture plugs were injected into the flow system at different temperatures. Residence time in the heated reactor was set at 33 min (flow rate = 0.3 mL/min) for each sample plug.

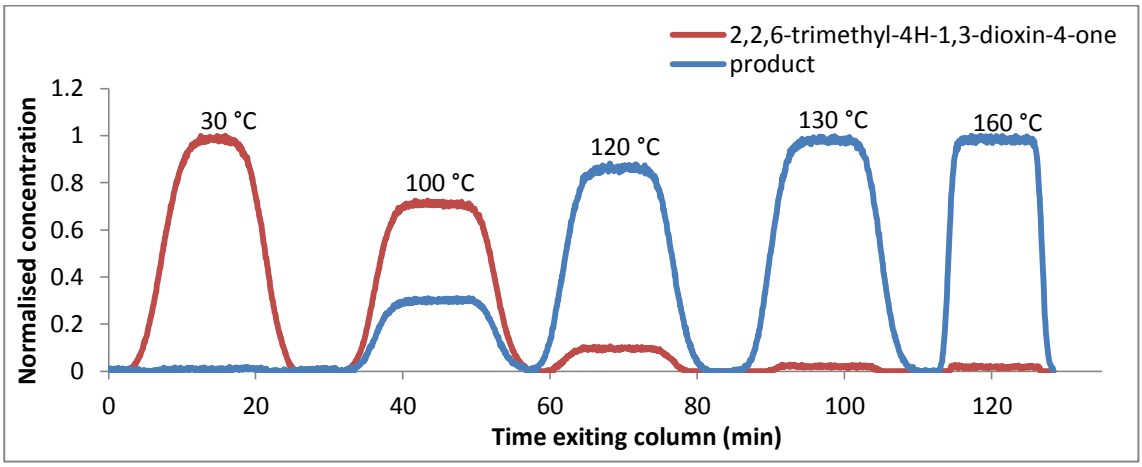

Figure 7.36: Series of 5 mL plugs injections of 2,2,6-trimethyl-4*H*-1,3-dioxin-4-one and EtOH in MeCN at 0.3 mL/min and at the indicated temperature through the 10 mL PFA loop followed by the 10 mL heated reactor. In-line IR detection and OPA processing using BORIS software. 0% and 100% conversion respectively conducted at 30 and 160 °C were performed to normalise the data.

According to the data obtained after processing of the IR spectra with BORIS software (Figure 7.36), the conversion for the dispersed reactions at 100 °C (Figure 7.37) was calculated using the following Equation 7.1.

$$\text{Conversion}_t = \frac{[\text{dioxinone}]_0 - [\text{dioxinone}]_t}{[\text{dioxinone}]_0} = 1 - \frac{[\text{dioxinone}]_t}{[\text{dioxinone}]_0}$$

$$\text{Conversion}_t = 1 - \frac{[\text{dioxinone}]_t}{[\text{dioxinone}]_t + [\text{product}]_t}$$

Equation 7.1: Formula used for the calculation of the conversion.

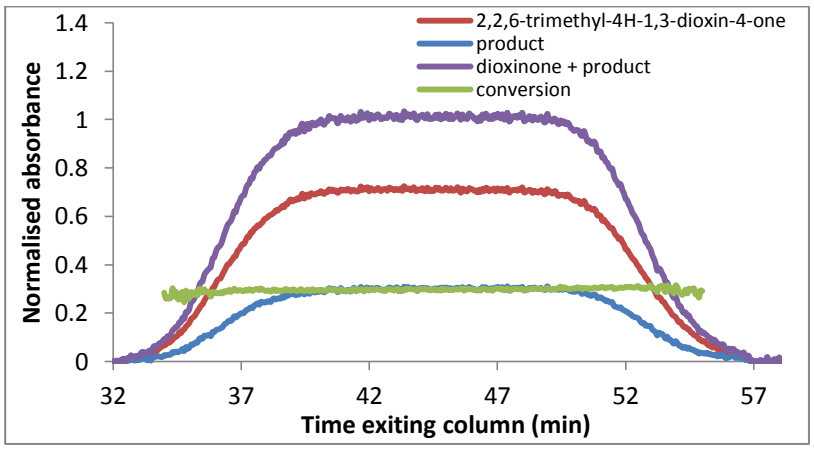

Figure 7.37: Zoom in on the sample plug injected into the flow system at 100 °C. Concentration profile of the starting material and the product. Calculation of the conversion according to the Equation 7.1.

From this graph (Figure 7.37), the reaction rate constant at 100 °C can be extracted by plotting $\ln[\mathbf{2.38}]_0$ *vs*. $\ln[\mathbf{2.38}]_t$.

Application of the concentration gradient methodology on a 2nd order reaction: Using the general procedure described above, the concentration gradient methodology was then applied to a 2nd order reaction. A solution of methyl acrylate (**5.2**, 7.20 mL, 80.0 mmol) and isoprene (**5.1**, 8.00 mL, 80.0 mmol) in 10 mL of toluene was prepared ([C] = 3.17 M). A 5 mL single plug of the reaction mixture was injected into the flow system at 200 °C. Residence time in the heated reactor was set at 33 min (flow rate = 0.3 mL/min). At the end of the reactor, an in-line IR spectrometer recorded the different spectra and the reaction mixture was collected in vials using the liquid handler (0.2 mL collected per vial). The spectra were processed using BORIS software by calibration-less methods (height of non-overlapping peaks processing) (Figure 7.41). After addition of 1 mL of DCM in each vials, GC analysis were performed. GC data (Area of each peak) were converted into molar units using calibration curves (Figures 7.38 and 7.39) and the concentration gradient profile of the methyl acrylate and the products were obtained (Figure 7.40). The isoprene was not seen on GC, probably due to an overlap with the solvent. The conversion profile was calculated using the following Equation 7.2.

$$\text{Conversion}_t = 1 - \frac{[\text{methyl acrylate}]_t}{[\text{methyl acrylate}]_t + [\text{products}]_t}$$

Equation 7.2: Formula used for the calculation of the conversion.

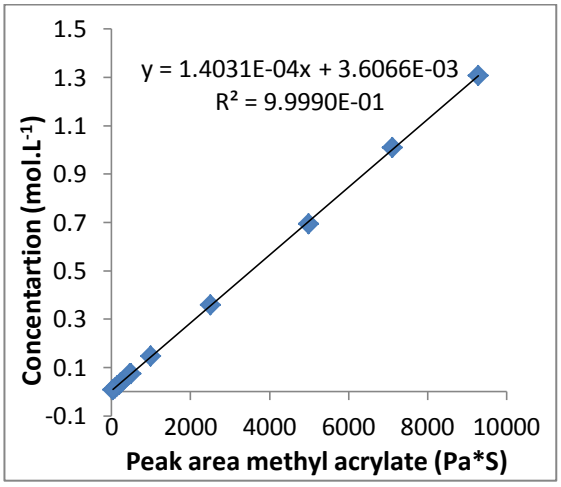

Figure 7.38: Calibration curve to get the concentration of methyl acrylate according to the peak area in GC.

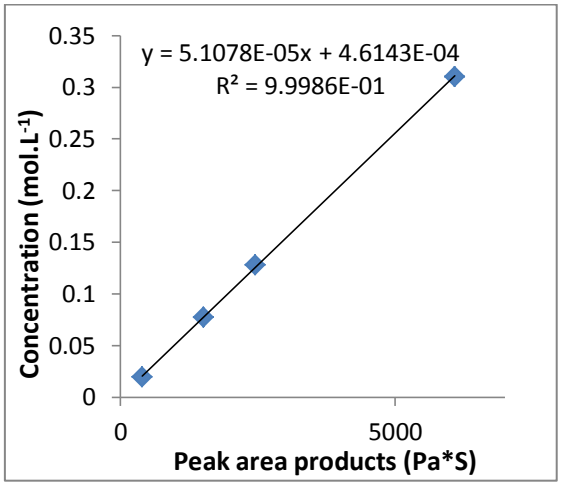

Figure 7.39: Calibration curve to get the concentration of products (3-methyl and 4-methyl isomers) according to the peaks area in GC.

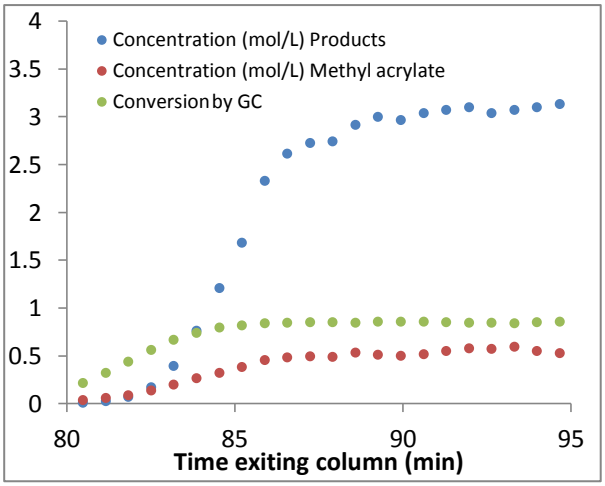

Figure 7.40: Concentration gradient profile of the methyl acrylate (**5.2**) and the products **5.3** + **5.4** obtained after conversion of the peak area (GC) into molar units using the calibration curves (Figures 7.38 and 7.39). Calculation of the conversion according to Equation 7.2.

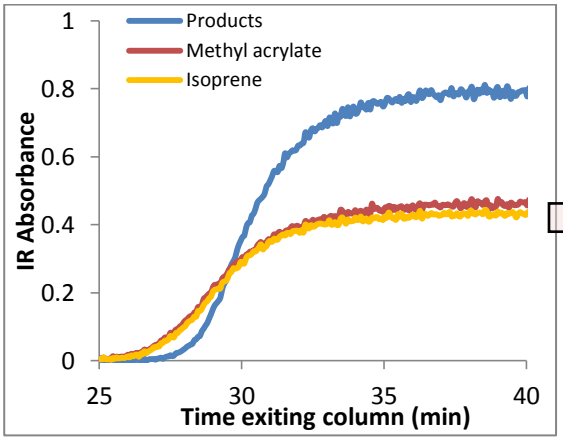

Figure 7.41: IR profile of the methyl acrylate, the isoprene and the products obtained after processing the spectra with BORIS (height of non-overlapping peaks processing at 898 nm for the isoprene, 1400 nm for the methyl acrylate and 2830 nm for the products).

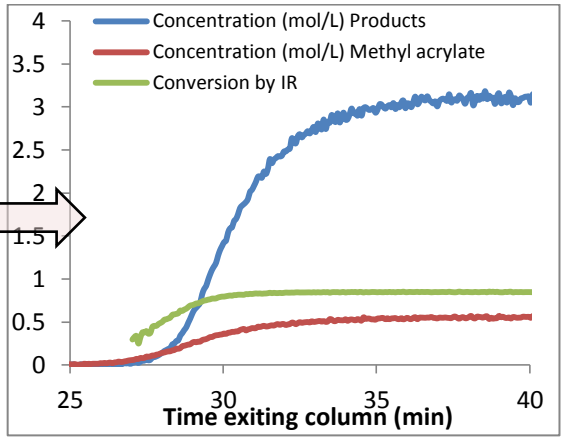

Figure 7.42: Concentration gradient profile of the methyl acrylate and the products obtained from the IR profile (Figure 7.41). The maximum IR absorbance of each curve was normalised with the maximum concentration obtained in Figure 7.40. Calculation of the conversion according to the Equation 7.2.

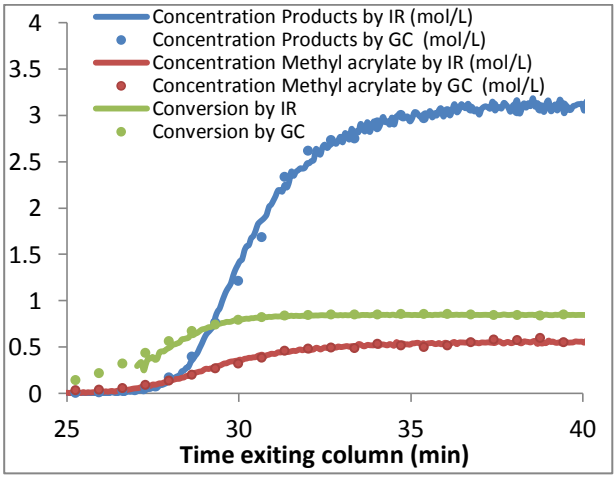

Figure 7.43: Good overlap between both IR (Figure 7.42) and GC (Figure 7.40) concentration gradient results.

From this graph (Figure 7.43), the reaction rate constant at 200 °C can be extracted by plotting $1/\ln[\mathbf{5.2}]_t$ *vs*. $1/\ln[\mathbf{5.2}]_0$.

7.2.4.2.4 Application of the concentration gradient methodology in flow: a novel process towards the fast optimisation of photochemical reaction conditions - [2 + 2] photocycloaddition (A + B → C)

Experimental set-up for the generation of the concentration gradient profile of the reagent to disperse (Reagent B) at the exit of the 10 mL loop (step 1): Using the flow machine (Vapourtec R2+/R4), the experiments were carried out using one single pump, a PFA loop (10 mL capacity, 1 mm i.d.), a 250 psi BPR and an in-line UV or IR spectrometer (Ocean Optics DH-2000-BAL spectrometer or alpha transmission FT-IR from Bruker).

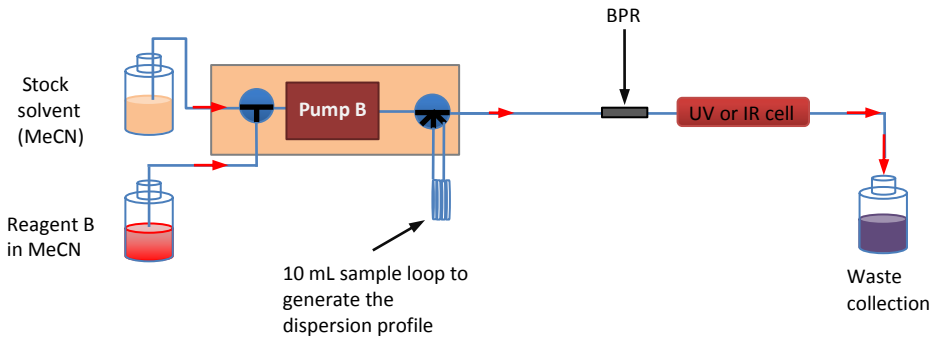

Figure 7.44: Flow set-up for the generation of concentration gradient profile.

General procedure for the generation of the concentration gradient profile of the reagent to disperse (Reagent B) at the exit of the 10 mL loop (step 1): In a 50 mL flask, the reagent to disperse was mixed with MeCN. The reaction mixture was degassed by sonication whilst being saturated with nitrogen. Solvent was pumped at the indicated flow rate (0.05 mL/min, 0.1 mL/min or 0.113 mL/min) and after few minutes, the feeding valve was switched to the reagent solution and 10 mL of the reaction mixture was injected. At the end of the sample plug injection, the feeding valve was returned to the solvent feed. The sample plug dispersed in the 10 mL PFA loop. In-line IR or UV detection was used and the data sampling rate was determined by the acquisition parameters. The spectra were processed using BORIS software by calibration-less methods (height of non-overlapping peaks processing).

Generation of the concentration gradient profile of the tetramethylehylene or the cyclohex-2-enone at 0.05, 0.1 or 0.113 mL/min.

Using the general procedure described above, the following concentration gradient profiles were obtained.

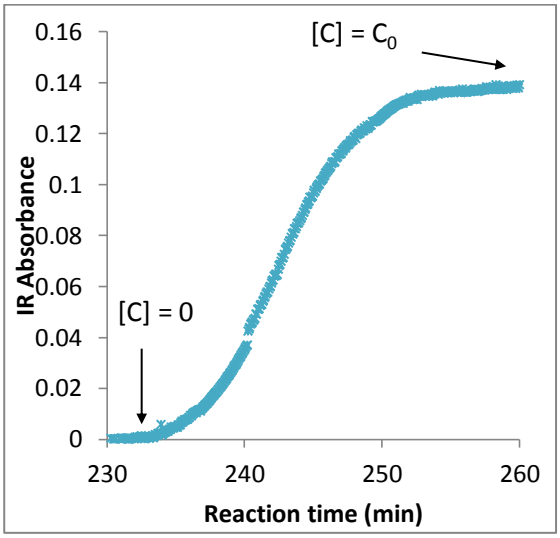

Figure 7.45: Concentration gradient profile of a 10 mL plug of tetramethylethylene in MeCN ($[C_0]$ = 0.4 M) after going through a 10 mL PFA loop at 0.05 mL/min (See general procedure above). In-line IR detection and height of non-overlapping peaks processing at 1160 nm.

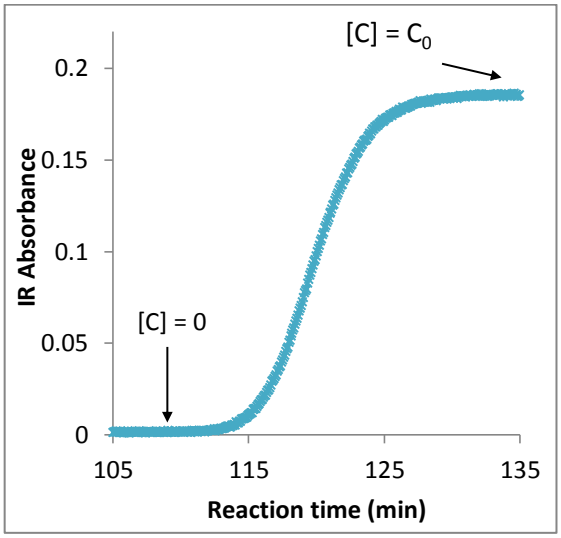

Figure 7.46: Concentration gradient profile of a 10 mL plug of tetramethylethylene in MeCN ($[C_0]$ = 0.5 M) after going through a 10 mL PFA loop at 0.1 mL/min (See general procedure above). In-line IR detection and height of non-overlapping peaks processing at 1160 nm.

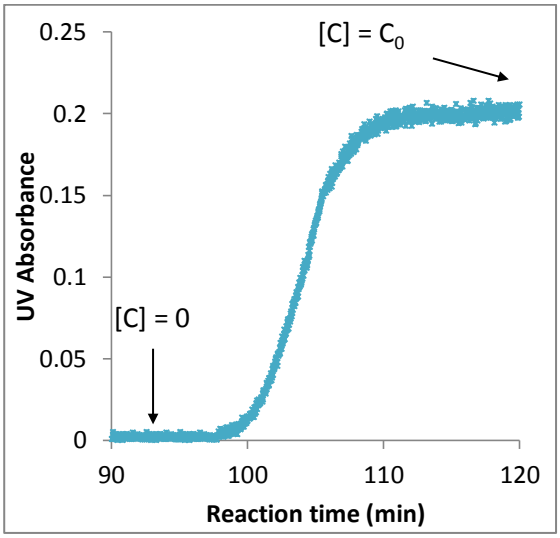

Figure 7.47: Concentration gradient profile of a 10 mL plug of tetramethylethylene in MeCN ($[C_0]$ = 0.1 M) after going through a 10 mL PFA loop at 0.113 mL/min (See general procedure above). In-line UV detection and height of non-overlapping peaks processing at 240 nm.

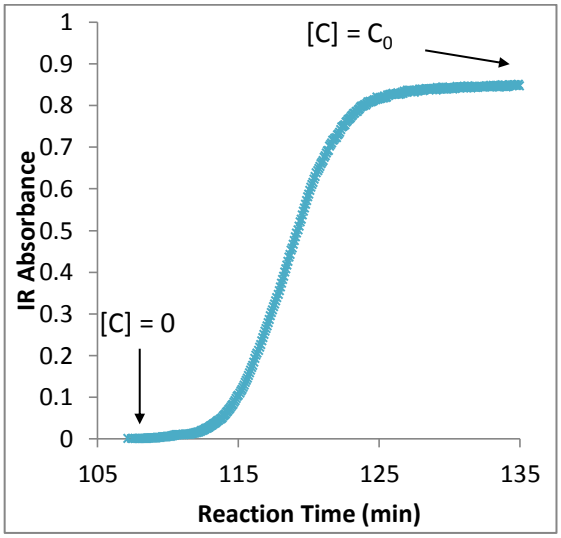

Figure 7.48: Concentration gradient profile of a 10 mL plug of cyclohex-2-enone in MeCN ($[C_0]$ = 0.1 M) after going through a 10 mL PFA loop at 0.1 mL/min (See general procedure above). In-line IR detection and height of non-overlapping peaks processing at 1680 nm.

Experimental set-up for the application of the concentration gradient methodology on the [2 + 2] photocycloaddition (step 2): Using the flow machine (Vapourtec R2+/R4), the experiments were carried out using two pumps, a PFA loop (10 mL capacity, 1 mm i.d.), a home-made coiled photoflow reactor (14.1, 28.0 or 31.8 mL capacity, 1 mm i.d.) equipped with a 9 or 36 W UV lamp (UV-A, B or C), a 250 psi BPR and GC vials for off-line analysis.

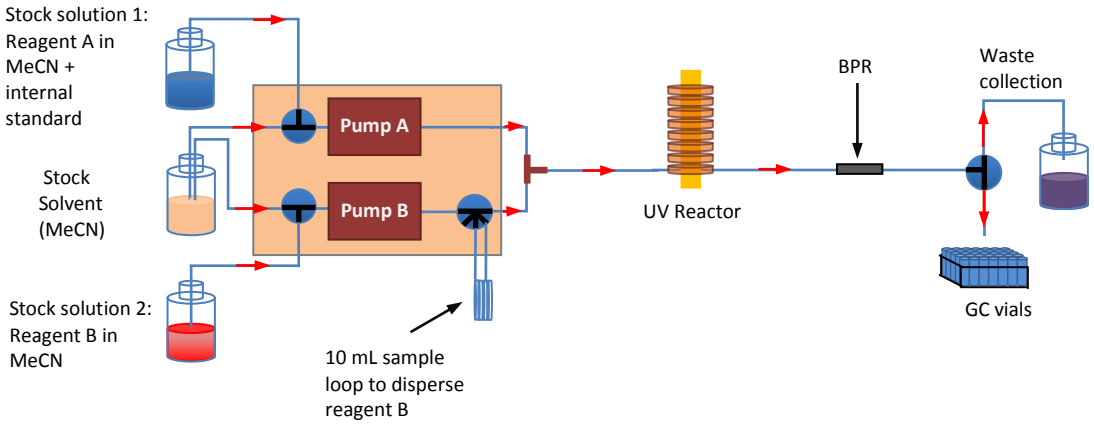

Figure 7.49: Flow set-up for the application of the concentration gradient methodology on the [2 + 2] photocycloaddition.

General procedure for the application of the concentration gradient methodology on the [2 + 2] photocycloaddition (step 2): In a 50 mL flask, the reagent A (no dispersion) was mixed with an internal standard (dibutyl ether) and MeCN (Stock solution 1). In the same way, in another 50 mL flask, the reagent B (dispersion) was mixed with MeCN (Stock solution 2). Each flask (Stock solution 1, 2 and Stock solvent) was degassed by sonication whilst being saturated with nitrogen. Before starting the reaction, solvent was pumped at the indicated flow rate and the indicated UV lamp (Philips 2-pin PL-S 9 W UV-A/B or C or Philips 4-pin PL-L 36 W UV-A/B or C) was switched on and left to warm up for 10-15 minutes. The water cooling system was turned on. Once the system was stable, the feeding valves (pump A and B) were switched to the stock solutions 1 and 2 (reagent A and B). The reagent A went straight to the UV reactor and the reagent B dispersed first in the 10 mL loop to form the gradient of concentration and went then to the UV reactor. Once 15 mL of solution 1 and 2 were injected into the flow system, the feeding valves were returned to the solvent feed. The reaction between a constant amount of A and a gradient amount of B occurred in the UV reactor. The reaction mixture was collected in vials and the sampling rate was precisely determined (1, 1.5 or 2 min collection per vial with addition of 1 mL of MeCN). The different samples were then analysed via off-line GC experiments.

General procedure for the processing of the GC data - Incorporation of the concentration gradient profile of the reagent to disperse and calculation of the conversion and the yield according to the experimental time (steps 3 and 4): From each GC spectrum generated, the different ratios Peak area compound/Peak area internal standard were calculated and plotted against the experimental time. The concentration gradient profile obtained in step 1 was incorporated with normalisation of the x and y-axes. The determination of the right position of this concentration gradient profile was the main difficulty. Explanations are highlighted for the experiments in Table 5.2, entries 1 and 2. The conversion and the yield for each GC analysis were calculated using equations 7.3 and 7.4 respectively.

$$\text{Conversion}_t = 1 - \frac{(\text{Peak area cyclohex} - 2 - \text{enone/ Peak area internal standard})_t}{(\text{Peak area cyclohex} - 2 - \text{enone/ Peak area internal standard})_0}$$

Equation 7.3: Formula used for the calculation of the conversion at a given moment.

$$\text{Yield}_t = \frac{\text{n(2 diastereoisomeres)}_t}{\text{n(2 diastereoisomeres)}_{theoretical}}$$

Equation 7.4: Formula used for the calculation of the yield at a given moment.

Vial	Weight IS (mg)	Weight 2 dia (mg)	Peak area 2 dia/Peak area IS	[2 dia]/[IS]
1	3.03	3.88	0.92497	1.53616
2	1.57	3.55	1.63331	2.69157
3	2.89	1.33	0.33242	0.50536
4	1.35	0.85	0.45480	0.75313

$$\frac{\text{Peak area 2 dia}}{\text{Peak area IS}} = \frac{\text{K(2 dia)}}{\text{K(IS)}} \text{ x } \frac{\text{[2 diastereoisomers]}}{\text{[IS]}}$$

K(2 dia)/K(IS) = 1.6583

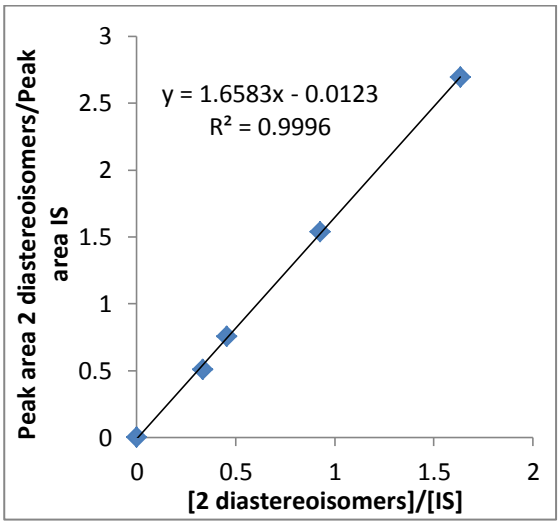

Figure 7.50: Calibration curve used for the calculation of the yield$_t$.

General procedure for the generation of the plots conversion *vs.* equivalents of dispersed reagent and yield *vs.* equivalents of dispersed reagent (step 5): Using the curves with the conversion, the yield and the concentration gradient profile plotted against the experimental time, 2 new plots can be generated: conversion *vs.* equivalents of dispersed reagent B and yield *vs.* equivalents of the dispersed reagent B. Indeed, for specific times, equivalents of reagent B, conversion and yield are aligned. Using these series of specific data, these 2 new plots can be obtained.

Concentration gradient results using the 28.0 mL photoflow reactor - UV-A (9 W):

Table 5.2, entry 2:

Entry	Reagent A	Reagent B	Internal Standard	Reagent A			Reagent B (dispersed)			IS	Reaction time (min)
				equiv.	[A][a] (M)	flow rate (mL/min)	equiv.	[B][b] (M)	flow rate (mL/min)	[IS][c] (M)	
2			dibutyl ether	1	0.051	0.1	19.6	1	0.1	0.044	140

[a] [A] Concentration of reagent A in the stock solution 1 (200.4 µL of reagent A were mixed with 0.30 mL of IS and 40 mL of MeCN). [b] [B] Concentration of reagent B in the stock solution 2 (18.0 mL of reagent B at 1 M in THF). [c] [IS] Concentration of Internal Standard in the stock solution 1 (0.30 mL of IS mixed with 200.4 µL of reagent A and 40 mL of MeCN).

Using these reaction conditions and the general procedures described above (steps 2, 3, 4 and 5), the following results were obtained. For this experiment, an overview of the data processing (steps 3, 4 and 5) was highlighted. This data processing is the same for the series of experiments with dispersion of tetra-methylethylene (Table 5.2, entries 1 and 2; Table 5.3, entries 1, 2, 3 and 4; Table 5.4, entries 1, 2, 3 and 4).

GC Vial	Exp. time (min)	Peak area cyclohex-2-enone$_t$	Peak area 2 diastereo-isomers$_t$	Peak area open cyclobu-tane$_t$	Peak area 2 dimers$_t$	Peak area IS$_t$	(Peak area cyclohex-2-enone/Peak area IS)$_t$	(Peak area 2 diastereo-isomers/Peak area IS)$_t$	(Peak area open cyclobutane/ Peak area IS)$_t$	(Peak area 2 dimers/Peak area IS)$_t$
7	9	118.5	0	0	17.7	160.2	0.73970038	0	0	0.110486891
8	10.5	116.8	0	0	18.3	159.7	0.73137132	0	0	0.114589856
9	12	113.1	0	0	17.9	152	0.74407895	0	0	0.117763158
10	13.5	145.3	0.42	0	20.9	191.2	0.75993724	0.00219665	0	0.109309623
11	15	116	1.93	0.24	19.2	159.3	0.72818581	0.01211551	0.001506591	0.120527307
12	16.5	134.4	7.2	0.94	20.8	183.3	0.73322422	0.03927987	0.005128205	0.113475177
13	18	107.5	15.9	2.1	19.6	164	0.65548781	0.09695122	0.012804878	0.119512195
14	19.5	122.2	40.4	5.4	20.7	198.8	0.61468813	0.20321932	0.027162978	0.104124748
15	21	92.8	63.1	8.5	17.6	175.7	0.52817302	0.35913489	0.048377917	0.100170746
16	22.5	77.7	94.9	12.5	14.8	176.1	0.44122658	0.53889835	0.070982396	0.084043157
17	24	60.6	121.4	15.6	11.7	170.8	0.35480094	0.71077283	0.091334895	0.068501171
18	25.5	41.9	125	15.9	7.9	146.8	0.28542234	0.85149864	0.108310627	0.053814714
19	27	38.8	154.9	19.8	7.6	164.5	0.23586626	0.94164134	0.120364742	0.046200608
20	28.5	32.2	158.7	20.4	6.5	158.2	0.20353982	1.00316056	0.128950695	0.041087231
21	30	34.6	193.8	24.6	7	181.8	0.19031903	1.06600660	0.135313531	0.03850385
22	31.5	28.6	178.2	22.7	5.8	165.2	0.17312349	1.07869249	0.137409201	0.035108959
23	33	30.8	204.3	25.8	6.4	183.5	0.16784741	1.11335150	0.140599455	0.034877384
24	34.5	29.5	200.4	25.4	5.9	178.8	0.16498881	1.12080537	0.142058166	0.032997763
25	36	26.3	186.2	23.6	5.4	169.3	0.15534554	1.0998228	0.139397519	0.031896043
26	37.5	27.6	199.9	25.3	5.7	177.7	0.15531795	1.12492966	0.142374789	0.032076533
27	39	28.4	205.1	26	5.8	181.6	0.15638767	1.12940529	0.143171806	0.031938326
28	40.5	25.9	190.9	24	5.4	168.7	0.15352697	1.13159455	0.142264375	0.032009484
29	42	32.3	232.6	29.4	6.6	206.8	0.15618956	1.12475822	0.142166344	0.031914894
30	43.5	23.6	175.8	22.1	4.9	157.8	0.14955640	1.11406844	0.140050697	0.031051965
31	45	28.1	207.4	26.3	5.9	181.6	0.15473568	1.14207049	0.144823789	0.032488987
32	46.5	30.6	225.1	28.6	6.3	196.7	0.15556685	1.14438231	0.145399085	0.03202847
33	48	26.1	193.3	24.5	5.4	172.4	0.15139211	1.12122970	0.142111369	0.031322506
34	49.5	28.1	206.2	25.9	5.8	182	0.15439560	1.13296703	0.142307692	0.031868132
35	51	25.7	192.7	24.5	5.6	171.2	0.15011682	1.12558411	0.143107477	0.03271028
36	52.5	24.1	182.6	22.9	5.1	159.7	0.15090795	1.14339386	0.143393863	0.031934878
37	54	24.6	185.9	23.6	5.2	163.3	0.15064299	1.13839559	0.14451929	0.031843233
38	55.5	24.3	182.6	23.1	5.1	164.1	0.14808044	1.11273614	0.140767824	0.031078611
39	57	29.5	216.6	27.3	6.2	189.9	0.15534492	1.14060032	0.143759874	0.032648763
40	58.5	26	193.6	24.5	5.4	170.9	0.15213575	1.13282621	0.143358689	0.031597425
41	60	26.2	195.9	24.8	5.5	171.3	0.15294804	1.14360771	0.144775248	0.032107414

Table 7.2: GC data obtained from the different vials. For this experiment, the sampling rate was 1.5 min (volume collected per GC vial = 0.3 mL) and 1 mL of MeCN was added in each vial before running the GC analysis (volume per GC vial = 1.3 mL).

From this Table 7.2 the following Figure 7.51 was obtained.

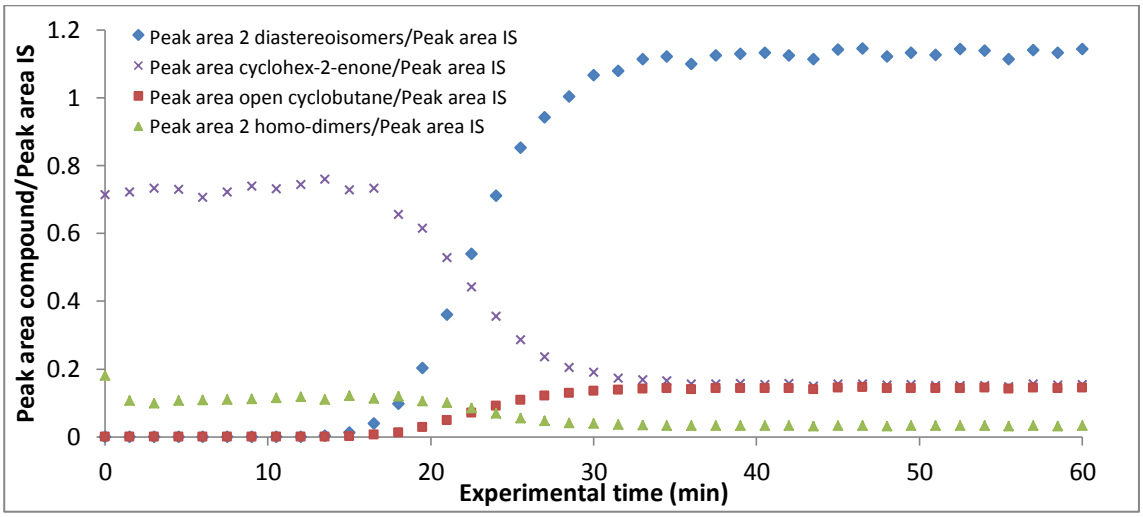

Figure 7.51: Plot of the different ratios Peak area compound/Peak area IS according to the experimental time.

As explained previously, the incorporation of the dispersion curve (Figure 7.46) was a major difficulty. After normalisation of the x and y-axes, the position of the dispersion curve was determined as follows: From the experiment with 5 equivalents of tetramethylethylene (Table 5.2, entry 1), the maximum ratio Peak area 2 diastereoisomers/Peak area IS (y = 0.50) was used as a first reference to determine the position of the dispersion curve on the x-axis (Figure 7.52). From this right position, the time (abscissa) corresponding to the maximum ordinate of the dispersion curve divided by 2 was determined (y = 1.14/2 = 0.57; x = 25.7 min). From this time (x = 25.7 min), the corresponding ratio Peak area 2 diastereoisomers/Peak area IS was calculated (y = 0.85) and converted into percentage (74.6 %) of the maximum (y = 1.14). For the different experiments performed with the double coiled 28.0 mL photoflow reactor, this percentage was used as a reference to determine the right position of the dispersion curve. For the other reactors, the same procedure was achieved.

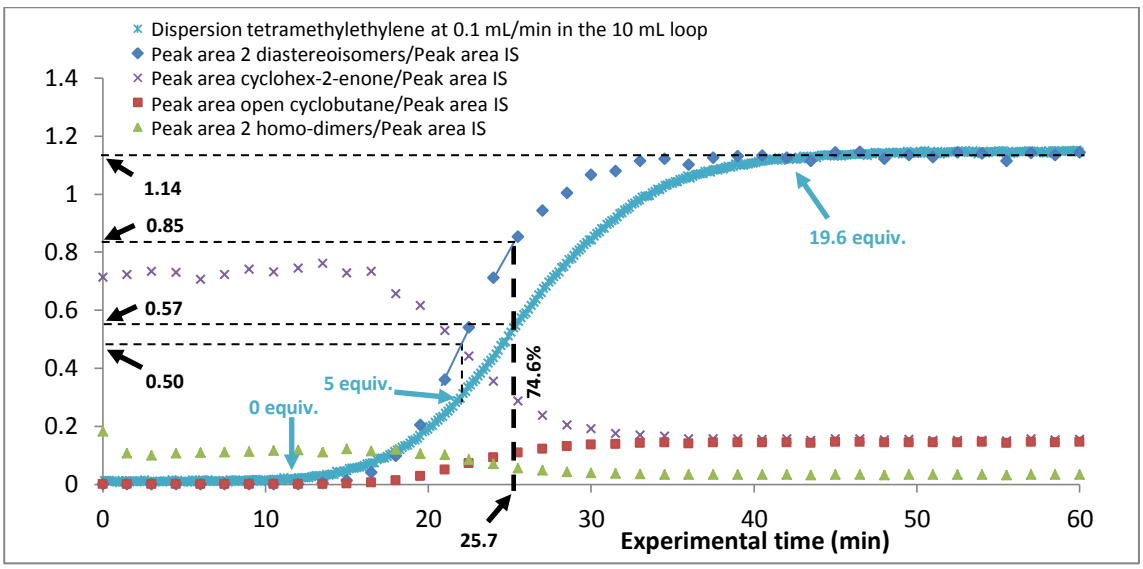

Figure 7.52: Determination of the position of the dispersion curve on the x-axis.

GC Vial	Exp. Time	(Peak area cyclohex-2-enone/ Peak area IS)$_t$	(Peak area 2 diastereo-isomers/ Peak area IS)$_t$	Conversion$_t$ [a]	[2 diastereoisomers]$_t$ [b] (mol/L)	n(2 diastereoisomers)$_t$ [c] (mol)	Yield$_t$ [d]
7	9	0.739700375	0	0.1497696	0	0	0
8	10.5	0.731371321	0	0.1593433	0	0	0
9	12	0.744078947	0	0.1447368	0	0	0
10	13.5	0.759937238	0.002196653	0.1265089	6.68944E-06	8.69627E-09	0.001136767
11	15	0.728185813	0.012115505	0.1630048	3.68952E-05	4.79638E-08	0.006269772
12	16.5	0.733224223	0.039279869	0.1572135	0.000119618	1.55504E-07	0.020327325
13	18	0.655487805	0.09695122	0.2465657	0.000295244	3.83818E-07	0.050172238
14	19.5	0.614688129	0.203219316	0.2934619	0.000618861	8.0452E-07	0.105165957
15	21	0.528173022	0.359134889	0.3929045	0.001093669	1.42177E-06	0.185852237
16	22.5	0.441226576	0.538898353	0.4928430	0.0016411	2.13343E-06	0.278879795
17	24	0.354800937	0.710772834	0.5921828	0.002164508	2.81386E-06	0.367824806
18	25.5	0.285422343	0.851498638	0.6719283	0.002593058	3.37098E-06	0.440650383
19	27	0.235866261	0.941641337	0.7288893	0.002867568	3.72784E-06	0.487299213
20	28.5	0.203539823	1.003160556	0.7660461	0.003054912	3.97139E-06	0.519135397
21	30	0.190319032	1.066006601	0.7812424	0.003246296	4.22019E-06	0.551658213
22	31.5	0.173123487	1.078692494	0.8010074	0.003284929	4.27041E-06	0.55822316
23	33	0.167847411	1.113351499	0.8070719	0.003390475	4.40762E-06	0.576159189
24	34.5	0.164988814	1.120805369	0.8103576	0.003413174	4.43713E-06	0.580016565
25	36	0.15534554	1.0998228	0.8214419	0.003349276	4.35406E-06	0.56915809
26	37.5	0.155317952	1.124929657	0.8214736	0.003425734	4.45345E-06	0.582150883
27	39	0.156387665	1.129405286	0.8202440	0.003439364	4.47117E-06	0.584467021
28	40.5	0.153526971	1.131594547	0.8235322	0.003446031	4.47984E-06	0.585599963
29	42	0.156189555	1.124758221	0.8204717	0.003425212	4.45278E-06	0.582062165
30	43.5	0.149556401	1.114068441	0.8280960	0.003392659	4.41046E-06	0.576530206
31	45	0.154735683	1.142070485	0.8221428	0.003477933	4.52131E-06	0.591021259
32	46.5	0.155566853	1.144382308	0.8211875	0.003484973	4.53046E-06	0.592217627
33	48	0.151392111	1.121229698	0.8259860	0.003414467	4.43881E-06	0.580236156
34	49.5	0.154395604	1.132967033	0.8225337	0.00345021	4.48527E-06	0.586310224
35	51	0.150116822	1.125584112	0.8274519	0.003427727	4.45605E-06	0.582489564
36	52.5	0.150907952	1.143393863	0.8265425	0.003481963	4.52655E-06	0.591706107
37	54	0.150642988	1.138395591	0.8268471	0.003466742	4.50676E-06	0.589119502
38	55.5	0.148080439	1.112736137	0.8297925	0.003388601	4.40518E-06	0.575840739
39	57	0.155344918	1.140600316	0.8214426	0.003473456	4.51549E-06	0.590260447
40	58.5	0.152135752	1.132826214	0.8251313	0.003449781	4.48472E-06	0.58623735
41	60	0.152948044	1.143607706	0.8241976	0.003482614	4.5274E-06	0.59181677

Table 7.3: Calculation of the conversion and the yield according to the experimental time.

[a] $\text{Conversion}_t = 1\text{-}\ \frac{(\text{Peak area cyclohex-2-enone/ Peak area internal standard})_t}{(\text{Peak area cyclohex-2-enone/ Peak area internal standard})_0}$

with (Peak area cyclohex-2-enone/Peak area internal standard)$_0$ = 0.87, determined from a GC of the initial stock solution 1 (200.4 µL of reagent A mixed with 0.30 mL of IS and 40 mL of MeCN).

[b] $[\text{2 diastereoisomers}]_t = \left(\frac{\text{Peak area 2 dia}}{\text{Peak area IS}}\right)_t \text{ x } \frac{[\text{IS}]}{\text{K(2 dia)/K(IS)}}$, the concentration of diastereoisomers in the corresponding GC vial.

with K(2 dia)/K(IS) = 1.6583, determined from the calibration curve (Figure 7.50).
[IS] = 0.00505 M, the concentration of IS in the GC vials after addition of 1 mL of MeCN.

[c] $\text{n(2 diastereoisomers)}_t = [\text{2 diastereoisomers}]_t \text{ x Volume per GC vial}$, the amount of diastereoisomers in the corresponding GC vial

with Volume per GC vial = Volume collected per GC vial + Volume added = 0.3 + 1 = 1.3 mL.

[d] $\text{Yield}_t = \frac{\text{n(2 diastereoisomeres)}_t}{\text{n(2 diastereoisomeres)}_{\text{theoretical}}} = \frac{[\text{2 diastereoisomeres}]_t \text{ x Volume per GC vial}}{[\text{limiting reagent}]_0 \text{ x Volume collected per GC vial}}$

with [limiting reagent]$_0$ = 0.0255 M, the concentration of the limiting reagent after the T-mixer (Calculations were performed with the cyclohex-2-enone as the limiting reagent even if the tetramethylethylene was the limiting one for a short period of time during the concentration gradient experiment).
Volume collected per GC vial = 0.3 mL (collection during 1 min and 30 seconds at 0.2 mL/min).

From Table 7.3, the following Figure 7.53 was obtained.

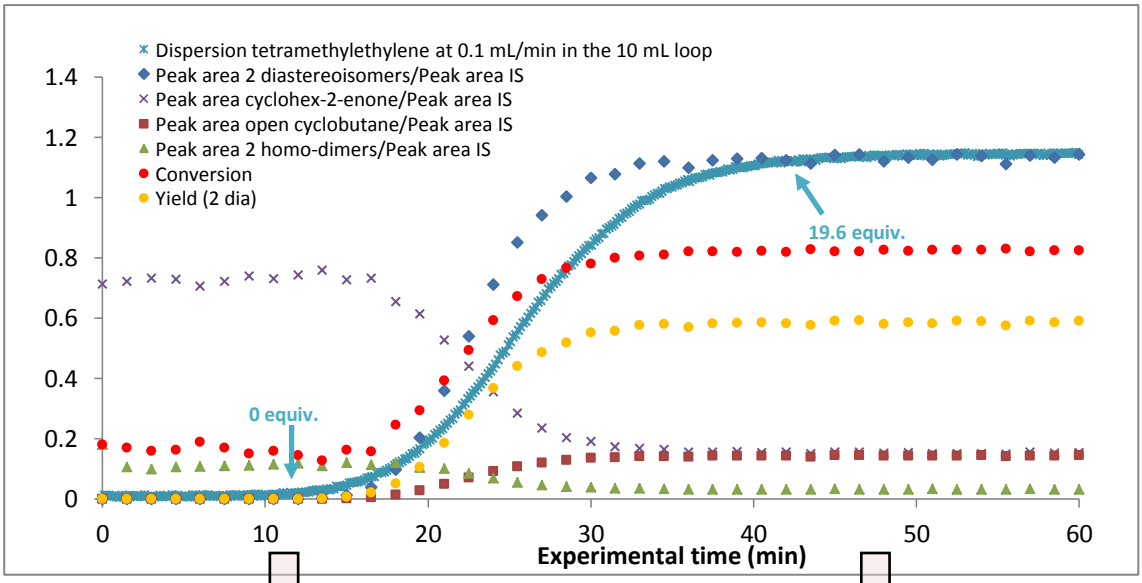

Figure 7.53: Ratios of the peak area of each compound over the peak area of the IS plotted against the experimental time. Evolution of the conversion and the yield according to the experimental time.

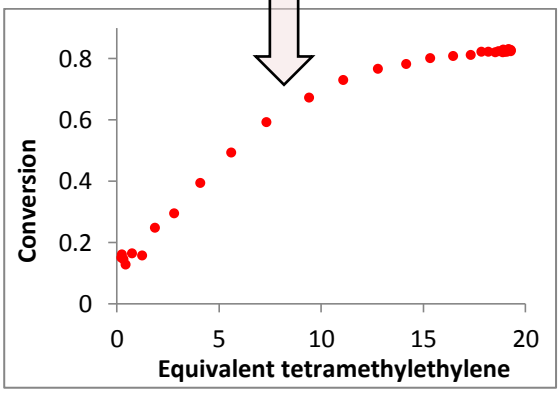

Figure 7.54: Evolution of the conversion according to the equivalent of tetramethylethylene.

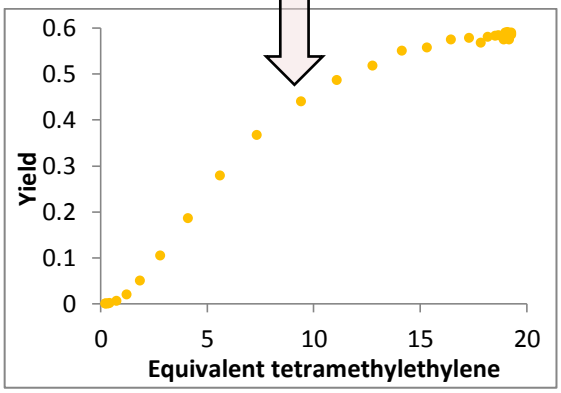

Figure 7.55: Evolution of the yield according to the equivalent of tetramethylethylene.

Finally, as explained in section 5.3.3.2.1, Figure 7.53 enabled the generation of Figures 7.54 and 7.55.

Table 5.2, entry 1:

Entry	Reagent A	Reagent B	Internal Standard	Reagent A			Reagent B (dispersed)			IS	Reaction time (min)
				equiv.	[A][a] (M)	flow rate (mL/min)	equiv.	[B][b] (M)	flow rate (mL/min)	[IS][c] (M)	
1	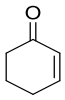		dibutyl ether	1	0.051	0.1	5	0.26	0.1	0.044	140

[a] [A] Concentration of reagent A in the stock solution 1 (200.4 µL of reagent A were mixed with 0.30 mL of IS and 40 mL of MeCN). [b] [B] Concentration of reagent B in the stock solution 2 (5.17 mL of reagent B at 1 M in THF were mixed with 14.83 mL of MeCN). [c] [IS] Concentration of Internal Standard in the stock solution 1 (0.30 mL of IS were mixed with 200.4 µL of reagent A and 40 mL of MeCN).

Using these reaction conditions and the general procedures described previously (steps 2, 3, 4 and 5), the following results were obtained.

For this experiment, after normalisation of the x and y-axes, the position of the dispersion curve was determined as follows: 74.6% of the maximum of the ratio Peak area 2 diastereoisomers/Peak area IS was calculated (y = 74.6% x 0.50 = 0.37) and the corresponding time (x = 25.4 min) was used to place the maximum of the dispersion curve dived by 2 (y = 0.50/2 = 0.25). For the other experiments with dispersion of tetramethylethylene, the same procedure was achieved.

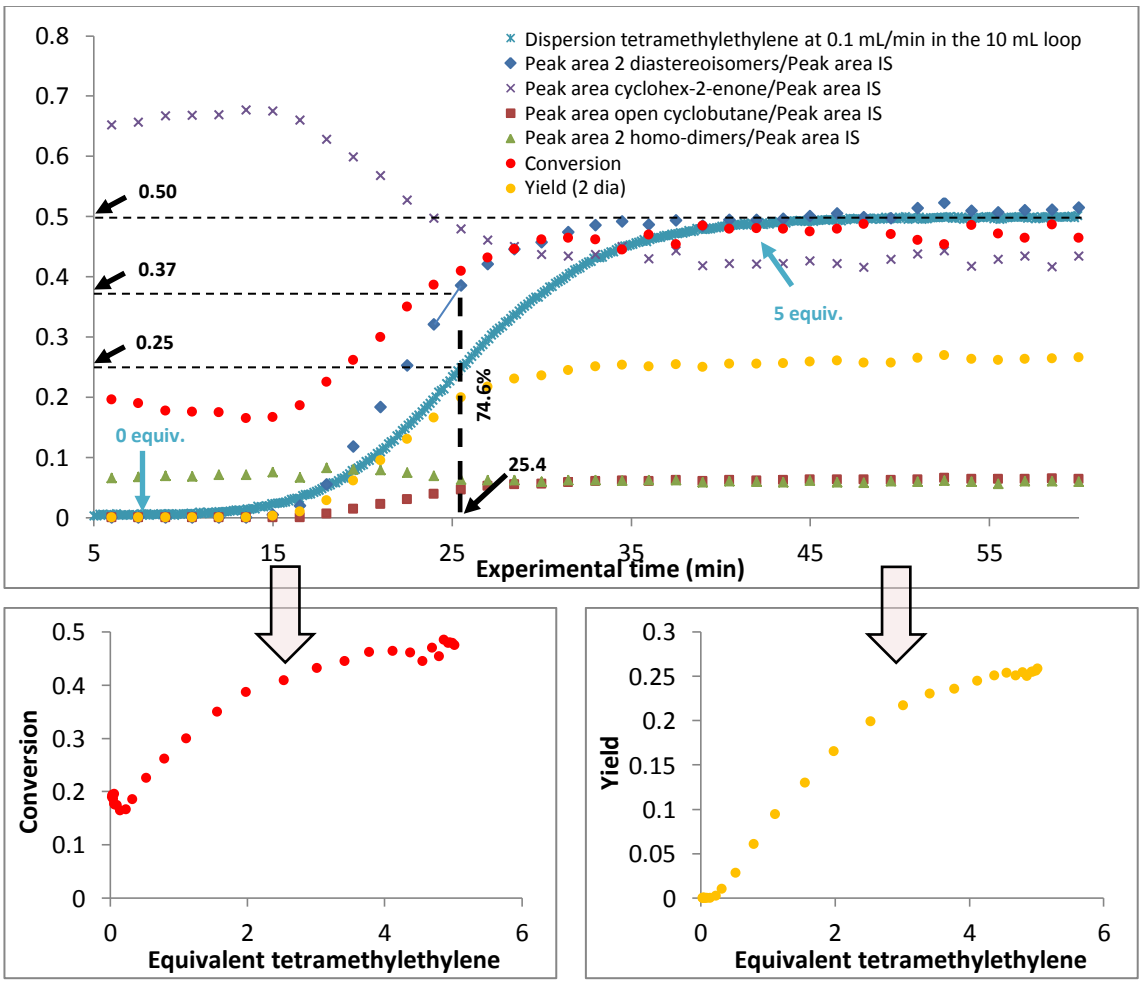

Concentration gradient results using the 14.1 mL photoflow reactor - UV-A (9 W):

Table 5.3, entry 2:

Entry	Reagent A	Reagent B	Internal Standard	Reagent A			Reagent B (dispersed)			IS	Reaction time
				equiv.	[A][a] (M)	flow rate (mL/min)	equiv.	[B][b] (M)	flow rate (mL/min)	[IS][c] (M)	(min)
2			dibutyl ether	1	0.051	0.05	19.6	1	0.05	0.044	140

[a] [A] Concentration of reagent A in the stock solution 1 (200.4 µL of reagent A were mixed with 0.30 mL of IS and 40 mL of MeCN). [b] [B] Concentration of reagent B in the stock solution 2 (15.0 mL of reagent B at 1 M in THF). [c] [IS] Concentration of Internal Standard in the stock solution 1 (0.30 mL of IS mixed with 200.4 µL of reagent A and 40 mL of MeCN).

Using these reaction conditions and the general procedures described previously (steps 2, 3, 4 and 5), the following results were obtained.

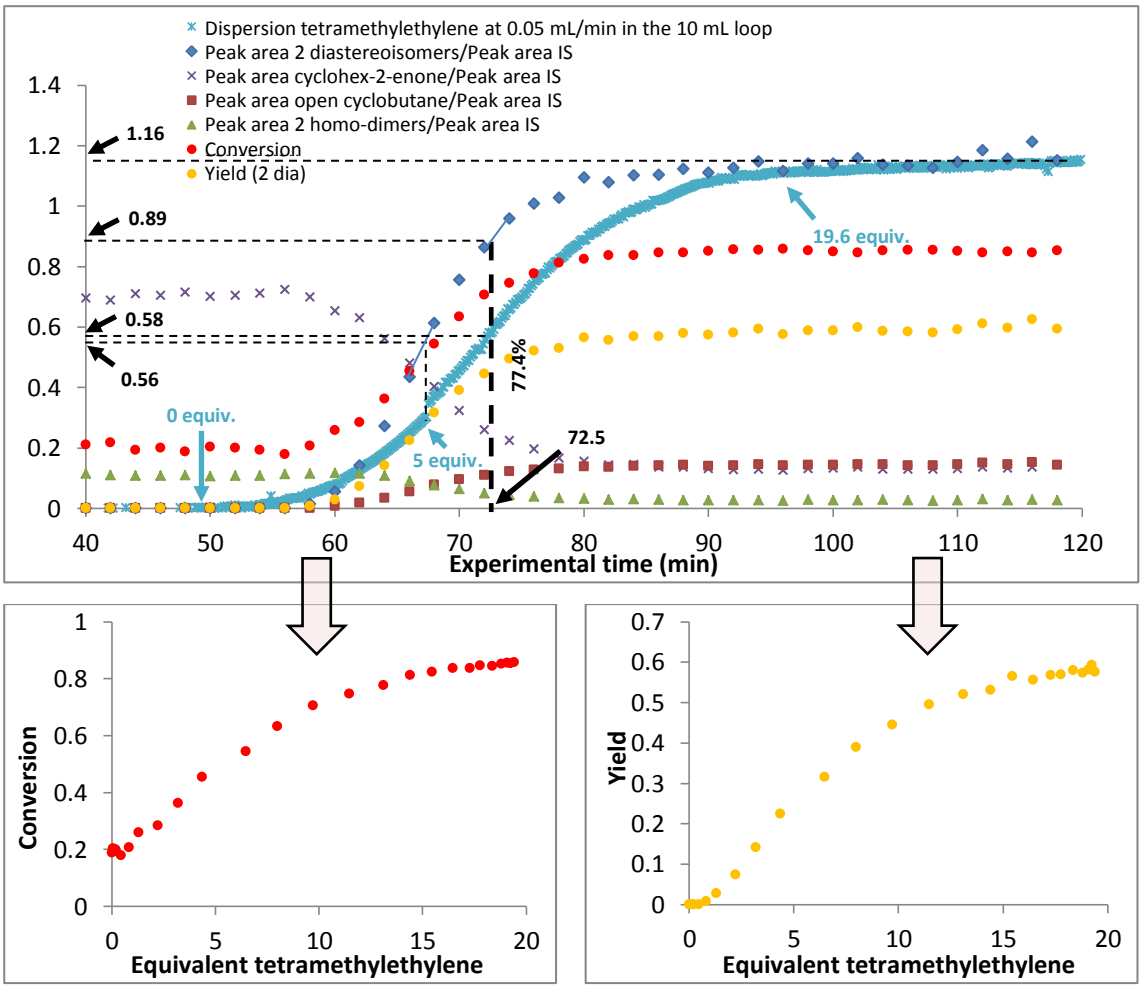

Table 5.3, entry 1:

Entry	Reagent A	Reagent B	Internal Standard	Reagent A			Reagent B (dispersed)			IS	Reaction time (min)
				equiv.	[A][a] (M)	flow rate (mL/min)	equiv.	[B][b] (M)	flow rate (mL/min)	[IS][c] (M)	
1	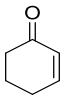		dibutyl ether	1	0.051	0.05	5	0.26	0.05	0.044	140

[a] [A] Concentration of reagent A in the stock solution 1 (200.4 µL of reagent A were mixed with 0.30 mL of IS and 40 mL of MeCN). [b] [B] Concentration of reagent B in the stock solution 2 (5.17 mL of reagent B at 1 M in THF were mixed with 14.83 mL of MeCN). [c] [IS] Concentration of Internal Standard in the stock solution 1 (0.30 mL of IS were mixed with 200.4 µL of reagent A and 40 mL of MeCN).

Using these reaction conditions and the general procedures described previously (steps 2, 3, 4 and 5), the following results were obtained.

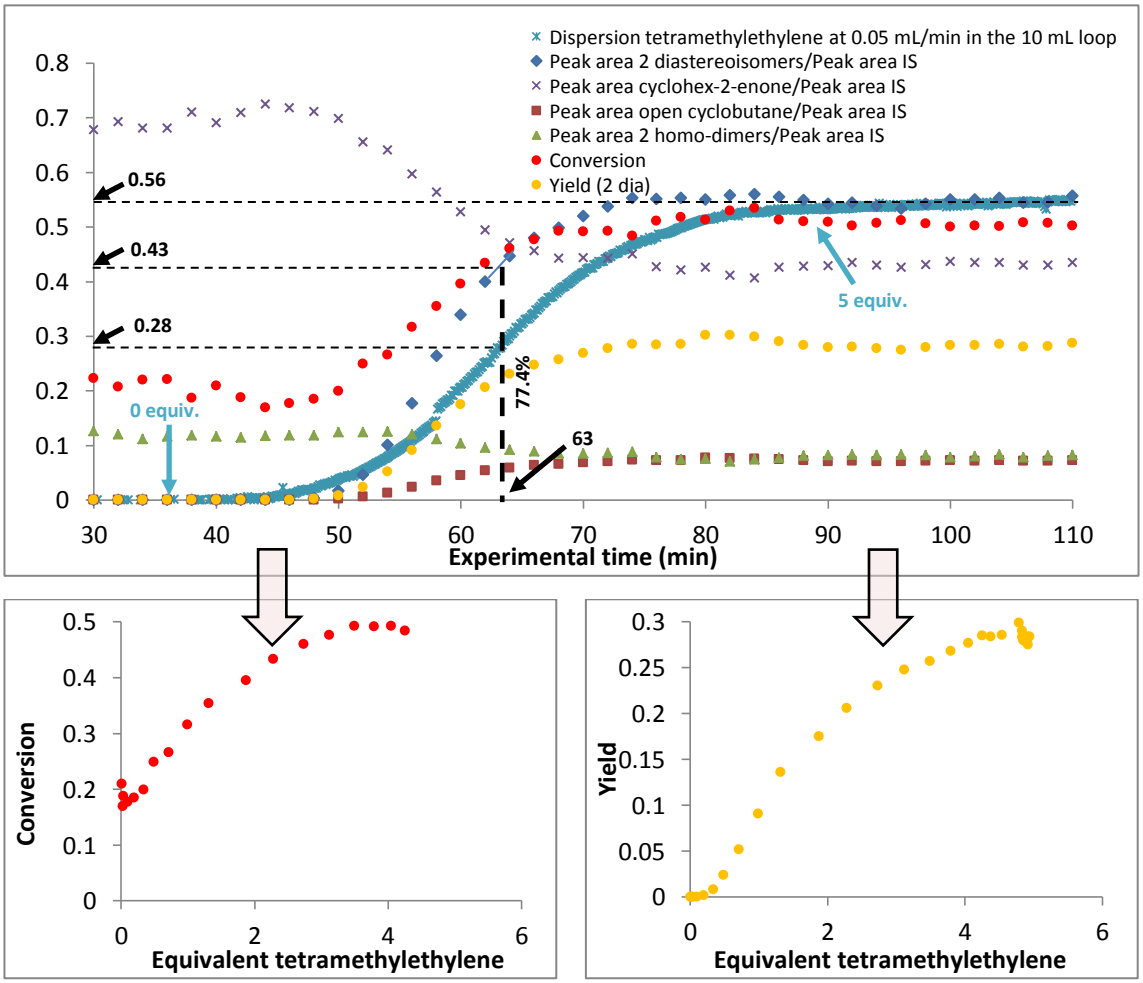

Table 5.3, entry 4:

Entry	Reagent A	Reagent B	Internal Standard	Reagent A			Reagent B (dispersed)			IS	Reaction time (min)
				equiv.	[A][a] (M)	flow rate (mL/min)	equiv.	[B][b] (M)	flow rate (mL/min)	[IS][c] (M)	
4	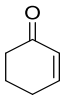		dibutyl ether	1	0.153	0.05	19.6	2.99	0.05	0.131	140

[a] [A] Concentration of reagent A in the stock solution 1 (600 µL of reagent A were mixed with 0.90 mL of IS and 39 mL of MeCN). [b] [B] Concentration of reagent B in the stock solution 2 (5.34 mL of pure reagent B were mixed with 9.66 mL of MeCN). [c] [IS] Concentration of Internal Standard in the stock solution 1 (0.90 mL of IS were mixed with 600 µL of reagent A and 39 mL of MeCN).

Using these reaction conditions and the general procedures described previously (steps 2, 3, 4 and 5), the following results were obtained.

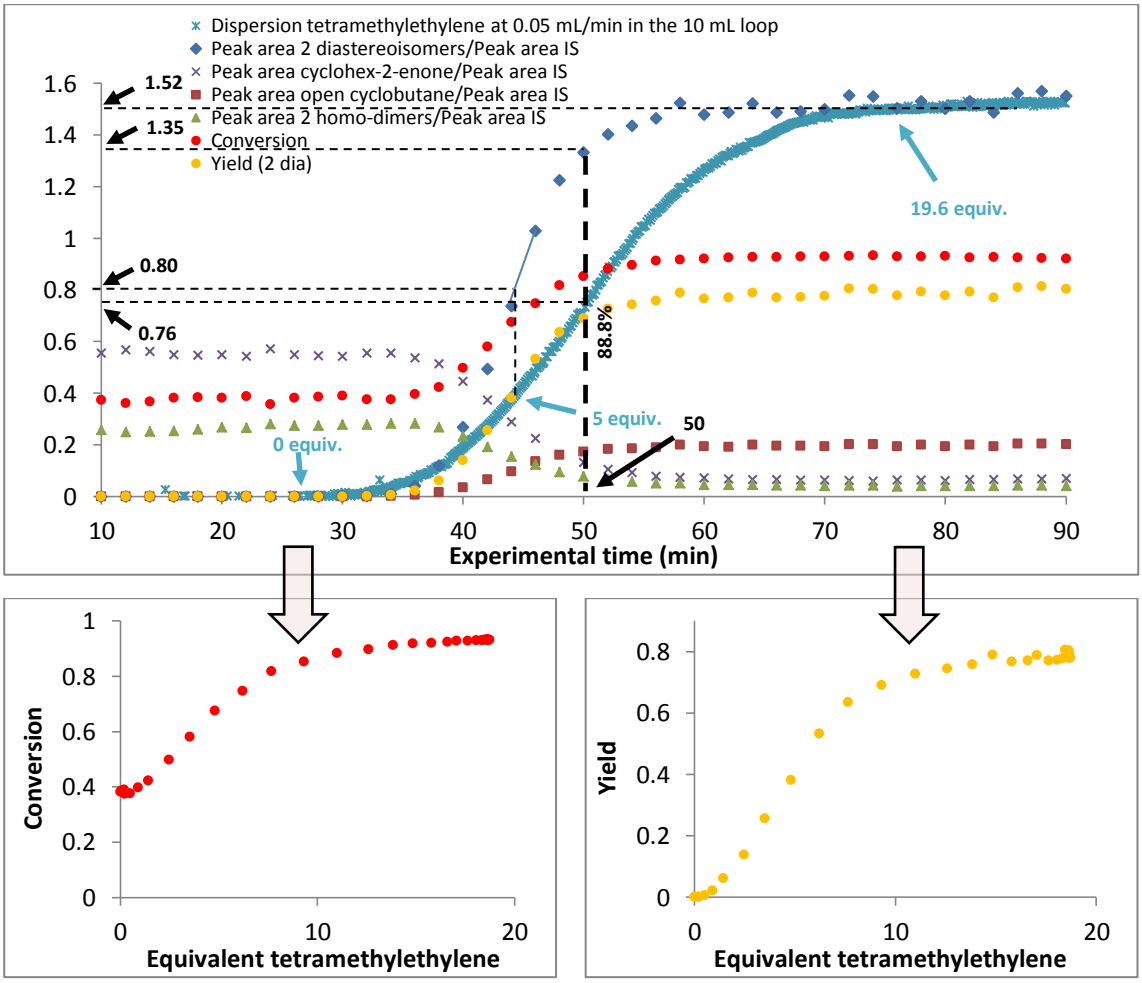

Table 5.3, entry 3:

Entry	Reagent A	Reagent B	Internal Standard	Reagent A			Reagent B (dispersed)			IS	Reaction time (min)
				equiv.	[A][a] (M)	flow rate (mL/min)	equiv.	[B][b] (M)	flow rate (mL/min)	[IS][c] (M)	
3	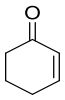		dibutyl ether	1	0.153	0.05	5	0.77	0.05	0.131	140

[a] [A] Concentration of reagent A in the stock solution 1 (600 µL of reagent A were mixed with 0.90 mL of IS and 39 mL of MeCN). [b] [B] Concentration of reagent B in the stock solution 2 (1.38 mL of pure reagent B were mixed with 13.62 mL of MeCN). [c] [IS] Concentration of Internal Standard in the stock solution 1 (0.90 mL of IS were mixed with 600 µL of reagent A and 39 mL of MeCN).

Using these reaction conditions and the general procedures described previously (steps 2, 3, 4 and 5), the following results were obtained.

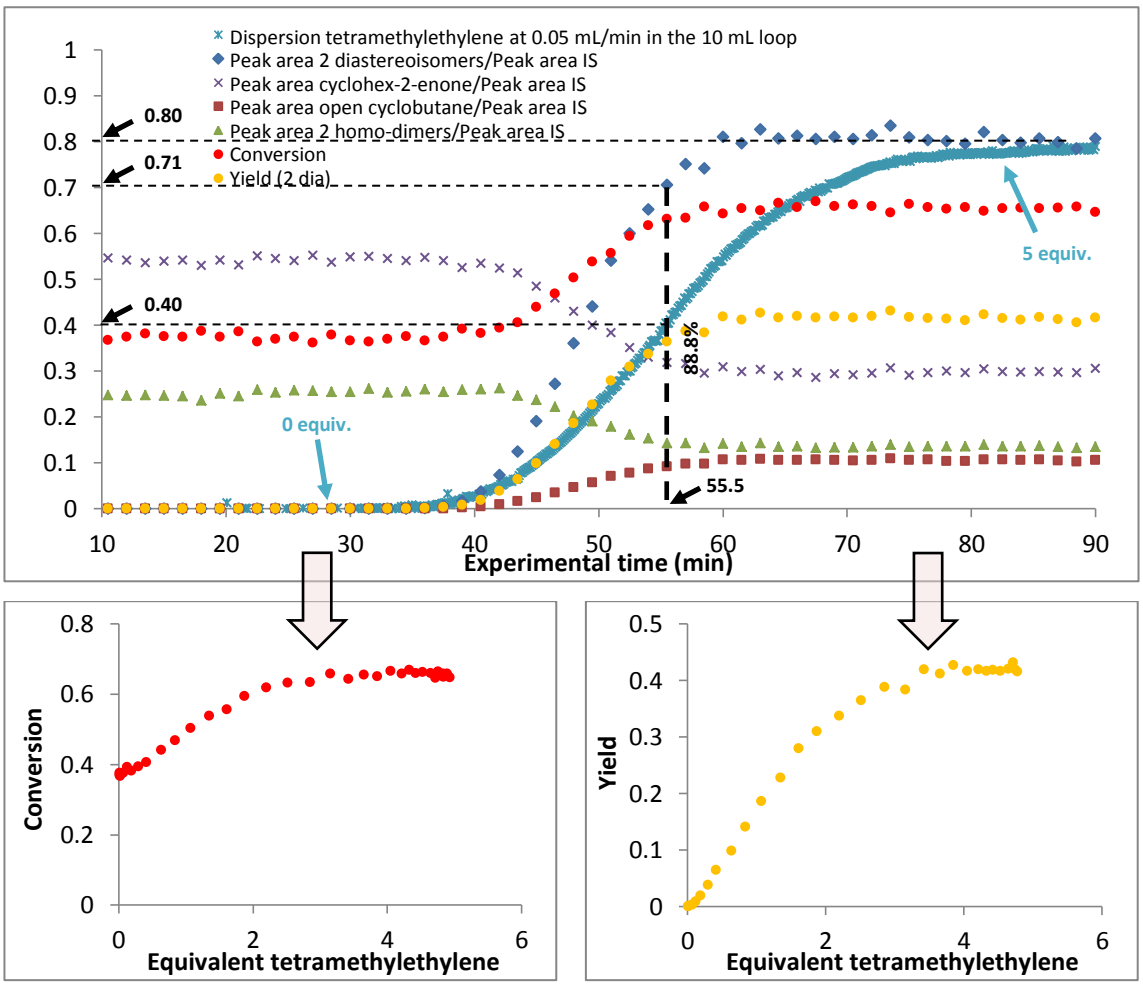

Concentration gradient results using the 31.8 mL photoflow reactor - UV-A (36 W):

Table 5.4, entry 2:

Entry	Reagent A	Reagent B	Internal Standard	Reagent A			Reagent B (dispersed)			IS	Reaction time
				equiv.	[A][a] (M)	flow rate (mL/min)	equiv.	[B][b] (M)	flow rate (mL/min)	[IS][c] (M)	(min)
2			dibutyl ether	1	0.051	0.113	19.6	1	0.113	0.044	140

[a] [A] Concentration of reagent A in the stock solution 1 (200.4 µL of reagent A were mixed with 0.30 mL of IS and 40 mL of MeCN). [b] [B] Concentration of reagent B in the stock solution 2 (2.38 mL of pure reagent B were mixed with 17.62 mL of MeCN). [c] [IS] Concentration of Internal Standard in the stock solution 1 (0.30 mL of IS were mixed with 200.4 µL of reagent A and 40 mL of MeCN).

Using these reaction conditions and the general procedures described previously (steps 2, 3, 4 and 5), the following results were obtained.

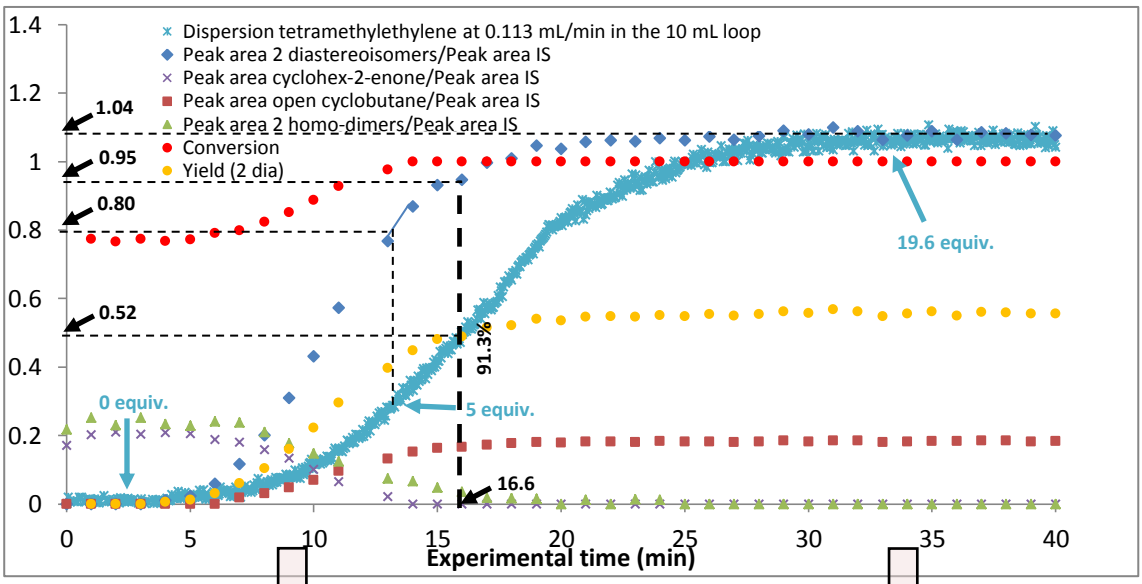

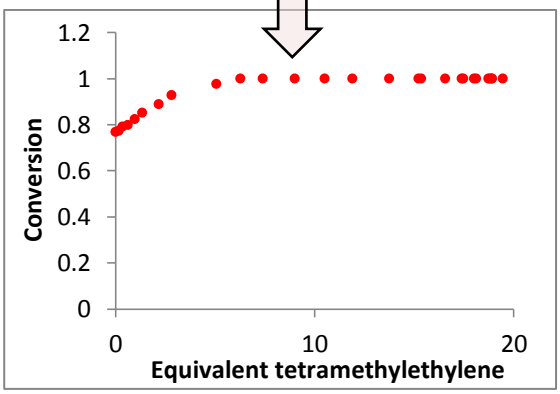

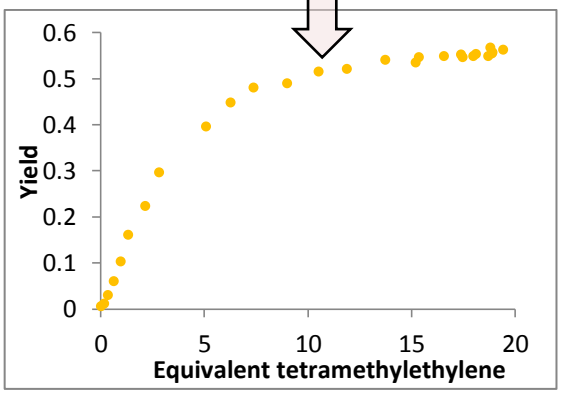

Table 5.4, entry 1:

Entry	Reagent A	Reagent B	Internal Standard	Reagent A			Reagent B (dispersed)			IS	Reaction time (min)
				equiv.	[A][a] (M)	flow rate (mL/min)	equiv.	[B][b] (M)	flow rate (mL/min)	[IS][c] (M)	
1	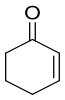		dibutyl ether	1	0.051	0.113	5	0.26	0.113	0.044	140

[a] [A] Concentration of reagent A in the stock solution 1 (200.4 µL of reagent A were mixed with 0.30 mL of IS and 40 mL of MeCN). [b] [B] Concentration of reagent B in the stock solution 2 (614 µL of pure reagent B were mixed with 19.4 mL of MeCN). [c] [IS] Concentration of Internal Standard in the stock solution 1 (0.30 mL of IS were mixed with 200.4 µL of reagent A and 40 mL of MeCN).

Using these reaction conditions and the general procedures described previously (steps 2, 3, 4 and 5), the following results were obtained.

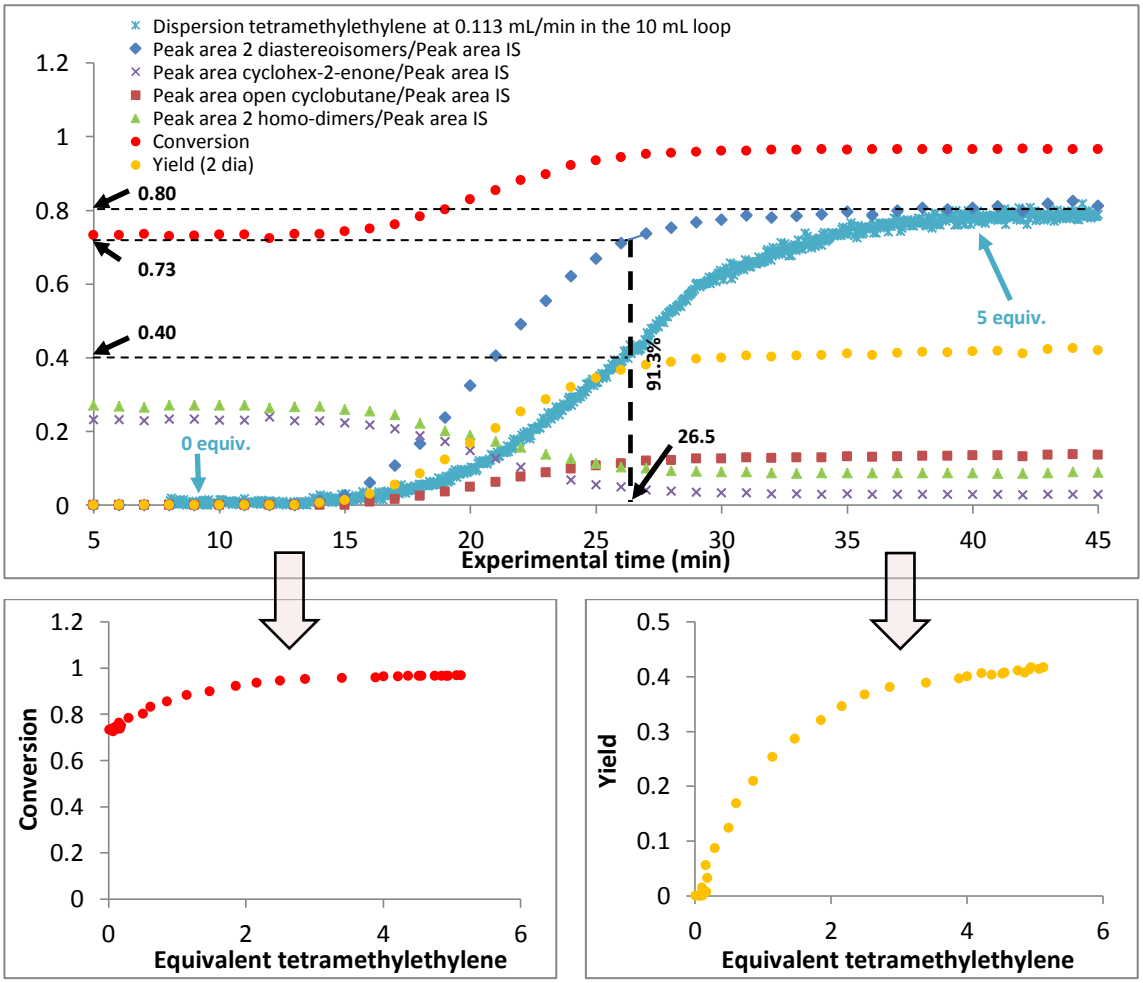

Table 5.4, entry 4:

Entry	Reagent A	Reagent B	Internal Standard	Reagent A			Reagent B (dispersed)			IS	Reaction time (min)
				equiv.	[A][a] (M)	flow rate (mL/min)	equiv.	[B][b] (M)	flow rate (mL/min)	[IS][c] (M)	
4	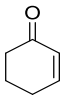		dibutyl ether	1	0.153	0.113	19.6	2.99	0.113	0.131	140

[a] [A] Concentration of reagent A in the stock solution 1 (600 µL of reagent A were mixed with 0.90 mL of IS and 39 mL of MeCN). [b] [B] Concentration of reagent B in the stock solution 2 (5.34 mL of pure reagent B were mixed with 9.66 mL of MeCN). [c] [IS] Concentration of Internal Standard in the stock solution 1 (0.90 mL of IS were mixed with 600 µL of reagent A and 39 mL of MeCN).

Using these reaction conditions and the general procedures described previously (steps 2, 3, 4 and 5), the following results were obtained.

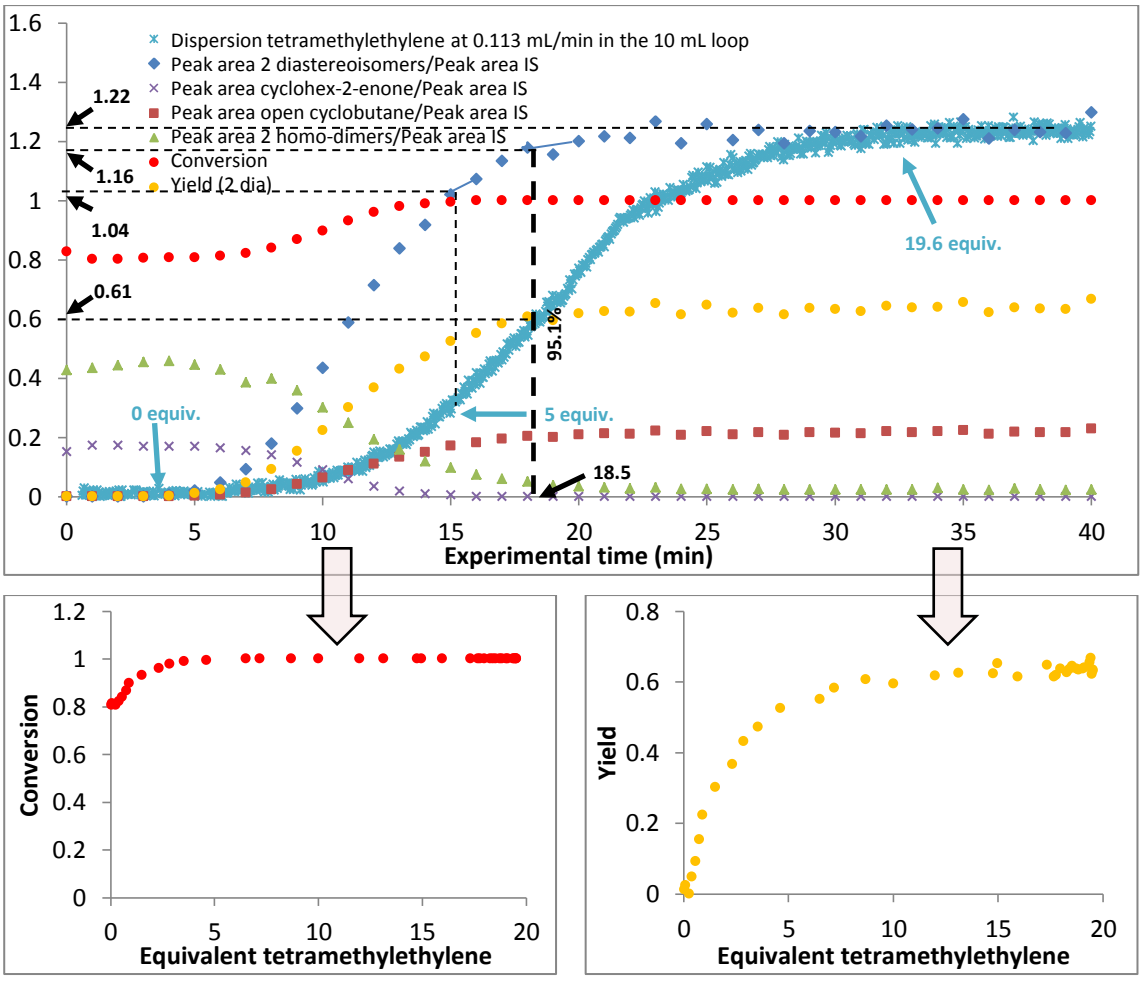

Table 5.4, entry 3:

Entry	Reagent A	Reagent B	Internal Standard	Reagent A			Reagent B (dispersed)			IS	Reaction time (min)
				equiv.	[A][a] (M)	flow rate (mL/min)	equiv.	[B][b] (M)	flow rate (mL/min)	[IS][c] (M)	
3	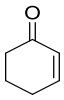		dibutyl ether	1	0.153	0.113	5	0.77	0.113	0.131	140

[a] [A] Concentration of reagent A in the stock solution 1 (600 µL of reagent A were mixed with 0.90 mL of IS and 39 mL of MeCN). [b] [B] Concentration of reagent B in the stock solution 2 (1.38 mL of pure reagent B were mixed with 13.62 mL of MeCN). [c] [IS] Concentration of Internal Standard in the stock solution 1 (0.90 mL of IS were mixed with 600 µL of reagent A and 39 mL of MeCN).

Using these reaction conditions and the general procedures described previously (steps 2, 3, 4 and 5), the following results were obtained.

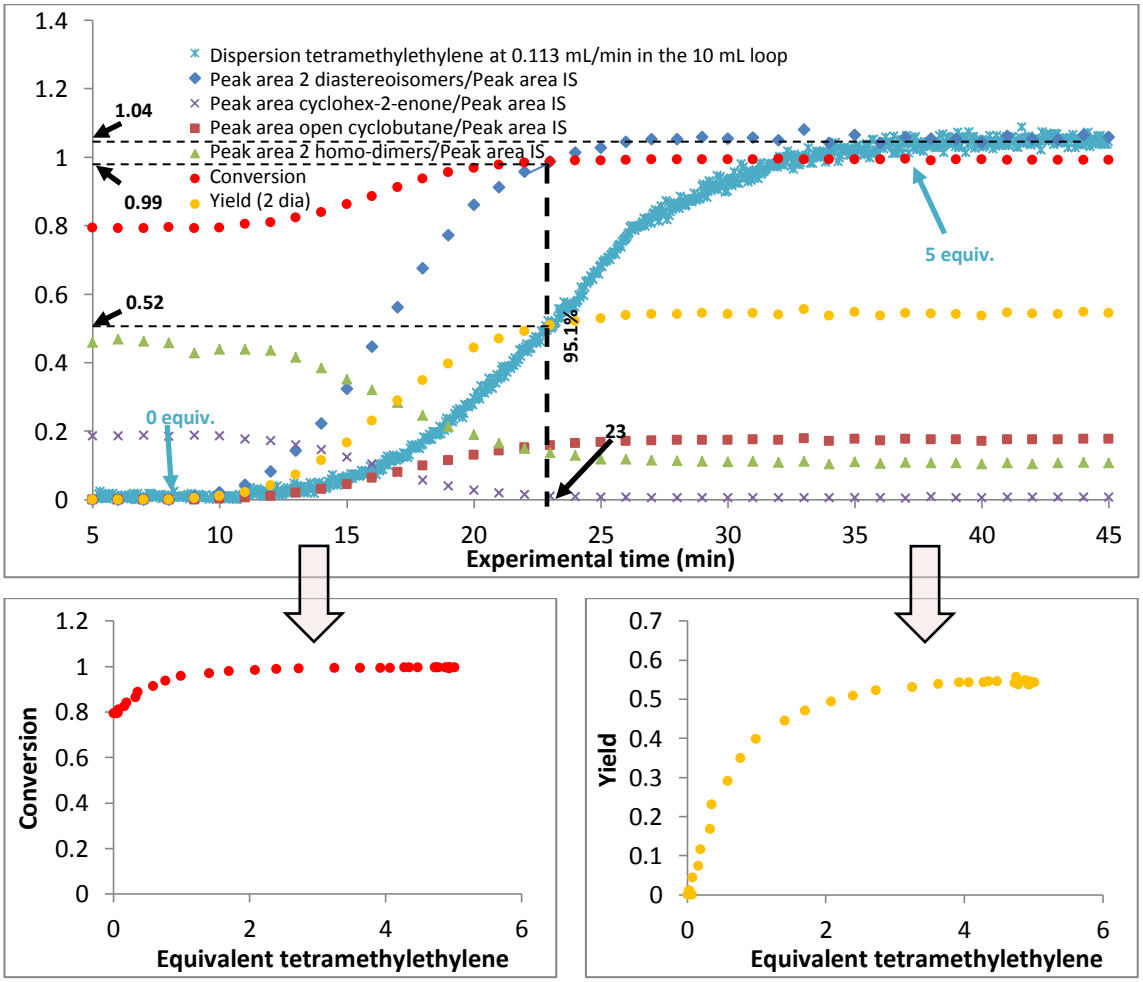

Concentration gradient results using the 28.0 mL photoflow reactor - UV-A (9 W):

Table 5.5, entry 1:

Entry	Reagent A	Reagent B	Internal Standard	Reagent A			Reagent B (dispersed)			IS	Reaction time (min)
				equiv.	[A][a] (M)	flow rate (mL/min)	equiv.	[B][b] (M)	flow rate (mL/min)	[IS][c] (M)	
1		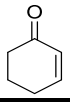	dibutyl ether	19.4	0.99	0.1	1	0.051	0.1	0.044	140

[a] [A] Concentration of reagent A in the stock solution 1 (14.74 mL of reagent A at 1 M in THF were mixed with 0.11 mL of IS). [b] [B] Concentration of reagent B in the stock solution 2 (200.4 µL of reagent B were mixed with 40.3 mL of MeCN). [c] [IS] Concentration of Internal Standard in the stock solution 1 (0.11 mL of IS were mixed with 14.74 mL of reagent A).

Using these reaction conditions and the general procedures described above (steps 2, 3, 4 and 5), the following results were obtained. For this experiment, an overview of the data processing (steps 3, 4 and 5) was highlighted as the dispersed reagent was the cyclohex-2-enone.

GC Vial	Time (min)	Peak area cyclohex-2-enone$_t$	Peak area 2 diastereo-isomers$_t$	Peak area open cyclobu-tane$_t$	Peak area 2 dimers$_t$	Peak area IS$_t$	(Peak area cyclohex-2-enone/Peak area IS)$_t$	(Peak area 2 diastereo-isomers/Peak area IS)$_t$	(Peak area open cyclo-butane/Peak area IS)$_t$	(Peak area 2 dimers/Peak area IS)$_t$
14	19.5	0	0	0	0	149.4	0	0	0	0
15	21	0	0	0	0	176.3	0	0	0	0
16	22.5	0	0	0	0	178.1	0	0	0	0
17	24	0	0	0	0	188.4	0	0	0	0
18	25.5	0	0	0	0	154.5	0	0	0	0
19	27	0	0	0	0	167.9	0	0	0	0
20	28.5	0.57	3.1	0.37	0	183	0.00311475	0.01694	0.002021858	0
21	30	1.1	7.1	0.84	0	199.9	0.00550275	0.035518	0.004202101	0
22	31.5	2.1	13.4	1.6	0	195.6	0.0107362	0.068507	0.008179959	0
23	33	3.1	20.6	2.5	0	171.3	0.01809691	0.120257	0.014594279	0
24	34.5	5.7	37.5	4.6	0	184.1	0.03096143	0.203694	0.02498642	0
25	36	9.7	59.8	7.4	0.25	196.1	0.04946456	0.304946	0.037735849	0.001275
26	37.5	21.3	122.8	15.3	1.65	264	0.08068182	0.465152	0.057954545	0.00625
27	39	19.8	113.7	14.1	1.76	179.5	0.11030641	0.633426	0.078551532	0.009805
28	40.5	24.6	137.2	17.2	2.6	191.6	0.12839248	0.716075	0.089770355	0.01357
29	42	23.9	135.6	17	2.8	171	0.13976608	0.792982	0.099415205	0.016374
30	43.5	25.1	144.5	18.1	3.1	170.8	0.1469555	0.846019	0.105971897	0.01815
31	45	32.6	189.1	23.6	4.2	216.5	0.15057737	0.873441	0.109006928	0.0194
32	46.5	31.5	179	22.2	4.1	200.3	0.1572641	0.89366	0.110833749	0.020469
33	48	28.2	163.1	20.5	3.9	184.5	0.15284553	0.884011	0.111111111	0.021138
34	49.5	31.4	181.6	22.7	4.1	202.9	0.15475604	0.895022	0.111877772	0.020207
35	51	30.6	178.6	22.3	4	197.1	0.15525114	0.906139	0.113140538	0.020294
36	52.5	33.1	193	24.1	4.6	214.2	0.15452848	0.901027	0.112511671	0.021475
37	54	28.3	166.5	20.8	3.7	185.6	0.15247845	0.897091	0.112068966	0.019935
38	55.5	28.1	167.4	21	3.8	190	0.14789474	0.881053	0.110526316	0.02
39	57	27.4	164.1	20.5	3.7	183.9	0.14899402	0.892333	0.111473627	0.02012
40	58.5	31.7	184.3	23	4.3	201.7	0.15716411	0.913733	0.114030739	0.021319
41	60	32.9	196.7	24.6	4.7	219.9	0.15674131	0.937113	0.117198666	0.022392

Table 7.4: GC data obtained from the different vials. For this experiment, the sampling rate was 1.5 min (volume collected per GC vial = 0.3 mL) and 1 mL of MeCN was added in each vial before running the GC analysis (volume per GC vial = 1.3 mL).

From Table 7.4, the following Figure 7.56 was obtained.

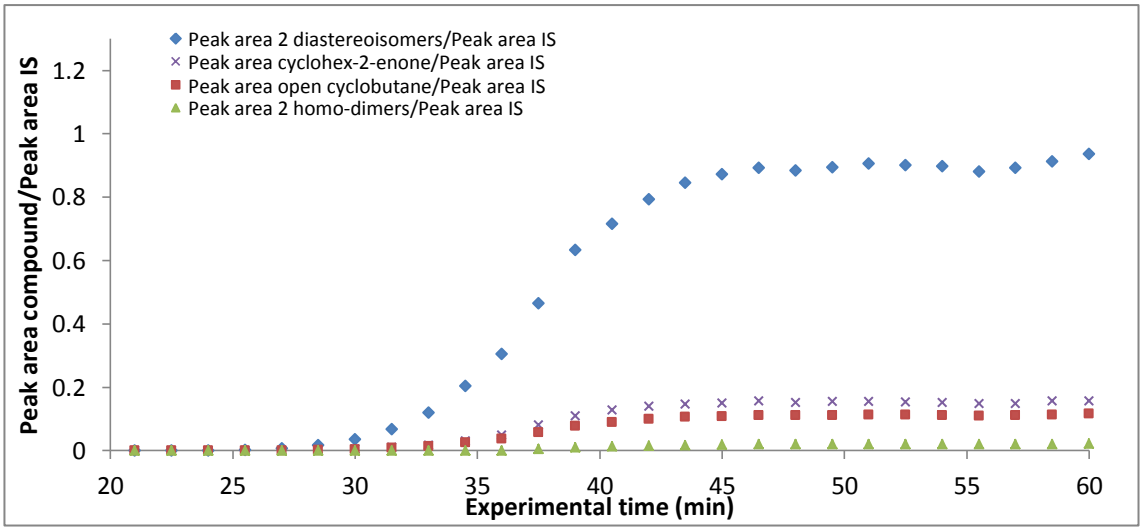

Figure 7.56: Plot of the different ratios Peak area compound/Peak area IS according to the experimental time.

The incorporation of the dispersion curve in Figure 7.57 was performed without using any references.

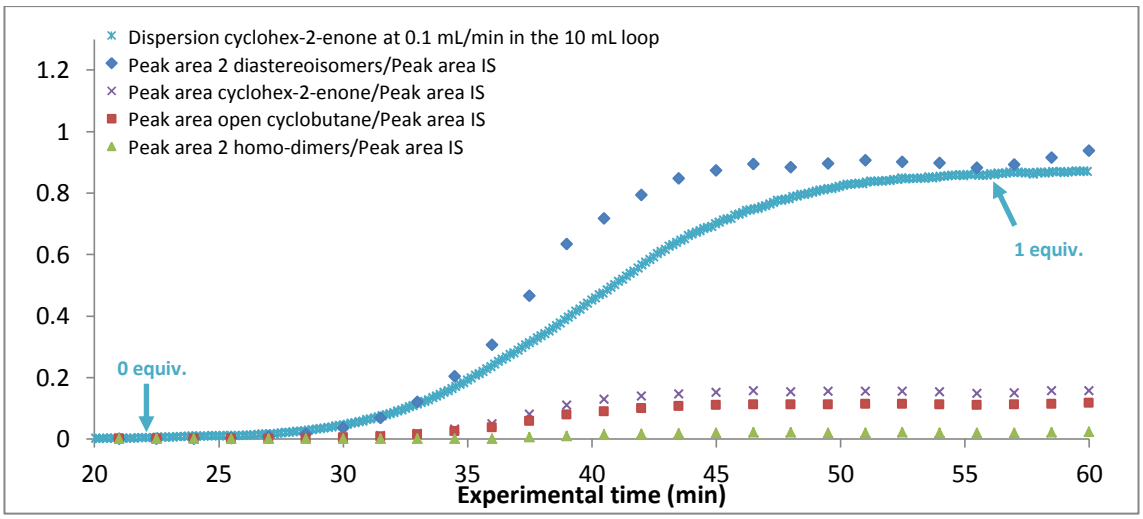

Figure 7.57: Incorporation of the dispersion curve.

GC Vial	Exp. time (min)	(Peak area cyclohex-2-enone/Peak area IS)$_t$	(Peak area cyclohex-2-enone/Peak area IS)$_{0\,t}$	Conversion$_t$ [a]	[ketone]$_{theo\,t}$ [b] (mol/L)	n(2 dia)$_{theo\,t}$ [c] (mol)	[2 dia]$_t$ [d] (mol/L)	n(2 dia)$_t$ [e] (mol)	Yield$_t$ [f]
14	19.5	0	0	/	0	0	0	0	/
15	21	0	0	/	0	0	0	0	/
16	22.5	0	0	/	0	0	0	0	/
17	24	0	0	/	0	0	0	0	/
18	25.5	0	0	/	0	0	0	0	/
19	27	0	0	/	0	0	0	0	/
20	28.5	0.0031148	0.027346	0.886097	0.000801527	2.40458E-07	5.3119E-05	7.1710E-08	0.298226
21	30	0.0055028	0.0452036	0.878266	0.001324932	3.9748E-07	0.00011137	1.5035E-07	0.378272
22	31.5	0.0107362	0.0719380	0.850758	0.002108528	6.32558E-07	0.00021482	2.9000E-07	0.458469
23	33	0.0180969	0.1131397	0.840048	0.003316164	9.94849E-07	0.00037709	5.0907E-07	0.511713
24	34.5	0.0309614	0.1696794	0.817530	0.004973361	1.49201E-06	0.00063873	8.6228E-07	0.577936
25	36	0.0494646	0.2435039	0.796863	0.006867886	2.06037E-06	0.00095623	1.2909E-06	0.626545
26	37.5	0.0806818	0.3130551	0.742275	0.009175752	2.75273E-06	0.00145859	1.9691E-06	0.715327
27	39	0.1103064	0.3959524	0.721414	0.011605502	3.48165E-06	0.00198626	2.6814E-06	0.770167
28	40.5	0.1283925	0.4742895	0.729295	0.01390159	4.17048E-06	0.00224542	3.0313E-06	0.726853
29	42	0.1397661	0.5655660	0.752873	0.016576935	4.97308E-06	0.00248658	3.3568E-06	0.675013
30	43.5	0.1469555	0.644752	0.772074	0.018695959	5.60879E-06	0.00265289	3.5814E-06	0.638535
31	45	0.1505774	0.6998620	0.784847	0.020513198	6.15396E-06	0.00273888	3.6975E-06	0.600832
32	46.5	0.1572641	0.7479571	0.789741	0.02192288	6.57686E-06	0.00280228	3.7830E-06	0.575211
33	48	0.1528455	0.7872271	0.805843	0.022896204	6.86886E-06	0.00277202	3.7422E-06	0.544812
34	49.5	0.154756	0.8133281	0.809724	0.023838928	7.15168E-06	0.00280655	3.7888E-06	0.529785
35	51	0.1552511	0.8337519	0.813792	0.024437557	7.33127E-06	0.00284141	3.8359E-06	0.523226
36	52.5	0.1545285	0.8492540	0.818042	0.024891928	7.46758E-06	0.00282538	3.8142E-06	0.510778
37	54	0.1524784	0.8544330	0.821544	0.025043726	7.51312E-06	0.00281304	3.7976E-06	0.505464
38	55.5	0.1478947	0.8601374	0.828056	0.025111765	7.53353E-06	0.00276275	3.7297E-06	0.495082
39	57	0.148994	0.8652011	0.827792	0.025359343	7.6078E-06	0.00279812	3.7774E-06	0.496526
40	58.5	0.1571641	0.8694948	0.819246	0.025485193	7.64556E-06	0.00286523	3.8680E-06	0.505923
41	60	0.1567413	0.87	0.819837	0.0255	7.65E-06	0.00293854	3.9670E-06	0.518567

Table 7.5: Calculation of the conversion and the yield according to the experimental time.

[a] $\text{Conversion}_t = 1 - \frac{(\text{Peak area cyclohex-2-enone/ Peak area internal standard})_t}{(\text{Peak area cyclohex-2-enone/ Peak area internal standard})_{0\,t}}$

with (Peak area cyclohex-2-enone/Peak area internal standard)$_{0\,t}$ calculated from the dispersion profile of the cyclohex-2-enone at 0.1 mL/min (x-axis scale doubled). Normalisation of the maximum at 0.87 (value obtained during the experiment Table 5.2, entry 2).

[b] $[\text{ketone}]_{\text{theo t}}$ the theoretical concentration of cyclohex-2-enone calculated from the dispersion profile of the cyclohex-2-enone at 0.1 mL/min (x-axis scale doubled). Normalisation of the maximum at 0.0255 M (concentration of cyclohex-2-enone in the stock solution 2 divided by 2).

[c] $\text{n(2 dia)}_{\text{theo t}} = [\text{ketone}]_{\text{theo t}} \text{ x Volume collected per GC vial}$

with Volume collected per GC vial = 0.3 mL (collection during 1 min and 30 seconds at 0.2 mL/min).

[d] $[\text{2 dia}]_t = \left(\frac{\text{Peak area 2 dia}}{\text{Peak area IS}}\right)_t \text{ x } \frac{[\text{IS}]}{\text{K(2 dia)/K(IS)}}$

with K(2 dia)/K(IS) = 1.6583, determined from the calibration curve (Figure 7.50).
[IS] = 0.00505 M, the concentration of IS in the GC vials after addition of 1 mL of MeCN.

[e] $\text{n(2 dia)}_t = [\text{2 dia}]_t \text{ x Volume per GC vial}$

with Volume per GC vial = 1.3 mL.

[f] $\text{Yield}_t = \frac{\text{n(2 dia)}_t}{\text{n(2 dia)}_{\text{theo t}}}$

From Table 7.5, the following Figure 7.58 was obtained.

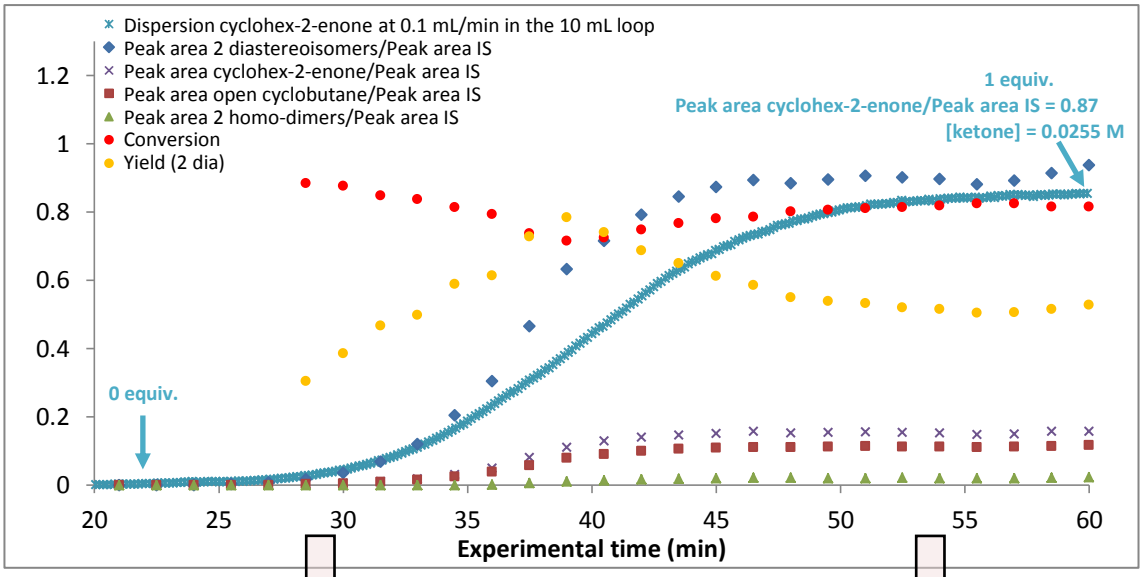

Figure 7.58: Ratios of the peak area of each compound over the peak area of the IS plotted against the experimental time. Evolution of the conversion and the yield according to the experimental time.

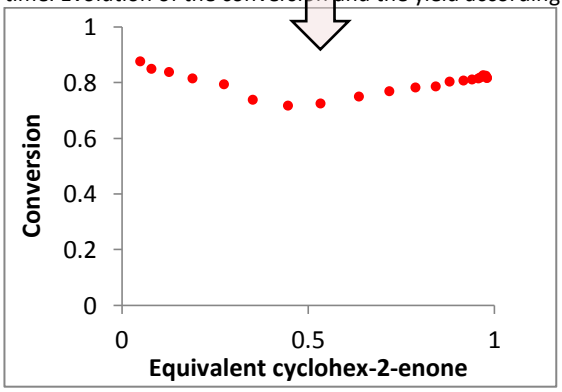

Figure 7.59: Evolution of the conversion according to the equivalent of cyclohex-2-enone.

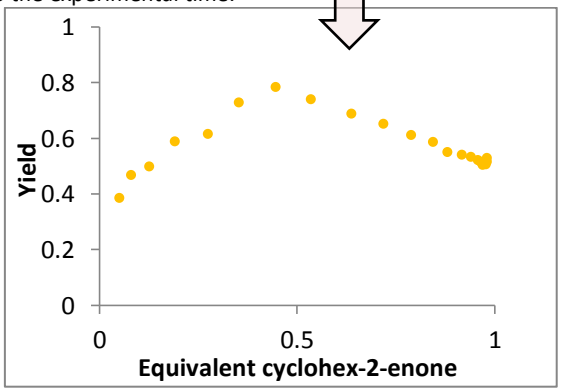

Figure 7.60: Evolution of the yield according to the equivalent of cyclohex-2-enone.

Finally, as explained in section 5.3.3.2.1, Figure 7.58 enabled the generation of Figures 7.59 and 7.60.

7.2.4.2.5 Application of the concentration gradient in flow: a novel process towards the fast optimisation of photochemical reaction conditions - photocyclisation of cis-stilbene (B → C)

Experimental set-up for the generation of the concentration gradient profile of the dispersed reagent B (cis-stilbene) at the exit of the 10 mL loop (step 1): Using the flow machine (Vapourtec R2+/R4), the experiment was carried out using one single pump, a PFA loop (10 mL capacity, 1 mm i.d.), a 250 psi BPR and an in-line UV spectrometer (Ocean Optics DH-2000-BAL spectrometer).

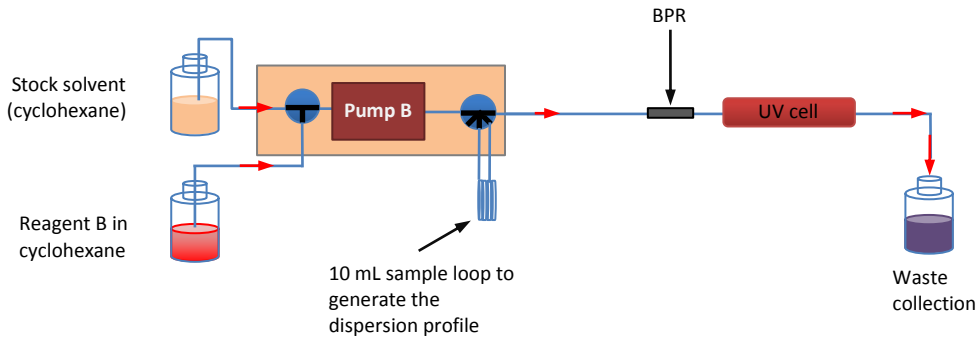

Figure 7.61: Flow set-up for the generation of concentration gradient profile.

Generation of the concentration gradient profile of the dispersed reagent B (cis-stilbene) at the exit of the 10 mL loop (step 1): In a 50 mL flask, 10.00 µL of cis-stilbene were mixed with 25 mL of cyclohexane ($[C_0]$ = 2.2 x 10^{-3} M). The reaction mixture was degassed by sonication whilst being saturated with nitrogen. Solvent was pumped at 0.353 mL/min and after few minutes, the feeding valve was switched to the reagent solution and 10 mL of the reaction mixture was injected. At the end of the sample plug injection, the feeding valve was returned to the solvent feed. The sample plug dispersed in the 10 mL PFA loop. In-line UV detection was used and the data sampling rate was determined by the acquisition parameters. The spectra were processed using BORIS software by calibration-less methods (height of non-overlapping peaks processing).

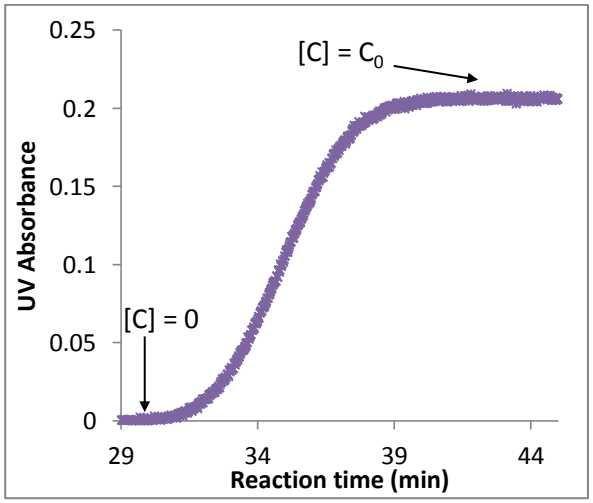

Figure 7.62: Concentration gradient profile of a 10 mL plug of cis-stilbene in cyclohexane ($[C_0]$ = 2.2 x 10^{-3} M) after going through a 10 mL PFA loop at 0.353 mL/min. In-line UV detection and height of non-overlapping peaks processing at 278 nm.

Experimental set-up for the application of the concentration gradient methodology on the photocyclisation of cis-stilbene (step 2): Using the flow machine (Vapourtec R2+/R4), the experiments were carried out using two pumps, a PFA loop (10 mL capacity, 1 mm i.d.), a home-made coiled photoflow reactor (31.8 mL capacity, 1 mm i.d.) equipped with a 36 W UV lamp (UV-A, B or C), a 250 psi BPR and GC vials for off-line analysis.

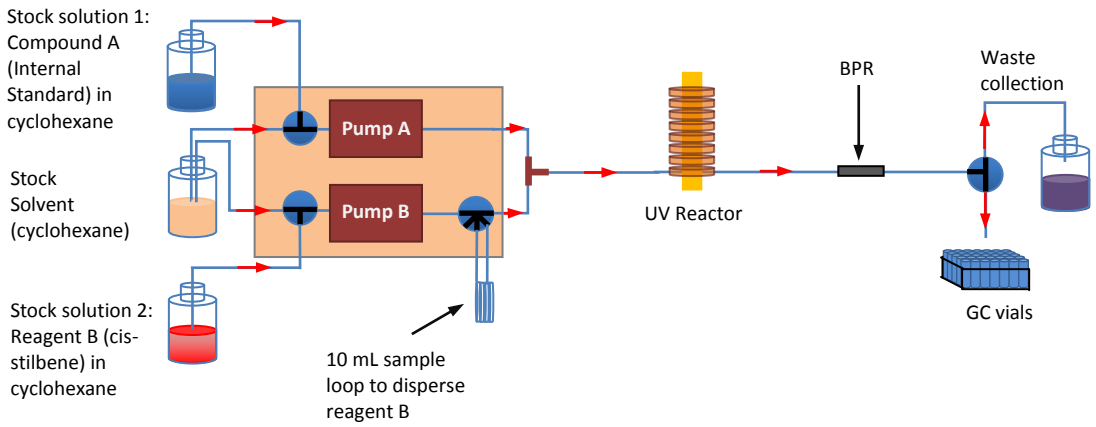

Figure 7.63: Flow set-up for the application of the concentration gradient methodology on the photocyclisation of cis-stilbene.

General procedure for the application of the concentration gradient methodology on the photocyclisation of cis-stilbene (step 2): In a 50 mL flask, compound A (Internal standard: dibutyl ether) was mixed with cyclohexane (Stock solution 1). In the same way, in another 50 mL flask, the reagent B to disperse (cis-stilbene) was mixed with cyclohexane (Stock solution 2). Each flask (Stock solution 1, 2 and Stock solvent) was degassed by sonication whilst being saturated with nitrogen. Before starting the reaction, solvent was pumped at the indicated flow rate and the indicated UV lamp (Philips 4-pin PL-L 36 W UV-A/B or C) was switched on and left to warm up for 10-15 minutes. The water cooling system was turned on. Once the system was stable, the feeding valves (pump A and B) were switched to the stock solutions 1 and 2 (compound A (IS) and reagent B). The compound A went straight to the UV reactor and the reagent B dispersed first in the 10 mL loop to form the gradient of concentration and went then to the UV reactor. Once 15 mL of solution 1 and 2 were injected into the flow system, the feeding valves were returned to the solvent feed. The reaction with different concentrations of reagent B occurred in the UV reactor. The reaction mixture was collected in vials and the sampling rate was precisely determined (20 seconds collection per vial with addition of 1 mL of hexane). The different samples were then analysed via off-line GC experiments.

General procedure for the processing of the GC data - Incorporation of the concentration gradient profile of the dispersed reagent and calculation of the conversion and the yield according to the reaction time (steps 3 and 4): From each GC spectrum generated, the different ratios Peak area compound/Peak area Internal Standard were calculated and plotted against the experimental time. The x-axis scale of the dispersion profile obtained in step 1 was doubled and the curve was incorporated with the different ratios previously calculated. The

accurate position of the dispersion curve was determined from the turn off light results (section 5.4.5, Figures 5.58, 5.60 and 5.62). The conversion and the yield for each GC analysis were calculated using equations 7.5 and 7.6 respectively.

$$\text{Conversion}_t = 1 - \frac{(\text{Peak area cis} - \text{stilbene/ Peak area internal standard})_t}{(\text{Peak area cis} - \text{stilbene/ Peak area internal standard})_{0\,t}}$$

Equation 7.5: Formula used for the calculation of the conversion at a given moment.

$$\text{Yield}_t = \frac{\text{n(phenanthrene)}_t}{\text{n(phenanthrene)}_{theoretical\ t}}$$

Equation 7.6: Formula used for the calculation of the yield at a given moment.

Vial	Weight IS (mg)	Weight product (mg)	Peak area product/ Peak area IS	[product]/[IS]
1	3.10	1.00	0.36288	0.23570
2	3.50	1.00	0.31694	0.20877
3	5.45	1.02	0.20580	0.13675
4	5.57	1.4	0.27316	0.18366

IS: dibutyl ether
Product: Phenanthrene

$$\frac{\text{Peak area product}}{\text{Peak area IS}} = \frac{\text{K(product)}}{\text{K(IS)}} \text{ x } \frac{\text{[product]}}{\text{[IS]}}$$

K(product)/K(IS) = 1.5261

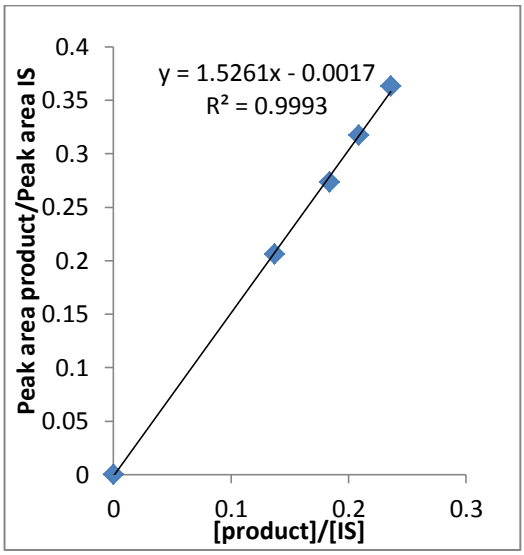

Figure 7.64: Calibration curve for the calculation of the yield$_t$.

General procedure for the generation of the plots conversion *vs.* initial concentration of the cis-stilbene and yield *vs.* initial concentration of the cis-stilbene (step 5): Using the curves with the conversion, the yield and the dispersion profile of the cis-stilbene plotted against the reaction time, 2 new plots can be generated: conversion *vs.* initial concentration of cis-stilbene and yield *vs.* initial concentration of cis-stilbene. Indeed, for specific times, initial concentration of the cis-stilbene, conversion and yield are aligned. Using these series of specific data, these 2 new plots can be obtained.

Concentration gradient results using the 31.8 mL photoflow reactor - UV-A (36 W):

Table 5.6, entry 1:

Entry	Compound A Internal Standard	Reagent B	Compound A (IS)		Reagent B (dispersed)		Reaction time (min)	UV lamp	UV reactor
			[A][a] (M)	flow rate (mL/min)	[B][b] (M)	flow rate (mL/min)			
1	dibutyl ether	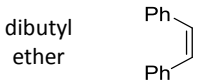	0.36	0.353	0.1	0.353	45	UV-A 36 W	Single coiled 31.8 mL

[a] [A] Concentration of compound A (Internal standard) in the stock solution 1 (1.5 mL of internal standard were mixed with 23 mL of cyclohexane). [b] [B] Concentration of reagent B in the stock solution 2 (445 µL of cis-stilbene was mixed with 58.0 mg of I_2 and 24.5 mL of cyclohexane).

Using these reaction conditions and the general procedures described above (steps 2, 3, 4 and 5), the following results were obtained. For this experiment, an overview of the data processing (steps 3, 4 and 5) was highlighted. This data processing is the same for the series of experiments with UV-A, B and C (Table 5.6, entries 1, 2 and 3).

GC vial	Exp. time (min)	Peak area cis-stilbene$_t$	Peak area phenanthrene$_t$	Peak area 2 dimers$_t$	Peak area IS$_t$	(Peak area cis-stilbene/Peak area IS)$_t$	(Peak area Phenanthrene/ Peak area IS)$_t$	(Peak area 2 dimers/Peak area IS)$_t$
1	0	0	9.3	0	484	0	0.019214876	0
2	0.333	0	23.0	0	881.6	0	0.026088929	0
3	0.667	0	41.4	0	1166.9	0	0.035478619	0
4	1	0	50.4	0	1117.2	0	0.045112782	0
5	1.333	0	60.3	3.2	1086.3	0	0.055509528	0.002945779
6	1.667	0	71.9	4.2	1082.6	0	0.066414188	0.003879549
7	2	0	96.7	9.3	1243.9	0	0.077739368	0.007476485
8	2.333	0	101.3	10.8	1139.5	0	0.088898640	0.009477841
9	2.667	2.6	116.0	14	1182.7	0.00219836	0.098080663	0.011837321
10	3	4.3	121.5	17.2	1163.2	0.003696699	0.104453232	0.014786795
11	3.333	5.2	126.9	20.6	1143.7	0.004546647	0.110955670	0.018011716
12	3.667	11.7	138.0	25.9	1201.2	0.00974026	0.114885115	0.021561772
13	4	28.2	185.1	43.1	1635.3	0.017244542	0.113190240	0.02635602
14	4.333	36.7	144.6	42.5	1285.8	0.028542542	0.112459169	0.033053352
15	4.667	48.5	123.9	43.9	1141.5	0.042487954	0.108541393	0.038458169
16	5	73.9	131.5	55	1246.9	0.059266982	0.105461545	0.044109391
17	5.333	90.4	117.4	60.8	1179.1	0.076668646	0.099567467	0.051564753
18	5.667	118.8	118.2	69.3	1222.2	0.097201767	0.096710849	0.056701031
19	6	160.3	127.1	84.4	1344.3	0.119244216	0.094547348	0.062783605
20	6.333	149.6	97.8	75.2	1069	0.139943873	0.091487371	0.070346118
21	6.667	201.1	112.1	98.3	1274.3	0.157812132	0.087969866	0.077140391
22	7	235.2	116.8	112.3	1358.8	0.173093906	0.085958198	0.082646453
23	7.333	107.8	49.8	51.8	590.1	0.182680902	0.084392476	0.087781732
24	7.667	253.1	109.3	122.5	1291.7	0.19594333	0.084617171	0.094836262
25	8	267.5	106.0	128.2	1297.3	0.206197487	0.081708163	0.098820627
26	8.333	286.8	107.7	139.4	1331.7	0.215363821	0.080874071	0.104678231
27	8.667	223	81.0	107.6	1007.4	0.221361922	0.080405003	0.106809609
28	9	297.4	105.0	145.5	1309.9	0.227040232	0.080158791	0.111077181
29	9.333	299.6	99.3	147.7	1286.8	0.232825614	0.077168169	0.114780852
30	9.667	326.4	106.6	163.7	1383	0.236008677	0.077078814	0.118365871
31	10	104.1	35.2	52.1	448.3	0.232210573	0.078518849	0.116216819
32	10.33	282	91.2	141.9	1180.7	0.238841365	0.077242314	0.120182942
33	10.67	315	101.2	157.2	1296.4	0.242980562	0.078062326	0.121258871
34	11	271.4	85.1	136.5	1108.4	0.244857452	0.076777337	0.123150487
35	11.33	282.6	90.1	143.4	1146.6	0.246467818	0.078580150	0.125065411
36	11.67	301.7	93.8	153.1	1224.8	0.246325931	0.076583932	0.125
37	12	370.5	113.9	188.8	1465.4	0.252831991	0.077726218	0.128838542
38	12.33	290.8	91.3	148	1172.9	0.247932475	0.077841248	0.126182965
39	12.67	351.4	108.0	179.6	1398.6	0.251251251	0.077220077	0.128414128
40	13	334.2	102.1	169.7	1319.5	0.253277757	0.077377795	0.128609322
41	13.33	270.6	82.9	137	1075.1	0.251697517	0.077109106	0.127430007
42	13.67	290.1	88.3	146.3	1144.7	0.253428846	0.077138115	0.127806412

43	14	291.6	90.7	147.2	1159	0.251596204	0.078257118	0.12700604
44	14.33	305.9	96.2	156.1	1213.5	0.252080758	0.079274825	0.128636176
45	14.67	428.3	134.5	220.5	1681.9	0.254652476	0.079969083	0.13110173
46	15	430.3	130.7	223.4	1667.1	0.258112891	0.078399616	0.134005159
47	15.33	384	115.5	198.1	1485.5	0.258498822	0.077751599	0.133355772
48	15.67	379.3	113.3	193.9	1480.7	0.256162626	0.076517863	0.130951577
49	16	343.2	105.5	174.4	1347.5	0.254693878	0.078293135	0.129424861
50	16.33	281.3	85.8	142.5	1111.1	0.253172532	0.077220772	0.128251283
51	16.67	376.5	114.6	192.9	1477.8	0.254770605	0.077547706	0.130531872
52	17	327.3	99.2	165.8	1283.3	0.255045586	0.077300709	0.129198161
53	17.33	350.6	106.3	178	1374.4	0.255093132	0.077342841	0.129511059
54	17.67	332	102.0	169.3	1305	0.25440613	0.078160920	0.129731801
55	18	322.8	99.1	163.5	1267.2	0.254734848	0.078203914	0.129024621
56	18.33	368.8	110.4	186.6	1429.2	0.25804646	0.077246012	0.130562552
57	18.67	390.3	117.6	198.6	1523.6	0.256169598	0.077185613	0.130349173
58	19	331.5	100.4	167	1306.2	0.253789619	0.076864186	0.127851784
59	19.33	268.8	81.8	134.3	1055.8	0.254593673	0.077476795	0.127202122
60	19.67	307.7	94.6	151.2	1213.9	0.253480517	0.077930637	0.124557212
61	20	369.4	113.2	185.1	1446.8	0.25532209	0.078241637	0.127937517

Table 7.6: GC data obtained from the different vials. For this experiment, the sampling rate was 20 seconds (volume collected per GC vial = 0.235 mL) and 1 mL of hexane was added in each vial before running the GC analysis (volume per GC vial = 1.235 mL).

From Table 7.6, the following Figure 7.65 was obtained.

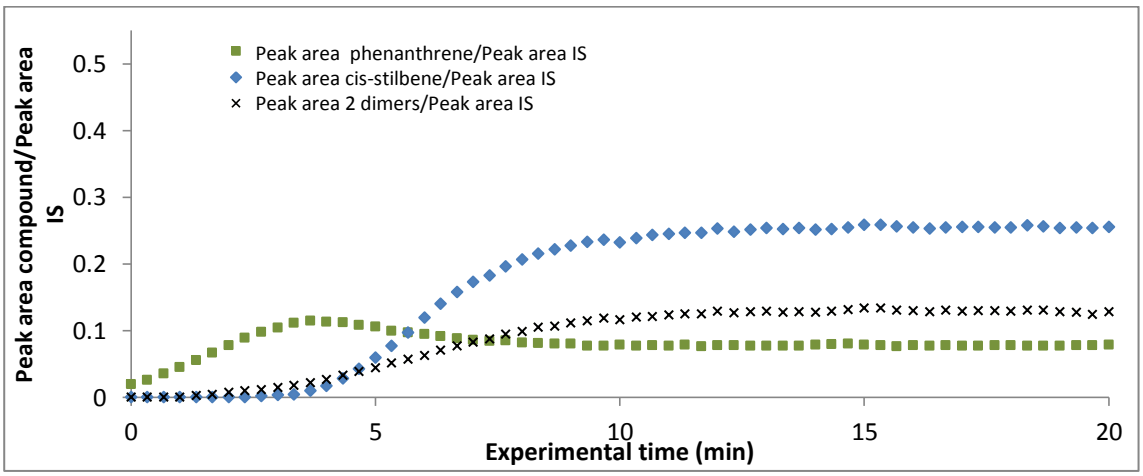

Figure 7.65: Plot of the different ratios Peak area compound/Peak area IS according to the experimental time.

The incorporation of the dispersion curve (Figure 7.62) in Figure 7.66 was performed in such a way that the increase of the phenanthrene correlates with the increase of the dispersed cis-stilbene.

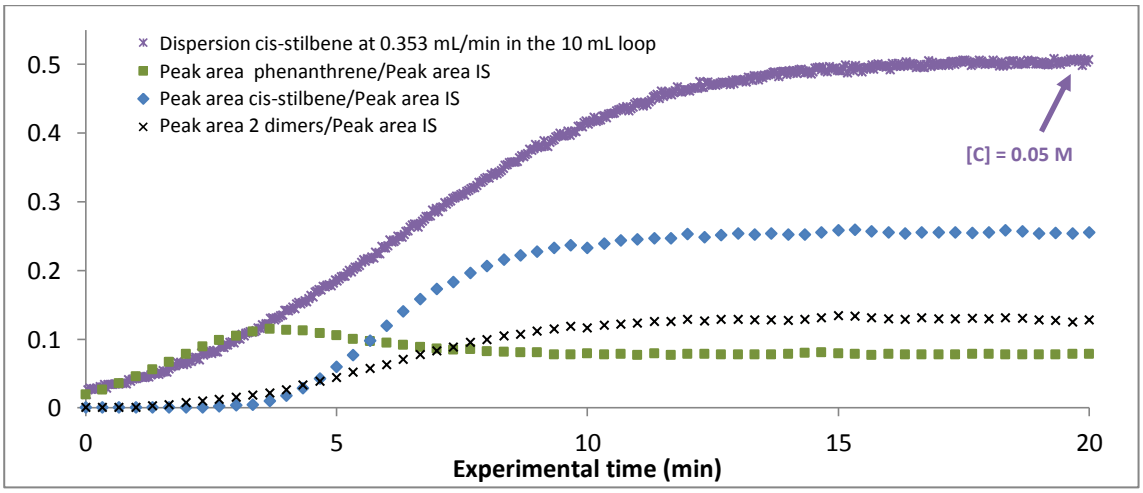

Figure 7.66: Incorporation of the concentration gradient profile.

GC vial	Exp. time (min)	(Peak area cis-stilbene/Peak area IS)$_t$	(Peak area cis-stilbene/Peak area IS)$_{0\ t}$	Conv.$_t$[a]	[cis-stilbene]$_{theo\ t}$[b] (mol/L)	n(phen.)$_{theo\ t}$[c] (mol)	[phen.]$_t$[d] (mol/L)	n(phen.)$_t$[e] (mol)	Yield$_t$[f]
1	0	0	0.018972	1	0.003349	7.870E-07	0.000433	5.344E-07	0.6791
2	0.33	0	0.029505	1	0.004169	9.796E-07	0.000585	7.219E-07	0.7370
3	0.67	0	0.034159	1	0.004914	1.155E-06	0.000797	9.849E-07	0.8528
4	1	0	0.042519	1	0.005548	1.304E-06	0.001012	1.249E-06	0.9583
5	1.33	0	0.050128	1	0.006255	1.470E-06	0.001245	1.537E-06	1.0460
6	1.67	0	0.056589	1	0.007531	1.770E-06	0.001491	1.841E-06	1.0404
7	2	0	0.066575	1	0.008819	2.072E-06	0.001744	2.154E-06	1.0392
8	2.33	0	0.079349	1	0.009681	2.275E-06	0.001995	2.464E-06	1.0829
9	2.67	0.002198	0.089954	0.975561	0.010858	2.552E-06	0.002202	2.719E-06	1.0656
10	3	0.003697	0.098751	0.962565	0.012002	2.821E-06	0.002345	2.896E-06	1.0267
11	3.33	0.004547	0.109808	0.958594	0.013867	3.259E-06	0.002491	3.076E-06	0.9440
12	3.67	0.00974	0.122422	0.920437	0.015011	3.527E-06	0.002578	3.184E-06	0.9026
13	4	0.017245	0.141444	0.878082	0.016821	3.953E-06	0.002540	3.137E-06	0.7936
14	4.33	0.028543	0.153108	0.813579	0.018056	4.243E-06	0.002523	3.116E-06	0.7345
15	4.67	0.042488	0.171571	0.752360	0.019754	4.642E-06	0.002436	3.009E-06	0.6482
16	5	0.059267	0.184168	0.678191	0.021157	4.972E-06	0.002367	2.923E-06	0.5879
17	5.33	0.076669	0.201487	0.619485	0.023075	5.423E-06	0.002234	2.759E-06	0.5087
18	5.67	0.097202	0.215799	0.549573	0.024722	5.810E-06	0.002171	2.681E-06	0.4615
19	6	0.119244	0.232396	0.486891	0.026269	6.173E-06	0.002122	2.621E-06	0.4246
20	6.33	0.139944	0.252168	0.445037	0.028391	6.672E-06	0.002053	2.535E-06	0.3800
21	6.67	0.157812	0.267939	0.411014	0.029875	7.021E-06	0.001974	2.438E-06	0.3472
22	7	0.173094	0.289593	0.402285	0.031206	7.333E-06	0.001929	2.382E-06	0.3248
23	7.33	0.182681	0.304729	0.400514	0.032845	7.718E-06	0.001893	2.337E-06	0.3028
24	7.67	0.195943	0.318303	0.384412	0.034114	8.017E-06	0.001899	2.346E-06	0.2926
25	8	0.206197	0.335016	0.384513	0.035664	8.381E-06	0.001833	2.264E-06	0.2702
26	8.33	0.215364	0.347958	0.381063	0.037068	8.711E-06	0.001814	2.241E-06	0.2572
27	8.67	0.221362	0.363775	0.391486	0.038251	8.989E-06	0.001805	2.229E-06	0.2480
28	9	0.22704	0.378096	0.399516	0.038865	9.133E-06	0.001800	2.223E-06	0.2434
29	9.33	0.232826	0.390163	0.403259	0.040484	9.514E-06	0.001732	2.139E-06	0.2249
30	9.67	0.236009	0.396419	0.404647	0.041651	9.788E-06	0.001730	2.136E-06	0.2182
31	10	0.232211	0.412937	0.437661	0.042606	1.001E-05	0.001761	2.174E-06	0.2172
32	10.3	0.238841	0.424843	0.437812	0.043378	1.019E-05	0.001733	2.141E-06	0.2100
33	10.67	0.242981	0.434578	0.440881	0.044506	1.046E-05	0.001752	2.163E-06	0.2069
34	11	0.244857	0.442459	0.446598	0.044615	1.048E-05	0.001722	2.127E-06	0.2029
35	11.33	0.246468	0.453959	0.457070	0.045328	1.065E-05	0.001764	2.179E-06	0.2046
36	11.67	0.246326	0.455071	0.458709	0.046359	1.089E-05	0.001718	2.122E-06	0.1948
37	12	0.252832	0.462342	0.453149	0.046297	1.088E-05	0.001744	2.154E-06	0.1980
38	12.33	0.247932	0.466322	0.468323	0.046734	1.098E-05	0.001747	2.157E-06	0.1964
39	12.67	0.251251	0.472234	0.467951	0.047408	1.114E-05	0.001733	2.140E-06	0.1921
40	13	0.253278	0.476682	0.468665	0.047572	1.118E-05	0.001737	2.145E-06	0.1919
41	13.33	0.251698	0.483567	0.479497	0.048086	1.130E-05	0.001731	2.138E-06	0.1892
42	13.67	0.253429	0.485239	0.477724	0.047730	1.122E-05	0.001731	2.138E-06	0.1906
43	14	0.251596	0.490472	0.487032	0.048206	1.133E-05	0.001756	2.169E-06	0.1914
44	14.33	0.252081	0.486844	0.482214	0.048171	1.132E-05	0.001780	2.198E-06	0.1942
45	14.67	0.254652	0.491703	0.482101	0.048811	1.147E-05	0.001795	2.217E-06	0.1932
46	15	0.258113	0.490099	0.473345	0.048867	1.148E-05	0.001760	2.173E-06	0.1892
47	15.33	0.258499	0.497871	0.480791	0.048781	1.146E-05	0.001745	2.156E-06	0.1880
48	15.67	0.256163	0.498447	0.486078	0.048727	1.145E-05	0.001717	2.120E-06	0.1852
49	16	0.254694	0.497567	0.488121	0.048580	1.142E-05	0.001751	2.163E-06	0.1894
50	16.33	0.253173	0.503713	0.497387	0.048823	1.147E-05	0.001733	2.140E-06	0.1866
51	16.67	0.254771	0.495516	0.485847	0.048954	1.150E-05	0.001741	2.150E-06	0.1869
52	17	0.255046	0.497991	0.487850	0.048795	1.147E-05	0.001735	2.143E-06	0.1869
53	17.33	0.255093	0.499335	0.489133	0.049192	1.156E-05	0.001736	2.144E-06	0.1854
54	17.67	0.254406	0.497711	0.488847	0.049061	1.153E-05	0.001754	2.166E-06	0.1879
55	18	0.254735	0.501762	0.492319	0.049120	1.154E-05	0.001754	2.167E-06	0.1877
56	18.33	0.258046	0.500424	0.484343	0.049057	1.153E-05	0.001734	2.141E-06	0.1857
57	18.67	0.25617	0.501025	0.488708	0.049174	1.156E-05	0.001732	2.140E-06	0.1851
58	19	0.25379	0.500383	0.492809	0.049482	1.163E-05	0.001725	2.130E-06	0.1832
59	19.33	0.254594	0.501578	0.492414	0.049666	1.167E-05	0.001739	2.148E-06	0.1840
60	19.67	0.253481	0.504718	0.497778	0.049876	1.172E-05	0.001749	2.160E-06	0.1843
61	20	0.255322	0.51	0.499368	0.05	1.175E-05	0.001756	2.168E-06	0.1845

Table 7.7: Calculation of the conversion and the yield according to the experimental time.

[a] $\text{Conv.}_t = 1 - \frac{(\text{Peak area cis-stilbene/ Peak area internal standard})_t}{(\text{Peak area cis-stilbene/ Peak area internal standard})_{0\,t}}$

with (Peak area cis-stilbene/Peak area internal standard)$_{0\,t}$ calculated from the concentration gradient profile of the cis-stilbene at 0.353 mL/min (x-axis scale doubled). Normalisation of the maximum at 0.51 (GC ratio obtained from a mixture of 445 µL of cis-stilbene, 1.5 mL of Internal standard and 50 mL of cyclohexane).

[b] $[\text{cis-stilbene}]_{\text{theoretical t'}}$ the theoretical concentration of cis-stilbene calculated from the concentration gradient profile of the cis-stilbene at 0.353 mL/min (x-axis scale doubled). Normalisation of the maximum at 0.05 M (concentration of cis-stilbene in the stock solution 2 divided by 2).

[c] $n(\text{phen.})_{\text{theoretical t}} = [\text{cis-stilbene}]_{\text{theoretical t}} \text{ x Volume collected per GC vial}$

with Volume collected per GC vial = 0.235 mL (collection during 20 seconds at 0.706 mL/min).

[d] $[\text{phen.}]_t = \left(\frac{\text{Peak area phenanthrene}}{\text{Peak area IS}}\right)_t \text{ x } \frac{[\text{IS}]}{\text{K(phenanthrene)/K(IS)}}$

with K(phenanthrene)/K(IS) = 1.5261, determined from the calibration curve (Figure 7.64).
[IS] = 0.03425 M, the concentration of IS in the GC vials after addition of 1 mL of hexane.

[e] $n(\text{phen.})_t = [\text{phen.}]_t \text{ x Volume per GC vial}$

with Volume per GC vial = 1.235 mL.

[f] $\text{Yield}_t = \frac{n(\text{phen.})_t}{n(\text{phen.})_{\text{theoretical t}}}$

From Table 7.7, the following Figure 7.67 was obtained.

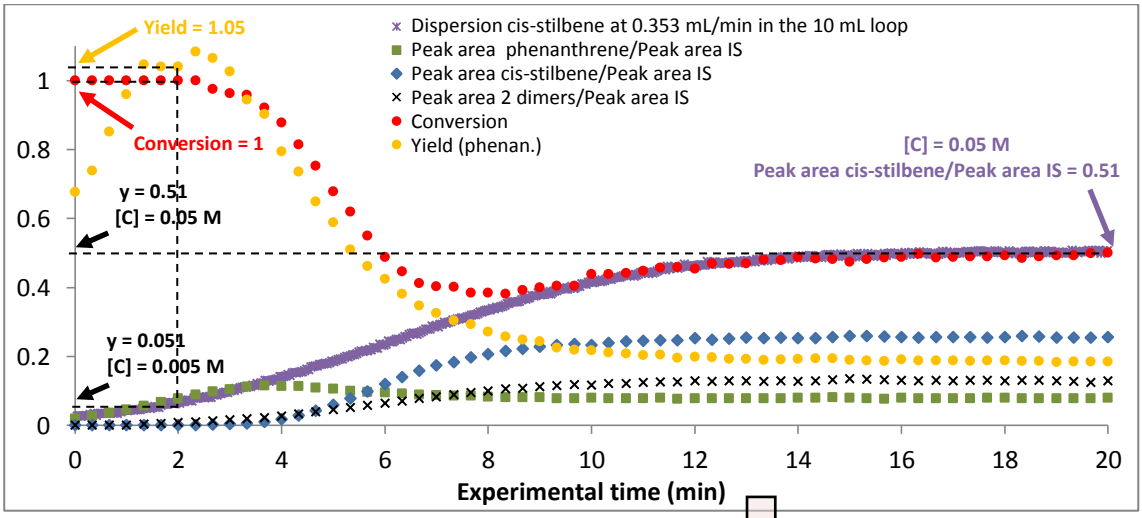

Figure 7.67: Ratios of the peak area of each compound over the peak area of the IS plotted against the experimental time. Evolution of the conversion and the yield according to the experimental time.

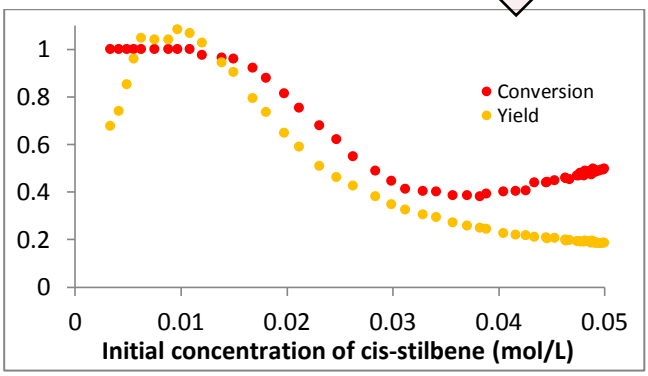

Figure 7.68: Evolution of the conversion and the yield according to the initial concentration of cis-stilbene.

To check that the dispersion curve is placed at the right position on the x-axis, the calculated conversion and yield at [C] = 0.005 M (1 and 1.05 respectively) were compared to the

conversion and yield obtained during the turn off light experiment with exactly the same conditions (Figure 5.58). The results are consistent (1 *vs.* 1 for the conversion and 1.05 *vs.* 1.03 for the yield).

Finally, as explained in section 5.3.4.2.1, Figure 7.67 enabled the generation of Figure 7.68.

Table 5.6, entry 2:

Entry	Compound A Internal Standard	Reagent B	Compound A (IS)		Reagent B (dispersed)		Reaction time (min)	UV lamp	UV reactor
			[A][a] (M)	flow rate (mL/min)	[B][b] (M)	flow rate (mL/min)			
2	dibutyl ether		0.36	0.353	0.1	0.353	45	UV-B 36 W	Single coiled 31.8 mL

[a] [A] Concentration of compound A (Internal standard) in the stock solution 1 (1.5 mL of internal standard were mixed with 23 mL of cyclohexane). [b] [B] Concentration of reagent B in the stock solution 2 (445 µL of cis-stilbene was mixed with 60.0 mg of I_2 and 24.5 mL of cyclohexane).

Using these reaction conditions and the general procedures described previously (steps 2, 3, 4 and 5), the following results were obtained.

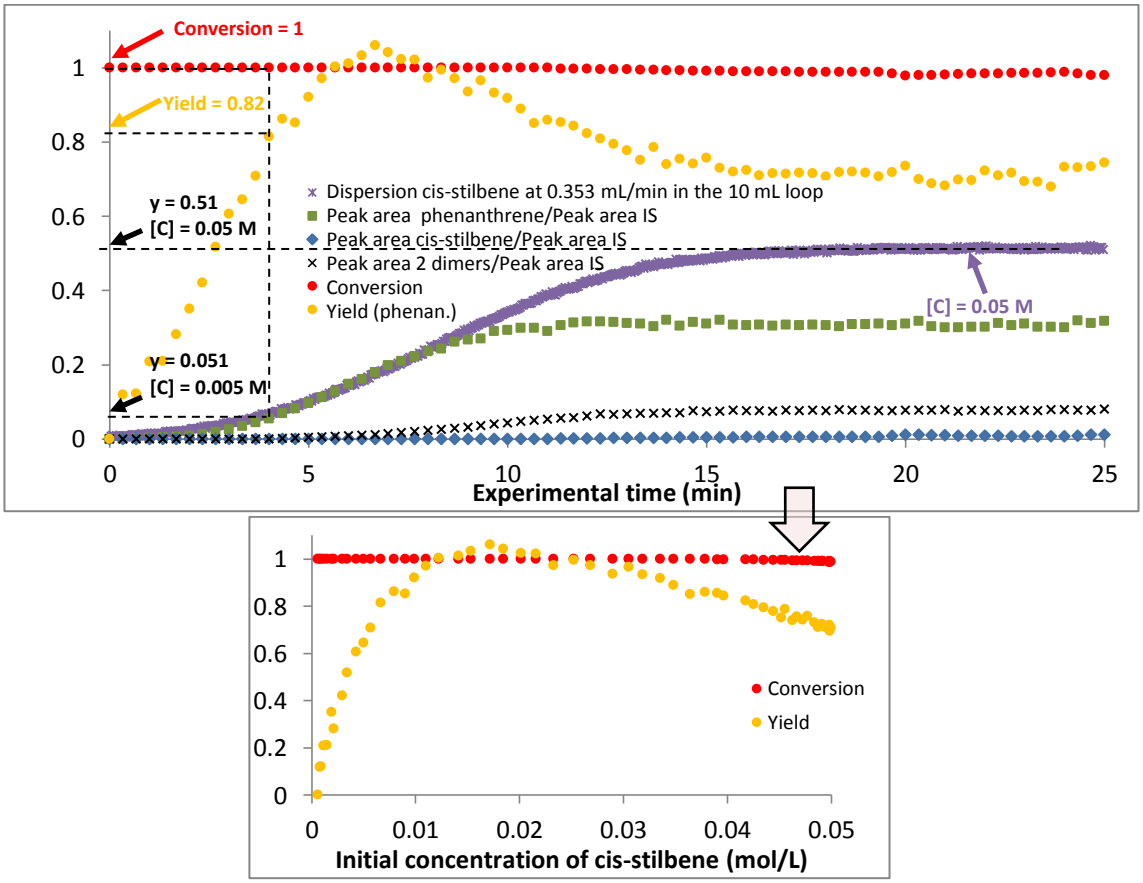

To check that the dispersion curve is placed at the right position on the x-axis, the calculated conversion and yield at [C] = 0.005 M (1 and 0.82 respectively) were compared to the conversion and yield obtained during the turn off light experiment with exactly the same conditions (Figure 5.60). The results are consistent (1 *vs.* 1 for the conversion and 0.82 *vs.* 0.84 for the yield).

Table 5.6, entry 3:

Entry	Compound A Internal Standard	Reagent B	Compound A (IS)		Reagent B (dispersed)		Reaction time (min)	UV lamp	UV reactor
			[A][a] (M)	flow rate (mL/min)	[B][b] (M)	flow rate (mL/min)			
3	dibutyl ether		0.36	0.353	0.1	0.353	45	UV-C 36 W	Single coiled 31.8 mL

[a] [A] Concentration of compound A (Internal standard) in the stock solution 1 (1.5 mL of internal standard were mixed with 23 mL of cyclohexane). [b] [B] Concentration of reagent B in the stock solution 2 (445 µL of cis-stilbene was mixed with 60.0 mg of I_2 and 24.5 mL of cyclohexane).

Using these reaction conditions and the general procedures described previously (steps 2, 3, 4 and 5), the following results were obtained.

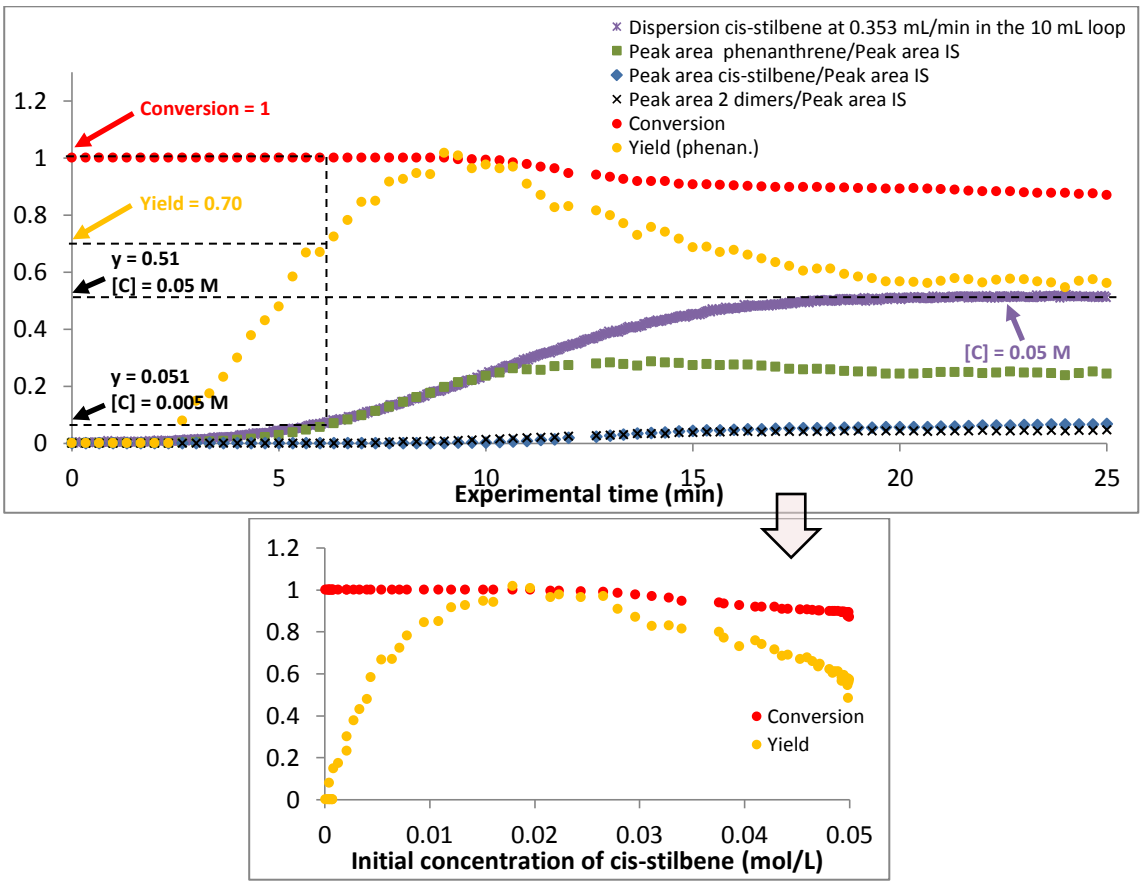

To check that the dispersion curve is placed at the right position on the x-axis, the calculated conversion and yield at [C] = 0.005 M (1 and 0.70 respectively) were compared to the conversion and yield obtained during the turn off light experiment with exactly the same conditions (Figure 5.62). The results are consistent (1 *vs.* 1 for the conversion and 0.70 *vs.* 0.68 for the yield).

7.2.4.3 GENERAL PROCEDURES: Turn off light experiments

7.2.4.3.1 Correction to apply to the turn off light methodology for the determination of the optimum reaction time

Experimental set-up for: Using the flow machine (Vapourtec R2+/R4), the experiments were carried out using one pump, a home-made coiled photoflow reactor (14.1 or 31.8 mL capacity, 1 mm i.d.) equipped with a 9 or 36 W UV-A lamp, a 250 psi BPR and a sample collector for off-line GC analysis.

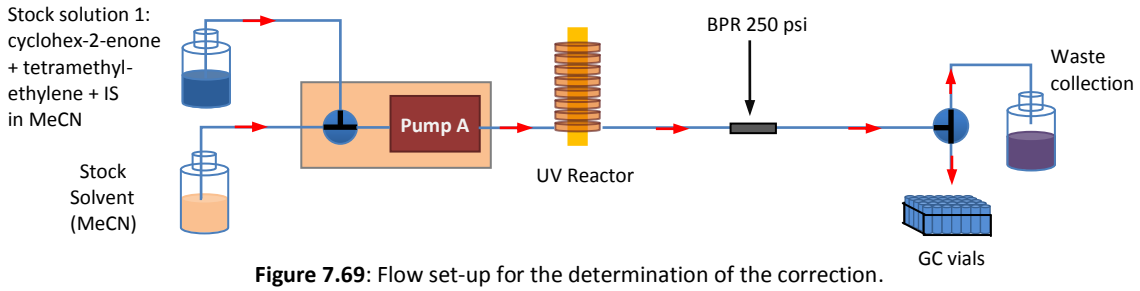

Figure 7.69: Flow set-up for the determination of the correction.

General procedure for the determination of the correction to apply to the turn off light methodology: In a 50 mL flask, cyclohex-2-enone (**5.7a**, 1 equiv.) was mixed with tetramethylethylene (**5.17**, 19.6 equiv.), dibutyl ether as an internal standard and MeCN (Stock solution 1). The reaction mixture was degassed by sonication whilst being saturated with nitrogen. The reaction mixture was injected into the photoflow reactor (UV lamp switched off) until it was entirely filled up. Then, the pump was turned off, the water cooling system was turned on, the indicated UV lamp (Philips 2-pin PL-S 9 W UV-A or Philips 4-pin PL-L 36 W UV-A) was switched on and the reaction was left to proceed during the indicated time. Once the time has passed, the UV lamp was turned off, the feeding valve was returned to the stock solvent, the content of the UV reactor was pushed out (0.5 or 1 mL/min) and it was collected in GC vials. The sampling rate was precisely determined (30 or 45 seconds collection per vial with addition of 1 mL of MeCN). The different samples were then analysed via off-line GC experiments.

General procedure for the processing of the GC data: From each GC spectrum generated, the ratios Peak area cyclohex-2-enone/Peak area IS and Peak area 2 diastereoisomers/Peak area IS were calculated and plotted against the volume eluted. This plot was used as a reference to calculate the efficiency of the UV lamp according to the area in the UV reactor.

Correction to apply to the turn off light methodology for the determination of the optimum reaction time (14.1 mL UV reactor):

Reagent A	Reagent B	Internal Standard	Reaction conditions							
			equiv. A	[A][a] (M)	equiv. B	[B][b] (M)	[IS][c] (M)	Reaction time (min)	UV lamp	UV reactor
		dibutyl ether	1	0.025	19.6	0.50	0.022	60	UV-A 9 W	Single coiled 14.1 mL

[a] [A] Concentration of reagent A in the stock solution 1 (98.7 µL of reagent A were mixed with 0.15 mL of IS, 2.38 mL of pure reagent B and 37.5 mL of MeCN). [b] [B] Concentration of reagent B in the stock solution 1. [c] [IS] Concentration of Internal Standard in the stock solution 1.

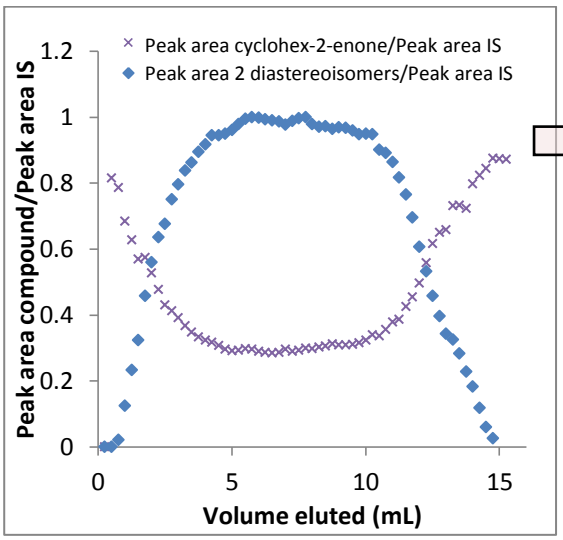

Figure 7.70: GC data (Peak area 2 diastereoisomers/Peak area IS) of the different vials collected at the exit of the reactor.

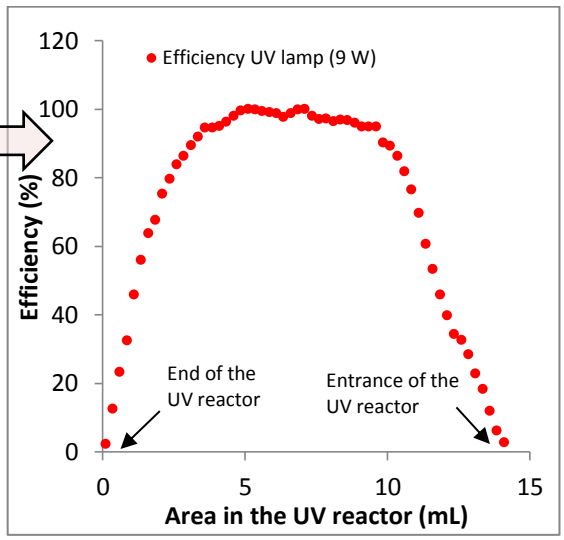

Figure 7.71: Conversion of the GC data into % efficiency of the lamp (normalisation of the max Peak area 2 diastereoisomers/Peak area IS at 100) according to the area in the UV reactor (14.1 mL).

Correction to apply to the turn off light methodology for the determination of the optimum reaction time (31.8 mL UV reactor):

Reagent A	Reagent B	Internal Standard	Reaction conditions							
			equiv. A	[A][a] (M)	equiv. B	[B][b] (M)	[IS][c] (M)	Reaction time (min)	UV lamp	UV reactor
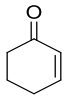		dibutyl ether	1	0.025	19.6	0.50	0.022	30	UV-A 36 W	Single coiled 31.8 mL

[a] [A] Concentration of reagent A in the stock solution 1 (118.3 µL of reagent A were mixed with 0.18 mL of IS, 2.85 mL of pure reagent B and 45 mL of MeCN). [b] [B] Concentration of reagent B in the stock solution 1. [c] [IS] Concentration of Internal Standard in the stock solution 1.

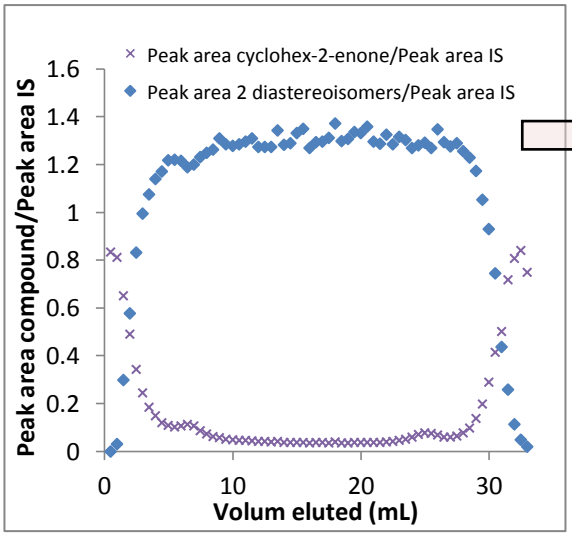

Figure 7.72: GC data (Peak area 2 diastereoisomers/Peak area IS) of the different vials collected at the exit of the reactor.

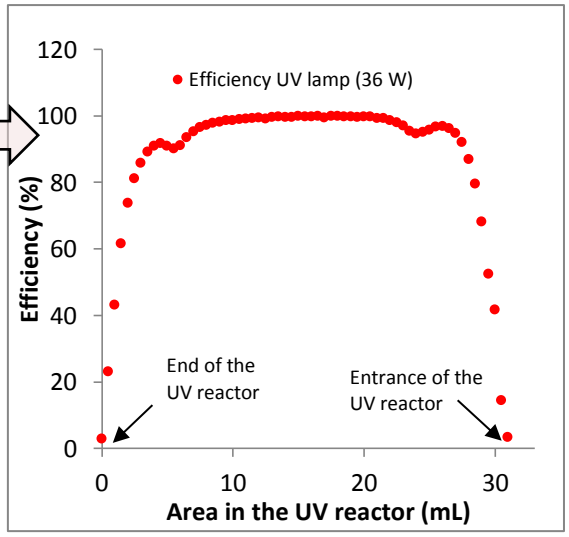

Figure 7.73: Conversion of the GC data into % efficiency of the lamp (inversion of the Peak area cyclohex-2-enone/Peak area IS curve and normalisation of the max at 100) according to the area in the UV reactor (31.8 mL).

7.2.4.3.2 Application of the turn off light methodology

Experimental set-up for the application of the turn off light methodology: Using the flow machine (Vapourtec R2+/R4), the experiments were carried out using one or two pumps, a home-made coiled photoflow reactor (14.1 or 31.8 mL capacity, 1 mm i.d.) equipped with a 9 or 36 W UV lamp (UV-A, B or C), a 250 psi BPR and a sample collector for off-line GC analysis.

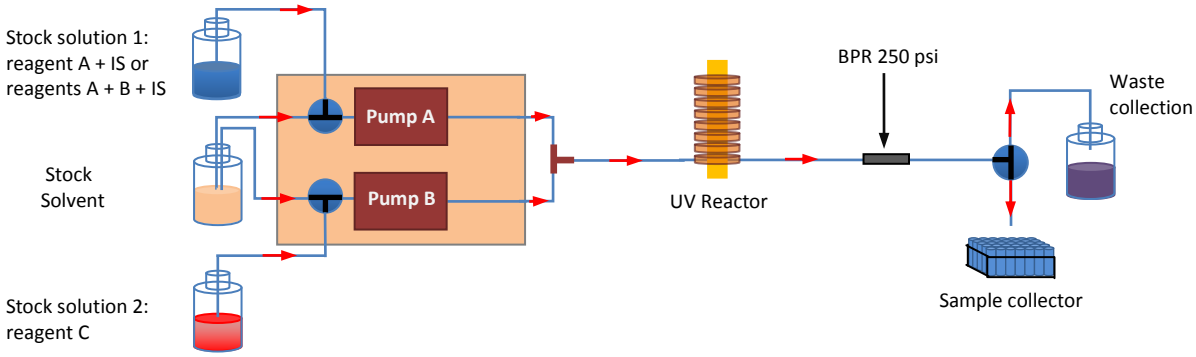

Figure 7.74: Flow set-up for turn off light methodology.

General procedure for the application of the turn off light methodology: In a 50 mL flask, the reagent A or the reagents A + B were mixed with an internal standard and the corresponding solvent (Stock solution 1). When indicated, in another 50 mL flask, the reagent C was mixed with the corresponding solvent (Stock solution 2). Each flask was degassed by sonication whilst being saturated with nitrogen or, when indicated, with O_2. Before starting the reaction, solvent was pumped at the indicated flow rate and the indicated UV lamp (Philips 2-pin PL-S 9 W

UV-A/B or C or Philips 4-pin PL-L 36 W UV-A/B or C) was switched on and left to warm up for 10-15 minutes. The water cooling system was turned on. Once the system was stable, the feeding valves (pump A or, when indicated, pump A and B) were switched to the stock solutions. Once the UV reactor was entirely filled up with the stock solutions, the UV lamp was switched off, the feeding valves were returned to the solvent feed, the content of the UV reactor was pushed out (0.5 or 1 mL/min) and it was collected in GC vials. The sampling rate was precisely determined (30 or 45 seconds collection per vial with addition of 0.5 or 1 mL of solvent). The different samples were then analysed via off-line GC experiments.

General procedure for the processing of the GC data: From each GC spectrum generated, the different ratios Peak area compound/Peak area Internal Standard were calculated and plotted. The conversion and the yield for each GC analysis were calculated using equations 7.7 and 7.8 respectively.

$$\text{Conversion}_t = 1 - \frac{(\text{Peak area reagent A/ Peak area internal standard})_t}{(\text{Peak area reagent A/ Peak area internal standard})_0}$$

Equation 7.7: Formula used for the calculation of the conversion at a given moment.

$$\text{Yield}_t = \frac{\text{n(product)}_t}{\text{n(product)}_{theoretical}} = \frac{[\text{product}]_t \text{ x Volume per GC vial}}{[\text{limiting reagent}]_0 \text{ x Volume collected per GC vial}}$$

Equation 7.8: Formula used for the calculation of the yield at a given moment.

Vial	Weight IS (mg)	Weight products (mg)	Peak area products/Peak area IS	[products]/[IS]
1	3.03	3.88	0.92497	1.53616
2	1.57	3.55	1.63331	2.69157
3	2.89	1.33	0.33242	0.50536
4	1.35	0.85	0.45480	0.75313

IS: dibutyl ether
Products: 7,7,8,8-tetramethylbicyclo[4.2.0]octan-2-one (2 diastereoisomers **5.18** and **5.19**)

$$\frac{\text{Peak area products}}{\text{Peak area IS}} = \frac{\text{K(products)}}{\text{K(IS)}} \text{ x } \frac{[\text{products}]}{[\text{IS}]}$$

K(products)/K(IS) = 1.6583

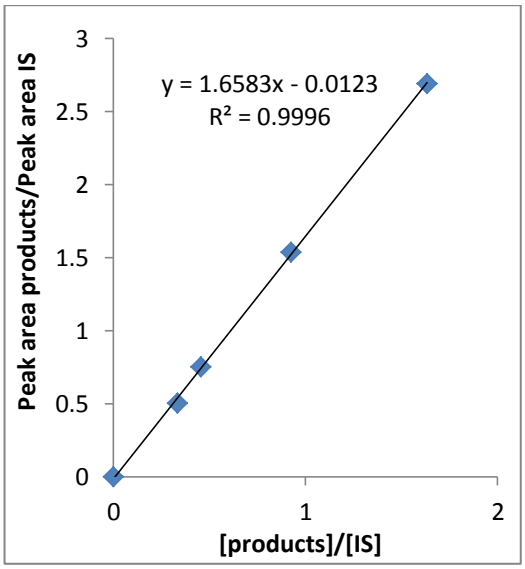

Figure 7.75: Calibration curve for the calculation of the yield$_t$ (7,7,8,8-tetramethylbicyclo[4.2.0]octan-2-one (2 diastereoisomers)).

Vial	Weight IS (mg)	Weight product (mg)	Peak area product/ Peak area IS	[product]/[IS]
1	3.10	1.00	0.36288	0.23570
2	3.50	1.00	0.31694	0.20877
3	5.45	1.02	0.20580	0.13675
4	5.57	1.4	0.27316	0.18366

IS: dibutyl ether
Product: Phenanthrene (**5.23**)

$$\frac{\text{Peak area product}}{\text{Peak area IS}} = \frac{\text{K(product)}}{\text{K(IS)}} \text{ x } \frac{\text{[product]}}{\text{[IS]}}$$

K(product)/K(IS) = 1.5261

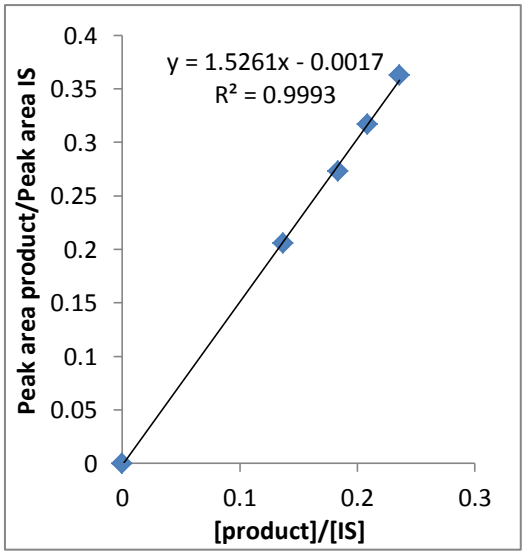

Figure 7.76: Calibration curve for the calculation of the yield$_t$ (phenanthrene).

Vial	Weight IS (mg)	Weight product (mg)	Peak area product/ Peak area IS	[product]/[IS]
1	7.53	2.12	0.42591	0.23424
2	16.20	2.00	0.19354	0.10272
3	25.07	1.27	0.06526	0.04215
4	38.65	1.42	0.04644	0.03057

IS: triethylene glycol dimethyl ether
Product: ethyl 2-cyano-2-(2-cyanophenyl)acetate (**5.32**)

$$\frac{\text{Peak area product}}{\text{Peak area IS}} = \frac{\text{K(product)}}{\text{K(IS)}} \text{ x } \frac{\text{[product]}}{\text{[IS]}}$$

K(product)/K(IS) = 1.849

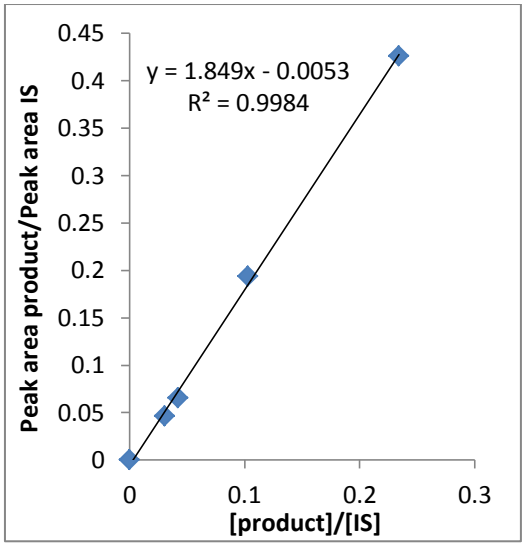

Figure 7.77: Calibration curve for the calculation of the yield$_t$ (ethyl 2-cyano-2-(2-cyanophenyl)acetate).

Turn off light results - [2 + 2] photocycloaddition between cyclohex-2-enone (**5.7a**) and tetramethylethylene (**5.17**)

Table 5.7, entry 1:

Entry	Reagent A	Reagent B	Internal Standard	Reaction conditions								
				equiv. A	[A][a] (M)	equiv. B	[B][b] (M)	[IS][c] (M)	flow rate (mL/min)	Reaction time (min)	UV lamp	UV reactor
1			dibutyl ether	1	0.025	19.6	0.50	0.022	0.058	243	UV-A 9 W	Single coiled 14.1 mL

[a] [A] Concentration of reagent A in the stock solution 1 (98.7 µL of reagent A were mixed with 0.15 mL of IS, 20 mL of reagent B at 1 M in THF and 20 mL of MeCN). [b] [B] Concentration of reagent B in the stock solution 1. [c] [IS] Concentration of Internal Standard in the stock solution 1.

For this experiment, an overview of the data processing was highlighted. This data processing is the same for the series of turn off light experiments described below.

GC vial	Time (min)	Volume in the Reactor (mL)[a]	Reaction Time (min)[b]	Peak area cyclohex-2-enone$_t$	Peak area 2 diastereoisomers$_t$	Peak area open cyclobutane$_t$	Peak area 2 dimers$_t$	Peak area IS$_t$
5	0	14.1	243.10345	0	4.1	0.46	0	2.5
6	0.5	13.85	238.79310	4.8	192.2	24.7	4.3	153.7
7	1	13.6	234.48275	4.3	170.5	21.9	4	134.8
8	1.5	13.35	230.17241	4.3	177.6	22.9	4.3	142.3
9	2	13.1	225.86206	4.2	170.1	21.9	3.9	136.1
10	2.5	12.85	221.55172	4.5	176.8	22.3	4.2	141.5
11	3	12.6	217.24137	4.7	186.6	24	4.7	148.9
12	3.5	12.35	212.93103	4.5	171.4	21.8	4.1	137.5
13	4	12.1	208.62068	4.7	176	22.7	4.2	141.7
14	4.5	11.85	204.31034	5.1	180.9	23.4	4.3	145.2
15	5	11.6	200	5.3	178.2	22.7	4.3	143.7
16	5.5	11.35	195.68965	5.5	175.4	22.7	4.3	141.8
17	6	11.1	191.37931	6	181.1	23.2	4.5	146.3
18	6.5	10.85	187.06896	6.4	177.8	22.8	4.5	144.3
19	7	10.6	182.75862	6.6	172	22	4.2	140.4
20	7.5	10.35	178.44827	7.5	180.3	23.3	4.5	150.4
21	8	10.1	174.13793	7.7	171.7	22	4.4	142
22	8.5	9.85	169.82758	9.2	182.1	23.6	4.7	153.5
23	9	9.6	165.51724	9.4	176.4	22.6	4.5	148
24	9.5	9.35	161.20689	9.7	166.4	21.2	4.2	140.4
25	10	9.1	156.89655	11.6	176.6	22.6	4.6	152.2
26	10.5	8.85	152.58620	12.9	178.7	23.1	4.7	152
27	11	8.6	148.27586	12.4	156.7	20	4.1	137.4
28	11.5	8.35	143.96551	16.2	180.4	23.2	4.9	159.7
29	12	8.1	139.65517	16	162.5	21	4.4	146.4
30	12.5	7.85	135.34482	16.8	156.1	20	4.2	141.8
31	13	7.6	131.03448	19.8	163.4	20.9	4.6	149.6
32	13.5	7.35	126.72413	22.6	166.2	21.3	4.7	156.3
33	14	7.1	122.41379	22	146	18.8	4.1	140.3
34	14.5	6.85	118.10344	25	146.6	18.7	4.1	144.7
35	15	6.6	113.79310	28.7	149.2	19.1	4.4	151.4
36	15.5	6.35	109.48275	32.3	152	19.5	4.5	155.2
37	16	6.1	105.17241	35.8	146.4	18.7	4.4	156.9
38	16.5	5.85	100.86206	38.2	141.2	18.1	4.3	153.5
39	17	5.6	96.55172	39.5	130.1	16.6	4.1	146.9
40	17.5	5.35	92.24137	43.5	126.4	16.2	3.9	151.1
41	18	5.1	87.93103	52.8	133.6	17.2	4.3	164.5
42	18.5	4.85	83.62068	52.5	116.2	14.9	3.8	152.8
43	19	4.6	79.31034	51.8	101.5	13	3.3	140.5
44	19.5	4.35	75	66.1	112.2	14.4	3.7	159.8
45	20	4.1	70.68965	66.7	96	12.3	3.2	152.1
46	20.5	3.85	66.37931	70.4	88.4	11.4	3	146.6
47	21	3.6	62.06896	75.6	79.5	10.3	2.8	149.7
48	21.5	3.35	57.75862	80.4	72	9.2	2.5	147.9
49	22	3.1	53.44827	88.9	64.6	8.3	2.16	154
50	22.5	2.85	49.13793	94.6	56.3	7.2	1.86	153.2
51	23	2.6	44.82758	100.1	48.7	6.3	1.56	154
52	23.5	2.35	40.51724	99.1	40.2	5.1	1.22	146.1
53	24	2.1	36.20689	108.7	34.8	4.4	0.99	153.7
54	24.5	1.85	31.89655	119.7	31	4.1	0.88	160.6
55	25	1.6	27.58620	109.9	22.5	2.9	0.6	140.8
56	25.5	1.35	23.27586	118.2	19.1	2.4	0.26	150.4
57	26	1.1	18.96551	120.2	15.2	1.9	0	148.5
58	26.5	0.85	14.65517	136.2	13	1.7	0	163
59	27	0.6	10.34482	136.6	9.2	1.1	0	158
60	27.5	0.35	6.034482	135.9	6.2	0.78	0	156.8
61	28	0.1	1.724137	131	3.6	0.43	0	152.8
62	28.5	0	0	138	2.06	0.26	0	157.4

Table 7.8: GC data obtained from the different vials. For this experiment, the sampling rate was 0.5 min with a flow rate of collection = 0.5 mL/min (volume collected per GC vial = 0.25 mL) and 1 mL of MeCN was added in each vial before running the GC analysis (volume per GC vial = 1.25 mL). [a] Volume in the reactor = Volume of the reactor - (Time x flow rate of collection) [b] Reaction Time = Volume in the reactor/flow rate of reaction.

GC vial	Reaction Time (min)	(Peak area cyclohex-2-enone/Peak area IS)$_t$	(Peak area 2 diastereo-isomers/Peak area IS)$_t$	(Peak area open cyclobutane/ Peak area IS)$_t$	(Peak area 2 dimer/Peak area IS)$_t$	Conversion$_t$ [a]	[2 dia]$_t$ [b] (M)	n(2 dia)$_t$ [c] (mol)	Yield$_t$ [d]
5	243.1034	0	1.64	0.184	0	1	0.004351	5.4393E-06	0.85996
6	238.7931	0.03123	1.250488	0.160703	0.027977	0.964104	0.003318	4.1474E-06	0.65572
7	234.4828	0.031899	1.264837	0.162463	0.029674	0.963334	0.003356	4.195E-06	0.66324
8	230.1724	0.030218	1.248067	0.160928	0.030218	0.965267	0.003312	4.1394E-06	0.65445
9	225.8621	0.03086	1.249816	0.160911	0.028655	0.964529	0.003316	4.1452E-06	0.65536
10	221.5517	0.031802	1.24947	0.157597	0.029682	0.963446	0.003315	4.1441E-06	0.65518
11	217.2414	0.031565	1.25319	0.161182	0.031565	0.963719	0.003325	4.1564E-06	0.65713
12	212.931	0.032727	1.246545	0.158545	0.029818	0.962382	0.003307	4.1344E-06	0.65365
13	208.6207	0.033169	1.242061	0.160198	0.02964	0.961875	0.003296	4.1195E-06	0.65130
14	204.3103	0.035124	1.245868	0.161157	0.029614	0.959628	0.003306	4.1321E-06	0.65329
15	200	0.036882	1.240084	0.157968	0.029923	0.957606	0.00329	4.1129E-06	0.65026
16	195.6897	0.038787	1.236953	0.160085	0.030324	0.955417	0.003282	4.1025E-06	0.64862
17	191.3793	0.041012	1.237867	0.158578	0.030759	0.95286	0.003284	4.1056E-06	0.64910
18	187.069	0.044352	1.232155	0.158004	0.031185	0.949021	0.003269	4.0866E-06	0.64610
19	182.7586	0.047009	1.225071	0.156695	0.029915	0.945967	0.003251	4.0631E-06	0.64239
20	178.4483	0.049867	1.198803	0.15492	0.02992	0.942682	0.003181	3.976E-06	0.62861
21	174.1379	0.054225	1.209155	0.15493	0.030986	0.937672	0.003208	4.0103E-06	0.63404
22	169.8276	0.059935	1.186319	0.153746	0.030619	0.931109	0.003148	3.9346E-06	0.62207
23	165.5172	0.063514	1.191892	0.152703	0.030405	0.926996	0.003162	3.9531E-06	0.62499
24	161.2069	0.069088	1.185185	0.150997	0.029915	0.920588	0.003145	3.9308E-06	0.62147
25	156.8966	0.076216	1.160315	0.148489	0.030223	0.912396	0.003079	3.8484E-06	0.60843
26	152.5862	0.084868	1.175658	0.151974	0.030921	0.90245	0.003119	3.8992E-06	0.61648
27	148.2759	0.090247	1.140466	0.14556	0.02984	0.896267	0.003026	3.7825E-06	0.59802
28	143.9655	0.10144	1.129618	0.145272	0.030683	0.883402	0.002997	3.7465E-06	0.59233
29	139.6552	0.10929	1.109973	0.143443	0.030055	0.87438	0.002945	3.6814E-06	0.58203
30	135.3448	0.118477	1.100846	0.141044	0.029619	0.86382	0.002921	3.6511E-06	0.57725
31	131.0345	0.132353	1.092246	0.139706	0.030749	0.84787	0.002898	3.6226E-06	0.57274
32	126.7241	0.144594	1.06334	0.136276	0.03007	0.8338	0.002821	3.5267E-06	0.55758
33	122.4138	0.156807	1.040627	0.133999	0.029223	0.819762	0.002761	3.4514E-06	0.54567
34	118.1034	0.172771	1.013131	0.129233	0.028334	0.801412	0.002688	3.3602E-06	0.53125
35	113.7931	0.189564	0.985469	0.126156	0.029062	0.78211	0.002615	3.2685E-06	0.51675
36	109.4828	0.208119	0.979381	0.125644	0.028995	0.760783	0.002599	3.2483E-06	0.51355
37	105.1724	0.228171	0.933078	0.119184	0.028043	0.737735	0.002476	3.0947E-06	0.48927
38	100.8621	0.24886	0.91987	0.117915	0.028013	0.713954	0.002441	3.0509E-06	0.48235
39	96.55172	0.26889	0.885636	0.113002	0.02791	0.690931	0.00235	2.9373E-06	0.46440
40	92.24138	0.287889	0.836532	0.107214	0.025811	0.669093	0.00222	2.7745E-06	0.43865
41	87.93103	0.320973	0.812158	0.104559	0.02614	0.631066	0.002155	2.6936E-06	0.42587
42	83.62069	0.343586	0.760471	0.097513	0.024869	0.605073	0.002018	2.5222E-06	0.39876
43	79.31034	0.368683	0.72242	0.092527	0.023488	0.576226	0.001917	2.396E-06	0.37881
44	75	0.413642	0.702128	0.090113	0.023154	0.524549	0.001863	2.3287E-06	0.36817
45	70.68966	0.438527	0.631164	0.080868	0.021039	0.495946	0.001675	2.0933E-06	0.33096
46	66.37931	0.480218	0.603001	0.077763	0.020464	0.448025	0.0016	1.9999E-06	0.31619
47	62.06897	0.50501	0.531062	0.068804	0.018704	0.419529	0.001409	1.7613E-06	0.27847
48	57.75862	0.543611	0.486815	0.062204	0.016903	0.37516	0.001292	1.6146E-06	0.25527
49	53.44828	0.577273	0.419481	0.053896	0.014026	0.336468	0.001113	1.3913E-06	0.21996
50	49.13793	0.617493	0.367493	0.046997	0.012141	0.290237	0.000975	1.2188E-06	0.19270
51	44.82759	0.65	0.316234	0.040909	0.01013	0.252874	0.000839	1.0488E-06	0.16582
52	40.51724	0.678303	0.275154	0.034908	0.00835	0.220342	0.00073	9.1259E-07	0.14428
53	36.2069	0.707222	0.226415	0.028627	0.006441	0.187101	0.000601	7.5094E-07	0.11872
54	31.89655	0.74533	0.193026	0.025529	0.005479	0.143299	0.000512	6.402E-07	0.10121
55	27.58621	0.78054	0.159801	0.020597	0.004261	0.102828	0.000424	5.3E-07	0.08379
56	23.27586	0.785904	0.126995	0.015957	0.001729	0.096662	0.000337	4.212E-07	0.06659
57	18.96552	0.809428	0.102357	0.012795	0	0.069623	0.000272	3.3948E-07	0.05367
58	14.65517	0.835583	0.079755	0.010429	0	0.03956	0.000212	2.6452E-07	0.04182
59	10.34483	0.864557	0.058228	0.006962	0	0.006256	0.000154	1.9312E-07	0.03053
60	6.034483	0.866709	0.039541	0.004974	0	0.003783	0.000105	1.3114E-07	0.02073
61	1.724138	0.85733	0.02356	0.002814	0	0.014563	6.25E-05	7.8141E-08	0.01235
62	0	0.876747	0.013088	0.001652	0	0	3.5E-05	4.3703E-08	0.00686

Table 7.9: Calculation of the conversion and the yield according to the reaction time.

[a] $\text{Conversion}_t = 1 - \frac{(\text{Peak area cyclohex-2-enone/ Peak area internal standard})_t}{(\text{Peak area cyclohex-2-enone/ Peak area internal standard})_0}$

with (Peak area cyclohex-2-enone/Peak area internal standard)$_0$ = 0.87, determined from a GC of the initial reaction mixture of the reagent with the IS (98.7 µL of reagent A mixed with 0.15 mL of IS, 20 mL of reagent B at 1 M in THF and 20 mL of MeCN).

[b] $[2\ \text{dia}]_t = \left(\frac{\text{Peak area 2 dia}}{\text{Peak area IS}}\right)_t \text{ x } \frac{[\text{IS}]}{\text{K(2 dia)/K(IS)}}$, the concentration of diastereoisomers in the corresponding GC vial.

with K(2 dia)/K(IS) = 1.6583, determined from the calibration curve (Figure 7.75).
[IS] = 0.00440 M, the concentration of IS in the GC vials after addition of 1 mL of MeCN.

[c] $n(2\ \text{dia})_t = [2\ \text{dia}]_t \text{ x Volume per GC vial}$, the amount of diastereoisomers in the corresponding GC vial.

with Volume per GC vial = 1.25 mL.

[d] $\text{Yield}_t = \frac{n(2\ \text{diastereoisomeres})_t}{n(2\ \text{diastereoisomeres})_{theoretical}} = \frac{[2\ \text{dia}]_t \text{ x Volume per GC vial}}{[\text{limiting reagent}]_0 \text{ x Volume collected per GC vial}}$

with $[\text{limiting reagent}]_0$ = $[\text{cyclohex-2-enone}]_0$ = 0.0253 M.
Volume collected per GC vial = 0.25 mL (collection during 30 seconds at 0.5 mL/min).

From Tables 7.8 and 7.9, the following Figure 7.78 was generated.

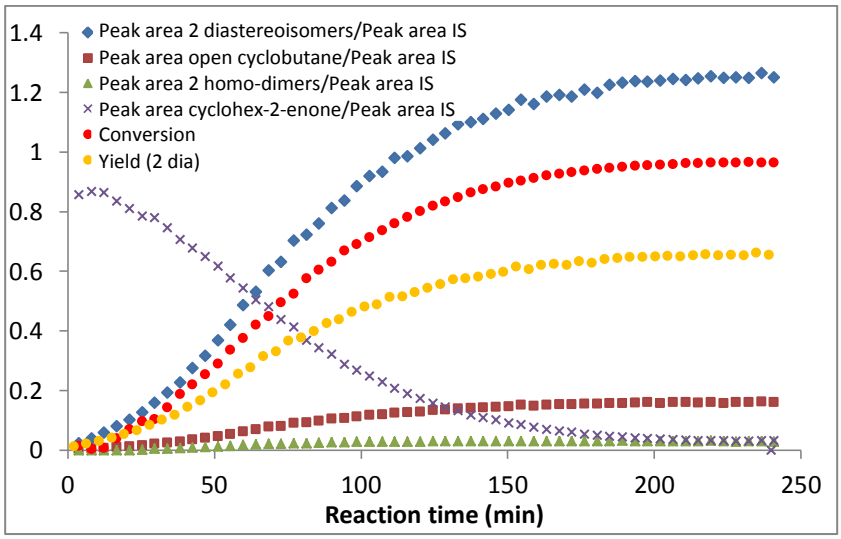

Figure 7.78: Evolution of Peak area compounds/Peak area IS, conversion and yield according to the reaction time (UV-A 9 W).

Finally, using the efficiency of the UV lamp data (Figure 7.71), the corrected reaction time was calculated (Table 7.10) and the final Figure 7.79 was generated.

GC vial	Volume in the reactor (mL)	Reaction Time (min)	Efficiency UV lamp (%)[a]	Corrected reaction time (min)[b]	Conversion$_t$	Yield$_t$
5	14.1	243.1034483	2.624309	176.2850435	1	0.85996
6	13.85	238.7931034	6.060606	176.1719267	0.964104	0.65572
7	13.6	234.4827586	11.80924	175.9106937	0.963334	0.66324
8	13.35	230.1724138	18.26858	175.4016749	0.965267	0.65445
9	13.1	225.862069	22.74395	174.6142363	0.964529	0.65536
10	12.85	221.5517241	28.36538	173.6338937	0.963446	0.65518
11	12.6	217.2413793	32.5835	172.4112479	0.963719	0.65713
12	12.35	212.9310345	34.25224	171.0067865	0.962382	0.65365
13	12.1	208.6206897	39.68579	169.5303968	0.961875	0.65130
14	11.85	204.3103448	45.79243	167.8198023	0.959628	0.65329
15	11.6	200	53.17516	165.8459909	0.957606	0.65026
16	11.35	195.6896552	60.61856	163.5539582	0.955417	0.64862
17	11.1	191.3793103	69.59022	160.9410894	0.95286	0.64910
18	10.85	187.0689655	76.46259	157.9415108	0.949021	0.64610
19	10.6	182.7586207	81.74098	154.6457098	0.945967	0.64239
20	10.35	178.4482759	86.31105	151.1223918	0.942682	0.62861
21	10.1	174.137931	89.20027	147.4020877	0.937672	0.63404
22	9.85	169.8275862	90.05413	143.5572484	0.931109	0.62207

23	9.6	165.5172414	94.80519	139.675605	0.926996	0.62499
24	9.35	161.2068966	94.87179	135.5891741	0.920588	0.62147
25	9.1	156.8965517	94.83261	131.4998726	0.912396	0.60843
26	8.85	152.5862069	95.95668	127.4122603	0.90245	0.61648
27	8.6	148.2758621	96.66667	123.2761966	0.896267	0.59802
28	8.35	143.9655172	96.86221	119.1095299	0.883402	0.59233
29	8.1	139.6551724	96.40387	114.9344347	0.87438	0.58203
30	7.85	135.3448276	97.18111	110.7790953	0.86382	0.57725
31	7.6	131.0344828	97.04433	106.5902542	0.84787	0.57274
32	7.35	126.7241379	97.86293	102.4073088	0.8338	0.55758
33	7.1	122.4137931	100	98.18907889	0.819762	0.54567
34	6.85	118.1034483	99.72087	93.87873406	0.801412	0.53125
35	6.6	113.7931034	98.76118	89.5804209	0.78211	0.51675
36	6.35	109.4827586	97.64997	85.32347332	0.760783	0.51355
37	6.1	105.1724138	98.72611	81.11442293	0.737735	0.48927
38	5.85	100.862069	98.97285	76.85898696	0.713954	0.48235
39	5.6	96.55172414	99.29923	72.59291566	0.690931	0.46440
40	5.35	92.24137931	99.78308	68.31277648	0.669093	0.43865
41	5.1	87.93103448	100	64.01178164	0.631066	0.42587
42	4.85	83.62068966	99.41558	59.70143681	0.605073	0.39876
43	4.6	79.31034483	97.89091	55.41628231	0.576226	0.37881
44	4.35	75	96.12626	51.19684657	0.524549	0.36817
45	4.1	70.68965517	94.95482	47.0534735	0.495946	0.33096
46	3.85	66.37931034	94.53125	42.96059335	0.448025	0.31619
47	3.6	62.06896552	94.41133	38.88597051	0.419529	0.27847
48	3.35	57.75862069	91.78571	34.81651679	0.37516	0.25527
49	3.1	53.44827586	89.40741	30.860236	0.336468	0.21996
50	2.85	49.13793103	86.17318	27.00646844	0.290237	0.19270
51	2.6	44.82758621	83.77358	23.29210704	0.252874	0.16582
52	2.35	40.51724138	79.54545	19.68117666	0.220342	0.14428
53	2.1	36.20689655	75.11848	16.25249327	0.187101	0.11872
54	1.85	31.89655172	67.57143	13.01462761	0.143299	0.10121
55	1.6	27.5862069	63.59551	10.10206603	0.102828	0.08379
56	1.35	23.27586207	55.94615	7.360880445	0.096662	0.06659
57	1.1	18.96551724	45.81498	4.949408545	0.069623	0.05367
58	0.85	14.65517241	32.3765	2.974625011	0.03956	0.04182
59	0.6	10.34482759	23.29131	1.579086132	0.006256	0.03053
60	0.35	6.034482759	12.48357	0.575150475	0.003783	0.02073
61	0.1	1.724137931	2.149791	0.037065379	0.014563	0.01235
62	0	0	0	0	0.014563	0.00686

Table 7.10: Calculation of the corrected reaction time according to the efficiency of the UV lamp (Figure 7.71). [a] Efficiency UV lamp data from Figure 7.71 [b] Corrected reaction $time_{vial\ n}$ = Corrected reaction $time_{vial\ n+1}$ + (reaction $time_{vial\ n}$ – reaction $time_{vial\ n+1}$) x (Efficiency UV $lamp_{vial\ n}$/100).

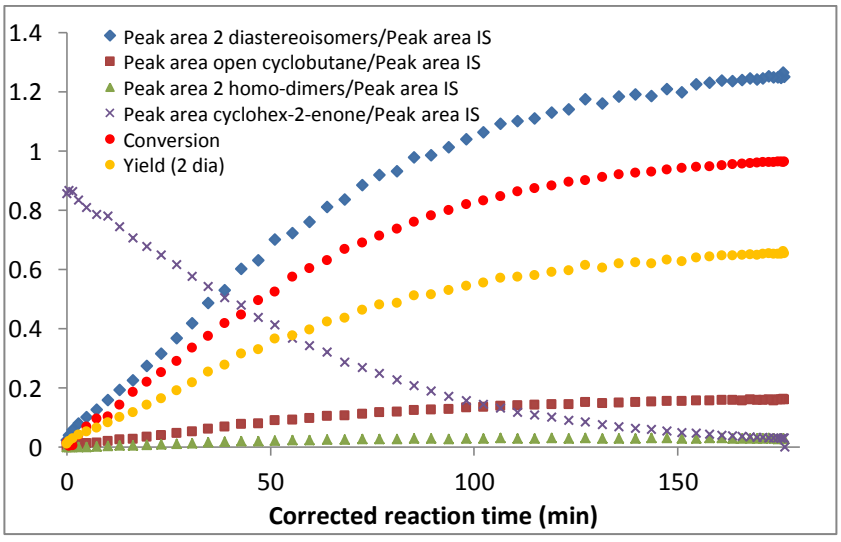

Figure 7.79: Evolution of Peak area compounds/Peak area IS, conversion and yield according to the corrected reaction time (UV-A 9 W).

Table 5.7, entry 2:

Entry	Reagent A	Reagent B	Internal Standard	Reaction conditions								
				equiv. A	[A][a] (M)	equiv. B	[B][b] (M)	[IS][c] (M)	flow rate (mL/min)	Reaction time (min)	UV lamp	UV reactor
2			dibutyl ether	1	0.025	19.6	0.50	0.022	0.058	243	UV-C 9 W	Single coiled 14.1 mL

[a] [A] Concentration of reagent A in the stock solution 1 (98.7 µL of reagent A were mixed with 0.15 mL of IS, 20 mL of reagent B at 1 M in THF and 20 mL of MeCN). [b] [B] Concentration of reagent B in the stock solution 1. [c] [IS] Concentration of Internal Standard in the stock solution 1.

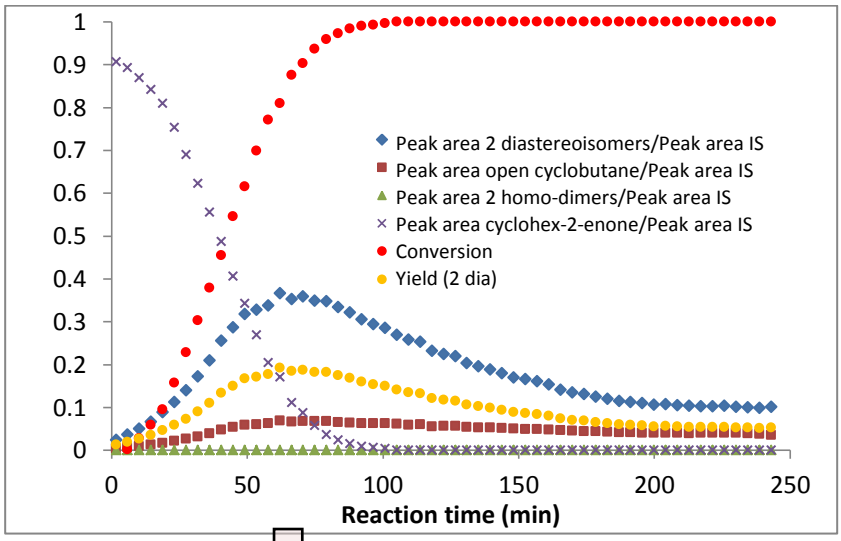

Figure 7.80: Evolution of Peak area compounds/Peak area IS, conversion and yield according to the reaction time (UV-C 9 W).

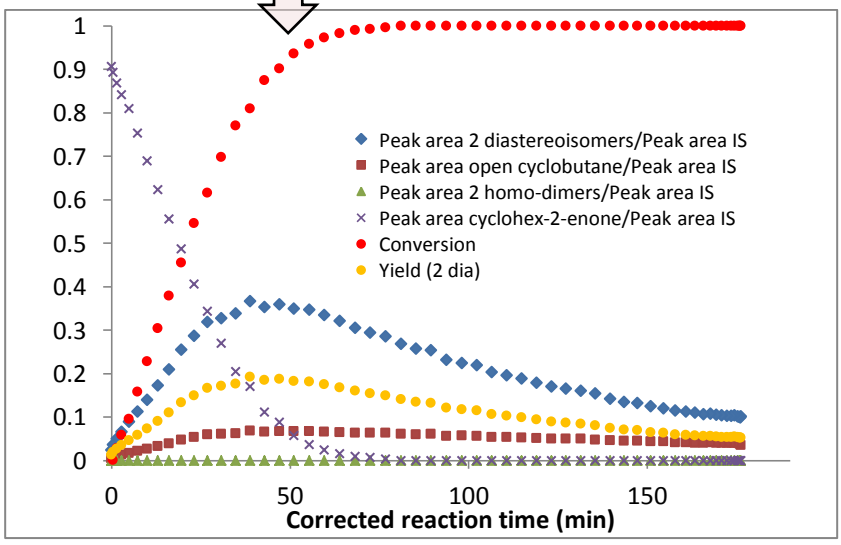

Figure 7.81: Evolution of Peak area compounds/Peak area IS, conversion and yield according to the corrected reaction time (UV-C 9 W).

Table 5.7, entry 3:

Entry	Reagent A	Reagent B	Internal Standard	Reaction conditions								
				equiv. A	[A][a] (M)	equiv. B	[B][b] (M)	[IS][c] (M)	flow rate (mL/min)	Reaction time (min)	UV lamp	UV reactor
3			dibutyl ether	1	0.025	19.6	0.50	0.022	0.133	239	UV-A 36 W	Single coiled 31.8 mL

[a] [A] Concentration of reagent A in the stock solution 1 (125.0 µL of reagent A were mixed with 0.19 mL of IS, 3.01 mL of pure reagent B and 47.9 mL of MeCN). [b] [B] Concentration of reagent B in the stock solution 1. [c] [IS] Concentration of Internal Standard in the stock solution 1.

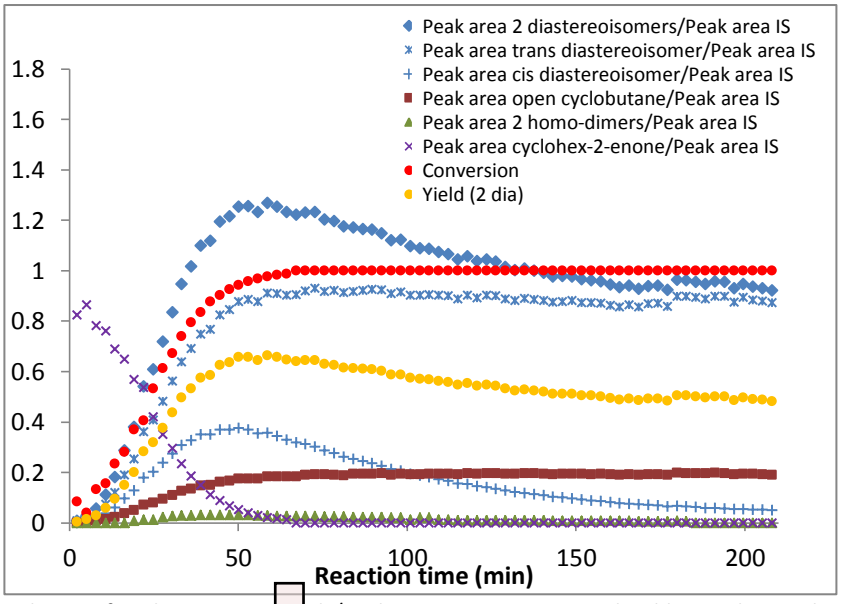

Figure 7.82: Evolution of Peak area compounds/Peak area IS, conversion and yield according to the reaction time (UV-A 36 W).

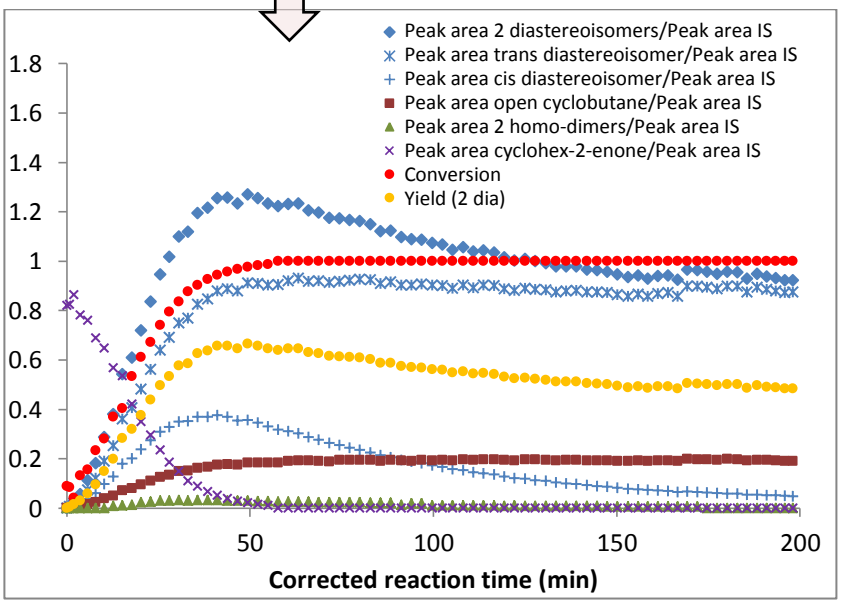

Figure 7.83: Evolution of Peak area compounds/Peak area IS, conversion and yield according to the corrected reaction time (UV-A 36 W).

Table 5.7, entry 4:

Entry	Reagent A	Reagent B	Internal Standard	Reaction conditions								
				equiv. A	[A][a] (M)	equiv. B	[B][b] (M)	[IS][c] (M)	flow rate (mL/min)	Reaction time (min)	UV lamp	UV reactor
4			dibutyl ether	1	0.025	19.6	0.50	0.022	0.133	239	UV-B 36 W	Single coiled 31.8 mL

[a] [A] Concentration of reagent A in the stock solution 1 (125.0 µL of reagent A were mixed with 0.19 mL of IS, 3.01 mL of pure reagent B and 47.9 mL of MeCN). [b] [B] Concentration of reagent B in the stock solution 1. [c] [IS] Concentration of Internal Standard in the stock solution 1.

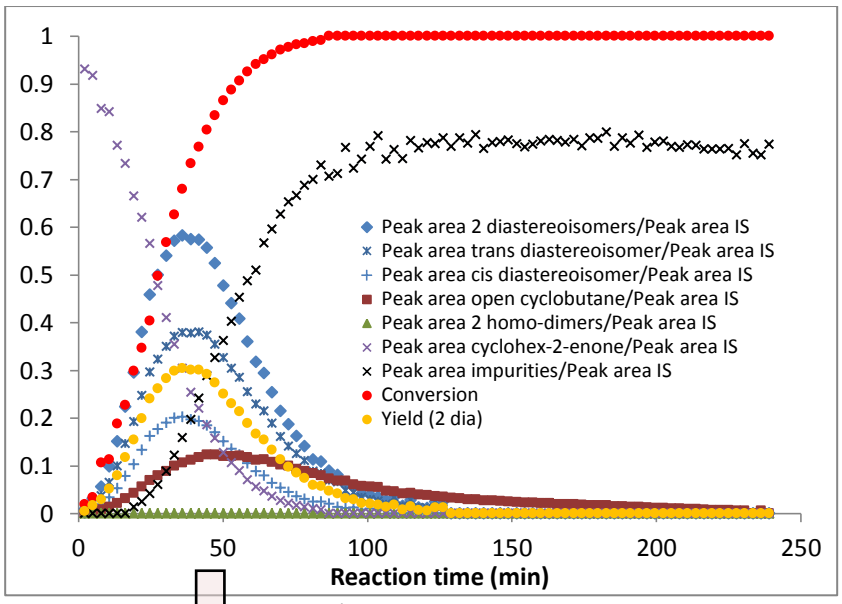

Figure 7.84: Evolution of Peak area compounds/Peak area IS, conversion and yield according to the reaction time (UV-B 36 W).

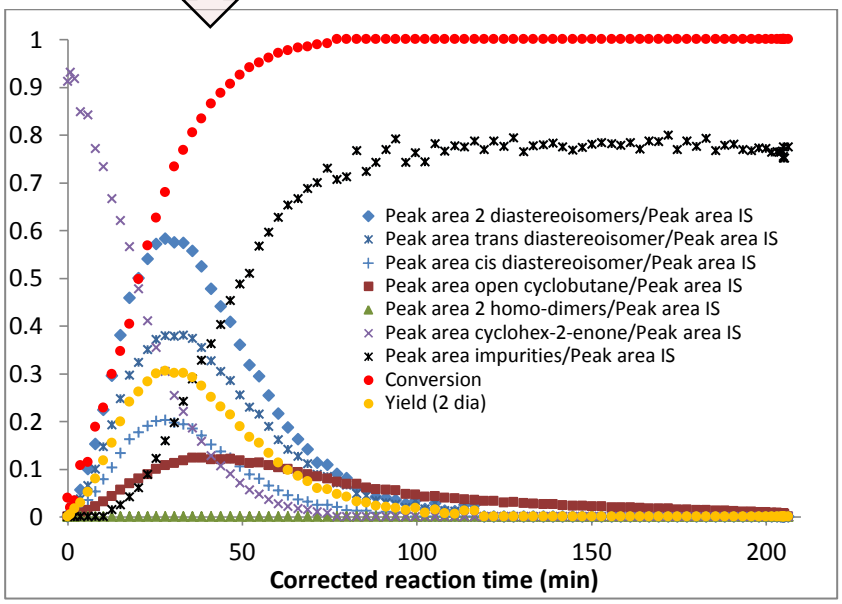

Figure 7.85: Evolution of Peak area compounds/Peak area IS, conversion and yield according to the corrected reaction time (UV-B 36 W).

Table 5.7, entry 5:

Entry	Reagent A	Reagent B	Internal Standard	Reaction conditions								
				equiv. A	[A][a] (M)	equiv. B	[B][b] (M)	[IS][c] (M)	flow rate (mL/min)	Reaction time (min)	UV lamp	UV reactor
5			dibutyl ether	1	0.025	19.6	0.50	0.022	0.133	239	UV-C 36 W	Single coiled 31.8 mL

[a] [A] Concentration of reagent A in the stock solution 1 (125.0 µL of reagent A were mixed with 0.19 mL of IS, 3.01 mL of pure reagent B and 47.9 mL of MeCN). [b] [B] Concentration of reagent B in the stock solution 1. [c] [IS] Concentration of Internal Standard in the stock solution 1.

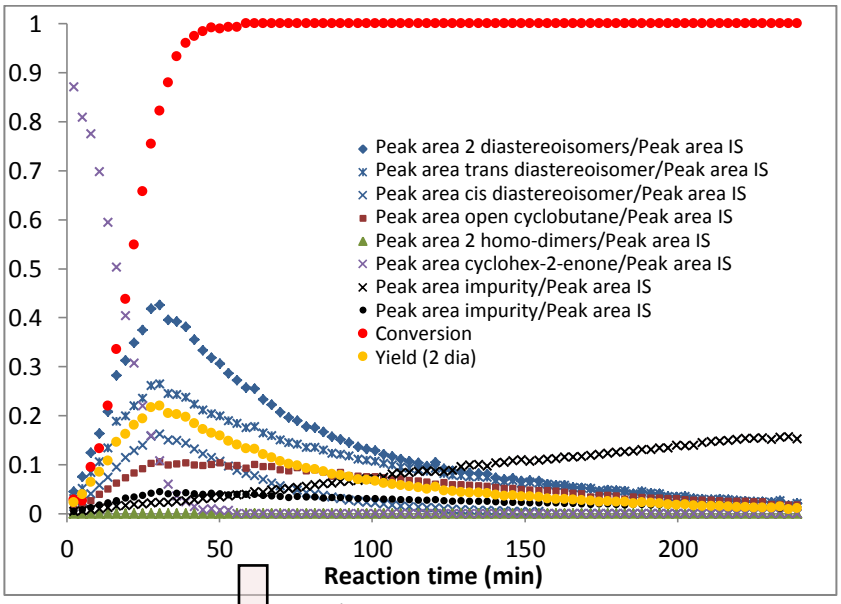

Figure 7.86: Evolution of Peak area compounds/Peak area IS, conversion and yield according to the reaction time (UV-C 36 W).

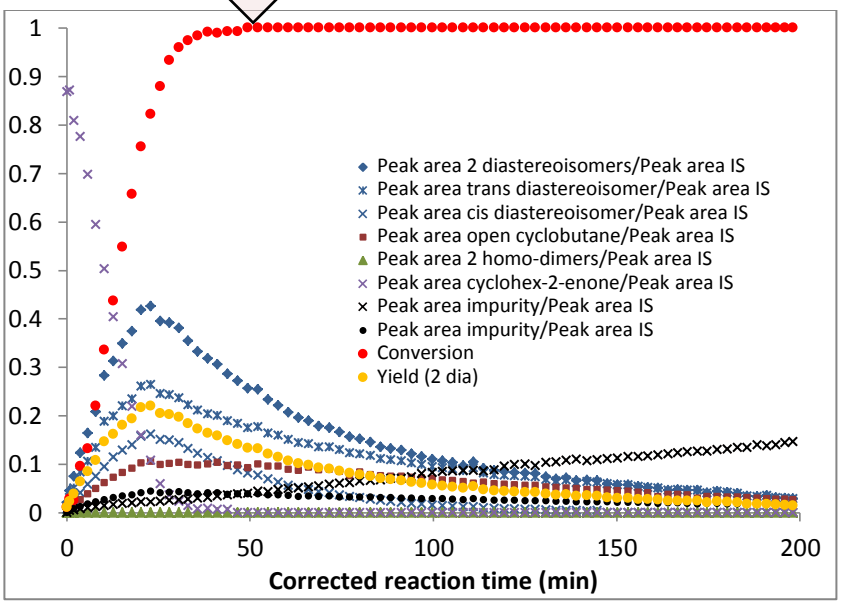

Figure 7.87: Evolution of Peak area compounds/Peak area IS, conversion and yield according to the corrected reaction time (UV-C 36 W).

Turn off light results - [2 + 2] photocycloaddition between 2,2,6-trimethyl-4*H*-11,3-dioxin-4-one (**2.38**) and tetramethylethylene (**5.17**)

Table 5.8, entry 1:

Entry	Reagent A	Reagent B	Internal Standard	Reaction conditions								
				equiv. A	[A][a] (M)	equiv. B	[B][b] (M)	[IS][c] (M)	flow rate (mL/min)	Reaction time (min)	UV lamp	UV reactor
1	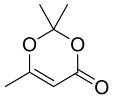		dibutyl ether	1	0.05	20	1	0.044	0.116	120	UV-C 9 W	Single coiled 14.1 mL

[a] [A] Concentration of reagent A in the stock solution 1 (133.6 µL of reagent A were mixed with 0.15 mL of IS, 2.39 mL of pure reagent B and 17.3 mL of MeCN). [b] [B] Concentration of reagent B in the stock solution 1. [c] [IS] Concentration of Internal Standard in the stock solution 1.

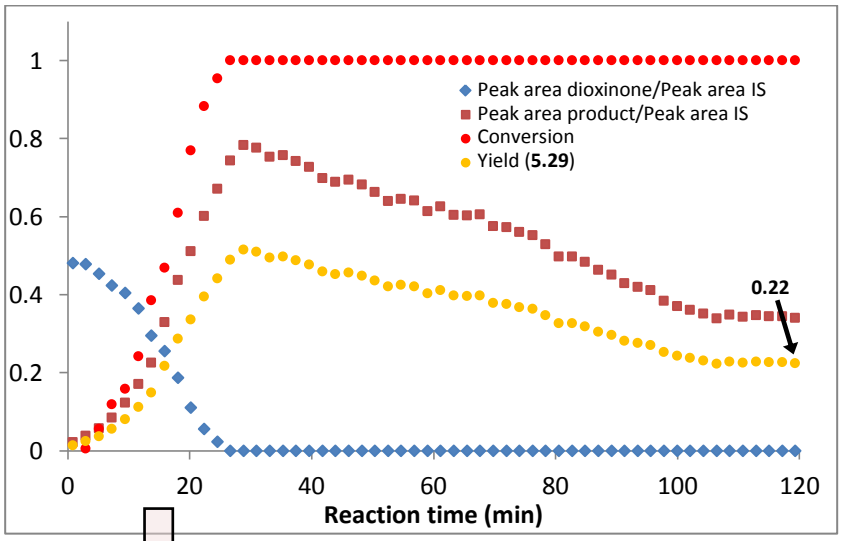

Figure 7.88: Evolution of Peak area compounds/Peak area IS, conversion and yield according to the reaction time (UV-C 9 W). The yield was calculated from the ratio Peak area product/Peak area IS normalised at 0.22 for a reaction time of 120 min. (During the preliminary experiment, the product was isolated in 22% yield after 120 min).

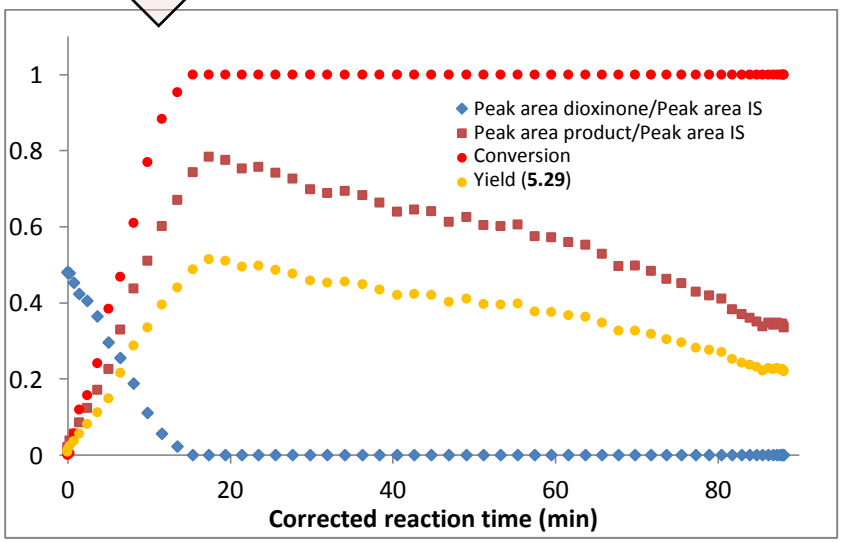

Figure 7.89: Evolution of Peak area compounds/Peak area IS, conversion and yield according to the corrected reaction time (UV-C 9 W).

Turn off light results - Photocyclisation of cis-stilbene

Table 5.9, entry 1:

Entry	Reagent A	Internal Standard	Reaction conditions					
			[A][a] (M)	[IS][b] (M)	flow rate (mL/min)	Reaction time (min)	UV lamp	UV reactor
1	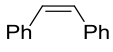	dibutyl ether	0.0050	0.018	0.707	45	UV-A 36 W	Single coiled 31.8 mL

[a] [A] Concentration of reagent A in the stock solution 1 (44.5 µL of reagent A were mixed with 0.15 mL of IS, 6.3 mg of iodine and 50 mL of cyclohexane, solution saturated with O_2). [b] [IS] Concentration of Internal Standard in the stock solution 1.

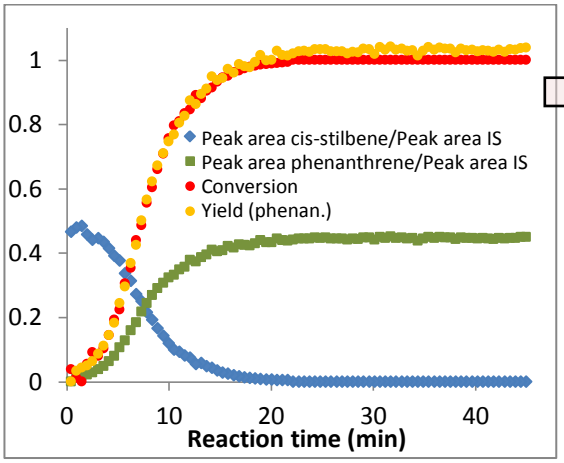

Figure 7.90: Evolution of Peak area compounds/Peak area IS, conversion and yield according to the reaction time (UV-A 36 W).

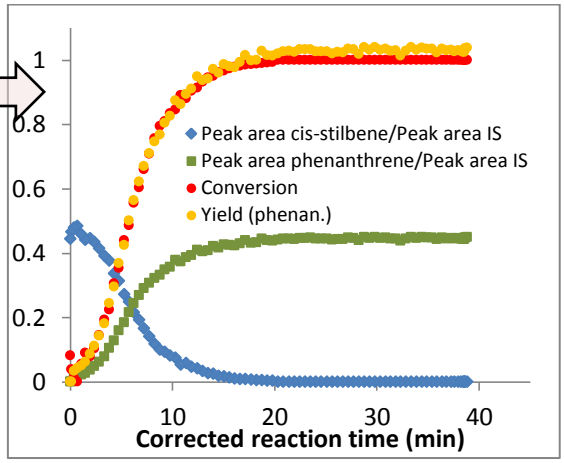

Figure 7.91: Evolution of Peak area compounds/Peak area IS, conversion and yield according to the corrected reaction time (UV-A 36 W).

Table 5.9, entry 2:

Entry	Reagent A	Internal Standard	Reaction conditions					
			[A][a] (M)	[IS][b] (M)	flow rate (mL/min)	Reaction time (min)	UV lamp	UV reactor
2	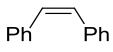	dibutyl ether	0.050	0.18	0.177	180	UV-A 36 W	Single coiled 31.8 mL

[a] [A] Concentration of reagent A in the stock solution 1 (445.0 µL of reagent A were mixed with 1.5 mL of IS, 63 mg of iodine and 48 mL of cyclohexane, solution saturated with O_2). [b] [IS] Concentration of Internal Standard in the stock solution 1.

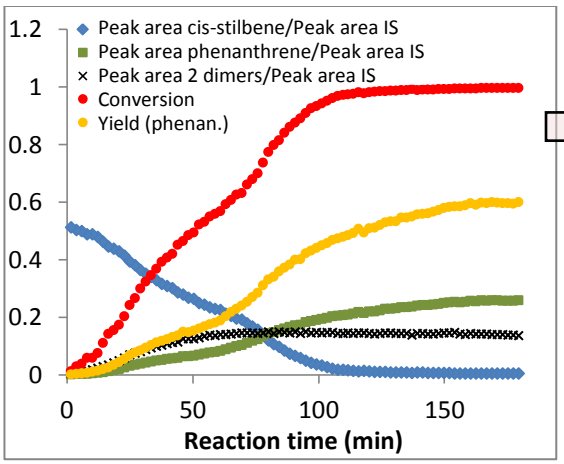

Figure 7.92: Evolution of Peak area compounds/Peak area IS, conversion and yield according to the reaction time (UV-A 36 W).

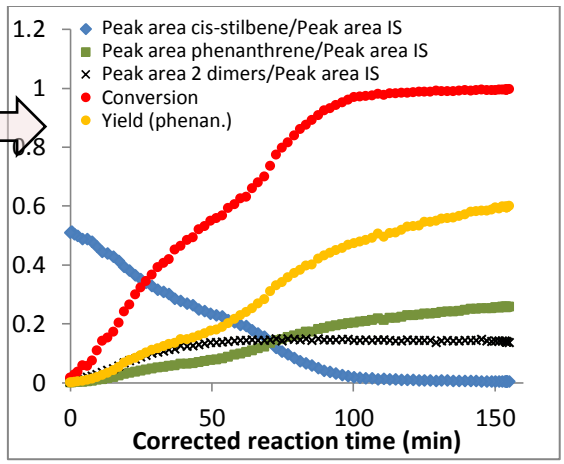

Figure 7.93: Evolution of Peak area compounds/Peak area IS, conversion and yield according to the corrected reaction time (UV-A 36 W).

Table 5.9, entry 3:

Entry	Reagent A	Internal Standard	Reaction conditions					
			[A][a] (M)	[IS][b] (M)	flow rate (mL/min)	Reaction time (min)	UV lamp	UV reactor
3	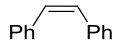	dibutyl ether	0.0050	0.018	0.707	45	UV-B 36 W	Single coiled 31.8 mL

[a] [A] Concentration of reagent A in the stock solution 1 (44.5 µL of reagent A were mixed with 0.15 mL of IS, 6.3 mg of iodine and 50 mL of cyclohexane, solution saturated with O_2). [b] [IS] Concentration of Internal Standard in the stock solution 1.

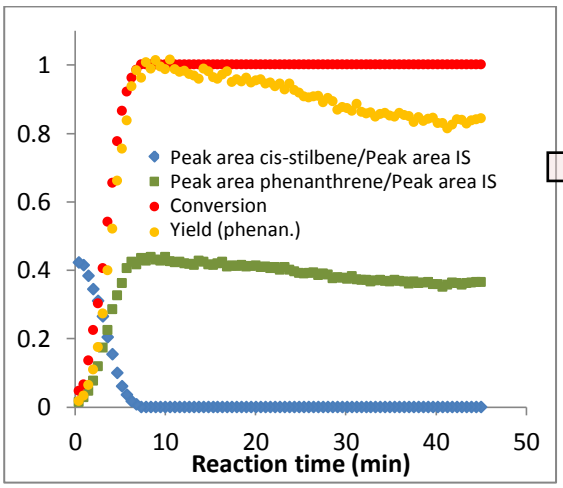

Figure 7.94: Evolution of Peak area compounds/Peak area IS, conversion and yield according to the reaction time (UV-B 36 W).

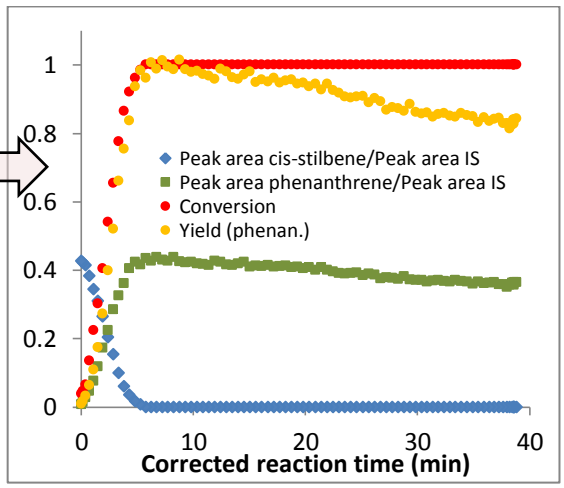

Figure 7.95: Evolution of Peak area compounds/Peak area IS, conversion and yield according to the corrected reaction time (UV-B 36 W).

Table 5.9, entry 4:

Entry	Reagent A	Internal Standard	Reaction conditions					
			[A][a] (M)	[IS][b] (M)	flow rate (mL/min)	Reaction time (min)	UV lamp	UV reactor
4	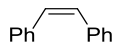	dibutyl ether	0.050	0.18	0.177	180	UV-B 36 W	Single coiled 31.8 mL

[a] [A] Concentration of reagent A in the stock solution 1 (445.0 µL of reagent A were mixed with 1.5 mL of IS, 63 mg of iodine and 48 mL of cyclohexane, solution saturated with O_2). [b] [IS] Concentration of Internal Standard in the stock solution 1.

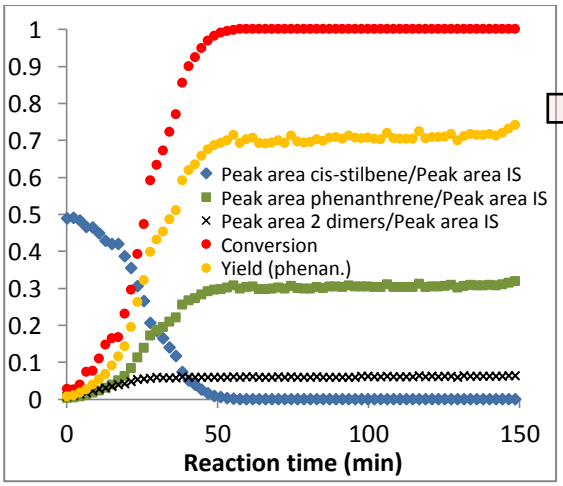

Figure 7.96: Evolution of Peak area compounds/Peak area IS, conversion and yield according to the reaction time (UV-B 36 W).

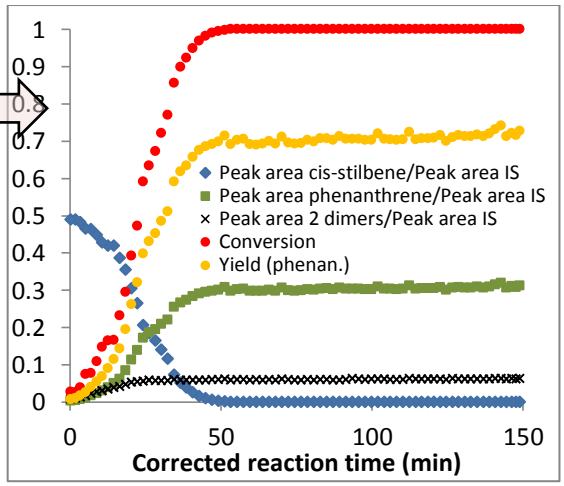

Figure 7.97: Evolution of Peak area compounds/Peak area IS, conversion and yield according to the corrected reaction time (UV-B 36 W).

Table 5.9, entry 5:

Entry	Reagent A	Internal Standard	Reaction conditions					
			[A][a] (M)	[IS][b] (M)	flow rate (mL/min)	Reaction time (min)	UV lamp	UV reactor
5	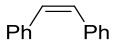	dibutyl ether	0.0050	0.018	0.707	45	UV-C 36 W	Single coiled 31.8 mL

[a] [A] Concentration of reagent A in the stock solution 1 (44.5 µL of reagent A were mixed with 0.15 mL of IS, 6.1 mg of iodine and 50 mL of cyclohexane, solution saturated with O_2). [b] [IS] Concentration of Internal Standard in the stock solution 1.

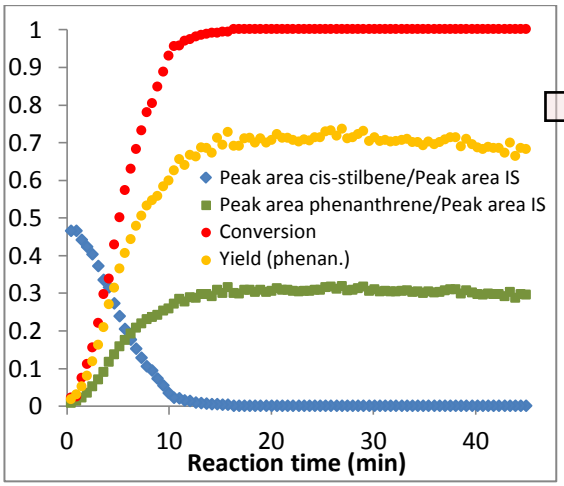

Figure 7.98: Evolution of Peak area compounds/Peak area IS, conversion and yield according to the reaction time (UV-C 36 W).

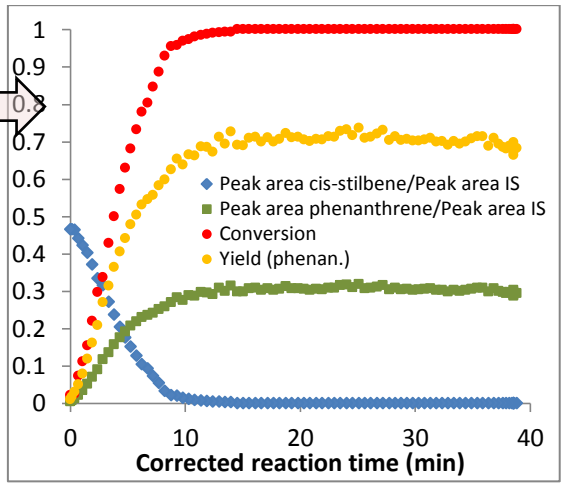

Figure 7.99: Evolution of Peak area compounds/Peak area IS, conversion and yield according to the corrected reaction time (UV-C 36 W).

Table 5.9, entry 6:

Entry	Reagent A	Internal Standard	Reaction conditions					
			[A][a] (M)	[IS][b] (M)	flow rate (mL/min)	Reaction time (min)	UV lamp	UV reactor
6	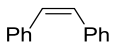	dibutyl ether	0.050	0.18	0.177	180	UV-C 36 W	Single coiled 31.8 mL

[a] [A] Concentration of reagent A in the stock solution 1 (445.0 µL of reagent A were mixed with 1.5 mL of IS, 67 mg of iodine and 48 mL of cyclohexane, solution saturated with O_2). [b] [IS] Concentration of Internal Standard in the stock solution 1.

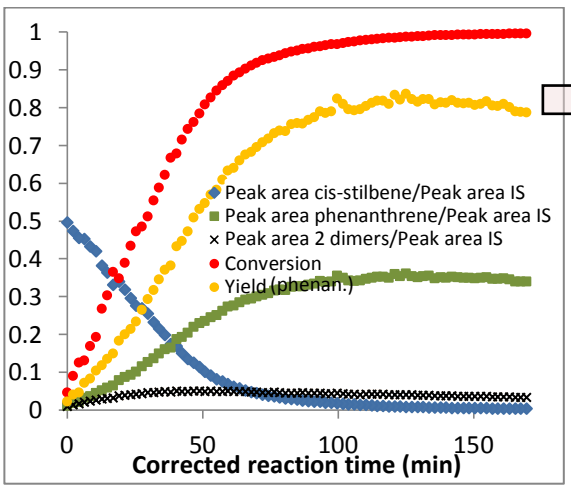

Figure 7.100: Evolution of Peak area compounds/Peak area IS, conversion and yield according to the reaction time (UV-C 36 W).

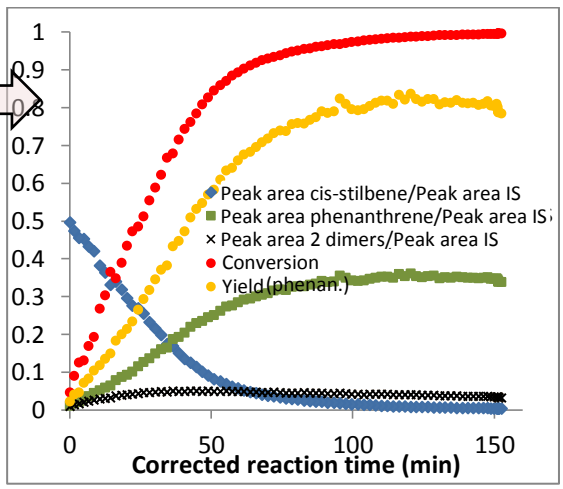

Figure 7.101: Evolution of Peak area compounds/Peak area IS, conversion and yield according to the corrected reaction time (UV-C 36 W).

Turn off light results - $S_{RN}1$ reaction

Table 5.10:

Reaction conditions											
Reagent A		Reagent B		IS		Reagent C			Reaction time (min)	UV lamp	UV reactor[e]
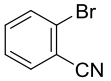		*t*-BuOK		Triethylene glycol dimethyl ether		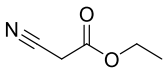					
Stock solution 1						Stock solution 2					
equiv. A	[A][a] (M)	equiv. B	[B][b] (M)	[IS][c] (M)	flow rate (mL/min)	equiv. C	[C][d] (M)	flow rate (mL/min)			
1	0.080	4	0.32	0.092	0.133	4	0.32	0.133	120	UV-B 36 W	Single Coiled 31.8 mL

[a] [A] Concentration of reagent A in the stock solution 1 (437 mg of reagent A were mixed with 1078 mg of *t*-BuOK, 0.5 mL of IS and 29.5 mL of DMSO). [b] [B] Concentration of reagent B in the stock solution 1. [c] [IS] Concentration of IS in the stock solution 1. [d] [C] Concentration of reagent C in the stock solution 2 (1.0 mL of reagent C was mixed with 29 mL of DMSO). [e] At the end of the UV reactor and before the collection in the GC vials, a flow of a solution of TFA in DMSO (5.1 mL of TFA in 200 mL of DMSO, same flow as the one inside the UV reactor) was injected in the reaction mixture.

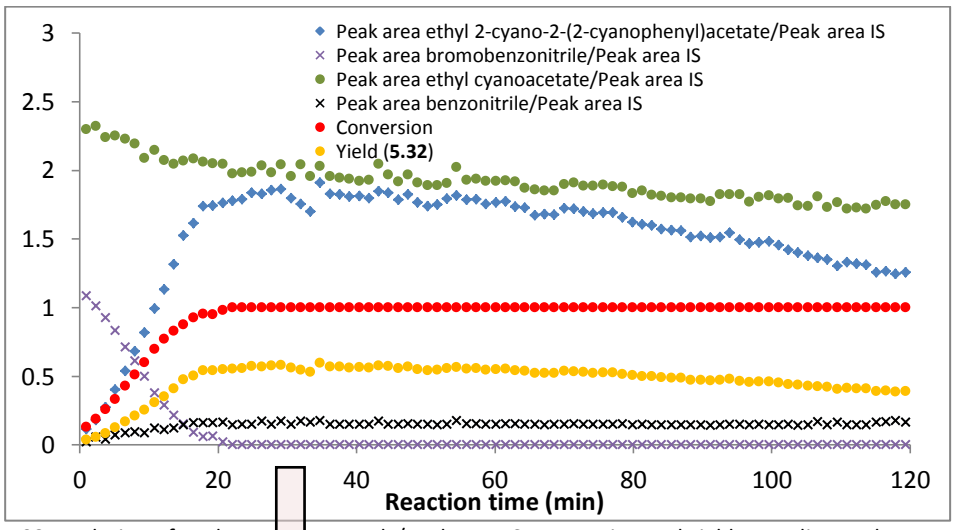

Figure 7.102: Evolution of Peak area compounds/Peak area IS, conversion and yield according to the reaction time (UV-B 36 W).

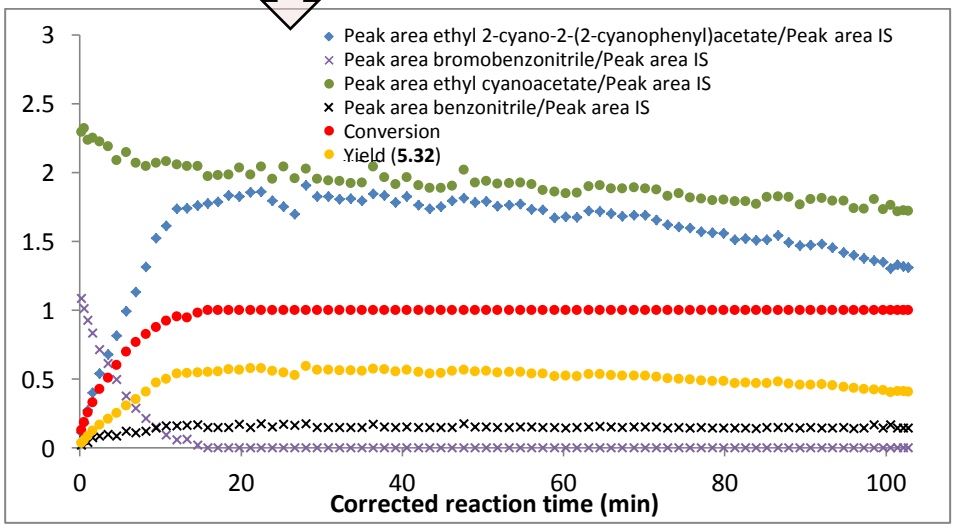

Figure 7.103: Evolution of Peak area compounds/Peak area IS, conversion and yield according to the corrected reaction time (UV-B 36 W).

8 References

1. Ley, S. V.; Baxendale, I. R., *Chimia* **2008,** *62* (3), 162-168.
2. (a) Riva, E.; Rencurosi, A.; Gagliardi, S.; Passarella, D.; Martinelli, M., *Chem. Eur. J.* **2011,** *17* (22), 6221-6226; (b) Newton, S.; Carter, C. F.; Pearson, C. M.; Alves, L. D.; Lange, H.; Thansandote, P.; Ley, S. V., *Angew. Chem., Int. Ed.* **2014,** *53* (19), 4915-4920.
3. Pashkova, A.; Greiner, L., *Chem. Ing. Tech.* **2011,** *83* (9), 1337-1342.
4. www.reaxys.com.
5. (a) Ahmed-Omer, B.; Brandt, J. C.; Wirth, T., *Org. Biomol. Chem.* **2007,** *5* (5), 733-740; (b) Mason, B. P.; Price, K. E.; Steinbacher, J. L.; Bogdan, A. R.; McQuade, D. T., *Chem. Rev.* **2007,** *107* (6), 2300-2318; (c) Ley, S. V., *Chem. Rec.* **2012,** *12* (4), 378-390.
6. Kulkarni, A. A., *Beilstein J. Org. Chem.* **2014,** *10*, 405-424.
7. (a) Leforestier, B.; Vogtle, M., *Synlett* **2016,** *27* (13), 1957-1962; (b) Baumann, M.; Baxendale, I. R.; Ley, S. V.; Nikbin, N.; Smith, C. D.; Tierney, J. P., *Org. Biomol. Chem.* **2008,** *6* (9), 1577-1586.
8. Harrowven, D. C.; Mohamed, M.; Goncalves, T. P.; Whitby, R. J.; Bolien, D.; Sneddon, H. F., *Angew. Chem., Int. Ed.* **2012,** *51* (18), 4405-4408.
9. www.vapourtec.com.
10. www.syrris.com.
11. www.uniqsis.com.
12. www.thalesnano.com.
13. (a) Kawaguchi, T.; Miyata, H.; Ataka, K.; Mae, K.; Yoshida, J., *Angew. Chem., Int. Ed.* **2005,** *44* (16), 2413-2416; (b) Ducry, L.; Roberge, D. M., *Org. Process Res. Dev.* **2008,** *12* (2), 163-167.
14. Mozharov, S.; Nordon, A.; Littlejohn, D.; Wiles, C.; Watts, P.; Dallin, P.; Girkin, J. M., *J. Am. Chem. Soc.* **2011,** *133* (10), 3601-3608.
15. Midorikawa, K.; Suga, S.; Yoshida, J., *Chem. Commun.* **2006,** (36), 3794-3796.
16. Nagaki, A.; Togai, M.; Suga, S.; Aoki, N.; Mae, K.; Yoshida, J., *J. Am. Chem. Soc.* **2005,** *127* (33), 11666-11675.
17. Baxendale, I. R.; Griffiths-Jones, C. M.; Ley, S. V.; Tranmer, G. K., *Chem. Eur. J.* **2006,** *12* (16), 4407-4416.
18. Fukuyama, T.; Shinmen, M.; Nishitani, S.; Sato, M.; Ryu, I., *Org. Lett.* **2002,** *4* (10), 1691-1694.
19. Liu, S. F.; Fukuyama, T.; Sato, M.; Ryu, I., *Org. Process Res. Dev.* **2004,** *8* (3), 477-481.
20. (a) Odille, F. G. J.; Stenemyr, A.; Ponten, F., *Org. Process Res. Dev.* **2014,** *18* (11), 1545-1549; (b) Brodmann, T.; Koos, P.; Metzger, A.; Knochel, P.; Ley, S. V., *Org. Process Res. Dev.* **2012,** *16* (5), 1102-1113.
21. Fernandez-Suarez, M.; Wong, S. Y. F.; Warrington, B. H., *Lab Chip* **2002,** *2* (3), 170-174.
22. Kim, H.; Nagaki, A.; Yoshida, J., *Nat. Commun.* **2011,** *2*.
23. Nagaki, A.; Kim, H.; Yoshida, J.-i., *Angew. Chem., Int. Ed.* **2008,** *47* (41), 7833-7836.
24. (a) Yoshida, J.-i.; Kim, H.; Nagaki, A., *Chemsuschem* **2011,** *4* (3), 331-340; (b) Nagaki, A.; Kim, H.; Yoshida, J.-i., *Angew. Chem., Int. Ed.* **2009,** *48* (43), 8063-8065.
25. (a) Belardi, J. K.; Micalizio, G. C., *Angew. Chem., Int. Ed.* **2008,** *47* (21), 4005-4008; (b) Canova, S.; Bellosta, V.; Bigot, A.; Mailliet, P.; Mignani, S.; Cossy, J., *Org. Lett.* **2007,** *9* (1), 145-148.
26. Bell, P. J. L.; Karuso, P., *J. Am. Chem. Soc.* **2003,** *125* (31), 9304-9305.
27. Choi, H. Y.; Veal, D. A.; Karuso, P., *J. Fluoresc.* **2006,** *16* (4), 475-482.
28. Chatterjee, S.; Karuso, P.; Boulange, A.; Franck, X.; Datta, A., *J. Phys. Chem. B* **2015,** *119* (20), 6295-6303.

29. Peixoto, P. A.; Boulange, A.; Ball, M.; Naudin, B.; Alle, T.; Cosette, P.; Karuso, P.; Franck, X., *J. Am. Chem. Soc.* **2014,** *136* (43), 15248-15256.
30. Peixoto, P. A.; Boulange, A.; Leleu, S.; Franck, X., *Eur. J. Org. Chem.* **2013,** (16), 3316-3327.
31. (a) Boulange, A., *PhD Thesis, University of Rouen* **2012**; (b) Peixoto, P., *PhD Thesis, University of Rouen* **2009**.
32. Katritzky, A. R.; Wang, Z. Q.; Wang, M. Y.; Hall, C. D.; Suzuki, K., *J. Org. Chem.* **2005,** *70* (12), 4854-4856.
33. Boulange, A.; Peixoto, P. A.; Franck, X., *Chem. Eur. J.* **2011,** *17* (37), 10241-10245.
34. Ramozzi, R.; Cheron, N.; Braida, B.; Hiberty, P. C.; Fleurat-Lessard, P., *New J. Chem.* **2012,** *36* (5), 1137-1140.
35. Ugi, S.; Werner, B.; Dömling, A., *Molecules* **2003,** *8*, 53-66.
36. Stephany, R. W.; Bie, M.; Drenth, W., *Org. Magn. Resonance* **1974,** *6* (1), 45-47.
37. Lieke, W., *Justus Liebigs Ann. Chem.* **1859,** *112* (3), 316-321.
38. Gautier, A., *Justus Liebigs Ann. Chem.* **1867,** *142* (3), 289-294.
39. Hofmann, A. W., *Justus Liebigs Ann. Chem.* **1867,** *144* (1), 114-120.
40. Grolla, A. A.; Podesta, V.; Chini, M. G.; Di Micco, S.; Vallario, A.; Genazzani, A. A.; Canonico, P. L.; Bifulco, G.; Tron, G. C.; Sorba, G.; Pirali, T., *J. Med. Chem.* **2009,** *52* (9), 2776-2785.
41. Desai, B.; Danks, T. N.; Wagner, G., *Tetrahedron Lett.* **2005,** *46* (6), 955-957.
42. Ugi, I.; Meyr, R., *Angew. Chem.* **1958,** *70* (22-23), 702-703.
43. Appel, R.; Kleinstuck, R.; Ziehn, K. D., *Angew. Chem., Int. Ed.* **1971,** *10* (2), 132.
44. Creedon, S. M.; Crowley, H. K.; McCarthy, D. G., *J. Chem. Soc., Perkin Trans. 1* **1998,** (6), 1015-1017.
45. Baldwin, J. E.; Oneil, I. A., *Synlett* **1990,** (10), 603-604.
46. Porcheddu, A.; Giacomelli, G.; Salaris, M., *J. Org. Chem.* **2005,** *70* (6), 2361-2363.
47. Kobayashi, G.; Saito, T.; Kitano, Y., *Synthesis-Stuttgart* **2011,** (20), 3225-3234.
48. Skorna, G.; Ugi, I., *Angew. Chem., Int. Ed. Engl.* **1977,** *16* (4), 259-260.
49. (a) Eckert, H.; Forster, B., *Angew. Chem., Int. Ed. Engl.* **1987,** *26* (9), 894-895; (b) Lopez, O.; Maza, S.; Ulgar, V.; Maya, I.; Fernandez-Bolanos, J. G., *Tetrahedron* **2009,** *65* (12), 2556-2566.
50. Weber, W. P.; Ugi, I. K.; Gokel, G. W., *Angew. Chem., Int. Ed.* **1972,** *11* (6), 530-531.
51. Okada, I.; Kitano, Y., *Synthesis-Stuttgart* **2011,** (24), 3997-4002.
52. Pirrung, M. C.; Ghorai, S., *J. Am. Chem. Soc.* **2006,** *128* (36), 11772-11773.
53. Ley, S. V.; Taylor, S. J., *Bioorg. Med. Chem. Lett.* **2002,** *12* (14), 1813-1816.
54. Gassman, P. G.; Guggenheim, T. L., *J. Am. Chem. Soc.* **1982,** *104* (21), 5849-5850.
55. Barton, D. H. R.; Bowles, T.; Husinec, S.; Forbes, J. E.; Llobera, A.; Porter, A. E. A.; Zard, S. Z., *Tetrahedron Lett.* **1988,** *29* (27), 3343-3346.
56. Passerini, M.; Simone, L., *Gazz. Chim. Ital.* **1921,** *51*, 126-129.
57. Faure, S.; Hjelmgaard, T.; Roche, S. P.; Aitken, D. J., *Org. Lett.* **2009,** *11* (5), 1167-1170.
58. Ugi, I.; Meyr, R.; Fetzer, U.; Steinbriickner, C., *Angew. Chem.* **1959,** *71* (11), 386.
59. Domling, A.; Ugi, I., *Angew. Chem., Int. Ed.* **2000,** *39* (18), 3168-3210.
60. Baumann, M.; Baxendale, I. R.; Ley, S. V.; Smith, C. D.; Tranmer, G. K., *Org. Lett.* **2006,** *8* (23), 5231-5234.
61. Bremner, W. S.; Organ, M. G., *J. Comb. Chem.* **2007,** *9* (1), 14-16.
62. Sharma, S.; Maurya, R. A.; Min, K. I.; Jeong, G. Y.; Kim, D. P., *Angew. Chem., Int. Ed.* **2013,** *52* (29), 7564-7568.
63. Salvador, C. E. M.; Pieber, B.; Neu, P. M.; Torvisco, A.; Andrade, C. K. Z.; Kappe, C. O., *J. Org. Chem.* **2015,** *80* (9), 4590-4602.
64. Birney, D. M.; Wiberg, K. B.; Berson, J. A., *J. Am. Chem. Soc.* **1988,** *110* (20), 6631-6642.
65. Birney, D. M.; Berson, J. A., *J. Am. Chem. Soc.* **1985,** *107* (15), 4553-4554.

66. (a) Simpson, C.; Price, J.; Holmes, G.; Adam, W.; Martin, H. D.; Bish, S., *J. Am. Chem. Soc.* **1990,** *112* (13), 5089-5094; (b) Buxton, J. P.; Simpson, C., *Chem. Phys.* **1986,** *105* (3), 307-316.
67. Birney, D. M.; Berson, J. A., *Tetrahedron* **1986,** *42* (6), 1561-1570.
68. Story, P. R.; Fahrenholtz, S. R., *Org. Synth.* **1964,** *44*, 12.
69. Story, P. R., *J. Org. Chem.* **1961,** *26* (2), 287-290.
70. Sletten, E. M.; Bertozzi, C. R., *J. Am. Chem. Soc.* **2011,** *133* (44), 17570-17573.
71. Lustgart. Rk; Winstein, S.; Brookhar.M, *J. Am. Chem. Soc.* **1972,** *94* (7), 2347-2363.
72. Srinivasu, P.; Gupta, S., *Patent* **2012**.
73. Tanida, H.; Tsuji, T., *J. Org. Chem.* **1964,** *29* (4), 849-852.
74. Bentley, T. W.; Llewellyn, G.; Norman, S. J.; Kemmer, R.; Kunz, U.; Christl, M., *Liebigs Ann. Recl.* **1997,** (1), 229-244.
75. Baird, W. C., *J. Org. Chem.* **1966,** *31* (7), 2411-2414.
76. Benito-Lopez, F.; Verboom, W.; Kakuta, M.; Gardeniers, J. G. E.; Egberink, R. J. M.; Oosterbroek, E. R.; van den Berg, A.; Reinhoudt, D. N., *Chem. Commun.* **2005,** (22), 2857-2859.
77. (a) Herzig-Marx, R.; Queeney, K. T.; Jackman, R. J.; Schmidt, M. A.; Jensen, K. F., *Anal. Chem.* **2004,** *76* (21), 6476-6483; (b) Floyd, T. M.; Schmidt, M. A.; Jensen, K. F., *Ind. Eng. Chem. Res.* **2005,** *44* (8), 2351-2358; (c) Leng, C. B.; Hiltner, J.; Pham, H.; Kelley, J.; Mach, M.; Zhang, Y. H.; Liu, Y., *Phys. Chem. Chem. Phys.* **2014,** *16* (9), 4350-4360; (d) Henry, C.; Bolien, D.; Ibanescu, B.; Bloodworth, S.; Harrowven, D. C.; Zhang, X. L.; Craven, A.; Sneddon, H. F.; Whitby, R. J., *Eur. J. Org. Chem.* **2015,** (7), 1491-1499.
78. Chaplain, G.; Haswell, S. J.; Fletcher, P. D. I.; Kelly, S. M.; Mansfield, A., *Aust. J. Chem.* **2013,** *66* (2), 208-212.
79. Song, H.; Ismagilov, R. F., *J. Am. Chem. Soc.* **2003,** *125* (47), 14613-14619.
80. (a) Wensink, H.; Benito-Lopez, F.; Hermes, D. C.; Verboom, W.; Gardeniers, H.; Reinhoudt, D. N.; van den Berg, A., *Lab Chip* **2005,** *5* (3), 280-284; (b) Xu, S.; Zhang, W.; Liu, X.; Han, X.; Bao, X., *J. Am. Chem. Soc.* **2009,** *131* (38), 13722-13727; (c) Sans, V.; Porwol, L.; Dragone, V.; Cronin, L., *Chem. Sci.* **2015,** *6* (2), 1258-1264; (d) Christianson, M. D.; Tan, E. H. P.; Landis, C. R., *J. Am. Chem. Soc.* **2010,** *132* (33), 11461-11463.
81. Singh, S.; de Leon, M. F.; Li, Z. J., *J. Phys. Chem. A* **2013,** *117* (42), 10863-10872.
82. (a) McMullen, J. P.; Jensen, K. F., *Org. Process Res. Dev.* **2011,** *15* (2), 398-407; (b) Reizman, B. J.; Jensen, K. F., *Org. Process Res. Dev.* **2012,** *16* (11), 1770-1782.
83. Bula, W. P.; Verboom, W.; Reinhoudt, D. N.; Gardeniers, H., *Lab Chip* **2007,** *7* (12), 1717-1722.
84. Luzgin, M. V.; Stepanov, A. G.; Arzumanov, S. S.; Rogov, V. A.; Parmon, V. N.; Wang, W.; Hunger, M.; Freude, D., *Chem. Eur. J.* **2005,** *12* (2), 457-465.
85. Mozharov, S.; Nordon, A.; Girkin, J. M.; Littlejohn, D., *Lab Chip* **2010,** *10* (16), 2101-2107.
86. Moore, J. S.; Jensen, K. F., *Angew. Chem., Int. Ed.* **2014,** *53* (2), 470-473.
87. Sato, M.; Ogasawara, H.; Oi, K.; Kato, T., *Chem. Pharm. Bull.* **1983,** *31* (6), 1896-1901.
88. Boulange, A.; Parraga, J.; Galan, A.; Cabedo, N.; Leleu, S.; Sanz, M. J.; Cortes, D.; Franck, X., *Bioorg. Med. Chem.* **2015,** *23* (13), 3618-3628.
89. Nahm, S.; Weinreb, S. M., *Tetrahedron Lett.* **1981,** *22* (39), 3815-3818.
90. Henegar, K. E.; Winkler, J. D., *Tetrahedron Lett.* **1987,** *28* (10), 1051-1054.
91. Haddad, N.; Rukhman, I.; Abramovich, Z., *J. Org. Chem.* **1997,** *62* (22), 7629-7636.
92. Eisenberg, S. W. E.; Kurth, M. J.; Fink, W. H., *J. Org. Chem.* **1995,** *60* (12), 3736-3742.
93. (a) Sato, M.; Ogasawara, H.; Komatsu, S.; Kato, T., *Chem. Pharm. Bull.* **1984,** *32* (10), 3848-3856; (b) Clemens, R. J.; Hyatt, J. A., *J. Org. Chem.* **1985,** *50* (14), 2431-2435.
94. Clemens, R. J.; Witzeman, J. S., *J. Am. Chem. Soc.* **1989,** *111* (6), 2186-2193.
95. Birney, D. M.; Xu, X. L.; Ham, S.; Huang, X. M., *J. Org. Chem.* **1997,** *62* (21), 7114-7120.

96. (a) Carvalho, A. R.; Brereton, R. G.; Thurston, T. J.; Escott, R. E. A., *Chemom. Intell. Lab. Syst.* **2004,** *71* (1), 47-60; (b) Thurston, T. J.; Brereton, R. G., *Analyst* **2002,** *127* (5), 659-668.
97. (a) Gourvenec, S.; Massart, D. L., *Anal. Bioanal. Chem.* **2004,** *380* (3), 373-375; (b) De Braekeleer, K.; Massart, D. L., *Chemom. Intell. Lab. Syst.* **1997,** *39* (2), 127-141.
98. (a) Zheng, X. T.; Gong, X. C.; Li, Q.; Qu, H. B., *Ind. Eng. Chem. Res.* **2012,** *51* (8), 3238-3245; (b) Hemmateenejad, B.; Javidnia, K.; Saeidi-Boroujeni, M., *J. Pharm. Biomed. Anal.* **2008,** *47* (3), 625-630; (c) De Luca, M.; Mas, S.; Ioele, G.; Oliverio, F.; Ragno, G.; Tauler, R., *Int. J. Pharm.* **2010,** *386* (1-2), 99-107; (d) Tauler, R.; Kowalski, B.; Fleming, S., *Anal. Chem.* **1993,** *65* (15), 2040-2047.
99. (a) Ruthven, D. M., *Chem. Eng. Sci.* **1971,** *26* (7), 1113; (b) Vandenberg, J. H. M.; Deelder, R. S., *Chem. Eng. Sci.* **1979,** *34* (11), 1345-1347.
100. Henry, C., *PhD Thesis, University of Southampton* **2014**.
101. Taylor, G., *Proc. R. Soc. London, A* **1953,** *219* (1137), 186-203.
102. Nagy, K. D.; Shen, B.; Jamison, T. F.; Jensen, K. F., *Org. Process Res. Dev.* **2012,** *16* (5), 976-981.
103. (a) Snyder, D. A.; Noti, C.; Seeberger, P. H.; Schael, F.; Bieber, T.; Rimmel, G.; Ehrfeld, W., *Helv. Chim. Acta* **2005,** *88* (1), 1-9; (b) Damm, M.; Glasnov, T. N.; Kappe, C. O., *Org. Process Res. Dev.* **2010,** *14* (1), 215-224; (c) Monbaliu, J.-C. M. R.; Cukalovic, A.; Marchand-Brynaert, J.; Stevens, C. V., *Tetrahedron Lett.* **2010,** *51* (44), 5830-5833; (d) Hornung, C. H.; Mackley, M. R.; Baxendale, I. R.; Ley, S. V., *Org. Process Res. Dev.* **2007,** *11* (3), 399-405; (e) Yokozawa, S.; Ohneda, N.; Muramatsu, K.; Okamoto, T.; Odajima, H.; Ikawa, T.; Sugiyama, J.-i.; Fujita, M.; Sawairi, T.; Egami, H.; Hamashima, Y.; Egi, M.; Akai, S., *RSC adv.* **2015,** *5* (14), 10204-10210.
104. Sauer, J., *Angew. Chem.* **1967,** *6*, 16-33.
105. Hosomi, A.; Saito, M.; Sakurai, H., *Tetrahedron Lett.* **1980,** *21* (4), 355-358.
106. Fischer, M., *Angew. Chem., Int. Ed. Engl.* **1978,** *17* (1), 16-26.
107. Knowles, J. P.; Elliott, L. D.; Booker-Milburn, K. I., *Beilstein J. Org. Chem.* **2012,** *8*, 2025-2052.
108. (a) Hook, B. D. A.; Dohle, W.; Hirst, P. R.; Pickworth, M.; Berry, M. B.; Booker-Milburn, K. I., *J. Org. Chem.* **2005,** *70* (19), 7558-7564; (b) Levesque, F.; Seeberger, P. H., *Org. Lett.* **2011,** *13* (19), 5008-5011; (c) Gutierrez, A. C.; Jamison, T. F., *Org. Lett.* **2011,** *13* (24), 6414-6417.
109. Galante, A. M. S.; Galante, O. L.; Campos, L. L., *Nucl. Instrum. Methods Phys. Res., Sect. A* **2010,** *619* (1-3), 177-180.
110. (a) Aillet, T.; Loubiere, K.; Dechy-Cabaret, O.; Prat, L., *Chem. Eng. Process.* **2013,** *64*, 38-47; (b) Horie, T.; Sumino, M.; Tanaka, T.; Matsushita, Y.; Ichimura, T.; Yoshida, J., *Org. Process Res. Dev.* **2010,** *14* (2), 405-410; (c) Anderson, B. G.; Bauta, W. E.; Cantrell, W. R., Jr., *Org. Process Res. Dev.* **2012,** *16* (5), 967-975.
111. (a) Yavorskyy, A.; Shvydkiv, O.; Hoffmann, N.; Nolan, K.; Oelgemoeller, M., *Org. Lett.* **2012,** *14* (17), 4342-4345; (b) Maskill, K. G.; Knowles, J. P.; Elliott, L. D.; Alder, R. W.; Booker-Milburn, K. I., *Angew. Chem., Int. Ed.* **2013,** *52* (5), 1499-1502; (c) Blackham, E. E.; Knowles, J. P.; Burgess, J.; Booker-Milburn, K. I., *Chem. Sci.* **2016,** *7* (3), 2302-2307.
112. (a) Suishu, T.; Shimo, T.; Somekawa, K., *Tetrahedron* **1997,** *53* (10), 3545-3556; (b) Corey, E. J.; Bass, J. D.; LeMahieu, R.; Mitra, R. B., *J. Am. Chem. Soc.* **1964,** *86* (24), 5570-5583; (c) Wilson, S. R.; Phillips, L. R.; Pelister, Y.; Huffman, J. C., *J. Am. Chem. Soc.* **1979,** *101* (24), 7373-7379; (d) Poplata, S.; Troster, A.; Zou, Y. Q.; Bach, T., *Chem. Rev.* **2016,** *116* (17), 9748-9815.
113. (a) Nicolaou, K. C.; Sarlah, D.; Shaw, D. M., *Angew. Chem., Int. Ed.* **2007,** *46* (25), 4708-4711; (b) Mascitti, V.; Corey, E. J., *J. Am. Chem. Soc.* **2006,** *128* (10), 3118-3119.
114. Ciamician, G.; Silber, P., *Ber.* **1908,** *41* (2), 1928-1935.
115. Fukuyama, T.; Kajihara, Y.; Hino, Y.; Ryu, I., *J. Flow Chem.* **2011,** *1* (1), 40-45.

116. Maradyn, D. J.; Weedon, A. C., *Tetrahedron Lett.* **1994,** *35* (44), 8107-8110.
117. (a) Batten, R. J.; Carless, H. A. J., *J. Chem. Soc. Chem. Comm.* **1985,** (17), 1146-1147; (b) Schuster, D. I.; Kaprinidis, N.; Wink, D. J.; Dewan, J. C., *J. Org. Chem.* **1991,** *56* (2), 561-567.
118. Yamashita, Y., *Sci. Technol. Adv. Mater.* **2009,** *10* (2), 024313.
119. Kubozono, Y.; Mitamura, H.; Lee, X.; He, X. X.; Yamanari, Y.; Takahashi, Y.; Suzuki, Y.; Kaji, Y.; Eguchi, R.; Akaike, K.; Kambe, T.; Okamoto, H.; Fujiwara, A.; Kato, T.; Kosugi, T.; Aoki, H., *Phys. Chem. Chem. Phys.* **2011,** *13* (37), 16476-16493.
120. Mallory, F. B.; Mallory, C. W., *Org. React.* **1984,** *30*, 1.
121. (a) Hernandez-Perez, A. C.; Vlassova, A.; Collins, S. K., *Org. Lett.* **2012,** *14* (12), 2988-2991; (b) McQuade, D. T.; O'Brien, A. G.; Dorr, M.; Rajaratnam, R.; Eisold, U.; Monnanda, B.; Nobuta, T.; Lohmannsroben, H. G.; Meggers, E.; Seeberger, P. H., *Chem. Sci.* **2013,** *4* (10), 4067-4070; (c) Okamoto, H.; Takane, T.; Gohda, S.; Kubozono, Y.; Sato, K.; Yamaji, M.; Satake, K., *Chem. Lett.* **2014,** *43* (7), 994-996.
122. Vicinelli, V.; Ceroni, P.; Maestri, M.; Lazzari, M.; Balzani, V.; Lee, S. K.; van Heyst, J.; Vogtle, F., *Org. Biomol. Chem.* **2004,** *2* (15), 2207-2213.
123. Talele, H. R.; Gohil, M. J.; Bedekar, A. V., *Bull. Chem. Soc. Jpn.* **2009,** *82* (9), 1182-1186.
124. Ohara, K.; Inokuma, Y.; Fujita, M., *Angew. Chem., Int. Ed.* **2010,** *49* (32), 5507-5509.
125. Baldwin, S. W.; Wilkinson, J. M., *J. Am. Chem. Soc.* **1980,** *102* (10), 3634-3635.
126. Beugelmans, R.; Boischoussy, M.; Boudet, B., *Tetrahedron* **1982,** *38* (23), 3479-3483.
127. Ley, S. V.; Smith, S. C.; Woodward, P. R., *Tetrahedron* **1992,** *48* (6), 1145-1174.
128. Giuliani, G.; Benedusi, A.; Milanese, A., *Patent* **2010**.
129. Goodreid, J. D.; Wong, K.; Leung, E.; McCaw, S. E.; Gray-Owen, S. D.; Lough, A.; Houry, W. A.; Batey, R. A., *J. Nat. Prod.* **2014,** *77* (10), 2170-2181.
130. Pini, E.; Bertacche, V.; Molinari, F.; Romano, D.; Gandolfi, R., *Tetrahedron* **2008,** *64* (37), 8638-8641.
131. (a) Schuurman, M. S.; Giegerich, J.; Pachner, K.; Lang, D.; Kiendl, B.; MacDonell, R. J.; Krueger, A.; Fischer, I., *Chem. Eur. J.* **2015,** *21* (41), 14486-14495; (b) Jones, C. H. W.; Jones, R. G.; Partingt.P; Roberts, R. M. G., *J. Organomet. Chem.* **1971,** *32* (2), 201-212.
132. Gassman, P. G.; Patton, D. S., *J. Am. Chem. Soc.* **1968,** *90* (26), 7276-7282.
133. Atkin, A. J.; Fairlamb, I. J. S.; Ward, J. S.; Lynam, J. M., *Organometallics* **2012,** *31* (16), 5894-5902.
134. Brennan, M. E.; Battiste, M. A., *J. Org. Chem.* **1968,** *33* (1), 324-332.
135. Jordan, R. W.; Le Marquand, P.; Tam, W., *Eur. J. Org. Chem.* **2008,** (1), 80-86.
136. Balducci, E.; Attolino, E.; Taddei, M., *Eur. J. Org. Chem.* **2011,** (2), 311-318.
137. (a) Tommasi, I.; Sorrentino, F., *Tetrahedron Lett.* **2005,** *46* (12), 2141-2145; (b) Kabalka, G. W.; Yang, K.; Wang, Z., *Synth. Commun.* **2001,** *31* (4), 511-517.
138. Gadge, S. T.; Bhanage, B. M., *Org. Biomol. Chem.* **2014,** *12* (30), 5727-5732.
139. Persson, T.; Nielsen, J., *Org. Lett.* **2006,** *8* (15), 3219-3222.
140. McDonald, S. L.; Wang, Q., *Chem. Commun.* **2014,** *50* (19), 2535-2538.
141. Sato, M.; Uehara, F.; Kamaya, H.; Murakami, M.; Kaneko, C.; Furuya, T.; Kurihara, H., *Chem. Commun.* **1996,** (9), 1063-1064.
142. May, A. E.; Hoye, T. R., *J. Org. Chem.* **2010,** *75* (17), 6054-6056.
143. Zarei, H. A.; Lavasani, M. Z.; Iloukhani, H., *J. Chem. Eng. Data* **2008,** *53* (2), 578-585.
144. Choi, H. Y.; Chi, D. Y., *Org. Lett.* **2003,** *5* (4), 411-414.
145. Mineno, M.; Sawai, Y.; Kanno, K.; Sawada, N.; Mizufune, H., *J. Org. Chem.* **2013,** *78* (12), 5843-5850.
146. (a) Gao, Q.; Li, S. Y.; Pan, Y. M.; Xu, Y. L.; Wang, H. S., *Tetrahedron* **2013,** *69* (19), 3775-3781; (b) Qian, H.; Ge, C. R.; Huang, M., *J. Chem. Res.* **2007,** (3), 160-161.
147. (a) Zhang, G. F.; Wen, X.; Wang, Y.; Mo, W. M.; Ding, C. R., *J. Org. Chem.* **2011,** *76* (11), 4665-4668; (b) Korsager, S.; Nielsen, D. U.; Taaning, R. H.; Skrydstrup, T., *Angew. Chem., Int. Ed.* **2013,** *52* (37), 9763-9766.

148. Sridhar, Y.; Srihari, P., *Eur. J. Org. Chem.* **2013,** (3), 578-587.
149. (a) Landers, B.; Berini, C.; Wang, C.; Navarro, O., *J. Org. Chem.* **2011,** *76* (5), 1390-1397; (b) Cogne-Laage, E.; Allemand, J. F.; Ruel, O.; Baudin, J. B.; Croquette, V.; Blanchard-Desce, M.; Jullien, L., *Chem. Eur. J.* **2004,** *10* (6), 1445-1455.
150. (a) Friedfeld, M. R.; Margulieux, G. W.; Schaefer, B. A.; Chirik, P. J., *J. Am. Chem. Soc.* **2014,** *136* (38), 13178-13181; (b) Eklund, L.; Axelsson, A. K.; Nordahl, A.; Carlson, R., *Acta Chem. Scand.* **1993,** *47* (6), 581-591; (c) Nakagawa, K.; Sawai, M.; Ishii, Y.; Ogawa, M., *Bull. Chem. Soc. Jpn.* **1977,** *50* (9), 2487-2488.
151. Taylor, A.; Eisenbraun, E. J.; Browne, C. E.; Holt, E. M., *Acta Crystallogr., Sect. C: Cryst. Struct. Commun* **1997,** *53*, 1963-1966.
152. Cecil, J. C.; Dyer, C. W.; Fleming, S. A.; Jessop, T. C., *Anal. Sci.* **1999,** *15* (9), 895-897.
153. Yang, J.; Dewal, M. B.; Shimizu, L. S., *J. Am. Chem. Soc.* **2006,** *128* (25), 8122-8123.
154. Barbero, N.; Martin, R., *Org. Lett.* **2012,** *14* (3), 796-799.
155. Ekomie, A.; Lefevre, G.; Fensterbank, L.; Lacote, E.; Malacria, M.; Ollivier, C.; Jutand, A., *Angew. Chem., Int. Ed.* **2012,** *51* (28), 6942-6946.
156. Fujiwara, Y.; Sumino, M.; Nozaki, A.; Okamoto, M., *Chem. Pharm. Bull.* **1989,** *37* (6), 1452-1457.
157. (a) Syamala, M. S.; Ramamurthy, V., *J. Org. Chem.* **1986,** *51* (19), 3712-3715; (b) Rao, K.; Hubig, S. M.; Moorthy, J. N.; Kochi, J. K., *J. Org. Chem.* **1999,** *64* (22), 8098-8104.